

https://dspace.org/

An investigation of the mineralisation and associated structures within the Grasvally area, South Africa

Acheampong, Kofi Osei

2020

https://hdl.handle.net/10539/31013

Downloaded from a DSpace repository. https://dspace.org/

UNIVERSITY OF THE WITWATERSRAND, JOHANNESBURG,
SCHOOL OF GEOSCIENCES



UNIVERSITY OF THE
WITWATERSRAND,
JOHANNESBURG

AN INVESTIGATION OF THE MINERALISATION AND ASSOCIATED STRUCTURES WITHIN THE GRASVALLY AREA, SOUTH AFRICA.

By: Kofi Osei Acheampong
571056

Supervisors: Prof. Judith A Kinnaird

Prof. Paul Nex

Declaration

I, *Kofi Osei Acheampong*, declare that this dissertation is my own, unaided work. It is being submitted for the Degree of Master of Science at the University of the Witwatersrand, Johannesburg. It has not been submitted before for any degree or examination at any other University.



K.O Acheampong

02 day of January 2020 at The University of the Witwatersrand

Abstract

The mafic rocks of the Bushveld Complex differ to the north and south of the Ysterberg-Planknek Fault, part of the array that is the Thabazimbi-Murchison Lineament. To the north, there is sporadic Lower Zone, succeeded by a PGE-Cu-Ni-bearing Platreef, Main Zone and Upper Zone successions. To the south is Lower Zone, the Grasvally Norite-Pyroxenite-Anorthosite (GNPA) member and Main Zone. This investigation on the farm of Grasvally aims to provide a better understanding of the mafic rocks south of Mokopane, in order to provide an improved understanding of the relationship between the geology and mineralisation of this region.

The farm Grasvally is situated approximately 20 km south of Mokopane. The geology of the Grasvally area comprises mainly mafic to ultramafic Bushveld rocks of Lower Zone to Main Zone affinity which were within sedimentary rocks of the Pretoria Group. The GNPA member was originally divided into two major sub-units but more recently it has been divided into the Lower Mafic Unit (LMF), the Lower Gabbronorite Unit (LGN) and the Mottled Anorthosite Unit (MANO). The GNPA member may be the equivalent to the Platreef to the north of the Ysterberg-Planknek Fault.

The Lower Zone displays little to no variation in Mg# indicative of no fractionation and continuous replenishment of magma. Two well-developed chromitites ~60 - 90 cm in thickness are intersected within the Lower Zone (LZ). These chromitite layers display the highest Cr_2O_3 within the Bushveld Complex and are not nearly as thick within the LZ anywhere else. The chromitites, disseminated chromite, pyrrhotite, chalcopyrite and minor pentlandite mineralisation are hosted within the harzburgites and pyroxenites of the LZ. The kink banding in olivine of the Lower Zone is indicative of high-pressure solid-state deformation. The Lower Zone also displays serpentinisation, which increases from east to west, possibly having occurred along fractures associated with this high-pressure high-temperature system.

Three-dimensional modelling of the area with the use of borehole logs, existing surface mapping and structural data proves the existence of a 70°W dipping fault which has brought the Transvaal sedimentary rocks, the marginal member and Critical Zone to the east of the fault in contact with the LZ. To the west of the fault the Lower Zone, LMF, MANO, and Upper Zone form a conformable sequence, shallowly dipping to the west. The Thabazimbi-Murchison Lineament may

have acted as a barrier to the flow of magma causing the GNPA member to be compartmentalised and to follow a different evolution from the Critical Zone magma in the eastern or western limbs or to the Platreef to the north.

Core logging indicated that the GNPA member overlies the Magaliesberg quartzites of the Pretoria Group and the Lower Zone to the east and the west of the farm respectively. Previous work (Smith *et al*., 2014) suggests PGE mineralisation is associated with sulphides and is not restricted to one lithological unit within the GNPA member. Within the LGN blebs (<1 cm) of fine-grained cumulus magnetite within norite have not been previously documented. Additionally, below this unit, within the LMF are disseminated to well-developed layers of chromite, as well as isolated pods of chromitite within norite and gabbronorite which are not easily correlated with the known stratigraphy. The boreholes also intersect a pyroxenite unit within the LMF that has visual similarities to the mineralisation and the same hanging and footwall as the UG 2 chromitite layer. This pyroxenite comprising orthopyroxene, interstitial plagioclase and clinopyroxene, hosts disseminations and a well-developed chromitite layer with associated disseminated to blebby pyrrhotite and chalcopyrite. The Pt/Pd ratios associated with chromitiferous pyroxenites and chromitites within the pyroxenites are similar to that of the UG2 whereas the Pt/Pd variation within the GNPA member is indicative of multiple influxes of magma.

Contents

Abstract iii

Table of Figures vii

List of Tables xv

Motivation for Research ii

CHAPTER 1 1

General Geology of the Bushveld Complex 1

1.1 Introduction 1

1.2 Magmatic Stratigraphy and Subdivisions of the Rustenburg Layered Suite 2

1.3 Location and Research Area 4

1.4 Aims 5

1.5 Methodology 6

1.5.4 Magnetic Susceptibility 7

CHAPTER 2 8

Geological Setting of the northern limb 8

2.1 Lower Zone 9

2.2 The Grasvally Norite-Pyroxenite-Anorthosite (GNPA) member 11

2.3 The Platreef 16

2.4 Structural deformation of the northern limb 16

2.5 Summary 22

CHAPTER 3 23

Geology of the Grasvally Area 23

3.1 Core Logging 23

3.2 Petrography 36

3.4 Magnetic Susceptibility (MS) 46

3.5 Discussion 49

3.6 Summary 55

CHAPTER 4 56

Geochemical Analysis 56
4.1 Introduction 56
4.2 Methodology 56
4.3 Major and Trace element geochemistry 57
4.4 Major oxide plots 60
4.5 Geochemical variations with depth 63
4.6 Discussion 79
CHAPTER 5 85
Three-Dimensional (3D) Modelling 85
5.1 Methodology 85
5.2 Modelling Process 90
5.3 Interpretation of three-dimensional Modelling 96
CHAPTER 6 103
Discussion 103
6.1 The stratigraphy of the Grasvally area 103
6.1.1 Footwall 103
6.1.2 Lower Zone 107
6.1.3 Marginal member 110
6.1.4 Critical Zone (GNPA member) 112
6.2 Correlative Marker Horizons 115
6.3 Mineralisation 118
CHAPTER 7 120
Conclusions 120
Further Recommendations 123
References ..... a
List of Appendices ..... a

Table of Figures

Chapter 1

Figure 1.1: Simplified geological map of the Bushveld Complex, which includes the Rustenburg Layered Suite, the Rooiberg Volcanics and the Lebowa Granite Suite adapted from McCreesh, 2018. Major structural features such as the Thabazimbi -Murchison Lineament and the Hout River Shear Zone (HRSZ) are included. 1

Figure 1.2: Geological map of the northern limb of the Rustenburg Layered Suite (RLS), showing the location of the research area on the farm of Grasvally. Adapted from Smith *et al*. (2014). 5

Chapter 2

Figure 2.1: The general geology of the northern limb of the Bushveld Complex showing the different stratigraphic units, surrounding rocks and structural features. Original map by van der Merwe (1979); colour map generated by Ashwal *et al*. (2005); from Kinnaird and McDonald (2005). 8

Figure 2.2: Differences between northern limb stratigraphy to the north and south of the Ysterberg-Planknek Fault Adapted from Smith *et al*. (2011). 9

Figure 2.3: Stratigraphic column of the northern limb Lower Zone south of the Ysterberg-Planknek Fault. Adapted from Hulbert (1983). 10

Figure 2.4: Differences in magmatic stratigraphy of Critical Zone, and its equivalents across the Bushveld Complex. Adapted from Smith *et al*. (2011). 12

Figure 2.5: Geological map of the lower portion of the northern limb. Adapted from McDonald *et al*. (2005). Idealised stratigraphic sections for key localities along the strike of the northern limb displaying the successively younger footwall rocks to the south, Lower Zone intersections as well as variations in the Critical Zone equivalent. 13

Figure 2.6: Stratigraphic column of the Rooipoort-Grasvally area. Adapted from Maier *et al*. (2008). 15

Figure 2.7: Granite-greenstone terrains of the Kaapvaal Craton displaying outline of the Bushveld Complex and Thabazimbi-Murchison Lineament modified after de Wit and Hart (1993). 17

Figure 2.8: Geological map of Tweefontein Hill showing the distribution of lithologies, faults and adits. Stippled lines show inferred geological contacts and solid lines are observed contacts (Nex, 2005). 19

Figure 2.9: Schematic lithostratigraphic column of the lower part of the Transvaal Supergroup in the Mokopane Area after SACS,Greer (1983) and Nex (2005). 20

Figure 2.10: Generalised geological map of the Grasvally-Zoetveld-Volspruit area showing the four generations of faults, modified after Hulbert (1983). Map of general geology of the northern limb after Ashwal *et al*. (2005). 21

Chapter 3

Figure 3.1: Borehole distribution on the farm Grasvally drilled by Samancor in 2004. Map modified after Hulbert (1983). 24

Figure 3.2: IUGS classification scheme for mafic rocks. The Grasvally rock types fall mainly in the orthopyroxenite, olivine orthopyroxenite and harzburgite fields (le Bas and Streckeisen, 1991). 25

Figure 3.3: Simplified geological logs of representative boreholes arranged in order from west to east. The brown line at the top of the boreholes represents the relative topographic elevation of the collars. 26

Figure 3.4: Simplified geological logs of representative boreholes arranged in order from south to north. The brown line at the top of the boreholes represents the relative topographic elevation of the collars. 27

Figure 3.5: Fresh dunite with disseminated chromite intersected in GVL 9 (a) in quarter core and (b) in full core. 29

Figure 3.6: Serpentinised harzburgite with net-textured pyrrhotite and specks of interstitially disseminated chalcopyrite. 30

Figure 3.7: Various harzburgites. (a) Poikilitic harzburgite with 1 cm oikocrysts of orthopyroxene and olivine chadacrysts. (b) Serpentinised harzburgite with interstitially disseminated pyrrhotite. (c) Harzburgite with even proportions of orthopyroxene and olivine. (d) Extremely serpentinised harzburgite with widely spaced orthopyroxene oikocrysts. 31

Figure 3.8: Various pyroxenites. (a) Coarse-grained feldspathic pyroxenite. (b) Altered coarse-grained feldspathic pyroxenite. (c) Fine-grained feldspathic pyroxenite with weathered mineralised sulphides. (d) Fine-grained pyroxenite with sulphide specks. 32

Figure 3.9: Norite package intersected in borehole GVL 2 cut by several quartzofeldspathic veins. 33

Figure 3.10: various xenoliths observed within the norites and gabbronorites in core GVL 2. (a) Chromitite pod with associated sulphides within gabbronorite. (b) Pyroxenite xenolith with interstitially disseminated sulphide specks. (c) Anorthosite xenolith within gabbronorite. All Samples are intersected in GVL 2. 34

Figure 3.11: Fine-grained magnetite bleb within norite intersected in borehole GVL 2. 34

Figure 3.12: variably textured mottled anorthosite unit grading from spotted to mottled to feldspathic pyroxenite back into mottled anorthosite intersected in borehole GVL 9. 35

Figure 3.13: Pyroxenite brecciated by quartzofeldspathic veins. 36

Figure 3.14: Photomicrographs of a serpentinised chromite-bearing harzburgite in both transmitted and reflected light. (a) serpentinised harzburgite in PPL with opaque chained chromite. (b) Serpentinised harzburgite in XPL dominated by secondary serpentine veins. (c) Serpentinised harzburgite in RL with chained chromite, chromite displaying atoll textures and interstitially disseminated pyrrhotite, chalcopyrite and magnetite. 37

Figure 3.15: Photomicrographs of a serpentinised dunite in both transmitted and reflected light. (a) Dunite in PPL with olivine and interstitially disseminated opaques. (b) Dunite in XPL with annealed olivine crystals displaying kink banding. (c) Dunite in RL with interstitially disseminated pyrrhotite and chromite (d) Serpentinised dunite in RL displaying interstitially disseminated blebs of pyrrhotite. (e) Serpentinised dunite in PPL with altered olivine and secondary biotite associated with pyrrhotite (opaque). (f) Serpentinised dunite in XPL displaying serpentinised and highly fractured olivine grains with secondary biotite associated with pyrrhotite (Opaque). 38

Figure 3.16: Photomicrographs of a mineralised pyroxenite in both transmitted and reflected light. (a) Pyroxenite in PPL displaying clinopyroxene with exsolution lamellae and annealed olivine and altered orthopyroxenes. (b) Pyroxenite with clinopyroxene displaying exsolution lamellae, olivine and orthopyroxene. (c) Pyroxenite in RL displaying chromite, interstitially disseminated pyrrhotite with lesser specks of disseminated chalcopyrite. 39

Figure 3.17: Photomicrographs of an altered gabbronorite in both transmitted and reflected light. (a) Gabbronorite in PPL with biotite associated with opaque magnetite. (b) gabbronorite in XPL with highly altered and fractured opx and cpx displaying exsolution lamellae. Sericitisation of feldspars is visible in places. (c) Gabbronorite in reflected light displaying grains of magnetite. 40

Figure 3.18: Photomicrographs of a norite in both transmitted and reflected light. (a) Highly fractured norite dominated by orthopyroxene in PPL. (b) Norite dominated by orthopyroxene, plagioclase with minor intercumulus clinopyroxene in XPL. (c) Blebby pyrrhotite with associated chalcopyrite and lesser interstitially disseminated chalcopyrite and pyrite specks. 41

Figure 3.19: Photomicrographs of an altered anorthosite in both transmitted and reflected light. (a) Anorthosite in PPL with dominant plagioclase crystals as well as darker coloured areas of alteration. (b) Anorthosite displaying dominant plagioclase crystals heavily altered to sericite, interstitial clinopyroxene as well as orthopyroxene. (c) Secondary veinlets of magnetite as well as interstitial magnetite is present associated with the sericitised zone. 42

Figure 3.20: Photomicrographs of a granofels in transmitted light displaying granophyric texture. (a) Photomicrograph of quartzofeldspathic vein displaying granophyric texture in XPL. (b) Quartzofeldspathic vein displaying granophyric texture in PPL. 43

Figure 3.21: Photomicrographs of various opaque minerals observed in core. Interstitially distributed cumulus chromite and lesser magnetite in XPL within feldspathic gabbronorite in PPL (a) and in RL (b). Gabbronorite dominated by feldspar with interstitial clinopyroxene with exsolution lamellae highly fractured and altered orthopyroxene with inclusions of feldspar (c). Interstitial intercumulus magnetite with associated biotite and minor specks of pyrite within gabbronorite (d). 44

Figure 3.22: (a) A large pyrrhotite with marginal chalcopyrite. Veinlets and specks of secondary magnetite. (b) Pyrrhotite, chalcopyrite, magnetite and chromite. (c) Interstitial pyrrhotite rimmed partially by chalcopyrite. (d) Chromitite grains displaying atoll texture with specks of interstitially disseminated pyrrhotite. 45

Figure 3.23: SM-30 Magnetic Susceptibility metre alongside pyroxenite quarter-core displaying susceptibility reading. 47

Figure 3.24: Magnetic susceptibility profiles (SI units) of selected holes GVL 3, GVL 11, GVL 2, GVL 9 and GVL 4 plotted against simplified geological logs. 48

Figure 3.25: Tentative correlations based on hand sample and thin section descriptions of boreholes arranged east to west. 50

Figure 3.26: Tentative correlations based on hand sample and thin section descriptions of boreholes arranged south to north. 50

Figure 3.27: Simplified lithological logs of chosen representative holes correlated with the stratigraphic subdivisions of de Klerk (2005). 53

Figure 3.28: Magnetic susceptibility signatures of boreholes GVL 3, 4,11,9, and 2 correlated with possible stratigraphic units. Stratigraphic units adapted from Hulbert (1983) and (de Klerk, 2005). 55

Chapter 4

Figure 4.1: Classification and nomenclature of gabbroic rocks based on the CIPW normative proportions calculated from the modal geochemistry of plagioclase (Plag), clinopyroxene (Cpx) and orthopyroxene (Opx) (after Streckeisen, 1976). 58

Figure 4.2: Classification and nomenclature of ultramafic rocks based on the CIPW proportions of olivine (Ol), orthopyroxene (Opx) and clinopyroxene (Cpx) (after Streckeisen, 1976). 59

Figure 4.3: Classification of samples K-1 to K-133 on a diagram showing MgO wt % against Al2O3 wt %. The classification parameters have been adopted from Hulbert (1983). Samples have been plotted according to the hand sample classification. 61

Figure 4.4: Classification of samples K-1 to K-133 on diagram showing MgO + FeO wt. % against CaO wt. %. The classification parameters have been adopted from Hulbert (1983). Samples have been plotted according to the hand sample classification. 61

Figure 4.5: Classification of samples K-1 to K-133 showing Al_2O_3 against CaO wt. %. The classification parameters have been adopted from Hulbert (1983). Samples have been plotted according to the hand sample classification. 62

Figure 4.6: Classification for samples K-1 to K-133 on a diagram showing MgO against CaO wt. %. The classification parameters have been adopted from Hulbert (1983). Samples have been plotted according to the hand sample classification. 62

Figure 4.7: Classification for samples K-1 to K-133 showing MgO + Fe_2O_3 against Al2O3 wt. %. The classification parameters have been adopted from Hulbert (1983). Samples have been plotted according to the hand sample classification. 63

Figure 4.8: Variations of the whole-rock Mg#, major and trace element ratios and trace element contents through borehole the GVL 3. Mg# and Cr (ppm) display generally decreasing trends up section as the package transitions into more leucocratic rocks. 64

Figure 4.9: Variations of the whole-rock Mg#, major and trace element ratios and trace element contents through borehole GVL 4. 65

Figure 4.10: Variations of the whole-rock Mg#, major and trace element ratios and trace element contents through borehole GVL 9. 66

Figure 4.11: Variations of the whole-rock Mg#, major and trace element ratios and trace element contents through borehole the GVL 5. Mg# displays little to no variation up section and is indicative of a lack of fractionation occurring within this package but perhaps a constant replenishment of magma. 67

Figure 4.12: Variations of the whole-rock Mg#, major and trace element ratios and trace element contents through borehole GVL 11. 70

Figure 4.13: Variations of the whole-rock Mg#, major and trace element ratios and trace element contents through borehole GVL 18. 71

Figure 4.14: Variations of the whole-rock Mg#, major and trace element ratios and trace element contents through part of borehole the GVL 2. The Mg# displays a decrease up section within the gabbronorite. The Cr displays a sharp increase in Cr at 210 m whereas the Cr is below 200m ppm elsewhere within this unit. 72

Figure 4.15: Whole rock Cr (ppm) and MgO (wt. %) for samples from boreholes GVL 2. GVL 3, GVL 4, GVL 9, GVL 11 and GVL 18 with the exclusion of Lower Zone samples. The classification fields are defined by the Cr/MgO ratios of 80 and 60 for the Critical Zone and Main Zone respectively (Seabrook *et al*., 2005). 75

Figure 4.16: Pt/Pd ratios for boreholes GVL 10, GVL 4 and GVL 15 plotted against depth. The chromitite seam markers are not to scale. Stippled line indicates average Pt/Pd ratio for the overall Platreef although different sills within the Platreef as a whole have distinctly different Pt/Pd ratios (1:1 Pt/Pd) (Kinnaird, 2005a). 76

Figure 4.17: Binary variation diagrams of Cu/Ni, and Cu/Pd ratios, showing data for the GNPA member pyroxenite from this study, plotted against Platreef and the Lower Zone peridotite, pyroxenite, and feldspathic pyroxenite after Yudovskaya (2013). Samples plotted against Sandsloot samples (a) and Turfspruit (b) showing that the GNPA samples display a similar distribution to that of the Platreef on Turfspruit. 78

Figure 4.18: Binary variation diagrams of Cu/Ni, and Pt/Pd ratios, showing data for the GNPA member pyroxenite from this study, plotted against Platreef and the Lower Zone peridotite, pyroxenite, and feldspathic pyroxenite after Yudovskaya (2013) Samples plotted against Sandsloot samples (a) and Turfspruit samples (b) showing the samples of the GNPA member are generally palladium dominated with displaying a similar distribution to the Platreef samples of Sandsloot. 78

Chapter 5

Figure 5.1: Modelling methodology framework followed to design a 3D geological model. 85

Figure 5.2: A topographic map of the Grasvally area with the geological map overlain, generated in Leapfrog Geo®. 86

Figure 5.3: Plan view of modelled area with boreholes incorporated. Draped map adapted from Hulbert (1983). 88

Figure 5.4: Simplistic depiction of model components. Wireframes or surfaces (a) which are representative of the lithological or stratigraphic boundaries which are then used to define the lithological or stratigraphic volumes (b). Modified after Ross *et al*. (2007). 88

Figure 5.5: Digitised contacts between stratigraphic units. Stratigraphic contacts are obtained from Hulbert 1983. 89

Figure 5.6: Digitised stratigraphic contacts with structural disks. Structural disks are a graphical representation of the orientation of each feature. The colour of structural disks based on the polarisation of each contact, red- positive, blue- negative, to influence the interaction of contacts with each other. The structural data was obtained from Hulbert 1983. 90

Figure 5.7: Orthographic view of all surfaces, vein surfaces dyke, marginal member and granite unit and intrusive surfaces of the Transvaal metasedimentary succession, the Lower Zone, Critical Zone, Main Zone, Upper Zone, and the alluvial cover, showing the differences between the surfaces used to create the deposit- type and erosive volumes compared to the vein type or intrusive volumes. 92

Figure 5.8: Orthographic view from the south of vein surfacing of dyke (yellow) marginal member (orange) and the granite body (pink). 93

Figure 5.9: Plan view of model with major faults introduced showing how the ENE-WNW faults further offset and compartmentalise the major stratigraphic units within the Grasvally area. 93

Figure 5.10: Orthographic view of the modelled geological volumes of the Grasvally area. Structural data obtained from Hulbert 1983. 94

Figure 5.11: Three-dimensional surfaces further constrained with the use of simplified borehole data showing the general orientation of the contacts as well as the dip of the volumes to east and the west of the major N-S trending fault. 95

Figure 5.12: Exploded view of Grasvally area with stratigraphic units and structural data projected from surface mapping. Orthographic exploded view is north looking. 96

Figure 5.13: Orthographic view of Transvaal volume from a south-west perspective. 97

Figure 5.14: Sectional view of Grasvally body looking south. Inferred boundaries in black stippled line, and fault in white stippled line. The orange unit represents gabbronorite which was interpreted as being part of the marginal member however modelling shows that within GVL 1 this gabbronorite is part of the Critical Zone. 98

Figure 5.15: Sectional view of Grasvally body looking south. Boundaries have been further constrained by the incorporation of simplified borehole data. 98

Figure 5.16: View of eastern section exposing the morphology and orientation of the marginal member and underlying Transvaal unit. 99

Figure 5.17: Sectional view looking east of the Main Zone volume generated from the mapping of Hulbert (1983) with the boreholes GVL 3 and GVL 15 plotted against it. 100

Chapter 6

Figure 6.1: A schematic diagram displaying the differences and similarities in stratigraphy between the eastern and western limbs of the Bushveld Complex, the Grasvally area, the Rooipoort Project (de Klerk, 2005) and the generalised northern limb Stratigraphy (Modified from Kinnaird *et al*. (2005)). 104

Figure 6.2: Comparison of cross sections of Grasvally area. (top) Interpreted cross sectional view A-B of the Grasvally area considering borehole data and structural data (Hulbert, 1983). The cross section is compared to the idealised section of Hulbert (1983) below to highlight the differences in stratigraphy in the east of the area. The lithologies have been simplified into stratigraphic units. 105

Figure 6.3: Interpretation of the footwall geometry through the use of gravity data taken along cross section E-F showing the complex nature of footwall lithologies (Barrett *et al*., 1978). The marginal member, Critical Zone and Main Zone have been represented within this diagram as one unit (seen in red) after Barrett *et al*. (1978). The dotted lines represent the chromitite layers within the Lower Zone. 106

Figure 6.4: Schematic diagram of marker horizons identified displaying the mottled anorthosite marker within the MANO, chromitite within the LMF, the marginal member with a distinct magnetic susceptibility, the Lower Zone - LMF boundary which is marked by an increase in feldspar as well as the chromitite layers within the Lower Zone that can be correlated between boreholes. 117

List of Tables

Chapter 3

Table 3.1: Average magnetic susceptibility values for Bellevue drill core (BV-1) after Ashwal *et al*. (2005). 46

Chapter 6

Table 6.1: Varying Pt:Pd ratios for pyroxenite packages from cores ATS57 and ATS26 on Turfspruit displaying variation in reef layers (Kinnaird, 2005b). 83

Acknowledgements

The Author would like to thank his supervisors, Prof. Judith Kinnaird and Prof. Paul Nex, for the help conceptualising this project and the constant priceless support and boundless knowledge provided along the way. The author honestly cannot thank his supervisors enough for never giving up on him when hope started to fade - without them this project would not have been possible. The author would also like to thank Dr. Marina Yudovskaya and Dr. Matthew McCreesh for the constant support in the field and for the free consultations.

The CIMERA (Centre of Excellence for Integrated Mineral and Energy Resource Analysis) and the S V Kearney Education Trust are also thanked for providing funding for the author and the project**.** Sylvania Platinum (Pty) Ltd is thanked for providing full access to their core yard, assay data as well as accommodating the author during lengthy field visits. The author would like to thank Rob Steen of Sylvania Platinum for sharing his knowledge on the area and support. The author is also greatly indebted to Given for saving the authors life and rescuing him from the ostrich attack.

The author would like to thank the staff from the University of the Witwatersrand Earth Lab for assistance with XRF sample preparation as well as conducting the XRF sample analyses. A special thanks to Mr. Caiphus Majola, Mr. Samuel Tshabalala and Mr. Joe Aphane for all their technical assistance with thin section preparation as well as invaluable motivation talks. Papa Joe sadly passed on before this thesis reached completion - still, I know you are proud.

Last and not least, the author would like to thank his family, for the emotional and financial support as well as patience with him as he pursued this dream.

Motivation for Research

Molengraaff (1901) together with other geologists of the Geological Survey were the first to map the Mokopane area in 1901. The discovery of PGEs in 1924 increased interest in the area and subsequently triggered widespread exploration and mining (Merensky, 1925) The most detailed study that included the mafic rocks and associated platinum mineralisation was carried out by Wagner (1929). In 1960 Mr S.P. Rautenbach discovered encouraging chromite mineralisation on the farms of Grasvally 293KR and Zoetveld 194KR which promoted further study of the area by De Villiers (1967). The discovery of some of the highest grade chromitite ore in the country led to the mining of the Grasvally area under Amcor and later Samancor until its closure in 1988.

A great contribution towards the understanding of the regional setting and stratigraphy of the northern limb was made by van der Merwe (1976, 1978) through detailed mapping of the entire northern limb. Van de Merwe (1978) further subdivided the layered sequence of mafic and ultramafic rocks into a Lower, Critical, Main and Upper Zone. Combining the available geological and geophysical data, van der Merwe (1978) concluded that the northern limb shares no physical connection to the eastern or western limbs of the Bushveld Complex. Furthermore, van der Merwe (1976, 1978) proposed that the Platreef continued south of Mokopane. This was later disproved by the discovery of the Kleinmeid Syncline in the mafic rocks on the northern part of the farm of Grasvally (Blaine, 1973).

An investigation was undertaken by Hulbert (1983) in order to determine the relationship between the ultramafic rocks of the Grasvally area and those of the Rustenburg Layered Suite (RLS), from both a structural as well as petrological perspective. Hulbert (1983) postulated the origin of the Grasvally body being the result of a horst structure flanked by two N-S-striking faults. In previous studies by Von Gruenewaldt *et al*. (1989); van der Merwe (1976, 2008) and Maier *et al*. (2008), the GNPA (Grasvally Norite-Pyroxenite Anorthosite) member had been assumed to correlate with the Platreef. The GNPA member has been further correlated with the Critical Zone of the eastern and western limbs (Von Gruenewaldt *et al*., 1989; van der Merwe 2008; Dunnett *et al.*, 2012; Grobler *et al*., 2012). This correlation has recently been challenged by McDonald *et al.*, (2005) based on the differences observed in lithologies, mineral textures, rare earth elements (REE), platinum group elements (PGE) and differences in the Mg# of orthopyroxene and olivine. The findings have opened discussion on the precise correlation on the GNPA member.

The GNPA member and its stratigraphy are still largely poorly understood due to the lack of surface outcrop, the structural complexity of the area as well as the lack of marker horizons. Re-evaluation of this deposit through current drilling and exploration by Sylvania Platinum Limited has provided the opportunity to further investigate the geology of this enigmatic area.

CHAPTER 1

General Geology of the Bushveld Complex

1.1 Introduction

The Bushveld Complex is located in South Africa (Figure 1.1) and contains the largest known ultramafic to mafic layered intrusion in the world (Rustenburg Layered Suite or RLS) (Eales and Cawthorn, 1996). The Complex is situated on the Kaapvaal craton and intruded a succession of sedimentary to metasedimentary rocks of the Transvaal Supergroup (Walraven *et al*., 1990; Barton *et al*., 1994; Cawthorn and Walraven, 1998). Recent geophysical studies using pre-existing gravity and magnetic data in conjunction with seismic and magnetotellurics have identified ultramafic to mafic rocks to the north of the Hout River Shear Zone increasing the areal extent from 65 000 km^2 to >90 000 km^2 (Finn *et al*., 2015).

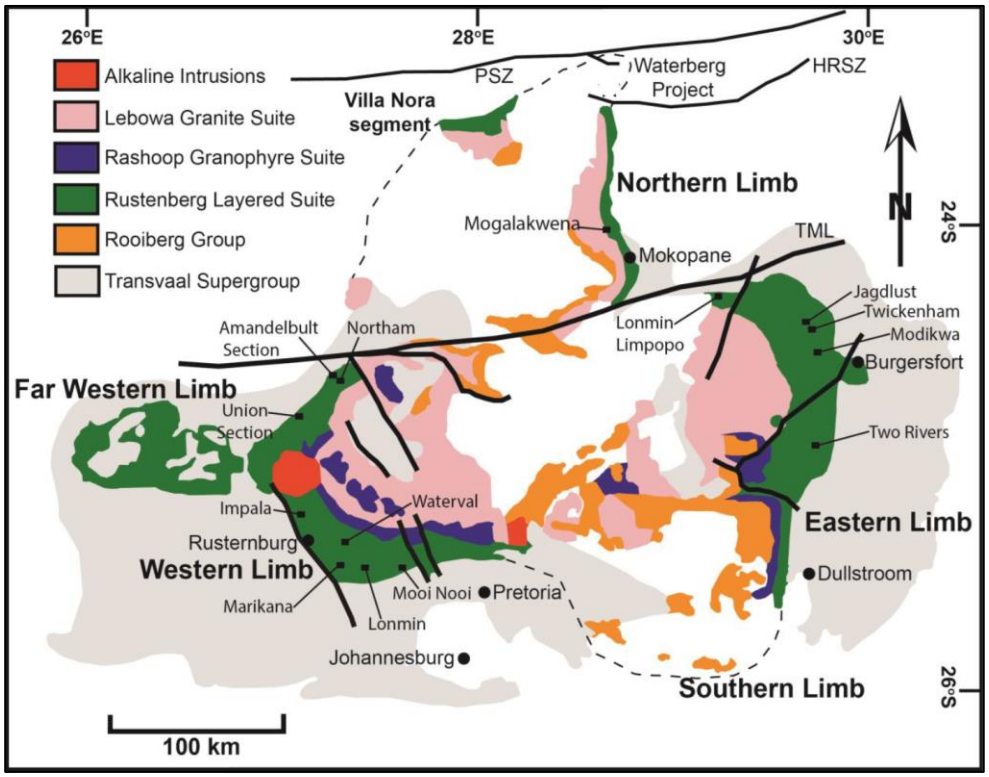

Figure 1.1: Simplified geological map of the Bushveld Complex, which includes the Rustenburg Layered Suite, the Rooiberg Volcanics and the Lebowa Granite Suite adapted from McCreesh, 2018. Major structural features such as the Thabazimbi -Murchison Lineament and the Hout River Shear Zone (HRSZ) are included.

An age of ~2.06 Ga was assigned by Walraven *et al.*, (1990), but more recently, Scoates and Friedman (2008) reported a U-Pb zircon age of 2054.4 ±1.3 Ma based on studies on the Merensky Reef. This was supported by the work of Zeh *et al.*, (2015) who analysed zircons located throughout the RLS and determined that final crystallisation from the floor (Marginal Zone) to the centre of the RLS (Upper Critical Zone and lower Main Zone) took place between 2055.91 ±0.26 and 2054.9 ±0.37 Ma and concluded that emplacement took place within 1.02 ±0.63 Ma.

1.2 Magmatic Stratigraphy and Subdivisions of the Rustenburg Layered Suite

The Bushveld Complex crops out as 4 limbs namely the far western, western, eastern and northern or Potgietersrus limbs (Figure 1.1). The fifth lobe, the south eastern or Bethal limb has no surface exposure as it is covered by younger sedimentary rocks (Eales and Cawthorn, 1996). The western limb and the, better exposed, eastern limb both show similarities in terms of rock types, mineral compositions, isotopic ratios and dip towards the centre of the complex (Cawthorn and Webb, 2001). Taking into account stratigraphic, petrologic and gravity models, Cawthorn and Webb (2001) and Finn *et al.*, (2015) concluded that these two limbs are probably connected at depth.

The RLS in the eastern and western limbs has been divided into five zones namely the Marginal (MaZ), Lower (LZ), Critical (CZ), Main (MZ) and Upper (UZ), based on traceable lithological markers as well as the disappearance and appearance of certain cumulus mineral phases (van der Merwe, 1976). The precise boundaries between these zones, however, are a topic of much debate (e.g. Kruger, 1990). Application of this zonal classification to the northern limb has met with much difficulty and so has been traditionally treated separately.

1.2.1 Marginal Zone

The Marginal Zone (MaZ) is a ~ 880 m thick sequence comprising predominantly medium-grained poorly layered noritic rocks (Eales and Cawthorn, 1996). This heterogeneous sequence forms the bottom contact of the Rustenburg Layered Suite (RLS) in some localities and is not always present (Kinnaird *et al.*, 2002). Although the Marginal Zone (MaZ) is the lowest unit of the RLS, it displays no chill margin and was thus interpreted by Eales and Cawthorn (1996) to suggest that the RLS formed as a series of multiple injections of magma.

1.2.2 Lower Zone

The Marginal Zone is overlain by an 800-1300 m thick package named the Lower Zone (LZ). The LZ comprises 3 subdivisions; Lower Pyroxenite subzone, the Harzburgite subzone, and the Upper pyroxenite subzone.

The maximum thickness of the Lower Zone is yet to be determined however recent work on the Clapham trough section of the Eastern limb has revealed over 900 m of ultramafic rocks, extending the maximum thickness to 2 400 m (Wilson and Chunnett, 2010; Wilson, 2012; Yudovskaya *et al.*, 2013). The LZ is an olivine-rich succession comprising dunite, harzburgite and pyroxenite lithologies, interpreted to be emplaced as a series of up to 37 cyclic units (Maier and Barnes, 1999; Kinnaird *et al*., 2002; Naldrett *et al*., 2009). These lithologies exist in the southern part of the northern limb (Hulbert and Von Gruenewaldt, 1982), with the thickest and most primitive succession of LZ located on the farms Grasvally, Volspruit and Zoetveld. This succession reaches a thickness of 1600 m.

1.2.3 Critical Zone

A 1300-1800 m thick package, the Critical Zone (CZ), overlies the Lower Zone. The CZ is subdivided into the lower (C_LZ) and upper (C_uZ) (Cawthorn and Webb, 2001). The lower Critical Zone comprises ultramafic orthopyroxenitic lithologies and hosts several chromitite seams (Lower Group) (Maier and Barnes, 1999; Kinnaird *et al*., 2002).

However, within the Grasvally area, the Lower Zone hosts two well-developed chromitite seams. The transition from the LZ into the C_uZ is demarcated by the appearance of mafic plagioclase-bearing lithologies associated with the Middle Group of chromitite seams (MG). The precise boundary is placed at the occurrence of the lowermost anorthosite layer sandwiched between the MG 2 and 3 seams (Maier and Barnes, 1999; Kinnaird *et al*., 2002). Above the MG the C_uZ contains a sequence of plagioclase –orthopyroxene cumulates capped by the Upper Group chromitite seams (UG), with the UG2 being the most significant in terms of economic Cr-Ni-Cu-PGE mineralization. Above the UG2, the Merensky and Bastard cyclic units are pyroxenitic rocks with significant chromitite, norite and anorthosite (Eales and Cawthorn, 1996). The Merensky Reef is mined for PGE and is roughly 1 m thick and yields grades of 4-6 g/ton, whereas the Bastard Reef has very low-grade PGE and is not mined (Eales and Cawthorn, 1996).The UG2 comprises chromitite layers which contain up to

approximately 5 ppm PGE. It is becoming more economically significant than the Merensky Reef as the Merensky Reef is being mined out (McLaren and De Villiers, 1982).

1.2.4 Main Zone

The Main Zone is the thickest unit within the Rustenburg Layered Suite reaching thicknesses of 3940 m in the Roossenekal area (Von Gruenewaldt, 1973). The MZ is made up predominantly of norites and gabbronorite characterised by low olivine-content and scarcity of anorthosite (Kinnaird *et al*., 2002). The Main Zone is poorly layered in comparison to the Critical Zone possibly due to fluctuations in magma compositions. Major changes in mineral composition trends occur in proximity to a marker horizon, a thin layer of orthopyroxenite termed the Pyroxenite Marker (PM) (Von Gruenewaldt,1973; Molyneux, 1974; Klemm *et al.*, 1985; Sharpe, 1985; Kruger *et al.*, 1987). The PM has been suggested to represent the transition from MZ to Upper Zone (Kruger, 1990), however the appearance of cumulus magnetite is widely accepted to represent the base of the UZ (Eales and Cawthorn, 1996) even though this boundary is not accompanied by changes in mineral composition trends (Von Gruenewaldt, 1973; Molyneux, 1974).

1.2.5 Upper Zone

The Upper Zone which overlies the MZ is approximately 2500 m thick and is the uppermost unit of the RLS. It comprises ferrogabbro, ferrodiorite, anorthosite and troctolite lithologies and is characterised by a high magnetic susceptibility due to the 25 magnetitite layers hosted within the unit (Wager and Brown, 1967). Individual magnetitite layers range in thickness from 0.1 m to 10 m, with a cumulative thickness of ~20.4 m (Harney and Von Gruenewaldt, 1995). The Main Magnetite layer which occurs near the base of the UZ is ~ 2 m thick and it is mined for its vanadium content (~1.3 % V_2O_3) (Kinnaird, 2005a). These titaniferous magnetite layers are of economic importance as they host just about half of the world's vanadium reserves (Kinnaird, 2005a).

1.3 Location and Research Area

The area of focus is within the Limpopo province of South Africa, on the farm of Grasvally about 20 km south of the town of Mokopane and the NE-striking sinistral Ysterberg-Planknek Fault (Figure 1.2). The farm and mineral rights are currently under the ownership of Sylvania Platinum Ltd. The Ysterberg-Planknek Fault is part of the fault array associated with the Thabazimbi-Murchison Lineament and is of significance as the Platreef has only been recognised north of the fault and is

absent to the south. To the south of the fault, is a body termed the Grasvally Norite-Pyroxenite-Anorthosite member (GNPA member), at a similar stratigraphic position to the Platreef, although they differ geochemically.

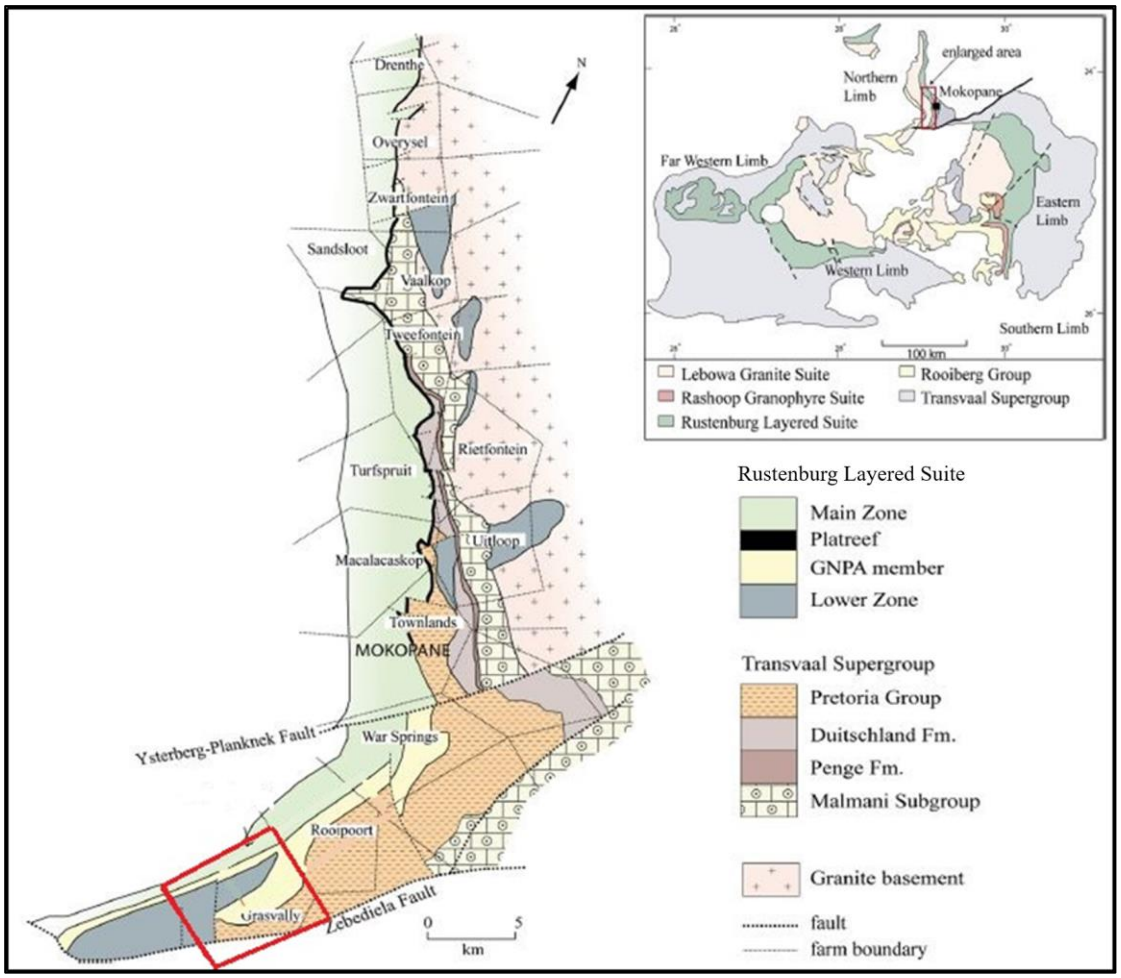

Figure 1.2: Geological map of the northern limb of the Rustenburg Layered Suite (RLS), showing the location of the research area on the farm of Grasvally. Adapted from Smith *et al.* (2014).

1.4 Aims

This research project aims to:

- create a sound stratigraphy through detailed analysis of the rock types on the farm Grasvally.
- find potential marker horizons within the sequence in order to correlate the geology of the area across boreholes and to enable the identification of structural features.

- determine if there are any relationships between structural features and mineralisation in the area.
- correlate the stratigraphy of the area with that of the northern limb north of Mokopane as well as the eastern and western limbs of the Bushveld Complex.

1.5 Methodology

In order to meet the requirements to accomplish the aims and objective of this project the following geological techniques were used: borehole core logging (mineralogy), measuring the magnetic susceptibility of lithologies downhole, polished thin section study (petrography), geochemical analysis (geochemistry) and three-dimensional implicit modelling. Using these different parameters within the methodology it was expected that it should be possible to make certain suggestions and conclusions that can be used to test the hypothesis that the GNPA is the equivalent to the Platreef across the Ysterberg-Planknek fault.

1.5.1 Core Logging

Twenty of the original borehole cores drilled on the farm of Grasvally were analysed over three field visits from the August 2015 to June 2017. The core was drilled by the contractor Geoserve and access to these cores was provided by Sylvania Platinum Limited. The core was logged in order to determine the lithological units and further to constrain lithological packages to an appropriate zone (or stratigraphic unit) based on the rock types present. This will aid in correlating the stratigraphy to that of the rest of the northern limb and the eastern and western limbs.

The structural aspects of the core have been analysed in order to aid in the interpretation of the structural history of the area and the relationship of the structures to the mineralisation.

Over one hundred 30 cm quarter-core samples were taken from the drill cores provided. The samples were taken from lithological units in which there was a visible change in lithology. Rock types that were difficult to identify in hand sample were also sampled in order to determine the lithology. The samples have been used for petrological and chemical analyses.

1.5.2 Petrography

From the samples collected, 133 polished thin sections were obtained and examined. The thin sections are representative of the various lithological units found in the area. In order to classify the

samples according to the exact mineralogy and to further correlate these with the greater northern limb stratigraphy, microstructures were also observed in order to add to the understanding of the structural implications.

1.5.3 Geochemical Analysis

The same samples that were selected for polished thin sections were used for bulk rock chemical analysis by X-Ray Fluorescence (XRF) of both major and trace elements. The geochemical data from the study area were used to compare with known geochemical signatures established for the RLS, for the purposes of lithological classification and correlation. In addition, certain elements provided information about mineralisation (e.g. Ni, Cu, Cr, Co, S), and backed up further assay data for PGE provided by Sylvania Platinum Ltd.

1.5.4 Magnetic Susceptibility

Magnetic susceptibility data was analysed on selected cores that displayed the most complete stratigraphy. Magnetic susceptibility measurements were taken at fixed 1 m intervals down the core. These measurements have been used to identify where there is a significant change in the magnetic susceptibility as this may indicate a change in lithological units. This method may also identify certain marker horizons that may be used to correlate lithological units across the boreholes.

1.5.5 Three-Dimensional Modelling

A three-dimensional geological model was created using integrated core log data undertaken in the field, data provided by the company and data from geological maps of the area. Leapfrog Geo® was used to create three-dimensional conceptual models from drillhole data and GIS data without the use of manual digitisation. The three-dimensional model was used to gain a better understanding of the GNPA member and its structures and possibly any correlation between the geological units and the structures.

CHAPTER 2

Geological Setting of the northern limb

The northern limb stratigraphy has traditionally followed the zonal subdivision established for the eastern and western limbs of the RLS (e.g. Van Der Merwe, 1979) but it has become clear from recent work that significant differences occur. Moreover, the Ysterberg-Planknek Fault (Figure 2.1) marks a major change in stratigraphy within the northern limb itself (Figure 2.2).

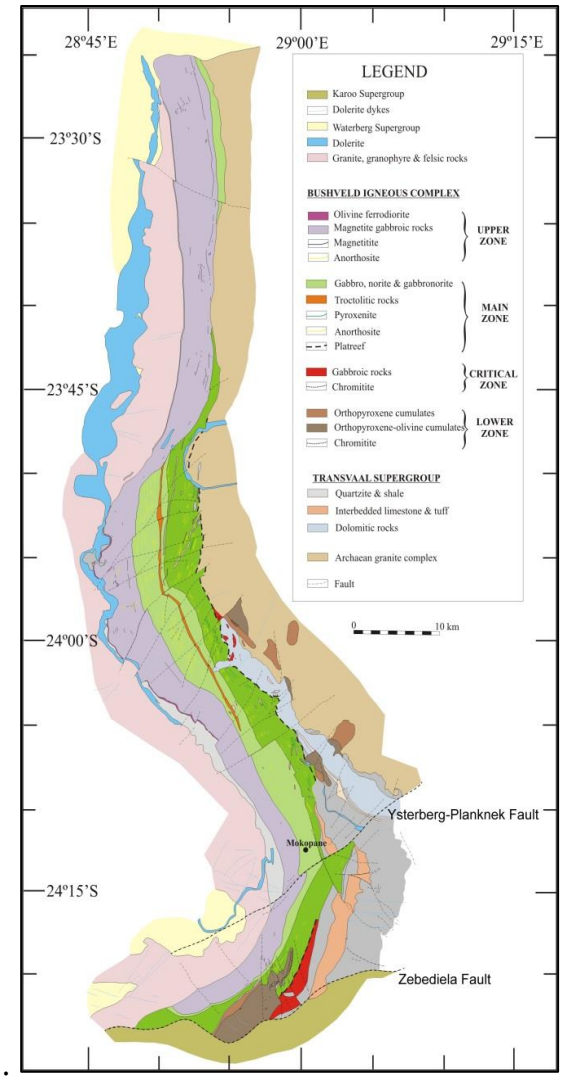

Figure 2.1: The general geology of the northern limb of the Bushveld Complex showing the different stratigraphic units, surrounding rocks and structural features. Original map by van der Merwe (1979); colour map generated by Ashwal *et al*. (2005); from Kinnaird and McDonald (2005).

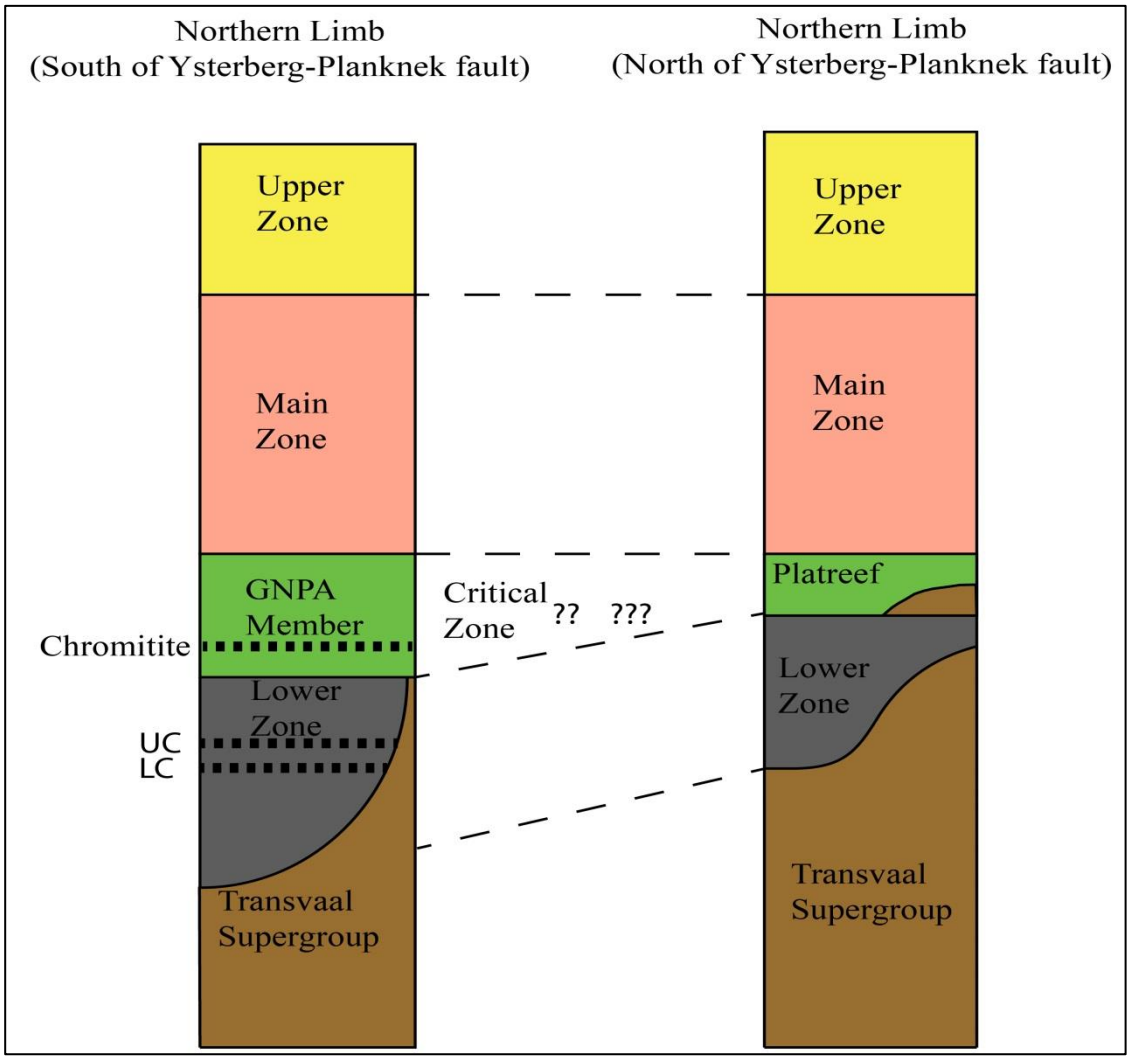

Figure 2.2: Differences between northern limb stratigraphy to the north and south of the Ysterberg-Planknek Fault Adapted from Smith *et al*. (2011).

2.1 Lower Zone

The Lower Zone south of the Y-P fault, is an 800-1600 m thick package of harzburgites and pyroxenites comprising up to 37 cyclic units (Hulbert and Von Gruenewaldt, 1982). In this area it has been subdivided into three subzones namely the Volspruit pyroxenite, Drummondlea harzburgite chromitite and the Moorddrift harzburgite pyroxenite (Figure 2.3). The Drummondlea subzone contains two chromitite seams that have the highest Cr# and Cr_2O_3 content in the RLS (Hulbert, 1983; Maier *et al*., 2013). Horizons with significant PGE mineralisation have been reported by Hulbert and Von Gruenewaldt (1982) in both the Volspruit and Drummondlea subzones.

To the north of the Ysterberg-Planknek Fault, the Lower Zone crops out as satellite bodies, (brown in Figure 2.1). Lower Zone of considerable thickness has been intersected in drill cores from the Sandsloot and Turfspruit area and has been further interpreted by Yudovskaya *et al.* (2013) as possibly extending deep beneath the Marginal Zone which is an irregular unit in this area. The Lower Zone is thought to have been emplaced before the Platreef as multiple magma batches which differentiated in the chamber, forming cyclic units of dunite, harzburgite and pyroxenite with compositional reversals at their bases (Yudovskaya *et al.*, 2013).

The Drummondlea harzburgite chromitite contains two chromitite seams of a higher grade in comparison to the rest of the Bushveld Complex (Hulbert and Von Gruenewaldt 1985). The Upper Chromitite and Lower Chromitite seam appear at 620 m and 690 m (Figure 2.3) respectively within the intersection studied by Hulbert (1983). The chromitite layers have the highest Cr# and Cr_2O_3 content in the Bushveld Complex (Hulbert, 1983; Maier *et al*., 2013).

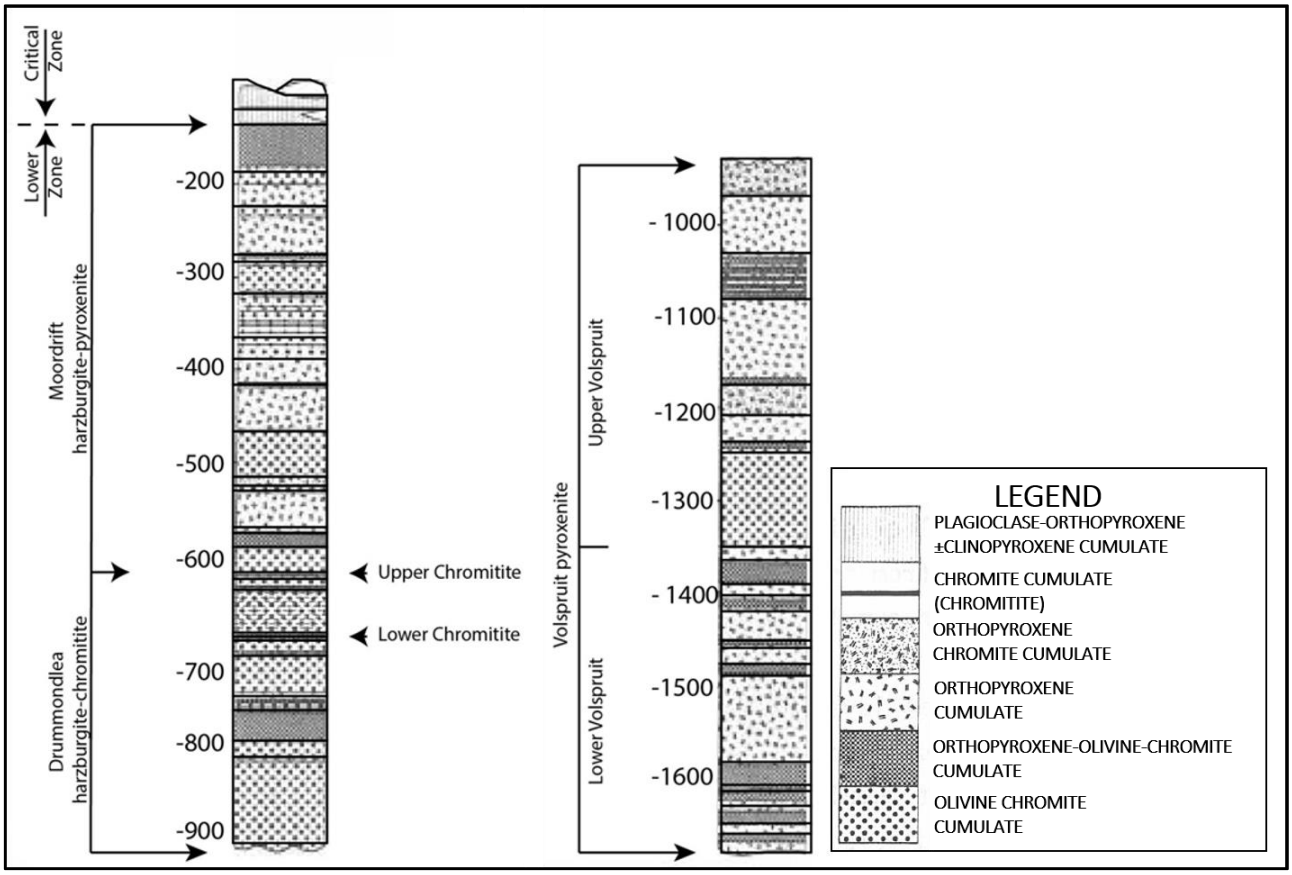

Figure 2.3: Stratigraphic column of the northern limb Lower Zone south of the Ysterberg-Planknek Fault. Adapted from Hulbert (1983).

2.2 The Grasvally Norite-Pyroxenite-Anorthosite (GNPA) member

The Grasvally Norite-Pyroxenite-Anorthosite or GNPA member is a package of PGE-bearing mafic cumulates that is only present between the Ysterberg-Planknek Fault in the north and the Zebediela Fault to the south (Hulbert, 1983) (Figure 2.5).

The GNPA forms a NE-striking body that extends for 30 km along strike and consists of gabbronorite, norite, anorthosite, pyroxenite and PGE-bearing chromitite and is cut by the north-south trending Grasvally Fault (Figure 2.5). To the east of the Grasvally Fault the GNPA member forms a syncline plunging to the south overlying the shales and quartzites of the Magaliesberg Quartzite Formation. To the west of the Grasvally Fault the GNPA member overlies gabbronorite, anorthosite, norite and pyroxenite of the Lower Zone (van der Merwe, 1976). The contact between the Lower Zone and the GNPA member is characterised by calc-silicate xenoliths which are of irregular occurrence and exhibit a chill margin of up to 7 m in thickness (de Klerk, 2005; Maier *et al*., 2008).

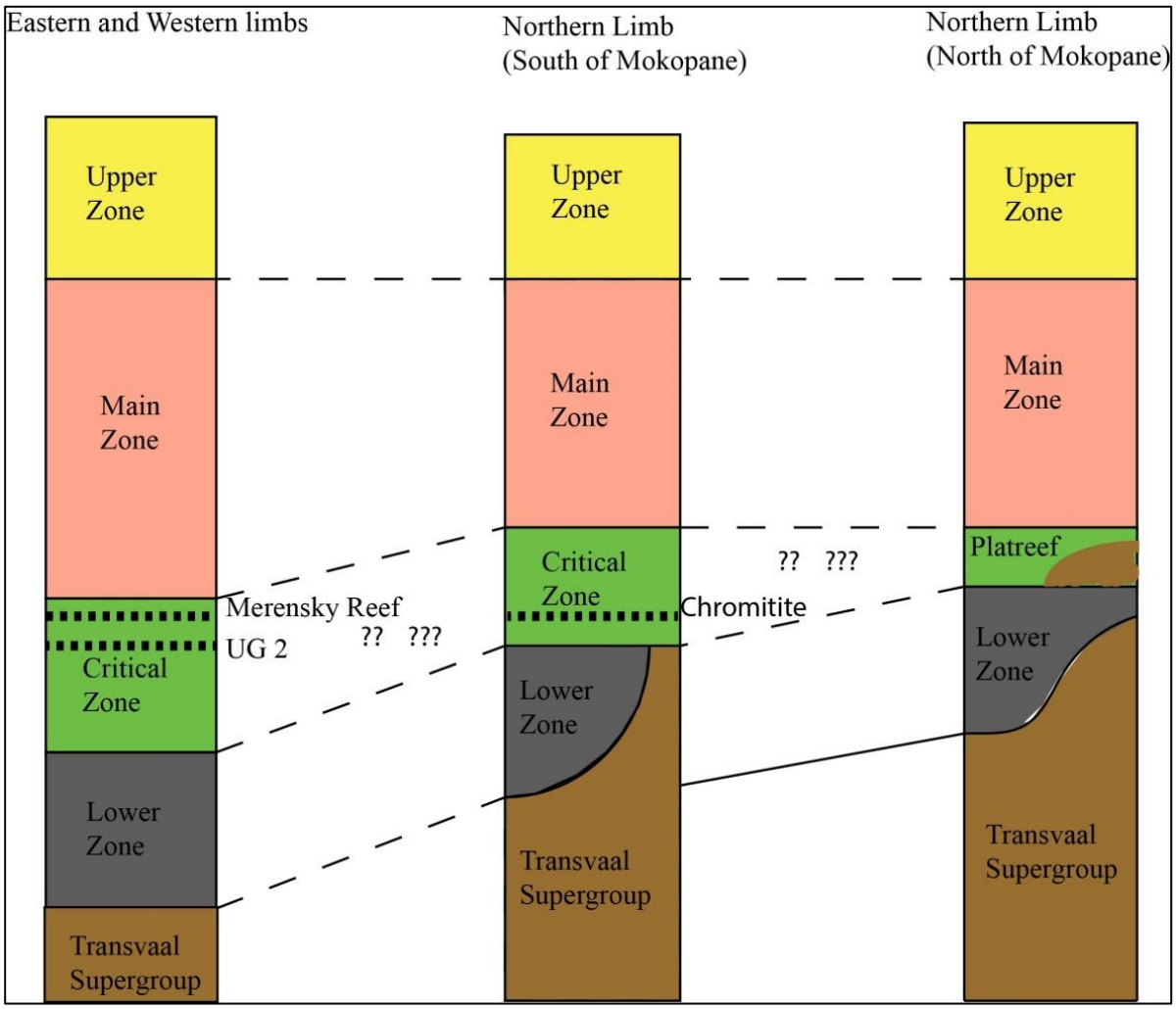

Figure 2.4: Differences in magmatic stratigraphy of Critical Zone, and its equivalents across the Bushveld Complex. Adapted from Smith *et al*. (2011).

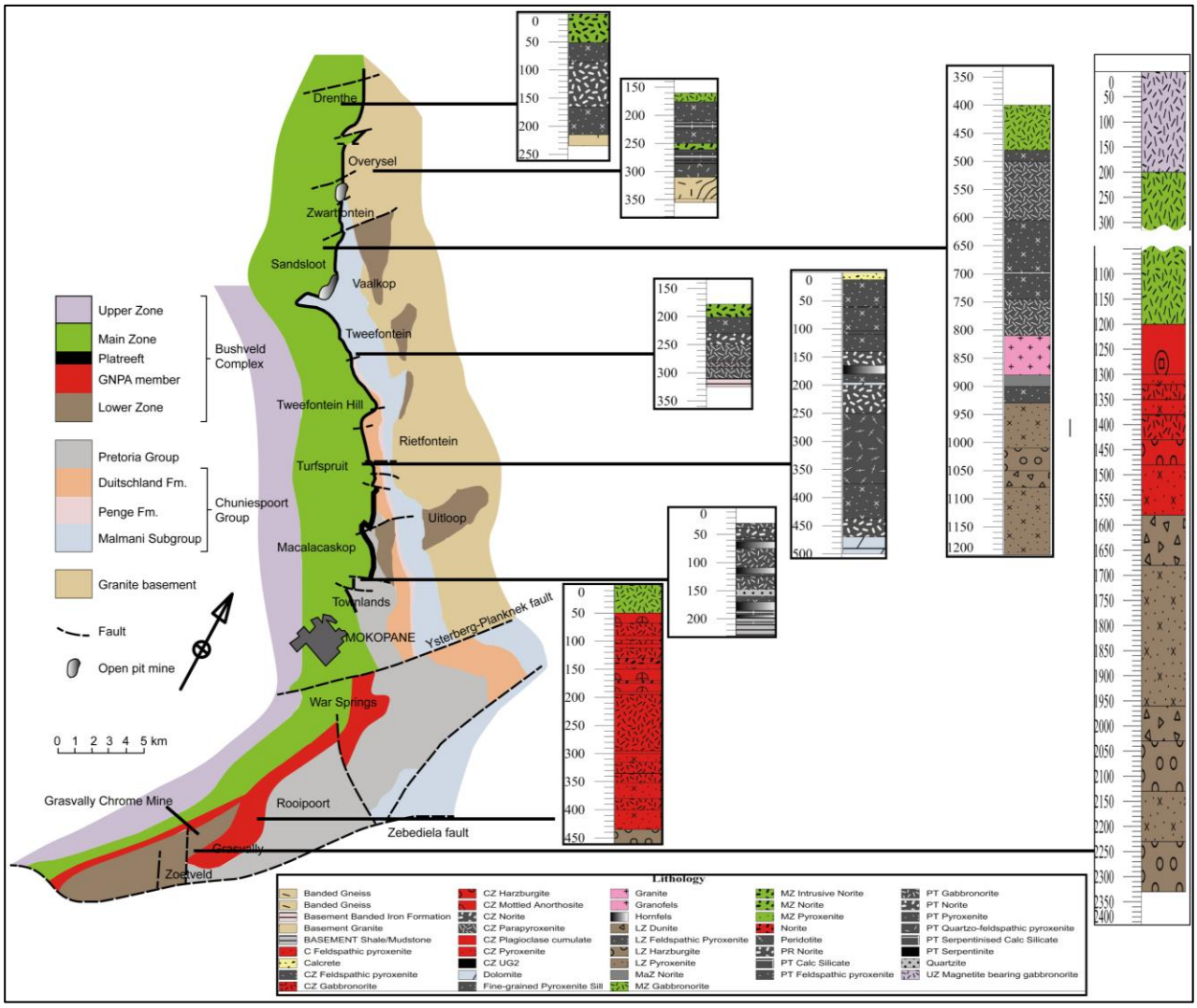

Figure 2.5: Geological map of the lower portion of the northern limb. Adapted from McDonald *et al.* (2005). Idealised stratigraphic sections for key localities along the strike of the northern limb displaying the successively younger footwall rocks to the south, Lower Zone intersections as well as variations in the Critical Zone equivalent.

The GNPA member has been subdivided into three subzones by de Klerk (2005) based on the appearance and disappearance of diagnostic cumulate phases. These are; the Lower Mafic Unit (LMF); the Lower Gabbronorite Unit (LGN); and the Mottled Anorthosite Unit (MANO) (Figure 2.6).

2.3.1 Marginal Zone

The Marginal Zone (MaZ) comprises fine to medium-grained gabbronorites and quartz-bearing gabbronorites ranging in thickness from a few centimetres to tens of metres (Hulbert 1983). The MaZ

is present where the overlying mafic package is in contact with the ultramafic and sedimentary floor rocks however exposure of the zone is very poor in the area. The MaZ is best exposed where the intrusion is in contact with the GNPA member from the northern boundary of farm Grasvally to the northern boundary of farm Zoetveld (van der Merwe, 2008). Rocks of the MaZ host xenoliths of carbonate rock, hornfels and quartzite, alluding to an intrusive nature (Hulbert, 1983). de Klerk (2005) postulated three stages in the development of the MaZ from borehole data where mafic rocks of the Grasvally Norite-Pyroxenite-Anorthosite member are in contact with the underlying ultramafics of the Grasvally body or sedimentary rocks of the Pretoria Group (van der Merwe, 2008). The first stage, which is close to the margin of the intrusion, displays a fine-grained chill over several metres (<40 m); the second is defined by a thin chill margin a few centimetres thick; while the third scenario, which is representative of deeper within the chamber, comprises a hybridised zone and is characterised by a brecciated zone with xenoliths of sedimentary rocks and ultramafic Bushveld rocks (van der Merwe, 2008).

2.3.2 Lower Mafic Unit

The LMF is dominated by fine to coarse-grained norites, gabbronorites, pyroxenites, feldspathic pyroxenites and less common pegmatitic feldspathic pyroxenites. The base of the LMF is marked by a fine-grained chilled margin irrespective of the underlying lithology (Hulbert, 1983; de Klerk, 2005). This chilled margin, ranging from a few centimetres to 20 m thick, is indicative of the Lower Zone cumulates having cooled significantly before the emplacement of the LMF (Smith *et al.*, 2011). The LMF hosts two PGE and base metal sulphide (BMS) bearing chromitites that are traceable along strike on the farms of Grasvally and the adjacent Rooipoort (Smith *et al.*, 2011). The chromitites are found near the basal contact of the LMF in the area of Grasvally studied by Hulbert (1983) and over 100 m above the LMF basal contact in the north on Rooipoort.

2.3.3 Lower Gabbronorite Unit

The LGN is characterised by homogeneous fine to medium-grained mela to leuco-gabbronorites. These gabbronorites contain xenoliths of pyroxenitic material entrained from the MANO and LMF with some sheared contacts also present. Due to the homogeneity of this unit and the petrographic similarities with the Main Zone, de Klerk (2005) postulated that the LGN represents a sill related to the Main Zone that intruded along the LMF-MANO contact.

2.3.4 Mottled Anorthosite Unit

The transition from the LGN to the MANO is marked by an increase in the proportion of plagioclase cumulates (Hulbert, 1983). The MANO is distinguished by occurrence of mottled, smottled (equally spotted and mottled texture) and spotted anorthosites with the orthopyroxene oikocrysts ranging in size from 20 to 60 mm (Hulbert, 1983).

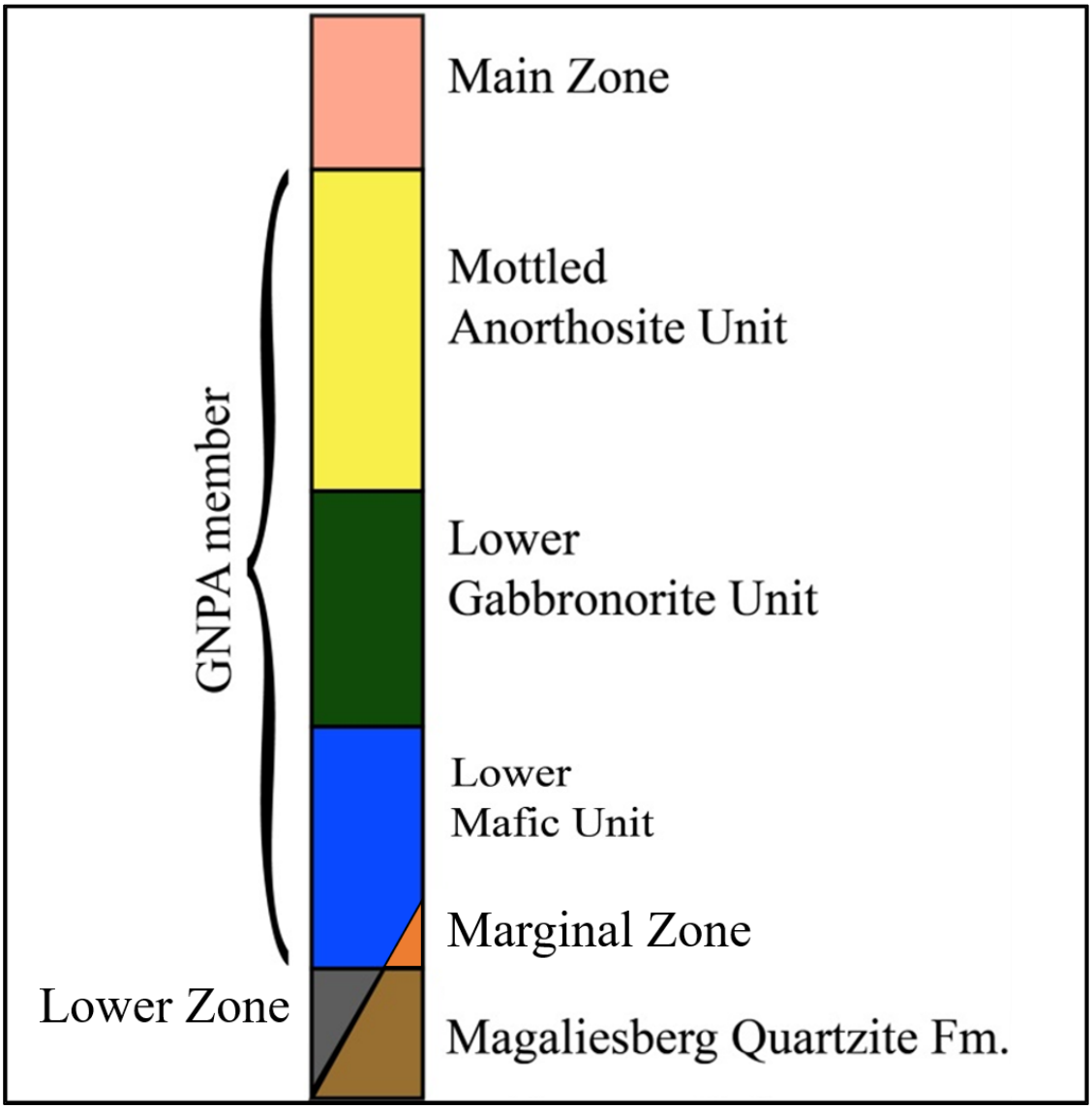

Figure 2.6: Stratigraphic column of the Rooipoort-Grasvally area. Adapted from Maier *et al*. (2008).

2.3 The Platreef

The Platreef appears to be restricted to the north of the Ysterberg-Planknek Fault and forms the lowest stratigraphic unit of the RLS for the most part of the northern limb (Kinnaird *et al*., 2005). It has been interpreted as the equivalent to the upper Critical Zone of the eastern and western limbs based on its stratigraphic position below the Main Zone (Figure 2.4) and the silicate geochemistry (van der Merwe, 1978; Kinnaird, 2005a; Maier *et al*., 2008; van der Merwe, 2008; Yudovskaya and Kinnaird, 2010), although this is disputed by McDonald *et al*., (2005). Mineralogically the unit is dominantly pyroxenitic and is irregularly mineralised in PGE, Cu and Ni. It was initially divided into A, B and C reefs (White, 1983; Barton *et al*., 1986). More recently the Platreef has been divided into four compositionally and chemically distinct feldspathic pyroxenite units with metasedimentary rocks and serpentinised peridotites interlayered between them (Kinnaird, 2005b). The complex structure and geochemical diversity of the Platreef points towards multiple discrete magmatic influxes (Kinnaird, 2005b), with metasedimentary material detached from the floor as pulses of magma flowed in and subsequently formed the layers that divide the feldspathic pyroxenite that dominate this package (Kinnaird, 2005b). As the Platreef is traced north, the basal contact rests on a transitional footwall, first on successively older strata of the Transvaal Supergroup and ultimately granitic basement in the north (Figure 2.5).

2.4 Structural deformation of the northern limb

The Kaapvaal Craton, into which the Bushveld Complex intruded, spans approximately 1.2 x 10^6 km^2 of Mid-Late Archaean rocks comprising mostly granitoids with intermingled greenstone belts, overlain by Late Archaean to Mesoproterozoic sedimentary as well as volcano-sedimentary basins (Good and De Wit, 1997). The Kaapvaal craton is subdivided into various terranes by tectonic contacts characterised by thrusts and strike-slip faults (Figure 2.7) (De Wit *et al.*, 1992; Good and De Wit, 1997). The prominent terrane boundaries associated with the terranes intruded by the Bushveld Complex are characterised by ENE-WSW trending structural lineaments such as the Thabazimbi-Murchison Lineament (TML) (Figure 2.7) (Good and De Wit, 1997).

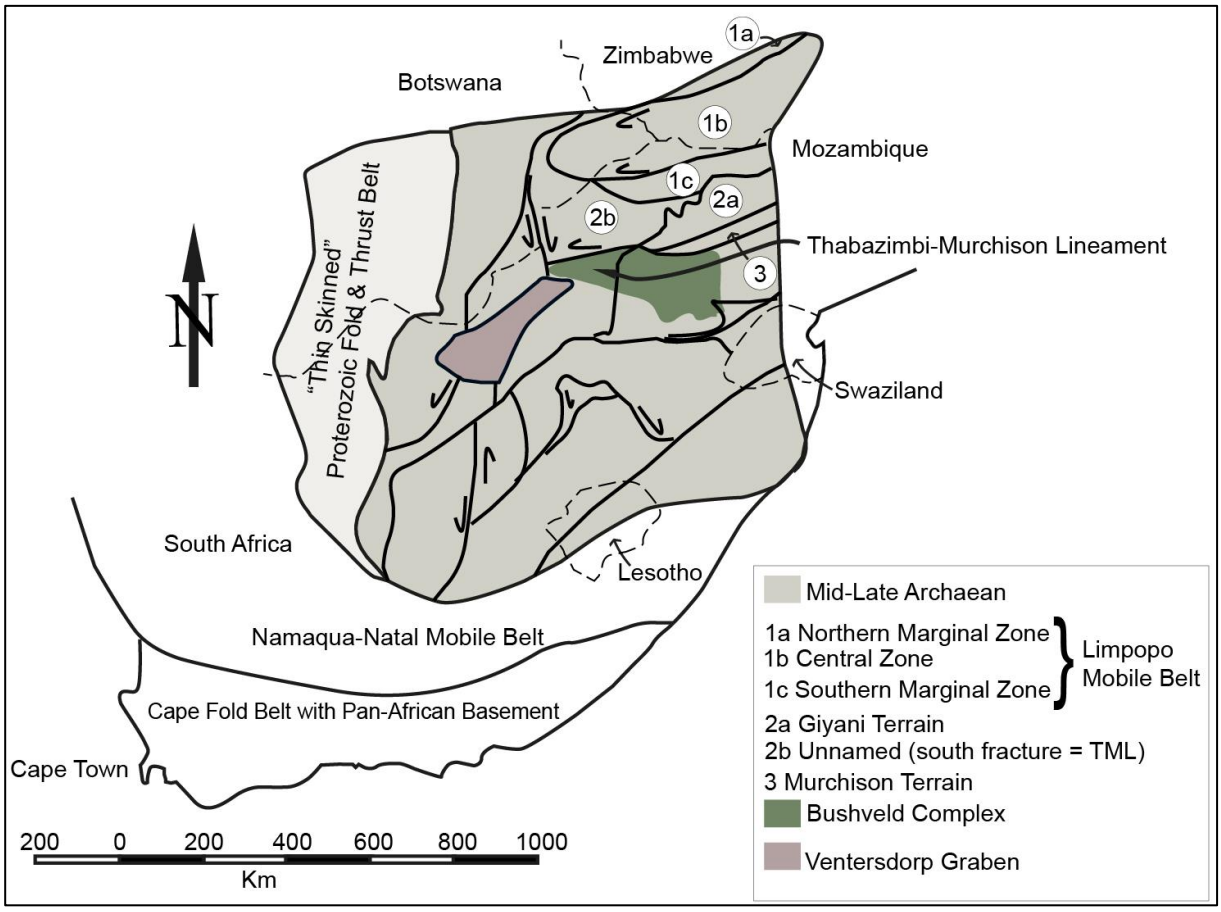

Figure 2.7: Granite-greenstone terrains of the Kaapvaal Craton displaying outline of the Bushveld Complex and Thabazimbi-Murchison Lineament modified after de Wit and Hart (1993).

The northern limb is structurally complicated by its proximity to the Thabazimbi-Murchison Lineament, which extends east-northeast west-southwest for more than 500 km (Figure 2.7) and has been active since 2960 Ma (Good and de Wit, 1997) to the present day. The northern limb can be subdivided into three sections based on such major structures and mineralisation; a northern section, central Platreef section and a southern GNPA section. The Platreef *sensu stricto* is bound by the Hout River shear zone to the north (Grobler and Whitfield, 1970), and the Ysterberg-Planknek Fault to the south (van der Merwe, 1976). To the north of the Hout River shear zone, Bushveld rocks have been intersected below a thick succession of Waterberg sediments. Drilling and further research in the area has revealed two mineralised packages, one with Main Zone affinity and one with lower Critical Zone or LZ affinity (Kinnaird *et al.*, 2017). The delineation of the structures within the northern limb and more locally to the south of Mokopane aims to draw a link between the structures in the area and the genesis of the ore bodies. For the scope of this study the northern section has been omitted.

2.4.1 General structural deformation of the central section of the northern limb

The structural deformation of the northern limb is well documented from work done on Tweefontein Hill (Figure 2.8) by Nex (2005). The mapping in the area delineated a major structure in the area noted in the Platreef, which sits unconformably on top of the Duitschland and the Penge Formation as part of the Chuniespoort Group of the Transvaal Supergroup (Figure 2.9). In the north, the Platreef generally strikes north-northwest with a dip of approximately 40° southwest with the strike shifting drastically to the south, striking north-south with the dip remaining constant (Nex, 2005). Massive to semi-massive base-metal sulphide mineralisation occurring towards the base of the Platreef within this structure, suggests that it formed in a footwall basin or downwarp during emplacement of the Platreef. The change in strike of the rocks is an expression of a south-west plunging synformal structure (Nex, 2005). The Malmani dolomites and the banded ironstones display different styles of folding due to the contrast in competencies. These folds are interpreted as two phases of ductile deformation; an early phase which resulted in upright folds with penetrative cleavage and a later phase of folding resulting in dominantly south-west plunging folds related to the major structure. Both sets of folding are overprinted by metamorphic textures attributed to the emplacement of the Bushveld Complex. Brittle deformation in the area is also observed in the form of north-northeast trending sub-vertical faults which offset contacts between the dolomites and the younger granite (Figure 2.8). The faults offsetting the granite is evidence that the brittle deformation postdates the emplacement of the Bushveld Complex (Nex, 2005). Minor granitic veins form a minor matrix to an ironstone breccia within the BIF. These are observed within the axial regions of some folds and are also in a north-south orientation.

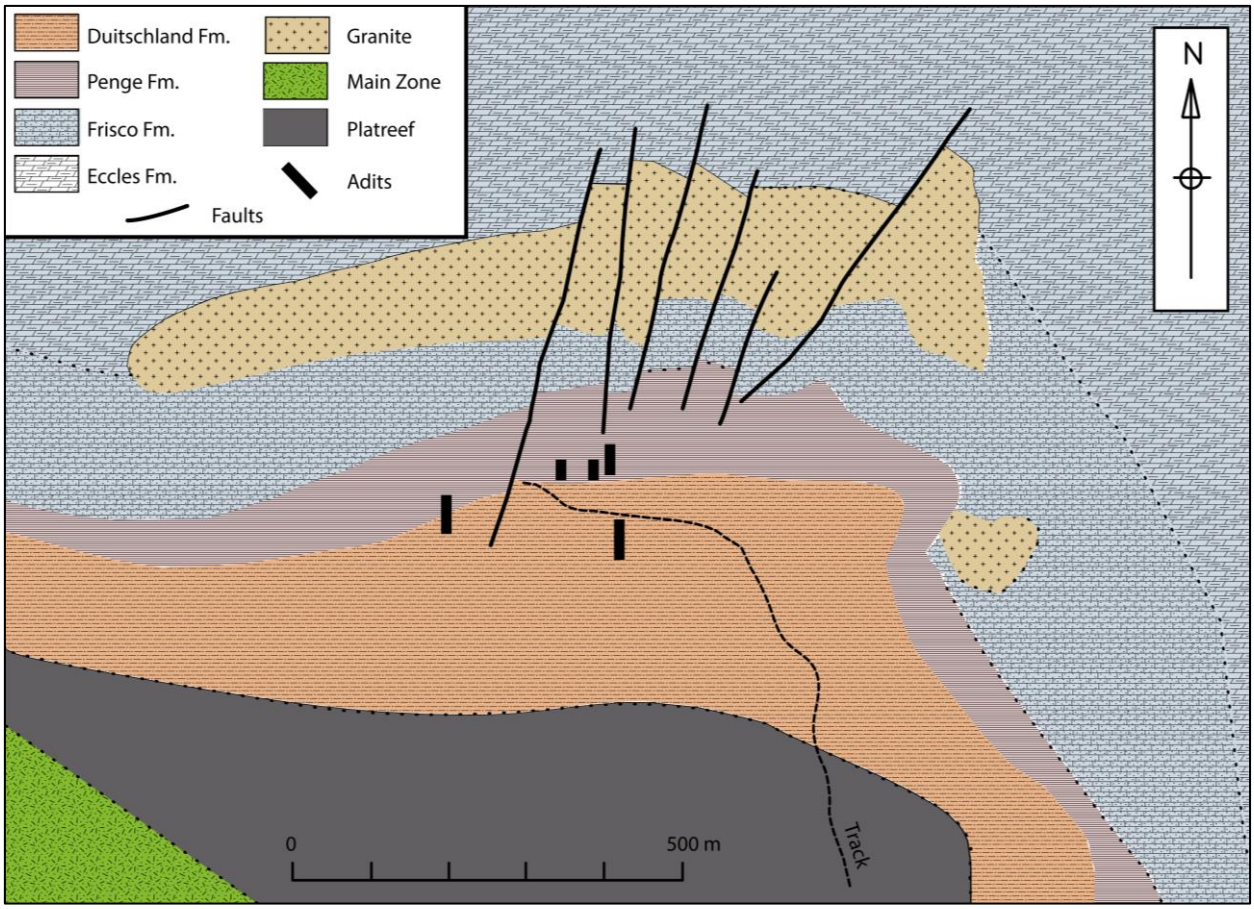

Figure 2.8: Geological map of Tweefontein Hill showing the distribution of lithologies, faults and adits. Stippled lines show inferred geological contacts and solid lines are observed contacts (Nex, 2005).

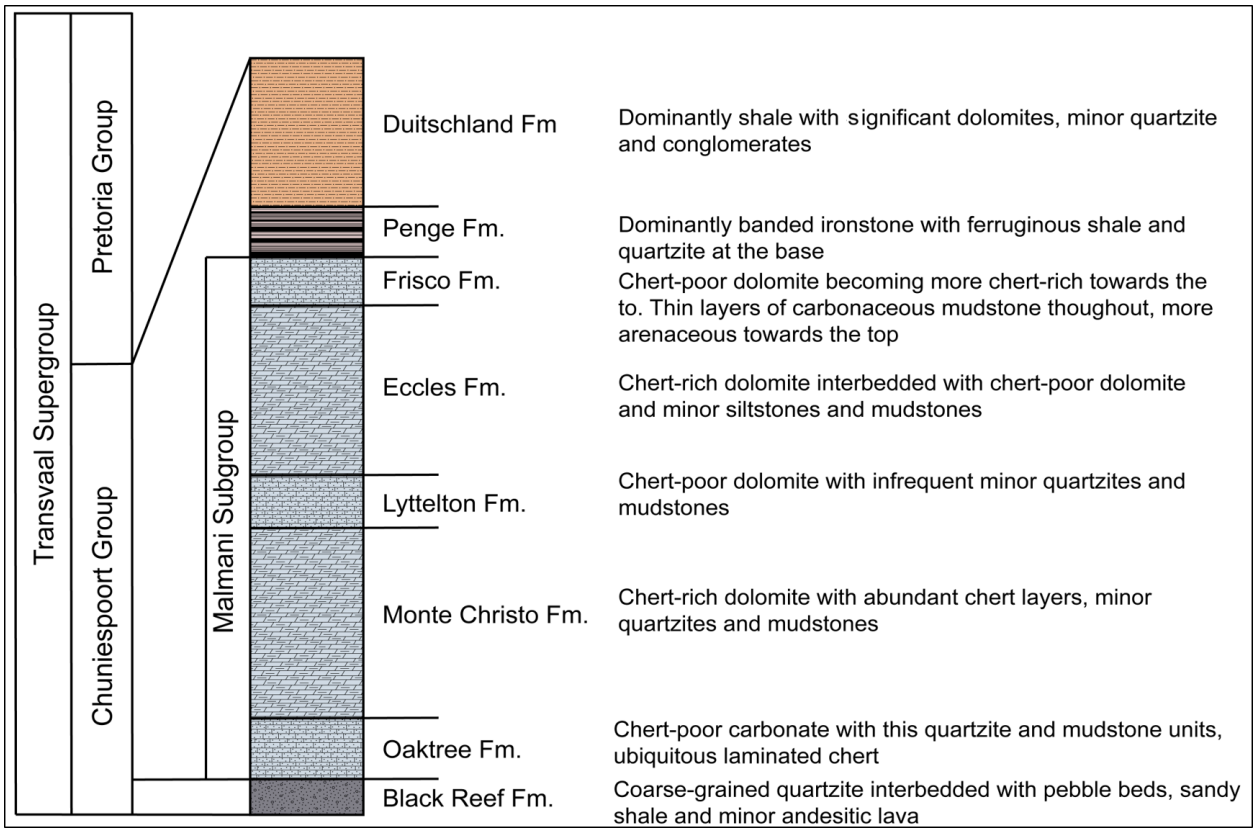

Figure 2.9: Schematic lithostratigraphic column of the lower part of the Transvaal Supergroup in the Mokopane Area after SACS,Greer (1983) and Nex (2005).

2.4.2 Structural Deformation within the Grasvally Area

The ultramafic to mafic body on the farm of Grasvally is bound to the north and the south by the Ysterberg-Planknek Fault and the Zebediela Fault (Figure 2.5). The Zebediela Fault is a surface expression of the Thabazimbi-Murchison Lineament which is thought to have acted as a boundary, compartmentalising the magma which formed the Bushveld Complex, allowing it to evolve separately to the north (Kruger, 2005; Yudovskaya *et al.*, 2013).

Hulbert (1983) noted four episodes of brittle deformation on the Grasvally farm which occurred after the emplacement and consolidation of the Rustenburg Layered Suite. This interpretation incorporates initial mapping on this area undertaken by Kynaston *et al.* (1911) and later improved by De Villiers (1967,1970) and van der Merwe (1976). Barret *et al.* (1978) conducted a gravity survey in order to further outline the structural events in the area.

The first generation of faulting was an episode of north-south trending reverse faults. This resulted in the horst-like block of Lower Zone (LZ) rocks being vertically displaced upwards by up to 800 m into the Critical Zone (Figure 2.10). Focusing on the distribution of the LZ chromitite layers, which

are confined to the horst-like block, reveals that the block was emplaced as a sequence of imbricate faults (Hulbert, 1983). The shear planes bounding and within the horst-like block are of variable orientation due to its imbricate nature, however they generally dip at ~70°W. The chromitites within the block display decreasing dip from 55°W in the north to 35°W in the south (Hulbert, 1983). The minimum collective vertical displacement across the studied area was calculated to be 1 350 m. van der Merwe (2008) disputed the presence of these bounding faults and noted the presence of one north-south trending fault, the Grasvally fault, along which the Lower Zone has been brought into contact with the Critical Zone. To the east of this fault a synformal structure, expressed on surface as a wedge-shaped outcrop, has been described (Blaine, 1973; Johnson, 1984a; Johnson, 1984b; de Klerk, 2005; van der Merwe, 2008).The axis of this syncline is orientated NNE and plunges 15°N (van der Merwe, 2008). The eastern limb of the syncline dips 25°W to 40°W and flattens out to 5°E towards the Grasvally fault (van der Merwe, 2008). The western limb of the syncline was noted by Hulbert (1983) towards the northern boundary of the farm Grasvally with Johnson (1984, 1984b) noting the same feature expressed by the dipping UG 2 layer on the eastern limits of the Grasvally Chrome Mine (van der Merwe, 2008).

The second generation of faulting is a WNW-ESE reverse block faulting system, resulting in a step-like displacement of the RLS (Figure 2.10). Tracing of the chromitites was used to determine the displacement of the different blocks (Figure 2.10). The reverse faulting in the south, noted on the farms of Zoetveld, Volspruit, and Vaalkop, exposed LZ lithologies from stratigraphic levels deeper than the chromitite layers (Hulbert, 1983).

The third generation of fault episodes is expressed by NE-SW striking faults. This resulted in the upfaulting of segments of Pretoria Group quartzites into the RLS (Figure 2.10). Similarly trending faults are present in the Waterberg Group to the southwest of Grasvally thus this generation is assumed to be post-Waterberg (Hulbert, 1983).

The final generation of faulting happened post-Karoo when Karoo basalts were brought into contact with LZ rocks along the Zebediela Fault (Figure 2.10).

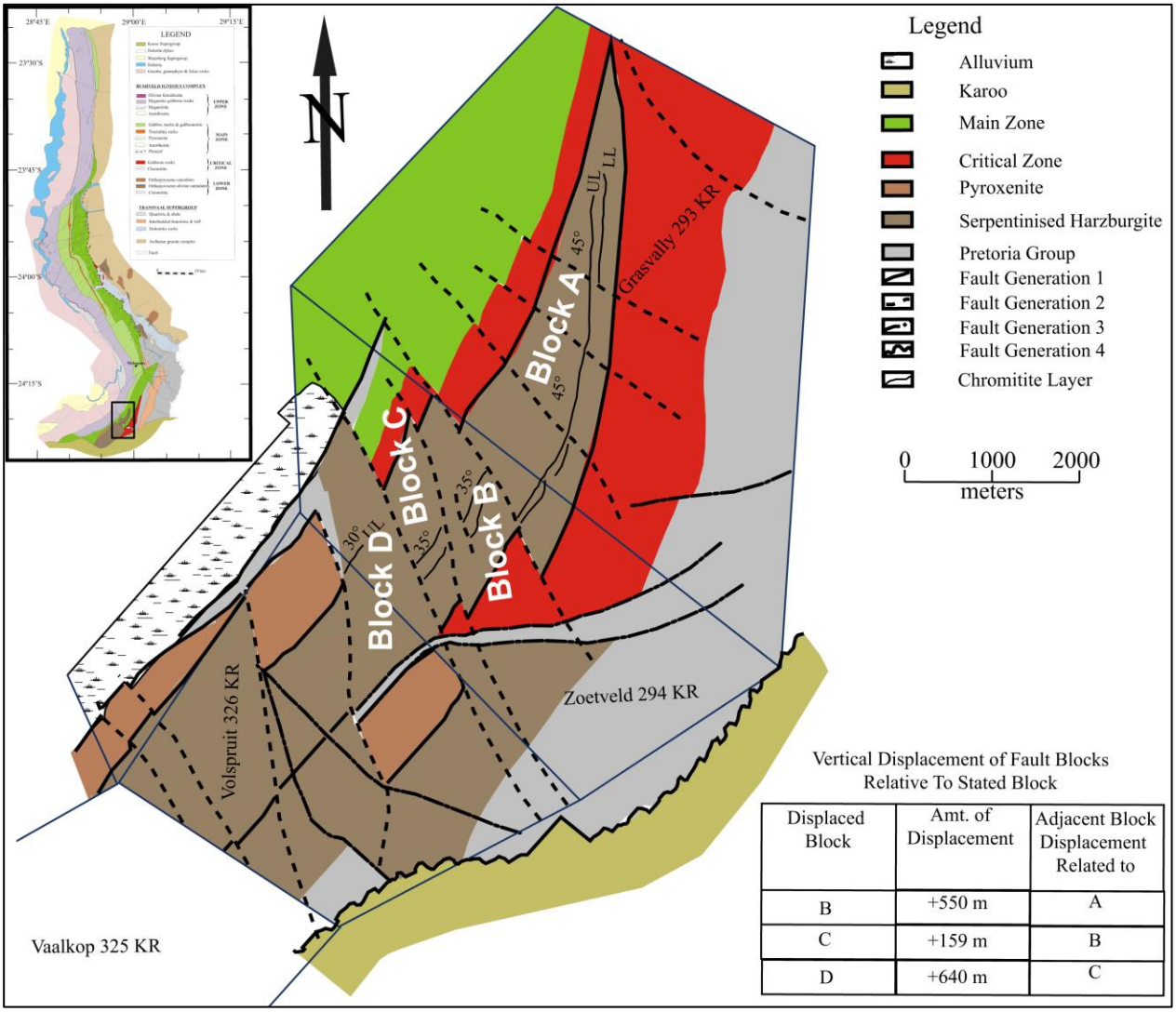

Figure 2.10: Generalised geological map of the Grasvally-Zoetveld-Volspruit area showing the four generations of faults, modified after Hulbert (1983). Map of general geology of the northern limb after Ashwal *et al*. (2005).

2.5 Summary

The northern limb to the south of the Ysterberg-Planknek Fault comprises similar stratigraphic units to that of the north. The LZ to the south is distinct due to the two chromitite layers as well as the PGE mineralisation. The GNPA member is correlated with the Platreef due to their similar stratigraphic position between the LZ and MZ. The GNPA member is distinct due to a UG2 like chromitite layer which occurs within the LMF. The Grasvally area is structurally complicated by four generations of brittle deformation which hinders correlation across the area.

CHAPTER 3

Geology of the Grasvally Area

The geology of the Grasvally area comprises mainly mafic to ultramafic rocks of the RLS, which were emplaced into sedimentary rocks of the Pretoria Group. Predictably, there has been extensive mineral exploration activity over the years, including 20 boreholes cores drilled in 2004 by Samancor on the farm of Grasvally and which were made available for this study by Sylvania Platinum Ltd. (Figure 3.1). The main objective of the core logging is to describe and classify each rock type based on distinctive features, textures, mineralogy, as well as physical properties. Such characterisation of the RLS in the study area will enable a correlation exercise with the known stratigraphy across the Ysterberg-Planknek Fault to the northern limb and also with the eastern and western limbs.

3.1 Core Logging

Sylvania Platinum Ltd made available 20 boreholes (GVL 1-GVL 20) whose localities define a north-south and an east-west array (Figure 3.1). These boreholes were collared in different lithologies and are relatively short, with a maximum depth of 641 m.

The boreholes were logged using a standardised logging system and were recorded in a field book, then subsequently transferred into an Excel spreadsheet. The lithological units were classified based on variations in mineral modes in accordance with IUGS classifications (Le Bas and Streckeisen, 1991) (Figure 3.2). Textural features, degree of alteration, deformation, the presence of xenoliths and enclaves, distinctive marker horizons (eg. chromitites) and mineralisation were also recorded. Since there were often cm scale subtle variations in mineralogy, texture, alteration throughout all the cores, some simplification and grouping was necessary to avoid small scale lithologic proliferation. The simplified lithological logs are presented in a west-east section (Figure 3.3) and a south-north section (Figure 3.4).

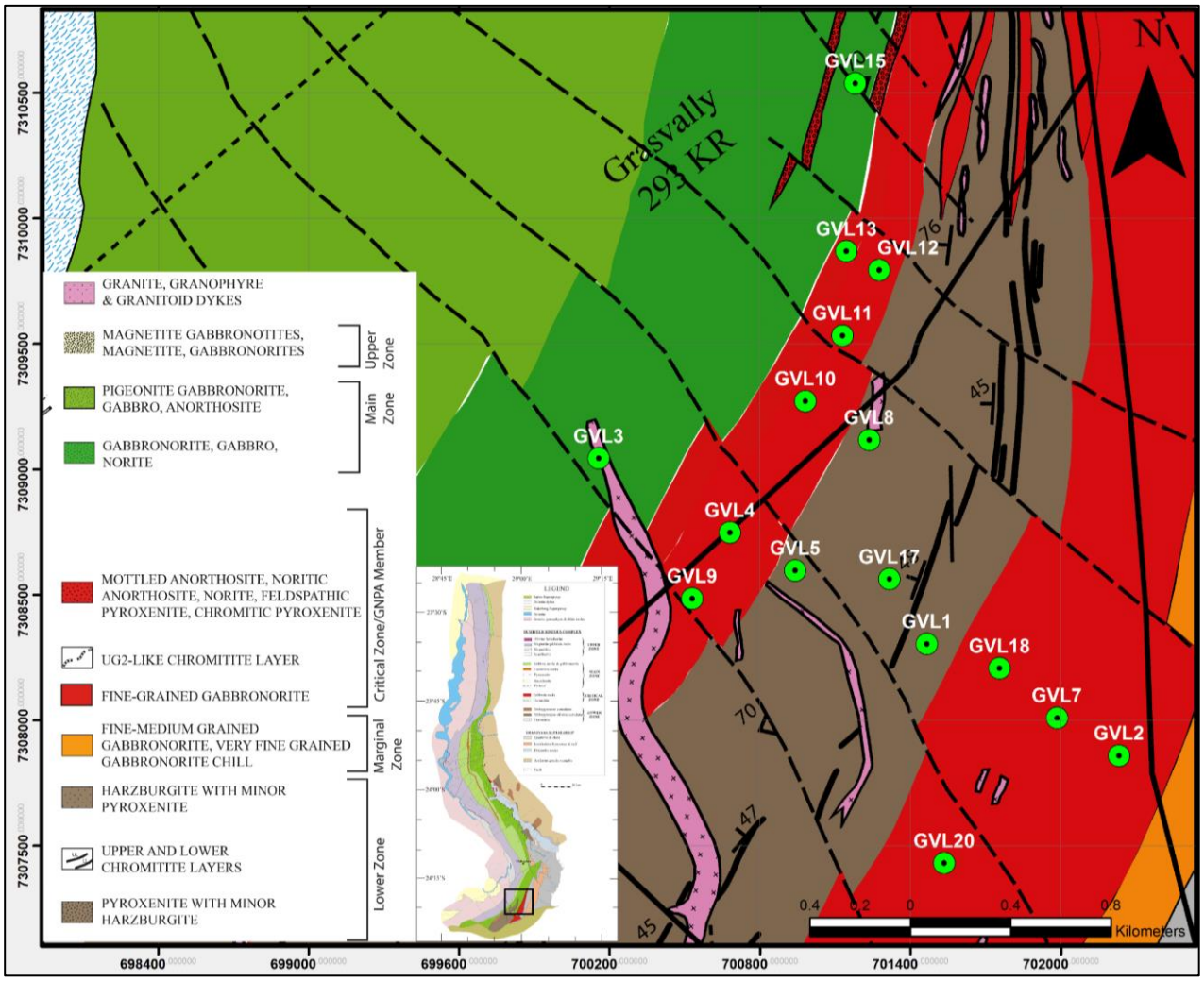

Figure 3.1: Borehole distribution on the farm Grasvally drilled by Samancor in 2004. Map modified after Hulbert (1983).

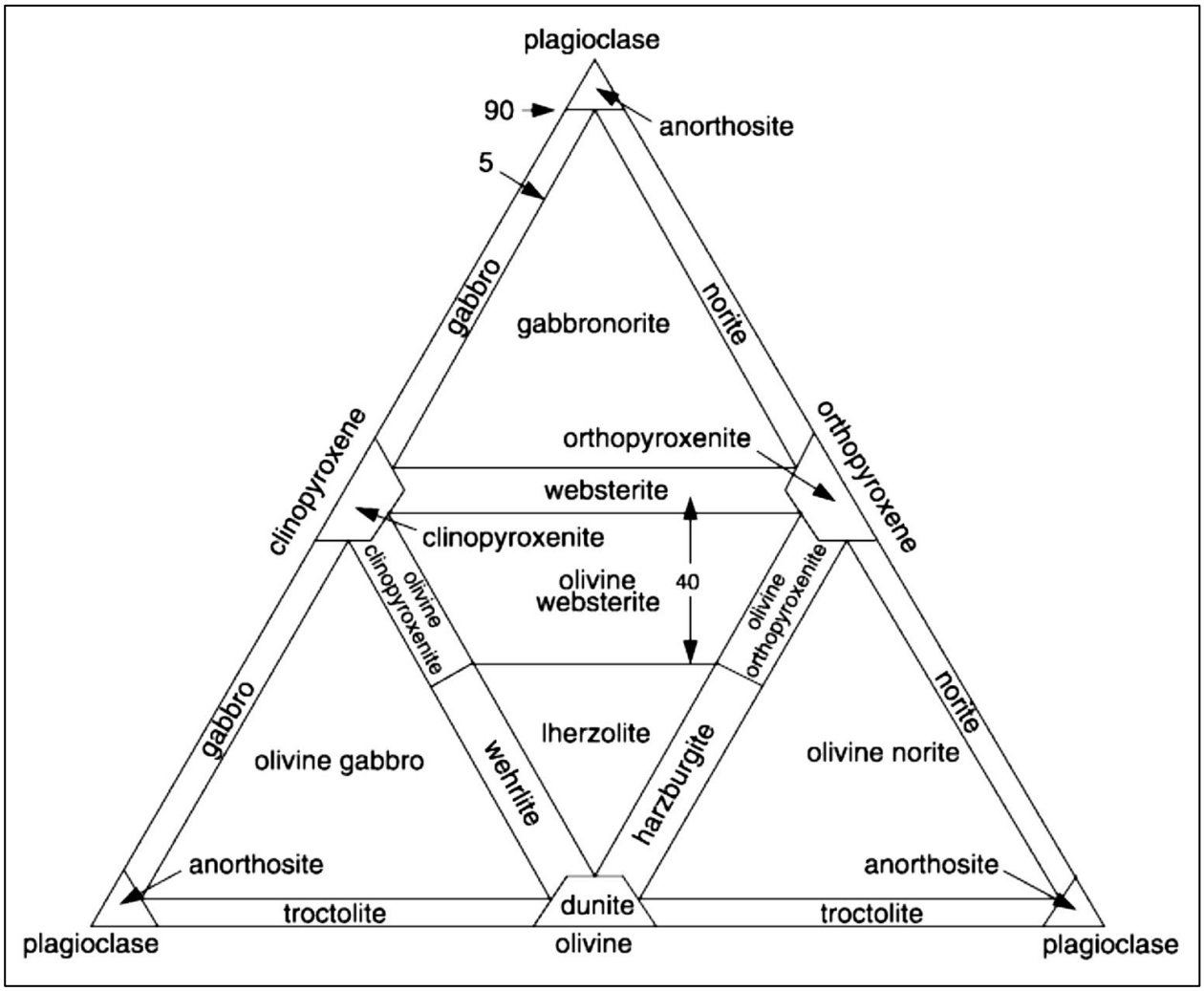

Figure 3.2: IUGS classification scheme for mafic rocks. The Grasvally rock types fall mainly in the orthopyroxenite, olivine orthopyroxenite and harzburgite fields (le Bas and Streckeisen, 1991).

3.1.1 Floor Rocks

The floor rocks comprise mainly quartzites and granofels formed by thermal metamorphism of the Pretoria Group (the former) and also early intrusives that are often contaminated with country rock (the latter). The equigranular quartzites are fine to medium-grained, pinkish-grey to reddish-brown in colour and are highly altered near the contact with the RLS. The reddish considered to be due to hematite.

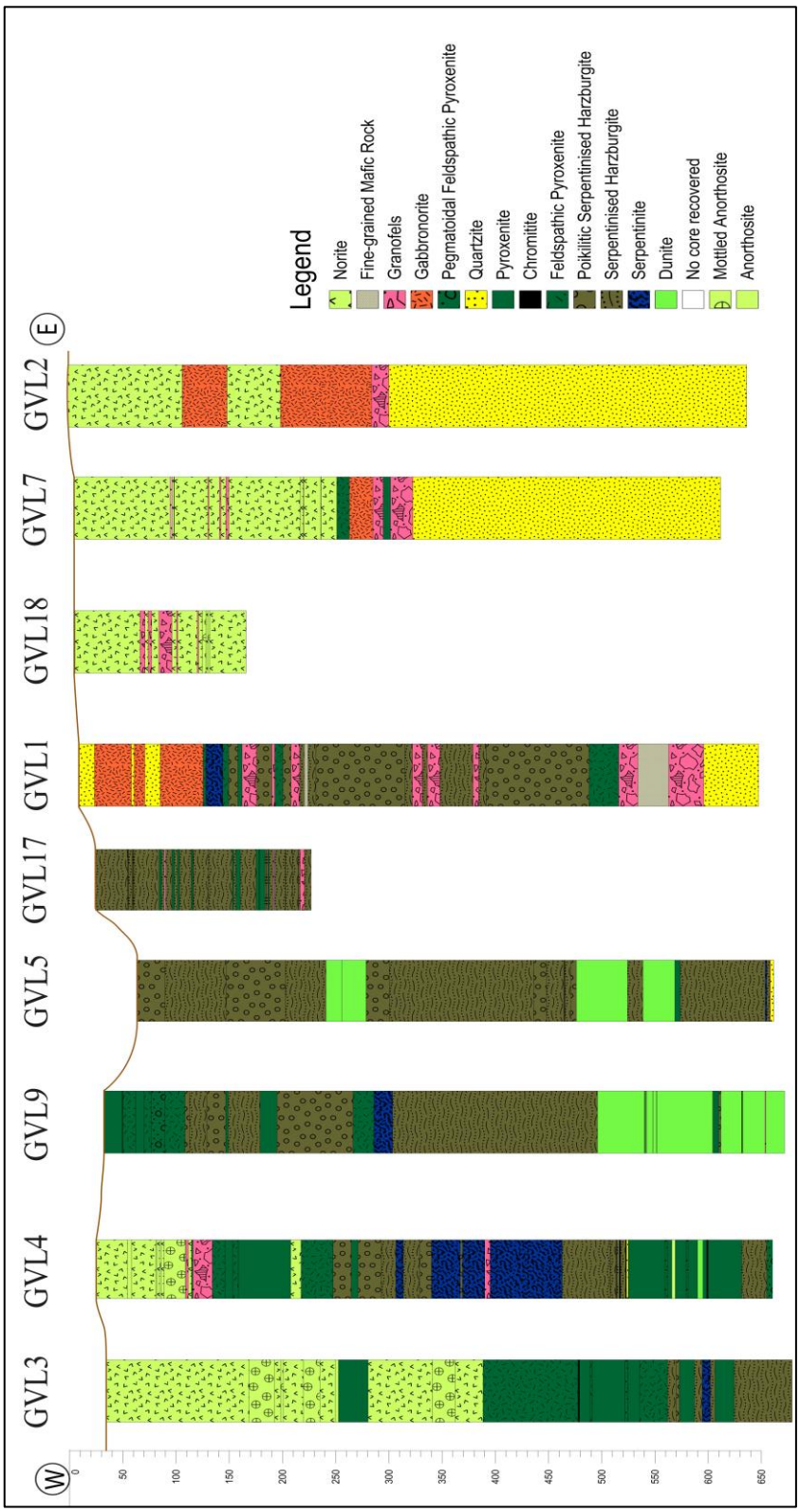

Figure 3.3: Simplified geological logs of representative boreholes arranged in order from west to east. The brown line at the top of the boreholes represents the relative topographic elevation of the collars.

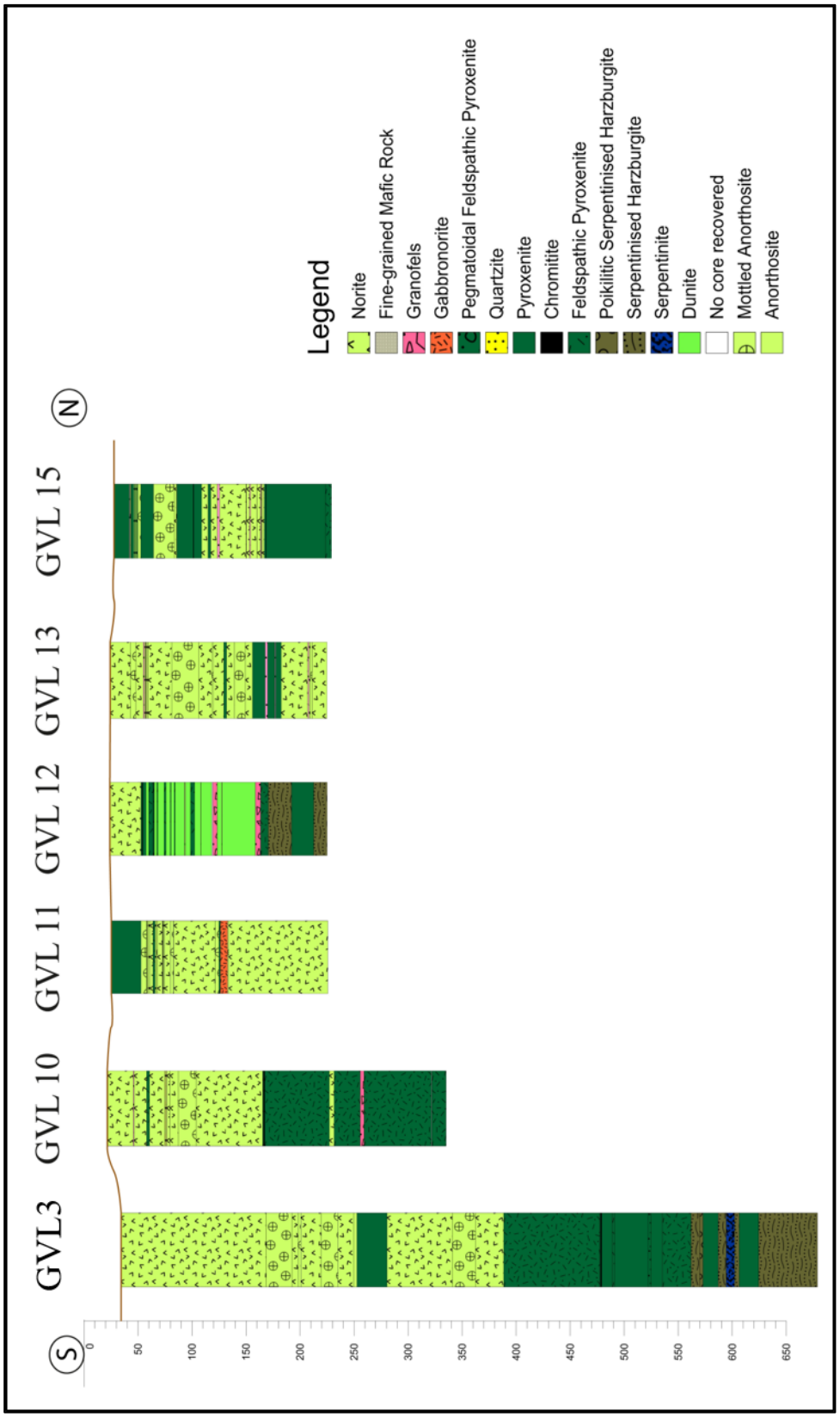

Figure 3.4: Simplified geological logs of representative boreholes arranged in order from south to north. The brown line at the top of the boreholes represents the relative topographic elevation of the collars.

There is no clear contact between the quartzites and the overlying RLS, rather an interfingering between metaigneous and metasedimentary material forming granofels, which can range in thickness from a few metres to tens of metres.

Quartzites are in contact with ultramafic rocks in boreholes GVL 1 and GVL 5 and also occur as xenoliths within ultramafics as seen in borehole GVL 1 (Figure 3.3). Boreholes GVL 2 and GVL 7 intersect quartzite at the base of norites (Figure 3.3). The holes to the north and northeast of the aforementioned boreholes do not intersect the quartzite but intersect a package of ultramafic rocks at depth (Figure 3.3 and Figure 3.4).

3.1.2 Ultramafic Package

Holes GVL 5, 6, 8, 9, 12, 17 and GVL 19 intersect an ultramafic package at depth comprising mainly variants of serpentinites, serpentinised harzburgites, dunites, serpentinised dunites and pyroxenites (Figure 3.3 and Figure 3.4). The package reaches apparent thicknesses of over 600 m. The thickness is interpreted as apparent as the strata is inclined, strata intersected perpendicular to the strike would be considered the true thickness.

Dunite:

Dunites encountered at the base of GVL 9 and GVL 5 are unusually fresh overall, despite several thin intercalations of serpentinised dunite, extremely serpentinised harzburgite and altered pyroxenites. These dunites are apple to army-green in colour, medium-grained and are extremely friable (Figure 3.5). The dunite consists of approximately 90 % cumulus olivine with disseminated chromite. The chromite also occurs as stringers to more developed layers as seen in borehole GVL 9 which displays two well-developed chromitite layers each with an apparent thickness of ~0.75 m.

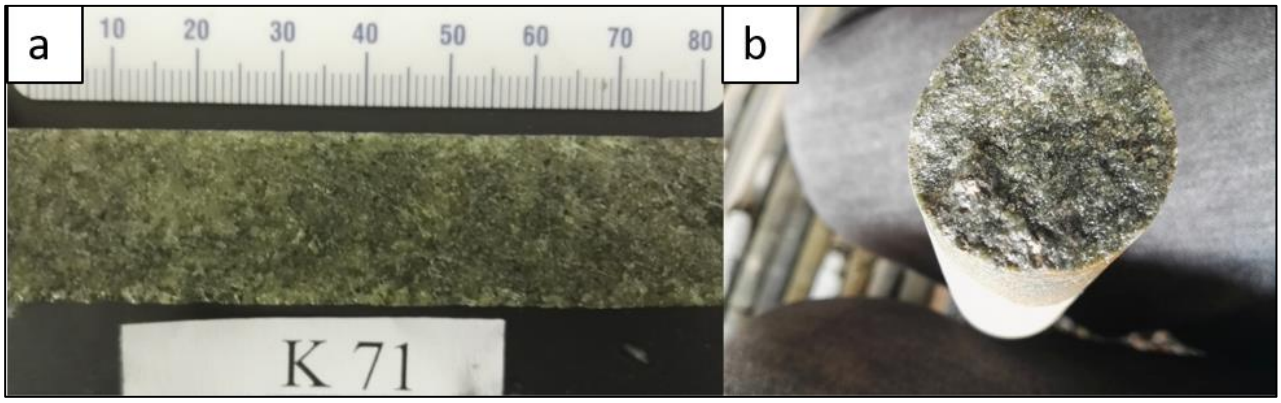

Figure 3.5: Fresh dunite with disseminated chromite intersected in GVL 9 (a) in quarter core and (b) in full core.

Harzburgite:

The harzburgites comprise cumulus olivine and orthopyroxene and are black to dark-grey in colour, fine- to medium-grained and are extensively serpentinised (Figure 3.6 and Figure 3.7). The harzburgites are differentiated based on the textural variations caused by the degree of serpentinisation as well as the size and distribution of the orthopyroxene oikocrysts (Figure 3.7), giving rise to a distinctive poikilitic texture. The oikocrysts vary in size, from 1 cm in diameter (Figure 3.7 a) to 5 cm (Figure 3.7 d). The harzburgites are mineralised in places with interstitially disseminated to net-textured pyrrhotite and minor chalcopyrite visible (Figure 3.6). The greatest variation within the harzburgites is observed in borehole GVL 4.

At 571.93 m to 594.20 m in borehole GVL 4 the harzburgite comprises evenly distributed orthopyroxene and olivine with interstitially disseminated chromite (Figure 3.7 c). The harzburgites also host well-developed chromitite layers as seen at 461.93 m to 462.86 m with an apparent thickness of 0.93 m.

The harzburgite grades upwards into a massive, entirely serpentinised harzburgite logged simply as a serpentinite (Figure 3.7 d). The serpentinite is completely black displaying relict olivine grains and interstitially disseminated pyrrhotite and chalcopyrite. The serpentinite units decrease in thickness from the west to the east (Figure 3.3).

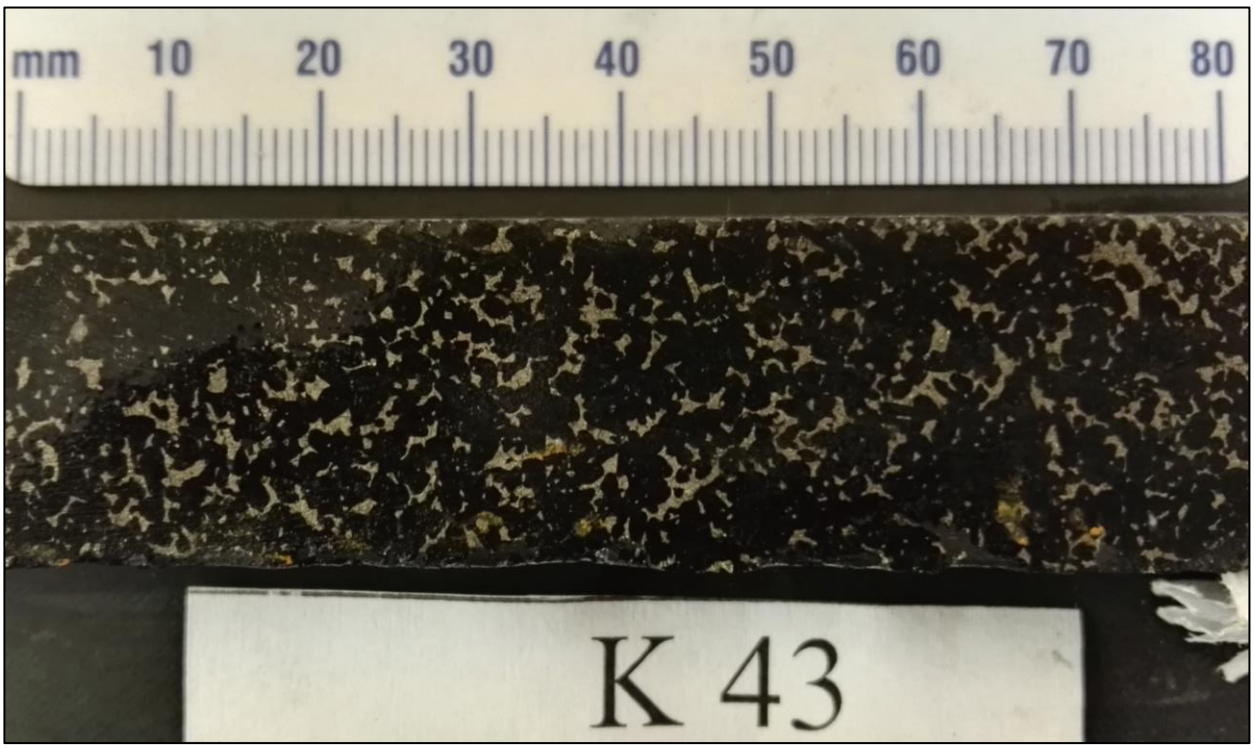

Figure 3.6: Serpentinised harzburgite with net-textured pyrrhotite and specks of interstitially disseminated chalcopyrite.

Poikilitic serpentinised harzburgites also occur within this ultramafic sequence. These harzburgites are characterised by oikocrysts of orthopyroxene ranging in size from 5 mm to 30 mm in diameter with olivine chadacrysts. The variety with smaller oikocrysts is seen in Figure 3.7 a. The oikocrysts of orthopyroxene also vary in colour from a light greenish-grey to very dark green. The dark green oikocrysts of orthopyroxene are made visible by the surrounding interstitial feldspar that occurs in some of the harzburgites with abundances of up to 15 %. Where the harzburgites have been serpentinised the presence of magnetite is noted by with the use of the magnetic pen. The magnetite is disseminated, however it forms centimetre thick bands in places. The relationship between serpentinisation and magnetite is not constant as some heavily serpentinised units have no magnetite present.

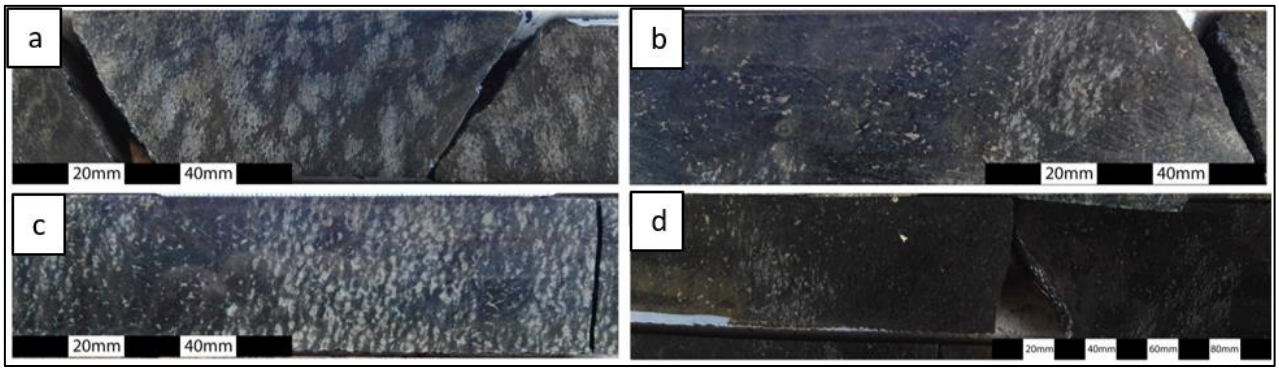

Figure 3.7: Various harzburgites. (a) Poikilitic harzburgite with 1 cm oikocrysts of orthopyroxene and olivine chadacrysts. (b) Serpentinised harzburgite with interstitially disseminated pyrrhotite. (c) Harzburgite with even proportions of orthopyroxene and olivine. (d) Extremely serpentinised harzburgite with widely spaced orthopyroxene oikocrysts.

Pyroxenite:

A variety of pyroxenites are intersected in this area ranging from fine-grained to pegmatoidal in texture (Figure 3.8). The pyroxenites are orthopyroxene dominated with feldspar abundances from 10 % in equigranular pyroxenites to 35 % in feldspathic and pegmatoidal feldspathic pyroxenites. Borehole GVL 9 intersects a pyroxenite unit with 10 % extremely altered olivine. The olivine-bearing pyroxenites are darker green in colour and are possibly chloritised as well as being serpentinised. The pyroxenites are often mineralised with up to 8 % interstitially disseminated specks and blebs of pyrrhotite with lesser chalcopyrite rimming the pyrrhotite. Chromite mineralisation is present as interstitially disseminated grains as well as well-developed stringers and layers as seen in GVL 4 at 540.88 m to 541.48 m which intersects a 0.60 m thick chromitite developed in pyroxenite. GVL 4 intersects pegmatoidal feldspathic pyroxenites mineralised in pyrrhotite, chalcopyrite as well as chromite at 103.08 m to 103.28 m and 105.48 m to 106.68 m.

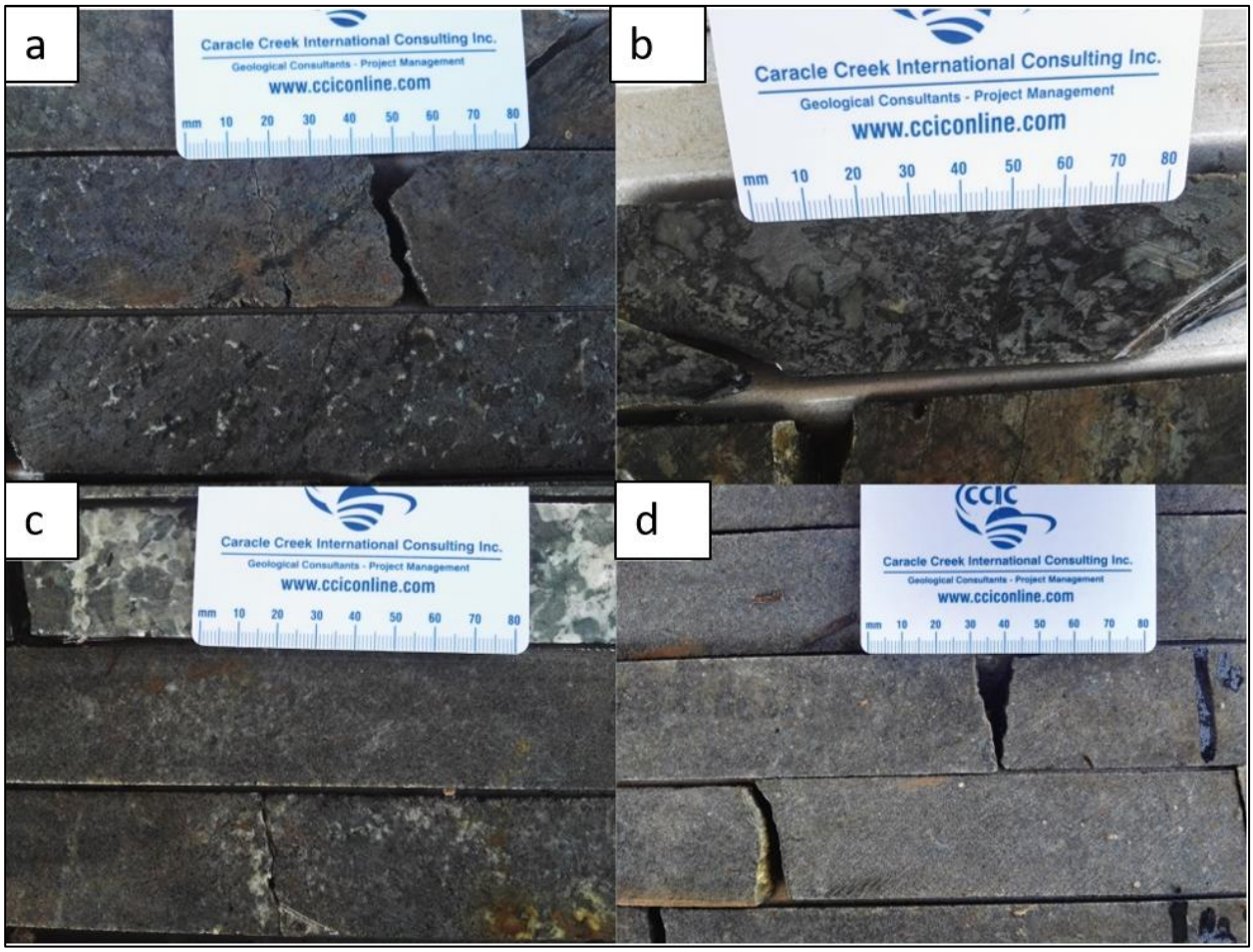

Figure 3.8: Various pyroxenites. (a) Coarse-grained feldspathic pyroxenite. (b) Altered coarse-grained feldspathic pyroxenite. (c) Fine-grained feldspathic pyroxenite with weathered mineralised sulphides. (d) Fine-grained pyroxenite with sulphide specks.

3.1.3 Norite Package

The ultramafic unit transitions into fine- to coarse-grained mafic lithologies comprising feldspathic pyroxenites, gabbronorites, norites and pyroxenites (Figure 3.9).

Gabbronorite:

GVL 1 intersects a fine-grained gabbronorite with quartzite xenoliths; this unit is similar to the fine-grained gabbronorite unit intersected at the base of borehole GVL 2. The gabbronorites are dark grey in colour and grade upwards into more medium-grained units with disseminated sulphide specks. At 74.97 m to 91.85 m there is a visibly sharp contact between the underlying gabbronorite and a shear zone characterised by recrystallised gabbronorite with flow textures and gabbronorite blocks within

it. GVL 2 intersects a gabbronorite unit at 222.00 m to 253.00 m with heavily disseminated chromite, pyrrhotite and chalcopyrite specks. This unit is also characterised by >1-3 cm chromitite pods with associated interstitial sulphides (Figure 3.10 a), fine to medium-grained pyroxenite xenoliths (Figure 3.10 b) with associated interstitially disseminated pyrrhotite and chalcopyrite as well as anorthosite fragments (Figure 3.10 c). The xenoliths are distributed about a metre apart. The gabbronorites are also characterised by the presence of phlogopite in proportions of up to 15 %.



Figure 3.9: Norite package intersected in borehole GVL 2 cut by several quartzofeldspathic veins.

Norite:

The norite units are classified as leuconorite, norite and melanorite based on the proportion of feldspar to pyroxene. The norites are fine to medium-grained with variable pyrrhotite and lesser chalcopyrite mineralisation. The norites are variably textured, and grade into melanorite and leuconorite (Figure 3.9). The norite displays similar mineralisation to that observed within other lithological units, dominated by interstitially disseminated pyrrhotite with associated less abundant chalcopyrite. The norite is altered in places with the feldspars displaying a light green tinge, possibly due to chloritisation.

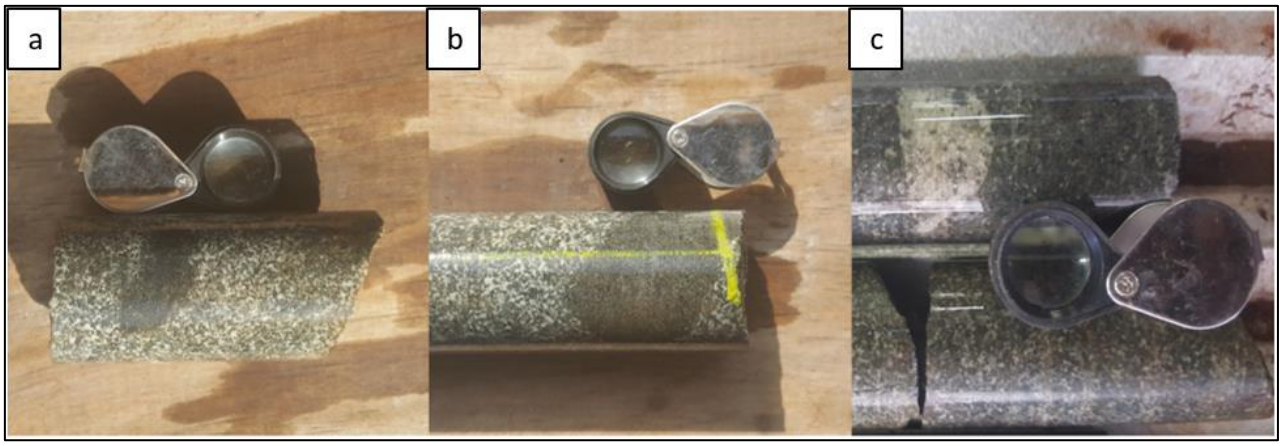

Figure 3.10: various xenoliths observed within the norites and gabbronorites in core GVL 2. (a) Chromitite pod with associated sulphides within gabbronorite. (b) Pyroxenite xenolith with interstitially disseminated sulphide specks. (c) Anorthosite xenolith within gabbronorite. All Samples are intersected in GVL 2.

GVL 2 intersects a 160 m thick medium to coarse-grained norite package intercalated with gabbronorite that is characterised by lightly disseminated as well as lenses of fine-grained cumulus magnetite or chromite (Figure 3.10). The grains are too fine-grained and oxidised to be identified on a millimetre scale, however, are visible when aggregated as laths or pods as seen in some norite intersections (Figure 3.11). The oxidation of the magnetite gives the norite a reddish colour in irregular patches. The magnetic pen was able to pick up the faint presence of magnetic minerals in places where the minerals were too fine-grained to identify on a millimetre scale.



Figure 3.11: Fine-grained magnetite bleb within norite intersected in borehole GVL 2.

3.1.4 Leucocratic unit

This unit comprises mostly spotted, smottled and mottled anorthosites (Figure 3.12) and is only intersected in the boreholes on the west of the farm (Figure 3.3). The spots and mottles of these

anorthosites are orthopyroxene oikocrysts ranging in diameter from 1 cm to 7 cm and the feldspar has a light greenish tinge possibly due to chloritisation. These anorthosites grade into norite, pyroxenite and back into mottled anorthosite units on a scale of tens of metres with less common feldspathic pyroxenite units and are commonly variably textured (Figure 3.12).The anorthosite units are cut by sharp, multiple, irregular quartzofeldspathic veins as well as quartz veins varying in thickness from a millimetre to a few centimetres. The mottled anorthosites are also mineralised, with specks of interstitial pyrrhotite present up to 4 % in places.



Figure 3.12: variably textured mottled anorthosite unit grading from spotted to mottled to feldspathic pyroxenite back into mottled anorthosite intersected in borehole GVL 9.

3.1.5 Quartzofeldspathic veins

All the rock types in the area are cut by quartzofeldspathic veins ranging in thickness from 1 mm to a few metres, brecciating the intruded rock type in places (Figure 3.13). These veins are white to milky white in colour and comprise equal proportions of quartz and feldspar. The quartzofeldspathic veins are mostly fine-grained but are locally pegmatoidal in a few places. The intrusion of this unit forms brecciated zones (Figure 3.13).

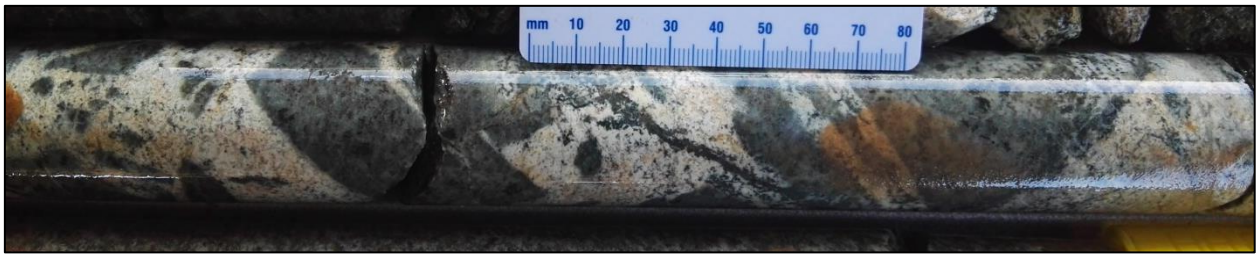

Figure 3.13: Pyroxenite brecciated by quartzofeldspathic veins.

3.2 Petrography

Sections of core described previously at the hand specimen scale were used to prepare thin sections for optical microscopy under transmitted and reflected light. Microscopic analysis helps considerably in clearing up ambiguities encountered with hand sample examination, both in terms of mineral identification and the integration of textural features, such as intercumulus and cumulus textures. Where cumulus plagioclase is seen within a pyroxene-bearing rock it is termed a norite, and where it is an intercumulus phase, a feldspathic pyroxenite (Hutchinson and Kinnaird, 2005). The detailed descriptions of samples K1-133 are found in Appendix D. The samples presented in this chapter represent key features in individual rock types.

3.2.1 Harzburgite

The harzburgite samples are moderately to extremely serpentinised. The olivine grains, roughly 3 mm in diameter, are highly fractured with serpentine veins within the fractures (Figure 3.14). The completely serpentinised samples comprise mostly serpentine veins and relict olivine cores. The alteration of these harzburgites has resulted in the growth of interstitially disseminated magnetite grains and veinlets within fractures and at the grain boundaries (Figure 3.14 c). Interstitial secondary biotite occurs associated with the alteration and magnetite (K-53). In some samples that have been completely serpentinised, there is no magnetite present.

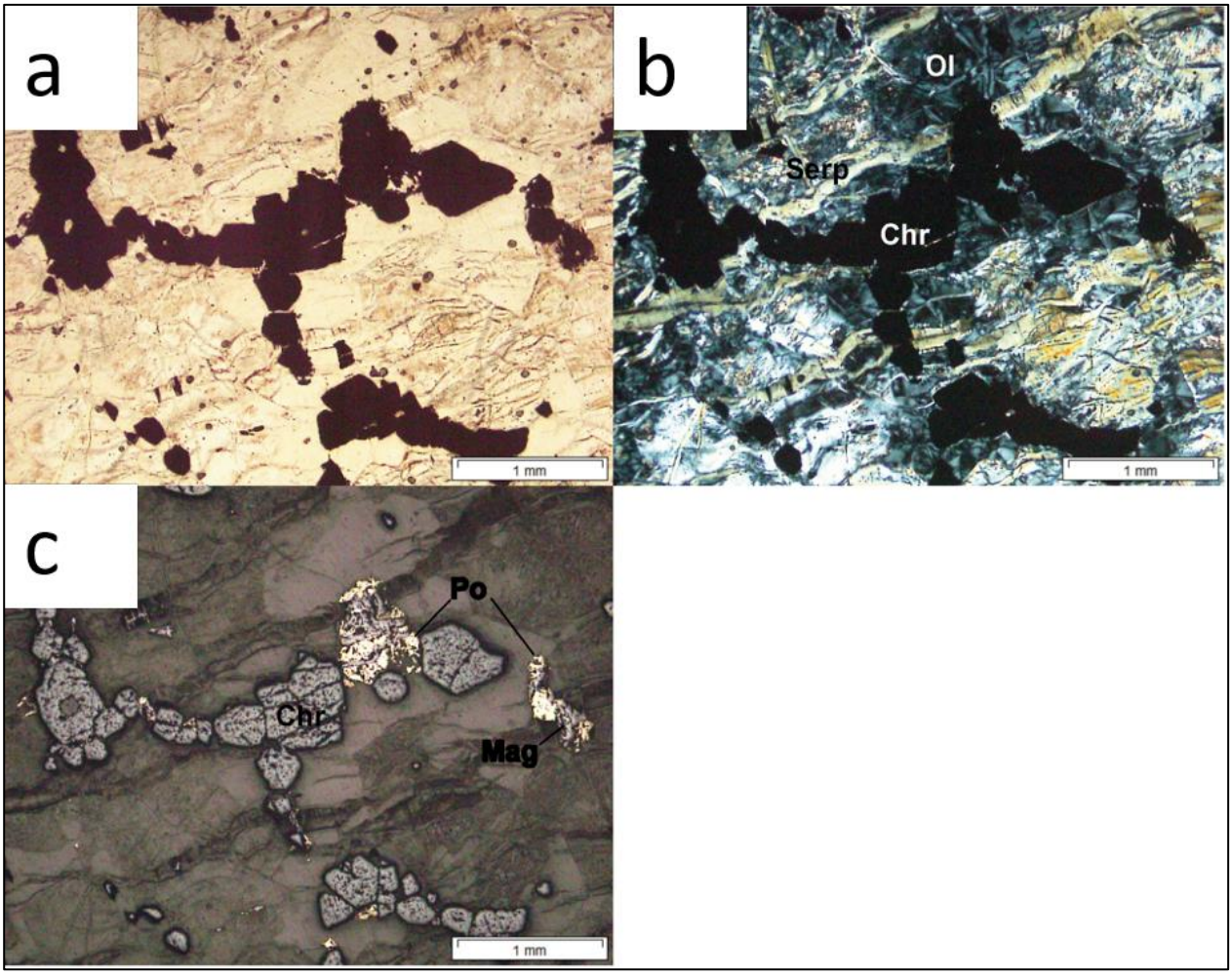

Figure 3.14: Photomicrographs of a serpentinised chromite-bearing harzburgite in both transmitted and reflected light. (a) serpentinised harzburgite in PPL with opaque chained chromite. (b) Serpentinised harzburgite in XPL dominated by secondary serpentine veins. (c) Serpentinised harzburgite in RL with chained chromite, chromite displaying atoll textures and interstitially disseminated pyrrhotite, chalcopyrite and magnetite.

3.2.2 Dunite

The dunite samples range from extremely pristine to completely serpentinised. Fresh unaltered dunite contains adcumulate annealed olivine crystals with triple junction boundaries (Figure 3.15 a), some showing kink-banding in crossed polars (Figure 3.15 b). The extremely serpentinised olivine crystals are very fractured and riddled with serpentine veins (Figure 3.15 f). The fresh dunites shows chromite, pyrrhotite and magnetite interstitially disseminated within the fractures (K-24) (K-73) (Figure 3.15 c). The minor interstitial orthopyroxene has been extremely altered (sericitisation) with > 1 % secondary biotite. The more altered biotite is dominated by interstitially disseminated pyrrhotite blebs with specks and veinlets of magnetite (Figure 3.15 d).

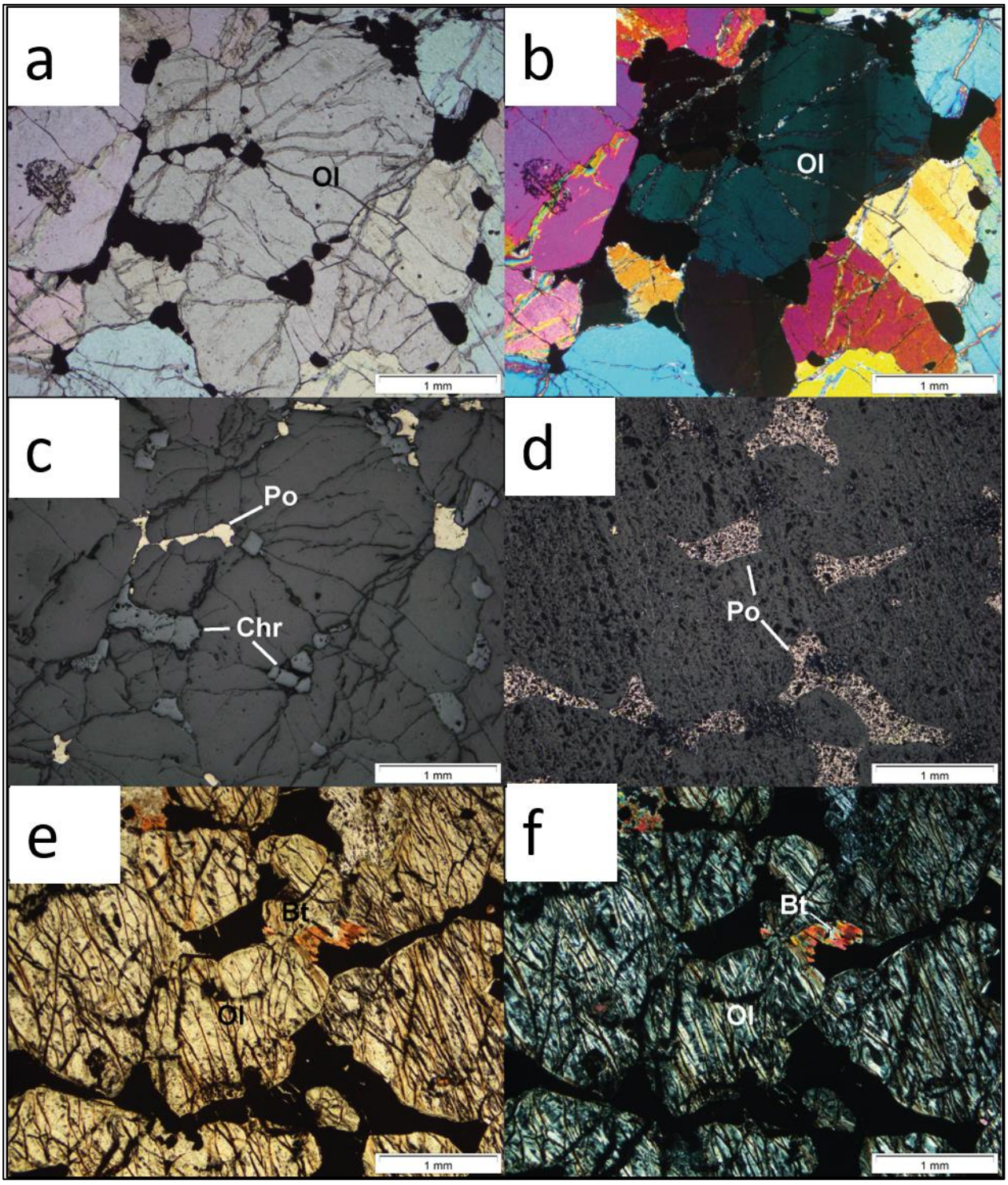

Figure 3.15: Photomicrographs of a serpentinised dunite in both transmitted and reflected light. (a) Dunite in PPL with olivine and interstitially disseminated opaques. (b) Dunite in XPL with annealed olivine crystals displaying kink banding. (c) Dunite in RL with interstitially disseminated pyrrhotite and chromite (d) Serpentinised dunite in RL displaying interstitially disseminated blebs of pyrrhotite. (e) Serpentinised dunite in PPL with altered olivine and secondary biotite associated with pyrrhotite (opaque). (f) Serpentinised dunite in XPL displaying serpentinised and highly fractured olivine grains with secondary biotite associated with pyrrhotite (Opaque).

3.2.3 Pyroxenite

The pyroxenites comprise dominantly cumulus orthopyroxene, with lower proportions of cumulus and intercumulus clinopyroxene and intercumulus feldspar (Figure 3.16). The proportion of feldspar ranges from 5 % to 35 %, samples with higher proportion of feldspar are termed feldspathic pyroxenite. The feldspar crystals are variably altered displaying patches of sericitisation to complete sericitisation in extremely altered samples. The cumulus orthopyroxene ranges in size from 1 mm to 13 mm and displays moderate alteration with blebby exsolution textures (Figure 3.16). The pyroxenite samples contain minor secondary biotite and chlorite (> 1 %). Some samples contain olivine (5 - 15 %) and have been termed olivine-bearing pyroxenites in Appendix D.

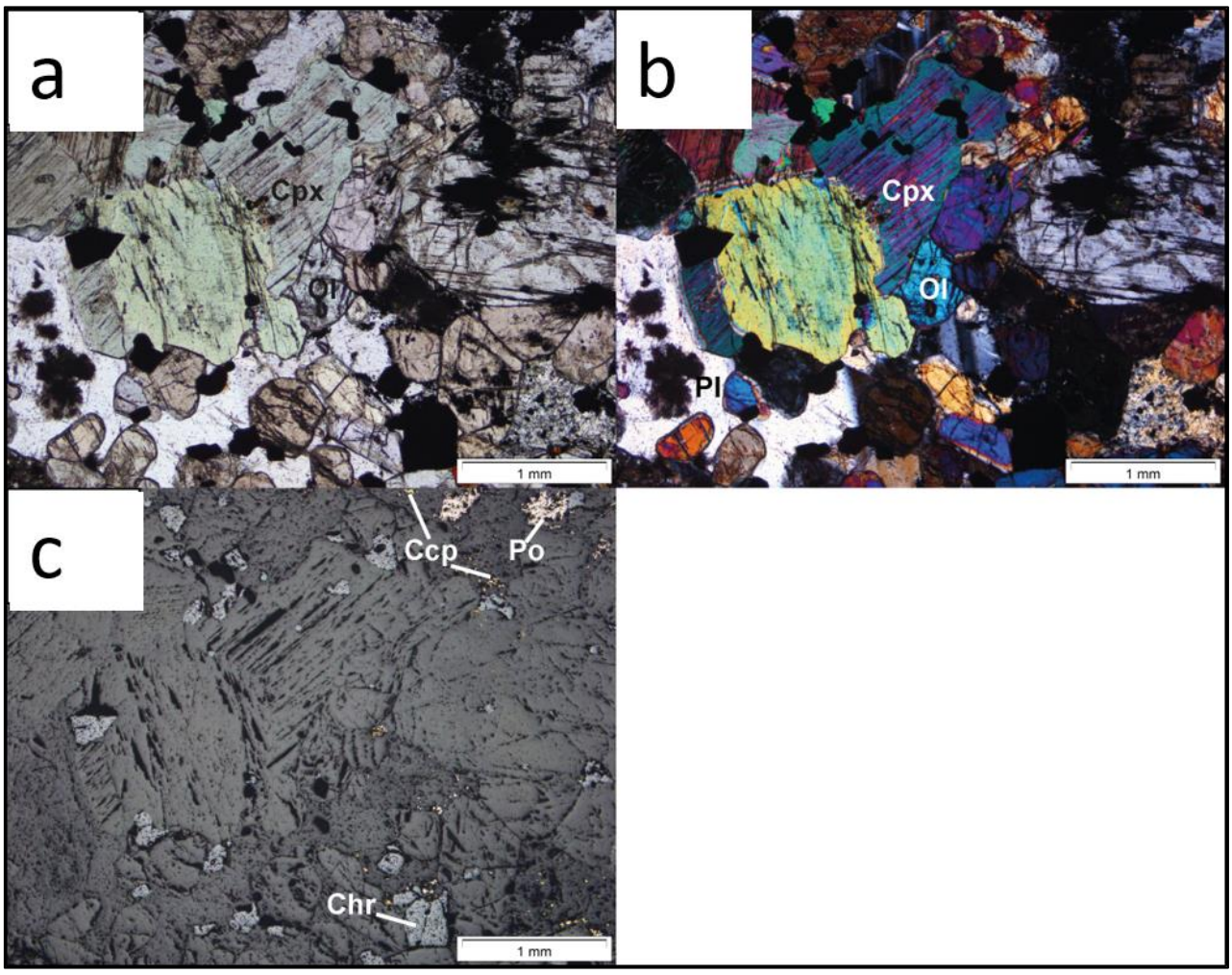

Figure 3.16: Photomicrographs of a mineralised pyroxenite in both transmitted and reflected light. (a) Pyroxenite in PPL displaying clinopyroxene with exsolution lamellae and annealed olivine and altered orthopyroxenes. (b) Pyroxenite with clinopyroxene displaying exsolution lamellae, olivine and orthopyroxene. (c) Pyroxenite in RL displaying chromite, interstitially disseminated pyrrhotite with lesser specks of disseminated chalcopyrite.

3.2.4 Gabbronorite

The gabbronorites are extremely altered in most cases with the samples displaying a grungy appearance. The feldspars are moderately to completely sericitised with secondary biotite forming in association with > 1 mm magnetite (Figure 3.17). The intercumulus clinopyroxene within the gabbronorites are > 1 mm to 8 mm in length and display patchy to well-developed exsolution lamellae (Figure 3.17 b). The < 2 mm orthopyroxene crystals are highly fractured and have a modal abundance of between 40 to 70 %.

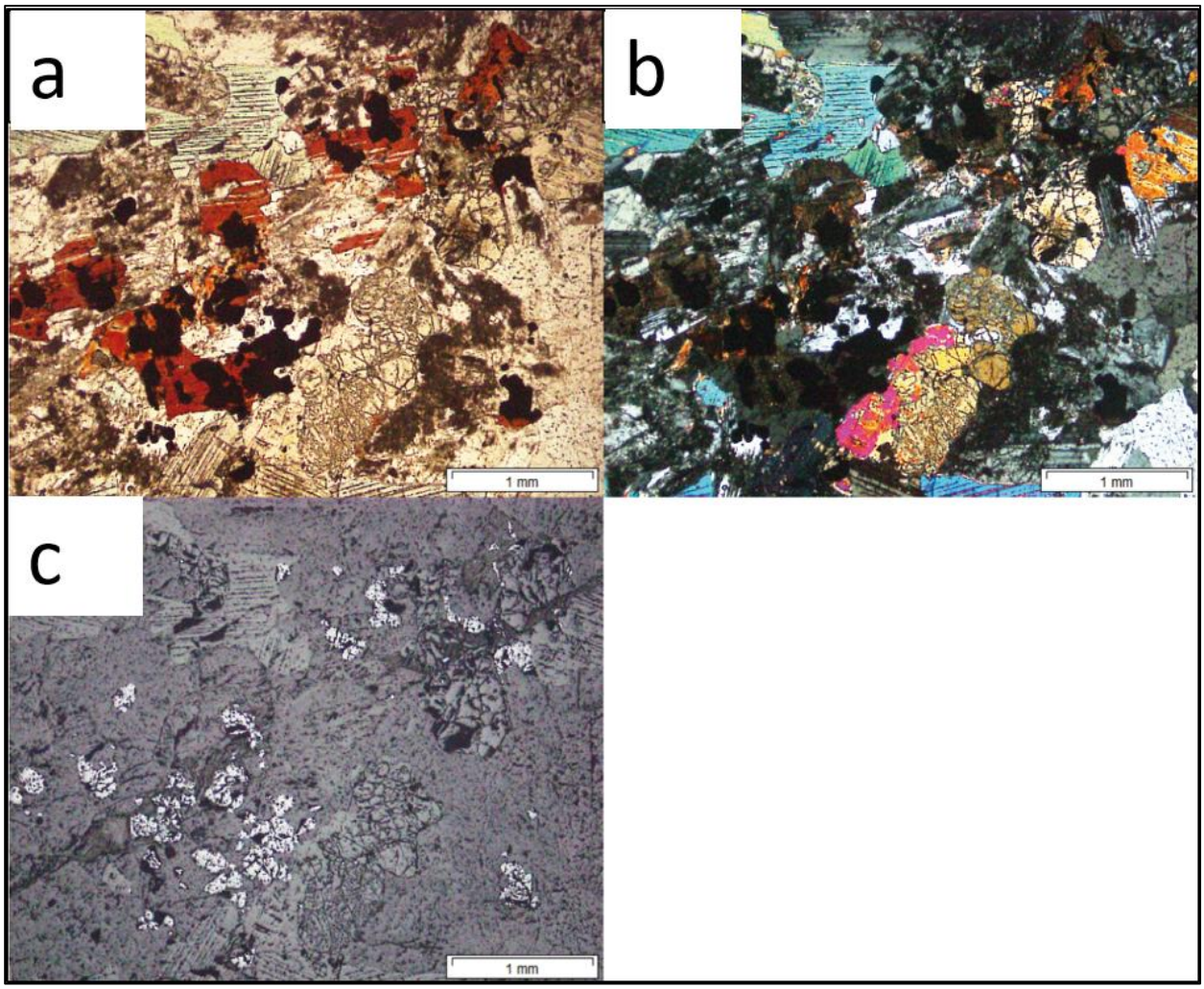

Figure 3.17: Photomicrographs of an altered gabbronorite in both transmitted and reflected light. (a) Gabbronorite in PPL with biotite associated with opaque magnetite. (b) gabbronorite in XPL with highly altered and fractured opx and cpx displaying exsolution lamellae. Sericitisation of feldspars is visible in places. (c) Gabbronorite in reflected light displaying grains of magnetite.

3.2.5 Norite

The norites differ in ratio of plagioclase to orthopyroxene ranging from leuco- to mela-norite. The cumulate feldspar crystals range in size from >1 mm to 3 mm along the short axis and display minor to extensive sericitisation. The orthopyroxenes display clinopyroxene exsolution blebs and more well-developed lamellae (Figure 3.18). Minor interstitial blebs of clinopyroxene also occur within the norite samples (K-01) (Figure 3.18).

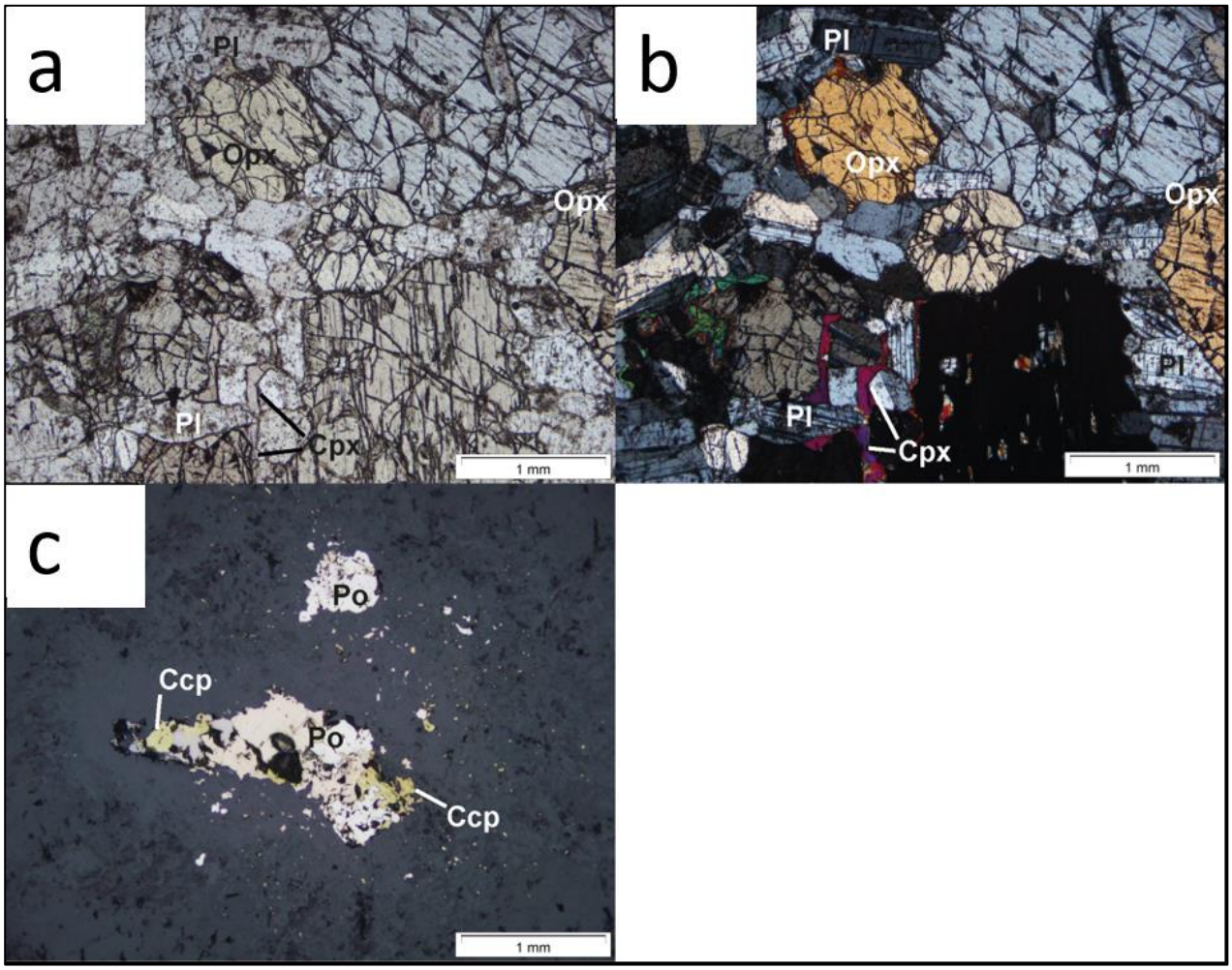

Figure 3.18: Photomicrographs of a norite in both transmitted and reflected light. (a) Highly fractured norite dominated by orthopyroxene in PPL. (b) Norite dominated by orthopyroxene, plagioclase with minor intercumulus clinopyroxene in XPL. (c) Blebby pyrrhotite with associated chalcopyrite and lesser interstitially disseminated chalcopyrite and pyrite specks.

3.2.6 Anorthosite

The anorthosites consist mainly of annealed, euhedral to subhedral feldspar crystals ranging from 1 mm to 4 mm crystals of which some display concentric compositional zoning (Sample K-29). The

mottled anorthosite samples comprise oikocrysts of clinopyroxene with exsolution lamellae and extensive chloritisation and sericitisation (Figure 3.19).

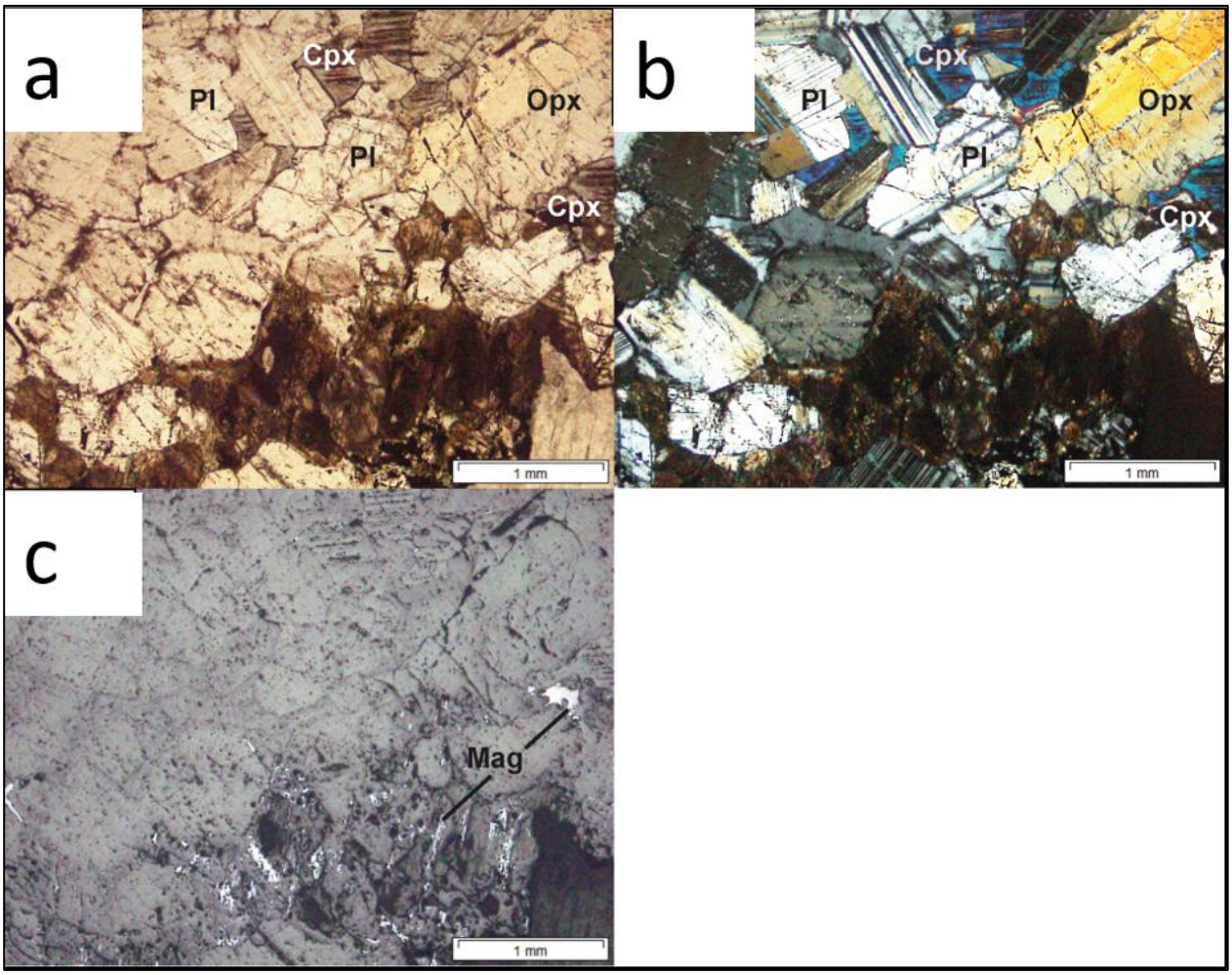

Figure 3.19: Photomicrographs of an altered anorthosite in both transmitted and reflected light. (a) Anorthosite in PPL with dominant plagioclase crystals as well as darker coloured areas of alteration. (b) Anorthosite displaying dominant plagioclase crystals heavily altered to sericite, interstitial clinopyroxene as well as orthopyroxene. (c) Secondary veinlets of magnetite as well as interstitial magnetite is present associated with the sericitised zone.

3.2.7 Granofels

In thin section the complex multi-component nature of the granofels contact zone confirms the hand specimen descriptions. Darker patches consist of brecciated mafic blocks that vary from 1 - 14 cm, while patches and lenses of lighter granitic material comprise equal parts of quartz and feldspar, the latter displaying moderate to extensive alteration to sericite. Grain sizes vary greatly and granophyric texture is common (Figure 3.20). Multiple milky-white veins cross cut the entire mixed assemblage.

Clearly the above features suggest that the contact granofels has developed during intrusion of RLS magmas into the Pretoria Group.

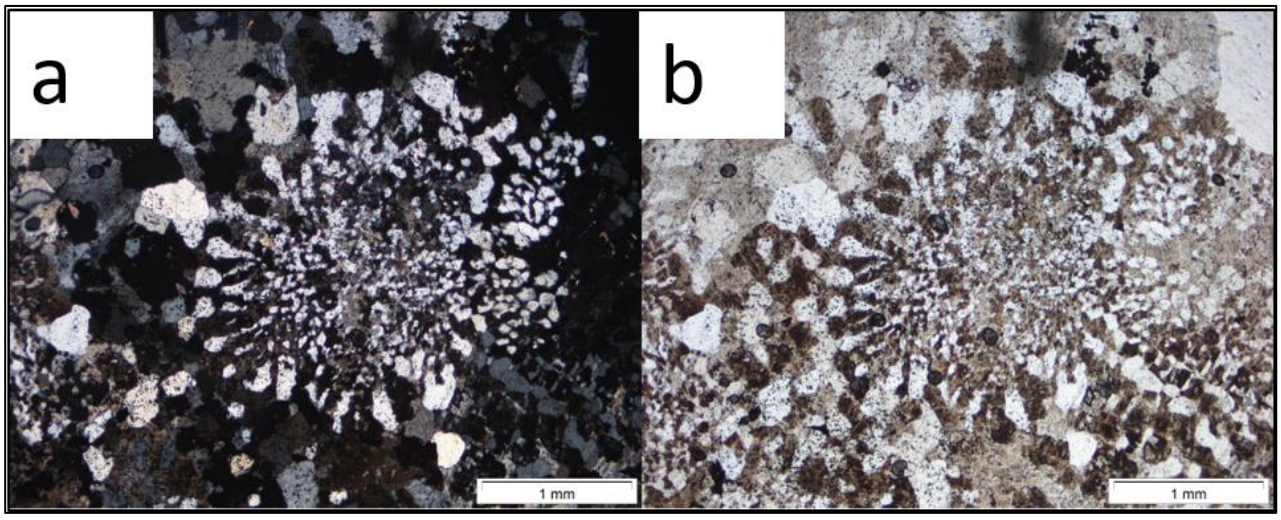

Figure 3.20: Photomicrographs of a granofels in transmitted light displaying granophyric texture. (a) Photomicrograph of quartzofeldspathic vein displaying granophyric texture in XPL. (b) Quartzofeldspathic vein displaying granophyric texture in PPL.

3.2.3 Mineralisation

The sulphide mineralisation within the area is not limited to one lithological or stratigraphic unit. The primary mineral assemblages are predominantly pyrrhotite, chalcopyrite, pentlandite and pyrite. Primary magnetite occurs within a few samples in borehole GVL 2 (K-29).

The primary magnetite along with ilmenite and chromite occur as pods within gabbronorites and norites (Figure 3.21). The chromite and magnetite crystals form aggregate grains with the magnetite occurring interstitially between the chromite, orthopyroxene and feldspars crystals (Figure 3.21 a). The ilmenite occurs as interstitial blebs to disseminated specks within the gabbronorites (Figure 3.21 c). The ilmenite often occurs with lesser magnetite specks and is associated with secondary biotite (Figure 3.21 c and Figure 3.21 d).

The magnetite-ilmenite mineralisation within the mottled anorthosites is associated with extensive alteration visible in association with biotite (K-92). Sulphide mineralisation textures vary from disseminated blebs to net-textured and this overall style is consistent within the different lithological units. Anorthosites, norites, gabbronorites, pyroxenites and harzburgites are mineralised at varying stratigraphic heights with the percentage of sulphides ranging between <1 to 10 %.

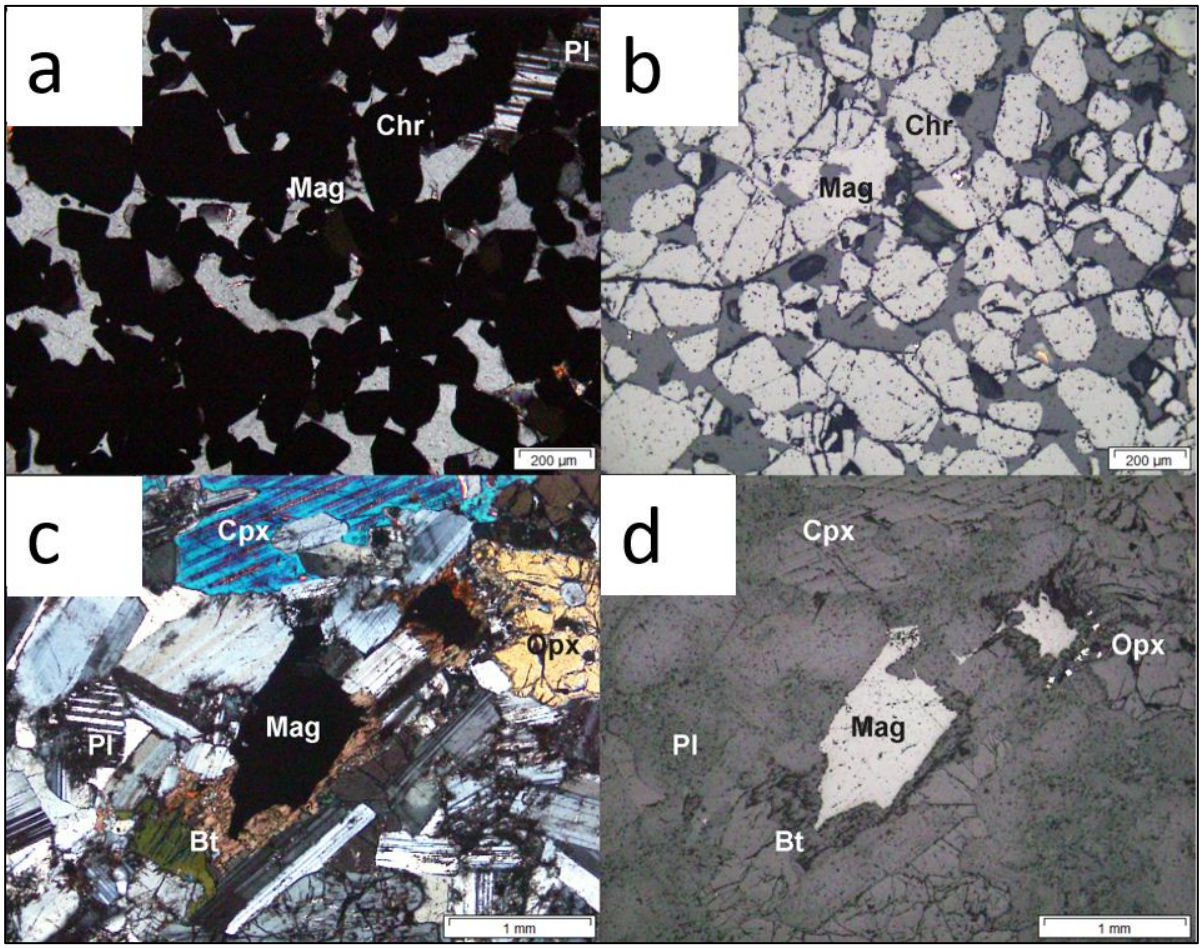

Figure 3.21: Photomicrographs of various opaque minerals observed in core. Interstitially distributed cumulus chromite and lesser magnetite in XPL within feldspathic gabbronorite (a) in PPL and (b) in RL. (c) Gabbronorite dominated by feldspar with interstitial clinopyroxene with exsolution lamellae highly fractured and altered orthopyroxene with inclusions of feldspar. (d) Interstitial intercumulus magnetite with associated biotite and minor specks of pyrite within gabbronorite.

The pyrrhotite blebs are rimmed by chalcopyrite as seen in Figure 3.22 c. Chromite grains display flame-like structures of pyrrhotite along the margins (K-20). The chromite mineralisation in this area is restricted to the gabbronorites, pyroxenites, harzburgites and dunites. The chromite occurs between cumulus grains forming aggregate chains of chromite and is also present within olivine grains as inclusions (2 - 15 %). The occurrence of chromite is, within some units, accompanied by the presence of sulphides, mainly pyrrhotite and chalcopyrite (Figure 3.22 b and Figure 3.22 d). The chromites within the serpentinised harzburgites accompanies olivine grains whose alteration has led to thin linings of secondary magnetite along contacts. Sulphide blebs dominated by chalcopyrite often occur along chromite-olivine contacts. Where chromite is more abundant, forming discontinuous stringers,

interstitial chalcopyrite is more widespread and not confined to olivine contacts (Figure 3.22 d). Some chromite grains display an atoll-texture, with the silicate material at their core (Figure 3.22 d).

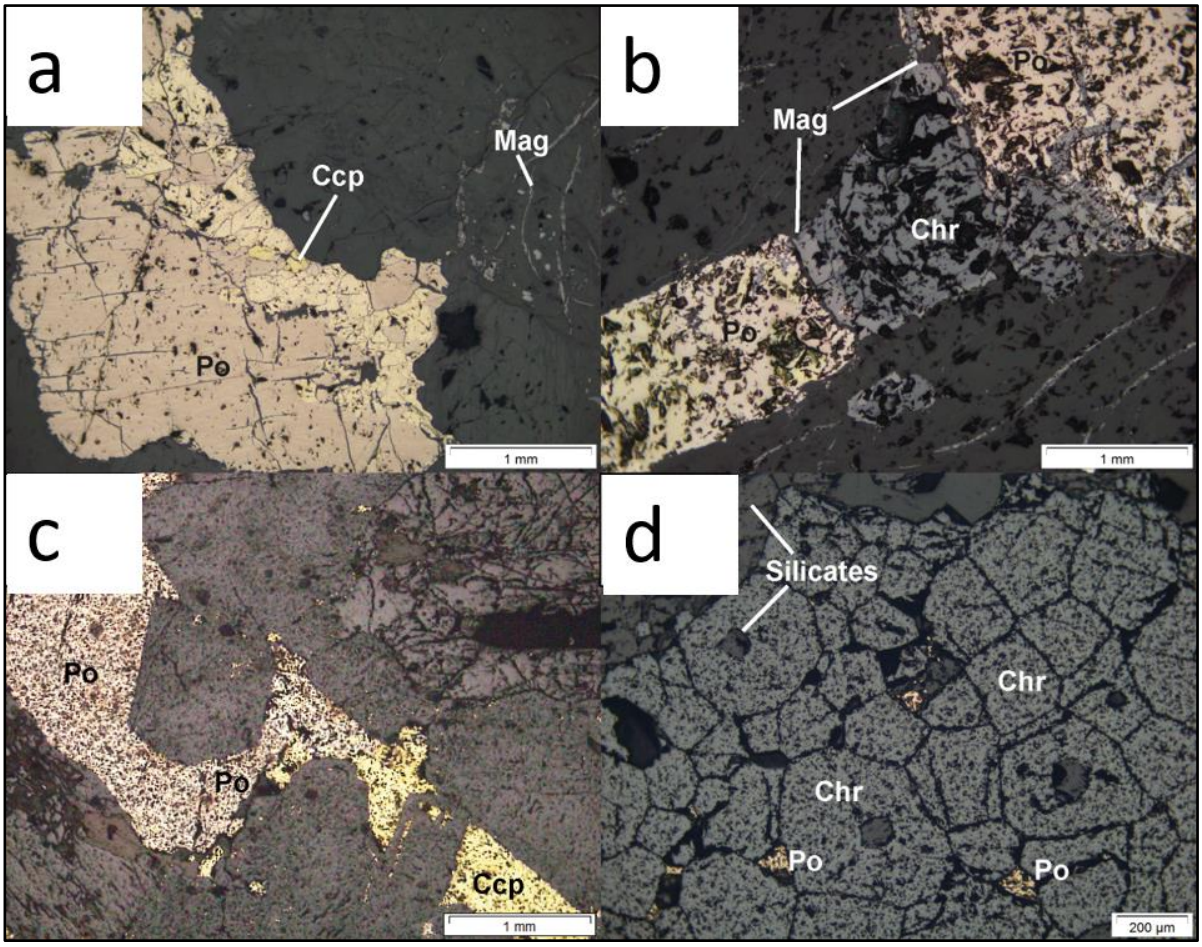

Figure 3.22: (a) A large pyrrhotite with marginal chalcopyrite. Veinlets and specks of secondary magnetite. (b) Pyrrhotite, chalcopyrite, magnetite and chromite. (c) interstitial pyrrhotite rimmed partially by chalcopyrite. (d) Chromitite grains displaying atoll texture with specks of interstitially disseminated pyrrhotite.

3.4 Magnetic Susceptibility (MS)

3.4.1 Introduction

The Grasvally area lacks good surface outcrops and the sub-surface is known to be complicated by faulting and the resulting horst-graben system. Attempts were made by Barrett *et al*. (1978) to constrain the structures in the area by integrating a gravity survey, surface mapping and borehole logs, but was hampered by the lack of useful marker horizons. This section aims to define possible marker horizons based on the magnetic susceptibility (MS) of the lithological units. The MS within igneous rocks is mainly controlled by the abundance of magnetite, which is known to vary within stratigraphic units of the RLS (Table 3.1) (Ashwal *et al*., 2005).

Table 3.1: Average magnetic susceptibility values for Bellevue drill core (BV-1) after Ashwal *et al.* (2005).

Unit	Average Magnetic Susceptibility (SI Units)
Titanomagnetite	1 - 50
Upper Zone	<0.1 - 5
Main Zone	<0.02

A SM-30 handheld magnetic susceptibility meter was used to record the measurements. The same boreholes sampled in previous chapters were selected for this method, apart from GVL 5. Measurements were taken at 50 cm spacing and 3 readings were taken for each point, averaged and recorded in Appendix E.

Where the core was either missing or extremely friable, the data point is omitted, and the nearest intact core was measured.



Figure 3.23: SM-30 Magnetic susceptibility meter alongside pyroxenite quarter-core displaying susceptibility reading.

3.4.2 Results

Magnetic susceptibility (MS) data, recorded in SI units, were collected on five selected cores and are plotted against stratigraphic height (Figure 3.24). The first MS profile (GVL-3) displays a decreasing trend with increasing stratigraphic height. The greatest variation is seen within the serpentinised harzburgite at the base, with a maximum of 0.021 at 610.02 m to 0 at 49.38 m. The interfingering and overlying pyroxenites display relatively lower, yet more constant values ranging from 0 to 0.003, while the overlying units of norite and mottled anorthosite display MS of 0 on average.

GVL 11 intersects mainly norites with minor gabbronorite. This unit displays no variation in MS with values averaging 0 with a maximum of 0.001. The pyroxenitic material at the top of the borehole could not be analysed as the core is too brittle and crumbly.

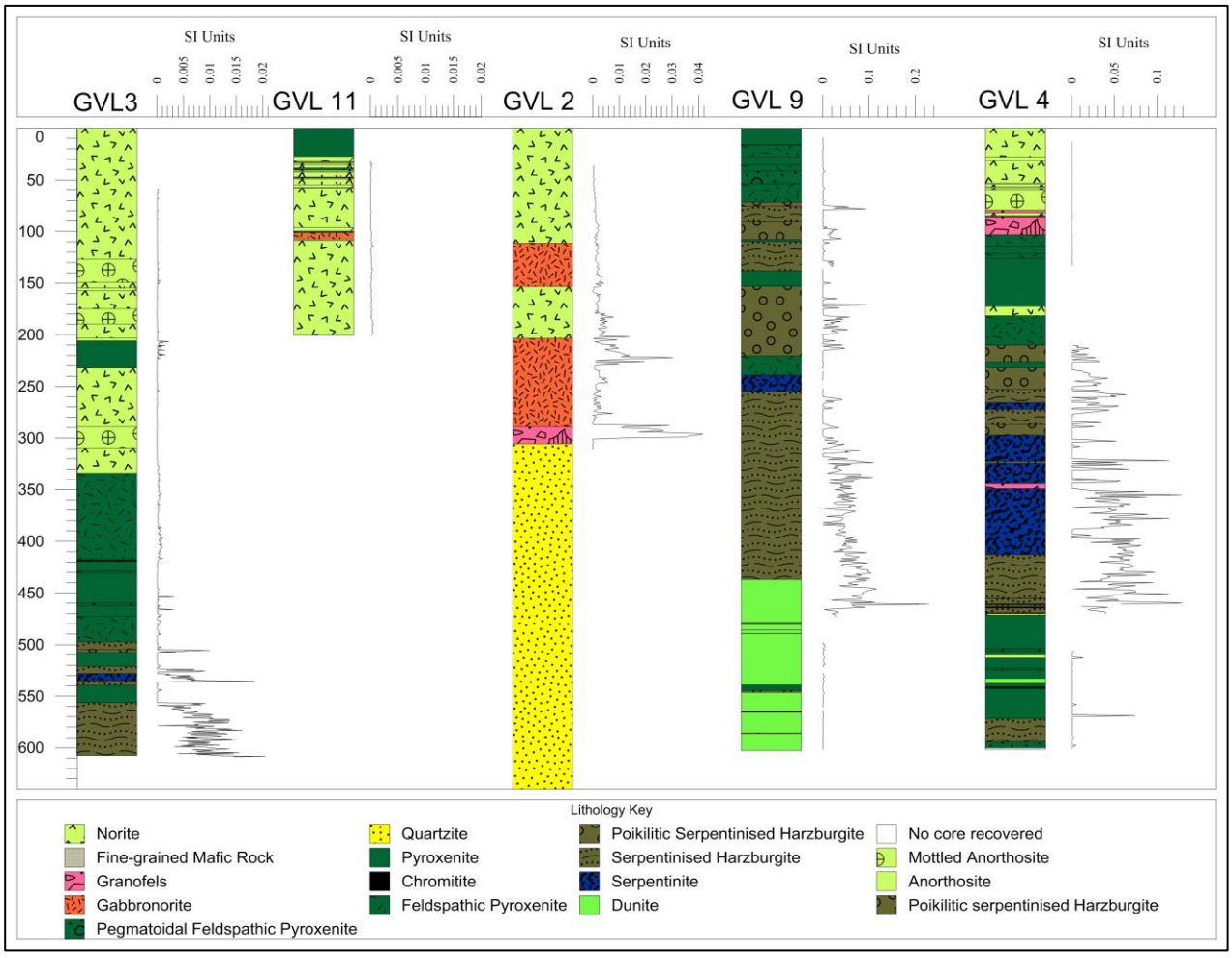

Figure 3.24: Magnetic susceptibility profiles (SI units) of selected holes GVL 3, GVL 11, GVL 2, GVL 9 and GVL 4 plotted against simplified geological logs.

Quartzite at the base of GVL 2 has a MS of 0, but which rises abruptly passing up into the overlying granofels unit ranging from 0.01 to 0.042. Above the granofels the interlayered norite and gabbronorite units display a generally decreasing trend in MS, with the lowermost gabbronorite unit displaying a high of 0.03. Overlying norite and gabbronorite units display an average MS of 0.003, with norite in this core having a higher MS value than those intersected in GVL 3 and GVL 11.

The dunite at the base of GVL 9 displays relatively low MS values with a spike of 0.23 at 461 m due to the presence of a magnetite band. From 437 to 473 m the dunite has relatively higher MS in comparison to the lower unit with a maximum value of 0.230 and minimum of 0.003. The relatively high and variable MS values continue throughout the overlying serpentinised harzburgite unit. The overlying and interfingering pyroxenite displays relatively lower values comparable with those intersected in GVL 3 and GVL 11.

3.5 Discussion

3.5.1 Stratigraphy

Based on the intersections with the floor rocks in GVL 1 and GVL 2, the quartzite at the base of the GNPA member slopes downwards towards the northwest as the GNPA member onlaps the quartzites in the west and the ultramafic rocks of the Lower Zone in the east (Figure 3.25). This transgressive relationship with the footwall is similar to that noted within the rest of the northern limb where the footwall changes to Archaean granite gneiss (Hall, 1932; van der Merwe, 1976; Button, 1976; Kinnaird *et al*., 2005). These quartzites are older than the intrusion as they occur as xenoliths within the layered body as seen in GVL 1 (Figure 3.3). The quartzites are consistent with the floor rocks described and mapped by Hulbert (1983). The intrusion lies uncomformably atop of the floor rocks with the noritic package in contact with the quartzites in the southeast and the ultramafic sequence in the northeast. The top of the quartzite units have been correlated across boreholes (Figure 3.25). This interpretation of the footwall is consistent with that of van der Merwe (1976) and Hulbert (1983) (Figure 3.27).

The ultramafic package comprising dunites, harzburgites, serpentinised harzburgites, pyroxenites and feldspathic pyroxenites is consistent with the detailed petrographic descriptions of the Lower Zone (LZ) rocks described in the area by Hulbert and Von Gruenewaldt (1982) and Hulbert (1983) (Figure 3.27). The presence of a thick, laterally extensive succession of LZ rocks is unique to this area south of the Ysterberg-Planknek Fault. To the north of the Ysterberg-Planknek Fault, the LZ occurs as sporadic isolated satellite bodies or offshoots hosted in country rocks of which their connectivity at depth is uncertain yet probable (van der Merwe, 1978; Yudovskaya *et al.*, 2013). The kink banding within the fresh olivines is noted within mantle peridotitic xenoliths and Ural-Alaskan complexes (Green and Radcliffe, 1972; Li *et al.*, 2012; Yudovskaya *et al.*, 2013).These features are generated through planar slip within the olivine lattice while undergoing high-temperature deformation (Yudovskaya *et al.*, 2013). The kink banding is not a common feature of layered intrusions although it has been noted within dunite of the Great Dyke and on the farm Turfspruit (Wilson, 1982; Yudovskaya *et al*., 2013).

The degree of serpentinisation of the harzburgites decreases from east to west and may possibly be structurally controlled (Figure 3.25). The extreme serpentinisation and other forms of alteration (chloritisation, sericitisation) make it difficult to determine the exact transition in intercumulus

plagioclase from 2 to 6 % which has also been suggested to mark the upper boundary of the LZ (Cameron, 1978).

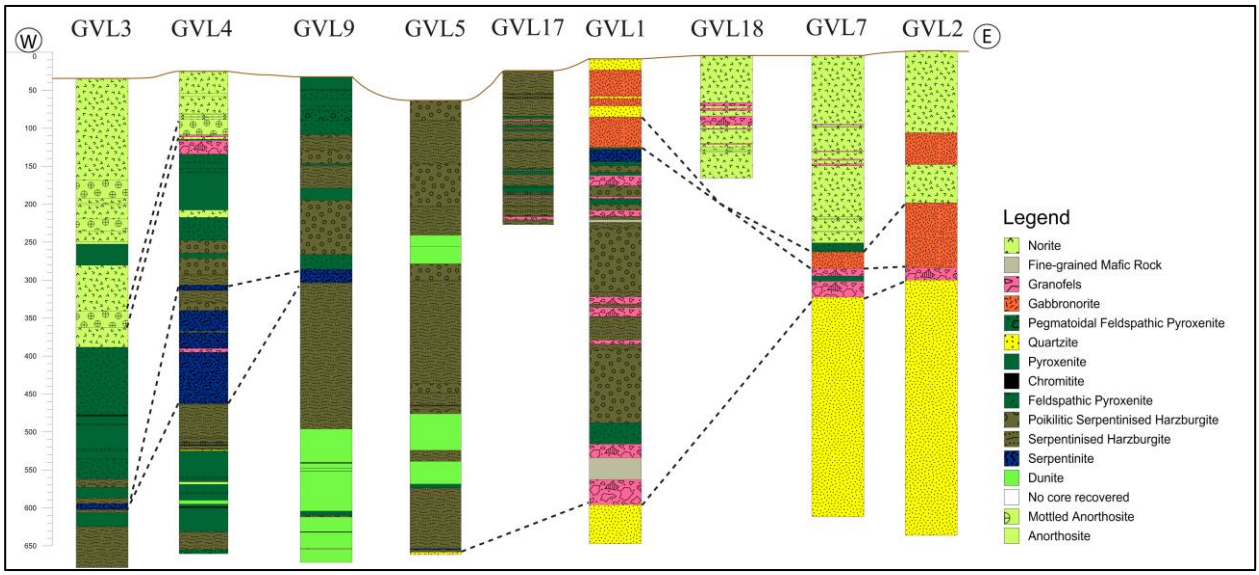

Figure 3.25: Tentative correlations based on hand sample and thin section descriptions of boreholes arranged from west to east.

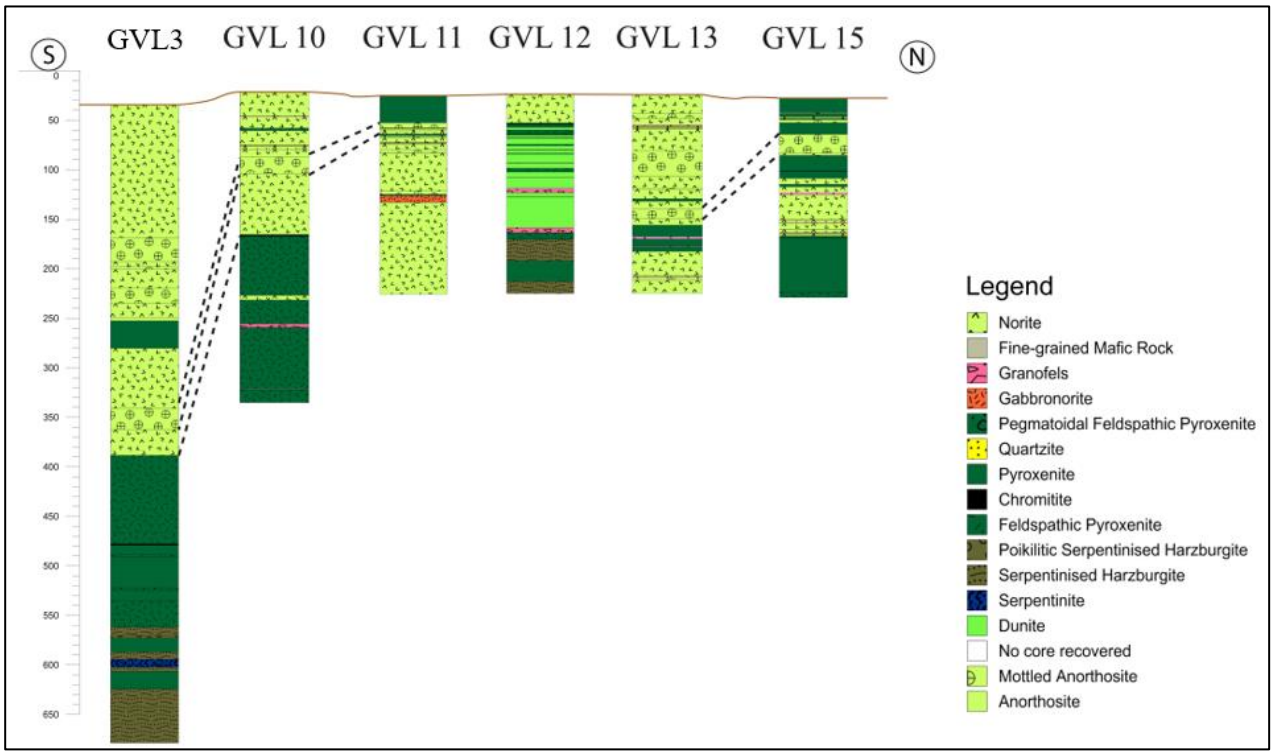

Figure 3.26: Tentative correlations based on hand sample and thin section descriptions of boreholes arranged from south to north.

The top of the LZ has been taken at the top of the last harzburgite unit (Figure 3.27) similar to the boundary suggested by Teigler and Eales (1996) for the western limb. The LZ hosts significant mineralisation in the form of two chromitite layers with an apparent thickness of ~60 cm hosted within pyroxenite and harzburgite. These chromitite layers are hosted within the Drummondlea subzone of the LZ which could be used as a stratigraphic marker for the boreholes in which the LZ is present (Hulbert, 1983). In comparison to the rest of the northern limb, although chromitites have been intersected within the LZ on Sandsloot, there is no comparison to the chromitites found in the Grasvally area as on Sandsloot and Turfspruit the chromitites are thin to disseminated and discontinuous (Yudovskaya *et al*., 2013). High chromite contents occur in the Basal Ultramafic Sequence (BUS) of the Clapham trough section of the eastern limb, but there it occurs in thin stringers and is thus not comparable to those encountered in the Grasvally area (Wilson, 2012). GVL 5 intersects a quartzite unit at the base of the LZ. This may mark the base of the LZ in this area. Further drilling would be recommended to determine the thickness of this quartzite unit as it may be a xenolith within the LZ.

The package of variably textured pyroxenites, feldspathic pyroxenites, chromitites and gabbronorites, directly above the LZ can be correlated with confidence with the LMF as described by de Klerk (2005) (Figure 3.27) or subzone 1 of Hulbert (1983). The LMF-LZ contact is marked by a fine-grained unit whereas in GVL 2, the Critical Zone equivalent is in contact with the footwall quartzites of the Pretoria Group. It is marked by interfingering granofels and quartzites, above which is fine-grained gabbronorite. The fine-grained unit is significant as it suggests that there was a gap in time between the intrusion of the LZ and the LMF, allowing the LZ to cool down significantly before the intrusion of the LMF, thus forming a fine-grained margin as this magma cooled against the pre-existing LZ. The LMF hosts one chromitiferous unit with associated sulphides. The chromitite bears a likeness to the UG 2 chromitite in terms of mineralisation style as originally interpreted by Hulbert (1983). The LMF hosts sporadic zones of disseminated pyrrhotite rimmed by chalcopyrite.

The leucocratic unit comprising mainly mottled and spotted anorthosites with intercalated gabbronorites and feldspathic pyroxenites, displays a sequence similar to subzone 2 of the Critical Zone described by Hulbert (1983), and the more recently defined MANO after de Klerk (2005). The MANO is observed on the west of the farm and not in the boreholes to the east of the study area (Figure 3.27). The MANO is also traced from south to north as it is present in most of the holes along

this section. The first mottled anorthosite of the MANO occurs a few metres above a pyroxenitic layer. The mottled anorthosite can tentatively be used to correlate between boreholes (Figure 3.25 and Figure 3.26). A prominent mottled anorthosite was used to the north on the farm War Springs in order to constrain the top contact of the mineralised reef that occurs within the MZ (Grobler *et al.*, 2005).

It is extremely difficult to differentiate between rocks of the Main Zone and those of the Lower Gabbronorite Unit (LGN) in hand sample as they both comprise fine- to medium-grained homogeneous gabbronorites, and norites. A notable difference between the MZ and the LGN are the xenoliths of pyroxenite and anorthosite from the LMF and MANO respectively within the LGN. These xenoliths support the hypothesis of de Klerk (2005) that the LGN is possibly the result of MZ magma which intruded along the LMF-MANO contact potentially causing the xenoliths to be entrained through either mechanical or thermal erosion.

The unit directly above the LGN in GVL 2 is a norite unit with blebs of fine-grained cumulus magnetite. The occurrence of primary titaniferous magnetite as well as the occurrence of primary ilmenite within fine-grained gabbronorites are distinctive features of the marginal member of the Critical Zone adjacent to the quartzite footwall as well as marking the base of the CZ (Hulbert, 1983). The gabbronorites intersected at the base of GVL 2 display interstitial ilmenite as well as magnetite. The distinctive feature noted in the core which is not explained in literature is the presence of pods of chromitite, magnetite and ilmenite within gabbronorites and norites intersected within GVL 2. The unit has been tentatively correlated with the marginal member of the Critical Zone adjacent to the sedimentary footwall (Figure 3.27).

The MANO is absent to the east of the LZ and is only present in the holes to the west of the LZ (Figure 3.27). The mineralisation in the area is not restricted to one lithological unit and is hosted mainly within the LZ and LMF. The LZ hosts chromite as well as PGE mineralisation which has a strong affinity to sulphides (Smith *et al.*, 2014). Mineralisation within the GNPA member is hosted within the LMF and the MANO.

The discontinuity of these units could be explained by displacement of units caused by fault generations 1 and 2 noted by Hulbert (1983) (Figure 2.10). The imbricate nature of the horst block, brought to surface by north-south trending reverse faulting, would make correlation of the LZ across boreholes difficult (Figure 2.10). The WNW-ESE trending reverse block faulting of fault generation

2 resulted in a step-like displacement making correlation of the GNPA member and LZ difficult from borehole to borehole (Figure 2.10).

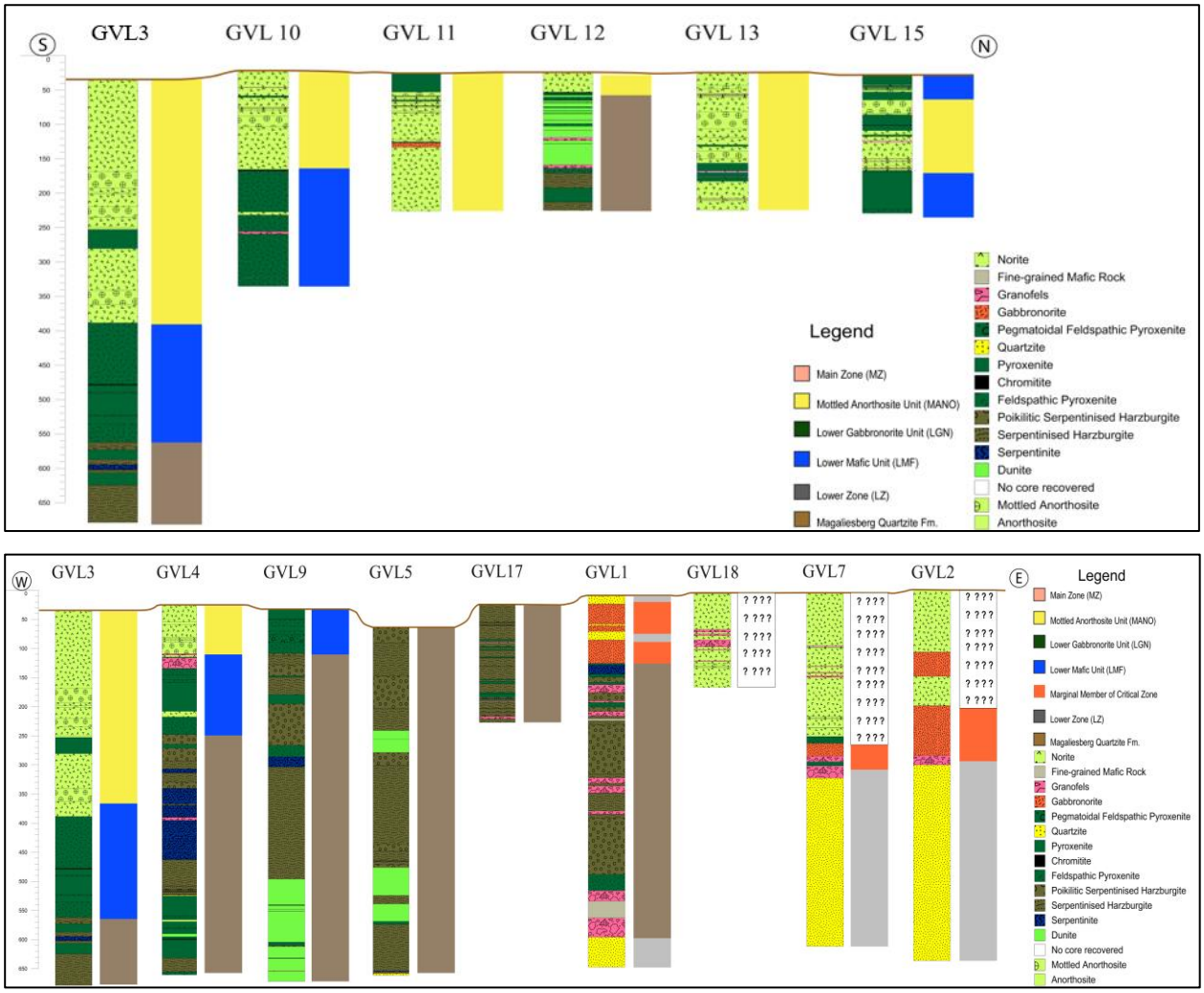

Figure 3.27: Simplified lithological logs of chosen representative holes correlated with the stratigraphic subdivisions of de Klerk (2005).

3.5.2 Magnetic Susceptibility

The magnetic susceptibility (MS) in the boreholes studied is controlled mainly by the presence of primary and secondary magnetite. The MS is also controlled by the abundance of magnetic minerals such as pyrrhotite and ilmenite. Due to the different signatures in MS a tentative correlation has been drawn between the studied boreholes and the stratigraphic units (Figure 3.28). The footwall quartzite displays no MS. The fresh dunite at the base of GVL 9 also displays relatively low to no MS. The dunite unit from 437.00 mm to 473.00 mm displays variable and relatively high MS. The MS within this unit is controlled mainly by the presence of secondary magnetite. The secondary magnetite is a

product of the serpentinisation of the olivine within these rocks. The MS of the harzburgite units is also attributed to the serpentinisation of olivine, similar to the MS highs noted within the troctolite horizon within the Bellevue core (Ashwal *et al.,* 2005). High MS values are attributed to extensive serpentinisation followed by the concentration of magnetite as laths or bands <1 cm to 2 cm thick.

The zones with no MS within the serpentinites are attributed to two factors; zones of brecciation and zones of complete serpentinisation. The serpentinite is brecciated in places by late quartzofeldspathic veins. The quartzofeldspathic dominated zones reflect the MS of the quartzofeldspathic veins (GVL 9). Where the precursor rock has been completely serpentinised, the magnetite has been concentrated elsewhere by the fluids, leaving the unit barren of magnetite.

The UZ contains an abundance of magnetite whereas the MZ has little to no magnetite (Nex *et al.*, 1998). The UZ-MZ boundary is signified by the presence of cumulus magnetite (Molyneux, 1974; SACS, 1980; Eales and Cawthorn, 1996; Knoper and Von Gruenewaldt, 1996). Ashwal *et al.* (2005) were able to detect the UZ-MZ boundary with the use of MS. The MZ typically displays MS values of <0.02 SI units and values up to 0.05 SI units (Ashwal *et al.*, 2005). The noritic package intersected in GVL 3, GVL 11 and GVL 9 displays far lower values (0.001 SI units) (Figure 3.28) than the values reported by Ashwal *et al.* (2005), therefore there are no packages intersected that are of MZ affinity as intersected in the north reported by de Klerk (2005).

The Critical Zone intersected within GVL 3, GVL 11 and GVL 9 displays little to no MS and no variation within the different subzones of the Critical Zone (Figure 3.28). Due to the lack of MS variability, it is not possible to differentiate between the MZ and the CZ as well as the subzones defined by Hulbert (1983) and de Klerk (2005) respectively (Figure 3.28).

The CZ-LZ boundary can be detected by MS differences if the boundary is taken at the last harzburgite unit.

The noritic and gabbroic package intersected in GVL 2 displays distinctly dissimilar MS signatures to the packages intersected in GVL 3, GVL 11 and GVL 4 (Figure 3.28). Thin section analysis suggests the MS is controlled by finely crystalline magnetite and ilmenite. The ilmenite is not visible on a millimetre scale and occurs as interstitially disseminated crystals within the norite and gabbronorite. The magnetite occurs within aggregate pods and laths of magnetite and chromite.

Based on the MS, this zone can be correlated with the marginal member of the Critical Zone defined by Hulbert (1983) (Figure 3.28).

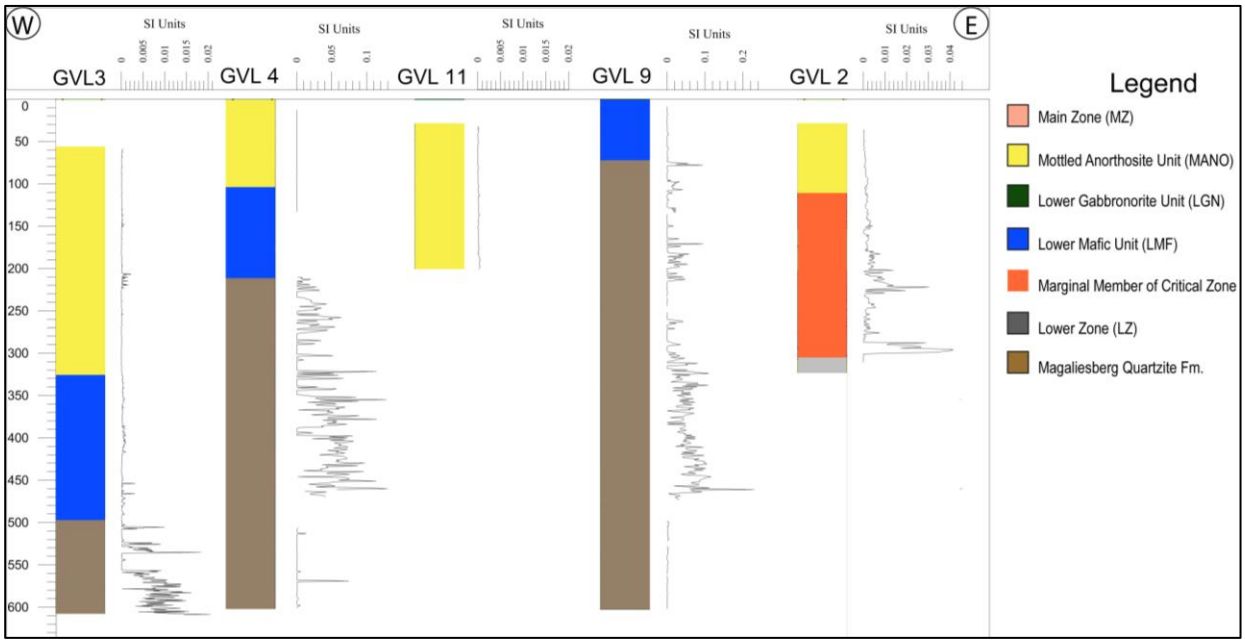

Figure 3.28: Magnetic susceptibility signatures of boreholes GVL 3, 4,11,9, and 2 correlated with possible stratigraphic units. Stratigraphic units adapted from Hulbert (1983) and (de Klerk, 2005).

3.6 Summary

The stratigraphy of the Grasvally area seems to vary greatly from east to west. The structural complexity of the area makes it difficult to correlate different layers across boreholes. The units do not seem completely continuous across the LZ and cannot be confidently correlated with the stratigraphic subdivisions proposed based on the lithological logging alone. The marginal member of the Critical Zone is evident to the east of Grasvally and is absent to the west. Due to the magnetic signature of the marginal member adjacent to the metasedimentary footwall, it too can be used as a potential marker horizon on the east of the farm Grasvally. On the west of the farm, the mottled anorthosites could potentially be used as a marker horizon. Throughout the package the chromitite layers could be used as marker horizons, provided the same chromitite layers are correlated. Magnetic susceptibility can be used to determine the LZ-CZ boundary and the Transvaal quartzite footwall-CZ boundary.

CHAPTER 4

Geochemical Analysis

4.1 Introduction

The same samples that were selected for thin section study were analysed for whole-rock geochemistry by XRF. A total of 131 samples were analysed from boreholes GVL 2, GVL 3, GVL 4, GVL 5, GVL 9, GVL 11 and GVL 18. The sample list and complete geochemical data is shown in Appendix B. The main objective of the geochemical analysis was to confirm field identification of the rock types based on the geochemical composition and to determine whether there were any particular anomalies that might be of use as geochemical marker horizons. In addition, depth profiles of the geochemical data through a borehole were also compiled to evaluate whether some of the stratigraphic units could potentially be correlated from borehole to borehole and to stratigraphic units throughout the RLS.

4.2 Methodology

Representative samples of 30 cm in length of quarter-core were selected, cut and appropriately packaged from the core provided by Sylvania Platinum Ltd. These samples were then crushed and milled to a fine powder in the crushing lab at the School of Geosciences at the University of the Witwatersrand. The equipment was stringently cleaned before and between samples to avoid contamination.

Sample powders for major element analysis were heated to 110°C to remove any moisture, then ashed at 1000°C to remove chemically bound volatiles such as CO_2 and H_2O+ (reported together as Loss on Ignition LOI). All Fe is oxidised to Fe_2O_3 during this ashing step. An aliquot of pre-ashed sample was mixed with a chemical flux, fused and pressed into a disk for major element analysis.

Pellets were pressed for trace element analyses by moistening 5g of powder with a few drops of binder solution (polyvinyl alcohol and water) in a silica mortar and pestle. The mixture was then placed in an aluminium cup and compacted by hydraulic press and left to dry. All equipment used was cleaned with acetone before and between samples to avoid contamination. A PANalytical PW2404 XRF instrument in the Earth laboratory, Bernard Price Building, University of the Witwatersrand was used for both major and trace element analyses.

Data on concentrations of 3 PGE (Pt, Pd and Rh) +Au as well as Cu + Ni data were provided by Sylvania Platinum Ltd. The samples were obtained from half-core with variable sample lengths ranging from 0.25 m to 0.3 m from NQ size diamond drill core. The sampled interval was selected based on where mineralisation was expected in relation to the assumed stratigraphic position. The samples were analysed for 3 PGE (Pt, Pd and Rh) +Au. The midpoint along the length of each sample was taken to create a discrete depth from which each sample point could be plotted against depth.

4.3 Major and Trace element geochemistry

Major oxide data obtained by XRF can be used to further refine the lithological characterisation of the variety of igneous rock types that occur within the boreholes of the Grasvally area. Particularly in those samples from strongly altered rocks were the primary igneous mineralogy is no longer visible in hand specimen or thin section. Such better clarification of lithological properties helps the approach to correlation across boreholes and stratigraphic analysis.

4.3.1 CIPW Normative Mineralogy

The CIPW normative calculation technique uses the major oxides to determine the primary igneous mineralogy of a rock and thus provides an alternative pathway to modal analysis and classification. This is particularly useful for the highly serpentinised ultramafic rocks and other altered rocks where secondary minerals replace pyroxenes and feldspars. The normative mineralogy is dominated by Olivine, Pyroxenes ("Hypersthene" = Opx; "Diopside" = Cpx) and Feldspar (=Plag) and can be plotted against the IUGS ternary diagrams (Le Bas and Streckeisen, 1991) for mafic rocks (Figure 4.1) and ultramafic rocks (Figure 4.2). The full list of samples and the respective classifications are represented in Appendix A.

When mafic rock compositions were plotted on the plagioclase-orthopyroxene-clinopyroxene ternary diagram the data plots mainly in the norite, gabbronorite and orthopyroxenite fields with a minority of samples plotting within the anorthosite field (Figure 4.1). The samples are generally clinopyroxene poor with five samples comprising more than 25 % Cpx.

Calculated modal mineralogy of samples of the ultramafic rocks from boreholes GVL 3, 4, 5 and GVL 9 plotted on the olivine-clinopyroxene-orthopyroxene diagram plot mainly within the harzburgite and dunite field (Figure 4.2). The ultramafic rocks intersected throughout GVL 9, GVL 5 and the lower portion of GVL 3 and GVL 4, between 334.00 m - 607.57 m and 107.71 m - 601.72

m comprise high proportions of olivine and orthopyroxene (Figure 4.2) with minor plagioclase (Figure 4.1). The ultramafic samples are also generally clinopyroxene poor, with 65 to 92 % olivine.

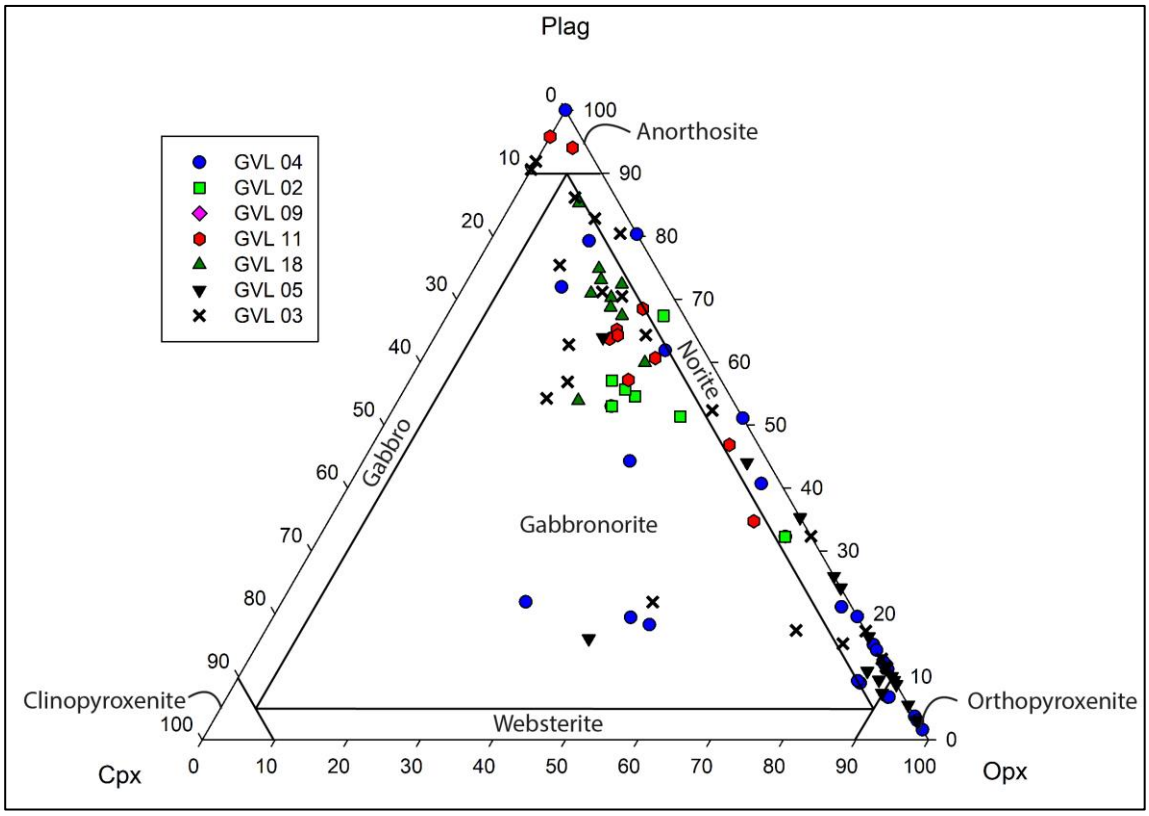

Figure 4.1: Classification and nomenclature of gabbroic rocks based on the CIPW normative proportions calculated from the modal geochemistry of plagioclase (Plag), clinopyroxene (Cpx) and orthopyroxene (Opx) (after Streckeisen, 1976).

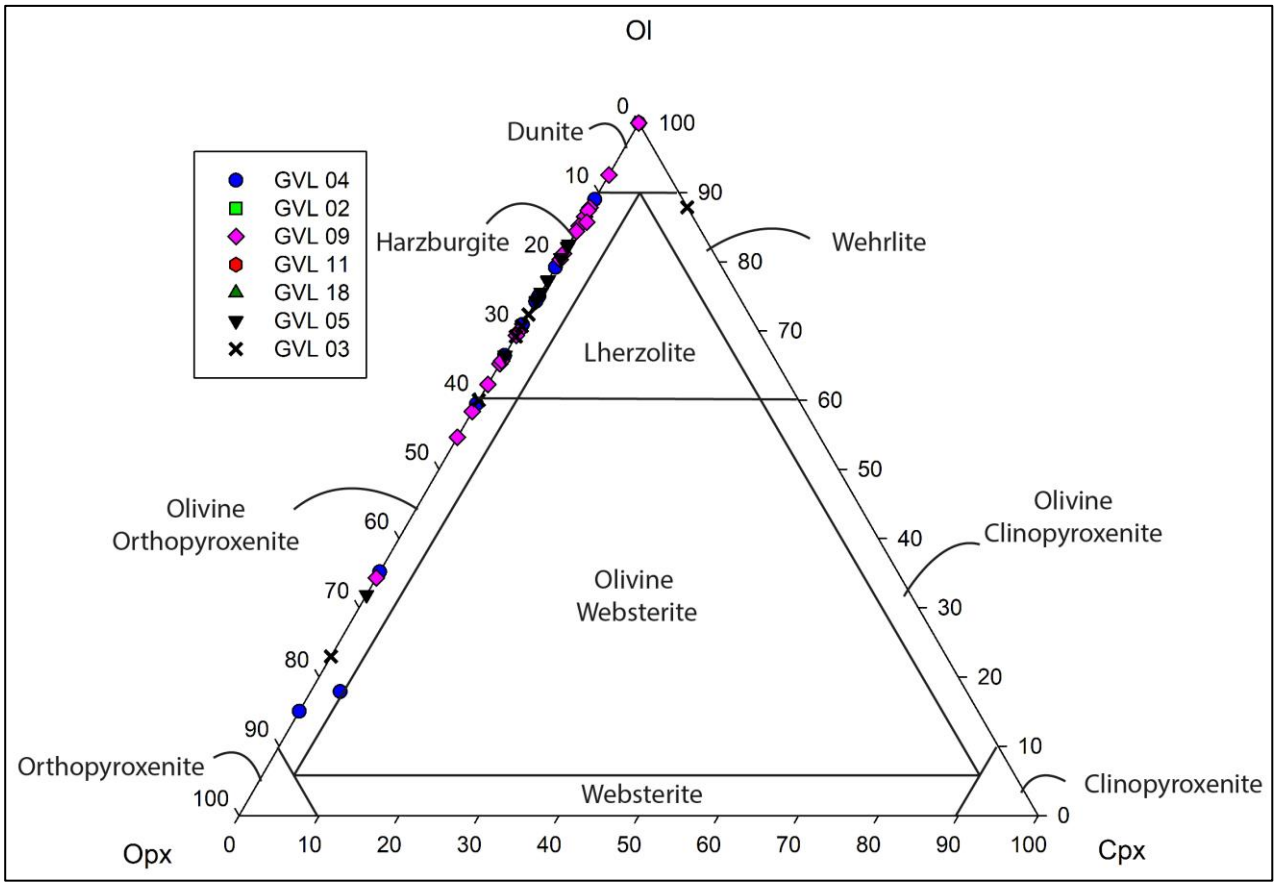

Figure 4.2: Classification and nomenclature of ultramafic rocks based on the CIPW proportions of olivine (Ol), orthopyroxene (Opx) and clinopyroxene (Cpx) (after Streckeisen, 1976).

4.3.1.1 Rock Names

After being plotted against the IUGS specified ternary diagrams, certain minor minerals were used in order to further distinguish between the rocks of different stratigraphic units. They could be either normative or visible and added as prefixes, such as magnetite-, chromite-, etc. The list of samples has been tabulated and presented in Appendix A.

4.3.1.2 CIPW normative interpretation

The samples that plot on the gabbroic classification diagram (Figure 4.1) plot as norites, gabbronorites and orthopyroxenites. This classification diagram does not discriminate between cumulus and intercumulus plagioclase – a distinction that is made by Bushveld Complex geologists, such that a rock with cumulus pyroxene and intercumulus plagioclase would be termed a feldspathic pyroxenite rather than a norite. Thus, certain samples from GVL 4 and GVL 3 which have been

classified as pyroxenites and orthopyroxenites in hand sample, plot modally as gabbronorites and norites (Figure 4.1).

The harzburgites, dunites and olivine orthopyroxenites are mostly representative of LZ samples as seen in GVL 3, GVL 4 GVL 5 and GVL 9. The samples from within the LZ contain very little to no feldspar (<10 %) and a great proportion of olivine content. The samples from within the Critical Zone and Main Zone display a higher abundance of feldspar (>10 %) with very little to no olivine content.

4.4 Major oxide plots

The rocks of the RLS are predominantly mafic to ultramafic in composition. As these rocks comprise mostly olivine (Ol), orthopyroxene (Opx), clinopyroxene (Cpx) and plagioclase (Plag), the average chemical compositions of these minerals are used to classify the rocks. These samples are plotted against mineral compositional data after Hulbert (1983). The Al_2O_3, CaO and Na_2O contents reflect the modal proportion of feldspars whilst the MgO and FeO values reflect the modal proportion of pyroxene and to a lesser extent by the amount of plagioclase feldspar. The CaO content is controlled largely by the amount of clinopyroxene in the rock. The presence of olivine within the rock has an effect on the relationship between $A1_2O_3$ and MgO (Eales *et al.*, 1986). The binary chemical compositions Al_2O_3 vs MgO, CaO vs MgO + FeO (total), CaO vs Al_2O_3, CaO vs MgO and Al_2O_3 vs MgO + FeO (total) content are plotted against each other for GVL 2, 3, 4, 5, 9, 11 and GVL 18 in Figure 4.3-Figure 4.7.

The scales have been selected to display the variations and trends within the data. For the graphs to be representative, the granitic veins and metasedimentary lithologies have been omitted from diagrams due to either very high or very low values that distort the plots. The petrographic (hand sample) classifications are compared to the chemical whole rock classification (Figure 4.3-Figure 4.7).

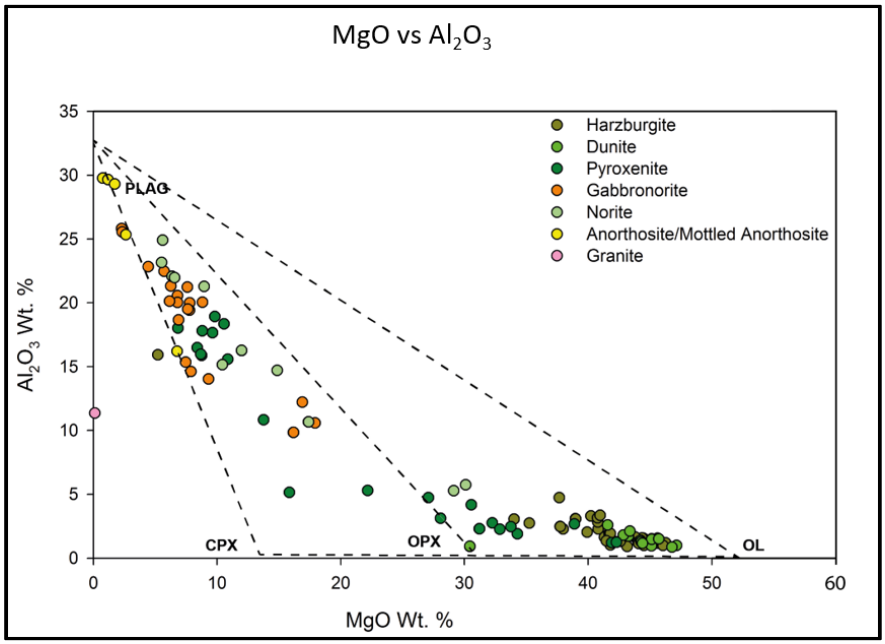

Figure 4.3: Classification of samples K-1 to K-133 on a diagram showing MgO wt % against Al_2O_3 wt %. The classification parameters have been adopted from Hulbert (1983). Samples have been coloured according to the hand sample classification.

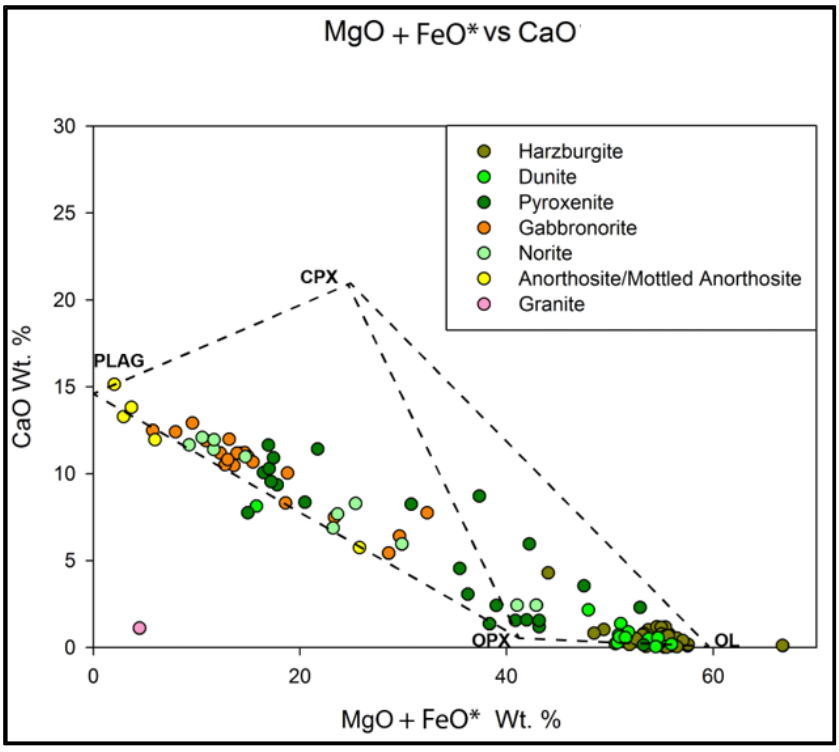

Figure 4.4: Classification of samples K-1 to K-133 on diagram showing MgO + FeO wt. % against CaO wt. %. The classification parameters have been adopted from Hulbert (1983). Samples have been coloured according to the hand sample classification.

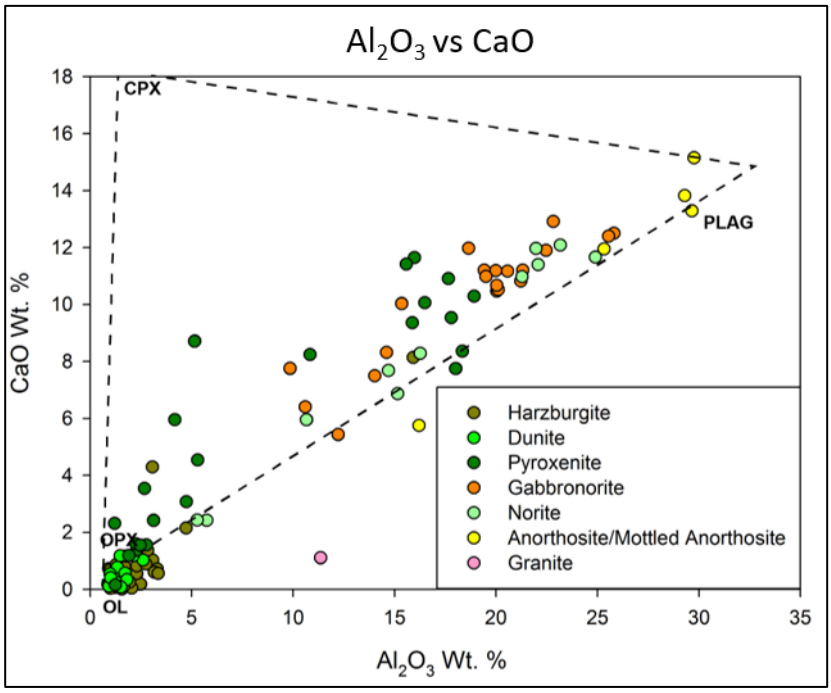

Figure 4.5: Classification of samples K-1 to K-133 showing Al_2O_3 against CaO wt. %. The classification parameters have been adopted from Hulbert (1983). Samples have been coloured according to the hand sample classification.

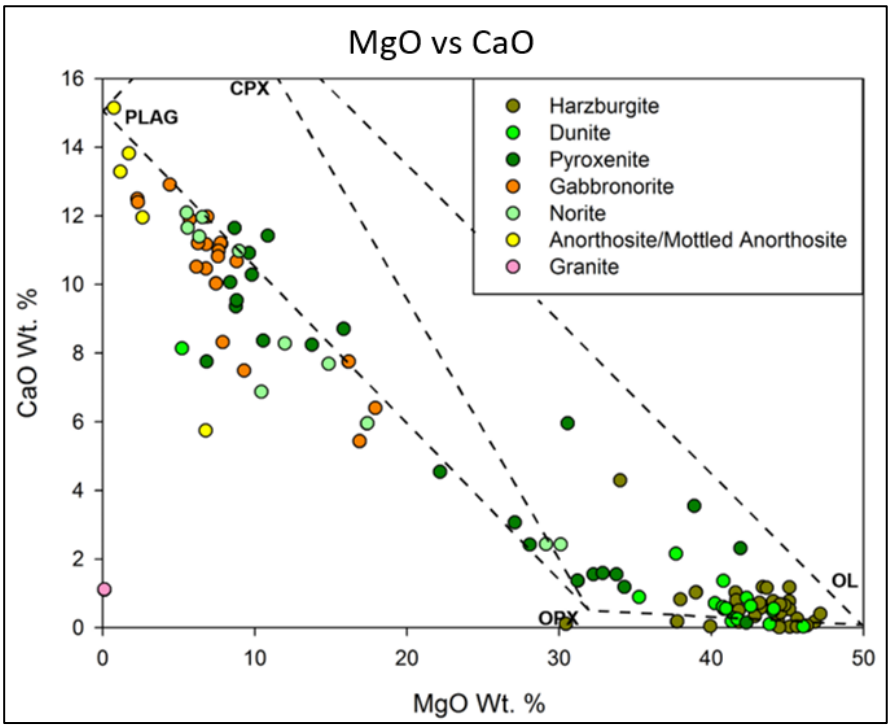

Figure 4.6: Classification for samples K-1 to K-133 on a diagram showing MgO against CaO wt. %. The classification parameters have been adopted from Hulbert (1983). Samples have been coloured according to the hand sample classification.

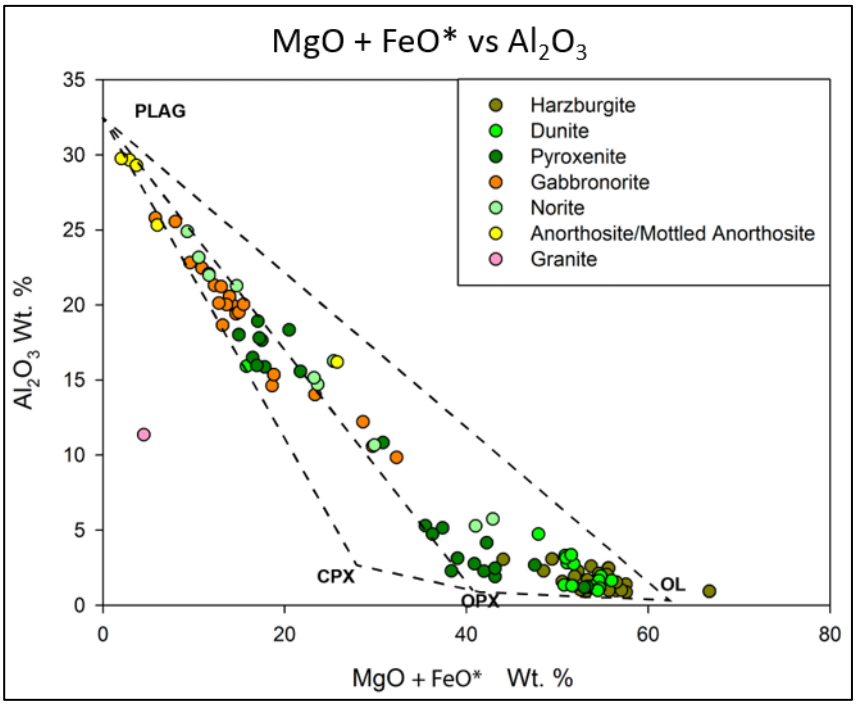

Figure 4.7: Classification for samples K-1 to K-133 showing MgO + Fe_2O_3 against Al_2O_3 wt. %. The classification parameters have been adopted from Hulbert (1983). Samples have been coloured according to the hand sample classification.

4.5 Geochemical variations with depth

Variations of selected major and trace elements with depth have been presented for boreholes GVL 2,3,4,5,9,11 and 18. The aim of the depth profiles is to geochemically characterise stratigraphic units to potentially correlate stratigraphic units from borehole to borehole and possibly with stratigraphic units of the greater Bushveld Complex.

4.5.1 Mg# variation

The Mg# (100*(molecular MgO/(MgO+FeO))) is used to determine how primitive the rocks are, with more primitive magma displaying higher Mg#. An upward increase in Mg# with height alludes to either an upward increase in the proportions of Mg rich phases or to new influxes of relatively more primitive magma. The Mg# displays a generally upward decreasing trend in cores GVL 3, GVL 4 and GVL 9 (Figure 4.8 , Figure 4.9 and Figure 4.10). The Mg# is constant for the harzburgites and dunites averaging an Mg# of 87 with a high of 93 and anomalous low outlier of 62 (Figure 4.11). At the transition from the harzburgite unit to the overlying pyroxenite there is a sharp decrease in Mg# as observed in GVL 3, 4 and 9 (Figure 4.8, Figure 4.9 and Figure 4.10).

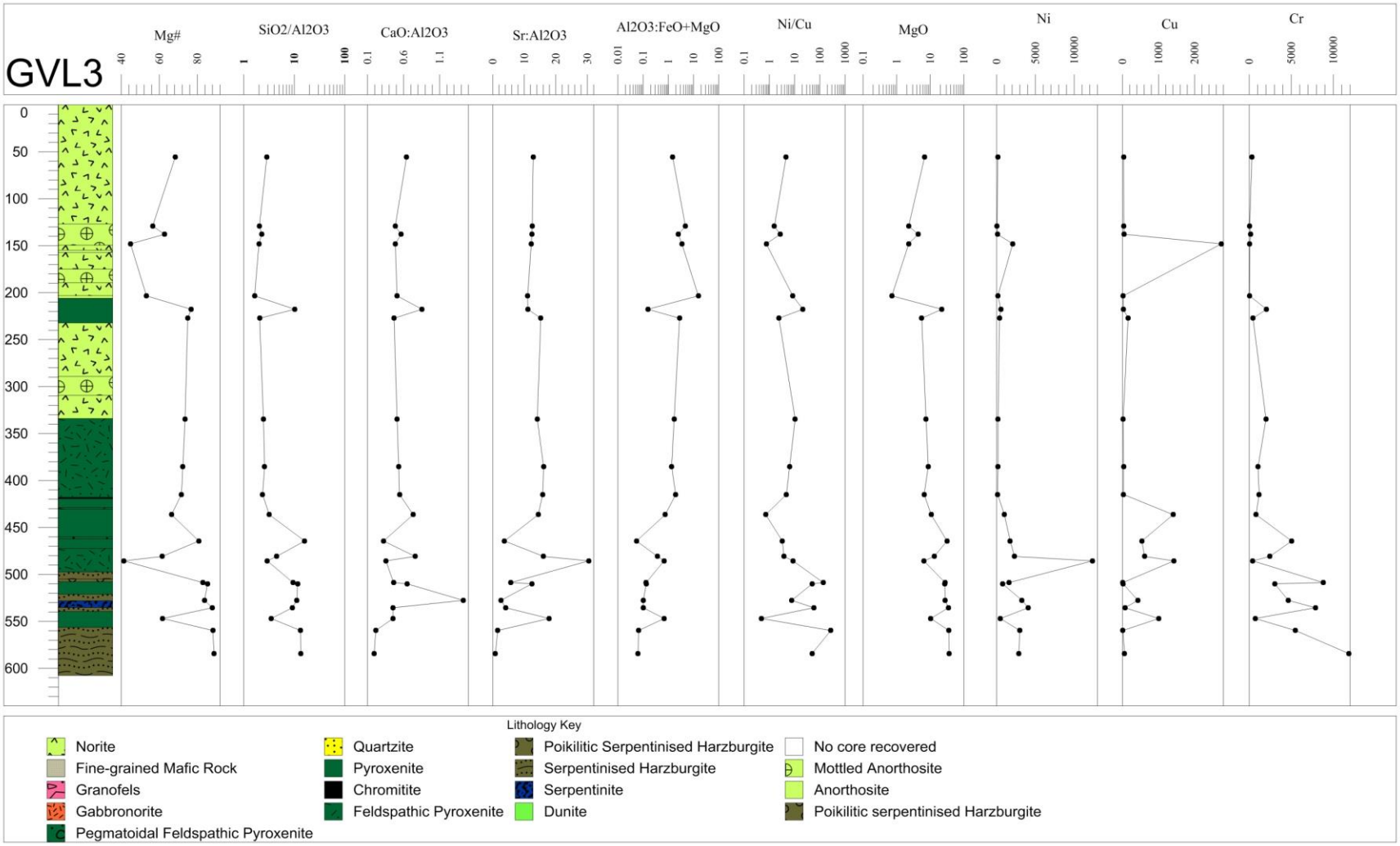

Figure 4.8: Variations of the whole-rock Mg#, major and trace element ratios and trace element contents through borehole GVL 3. Mg# and Cr (ppm) display generally decreasing trends up section as the package transitions into more leucocratic rocks.

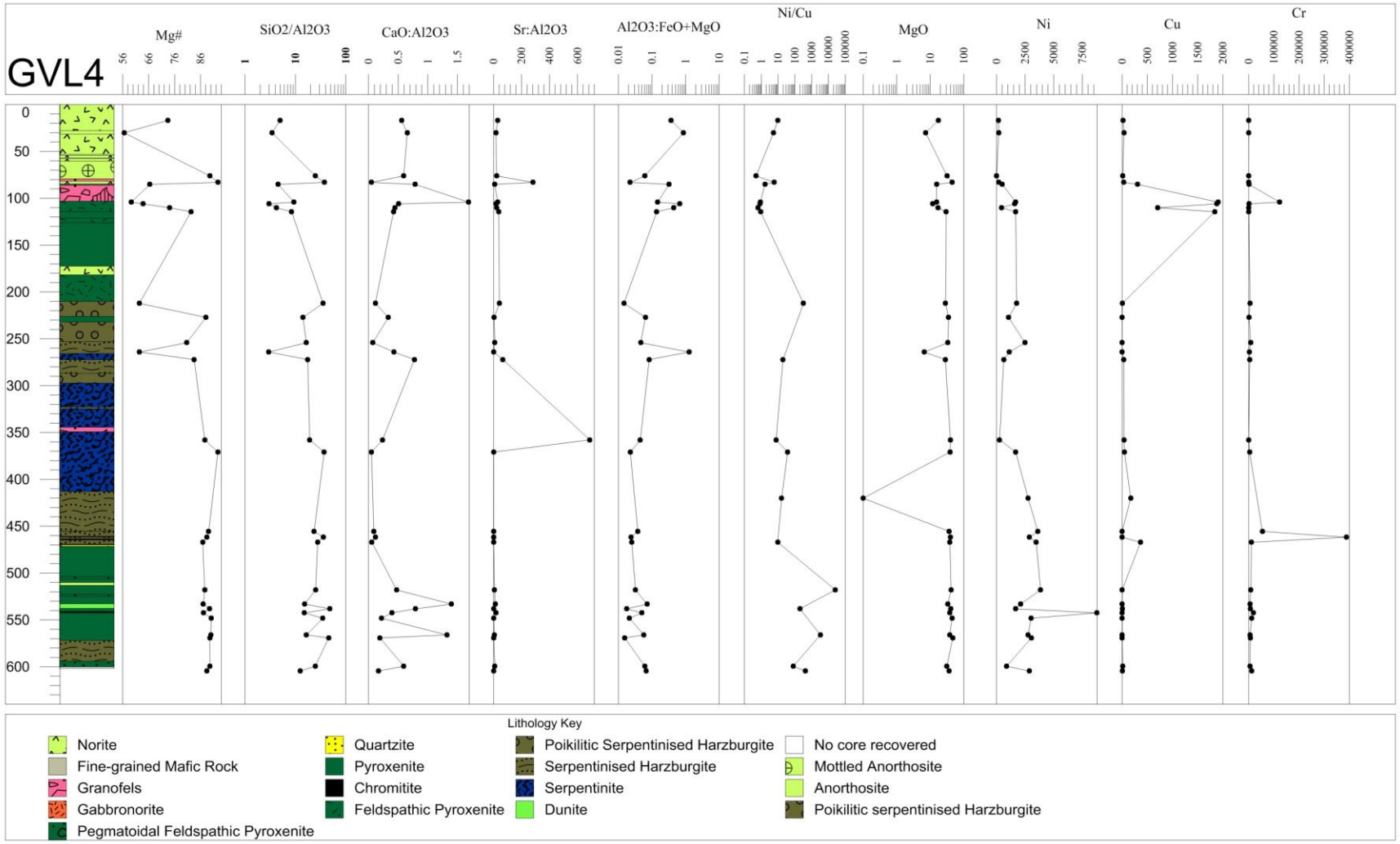

Figure 4.9: Variations of the whole-rock Mg#, major and trace element ratios and trace element contents through borehole GVL 4.

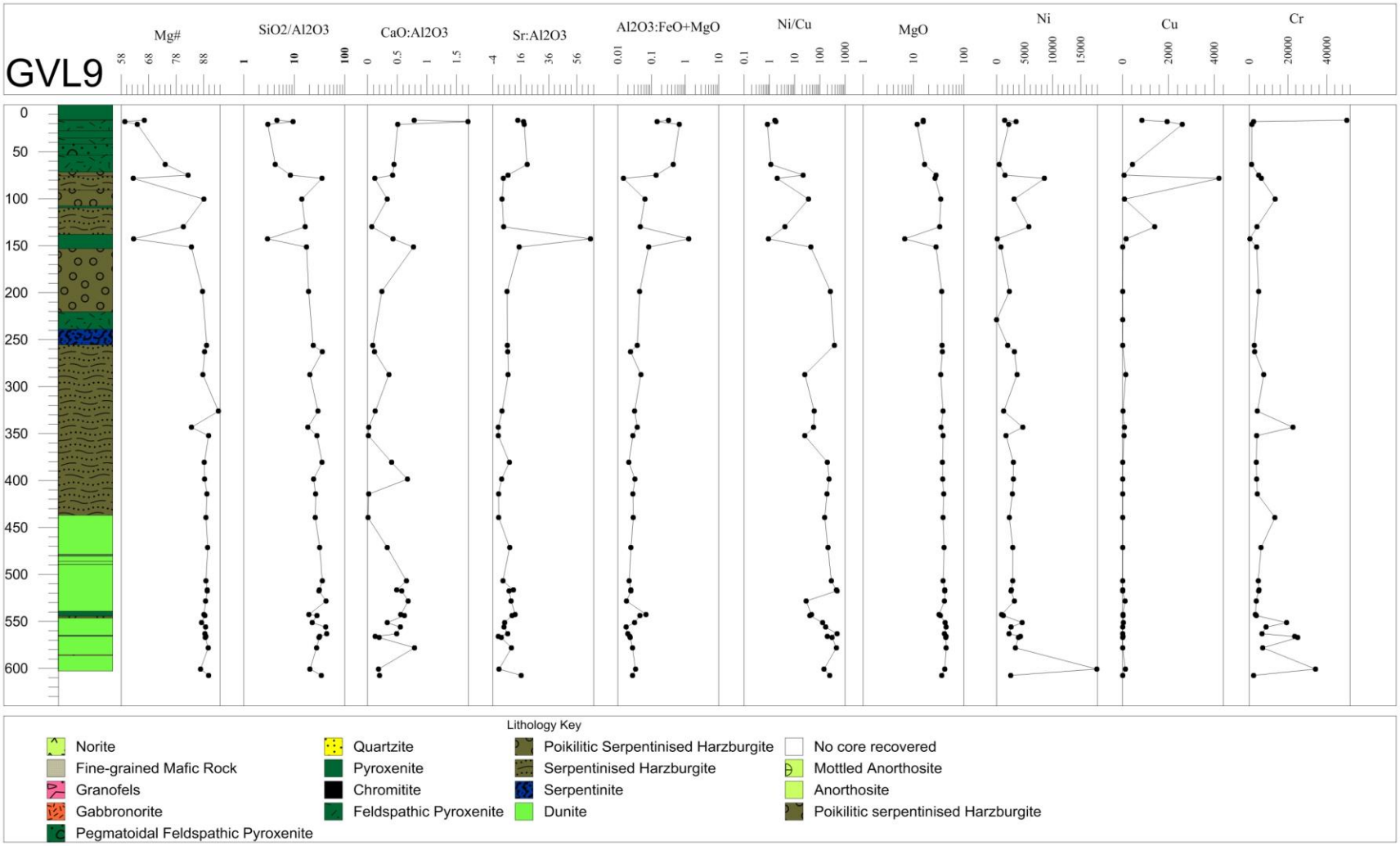

Figure 4.10: Variations of the whole-rock Mg#, major and trace element ratios and trace element contents through borehole GVL 9.

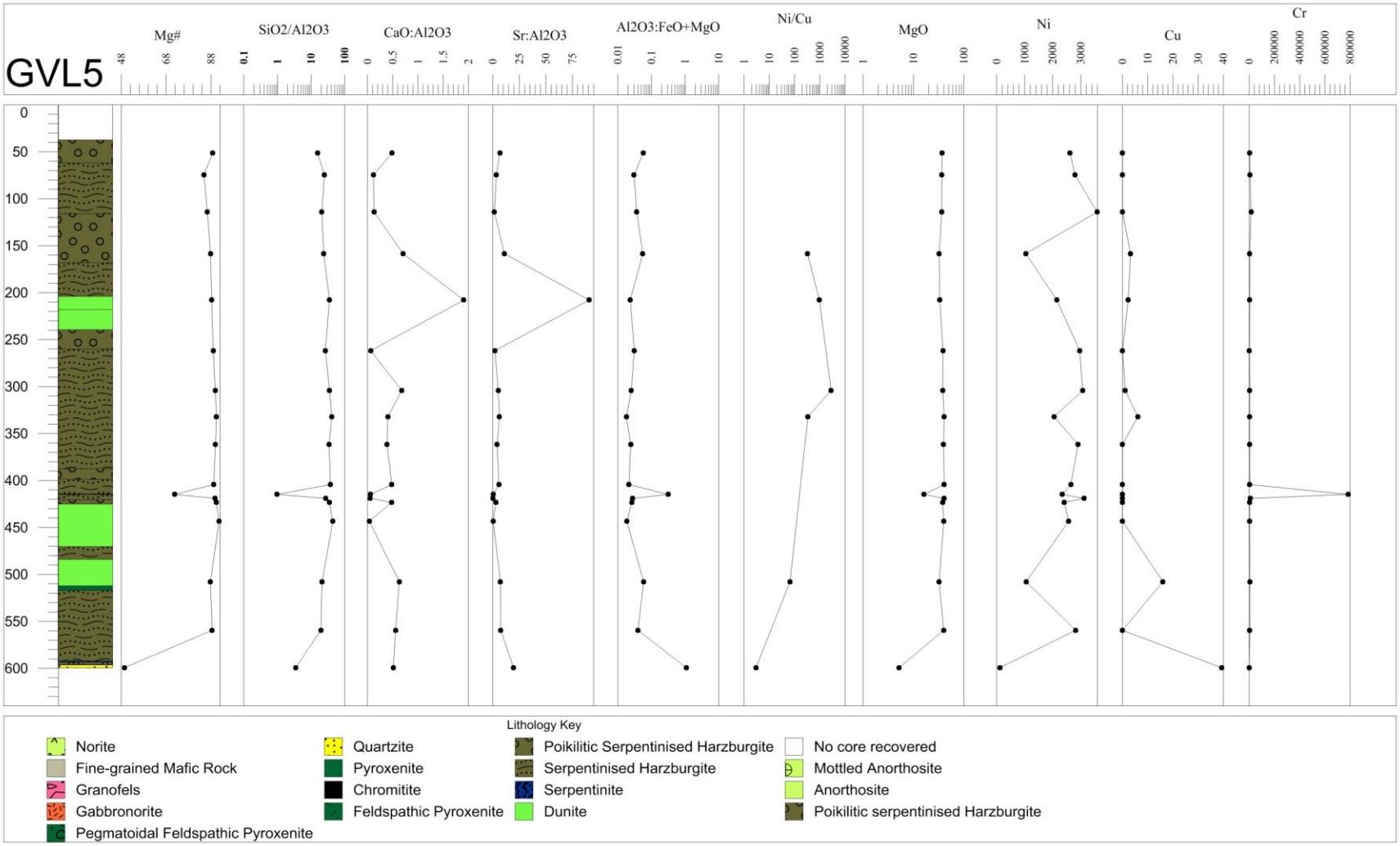

Figure 4.11: Variations of the whole-rock Mg#, major and trace element ratios and trace element contents through borehole GVL 5. Mg# displays little to no variation up section and is indicative of a lack of fractionation occurring within this package but perhaps a constant replenishment of magma.

The Mg# of the pyroxenites ranges from 89 to 56 with an increase in Mg# from the base of the pyroxenite upwards over the first 20 m in GVL 3 (Figure 4.8). The pyroxenite-harzburgite boundary is marked by a decrease in Mg# with increasing height (Figure 4.8 and Figure 4.9). The noritic package displays an upward increase in Mg# (Figure 4.8, Figure 4.12 and Figure 4.13).

4.5.2 SiO_2/Al_2O_3 variation

The ratio of SiO_2 to Al_2O_3 is largely controlled by the proportion of feldspar in the unit sampled. Lower values are indicative of an increase in feldspar with a relatively higher ratio being indicative of a lower feldspar content.

The ultramafic package intersected in GVL 5 displays very little variation in SiO_2/Al_2O_3 with values averaging 29.39 (Figure 4.11). The low value of 0.97 at 414.80 m is explained by the extremely high chromite content and the 3.45 value at 599.29 m is due to this unit being composed largely of feldspar and quartz (Figure 4.11). GVL 9 displays a general upward decrease in the SiO_2/Al_2O_3 ratio (Figure 4.10). The values range from 43.65 at 563.19 m within the dunite unit to 2.98 at 20.88 m within the feldspathic pyroxenites (Figure 4.10). GVL 3 displays two upward decreasing trends in SiO_2/Al_2O_3 (Figure 4.8) with a high value of 16.06 within the pyroxenite at 464.40 m. The ratio decreases to 2.05 at 227.24 m and remains fairly constant up section with the exception of the pyroxenite interval at 217.67 m depth which displays a high of 10.22 (Figure 4.8).

4.5.3 Sr/Al_2O_3 variation

The Sr (ppm)/Al_2O_3 (Wt. %) ratio has been used within the context of the Bushveld Complex to identify new influxes of magma (Kinnaird, 2005b) and to differentiate between different cyclic units based on distinctive ranges in Sr content (Eales *et al.*, 1986).

The Sr/Al_2O_3 of the harzburgite-dunite unit produces a fairly constant trend and is relatively low with values averaging 4.61. The minimum of 0.09 is associated with a chromitite layer which occurs at 419.01m. An anomalous high of 90.80 occurs at the upper contact of a dunite unit at 207.88 m (Figure 4.11). The pyroxenite unit displays a relatively higher Sr/Al_2O_3 ratio in comparison to the harzburgite-dunite unit. The transition from the harzburgite-dunite unit to the pyroxenite unit is marked by a spike in Sr/Al_2O_3 (30.43) above which the ratio varies sporadically ranging from 3.72 at 464.40 m to 16.11 at 385.15 m (Figure 4.8). The norite mottled anorthosite package displays fairly constant Sr/Al_2O_3 values from 15.23 at the base of the pyroxenite (227.24

m) stratigraphically above which the values tend towards the mean of 12.48 (Figure 4.8). Within the gabbronorite unit above the quartzite in GVL 2 the values display no notable trend with values from 14.18 to 22.94 (Figure 4.14).

4.5.4 Al_2O_3/FeO+MgO Variation

Variation in the Al_2O_3/FeO+MgO ratio is indicative of the variation in pyroxene to plagioclase proportions and which may suggest an influx of new magma into the system (Kinnaird, 2005b).

The harzburgite-dunite package displays little variation with respect to the Al_2O_3/FeO+MgO ratio with a mean of 0.03 ranging from 0.02 to 0.05 with an anomalous high of 0.32 associated with a chromitite layer at 414.80 in GVL 5 (Figure 4.11). The pyroxenite displays higher Al_2O_3/FeO+MgO ratios (mean 0.98) than those within the underlying harzburgite package (Figure 4.10). The pyroxenite package displays a general increasing trend with increasing stratigraphic height from 0.68 at 485.56 m to 1.70 at 334.66 m (Figure 4.8). The increase in Al_2O_3/FeO+MgO with increasing stratigraphic height continues across the transition from the pyroxenitic package into the norite-mottled anorthosite package with a break in the trend associated with the pyroxenite (206.00 m to 232.26 m) and mottled anorthosite (174.88 m to 189.46 m). The pyroxenite displays a peak of 15.55 towards the centre while the mottled anorthosite displays an inverted trend with a low of 2.51.

4.5.5 Ni Variation

The variation in Ni content has been used to define different lithological packages. The Ni (ppm) is the total Ni and there has been no differentiation between Ni in sulphide or Ni in silicate. The harzburgite and dunite units display the highest Ni values ranging from 0.1 % to 0.36 %. Within the dunite-harzburgite unit the Ni values are fairly constant with an average of 0.25 % in GVL 5 (Figure 4.11) and an average Ni of 0.36 % in GVL 9 except for an anomalous high of 1.79 % at 600.74 m depth associated with a dunite layer (Figure 4.10) and low values of approximately 0.09 % associated with a pyroxenite at 542.48 m depth.

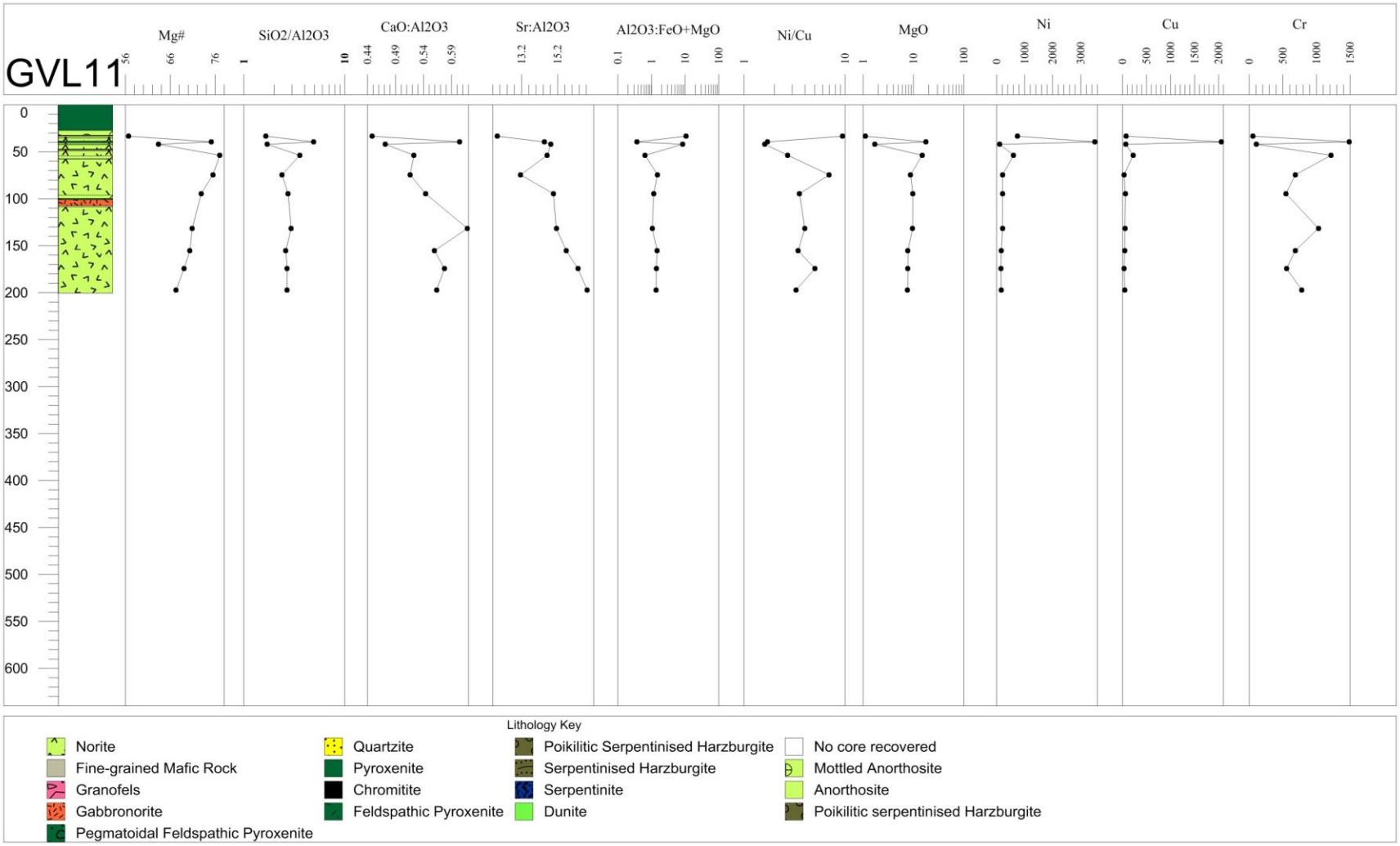

Figure 4.12: Variations of the whole-rock Mg#, major and trace element ratios and trace element contents through borehole GVL 11.

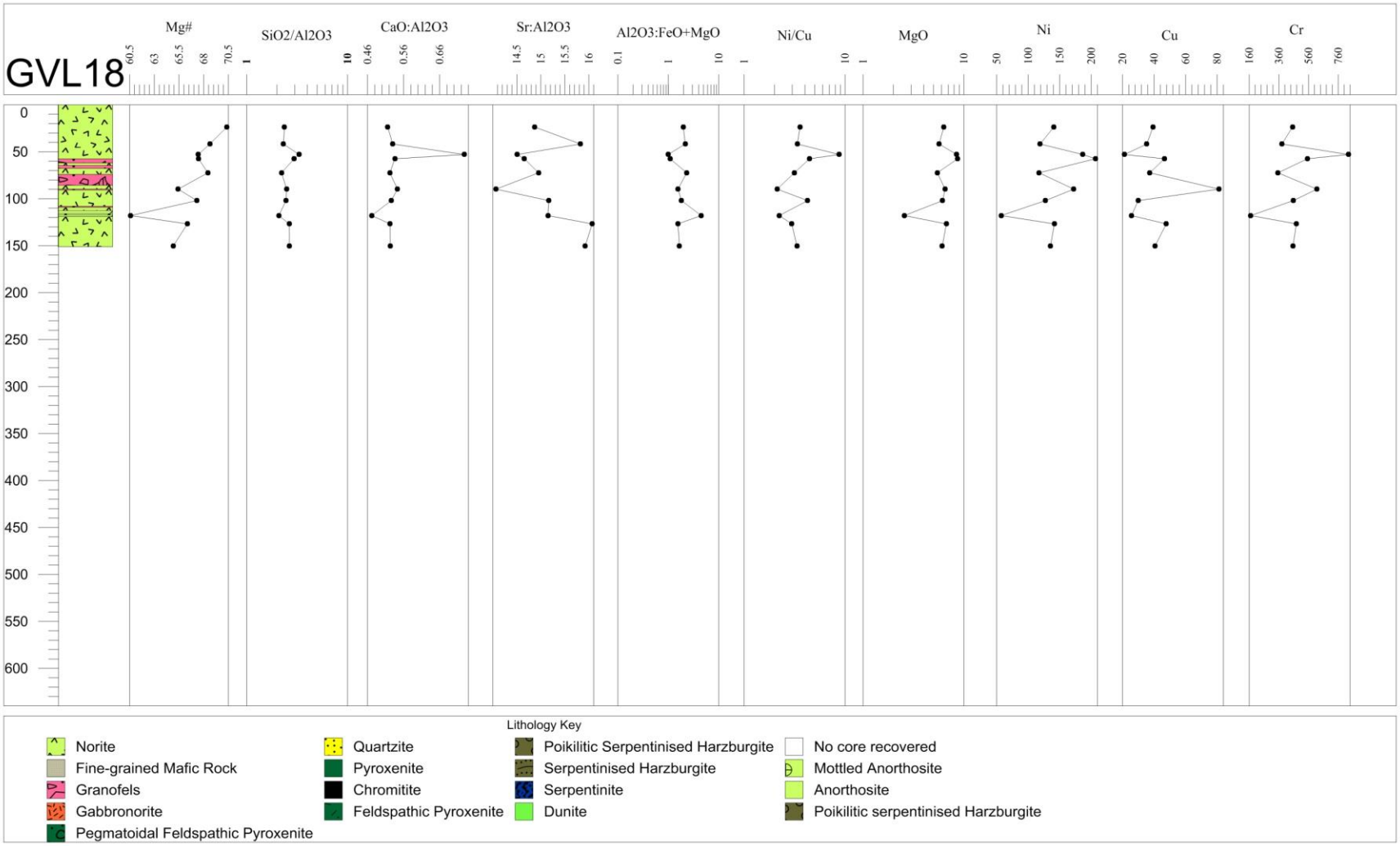

Figure 4.13: Variations of the whole-rock Mg#, major and trace element ratios and trace element contents through borehole GVL 18.

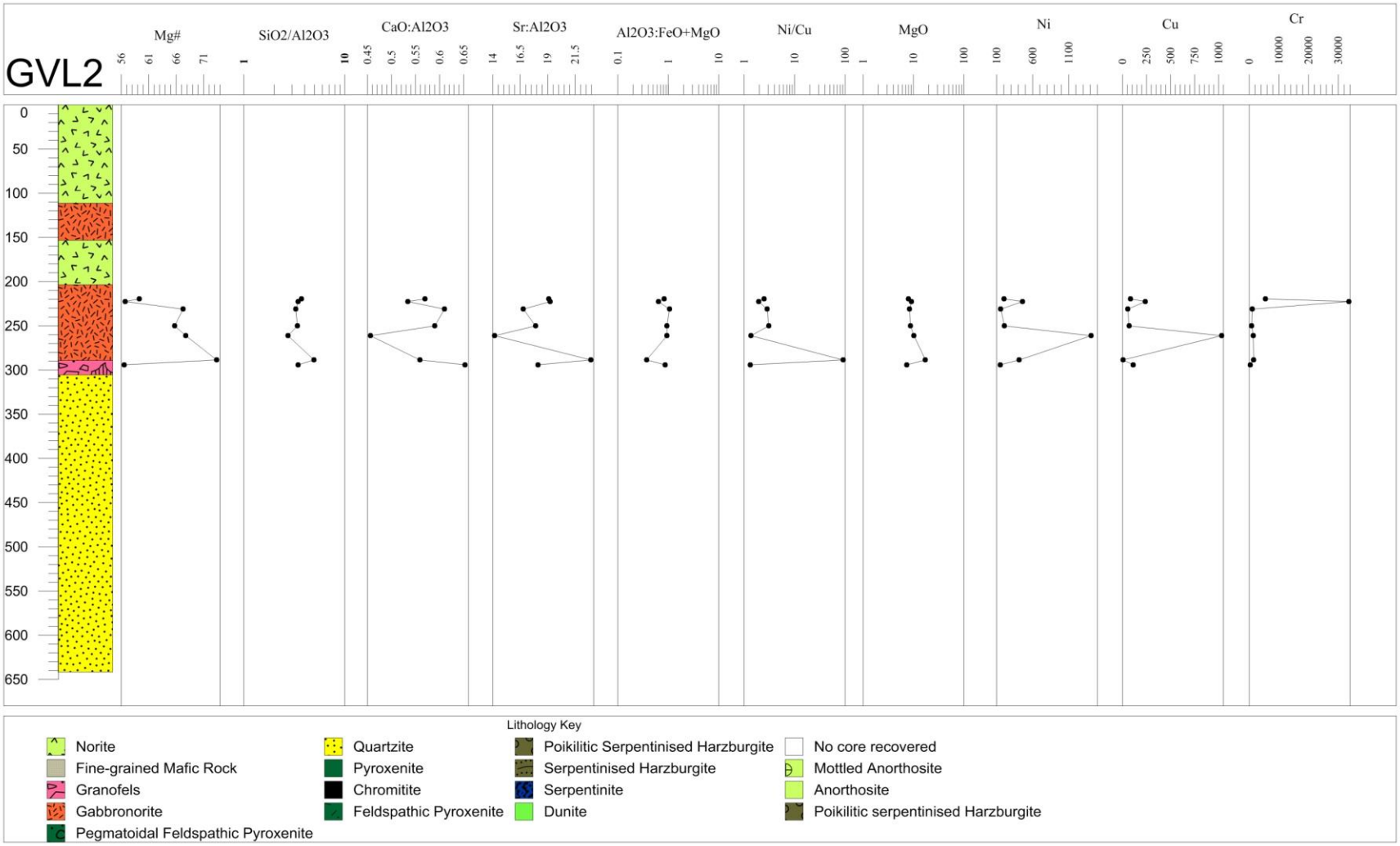

Figure 4.14: Variations of the whole-rock Mg#, major and trace element ratios and trace element contents through part of borehole the GVL 2. The Mg# displays a decrease up section within the gabbronorite. The Cr displays a sharp increase in Cr at 210 m whereas the Cr is below 200m ppm elsewhere within this unit.

The overlying pyroxenite displays an erratic variation in Ni concentration. There is a general upward increase in Ni % within the pyroxenites in GVL 9 from 10.28 ppm to 150.58 ppm and within the pyroxenites intercalated within harzburgite (at 142.71m and 229.02 m) where there is an anomalous high of, to 0.35 % at 17.88 m (Figure 4.10). GVL 3 displays a general decrease in Ni concentration, from 1.24 % to 0.01 %, with increasing stratigraphic height over the interval 485.56 m to 414.89 m (Figure 4.8). The pyroxenitic unit displays a relatively constant Ni concentration with an average 269.7 ppm and variation from 414.89 m to 203.40 m. The Ni concentration within the norite-mottled anorthosite package displays a relatively constant Ni concentration of approximately 110.7 ppm with an outlier high of 0.21 % at the base of the mottled anorthosite at 148.03 m (Figure 4.8).

4.5.6 Cu Variation

The harzburgite-dunite unit displays variable Cu concentrations with respect to stratigraphic height. The harzburgite-dunite package displays an average of 1.8 ppm with most of the samples reflecting no Cu content at all (Figure 4.11). The peak of 39.3 ppm at the base of GVL 5 is associated with the quartzite unit intersected at the base (Figure 4.11). GVL 9 displays a constant Cu distribution trend with a relatively higher average of 80.75 ppm, this includes the anomalous high of 1411.61 ppm (0.14 %). The boundary between the harzburgite-dunite unit and the overlying pyroxenite dominated unit is marked by a sharp increase in Cu (0.42 %) at 78.41 m in GVL 9 (Figure 4.10). The overlying pyroxenite unit displays a generally decreasing Cu profile with increasing stratigraphic height, averaging 0.1 % over the lowermost 75.00 m and dropping off to 25 ppm over the uppermost section of the pyroxenite. The pyroxenitic package however displays the highest Cu values relative to the other units averaging 0.06 %. The mottled anorthosite-norite package displays relatively low Cu values (<100 ppm) with two peaks of 0.01 % and 0.27 %, at the base of the pyroxenite and mottled anorthosite respectively (Figure 4.8).

4.5.7 Cr Variation

In GVL 5, the Cr variation within the harzburgite unit is fairly constant with an average of 0.48 % excluding the high values of 1.56 % and 78.42 % in the chromite-rich horizons which occur at 414.80 m and 114.16 m respectively or the low value of 0.17 % at 261.77 m (Figure 4.11).

In GVL 3, the pyroxenite unit above the harzburgite, displays a relatively constant Cr distribution which is significantly lower than the underlying harzburgite. The pyroxenite unit has an average Cr content of 0.18 % with a maximum of 0.51 % at 464.40 m approximately 10 m below a chromitite band and a minimum of 0.04 % which occurs directly above the harzburgite-pyroxenite contact (Figure 4.8). The overlying noritic unit displays a general increase in Cr with increasing stratigraphic height, above which the Cr values are erratic (Figure 4.10). Overall the pyroxenite in core GVL 3 displays a decreasing Cr % with increasing stratigraphic height, from 0.14 % at 485.56 m to 18.53 % at 334.66 m and averaging 0.06 % (Figure 4.8).

4.5.8 Cr/MgO Ratios

The Cr/MgO ratio of the Bushveld rocks has been used to differentiate between the different zones, particularly the Critical Zone (Cr/MgO typically >100) and the Main Zone (Cr/MgO typically <60) rocks (Seabrook *et al.*, 2005; Smith *et al.*, 2011). The ratio is used in this study in order to distinguish between Main Zone, MANO and LMF rocks, and for this reason Lower Zone samples have been omitted from Figure 4.15.

Most of the samples plot within the Critical Zone classification field with a few exceptions from GVL 3 and GVL 4. The two GVL 4 samples with the lowest Cr ppm content are in close proximity to the granofels layer. Samples K-112- K-115 of borehole GVL 5 from depths 55.16 m to 148.03 m plot within the MZ field whereas sample K117 from a greater depth, plots within the CZ classification field. Samples from GVL 18 are spread along the CZ-MZ classification boundary.

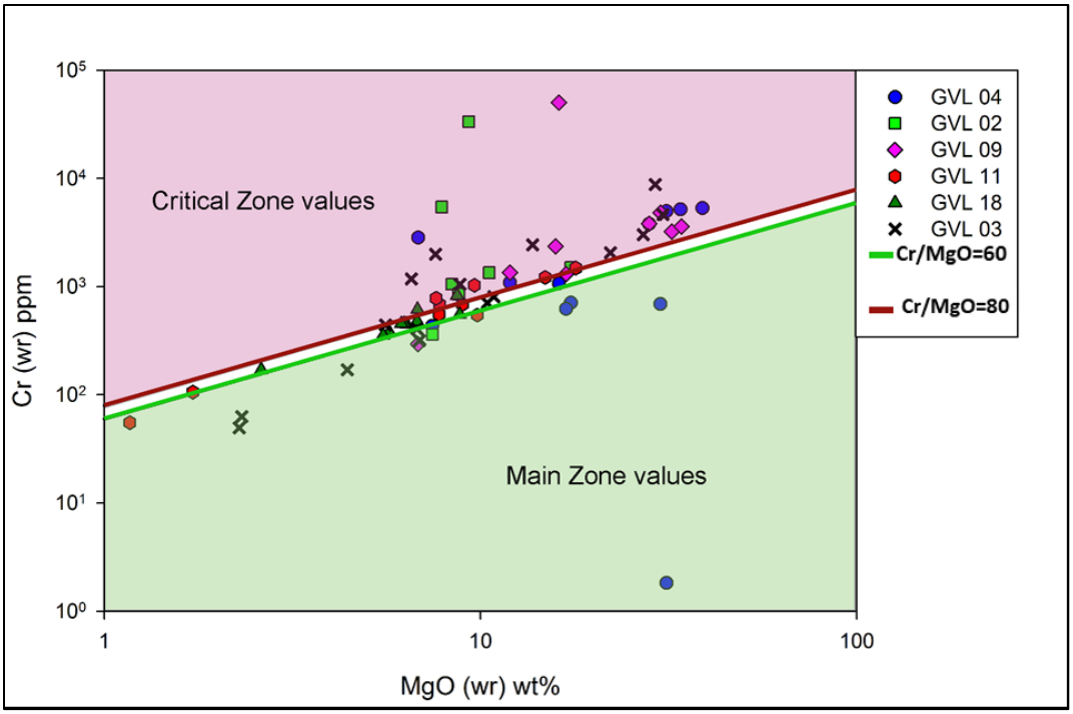

Figure 4.15: Whole rock Cr (ppm) and MgO (wt. %) for samples from boreholes GVL 2. GVL 3, GVL 4, GVL 9, GVL 11 and GVL 18 with the exclusion of Lower Zone samples. The classification fields are defined by the Cr/MgO ratios of 80 and 60 for the Critical Zone and Main Zone respectively (Seabrook *et al.*, 2005).

4.5.9 PGE

Overall, the PGE grade is quite low with grades varying from below detection limit within the norites to ranging between 0.004 and 2.66 g/t within the pyroxenites (Figure 4.16). The Pt/Pd ratio has been used in order to discriminate between the well-known reefs of the Bushveld Complex (Kinnaird, 2005a), however the Pt/Pd ratio differs with geographical location (Appendix F).

The Pt/Pd ratio of GVL 10 displays two trends (Figure 4.16). The Pt/Pd ratio is fairly constant within the feldspathic pyroxenite with an average of 0.5 between 301.25 m and 148.8 m (Figure 4.16). From 148.5 m to 142.6 m there is a general upward increase in the Pt/Pd ratio which coincides with the presence of a chromitite layer at the top of the pyroxenite (Figure 4.16). The Pt/Pd ratio within this chromite rich unit is distinctly higher, ranging from 0.7 to 1.4 with an average of 1.0.

The Pt/Pd ratio of GVL 4 displays a similar trend to that within GVL 10. From 105.81 to 103.60 m there is a general increase in Pt/Pd ratios from 0.4 to 0.7 with the highest value of 1.3 associated with a high chromium content within the feldspathic pyroxenite (Figure 4.16). From 84.9 to 86.32

the Pt/Pd ratios of the feldspathic pyroxenite are relatively higher ranging from 1 to 2.75 with an average of 1.9. The norite unit at the top of GVL 4 displays similar Pt/Pd ratios to the pyroxenite intersected in GVL 10 with an average ratio of 0.4.

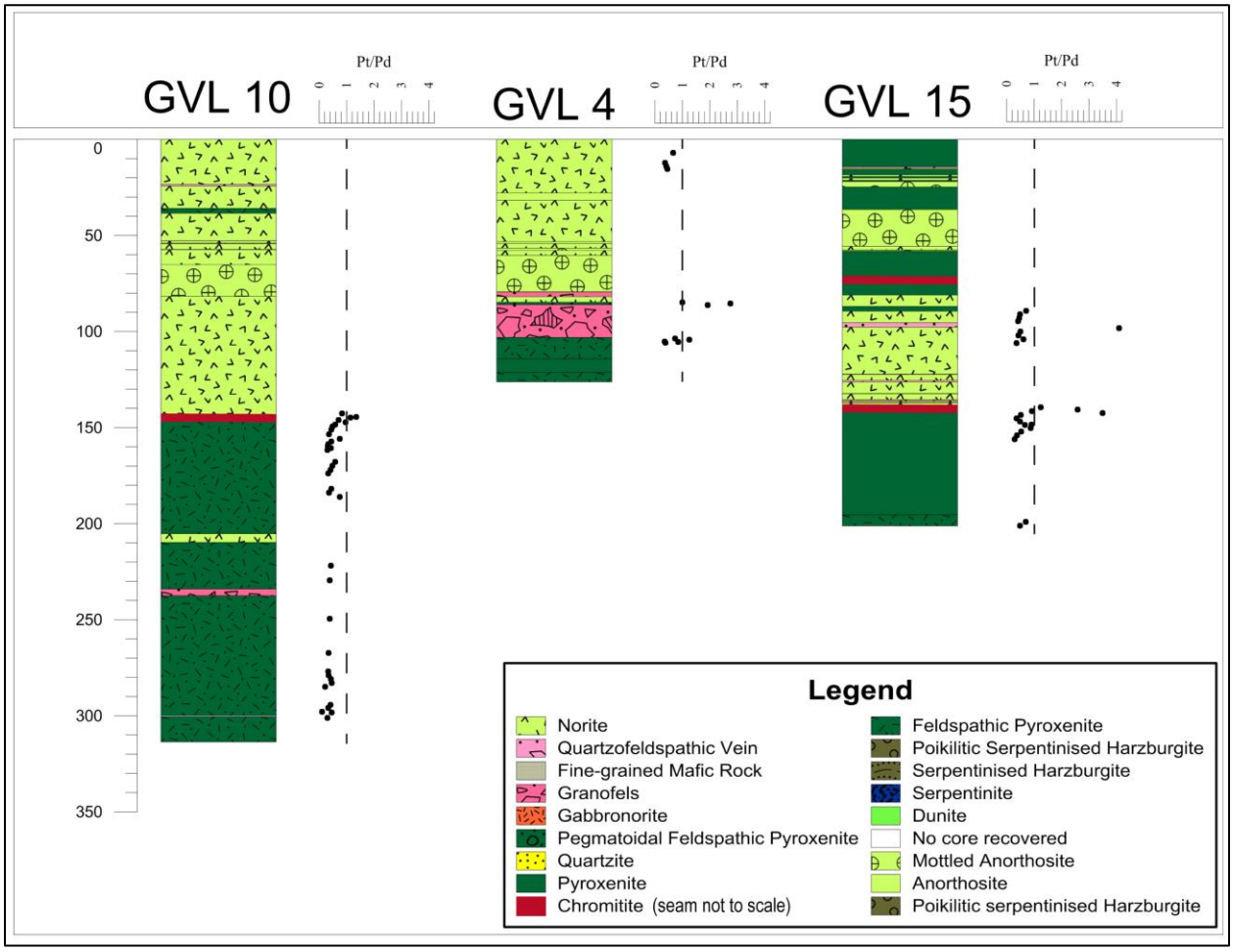

Figure 4.16: Pt/Pd ratios for boreholes GVL 10, GVL 4 and GVL 15 plotted against depth. The chromitite seam markers are not to scale. Stippled line indicates average Pt/Pd ratio for the overall Platreef although different sills within the Platreef as a whole have distinctly different Pt/Pd ratios (1:1 Pt/Pd) (Kinnaird, 2005a).

The feldspathic pyroxenite at 200 m has a similar Pt/Pd signature to the feldspathic pyroxenite intersected in GVL 10 as well as the noritic package intersected in GVL 4. The noritic package between 106.00 m and 89.25m has an average Pt/Pd ratio of 0.5 excluding one outlier sample with a ratio of 4.2 which is associated with a granofels layer, but the overall PGE content of this rock is low making the ratio somewhat unreliable.

The pyroxenite unit from 139.58 to 156.00 m displays three discrete trends. Within the interval 156.00 m to 150.25 m there is an upward increase in Pt/Pd ratio from 0.3 to 0.9. From 148.75 m to 145.25 m there is an upward decrease in Pt/Pd ratio from 0.7 to 0.4. There is an upward increase in Pt/Pd ratio from 0.5 to 1.23. The final increase in Pt/Pd ratio coincides with the presence of a chromitite layer. The relatively high Pt/Pd values of 3.5 and 2.6, which occur at 142.45 m and 140.63 m respectively, are at the base and within the chromitite seam.

4.5.10 Cu/Pd vs Cu/Ni and Pt/Pd vs Cu/Ni

PGE data and accompanying Cu and Ni values were only available for intersections GVL 4 and GVL 14 and have been plotted against published data from the Platreef.

The Cu/Ni ratio displays a variation within the GNPA member ranging from 0.72 to 0.43 at 73.75 m and 150.35 m respectively and within GVL 14 averaging 0.55 (Figure 4.17 and Figure 4.18). Within GVL 4 the Cu/Ni ratio ranges from 1.37 to 0.25 at 105.46 m and 7.04 m respectively averaging 0.74 (Figure 4.17 and Figure 4.18). The Cu/Pd ratio displays a low of 1340.48 and a maximum of 6577.78 at 103.60 m and 7.04 m averaging 2981 (Figure 4.17). Within GVL 14 the Cu/Pd ratio ranges from 1576.92 at 150.35 m to 3165.47 at 73.75 m averaging 2303.13. GVL 4 displays Cu/Pd ratios ranging from 90 000 at 84.90 m to 1340.48 at 103.60 m averaging 11 463. 39. The Pt/Pd ratios for GVL 14 range from 1.17 at 74.50 m to 0.31 at 1.408 m, averaging 0.61 (Figure 4.18). The Pt/Pd ratio for GVL 4 ranges from 2.75 at 268.85 m to 0.35 at 105.46, averaging 0.98.

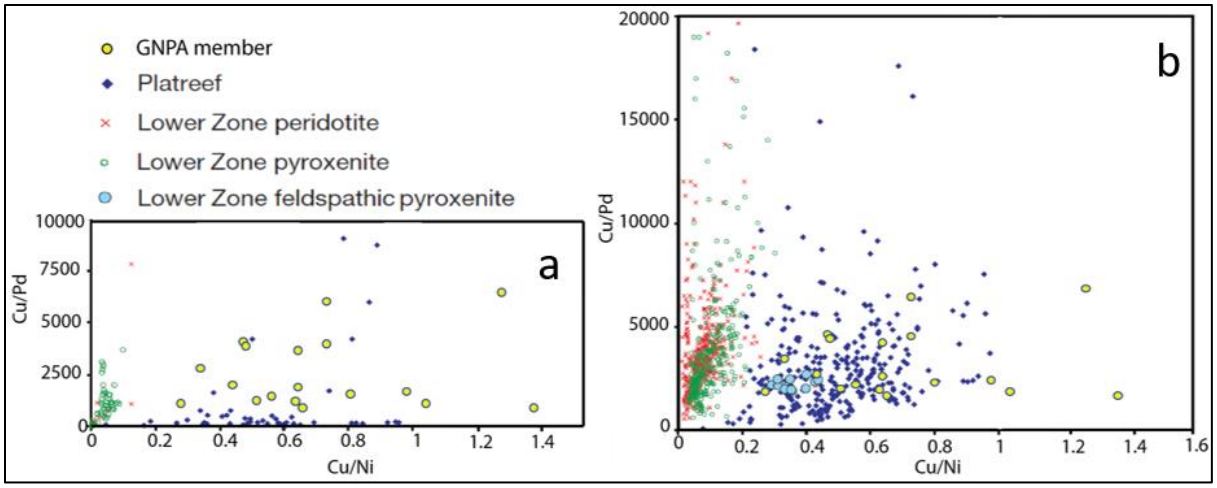

Figure 4.17: Binary variation diagrams of Cu/Ni, and Cu/Pd ratios, showing data for the GNPA member pyroxenite from this study, plotted against Platreef and the Lower Zone peridotite, pyroxenite, and feldspathic pyroxenite after Yudovskaya (2013). Samples plotted against (a) Sandsloot samples and (b) Turfspruit showing that the GNPA samples display a similar distribution to that of the Platreef on Turfspruit.

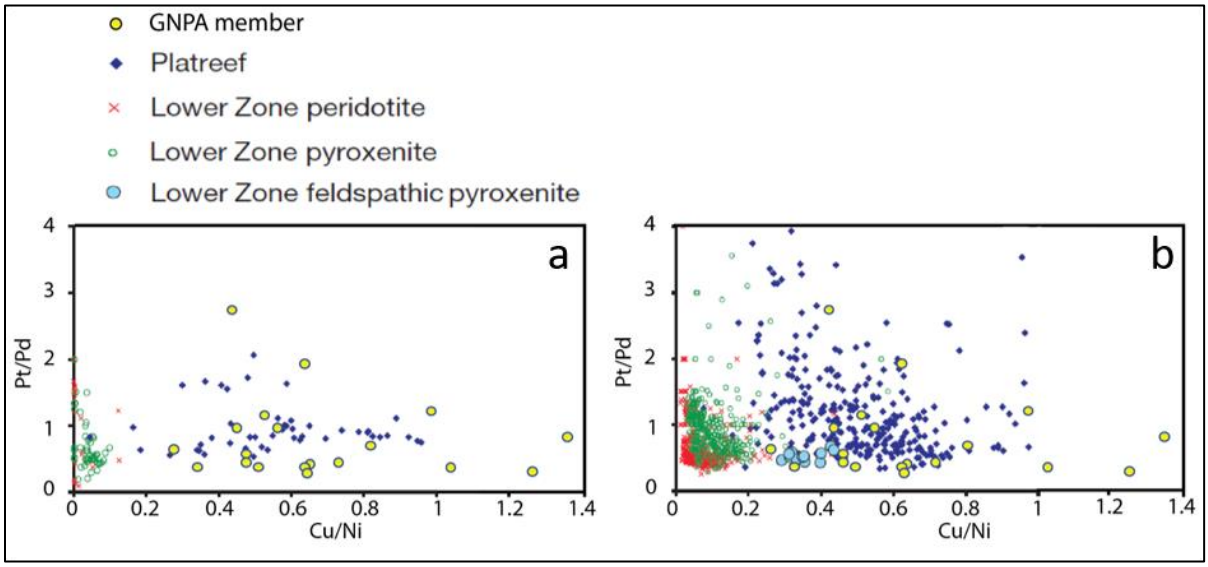

Figure 4.18: Binary variation diagrams of Cu/Ni, and Pt/Pd ratios, showing data for the GNPA member pyroxenite from this study, plotted against Platreef and the Lower Zone peridotite, pyroxenite, and feldspathic pyroxenite after Yudovskaya (2013) Samples plotted against (a) Sandsloot samples and (b) Turfspruit samples showing the samples of the GNPA member are generally palladium dominated with a similar distribution to the Platreef samples of Sandsloot.

4.6 Discussion

As the stratigraphy of the Grasvally area contrasts with that described elsewhere in the Bushveld Complex, it is important to evaluate the geochemical variations of the different rock types as well as across different stratigraphic units. Significant changes in geochemistry are seen at the transition between the ultramafic rocks and the overlying mafic package. The main geochemical variations occur between the various pyroxenites, gabbronorites, norites and anorthosites with sporadic mineralisation occurring within the Critical Zone equivalent unit. The rock types intersected are characterised according to their geochemical characteristics and further discussed in order of the stratigraphic units intersected with increasing stratigraphic height.

4.6.1 Key geochemical observations

The footwall in the Grasvally area comprises Pretoria Group quartzites with the CaO/Al_2O_3 ratio being close to that of plagioclase (0.6, Kinnaird, 2005b), indicative of the succession being devoid of calc-silicates and carbonate assimilated rocks (Kinnaird, 2005b).

The gabbronorite marginal member, only intersected in the east of the Grasvally area, displays no clear major element trends (Figure 4.14). Above that, the Mg# displays a decreasing trend with increasing stratigraphic height which is indicative of a normal fractionating sequence with two resets occurring at 231.15 m and 219.35 m. These resets are possibly due to an influx of new magma into the system or may be due to an increase in cumulus pyroxene or olivine. The SiO_2/Al_2O_3 and Al_2O_3/FeO+MgO ratios are fairly constant throughout the Critical Zone equivalent unit, however, the ratio of $Sr:Al_2O_3$ varies greatly throughout this unit.

Emplaced above the quartzite in the west of Grasvally area, is a sequence of dunites, harzburgites and orthopyroxenites correlated with the LZ. Harzburgite and dunite are the most primitive rock types and have the highest Cr content, with elevated Cr values being indicative of chromitite seams of which two are intersected within this package (Hulbert, 1983). This unit is characterised by an extremely low plagioclase content (<2 wt. %) and is geochemically characterised by low Al_2O_3 and elevated MgO in comparison with the pyroxenite packages intersected in the Grasvally area (Figure 4.8 and Figure 4.9). The Ni content within these LZ ultramafic rocks is high, relative to the rest of the stratigraphic units in the area, although there is no distinction between Ni in silicate and Ni in sulphide. The Cu content, indicative of sulphides, within this unit is low. The pyroxenites

with a relatively high MgO content (28 - 48 wt. % MgO), high Cr/MgO ratio (of Critical Zone values after Seabrook *et al*., 2005) and lower Al_2O_3 wt% (~<5% wt. % Al_2O_3), are interpreted as pyroxenites of the LZ (Figure 4.3). The relatively elevated MgO content is attributed to the presence of olivine within these rocks. The geochemistry of the harzburgites and dunites of this unit displays no significant variation, which together with the consistent Mg# suggests that the lithologies that the lithologies were from the same magma source (Hulbert, 1983).

The overlying package comprises various orthopyroxenites, pyroxenites, gabbronorites, norites and anorthosites. Geochemical classifications of these rock types do not differentiate between gabbronorites and feldspathic pyroxenites and between norites and mottled anorthosites. This package has been correlated with the Critical Zone based on stratigraphic position. The transition from the underlying harzburgite-dunite package to the overlying pyroxenite package is marked by a sharp decrease in Mg#, SiO_2/Al_2O_3, Cr content and a sharp increase in Ni, Cu content and Sr/Al_2O_3 ratio (Figure 4.8). The transition is also marked by a sharp change in Sr/Al_2O_3 which is possibly indicative of an influx of new magma. The increase in Ni and Cu across this boundary into the overlying CZ equivalent also suggests an influx of new magma that was not as depleted in Ni and Cu as the underlying LZ.

The stratigraphic unit overlying the LZ can be divided into a lower mafic orthopyroxenite-dominated unit (LMF or subzone 1) and an upper leucocratic gabbronorite, norite, mottled anorthosite and anorthosite dominated unit (MANO or subzone 2) (Hulbert, 1983; de Klerk 2005; Smith *et al.*, 2014). The LMF displays a decrease in Mg# up section which is indicative of a differentiating sequence (Figure 4.8). The marked decrease in SiO_2/Al_2O_3 is indicative of an increase in feldspar which is comparatively deficient in the underlying ultramafic LZ unit. An anomalous peak in Cr is correlated with a chromitiferous unit hosted within the pyroxenite in core GVL 9 at 16.51 m depth. The peak in Cr coincides with a peak in Cu and Ni which suggests sulphides are occurring in association with the chromitite. Where the chromitite layer occurs the Pt/Pd ratio is ~1 and < 1 within the rest of the pyroxenite unit (Figure 4.16). The LMF transitions upwards into a more leucocratic unit comprising gabbronorites, norites, mottled anorthosites and anorthosites. This transition is also marked by a Pt/Pd ratio of ~0.6 which differs from that of the underlying pyroxenite dominated unit (~1). The Cu, Ni and Cr peaks within mottled anorthosites are attributed to the presence of sulphides as well as sporadic occurrences of disseminated chromite

throughout the package even though the major trend displays a decrease in Cr content up section concomitant with increasing plagioclase. As these lithologies are similar to those of the Main Zone, the Cr/MgO ratio is used to identify the boundary between this stratigraphic unit and the overlying Main Zone (Figure 4.15).

4.6.2 Comparison with the rest of the RLS

The footwall in the Grasvally area comprises quartzite of the Pretoria Group which is the same as that noted by previous work in the same area (Hulbert, 1983), as well as in most localities of the Bushveld Complex (Barnes and Maier, 2002), and further north approaching the Ysterberg-Planknek Fault (Smith *et al*., 2014). North of the Ysterberg-Planknek Fault, the footwall transitions down through the lithologies of the Chuniespoort Group to the basement granites in the north towards Overysel. The assimilation of footwall carbonates, calc-silicates and shales to the north of the Ysterberg-Planknek Fault introduces contamination or hybridisation typical of the Platreef (van der Merwe, 1976; Mostert, 1982; Gain and Mostert, 1982; Buchanan *et al*., 1981 and Cawthorn *et al*., 1985) such as elevated CaO/Al_2O_3 ratios above that of plagioclase (Kinnaird, 2005b). The intersection of quartzite at the base of GVL 5, interpreted as footwall, displays elevated Cu values which could be indicative of local sulphide enrichment as observed further north at the footwall-Platreef interface where massive chalcopyrite zones have been observed (Sharman *et al*., 2013). Further analysis of samples at this interface as well as the contact between the footwall and the overlying Critical Zone equivalent is required to determine the relationship between these units and possible PGE mineralisation.

The thick ultramafic unit intersected in the study area is consistent with the data reported for the Lower Zone previously on Grasvally (Hulbert and Von Gruenewaldt, 1982 and Hulbert, 1983), Sandsloot and Turfspruit (Yudovskaya *et al.*, 2013) as well as on the Clapham section (Wilson, 2012) on the eastern limb. The constant Mg# contrasts with trends of large-scale cyclic units in some layered intrusions which display reversals in Mg# near the base of the dunite layers such as the Great Dyke (Wilson, 1982) and Muskox intrusion (Irvine, 1980). A significant difference noted within the LZ on Grasvally from anywhere else in the RLS is the peaks in Cr values which are representative of the thick chromitite layers that occur within the LZ. Chromite is present as disseminations on the farms of Sandsloot and Turfspruit (Yudovskaya *et al*, 2013), rather than as well-developed chromitite layers. In addition, the chromite of the Grasvally LZ has the highest Cr

content, (Hulbert and Von Gruenewaldt, 1982). The LZ of the Grasvally area is further dissimilar to LZ bodies to the north of the Ysterberg-Planknek Fault (e.g. the Uitloop and Zwartfontein bodies) and of the eastern and western limbs due to the presence of Ni-PGE mineralisation (Yudovskaya *et al.*, 2013). The occurrence of stratiform PGE mineralisation in the Lower Zone is unique to the Grasvally area and does not occur anywhere else in the Bushveld Complex (van der Merwe, 1976, Hulbert and Von Gruenewaldt,1982; Hulbert, 1983, van der Merwe, 1998).

The unit of various pyroxenites, gabbronorites and pyroxenites overlying the LZ has, in the past, been correlated with the Critical Zone for the most part due to its stratigraphic position. This stratigraphic unit is similar to that correlated with the Platreef to the north and the Critical Zone elsewhere in the Bushveld Complex as its Cr/MgO ratio displays that of Critical Zone affinity and the overlying (hanging wall) rocks are of Main Zone affinity (Seabrook *et al.*, 2005; Smith, 2014). The distribution of the GNPA member samples on the Cu/Pd vs Cu/Ni binary diagram is similar to the Platreef samples. The Cu/Ni ratio seems to be related to the higher amount of interstitial liquid in the plagioclase-rich cumulate rocks whereas Cu/Pd ratio, in comparison does not appear to be controlled by the same process due to the plagioclase-depleted LZ rocks displaying similar distributions to this package. The GNPA member samples are of a similar geochemical affinity to that of the Platreef samples from both Sandsloot and Turfspruit based on the data of Cu/Ni, Cu/Pd and Pt/Pd ratios.

The LMF has been separated from the underlying LZ due to variations in geochemical trends up-section that are not seen within the LZ. Geochemical reversals (Sr/Al_2O_3, SiO_2/Al_2O_3) seen within this stratigraphic unit have been used to differentiate between different pyroxenitic units as well as to indicate new influxes of magma comparative to that seen within the northern limb north of the Ysterberg-Planknek Fault (Kinnaird *et al.*, 2005)

The Pt/Pd ratio through the CZ in the Grasvally area is averaged at ~1:1 for the whole GNPA or CZ package. This is similar to the ratio for the Platreef as a whole however, throughout the CZ unit on Grasvally, the Pt:Pd ratio varies between pyroxenitic units indicative of separate ‘reeflets’ that occur within this package akin to the variability in Pt:Pd ratio seen within the Platreef (Table 4.1) (Kinnaird *et al.*, 2005).

Table 4.1: Varying Pt:Pd ratios for pyroxenite packages from cores ATS57 and ATS26 on Turfspruit displaying variation in reef layers (Kinnaird, 2005b).

BHID - ATS57	Thickness	Pt:Pd
IV. Top pyroxenite	45	2.2
III. Upper Middle	64	2
II. Lower Middle	67.3	0.62
I. Basal pyroxenite	26	1.05
Average		1.4675

BHID - ATS26	Thickness	Pt:Pd
IV. Top pyroxenite	38	2
III. Upper Middle	165	1
II. Lower Middle	94	0.78
I. Basal pyroxenite	59	1.01
Average		1.1975

The increase in Pt:Pd ratio in association with the chromitite layer is similar to that observed to the north of the farm of Turfspruit where the main chromitite is intersected within the Flatreef package (Grobler *et al.*, 2019). The chromitite seam intersected within the LMF has, in the past, been dubbed "UG2-like" and thus correlated with the UG2 reef of the eastern and western limb (Hulbert, 1983). The upper section of the Platreef on Turfspruit, which comprises chromitites comparable to that intersected within the LMF, shows good grade within the pegmatoidal pyroxenite and harzburgite package beneath the lower chromitite stringer and a poor correlation with grade and the upper Cr stringer on Turfspruit (Kekana, 2014). This "UG2-like" chromitite layer as well as the cyclic nature of this stratigraphic unit has prompted several correlations of this unit with the upper Critical Zone (Hulbert, 1983; van der Merwe, 1978 and 2008; Grobler *et al.*, 2012 and 2019). These correlations, as well as Merensky Reef style mineralisation on Turfspruit have suggested correlation between the Platreef, the mineralised unit intersected on Grasvally and the upper Critical Zone however, this is discounted due to differences in composition of parental magma of the units (McDonald *et al.*, 2005). Due to the position above the footwall and Lower Zone, it is suggested that the mineralised package of various pyroxenites, gabbronorites, feldspathic pyroxenites, norites and mottled anorthosites on Grasvally may merge at depth with the Platreef towards the Ysterberg-Planknek Fault or it is an analogue of the Platreef which has evolved differently due to separate staging chambers and the compartmentalisation due to the Thabazimbi Murchison Lineament (Smith, 2014).

4.6.3 Summary

Major whole rock geochemistry is used to characterise the different lithological groups encountered on the farm of Grasvally, apart from lithologies which are only distinguishable due to differences in cumulate and intercumulus phases. Whole rock geochemistry and downhole

geochemical variations were used to characterise lithological units and separate stratigraphic units into the metasedimentary footwall, an ultramafic package which has been correlated with the Lower Zone despite key differences, a mafic chromitite-bearing unit which develops into a more leucocratic unit that has been equated with the Platreef to the north, and also with the upper Critical Zone of the eastern and western limbs.

CHAPTER 5

Three-Dimensional (3D) Modelling

With software that is now generally available and relatively easy to use, lithological details obtained from the core logs, integrated with the surface lithological mapping data of Hulbert (1983), can be analysed in the computer program Leapfrog Geo® to obtain a 3D display of the Grasvally geology. Cross sections were primarily anchored by the N-S and E-W trends of the drill holes, and which revealed the subsurface structure and the effect of the generation 1 faults. It was anticipated that such a 3D model would also aid in the understanding of the GNPA member and its status within the Rustenburg Layered Suite.

5.1 Methodology

The process of modelling the area mapped by Hulbert (1983) incorporated the use of various data sources to construct surface topography and geological volumes. Digitised topographic maps were augmented by 90 m Shuttle Radar Topography Mission (SRTM) elevation maps to generate the land surface features. Digitised geological maps provided surface contacts and fault traces to which was added lithological and structural elements extracted from the borehole core logs (Figure 5.1).

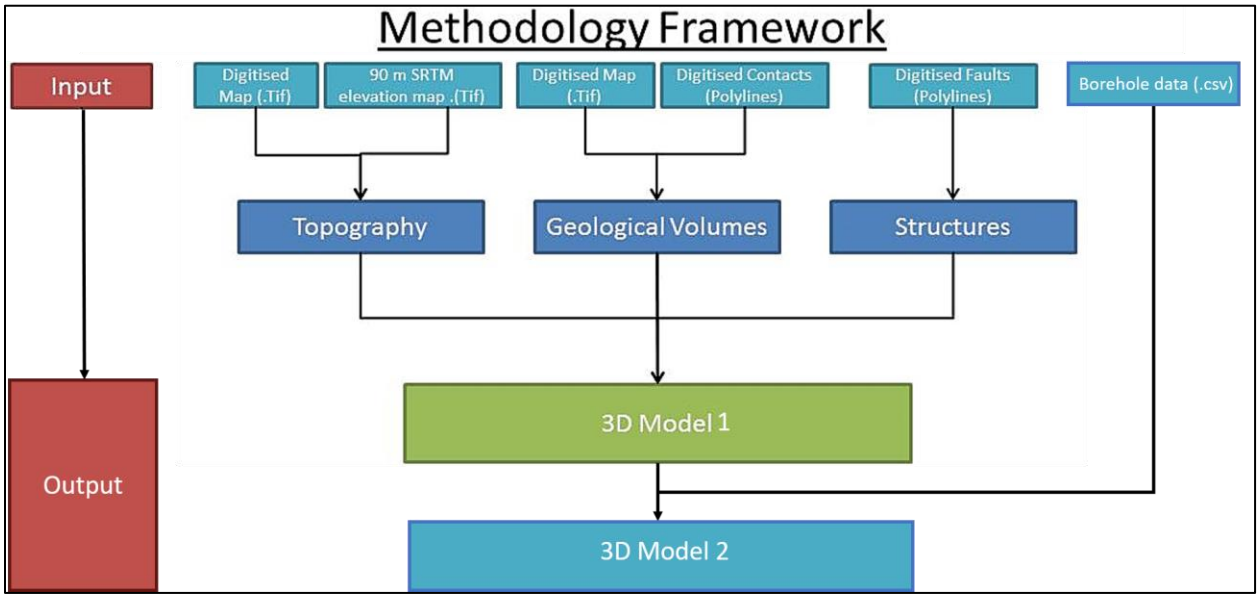

Figure 5.1: Modelling methodology framework followed to design a 3D geological model.

5.1.1 Surface information: topographic data and geological maps

The Grasvally area, which includes the adjacent farms of Rooipoort, Jaagbaan, Rondeboschje, Cyferkuil, Vaalkop, Volspruit and Zoetveld, was mapped in detail by Hulbert (1983) and he provided the comprehensive map that was digitised with the use of Adobe Illustrator CS6 (Appendix G), in order to convert it into a format suitable for computerised three-dimensional modelling. The map was then georeferenced using 20 points to prevent any distortion in ArcMap 10.2.2. Structural data extracted from the map generated by Hulbert (1983) was augmented by information gathered from van der Merwe (1976, 2008). The topography of the upper surface of the model is shown in Figure 5.2.

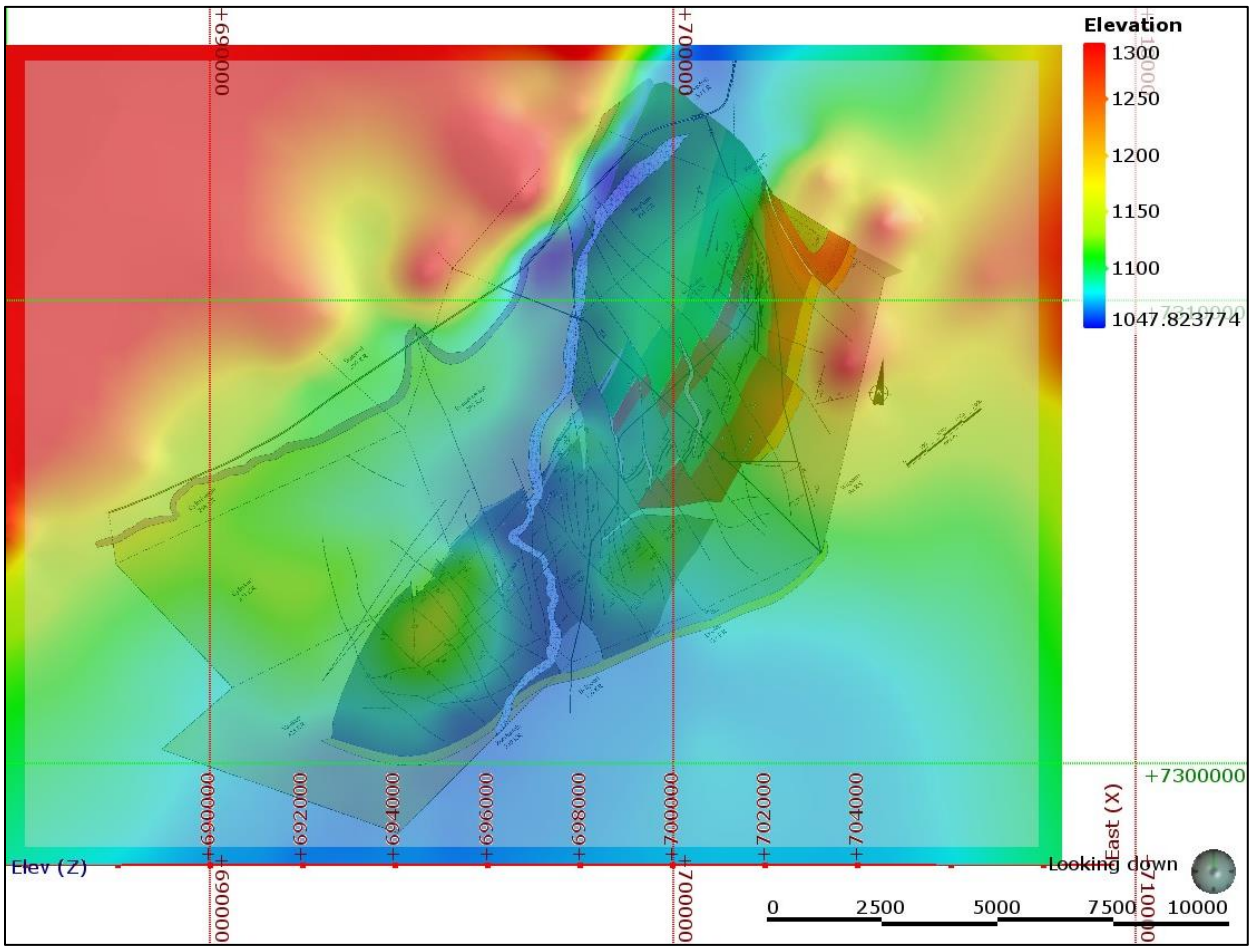

Figure 5.2: A topographic map of the Grasvally area with the geological map overlain, generated in Leapfrog Geo®.

5.1.2 Borehole Information

The borehole database for this study is limited to the 20 boreholes provided by Sylvania Platinum Ltd. Three boreholes were omitted due to a significant number of missing core trays which would be problematic when modelling. The boreholes are subvertical and the collar x-y-z coordinates were provided by Sylvania Platinum Ltd.

5.1.3 Geomodelling

Two geological models were created; one using only surface mapping and structural data (Figure 5.1), the second including borehole data (Figure 5.1). The purpose of the first model is to give preliminary insight into the GNPA body and Rustenburg Layered Suite south of the Ysterberg-Planknek Fault. The second model, which incorporates borehole data, aims to give an in-depth view of the effects of structures on the GNPA member as well as to provide an understanding of morphology of the LZ and GNPA member at depth. Note that the areal extent of the second model was restricted to the extent of the borehole distribution (Figure 5.3) and not the entire area as mapped by Hulbert (1983).

5.1.4 Geological volumes

Geological volumes are three dimensional representations of lithological or stratigraphic units (Figure 5.4). Model 1 required a total of 10 geological volumes to be created, one volume for each of the simplified stratigraphic units (Transvaal metasedimentary rocks, Lower Zone, Marginal member, Critical Zone, Main Zone, Upper Zone, Granite, Dyke, Alluvium and unknown lithology/empty volume). These volumes were generated in LeapFrog Geo® using lithological contacts between units (Figure 5.4). The volumes were constrained at surface level by the topography (Figure 5.2). The volumes were generated using modelling algorithms based on the chronological order of the lithological packages. The basal extent of the model was set on the depth of the longest borehole. Model 2 required a total of 6 geological volumes (Transvaal metasedimentary rocks, Lower Zone, Marginal member, Critical Zone, Main Zone and Granite) to be created with the use of the same algorithm with the same vertical extents.

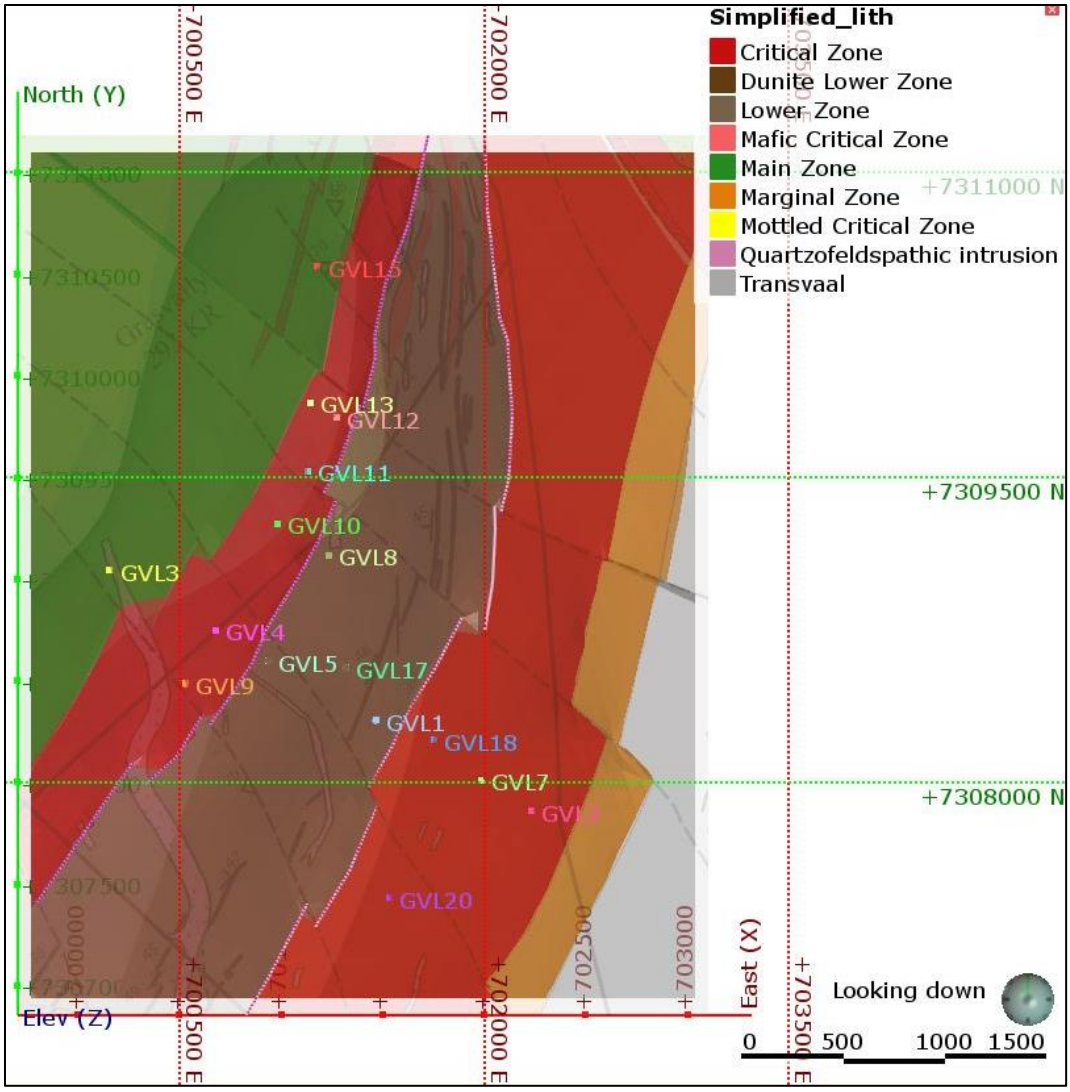

Figure 5.3: Plan view of modelled area with boreholes incorporated. Draped map adapted from Hulbert (1983).

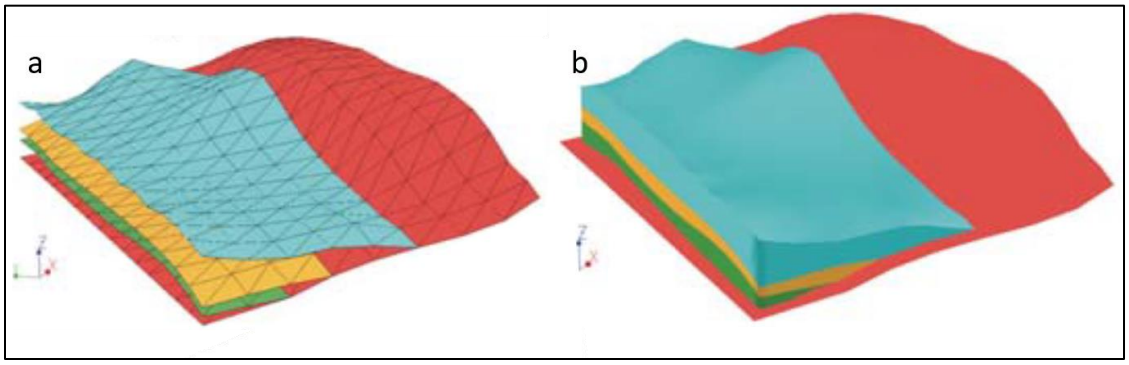

Figure 5.4: Simplistic generic depiction of model components. (a) Wireframes or surfaces which are representative of the lithological or stratigraphic boundaries which are then used to define (b) the lithological or stratigraphic volumes. Modified after Ross *et al.* (2007).

5.1.5 Surfaces

Surfaces are used to define the geological model volumes (Figure 5.4). The surfaces were created using the digitised geological contacts (Figure 5.5) from the geological map by Hulbert (1983). Supplementary surfaces were created from the digitised structural information such as polylines (Figure 5.5), GIS lines and orientation disks (Figure 5.6). Orientation or structural disks are a feature of LeapFrog Geo® which allows one to allocate an orientation to a digitised feature such as faults, lithological units and contacts (Figure 5.6). Each individual contact is assigned the same polarisation in order for the contacts to behave in a similar manner.

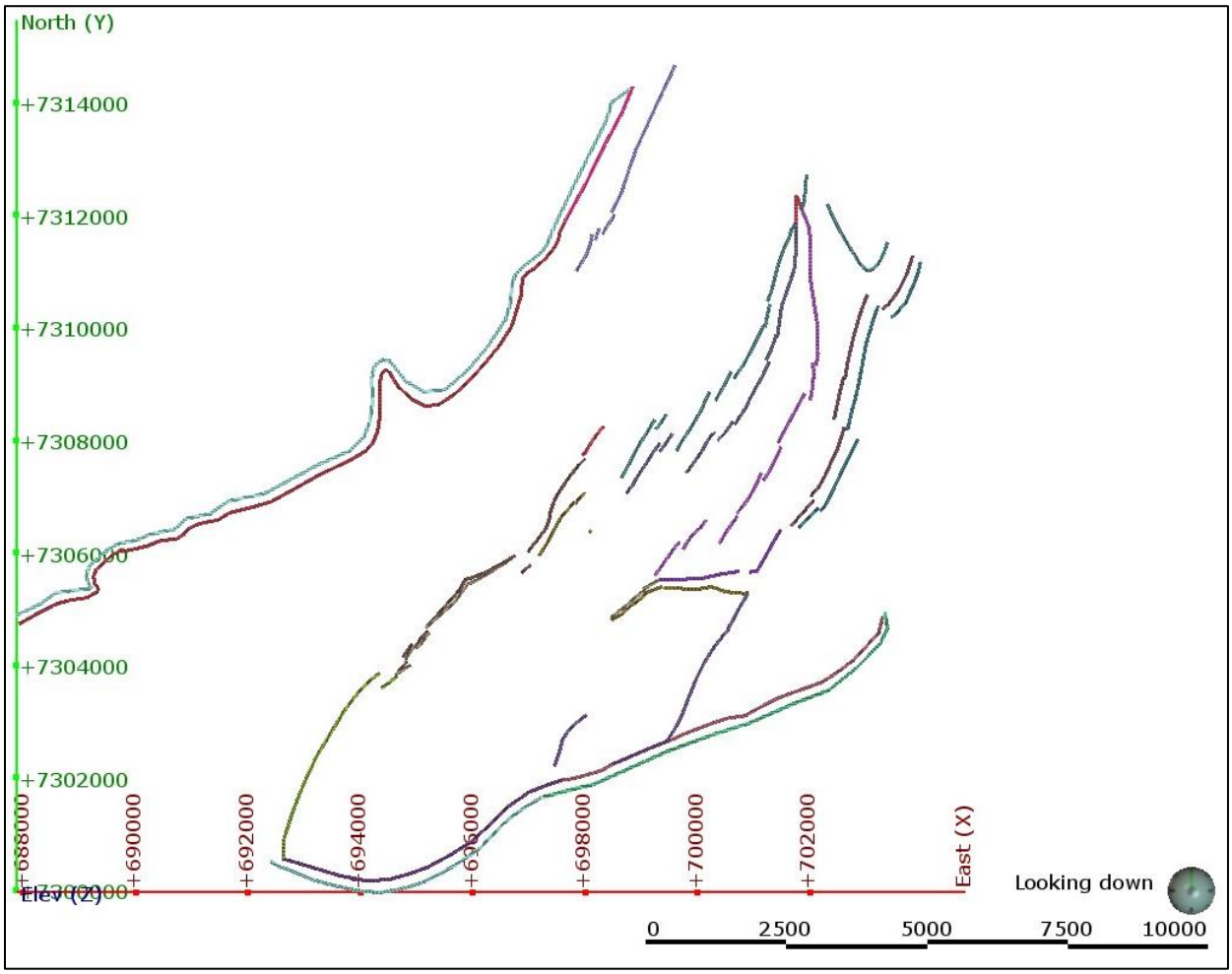

Figure 5.5: Digitised contacts between stratigraphic units. Stratigraphic contacts were obtained from Hulbert (1983).

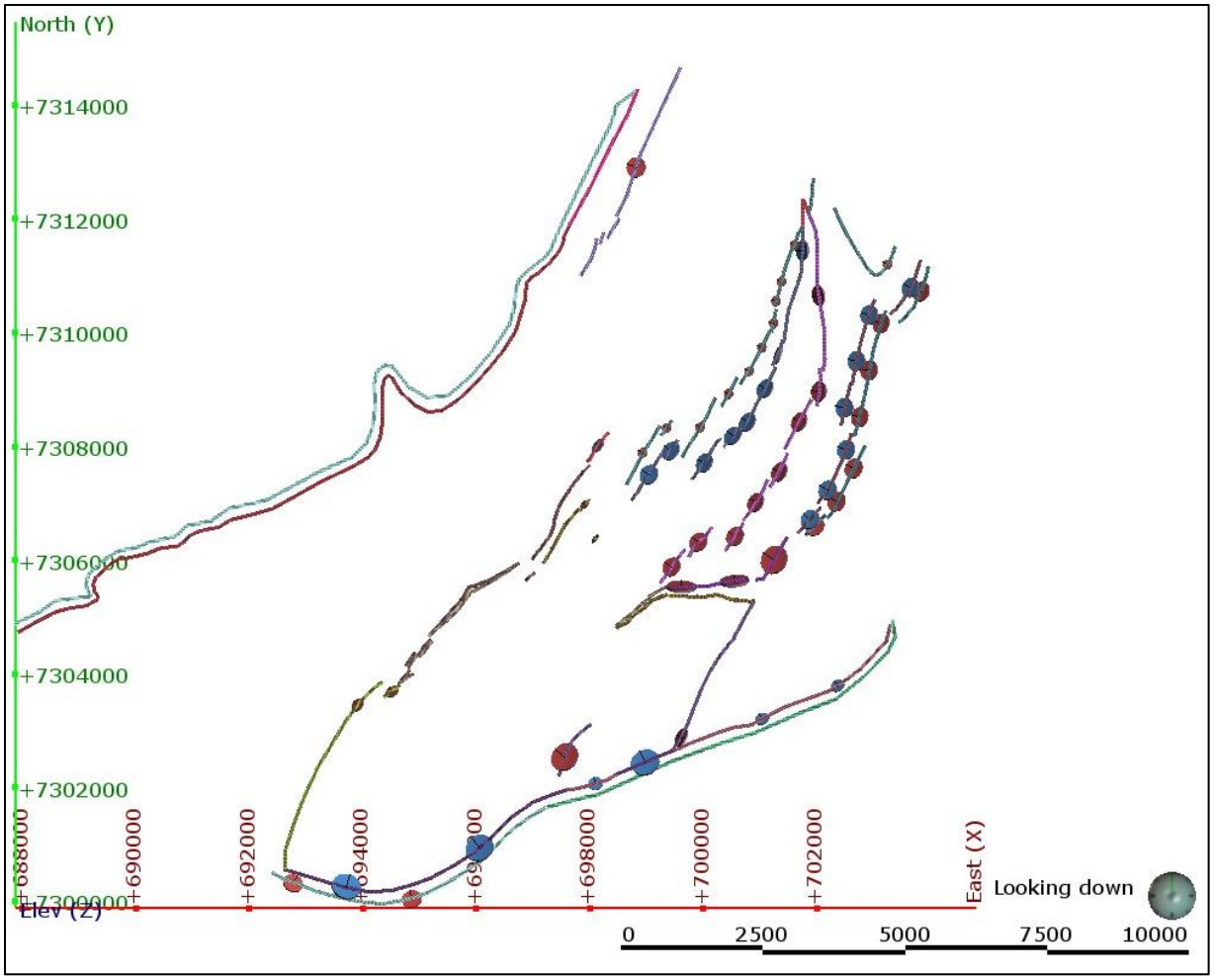

Figure 5.6: Digitised stratigraphic contacts with structural disks. Structural disks are a graphical representation of the orientation of each feature. The colour of the structural disks is based on the polarisation of each contact, red- positive, blue- negative, to influence the interaction of contacts with each other. The structural data was obtained from Hulbert (1983).

5.2 Modelling Process

In order to generate a 3-dimensional model, several data formats were incorporated to generate a topographical surface, the geological volumes and the structural features (Figure 5.1).

The topographical surface was created through the use of a triangulated mesh on Leapfrog Geo® (Figure 5.2). The triangulated mesh, which is an editable mesh using Delaunay triangulation as opposed to interpolated triangulation as the preferred algorithm, is capable of incorporating more points. An SRTM image of the area with a resolution of 90 m was used to generate the points needed to create the mesh. The topographic map was then overlain with the map of the area to generate the top surface of the model (Figure 5.2).

The structures in the area had to be simplified and only major faults with known or visible displacement were included. Faults within a single stratigraphic unit have been omitted as the effects or displacement along these faults cannot be interpreted. The faults were individually digitised in Leapfrog Geo® and the orientation of these faults have been sourced from the map produced by Hulbert (1983) and snapped to each individual fault with the use of orientation disks.

The geological volumes were constructed from the geological contacts. The contacts were digitised in ArcMap and imported into Leapfrog Geo® in the form of shape files. Leapfrog Geo® uses the contacts as well as structural information to generate 3D surfaces which are then used to create the individual surfaces (Figure 5.7)

LeapFrog Geo® allows for geological volumes to be created or categorised as either a deposit, erosional volume, an intrusive volume or vein volume. LeapFrog Geo® applies certain controls to each of the volume categories to dictate the behaviour of the volume in 3D space, the relationship between the individual unit and the units it is in contact with. A deposit within LeapFrog Geo® is a volume that lies conformably atop another geological volume, an erosional volume is a volume that acts unconformably in that it cuts across other geological volumes. Vein or intrusive volumes act as veins in that these volumes crosscut several geological volumes, in space, as a vein, dyke or sill would. LeapFrog Geo® simplifies geological relationships into these classes or volume groupings in order to predict the relationships between different volumes. The dyke in the south, the marginal member as well as the granite body in the north have all been modelled as veins using strictly the stratigraphic contacts as well as the structural data available (Figure 5.8). The Transvaal metasedimentary succession, the Lower Zone, Critical Zone, Main Zone, Upper Zone and the alluvial cover surfaces were all modelled as intrusive surfaces. These surfaces were generated using the lithological contacts, structural discs as well as topographic extents (Figure 5.6).

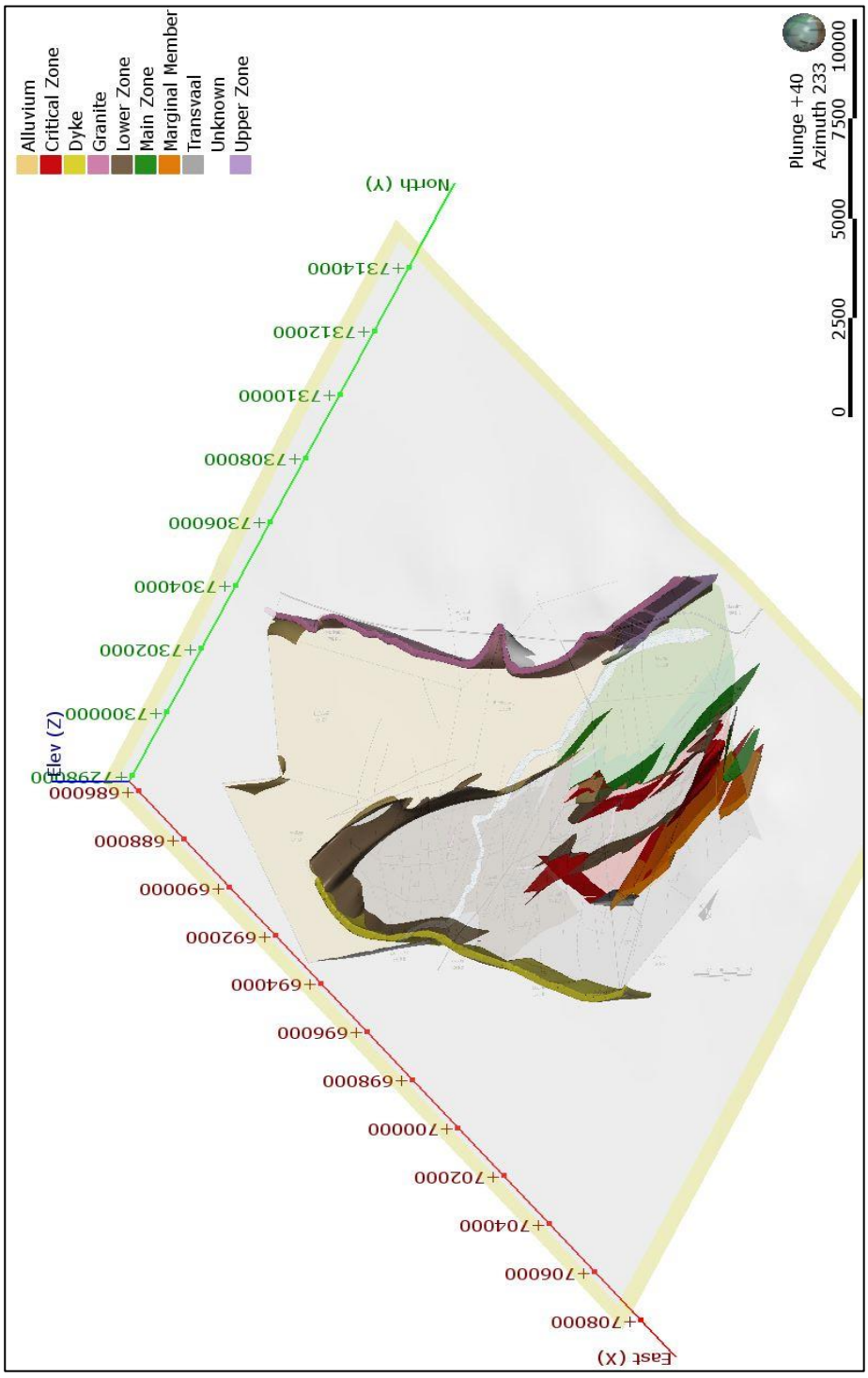

Figure 5.7: Orthographic view of all surfaces, vein surfaces of the dyke, marginal member and granite unit and intrusive surfaces of the Transvaal metasedimentary succession, the Lower Zone, Critical Zone, Main Zone, Upper Zone, and the alluvial cover, showing the differences between the surfaces used to create the deposit- type and erosive volumes compared to the vein type or intrusive volumes.

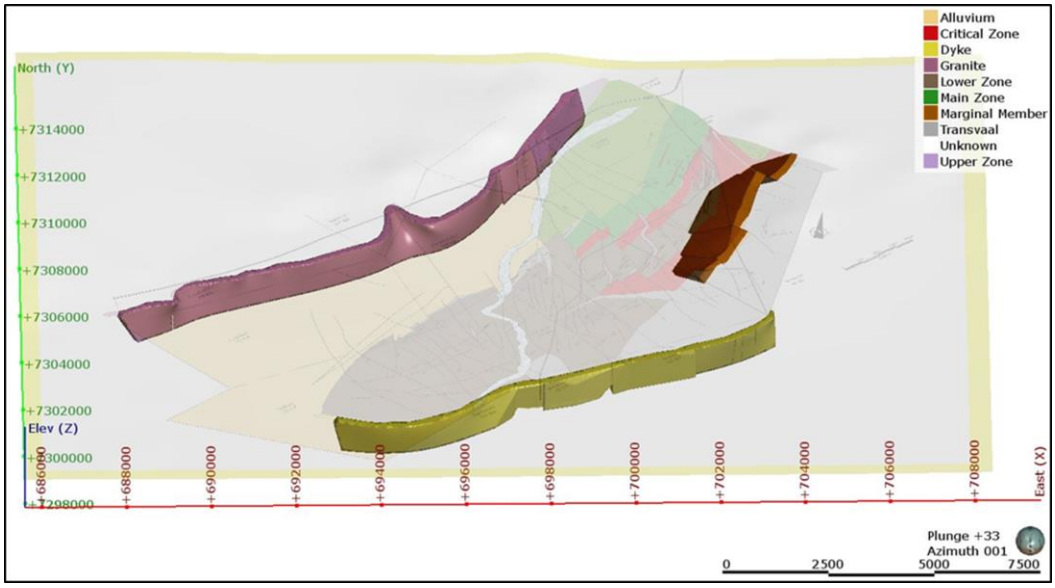

Figure 5.8: Orthographic view from the south of vein-type surfacing of dyke (yellow) marginal member (orange) and the granite body (pink).

The various surfaces were used to generate the first three-dimensional model (Figure 5.9 and Figure 5.10) that honoured the lithological and structural data of Hulbert (1983). The model represents the structural interpretation, however, it does not have any structural controls or data at depth.

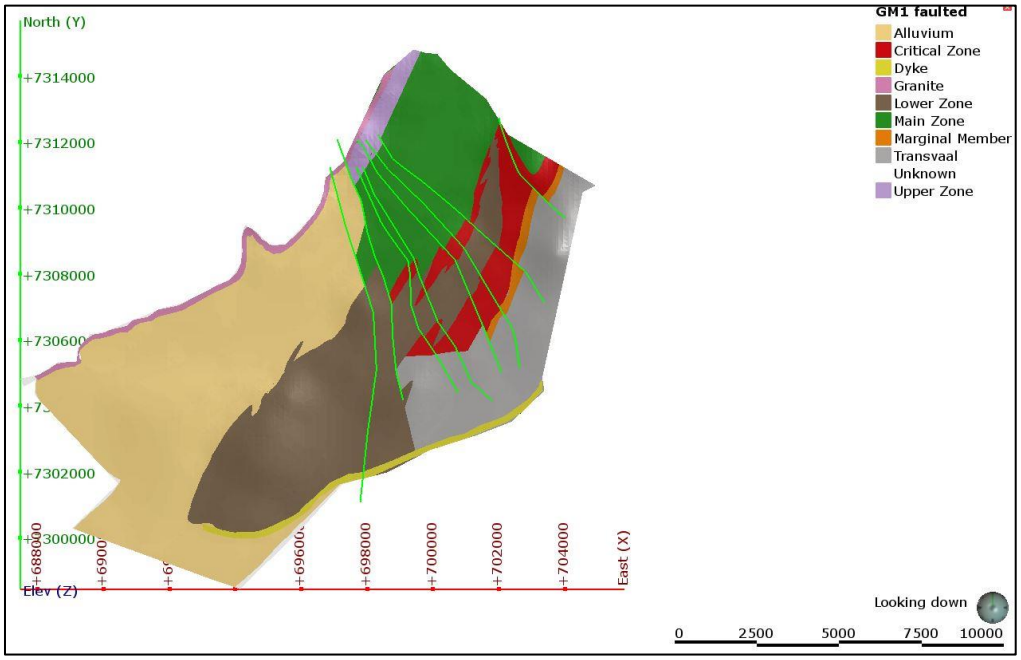

Figure 5.9: Plan view of model with major faults introduced showing how the ENE-WNW faults further offset and compartmentalise the major stratigraphic units within the Grasvally area.

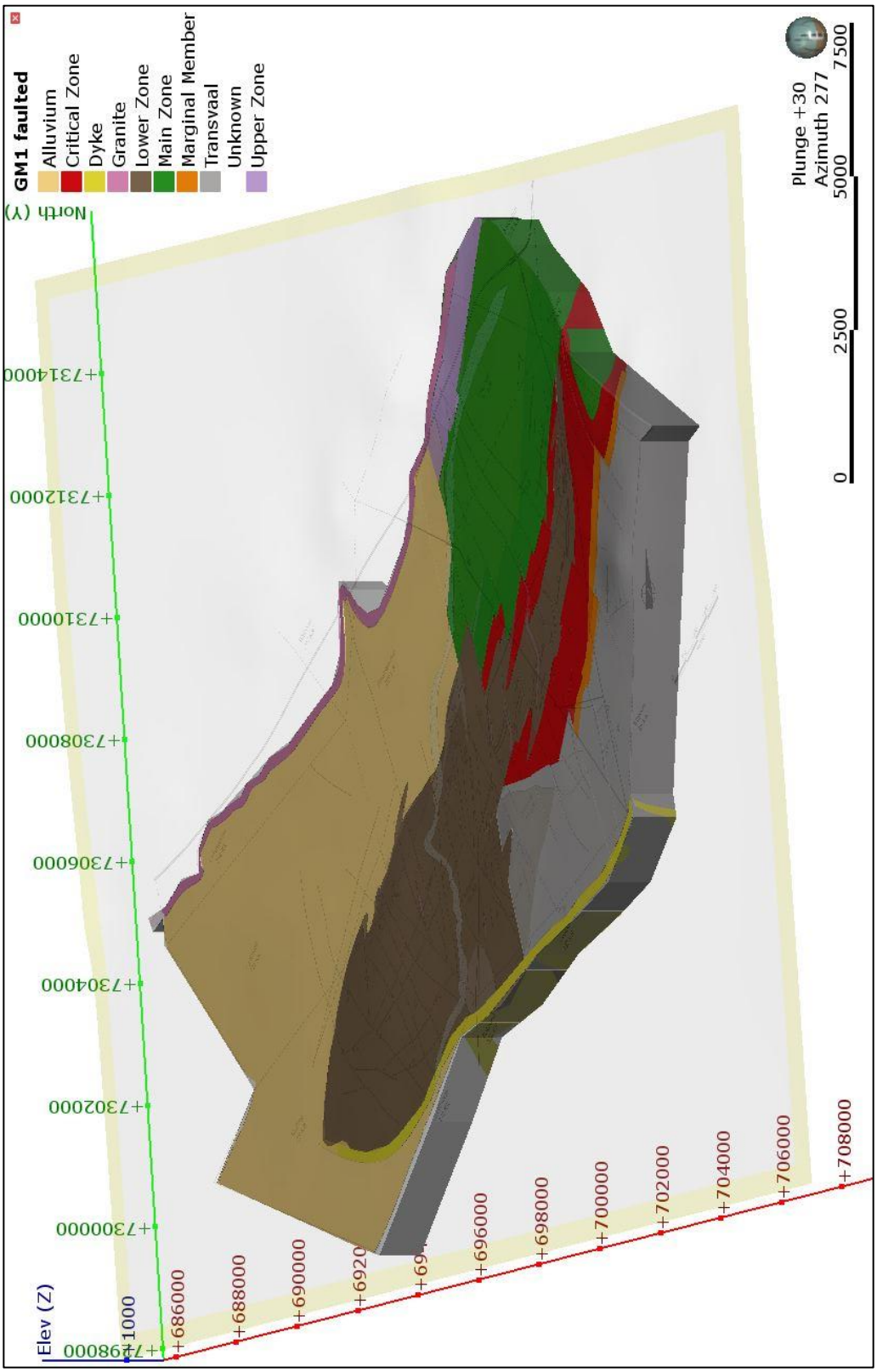

Figure 5.10: Orthographic view of the modelled geological volumes of the Grasvally area. Structural data obtained from Hulbert (1983).

The borehole data was then introduced to the model to further constrain the distribution of the various stratigraphic units. The lithological logs have been simplified and packaged into stratigraphic units in order to compare the data to that of Hulbert (1983). The lithological units have been packaged into Transvaal, Lower Zone, Marginal Member, Mafic Critical Zone, Mottled Critical Zone, and Main Zone (Figure 5.11). Three-dimensional surfaces were generated (Figure 5.11) for each unit with the use of the contacts and structural data as mapped by Hulbert (1983) and the logging data compiled within this study.

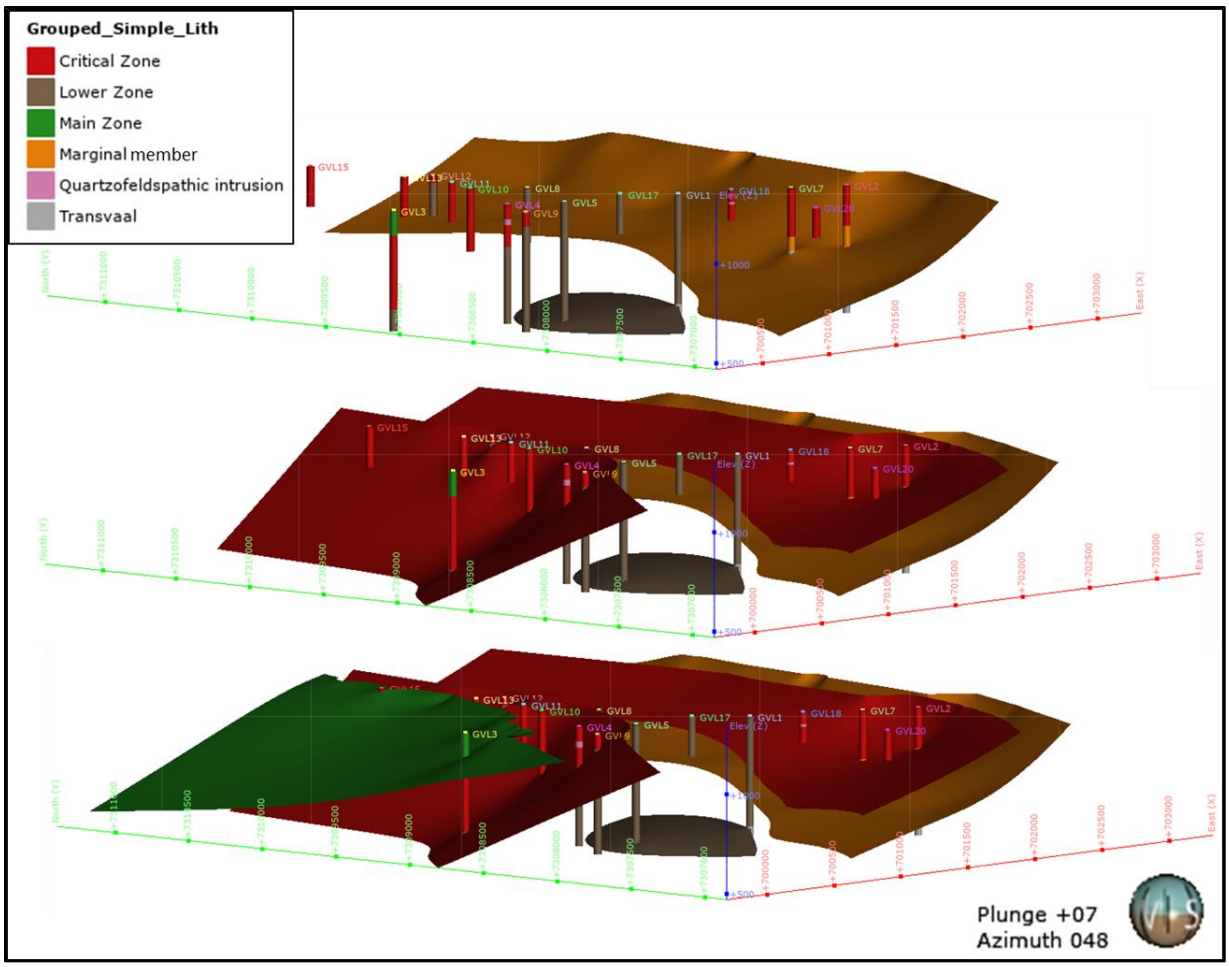

Figure 5.11: Three-dimensional surfaces further constrained with the use of simplified borehole data showing the general orientation of the contacts as well as the dip of the volumes to the east and to the west of the major N-S trending fault.

The three-dimensional model was then generated from these surfaces following the same procedure as with the model for the greater area. The borehole data constrains the volumes at depth, proving insight into the morphology of the RLS in this area and the effect of the structures (Figure 5.12).

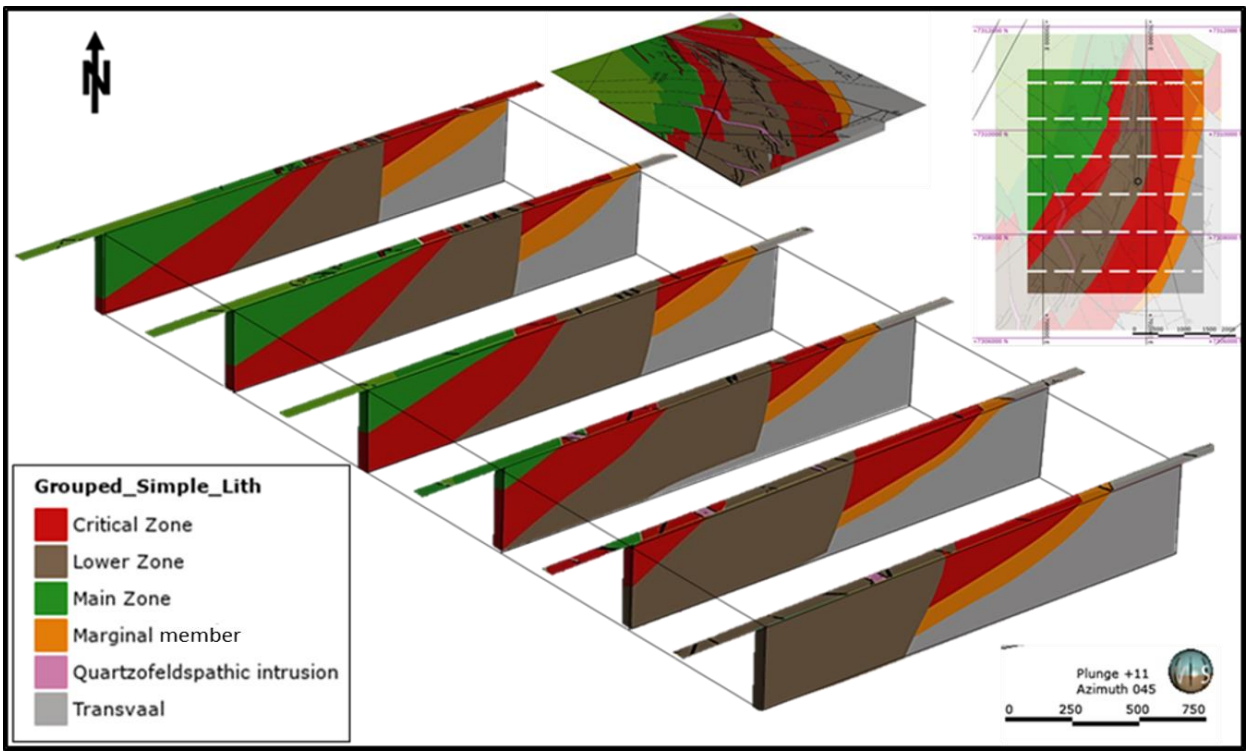

Figure 5.12: Exploded view of the Grasvally area with stratigraphic units and structural data projected from surface mapping. Orthographic exploded view is to the north.

5.3 Interpretation of three-dimensional Modelling

The stratigraphy comprises nine units which are separated by geological contacts. The geological model was generated through the framework outlined in Figure 5.1.

This section aims to summarise the findings of the geological modelling as well as providing comparisons to known published works. The findings of the modelling are discussed in terms of the structural interpretation and the structural features.

5.3.1 Stratigraphic Interpretation

On the comparison of the simplistic model, based only on the surface structural mapping (Hulbert, 1983), and the model generated by incorporating the core logging undertaken in this study, several key features are noted:

The dip of the footwall to the east of the area, which comprises quartzites of the Magaliesberg Formation of the Transvaal Supergroup, displays a flattening as the quartzites are intersected at

shallower depths within the core, at 305.51 m, 315.60 m, and at 522.00 m in GVL 2, GVL 7 and GVL 1, respectively. The dip of the footwall shallows from the east to the west from ~30° W (Hulbert, 1983) to ~5° W between boreholes GVL 2 and GVL 7 (Figure 5.13).

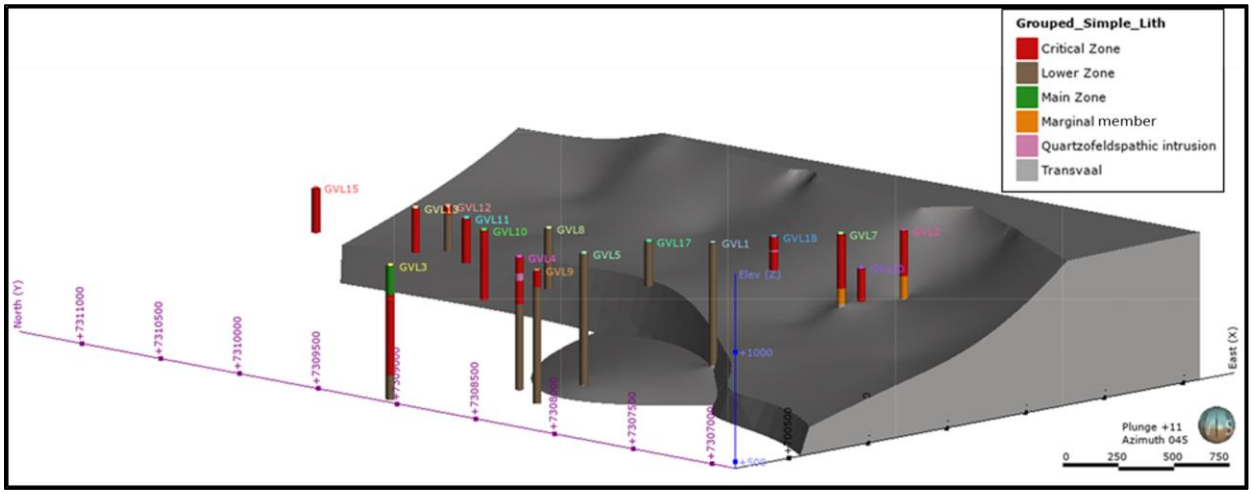

Figure 5.13: Orthographic view of Transvaal volume from a south-west perspective.

GVL 1 and GVL 5 display significantly deeper Transvaal intersections at 552.00 m and 568.48 m respectively in comparison to boreholes GVL 2 and GVL 7 at 305.51 m and 315.6 m respectively. This is interpreted as the result of a north-south trending fault running between boreholes GVL 7 and GVL 1 (Figure 5.14 and Figure 5.15).

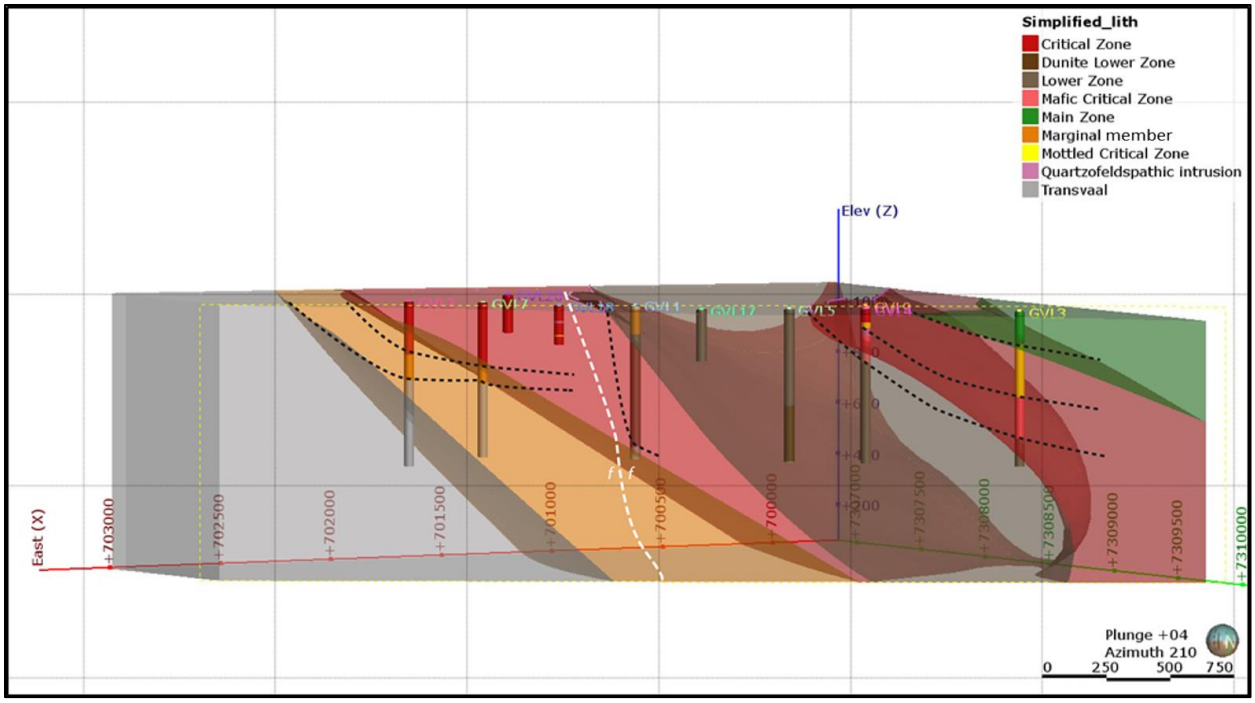

Figure 5.14: Sectional view of the Grasvally body looking south. Inferred boundaries in black stippled lines, and fault in white stippled line. The orange unit represents gabbronorite which was interpreted as being part of the marginal member however modelling shows that within GVL 1 this gabbronorite is part of the Critical Zone.

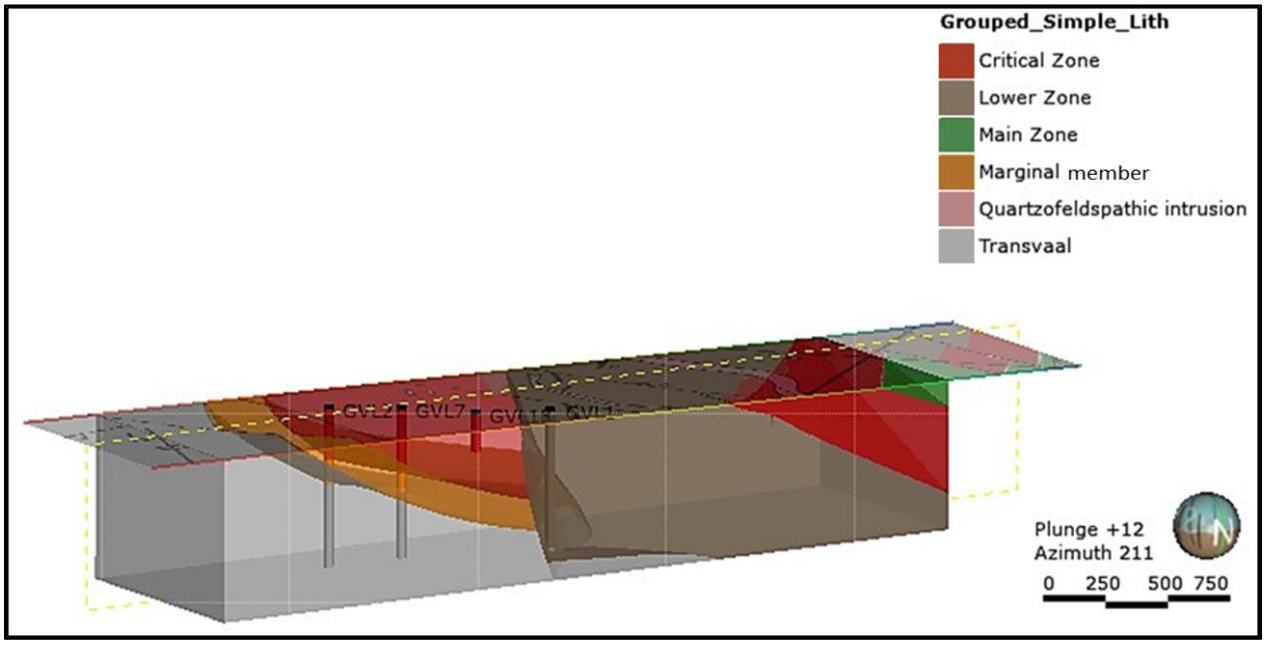

Figure 5.15: Sectional view of the Grasvally body looking south. Boundaries have been further constrained by the incorporation of simplified borehole data.

The western block of the Transvaal unit displays a downthrow of ~180 m (Figure 5.13). This fault has been correlated with the Grasvally Fault - a N-S trending reverse fault (Hulbert, 1983, Verbeek and Lomberg, 2005), however, analyses of the 3D model shows that although the fault orientation is N-S, the sense of movement along this fault is normal. To the east of the fault, the overlying marginal member and Critical Zone also display a conformable shallowing dip with depth consistent with the orientation being controlled by the footwall (Figure 5.14 and Figure 5.15).

To the east of the area, the boundary between the Lower Zone and Critical Zone dips approximately 70° W which contrasts with the average 45° W dip of the Lower Zone which was inferred from the orientation of the chromitites (Hulbert, 1983) (Figure 5.14 and Figure 5.15). The orientation of the LZ - CZ contact in the east is interpreted as being controlled by the north-south trending fault (Figure 5.14 and Figure 5.15) along which the Lower Zone is suggested to have been uplifted (Hulbert and Von Gruenewaldt, 1982; Hulbert, 1983; Hulbert and Von Gruenewaldt, 1985). This is congruent with the general 70° W orientation of shear planes noted in association with this structure (Hulbert, 1983). The boundary between the Lower Zone and Critical Zone to the west is shallower, displaying a dip of ~45° W which is within the range of the chromitites as observed by Hulbert (1983) as well as the orientation within the northern limb.

The boundary between the Critical Zone and the Main Zone is slightly shallower than the underlying LZ - CZ boundary at ~30° W (Figure 5.16) which is in agreement with the dip recorded by Hulbert (1983) as 28° W (Figure 5.14 and Figure 5.15).

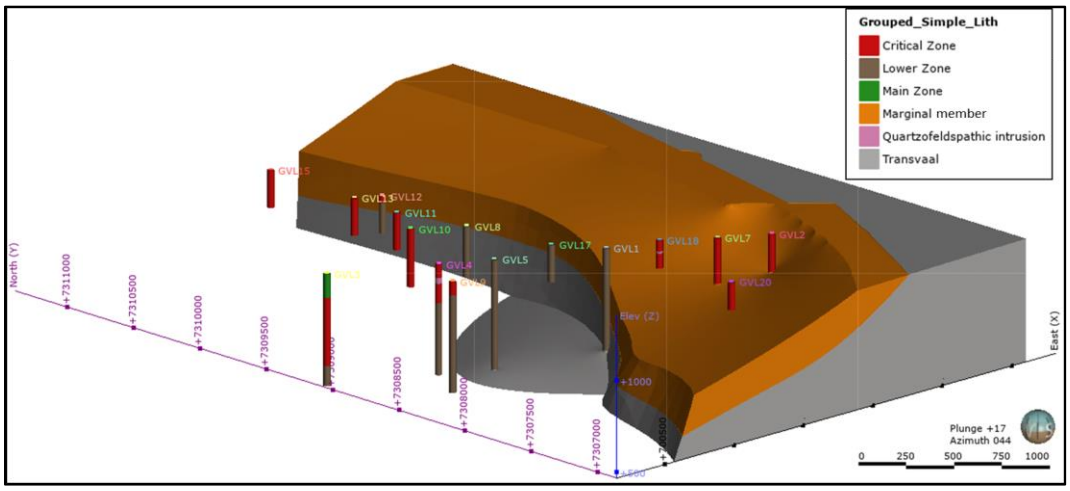

Figure 5.16: View of eastern section exposing the morphology and orientation of the marginal member and underlying Transvaal unit.

The gabbronorite intersected at the top of GVL 1 which was previously interpreted within this study, based solely from field descriptions of the lithology, as the same as that within the marginal member does not correlate with the position of the marginal member volume generated in both models. This unit is therefore interpreted as being different from the Maz and being possibly a portion of country rock assimilate preserved along the CZ-LZ boundary. The gabbronorite is only reported by Hulbert, (1983) to occur below the Critical Zone and overlying the Transvaal metasedimentary rocks therefore the gabbronorite unit is interpreted as marking the transitional zone between the LZ and CZ as LZ in GVL 1 (Figure 5.13).

The dip of the Main Zone, at approximately 30° W (Hulbert, 1983) holds true as both geological models intersect the Main Zone in borehole GVL 3 at the same height (Figure 5.17). Borehole GVL 15 is collared in lithologies of the Critical Zone; this is in contrast with the work of Hulbert (1983) who mapped Main Zone lithologies at this location (Figure 5.3). GVL 15 being collared in the Critical Zone instead of the Main Zone is interpreted as an increase in horizontal displacement westwards by an additional 113 m along the WNW-ESE trending reverse faults (Figure 5.10).

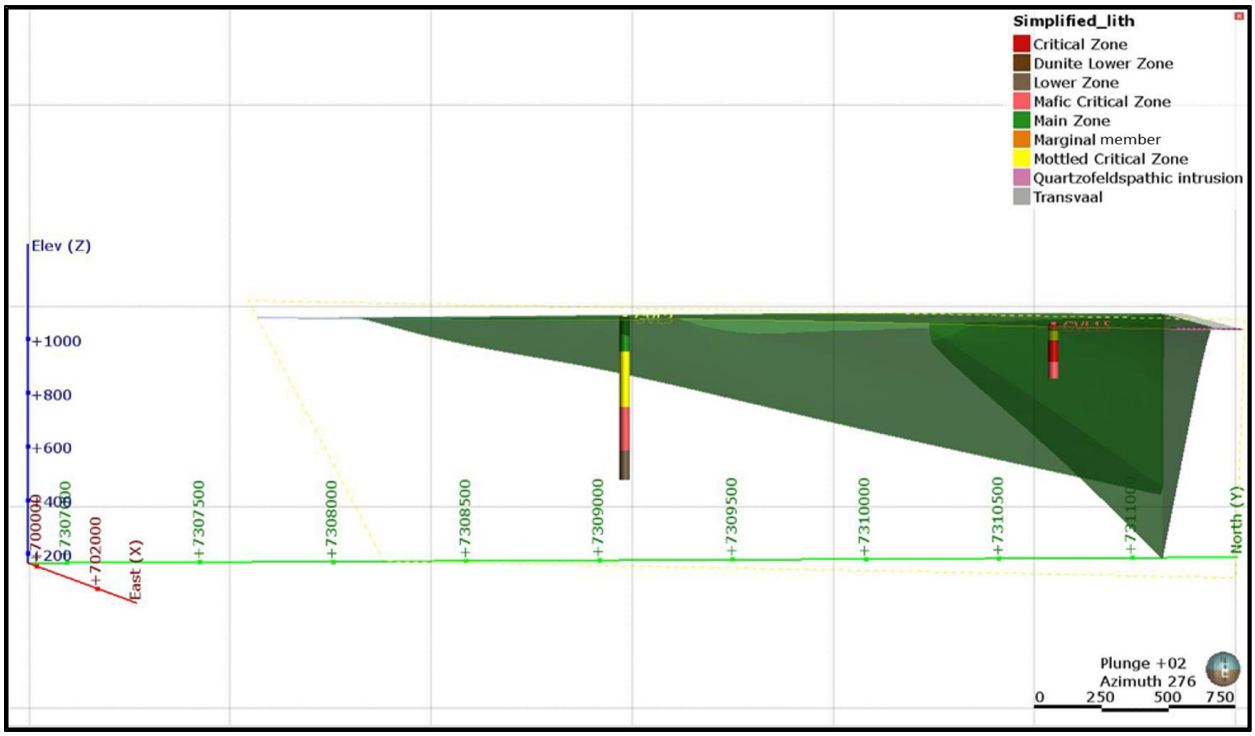

Figure 5.17: Sectional view looking east of the Main Zone volume generated from the mapping of Hulbert (1983) with the boreholes GVL 3 and GVL 15 plotted against it.

The dip of the Lower Zone in the west between boreholes GVL 4 and GVL 13 has been generated with the incorporation of the surface data and borehole data however it is highly reliant on the software algorithm to determine the dip at depth as the boreholes (GVL 4, GVL 10, GVL 11 and GVL 13) were not drilled deep enough to intersect the Lower Zone beneath the Critical Zone or did not intersect any critical marker horizons that could be used for correlation. The general dip for the LZ is ~35°W.

5.3.2 Structural features

The main structural features within block A (Figure 2.10) are fault generations 1 and 2 as detailed by Hulbert (1983). The first generation of faults brought the LZ to surface as a horst block sandwiched between the CZ to the east and to the west. The faults are generally north-south orientated reverse faults along the contact between the LZ and the CZ. The vertical displacement caused by this event is up to 800 m, as the LZ has been thrust upward into the CZ (Hulbert, 1983). The exact displacement within block A cannot be determined due to the extensive and varying serpentinisation of the LZ. The 3D modelling revealed a downthrow of at least 180 m within the western block which contradicts the findings of Hubert (1983). The contact between the Lower Zone and the Transvaal metasedimentary succession has never been observed, however sedimentary rocks intersected at the base of GVL 5 show a shallowing of the dip of Transvaal footwall rocks to ~5°W. The quartzite intersected beneath the LZ could possibly also be a xenolith and not a representation of the footwall and its orientation. The Critical Zone chill above the sedimentary rocks, the marginal member, displays a dip of approximately 40°W and the overlying mafic and ultramafic package displays a dip of 20 to 25°W.

The major finding from this study contrasts with interpretations from previous work. In Figure 5.5 and Figure 5.15 only a single major fault occurs, which trends north-south. This inferred singular fault is not consistent with the Lower Zone having resulted from a horst structure between two north-south trending faults as suggested in earlier work (Hulbert and Von Gruenewaldt, 1982; Hulbert, 1983; Hulbert and Von Gruenewaldt, 1985). This interpretation of a single fault is supported by drilling on Rooipoort to the north, where the presence of a single northerly striking fault, the Grasvally fault, has been demonstrated (de Klerk, 2005; van der Merwe, 2008) and no fault intersected on the western side of the Grasvally body on the farms of Moorddift, Jaagbaan, and Grasvally (van der Merwe, 2008). On the western margin, the Critical Zone - Lower Zone

boundary dip is approximately 45° W (Figure 5.15), which is similar to that of the rest of the northern limb suggesting the relationship to be conformable and does not support the LZ being brought to surface as a horst-like block. The Lower Zone with the Grasvally chromitite layers has been intersected by exploration boreholes on Moorddrift at depths of 1 250 m, underlying Critical Zone rocks. This suggests that the Lower Zone plunges to the north (van der Merwe, 1978, 2008) and is tentatively projected to continue north of the Ysterberg-Planknek Fault.

5.3.3 Summary

The 3D modelling of the Grasvally area provides insight into the morphology and orientation of the individual stratigraphic units. To the west of the LZ, the units follow a conformable stratigraphic order of LZ, CZ to MZ with increasing height (Figure 5.12). The units dip ~35°W which is consistent with the average dip angles observed within the shallow western dip of the northern limb (45°W to 10°W) (van der Merwe, 1978, 2008). The stratigraphy in the west is complicated by the planar offsets exceeding 650 m along strike-slip faults (Figure 5.9) which hinder correlation of units between boreholes.

The most notable feature is the CZ-LZ contact to the east of LZ. The modelling of the area based solely from structural data including surface mapping (Hulbert, 1983) supports the interpretation of the LZ as being a horst-like body, brought to surface along two steeply dipping north-south trending faults. When the data is further constrained with the use of borehole logging data, the steep 70°W dipping fault to the east of the LZ is apparent due to the down-throw within the Transvaal unit of ~180 m along a normal fault (Figure 5.16). This fault could have acted as a pathway for the MANO to intrude, bringing the MANO and marginal member into contact with the LZ, unconformably at this steep an angle.

CHAPTER 6

Discussion

The Grasvally area displays a distinctly different stratigraphy to the rest of the RLS and is bound by two surface expressions of the Thabazimbi-Murchison lineament, the Zebediela Fault to the south and the Ysterberg-Planknek Fault to the north (Figure 2.5). The area is further complicated by four generations of faulting which has made the correlation of layers in the Grasvally area difficult (Figure 2.10). Extensive serpentinisation has contributed to the lack of clear marker horizons within the mafic and ultramafic units. Nevertheless, the results of this study contributes to (i) the greater understanding of the RLS in the Grasvally area, (ii) determining key marker horizons in order to allow for correlation of units as well as (iii) the impact of the structural features on the magmatic history of the GNPA and LZ in this part of the northern limb.

6.1 The stratigraphy of the Grasvally area

The Ysterberg-Planknek Fault has clearly exerted a strong control on the development of the RLS in the northern limb. While ultramafic sequences interpreted as LZ seem to be present both north and south of the Y-P fault, that in the Grasvally area contains chromitites that are more primitive than any in the CZ elsewhere in the RLS. Pyroxenitic, noritic to anorthositic rocks stratigraphically overlying the LZ that would traditionally be classified as CZ include the GNPA south of the Y-P fault and the Platreef to the north (Figure 2.5). As the GNPA member is seen to plunge to the north, it is thought that the GNPA member and the Platreef could merge at depth. The GNPA member of Grasvally has been correlated with the Platreef to the north due to the similar stratigraphic position of these units (McDonald *et al*., 2005; Maier *et al*., 2008; van der Merwe 2008, Smith *et al*., 2014). This study made use of geochemical variations as well as key marker horizons in order to define and compare the stratigraphy of the Grasvally area with the rest of the RLS (Figure 6.1).

6.1.1 Footwall

Based on the intersections with the floor rocks in GVL 1 and GVL 2, the quartzite at the base of the RLS dips towards the northwest where it is unconformably overlain by ultramafic rocks of the Lower Zone (LZ) (Figure 5.13). The Transvaal metasediments-RLS discordant contact is intersected on both sides of the N-S trending fault. To the west of the N-S trending fault, the

footwall- RLS contact shallows in dip from east (~30° W) to west (~5° W) with the Critical Zone equivalent overlying this unit (Figure 6.2).

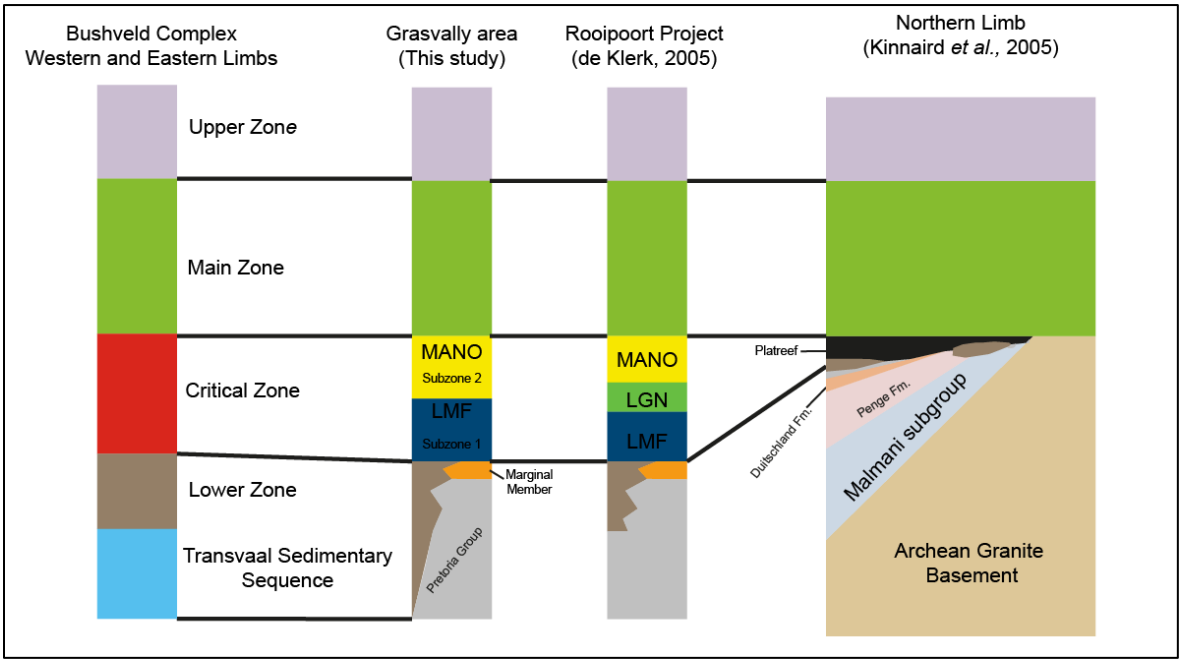

Figure 6.1: A schematic diagram displaying the differences and similarities in stratigraphy between the eastern and western limbs of the Bushveld Complex, the Grasvally area, the Rooipoort Project (de Klerk, 2005) and the generalised northern limb stratigraphy (Modified from Kinnaird *et al.* (2005)).

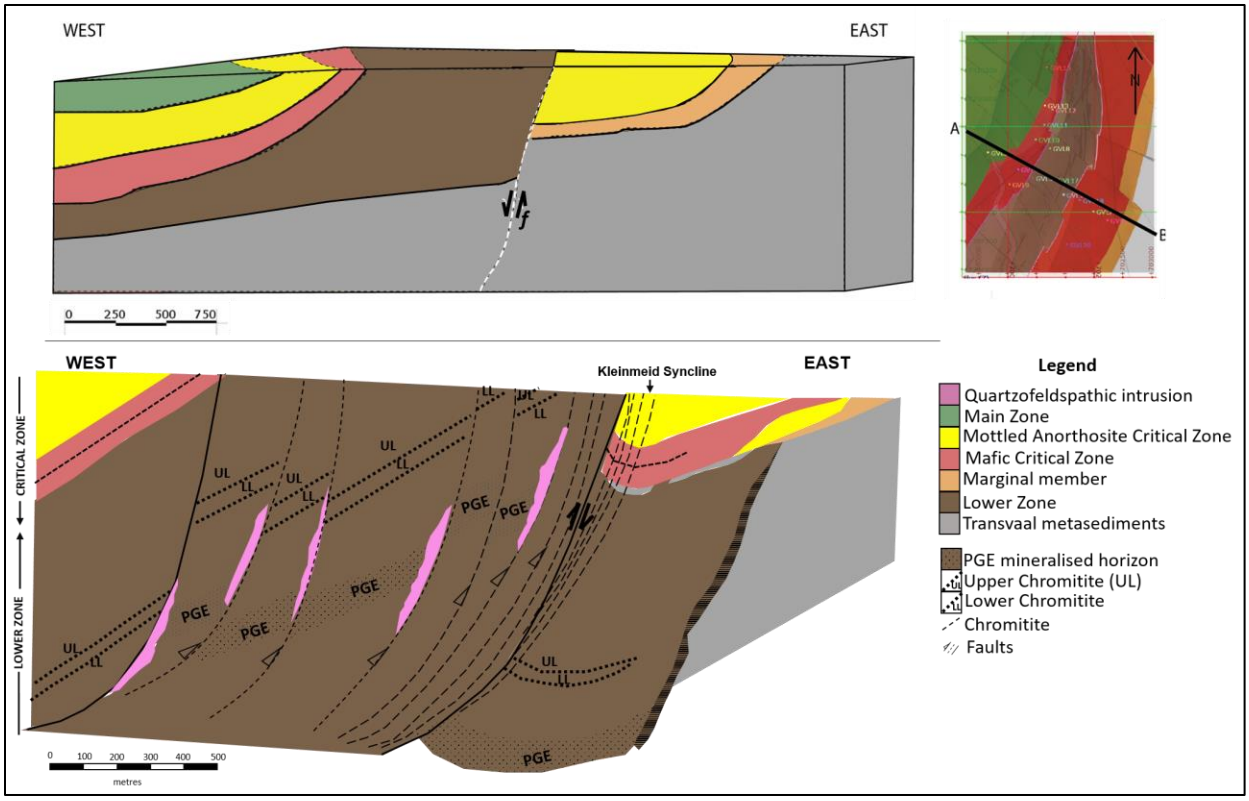

Figure 6.2: Comparison of cross sections of the Grasvally area. (top) Interpreted cross sectional view A-B of the Grasvally area considering borehole data and structural data (Hulbert, 1983). The cross section is compared to the adapted idealised section of Hulbert (1983) and highlights the differences in stratigraphy in the east of the area. The lithologies have been simplified into stratigraphic units.

Gravity surveys undertaken by Barrett *et al.* (1978) depict a more complex footwall morphology due to the presence of numerous strike-slip and normal faults which cause duplications of layers in the overlying strata as well as blocks of footwall to be thrust into the overlying LZ lithologies (Figure 6.3).The spacing of the boreholes, along with the vertical orientation of the drilling, would make it difficult to intersect steeply dipping faults observed within this area (Figure 2.10) and thus the step-like nature of the floor rocks was not observed in the modelling interpretation within this study (Figure 6.2). The Transvaal intersection in GVL 1 may be one of these step-like blocks which has been downthrown by 180 m, or it may be the result of a larger fault which separates the eastern and western blocks (Figure 5.15). If this intersection is the result of the major north-south trending fault, the Grasvally Fault, the downthrow in the western block would suggest movement resulting from normal faulting as opposed to reverse faulting as initially interpreted by Hulbert (1983).

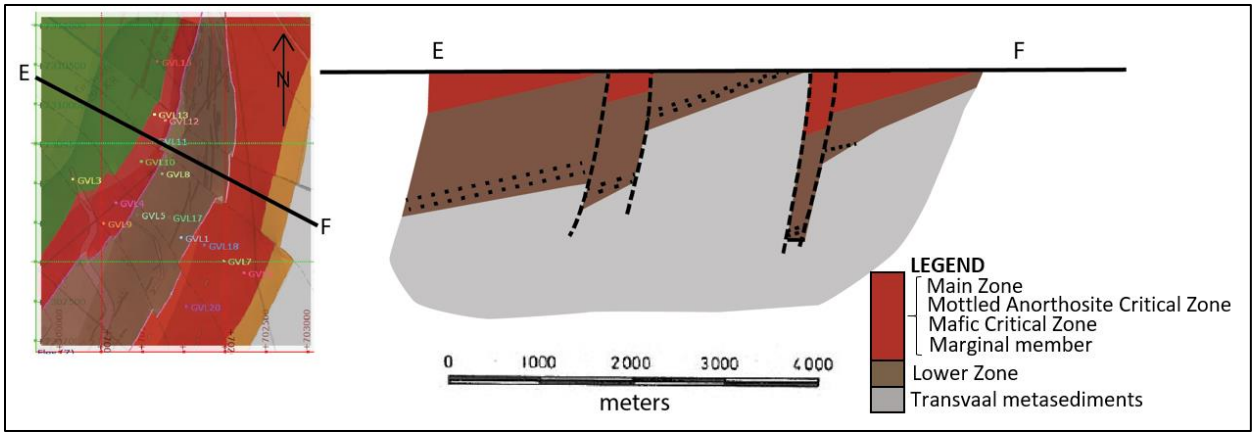

Figure 6.3: Interpretation of the footwall geometry through the use of gravity data taken along cross section E-F showing the complex nature of footwall lithologies (Barrett *et al.*, 1978). The marginal member, Critical Zone and Main Zone have been represented within this diagram as one unit (seen in red) after Barrett *et al.* (1978). The dotted lines represent the chromitite layers within the Lower Zone.

The footwall in the Grasvally area is interpreted as Pretoria Group quartzites which is the youngest footwall relative to the rest of the northern limb. The quartzites are consistent with the floor rocks described and mapped by Hulbert (1983). The northern limb, including the Grasvally area, displays a transgressive relationship with the footwall aging in a northerly direction (Hall, 1932; van der Merwe, 1976, 2008; Button, 1976; Kinnaird *et al*., 2005). These quartzites are also noted to occur as xenoliths, mechanically entrained within the layered body as seen in GVL 1 (Figure 3.3) and the idealised section of the area by Hulbert (1983).

The quartzites display low magnetic susceptibility values in comparison to the overlying gabbronorites in the east and the dunite and harzburgites of the LZ to the west (Figure 3.28). The low magnetic susceptibility is due to the quartzites being relatively pure quartz arenites, with the exception of the samples bearing magnetite and ilmenite that would have contributed negligibly to the contamination of the Rustenburg Layered Suite. To the north, on the farm of Rooipoort and further north of the Ysterberg-Planknek Fault, calc-silicates are seen to occur as xenolithic bodies which are a source for contamination, however, these do not occur within the Grasvally area. Quartzite intersected at the base of the LZ (core GVL 5) is interpreted as a raft or xenolithic body within the LZ as seen within GVL 1 (at depths of 0 m - 13. 85 m, 46.53 m - 48.95 m and 58.36 m - 71.98 m) rather than an *in-situ* footwall intersection beneath the LZ. Deeper drilling is recommended in order to verify this.

The quartzite intersected at the base of the LZ displays a slightly different magnetic signature (~0.03 SI units) in comparison to that of the quartzites (0.00 SI units) that occur as confirmed xenoliths (GVL 1) and beneath the CZ in the east of the area (GVL 2). The slightly elevated magnetic susceptibility is due to finely disseminated magnetite and ilmenite within the quartzite. The quartzite-LZ contact displays anomalously high Cu values. The elevated Cu horizon is similar to that observed at the Platreef-footwall contact further to the north where more well-defined massive chalcopyrite is found (Sharman *et al*, 2013) These sulphides are generally not associated with PGEs, unlike the rest of the Bushveld Complex, due to post-emplacement hydrothermal remobilisation of PGEs (Hutchinson and McDonald, 2008).

6.1.2 Lower Zone

The ultramafic package comprising dunites, harzburgites, serpentinised harzburgites and pyroxenites is consistent with the detailed petrographic descriptions of the Lower Zone (LZ) rocks described in the area by Hulbert and Von Gruenewaldt (1982) and Hulbert (1983) (Figure 3.27). The LZ is characterised by two prominent chromitite layers, a low proportion of interstitial plagioclase, a high Mg# as well as relatively low concentrations of sulphide Ni and Cu.

The low proportion of interstitial plagioclase is comparable to that of the Clapham section of the eastern limb and for the LZ elsewhere in the Bushveld Complex which ranges from approximately 2 to 6 wt. % (Cameron, 1978; Lee and Tredoux, 1986; Teigler, 1990). Due to the low proportion of interstitial plagioclase in the LZ, an increase from 6 to 8 wt. % has previously been used to denote the transition from LZ to Critical Zone as observed in the Jaglust area of the eastern limb (Cameron, 1978). This proved an inconsistent marker horizon in the Grasvally area as a transition of 2-6% is not always easily observed in heavily serpentinised ultramafic rocks such as those intersected within this area. In the Grasvally area the top of the uppermost harzburgite unit has been taken as the top of the LZ (Figure 3.27), as suggested by Teigler and Eales (1996) for the western limb - this has allowed for a more consistent definition across boreholes irrespective of alteration. This transition is also marked geochemically by a decrease in Mg#, SiO_2/Al_2O_3 ratio and Cr content and an increase in Cu content and Sr/Al_2O_3 ratio. Above this harzburgite, the transition is visually marked by a more fine-grained pyroxenite which marks the base of the Critical Zone (Hulbert, 1983), indicative of significant cooling of the LZ having taken place before emplacement of the CZ.

Using the uppermost harzburgite as the marker for the top of the LZ sequence, the LZ package within the studied core reaches a thickness of ~1100 m whereas Hulbert (1983) reported a thickness of 1600 m. Yudovskaya *et al.* (2013) reported thicknesses of up to 800 m for the LZ underlying the Platreef and thicknesses of 1300 m were reported for the Olifants River Trough of the eastern limb (Cameron, 1978). The relative thickness of the LZ within the Grasvally area is suggested to be due to its close proximity to a feeder system for the northern limb associated with a gravity high, to the northwest of this deposit (van der Merwe, 1978; Finn *et al.*, 2015). The Thabazimbi-Murchison Lineament (TML), which forms the boundary of this deposit to the south and north, has also been suggested by various authors as a possible feeder system (White, 1994; Kinnaird, 2004; Kruger, 2005; Kinnaird, 2008) making the position of the Grasvally deposit favourable to the two suggested feeder systems.

The LZ to the east abuts unconformably against Transvaal quartzites, the marginal member and the MANO of the CZ (Figure 5.12). This 70°W dipping contact coincides with the Grasvally Fault which was initially interpreted as one of two N-S dipping faults along which the LZ was brought to surface (Hubert, 1983). However, this was later interpreted as a singular fault along which the LZ abutted (van der Merwe, 2003). This fault could have acted as a plane along which CZ magma intruded preferentially, forming the MANO to the east and west of the LZ and enveloping the LZ (Figure 5.15).

The LZ rocks also display distinctly elevated Mg# (93), these are some of the most primitive values recorded within the Bushveld Complex and are comparable to the values determined within the Grasvally area by Hulbert and Von Gruenewaldt (1985). These primitive Mg# are comparable to those observed within the Sandsloot and Turfspruit areas within the northern limb to the north of the Ysterberg-Planknek Fault (Yudovskaya *et al*, 2013) as well as the Basal Ultramafic Sequence (BUS) intersected at the base of the LZ in the Clapham section of the eastern limb (Wilson, 2012, Wilson, 2015). Subdivisions within the LZ in the cores examined from the Grasvally area are extremely hard to determine due to the extensive serpentinisation of the original lithology as well as visually indistinct units.

The presence of a thick, laterally extensive succession of LZ rocks is unique to this area south of the Ysterberg-Planknek Fault. To the north of the Ysterberg-Planknek Fault, the LZ was originally identified as sporadic isolated satellite bodies or offshoots hosted in country rocks with their

connectivity at depth uncertain (van der Merwe, 1978), however, Yudovskaya *et al.*, (2013) have more recently defined thick LZ packages underlying the Platreef on the farms of Sandsloot and Turfspruit. The LZ intersected on Turfspruit is 800 m thick and extends for over 2 km (Yudovskaya *et al*, 2013) demonstrating that the LZ to the north of the Ysterberg-Planknek Fault is more extensive than previously thought and may expand at depth. Is it also possible these thick units may be interconnected with the known satellite bodies at depth (Yudovskaya *et al.*, 2013) forming bodies similar in size to that south of the Ysterberg-Planknek Fault.

The LZ package is heavily faulted and serpentinised with the degree of serpentinisation of the harzburgites increasing from west to east, a feature that may possibly be structurally controlled (Figure 3.25). The imbricate north-south trending reverse fault, fault generation 1, may have acted as pathways for hydrothermal fluids to interact with the LZ rocks. The degree of serpentinisation may vary considerably due to the abundance of pathways available for fluid flow. The degree of serpentinisation could also have been controlled by the build-up of pressure which in turn could have caused micro-cracking, and the propagation of joints and faults (Malvoisin *et al.*, 2017). An environment of high pressure is inferred from the presence of kink-banding and excessive faulting, which could have forced the fluids along these pathways. The kink banding within olivine of the fresh dunites, akin to those noted within mantle peridotitic xenoliths and Ural-Alaskan Complexes, is not a common feature of layered intrusions although it has been noted within dunite of the LZ elsewhere in the Bushveld Complex on the farm of Turfspruit and also within the Great Dyke further north (Wilson, 1982; Yudovskaya *et al.*, 2013). This suggests that the LZ to the south of the Ysterberg-Planknek Fault has undergone similar solid-state deformation as the LZ to the north of the Ysterberg-Planknek fault (Yudovskaya *et al.*, 2013).

The LZ intersected in this area differs from that in the eastern and western limbs of the Bushveld Complex due to the presence of two thick chromitite seams which occur within the Drummondlea Harzburgite Chromitite subzone (Hulbert, 1983). These two chromitite layers have apparent thicknesses of ~0.60 m within the pyroxenite and ~0.93 m within the harzburgite. These chromitite layers can be used as stratigraphic markers within the LZ, below which a notable zone of PGE mineralisation occurs (Hulbert, 1983) (Figure 6.2). These chromitites are reported to have the highest Cr_2O_3 content (45.52 % and 40.82 % within the lower and upper chromitite respectively) of anywhere in the Bushveld Complex. Elsewhere in the Bushveld Complex, within the LZ, thin

to disseminated discontinuous chromitite stringers are documented from Overysel, through Zwartfontein to Sandsloot by Jones (2006) while disseminated (<10 %) cumulus chromite has been identified on Tweefontein and Turfspruit to Macalacaskop by Yudovskaya *et al.* (2013) and Grobler *et al.* (2019) north of the Ysterberg-Planknek Fault, and in the Basal Ultramafic Sequence (BUS) of the Clapham trough section of the eastern limb host (Wilson, 2012).

The magnetic susceptibility (MS) within the LZ is relatively high and is attributed to the serpentinisation of olivine, similar to the MS highs noted within the troctolite horizon of the Bellevue core (Ashwal *et al.*, 2005). High MS values are attributed to extensive serpentinisation followed by the concentration of magnetite as laths or bands <1 cm to 2 cm thick. Zones where there is no MS in the LZ rocks possibly signify zones where the precursor rock has been completely serpentinised and any resultant magnetite has been mobilised elsewhere by the fluids, leaving the unit barren of magnetite.

The minor elements, Ni, and Cr display varied proportions through the section due to the abundance of olivine and chromite respectively, however the LZ is seen to be characteristically depleted in Cu, Ni in sulphide form and PGE's (McDonald and Holwell, 2007).

The contact between the LZ and the Critical Zone is marked by a fine-grained pyroxenite, and to the east of the LZ the footwall- CZ boundary is marked by a unique package of gabbronorites and norites; the marginal member.

6.1.3 Marginal member

The contact between the LZ and the Critical Zone to the east of the LZ is marked by a unique package of gabbronorites and norites termed the marginal member. This package is only intersected on the east of the farm, overlying the Pretoria Group quartzites. The marginal member observed is correlated to that of Hulbert (1983) and the Marginal Zone as defined by de Klerk (2005) and van der Merwe (2008) (Figure 6.1). The Marginal Zone of the eastern and western limbs occurs below the LZ and is not directly correlated with the marginal member as they occur at different stratigraphic positions.

The gabbronorites are fine-grained, dark grey in colour and grade upwards into more medium-grained units with disseminated sulphide specks. The fine-grained gabbronorite with quartzite xenoliths is separated from the underlying quartzites by a granofels formed due to the mixing of

the gabbronorite and quartzite. The marginal member as described, only occurs above the quartzites and not where the CZ unconformably overlies the LZ (Hulbert, 1983).

The marginal gabbronorite displays no clear major element trends. This could be a result of contamination due to the mixing between the marginal member magma and the underlying quartzite. The Mg# decreases up section (73.37 at 288.61 m - 59.29 at 219.55 m) indicative of a normal fractionating sequence with two resets occurring at 231.15 and 219.35 m. These resets are seen as a change from a decreasing to an increasing trend in Mg# and are possibly the result of an influx of new magma into the system. The SiO_2/Al_2O_3 and Al_2O_3/FeO+MgO ratios are fairly constant throughout the unit, however the ratio of Sr/Al_2O_3 varies greatly throughout this unit. The marginal member gabbronorite displays a distinct magnetic susceptibility profile as it has much higher MS values in comparison to the gabbronorites of the Critical Zone. The magnetic susceptibility signature is due to the pods of fine-grained chromite with interstitially disseminated ilmenite and magnetite. The disseminated ilmenite is present throughout the unit and persists into the overlying CZ which is visible in hand sample as oxidised rusted specks and as fine disseminated intercumulus grains under reflected light.

The upper more medium-grained portion of this gabbronorite comprises notable disseminated chromite, pyrrhotite and chalcopyrite specks. The gabbronorites are also characterised by the presence of phlogopite in proportions of up to 15 %. The presence of xenoliths of anorthosite, possibly from the MANO or subzone 2 (Figure 3.10 c), and angular pyroxenite xenoliths with associated interstitially disseminated pyrrhotite and chalcopyrite as well as anorthosite fragments (Figure 3.10 b) which are interpreted as being from the LMF (subzone 1) or the LZ, are indicative of an intrusion of magma post solidification of the Critical Zone to form the marginal member. The presence of heavily disseminated chromite, pyrrhotite and chalcopyrite is interpreted as being a result of either (i) a later CZ sill which intruded preferentially along the footwall-LZ contact, or (ii) Main Zone magma intruding preferentially along the marginal member - footwall quartzite boundary as is reported to occur at the LMF-MANO boundary on the farm of Rooipoort (de Klerk, 2005).

6.1.4 Critical Zone (GNPA member)

The Critical Zone in the study area comprises two subzones. A lower mafic dominated package termed Subzone 1 (Figure 6.) which comprises varieties of dunites, harzburgites and pyroxenites. Subzone 2 is a leucocratic unit which comprises varieties of pyroxenites, gabbronorites, norites, mottled anorthosites and anorthosites (Figure 6.).

Subzone 1

The package of variably textured pyroxenites, feldspathic pyroxenites, chromitites and gabbronorites, directly above the LZ can be correlated with confidence with the Lower Mafic Unit (LMF) of the Grasvally Norite-Pyroxenite-Anorthosite (GNPA) member as described by de Klerk (2005) on Rooipoort or subzone 1 of Hulbert (1983) for the Grasvally area (Figure 3.27).

The pyroxenite package has been taken as the base of the LMF and subsequently the base of the GNPA member, as it displays a sharp decrease in Mg# SiO_2/Al_2O_3, MgO and Cr content and a sharp increase in Ni, Cu, Sr/Al_2O_3 compared to the underlying LZ (Figure 4.8, Figure 4.9, Figure 4.10). This pyroxenite is seen to be visually distinct as it is fine-grained at the contact with the LZ and is interpreted as a textural result of CZ magma intruding and being emplaced above an already cooling LZ. The transition from LZ to the LMF or Subzone 1 is marked by a visible increase in feldspar content up-section as the Lower Zone is generally deficient in feldspar. Due to extensive serpentinisation, the increase in feldspar is only evident when >15 %, thus this transition does not serve as a very accurate marker horizon. The modal abundance of clinopyroxene within the GNPA member is relatively higher in comparison to the underlying LZ ranging from <5 % to 40 % cpx which is similar to the values reported for the GNPA member by Smith *et al.* (2014) but contrasts to the values (<10 %) for the upper Critical Zone (Cameron 1982; Maier and Barnes 1998). The LMF or subzone 1 is further distinguished from the LZ due to its lower magnetic susceptibility (0 to 0.003 SI Units) (Figure 3.24) which contrasts with the relatively high magnetic susceptibility of the LZ which varies significantly due to serpentinisation.

The mineralisation within this subzone is associated with the pyroxenites and feldspathic pyroxenites. Sulphides within the GNPA member are not confined to a particular lithological unit but are distributed in a varied manner throughout the package (Smith *et al.*, 2014). This is in

contrast to the upper Critical Zone elsewhere in the Bushveld Complex as mineralisation in the eastern and western limbs occurs in discrete layers.

de Klerk (2005) noted five mineralised horizons within the LMF, of which four display a correlation with elevated chrome values. The Critical Zone on Grasvally is a palladium-dominated deposit, with a ratio of approximately 1:2 Pt:Pd on average (Figure 4.16). The average Pt:Pd ratio does not depict the variation in Pt:Pd ratios as is seen within the varying composite reefs that make up the Platreef (Kinnaird, 2005b) (Table 6.1).

The ratio within the LMF is very similar to that observed within the Lower Middle Pyroxenite of the Platreef intersected on Turfspruit (Table 6.1) (Kinnaird, 2005b). The LMF and the MANO on the farm of Rooipoort also display differences in Pt/Pd, with ~ 1:2 in the LMF and ~1:1 in the MANO (Maier *et al.,* 2008). McDonald and Holwell (2011) and Smith *et al.* (2014) also reported Pd dominant results. Within this study the general Pt:Pd ratio ranges from approximately 1:2 to 1:1 where chromitite layers occur (Figure 4.16). The Pt:Pd ratios are dissimilar to that of the ~1 m thick chromitite (~1.9) occurring within subzone 1 observed by Hulbert (1983) which has been thought to be the equivalent within to the UG2 within the upper Critical Zone (Van der Merwe, 1976; van der Merwe, 1978; Hulbert, 1983).This UG-2 like chromitite is correlated with the L3 mineralised unit of de Klerk (2005) which similarly hosts a ~1 m thick chromitite and associated PGE mineralisation. As the Pt:Pd ratio is a function of the mantle source of which the magma is derived, the GNPA member is interpreted as being derived from the same source as the Platreef in the northern limb north of the Ysterberg-Planknek Fault.

de Klerk (2005) noted a broad zone of mineralisation within the LMF associated with disseminated sulphides and no elevated Cr values. This zone of mineralisation (termed the LSB) is marked by an increase in base metals, predominantly Ni (de Klerk, 2005). Based on the petrographic analysis, chalcopyrite occurs as rims around pyrrhotite which is the dominant sulphide. Within this area, Ni (ppm) is used as an indicator of sulphide mineralisation and as a geochemical marker for this mineralised horizon as described by de Klerk (2005). Typically, ultramafic rocks comprise an abundance of silicate-hosted Ni, with pyroxenites and peridotites averaging 1 500 ppm and 2 000 to 3 000 ppm background nickel respectively and peaks of up to 4 000 to 6 000 ppm indicative of sulphide mineralisation (Yudovskaya *et al.,* 2013). The low Cu concentrations are linked to the

lower abundance of chalcopyrite and other Cu-bearing sulphides in comparison to the Ni-bearing sulphides.

Subzone 2

The MANO or subzone 2 is a lithological package of dominantly leucocratic rock types comprising anorthosites, mottled anorthosites, norites, gabbronorites and pyroxenites. This subzone has no notable magnetic susceptibility, with the most notable feature being the mottled anorthosite units which occur within it.

The Mg# displays an upward decreasing trend which is interpreted as a normal differentiating sequence. The differentiating sequence is terminated where pyroxenites and mottled anorthosites are present. The relatively elevated Mg# of the mottled anorthosites and pyroxenites could be due to higher proportions of Mg within these rock types in comparison to the leuco-gabbronorites. The pyroxenites within the MANO or subzone 2 are interpreted as being representative of a magma replenishment.

The visually distinct mottled anorthosite units with oikocrysts of clinopyroxene form up to ~ 30 m thick packages. Within the northern limb to the north of the Ysterberg-Planknek Fault, the contact between the Platreef and the Main Zone is marked by what is informally termed the "Disturbed Main Zone" (Yudovskaya *et al*, 2013) which comprises similar lithologies as the MANO and as well as those of the upper Critical Zone within the eastern and western Limbs of the Bushveld Complex. The mottled anorthosites within the MANO are suggested as stratigraphic markers within the Grasvally area, in the same context as the Giant Mottled Anorthosite is used in the eastern and western limbs as it occurs at the top of the Bastard Cyclic Unit which is the uppermost cyclic unit in the Critical Zone (SACS, 1980). The mottled anorthosite units, similar to the Giant Mottled Anorthosite unit, do not mark the Critical Zone - Main Zone boundary, whereas the Platreef - Main Zone boundary is generally marked by a mottled anorthosite (SACS, 1980).

The presence of subzones 1 and 2 to the west of the LZ is correlated with the far east of the section by Hulbert (1983) where subzone 2 directly overlies the marginal member (Figure 6.2). It is suggested that the CZ intruded preferentially along the fault adjacent to the LZ (Figure 6.2). The section could be representative of the east of the Kleinmeid Syncline which could explain the

presence of the ultramafic rocks of the LMF or subzone 1 to the west of the Lower Zone / Grasvally fault and not to the east. The MANO or subzone 2 unit seen to the east of the Lower Zone dips toward the west (35° W). This is in agreement with the dip of the eastern limb of the Kleinmeid syncline (25° to 40° W), although towards the Grasvally fault the dip shallows to 5° W whereas it is documented to be 5°E by van der Merwe, (2008).

6.2 Correlative Marker Horizons

Visual characteristics, mineralogy, chemistry and magnetic susceptibility of lithological units were used in order to determine marker horizons which would facilitate the correlation of stratigraphic and lithological units within the Grasvally area. The proposed marker horizons for the Grasvally area are summarised graphically in Figure 6.4.

The upper and lower chromitites occur within the upper 100 m of the Drummondlea harzburgite-chromitite subzone of the Lower Zone. The lateral continuity of the upper and lower chromitites enables a correlation of these units across the WNW-ESE trending reverse faults (Hulbert 1983). These chromitites are a key marker horizon for determining the relative position of the mineralised PGE horizon of the LZ. This marker is ineffective in cases where only the upper 600 m of the Lower Zone, the Moordrift harzburgite-pyroxenite subzone, is intersected. The transition from LZ to CZ is taken at the top of the uppermost harzburgite. This unit is distinct and easier to identify, even within serpentinised units, in comparison to the 2-6 % increase in feldspar suggested by Cameron (1987).

The marginal member is a distinct fine-grained gabbronorite and norite unit that underlies the Critical Zone above the Magaliesberg quartzite. The contrast in grain size between the marginal member and the overlying medium-grained gabbronorites allows for visual correlation in hand specimen and core. This unit also displays a distinct magnetic susceptibility signature (0.01 to 0.042 SI units) in comparison to norites intersected at different stratigraphic heights (GVL 3, GVL 4, and GVL 11) (Figure 3.28). This is a significant feature as the magnetic susceptibility of this unit can be used to differentiate it from other noritic units and allows for correlation of this stratigraphic unit between boreholes. This unit is significant in defining the base of the Critical Zone to the east of the Lower Zone outcrop and is laterally traceable across the WNW-ESE trending reverse faults (Hulbert 1983).

The LMF or subzone 1 is a distinct unit in which the ~ 1 m chromitite is also suggested as a potential marker horizon, similar to other distinct chromitite reefs of the eastern and western limbs of the Bushveld Complex (e.g. UG2 Reef).

The mottled anorthosite units are also good potential marker horizons to correlate units within the MANO or sub zone 2 of the Critical Zone within boreholes GVL 3, GVL 4, GVL 5, GVL 10, GVL 13 and GVL 15 (Figure 3.3 and Figure 3.4). The mottled anorthosite unit represents the top of the Critical Zone and can be used as to correlate the MANO or subzone 2 to the west of the LZ (Figure 6.1 and Figure 6.4).

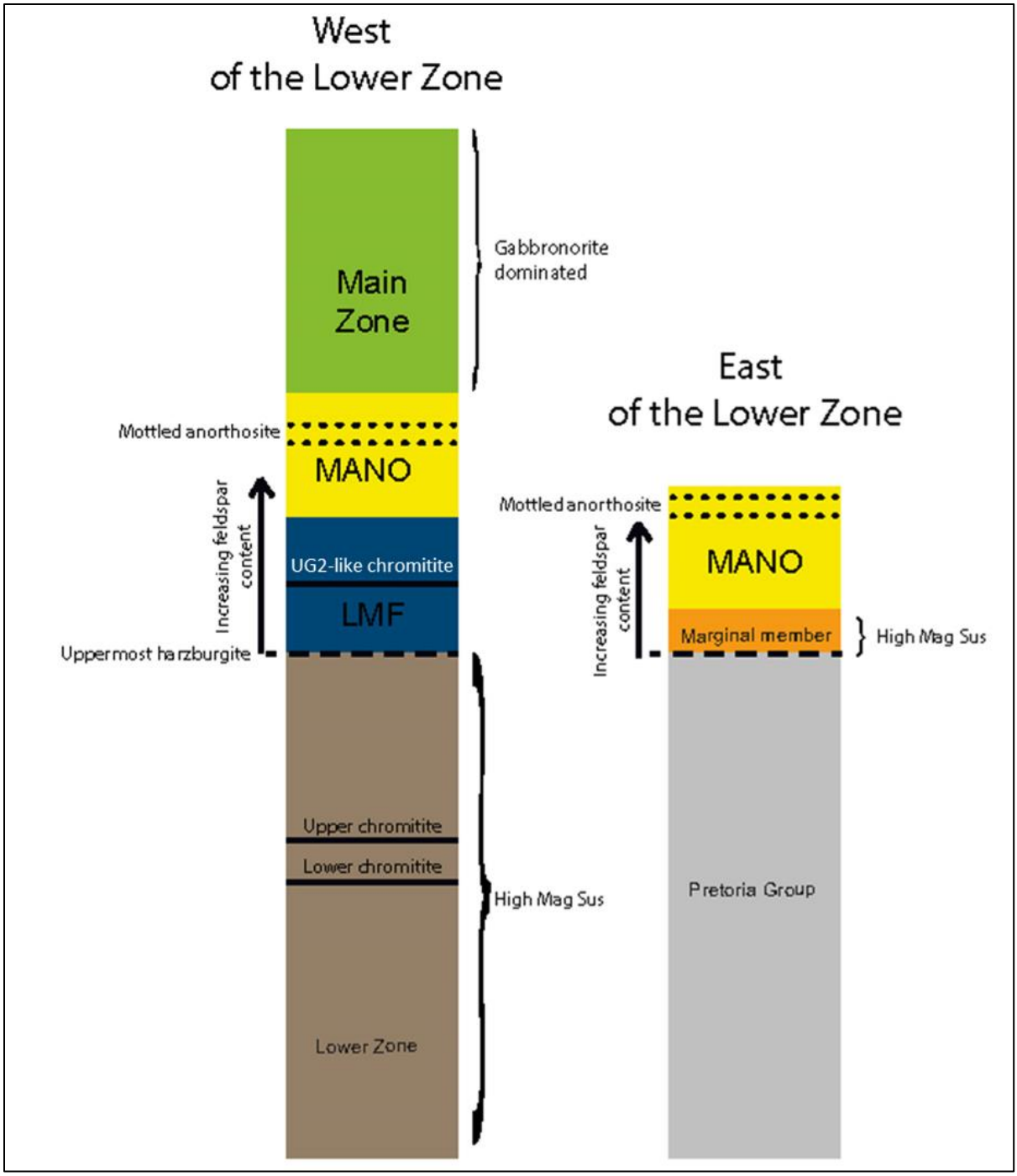

Figure 6.4: Schematic diagram of marker horizons identified, showing the mottled anorthosite marker within the MANO, the chromitite within the LMF, the marginal member with a distinct magnetic susceptibility, the Lower Zone - LMF boundary which is marked by an increase in feldspar, and the chromitite layers within the Lower Zone. These can be correlated between boreholes.

6.3 Mineralisation

Mineralisation within the Grasvally area occurs within the LZ, and within both of the subzones of the GNPA member. The LZ hosts a PGE horizon within the Volspruit pyroxenite which is stratigraphically identified as occurring within the pyroxenitic body below the distinct upper and lower chromitites.

The chromitites within the LZ are the highest grade chromitites in the Bushveld Complex averaging 54 % Cr_2O_3 (Hulbert and Von Gruenewaldt, 1982). This occurrence of chromitites up to 1 m thick within the LZ is unique to the Grasvally area as chromite only occurs as thin to disseminated bands within the LZ north of the Ysterberg-Planknek Fault. Whilst the chromitites have been mined in the past for their chromium content, there has been no recorded extraction of PGE's. However, the faulted nature of the area, has been a limiting factor in more recent mining of the area, although the old mine dumps are being re-processed by Sylvania.

The GNPA member hosts nine mineralised units within the LMF/subzone 1 and the MANO/subzone 2. The LMF hosts five mineralized units, namely the L1, L2, L3, LSB and LS (de Klerk, 2005). The L1, L2, L3, which fall under the broader LS group, are all associated with elevated chrome values. The Pt:Pd ratios are dissimilar to that of those occurring within subzone 1 observed by Hulbert (1983). This reinforces the differences between the GNPA member and the upper Critical Zone, which have been thought to be the equivalent (van der Merwe, 1976; van der Merwe, 1978; Hulbert, 1983).

The mineralisation within subzone 1 of the Critical Zone is associated with pyroxenites and feldspathic pyroxenites. This is in contrast to the upper Critical Zone elsewhere in the Bushveld Complex where mineralisation in the eastern and western limbs occurs in discrete chromitite layers or in the Merensky Reef. In Subzone 1, generally the Pt:Pd ratio is approximately 1:2 (<1), which concurs with the finding of McDonald and Holwell (2011) and Smith *et al.* (2014). The general Pt:Pd ratio changes from approximately 1:2 to 1:1 where chromitite layers occur (Figure 4.16). This means that mineralisation at Grasvally differs from the Merensky Reef where platinum is dominant with a typical ratio of 2:1 Pt:Pd or for the UG2 which is also largely platinum dominant except for north of the Steelpoort Fault (Anglo American, 2008). However, the Platreef is overall a palladium-dominated deposit (Figure 4.16) although the platinum to palladium ratio varies in the

different Platreef sills with only the upper sill showing a dominance of platinum (Kinnaird, 2005b). So, Subzone 1 has similarities in terms of Pt:Pd ratio with the lower parts of the Platreef.

CHAPTER 7

Conclusions

The stratigraphy of the Grasvally area is extremely complicated when compared to the rest of the Bushveld Complex due to its proximity to the long-lived Thabazimbi-Murchison lineament which has been active from 2.5 Ga to the present day (Good and de Wit, 2005). The major N-S trending fault plus an array of WNW-ENE trending faults which are semi parallel to the TML compartmentalise the Bushveld-aged rocks of the northern limb south of the Ysterberg-Planknek fault causing it to evolve differently to the rest of the northern limb to the north.

The LZ is approximately 1300 m thick and has been subdivided into three subzones namely the Volspruit pyroxenite, the Drummondlea harzburgite chromitite and the Moordrift harzburgite pyroxenite. The LZ in this area is thicker than that to the north of the Ysterberg-Planknek Fault and comprises significantly more primitive (Mg-rich) dunites and harzburgites than elsewhere in the Bushveld Complex. The LZ is not directly comparable to that elsewhere in the Bushveld Complex due to the presence of thick chromitite layers which only occur as disseminated layers, to thin bands at best, in the rest of the complex. The chromitites in this area are of the highest grade within the Bushveld Complex and have been mined in the past.

The stratigraphy of the area is further complicated by the LZ being flanked to the east and the west by an analogue of the CZ - the GNPA member. The LZ is unconformably overlain to the west by the GNPA member - a mineralised package comprising two subzones: The LMF or subzone 1 consists of dunites, harzburgites, chromitites, various pyroxenites and gabbronorites and a leucocratic subzone dominated by norites, gabbronorites and pronounced mottled anorthosite units. To the east of the LZ the felsic subzone 2 or the MANO, of the GNPA member has been brought into contact with the LZ along a steep~70°W dipping fault which probably facilitated access for the magma intrusion that created this subzone.

The GNPA member is a 400 - 800 m thick package comprising varieties of mafic rock types (dunites, harzburgites and pyroxenites) and more leucocratic rock types (pyroxenites, gabbronorites, norites, mottled anorthosites and anorthosites) and is subdivided into two zones, the Mottled Anorthosite (MANO) and the Lower Mafic Unit (LMF), respectively. The GNPA

member is a product of multiple magma impulses marked by sharp increases in Mg# followed by a normal fractionating trend up-section. The uppermost section of the GNPA member is correlated throughout the area based on the occurrence of three mottled anorthosite layers that occur within the MANO or subzone 2 as well as a distinctly mineralised pyroxenitic unit of the LMF or subzone 1 which hosts a chromitite unit which can be used to correlate this mineralised unit across boreholes.

Two generations of faults offset the subzones of the LZ and CZ. The geology is further complicated by the extensive serpentinisation which makes correlation of lithologies across boreholes extremely difficult. The stratigraphic units can be correlated from borehole to borehole only by using the contacts between the LZ-CZ and the CZ-MZ, where present and additionally by mottled anorthosite units or the chromitite layers.

The GNPA member intersected in this area is correlated with that studied by de Klerk (2005) further north on Rooipoort, however, on Grasvally the LGN unit of de Klerk is not present. The LMF is overlain by the MANO with no evident LGN intersected within any of the boreholes. This may be due to the fact that the Grasvally area is further away from the feeder of the LGN magma thus the injection of magma, such that the LGN, which is of MZ affinity, did not intrude this area further south.

The GNPA member as described in this study may be correlated to the Platreef in the north based on Pt:Pd ,Cu/Pd vs Cu/Ni and Pt/Pd vs Cu Ni ratios, however it may differ in terms of the degree of contamination by the underlying footwall and separation of the reef in the north by metasedimentary interlayers (Kinnaird, 2005b), The Pt:Pd ratios of the GNPA member are similar to those of the northern limb represented by the Platreef (~ 1:1) rather than the reefs of the eastern and western limbs which display distinctly different ratios (~ 2:1). The variations in the Pt:Pd ratios with increasing stratigraphic height may also be indicative of the GNPA member forming as a result of several magma impulses. The GNPA member is palladium dominant in comparison to the reefs of the eastern and western limbs which are generally platinum dominant.

The 3D geological model confirms the occurrence of the Grasvally Fault along which the Critical Zone is brought into contact with the LZ to the east of the body. The MANO or subzone 2 could have intruded preferentially along this fault. The MANO could also have been brought into contact

with the LZ as a result of reverse faulting. The proposed horst-like uplift of the LZ is rejected as no fault is observed to the west but rather there is a conformable sequence of LZ-CZ-MZ. The presence of the Kleinmeid syncline cannot be verified based on intersections to the east of the Grasvally Fault and the drilling of inclined tightly spaced holes is recommended to expose this feature.

Further Recommendations

A better understanding of the geochemical profile in this area is the next step in fully understanding the stratigraphy of the area. Certain sections of significant boreholes were not available to be sampled for this study and without this information the full geochemical profile through the stratigraphy cannot be determined which might allow for correlation of boreholes according to geochemical signatures.

Sr isotope studies have been used in the past (e.g. Seabrook *et al.,* 2005) to characterise different reefs within the Bushveld Complex, a similar approach is suggested for further studies in order to distinguish between the mineralised packages within the Grasvally area as well as to correlate these packages to those within the rest of the Bushveld Complex.

A more comprehensive study incorporating mineral chemistry of chromitites would allow for correlation and comparison of chromitites with that elsewhere in the Bushveld Complex as well as across structural trends.

A more focused study on the PGE signatures and distribution within the CZ would allow for better correlation with the Platreef to the north and to the UG2 and Merensky Reefs.

A study incorporating orientated drill core data or borehole televiewer data would aid in determining the orientation of contacts, joints and faults in order to corroborate the surface mapping undertaken by van der Merwe (1976), Hulbert (1983) and van der Merwe (2008).

Deeper drilling into the Lower Zone would aid in determining the footwall underlying the Lower Zone towards the GVL 5 drillhole (Figure 3.1).

Several maps of the GNPA member on Grasvally display striking differences especially on the eastern Lower Zone – GNPA member contact. Remapping of this contact is recommended to clarify the exact relationship at surface.

References

Ashwal, L. D., Webb, S. J., and Knoper, M. W., 2005, Magmatic stratigraphy in the Bushveld Northern Lobe: continuous geophysical and mineralogical data from the 2950 m Bellevue drillcore: South African Journal of Geology, v. 108, no. 2, p. 199-232.

Anglo American, 2008. Platinum Map of Southern Africa. 3rd Edition, 1. South Africa: Books on the Wall.

Barnes, S.-J., and Maier, W. D., 2002, Platinum-group element distributions in the Rustenburg layered suite of the Bushveld Complex, South Africa: The geology, geochemistry, mineralogy and mineral beneficiation of platinum-group elements, v. 54, p. 431-458.

Barrett, D., Jacobsen, J., McCarthy, T., and Cawthorn, R., 1978, The Structure of the Bushveld Complex South of Potgietersrus, as Revealed by a Gravity Survey Trans geol Soc. S. Afr, v. 81, p. 271-276.

Barton, J., Cawthorn, R. G., and White, J., 1986, The role of contamination in the evolution of the Platreef of the Bushveld Complex: Economic Geology, v. 81, no. 5, p. 1096-1104.

Barton, J., Holzer, L., Karnber, B., Doig, R., Kramers, J., and Nyfeler, D., 1994, Discrete metamorphic events in the Limpopo belt, southern Africa: implications for the application of PT paths in complex metamorphic terrains: Geology, v. 22, no. 11, p. 1035-1038.

Blaine, J. L., 1973, Report on the Potgietersrus project, Potgietersrus, Northern Transvaal: Falconbridge, 1323.

Buchanan, D.L., Nolan, J., Suddaby, P., Rouse, J.E., Viljoen, M.J. and Davenport, J.W.J., 1981. The genesis of sulfide mineralization in a portion of the Potgietersrus Limb of the Bushveld Complex. *Economic Geology*, *76*(3), pp.568-579

Button, A., Stratigraphy and relations of the Bushveld floor in the eastern Transvaal 1976, Geological Society of South Africa.

Cameron, E. N., 1978, The lower zone of the eastern Bushveld Complex in the Olifants River trough: Journal of Petrology, v. 19, no. 3, p. 437-462.

Cawthorn, R., 2004, Origin of variation of Pt/Pd values in the UG2 chromitite layer, Bushveld Complex: Geoscience Africa, University of the Witwatersrand, p. 110-113.

Cawthorn, R., and Webb, S., 2001, Connectivity between the western and eastern limbs of the Bushveld Complex: Tectonophysics, v. 330, no. 3, p. 195-209.

Cawthorn, R. G., and Walraven, F., 1998, Emplacement and crystallization time for the Bushveld Complex: Journal of Petrology, v. 39, no. 9, p. 1669-1687.

Clarke, B., Uken, R., and Reinhardt, J., 2009, Structural and compositional constraints on the emplacement of the Bushveld Complex, South Africa: Lithos, v. 111, no. 1, p. 21-36.

de Klerk, L., Bushveld stratigraphy on Rooipoort, Potgietersrus limb, in Proceedings Workshop on Platinum exploration and exploitation in Africa2005.

de Villiers, J., 1970, The structure and petrology of the mafic rocks of the Bushveld Complex south of Potgietersrus: Geological Society of South Africa, Special Publication, v. 1, p. 23-35.

de Villiers, J. S., 1967, The Geology of the Area South of Potgietersrus with Special Reference to the Chromite Deposits, Ph.D Thesis, University of the Witwatersrand. 124 pp.

de Wit, M. J., de Ronde, C. E., Tredoux, M., Roering, C., Hart, R. J., Armstrong, R. A., Green, R. W., Peberdy, E., and Hart, R. A., 1992, Formation of an Archaean continent: Nature, v. 357, no. 6379, p. 553-562.

de Wit, M. J., and Hart, R. A., 1993, Earth's earliest continental lithosphere, hydrothermal flux and crustal recycling: Lithos, v. 30, no. 3-4, p. 309-335.

Dunnett, T., Grobler, D., Simmonotti, N., and Mapeka, J., Lithological variations within Upper Critical Zone stratigraphy, Turfspruit 241KR, northern limb, Bushveld Complex, in Proceedings Platreef Workshop, 5th, Mokopane, South Africa, 9th-11th November 2012, Abstracts2012.

Eales, H., and Cawthorn, R., 1996, The bushveld complex: Developments in Petrology, v. 15, p. 181-229.

Eales, H., Marsh, J., Mitchell, A., de Klerk, W., Kruger, F., and Field, M., 1986, Some geochemical constraints upon models for the crystallization of the Upper Critical Zone-Main Zone interval, northwestern Bushveld Complex: Mineralogical Magazine, v. 50, no. 358, p. 567-582.

Finn, C. A., Bedrosian, P. A., Cole, J. C., Khoza, T. D., and Webb, S. J., 2015, Mapping the 3D extent of the Northern Lobe of the Bushveld layered mafic intrusion from geophysical data: Precambrian Research, v. 268, p. 279-294.

Gain, S.B. and Mostert, A.B., 1982. The geological setting of the platinoid and base metal sulfide mineralization in the Platreef of the Bushveld Complex in Drenthe, north of Potgietersrus. *Economic Geology*, *77*(6), pp.1395-1404.

Good, N., and De Wit, M. J., 1997, The Thabazimbi-Murchison lineament of the Kaapvaal craton, South Africa: 2700 Ma of episodic deformation: Journal of the Geological Society, v. 154, no. 1, p. 93-97.

Green, H., and Radcliffe, S., 1972, Dislocation mechanisms in olivine and flow in the upper mantle: Earth and Planetary Science Letters, v. 15, no. 3, p. 239-247.

Greer, S.E., 1980. The stratigraphy and sedimentology of the Potgietersrus area with particular reference to the Malmani Subgroup, Unpublished MSc thesis, University of the Witwatersrand, pp. 1–162.

Grobler, N., and Whitfield, G., 1970, The olivine-apatite magnetitites and related rocks in the Villa Nora occurrence of the Bushveld Igneous Complex: Geological Society of South Africa, Special Publication, l, p. 1161-1177.

Grobler, D.F., Brits, J.A.N., Maier, W.D. and Crossingham, A., 2019. Litho-and chemostratigraphy of the Flatreef PGE deposit, northern Bushveld Complex. *Mineralium Deposita*, *54*(1), pp.3-28.

Hall, A. L., 1932, The Bushveld igneous complex of the central Transvaal, *Mem. geol. Surv. Un. S.Afr*. No. 28.

Harney, D. M., and Von Gruenewaldt, G., 1995, Ore-forming processes in the upper part of the Bushveld complex, South Africa: Journal of African Earth Sciences, v. 20, no. 2, p. 77-89.

Hiemstra, S., 1986, The distribution of chalcophile and platinum-group elements in the UG-2 chromitite layer of the Bushveld Complex: Economic Geology, v. 81, no. 5, p. 1080-1086.

Hulbert, L., and Von Gruenewaldt, G., 1985, Textural and compositional features of chromite in the lower and critical zones of the Bushveld Complex south of Potgietersrus: Economic Geology, v. 80, no. 4, p. 872-895.

Hulbert, L. J., 1983, A petrological investigation of the Rustenburg layered suite and associated mineralization south of Potgietersrus. *Unpub* (Doctoral dissertation, D. Sc. dissertation, Univ. Pretoria).

Hulbert, L. J., and Von Gruenewaldt, G., 1982, Nickel, copper, and platinum mineralization in the Lower Zone of the Bushveld Complex, south of Potgietersrus: Economic Geology, v. 77, no. 6, p. 1296-1306.

Hutchinson, D., and Kinnaird, J. A., 2005, Complex multistage genesis for the Ni-Cu-PGE mineralisation in the southern region of the Platreef, Bushveld Complex, South Africa: Applied Earth Science, v. 114, no. 4, p. 208-224.

Hutchinson, D. and McDonald, I., 2008. Laser ablation ICP-MS study of platinum-group elements in sulphides from the Platreef at Turfspruit, northern limb of the Bushveld Complex, South Africa. *Mineralium Deposita*, *43*(6), p.695.

Irvine, T.N., 1980. Magmatic density currents and cumulus processes. *American Journal of Science*, *280*(Jackson Volume), pp.1-58.

Johnson, R., 1984a, Moorddrift and Jaagbaan platinum, Potgietersrus area. Morex SA. Report 1/84.

Johnson, R., 1984b, Past borehole information. Morex SA. Internal report.

Kekana, S. M., 2014, An investigation of mineralisation controls in the upper section of the Platreef in the southern sector, on Turfspruit, Northern Limb, Bushveld Complex, South Africa. MSc thesis, University of the Witwatersrand, pp. 128

Kinnaird, J.A., Kruger, F.J., Nex, P.A.M. and Cawthorn, R.G., 2002. Chromitite formation—a key to understanding processes of platinum enrichment. *Applied Earth Science*, *111*(1), pp.23-35.

Kinnaird, J., Yudovskaya, M., Naldrett, A., Botha, M., and Chunnett, G., 2012. PGE mineralisation in the Main Zone of the northern limb of the Bushveld Complex, in Proceedings 12th International Ni-Cu-(PGE) Symposium, Guiyang, China. Abstracts, p. 73-76.

Kinnaird, J. A., 2005a, The Bushveld large igneous province. http://www.largeigneousprovinces.org/LOM.htlm [January 2016].

Kinnaird, J. A., 2005b, Geochemical evidence for multiphase emplacement in the southern Platreef: Applied Earth Science, v. 114, no. 4, p. 225-242.

Kinnaird, J. A., Hutchinson, D., Schurmann, L., Nex, P., and de Lange, R., 2005, Petrology and mineralisation of the southern Platreef: northern limb of the Bushveld Complex, South Africa: Mineralium Deposita, v. 40, no. 5, p. 576-597.

Kinnaird, J.A. and McDonald, I., 2005. An introduction to mineralisation in the northern limb of the Bushveld Complex. Appl Earth Sci (Trans Inst Min Metall B) 114:B194–B198

Kinnaird, J.A., Yudovskaya, M., McCreesh, M., Huthmann, F. and Botha, T.J., 2017. The Waterberg platinum group element deposit: atypical mineralization in mafic-ultramafic rocks of the Bushveld Complex, South Africa. Economic Geology, 112(6), pp.1367-1394.

Klemm, D.D., Henckel, J., Dehm, R.M. and Von Gruenewaldt, G., 1985. The geochemistry of titanomagnetite in magnetite layers and their host rocks of the eastern Bushveld Complex. Economic Geology, 80(4), pp.1075-1088.

Knoper, M.W. and von Gruenewaldt, G., 1996. The Bellevue (BV-1) borehole core log: 2· 9 km of Bushveld Complex stratigraphy (northern lobe). Potgietersus. Available online at: http://rockscape. org.

Kruger, F.J., Cawthorn, R.G. and Walsh, K.L., 1987. Strontium isotopic evidence against magma addition in the Upper Zone of the Bushveld Complex. Earth and Planetary Science Letters, 84(1), pp.51-58.

Kruger, F.J., 1990. The stratigraphy of the Bushveld Complex: a reappraisal and the relocation of the Main Zone boundaries. South African Journal of Geology, 93(2), pp.376-381.

Kruger, F. J., 2005, Filling the Bushveld Complex magma chamber: lateral expansion, roof and floor interaction, magmatic unconformities, and the formation of giant chromitite, PGE and Ti-V-magnetitite deposits: Mineralium Deposita, v. 40, no. 5, p. 451-472.

Kynaston, H., Mellor, E., and Hall, A., 1911. The Geology of the Country Round Potgietersrust. An Explanation of Sheet 7 (Potgietersrust), Geol. Surv. S. Afr., Pretoria, 62 pp.

Le Bas, M., and Streckeisen, A. L., 1991, The IUGS systematics of igneous rocks: Journal of the Geological Society, v. 148, no. 5, p. 825-833.

Li, C., Thakurta, J., and Ripley, E. M., 2012, Low-Ca contents and kink-banded textures are not unique to mantle olivine: evidence from the Duke Island Complex, Alaska: Mineralogy and Petrology, v. 104, no. 3-4, p. 147-153.

Maier, W.D., de Klerk, L., Blaine, J., Manyeruke, T., Barnes, S.J., Stevens, M.V.A. and Mavrogenes, J.A., 2008. Petrogenesis of contact-style PGE mineralization in the northern lobe of the Bushveld Complex: comparison of data from the farms Rooipoort, Townlands, Drenthe and Nonnenwerth. *Mineralium Deposita*, *43*(3), pp.255-280.

Maier, W.D., Barnes, S.J. and Groves, D.I., 2013. The Bushveld Complex, South Africa: formation of platinum–palladium, chrome-and vanadium-rich layers via hydrodynamic sorting of a mobilized cumulate slurry in a large, relatively slowly cooling, subsiding magma chamber. *Mineralium Deposita*, *48*(1), pp.1-56.

Malvoisin, B., Brantut, N., and Kaczmarek, M.-A., 2017, Control of serpentinisation rate by reaction-induced cracking: Earth and Planetary Science Letters, v. 476, p. 143-152.

Manyeruke, T. D., Maier, W. D., and Barnes, S.-J., 2005, Major and trace element geochemistry of the Platreef on the farm Townlands, northern Bushveld Complex: South African Journal of Geology, v. 108, no. 3, p. 381-396.

McCarthy, T.S., Cawthorn, R.G., Wright, C.J. and McIver, J.R., 1985. Mineral layering in the Bushveld Complex; implications of Cr abundances in magnetite from closely spaced magnetitite and intervening silicate-rich layers. *Economic Geology*, *80*(4), pp.1062-1074.

McDonald, I., Holwell, D. A., and Armitage, P. E., 2005, Geochemistry and mineralogy of the Platreef and "Critical Zone" of the northern lobe of the Bushveld Complex, South Africa: implications for Bushveld

stratigraphy and the development of PGE mineralisation: Mineralium Deposita, v. 40, no. 5, p. 526-549.

McDonald, I. and Holwell, D.A., 2011. Geology of the northern Bushveld Complex and the setting and genesis of the Platreef Ni-Cu-PGE deposit. *Reviews in Economic Geology*, (17), pp.297-327.

McLaren, C. H., and De Villiers, J. P., 1982, The platinum-group chemistry and mineralogy of the UG-2 chromitite layer of the Bushveld Complex: Economic Geology, v. 77, no. 6, p. 1348-1366.

Merensky, H., 1925. The platinum occurrence on the properties of Potgietersrus Platinums Limited Report to the Directors. London and Rhodesia Mining and Land Company Limited, Johannesburg. p. 6.

Molengraaff, G. A. F., 1901, Geologie de la Republique S. Africaine. Bulletin of the Geolog-ical Society of France 1, 13–92.

Molyneux, T., 1974, A geological investigation of the Bushveld Complex in Sekhukhuneland and part of the Steelpoort valley: South African Journal of Geology, v. 77, no. 3, p. 329-338.

Nex, P., Kinnaird, J., Ingle, L., Van der Vyver, B., and Cawthorn, R., 1998, A new stratigraphy for the Main Zone of the Bushveld Complex, in the Rustenburg area: South African Journal of Geology, v. 101, no. 3, p. 215-223.

Nex, P. A., 2005, The structural setting of mineralisation on Tweefontein Hill, northern limb of the Bushveld Complex, South Africa: Applied Earth Science, v. 114, no. 4, p. 243-251.

Ross, M., Martel, R., Parent, G. and Smirnoff, A., 2007. Geomodels as a key component of environmental impact assessments of military training ranges in Canada. In Three-dimensional geological mapping for groundwater applications, Workshop Extended abstracts: Minnesota Geological Survey, Open-File Report pp. 07-4.

SACS, 1980, Stratigraphy of South Africa. Part 1: Lithostratigraphy of the Republic of South Africa, South West Africa/ Namibia and the Republic of Bophuthatswana, Transkei and Venda., p. 690.

Scoates, J. S., and Friedman, R. M., 2008, Precise age of the platiniferous Merensky Reef, Bushveld Complex, South Africa, by the U-Pb zircon chemical abrasion ID-TIMS technique: Economic Geology, v. 103, no. 3, p. 465-471.

Scoon, R. N., and Teigler, B., 1994, Platinum-group element mineralization in the critical zone of the western Bushveld Complex; I, Sulfide poor-chromitites below the UG-2: Economic Geology, v. 89, no. 5, p. 1094-1121.

Seabrook, C. L., Cawthorn, R. G., and Kruger, F. J., 2005, The Merensky Reef, Bushveld Complex: mixing of minerals not mixing of magmas: Economic Geology, v. 100, no. 6, p. 1191-1206.

Sharpe, M.R., 1985. Strontium isotope evidence for preserved density stratification in the main zone of the Bushveld Complex, South Africa. Nature, 316(6024), pp.119-126.

Sharman, E.R., Penniston-Dorland, S.C., Kinnaird, J.A., Nex, P.A.M., Brown, M. and Wing, B.A., 2013. Primary origin of marginal Ni-Cu-(PGE) mineralization in layered intrusions: δ33S evidence from the Platreef, Bushveld, South Africa. *Economic Geology*, *108*(2), pp.365-377.

Smith, J., Holwell, D., and McDonald, I., 2011, The mineralogy and petrology of platinum-group element-bearing sulphide mineralisation within the Grasvally Norite-Pyroxenite-Anorthosite (GNPA) member,

south of Mokopane, northern Bushveld Complex, South Africa: Applied Earth Science: Transactions of the Institutions of Mining and Metallurgy: Section B, v. 120, no. 4, p. 158-174.

Smith, J., Holwell, D. A., and McDonald, I., 2014, Precious and base metal geochemistry and mineralogy of the Grasvally Norite-Pyroxenite-Anorthosite (GNPA) member, northern Bushveld Complex, South Africa: implications for a multistage emplacement: Mineralium Deposita, v. 49, no. 6, p. 667-692.

Streckeisen, A., 1976, To each plutonic rock its proper name: Earth-science reviews, v. 12, no. 1, p. 1-33.

Teigler, B., and Eales, H., 1993, Correlation between chromite composition and PGE mineralization in the Critical Zone of the western Bushveld Complex: Mineralium Deposita, v. 28, no. 5, p. 291-302.

Teigler, B., and Eales, H. V., 1996, The Lower and Critical Zones of the western limb of the Bushveld Complex as intersected by the Nooitgedagt boreholes. Bull. Geol. Surv. S. Afri., 111, 126 pp.

van der Merwe, M., 1976, The layered sequence of the Potgietersrus limb of the Bushveld Complex: Economic Geology, v. 71, no. 7, p. 1337-1351.

van der Merwe, M. J., 1978, The geology of the basic and ultramafic rocks of the Potgietersrus limb of the Bushveld Complex: Unpublished PhD thesis, University of the Witwatersrand, Johannesburg.

van der Merwe, M. J., 2008, The geology and structure of the Rustenburg Layered Suite in the Potgietersrus/Mokopane area of the Bushveld Complex, South Africa: Mineralium Deposita, v. 43, no. 4, p. 405-419.

Verbeek, J., Lomberg, M.M.K., Global–Johannesburg, R.S.G. and Global–Perth, R.S.G., 2005. Independent Technical Report on the Central African Mineral Properties of TEAL Exploration & Mining Incorporated.

Viljoen, M., and Schurmann, L., 1998, Platinum-group metals. In: Wilson MGC, Anhaeusser CR (eds) The mineral resources of South Africa. Coun Geosci Handbook 16:532-568.

Von Gruenewaldt, G., 1973, The main and upper zones of the Bushveld Complex in the Roossenekal area, eastern Transvaal: Transactions of the Geological Society of South Africa, v. 76, p. 207-227.

Von Gruenewaldt, G., Hulbert, L.J. and Naldrett, A.J., 1989. Contrasting platinum-group element concentration patterns in cumulates of the Bushveld Complex. Mineralium deposita, 24(3), pp.219-229.

Von Gruenewaldt, G., Horsch, H., Dickst, D. and de Wet, J., 1990. PGE mineralization in the western sector of the eastern Bushveld Complex. Mineralogy and Petrology, 42(1-4), pp.71-95.

Wagner, P.A. 1929, The Platinum Deposits and Mines of South Africa. Oliver and Boyd, Edinburgh. 326 pp.

Wager, L.R. and Brown, G.M., 1967. Layered igneous rocks. WH Freeman. Oliver& Boyd, Edinburgh and London. Pp 588.

Wagner, P. A., 1929, The platinum deposits and mines of South Africa: Edinburgh, Oliver and Boyd, p.326.

Walraven, F., Armstrong, R., and Kruger, F., 1990, A chronostratigraphic framework for the north-central Kaapvaal craton, the Bushveld Complex and the Vredefort structure: Tectonophysics, v. 171, no. 1, p. 23-48.

White, J., 1983. The geology and mineralization of the Platreef of the Potgietersrus Limb of the Bushveld Complex. In Programme with Abstracts: Symposium on the Bushveld Complex. University of Pretoria (pp. 102-105).

Wilson, A., 1982, The geology of the Great 'Dyke', Zimbabwe: the ultramafic rocks: Journal of Petrology, v. 23, no. 2, p. 240-292.

Wilson, A., and Chunnett, G., 2010, New Insight into the stratigraphy, emplacement and evolution of the basal ultramafic succession in the Eastern Bushveld Complex, South Africa: Abstracts of 11 Platinum Symposium, Sudbury, June 21–24, Ontario Geological Survey, Miscellaneous Release–Data, p.269.Wilson, A. H., 2012, A chill sequence to the Bushveld Complex: insight into the first stage of emplacement and implications for the parental magmas: Journal of Petrology, v. 53, no. 6, p. 1123-1168.

Wilson, A.H., 2015. The earliest stages of emplacement of the eastern Bushveld Complex: development of the Lower Zone, Marginal Zone and Basal Ultramafic Sequence. *Journal of Petrology*, *56*(2), pp.347-388.

Yudovskaya, M. A., and Kinnaird, J. A., 2010, Chromite in the Platreef (Bushveld Complex, South Africa): occurrence and evolution of its chemical composition: Mineralium Deposita, v. 45, no. 4, p. 369-391.

Yudovskaya, M. A., Kinnaird, J. A., Sobolev, A. V., Kuzmin, D. V., McDonald, I., and Wilson, A. H., 2013, Petrogenesis of the Lower Zone olivine-rich cumulates beneath the Platreef and their correlation with recognized occurrences in the Bushveld Complex: Economic Geology, v. 108, no. 8, p. 1923-1952.

Zeh, A., Ovtcharova, M., Wilson, A. H., and Schaltegger, U., 2015, The Bushveld Complex was emplaced and cooled in less than one million years-results of zirconology, and geotectonic implications: Earth and Planetary Science Letters, v. 418, p. 103-114.

List of Appendices

Appendix A: CIPW Normative sample classifications

Appendix: B: Geochemical analysis

Appendix C: Assay data

Appendix D: Core logs

Appendix E: Magnetic susceptibility readings

Appendix F: Bushveld Complex Pt:Pd ratios

Appendix G: Map of Grasvally area. Modified after Hulbert (1983)

Appendix A

BHID	Depth	Sample No.	Rock type based on CIPW Norm
GVL-04	16.95	K 1	magnetite bearing mela norite
GVL-04	30.15	K 2	magnetite bearing Gabbronorite
GVL-04	76.15	K 5	Magnetite bearing orthopyroxenite
GVL-04	83.05	K 6	Harzburgite
GVL-04	85.15	K 7	Olivine bearing gabbronorite
GVL-04	104.15	K 8	chromite and Magnetite bearing gabbronorite
GVL-04	105.95	K 9	Olivine gabbronorite
GVL-04	110.15	K 10	Olivine bearing gabbronorite
GVL-04	114.45	K 11	Olivine bearing norite
GVL-04	212.15	K 12	chromite bearing Dunite
GVL-04	227.15	K 13	Harzburgite
GVL-04	254.15	K 14	chromite bearing Harzburgite
GVL-04	264.15	K 15	Olivine bearing gabbronorite/ Olivine websterite
GVL-04	272.15	K 16	Olivine bearing orthopyroxenite
GVL-04	357.85	K 17	Harzburgite
GVL-04	420.15	K 18	Granite
GVL-04	455.54	K 19	chromite bearing Harzburgite
GVL-04	461.75	K 20	Olivine orthopyroxenite (75.83 chromite- chromitite)
GVL-04	467.15	K 21	chromite bearing Dunite
GVL-04	517.95	K 22	Chromite bearing Harzburgite
GVL-04	533.15	K 23	Chromite bearing Lherzolite
GVL-04	538.15	K 24	Chromite bearing Harzburgite
GVL-04	542.5	K 25	chromite bearing dunite
GVL-04	548.15	K 26	Chromite bearing harzburgite
GVL-04	566.05	K 27	Olivine Gabbronorite/Chromite bearing lherzolite
GVL-04	569.15	K 28	Olivine bearing dunite
GVL-02	219.55	K 29	Magnetite-ilmenite-chromite bearing Gabbronorite
GVL-02	222.55	K 30	Magnetite-ilmenite-chromite bearing Gabbronorite
GVL-02	231.15	K 31	Magnetite bearing Gabbronorite
GVL-02	250.15	K 32	Magnetite bearing Gabbronorite
GVL-02	261.16	K 33	Olivine leuco-gabbronorite
GVL-02	288.61	K 34	Magnetite bearing norite
GVL-02	294.16	K 35	Magnetite ilmenite bearing gabbronorite
GVL-04	599.38	K 36	chromite magnetite bearing orthopyroxenite
GVL-04	370.87	K 37	Harzburgite
GVL-09	16.37	K 38	Chromite olivine bearing feldspathic gabbronorite
GVL-09	17.88	K 39	olivine bearing feldspathic gabbronorite
GVL-09	20.88	K 40	Olivine bearing leuconorite
GVL-09	63.45	K 41	Olivine orthopyroxenite
GVL-09	74.85	K 42	Chromite bearing Olivine Orthopyroxenite
GVL-09	78.41	K 43	Chromite bearing Dunite
GVL-09	100.5	K 44	Chromite bearing harzburgite
GVL-09	129.97	K 45	Harzburgite
GVL-09	142.71	K 46	Lherzolite/Olivine Gabbronorite
GVL-09	151.54	K 47	olivine bearing Orthopyroxenite
GVL-09	198.62	K 48	Chromite bearing Harzburgite
GVL-09	229.02	K 49	Granite
GVL-09	256.06	K 50	Harzburgite
GVL-09	262.84	K 51	Harzburgite

GVL-09	287.21	K 52	Chromite bearing Harzburgite

Appendix A

BHID	Depth	Sample No.	Rock type based on CIPW Norm
GVL-09	326.26	K 53	Harzburgite
GVL-09	343.33	K 54	Chromite bearing harzburgite
GVL-09	352.34	K 55	Harzburgite
GVL-09	380.72	K 56	Dunite
GVL-09	398.57	K 57	Harzburgite
GVL-09	414.41	K 58	Harzburgite
GVL-09	439.31	K 59	Chromite bearing Harzburgite
GVL-09	471.46	K 60	Chromite bearing harzburgite
GVL-09	506.8	K 61	Chromite bearing harzburgite
GVL-09	516.67	K 62	Chromite bearing harzburgite
GVL-09	517.47	K 63	Chromite bearing Dunite
GVL-09	528.31	K 64	Harzburgite
GVL-09	542.58	K 65	Olivine bearing orthopyroxenite
GVL-09	543.77	K 66	Olivine bearing orthopyroxenite
GVL-09	551.31	K 67	Chromite bearing Dunite
GVL-09	556.16	K 68	Chromite bearing dunite
GVL-09	563.19	K 69	Chromite bearing harzburgite
GVL-09	566.03	K 70	Chromite bearing dunite
GVL-09	567.3	K 71	Chromite bearing dunite
GVL-09	578.07	K 72	Chromite bearing dunite
GVL-09	600.74	K 73	Chromite bearing dunite
GVL-09	607.48	K 74	Harzburgite
GVL-11	33.39	K 75	olivine and clinopyroxene Anorthosite
GVL-11	39.54	K 76	Olivine bearing gabbronorite
GVL-11	42.05	K 77	opx cpx olivine Anorthosite
GVL-11	53.74	K 78	Magnetite bearing norite
GVL-11	74.52	K 79	Olivine bearing leuconorite
GVL-11	94.66	K 80	Magnetite bearing Gabbronorite
GVL-11	131.62	K 81	Magnetite leucogabbronorite
GVL-11	155.23	K 82	leucogabbronorite
GVL-11	174.4	K 83	leucogabbronorite
GVL-11	197.23	K 84	leucogabbronorite
GVL-18	23.67	K 85	Leuconorite
GVL-18	41.73	K 86	leucogabbronorite
GVL-18	52.95	K 87	Magnetite bearing Gabbronorite
GVL-18	57.45	K 88	magnetite bearing leucogabbronorite
GVL-18	72.41	K 89	Leuconorite
GVL-18	89.8	K 90	Leucogabbronorite
GVL-18	102.02	K 91	Leucogabbronorite
GVL-18	117.93	K 92	leucogabbronorite/mottled anorthosite
GVL-18	126.81	K 93	Leucogabbronorite
GVL-18	150.4	K 94	Leucogabbronorite
GVL-05	51.26	K 95	Harzburgite
GVL-05	74.71	K 96	Chromite bearing Harzburgite
GVL-05	114.16	K 97	Chromite bearing Harzburgite
GVL-05	158.49	K 98	Olivine orthopyroxenite
GVL-05	207.88	K 99	Lherzolite
GVL-05	261.77	K 100	Harzburgite
GVL-05	304.24	K 101	Harzburgite

GVL-05	332.11	K 102	Dunite

Appendix A

BHID	**Depth**	**Sample No.**	**Rock type based on CIPW Norm**
GVL-05	361.54	K 103	Harzburgite
GVL-05	404.31	K 104	Harzburgite
GVL-05	414.8	K 105	Chromitite/orthopyroxenite
GVL-05	419.01	K 106	Dunite
GVL-05	423.23	K 107	Harzburgite
GVL-05	443.39	K 108	Harzburgite
GVL-05	507.82	K 109	Olivine orthopyroxenite
GVL-05	559.49	K 110	Dunite
GVL-05	599.29	K 111	Ilmenite-magnetite bearing Gabbronorite
GVL-03	55.59	K 112	Gabbronorite
GVL-03	129.21	K 113	Leucogabbronorite
GVL-03	137.82	K 114	Leucogabbronorite
GVL-03	148.03	K 115	Leucogabbronorite
GVL-03	203.4	K 116	Anorthosite/Diopside bearing anorthosite
GVL-03	217.67	K 117	Melagabbronorite
GVL-03	227.24	K 118	Olivine bearing leuconorite
GVL-03	334.66	K 119	Olivine bearing leucogabbronorite
GVL-03	385.15	K 120	Leucogabbronorite
GVL-03	414.89	K 121	Norite
GVL-03	436.35	K 122	Olivine bearing gabbronorite
GVL-03	464.4	K 123	Harzburgite
GVL-03	480.84	K 124	Olivine Gabbronorite
GVL-03	485.56	K 125	Wehrlite/Troctolite/Olivine bearing Anorthosite
GVL-03	508.67	K 126	Olivine melanorite
GVL-03	509.98	K 127	Melanorite/Orthopyroxenite
GVL-03	527.57	K 128	Lherzolite/Olivine Gabbronorite
GVL-03	535.46	K 129	Harzburgite
GVL-03	546.93	K 130	Norite
GVL-03	559.69	K 131	Harzburgite
GVL-03	584.19	K 132	Harzburgite
GVL-04	604.58	K 133	Harzburgite

Appendix B: Major Element Geochemical Data

Table 1:

BHID	Depth	Sample No.	SiO2	Al_2O_3	Fe_2O_3	FeO	MnO	MgO	CaO	Na_2O	K_2O	TiO_2	P_2O_5	Cr_2O_3	NiO	total
GVL-04	16.95	K1	52.79	10.67	1.25	10.12	0.23	17.38	5.95	0.54	0.49	0.22	0.05	0.24	0.06	100.00
GVL-04	30.15	K2	53.06	15.35	1.13	9.19	0.17	7.45	10.04	1.87	0.90	0.65	0.11	0.06	0.02	100.01
GVL-04	76.15	K5	56.85	2.30	0.72	5.78	0.14	31.21	1.36	0.26	0.29	0.09	0.02	0.87	0.12	100.01
GVL-04	83.05	K6	44.41	1.19	0.73	5.85	0.11	46.28	0.06	0.07	0.01	0.04	0.02	0.95	0.29	100.00
GVL-04	85.15	K7	44.60	9.86	1.61	13.07	0.23	16.17	7.76	0.92	0.09	0.54	0.01	4.95	0.19	100.00
GVL-04	104.15	K8	48.35	5.15	2.15	17.45	0.28	15.84	8.71	0.74	0.17	0.29	0.02	0.41	0.46	100.02
GVL-04	105.95	K9	48.45	16.26	1.34	10.86	0.13	11.98	8.29	1.58	0.43	0.12	0.02	0.22	0.31	99.99
GVL-04	110.15	K10	51.53	12.22	1.17	9.48	0.16	16.89	5.43	0.83	1.78	0.18	0.02	0.22	0.07	100.00
GVL-04	114.45	K11	48.22	5.75	1.27	10.36	0.16	30.10	2.42	0.12	0.17	0.13	0.03	1.07	0.21	100.02
GVL-04	212.15	K12	32.77	0.93	3.63	29.39	0.12	30.43	0.11	-0.05	0.05	0.07	0.02	1.29	1.25	100.00
GVL-04	227.15	K13	43.61	3.08	1.04	8.46	0.14	38.99	1.03	0.04	0.06	0.09	0.03	2.97	0.45	100.00
GVL-04	254.15	K14	40.89	2.48	1.78	14.48	0.14	37.73	0.18	0.21	0.05	0.05	0.02	0.95	1.03	99.99
GVL-04	264.15	K15	53.26	18.02	0.81	6.58	0.12	6.83	7.75	1.88	4.45	0.20	0.02	0.05	0.02	100.00
GVL-04	272.15	K16	54.73	3.13	1.09	8.87	0.19	28.07	2.42	0.24	0.37	0.12	0.02	0.66	0.10	100.01
GVL-04	357.85	K17	44.02	2.29	1.15	9.24	0.12	40.82	0.54	0.06	0.12	0.07	0.02	1.24	0.32	100.01
GVL-04	420.15	K18	74.95	11.36	0.43	3.55	0.07	0.12	1.10	3.18	4.90	0.31	0.04	0.00	0.00	100.00
GVL-04	455.54	K19	45.45	1.93	1.01	8.17	0.12	41.80	0.17	0.09	0.23	0.05	0.03	0.64	0.31	99.99
GVL-04	461.75	K20	44.77	1.25	1.10	8.88	0.08	42.29	0.15	0.06	0.17	0.04	0.03	0.70	0.48	100.00
GVL-04	467.15	K21	38.63	1.40	1.33	10.77	0.13	44.24	0.08	0.03	0.01	0.05	0.02	2.71	0.60	100.00
GVL-04	517.95	K22	42.53	1.69	1.17	9.44	0.18	41.63	0.80	0.11	0.24	0.05	0.03	1.64	0.49	100.00
GVL-04	533.15	K23	46.93	3.07	1.00	8.13	0.16	34.00	4.29	0.35	0.61	0.11	0.03	1.03	0.28	100.00
GVL-04	538.15	K24	44.04	0.91	1.01	8.09	0.18	43.16	0.72	0.08	0.12	0.04	0.02	1.43	0.21	100.01
GVL-04	542.50	K25	39.15	2.61	1.22	9.82	0.20	41.58	1.02	0.23	0.09	0.04	0.02	2.85	1.18	100.02
GVL-04	548.15	K26	40.97	1.17	0.98	7.98	0.16	45.63	0.25	0.07	0.02	0.04	0.02	2.32	0.37	100.00
GVL-04	566.05	K27	44.34	2.68	0.87	6.98	0.13	38.88	3.55	0.13	0.89	0.09	0.02	1.10	0.36	100.02
GVL-04	569.15	K28	40.24	0.88	1.09	8.75	0.17	46.77	0.17	0.14	0.07	0.04	0.02	1.31	0.37	100.00
GVL-02	219.55	K29	54.28	14.61	1.07	8.69	0.17	7.89	8.32	2.36	0.81	0.69	0.12	0.96	0.03	100.00
GVL-02	222.55	K30	48.44	14.03	1.41	11.37	0.19	9.30	7.49	1.87	0.66	0.80	0.08	4.30	0.06	100.00
GVL-02	231.15	K31	53.97	16.49	0.81	6.55	0.13	8.39	10.06	2.22	0.74	0.36	0.06	0.18	0.02	99.99
GVL-02	250.15	K32	53.80	15.87	0.90	7.32	0.15	8.76	9.36	2.42	0.69	0.45	0.08	0.14	0.03	99.98

Appendix B: Major Element Geochemical Data

Table 2:

BHID	Depth	Sample No.	SiO2	Al_2O_3	Fe_2O_3	FeO	MnO	MgO	CaO	Na_2O	K_2O	TiO_2	P_2O_5	Cr_2O_3	NiO	total
GVL-02	261.16	K33	50.14	18.34	1.00	8.04	0.12	10.55	8.36	1.95	0.90	0.17	0.03	0.21	0.21	100.01
GVL-02	288.61	K34	52.80	10.66	1.25	10.12	0.23	17.38	5.96	0.54	0.49	0.22	0.05	0.24	0.06	100.01
GVL-02	294.16	K35	53.06	15.35	1.14	9.19	0.18	7.46	10.03	1.87	0.89	0.65	0.11	0.06	0.02	100.01
GVL-04	599.38	K36	56.84	2.30	0.71	5.78	0.14	31.20	1.37	0.26	0.29	0.09	0.02	0.88	0.12	100.01
GVL-04	370.87	K37	44.41	1.19	0.72	5.85	0.11	46.28	0.06	0.07	0.01	0.05	0.02	0.95	0.29	100.01
GVL-09	16.37	K38	44.60	9.86	1.62	13.07	0.23	16.16	7.75	0.94	0.09	0.54	0.01	4.96	0.19	100.01
GVL-09	17.88	K39	48.36	5.15	2.15	17.45	0.27	15.84	8.70	0.75	0.17	0.28	0.02	0.41	0.46	100.01
GVL-09	20.88	K40	48.46	16.26	1.34	10.86	0.13	11.98	8.28	1.58	0.43	0.12	0.02	0.22	0.31	100.01
GVL-09	63.45	K41	51.51	12.22	1.17	9.49	0.16	16.89	5.43	0.84	1.79	0.18	0.02	0.21	0.07	99.99
GVL-09	74.85	K42	48.22	5.74	1.28	10.36	0.16	30.10	2.42	0.12	0.17	0.13	0.03	1.07	0.21	100.01
GVL-09	78.41	K43	32.77	0.93	3.62	29.38	0.12	30.43	0.11	-0.05	0.05	0.08	0.02	1.29	1.25	100.01
GVL-09	100.50	K44	43.60	3.08	1.04	8.46	0.15	38.97	1.03	0.04	0.06	0.09	0.03	2.97	0.46	99.98
GVL-09	129.97	K45	40.90	2.48	1.79	14.49	0.13	37.75	0.18	0.21	0.05	0.05	0.02	0.95	1.02	100.00
GVL-09	142.71	K46	53.25	18.01	0.82	6.58	0.13	6.83	7.75	1.89	4.45	0.20	0.02	0.05	0.02	100.00
GVL-09	151.54	K47	54.74	3.13	1.09	8.87	0.19	28.06	2.42	0.25	0.37	0.11	0.02	0.66	0.10	100.02
GVL-09	198.62	K48	44.02	2.29	1.14	9.25	0.12	40.83	0.55	0.06	0.12	0.07	0.02	1.24	0.31	100.02
GVL-09	229.02	K49	74.96	11.36	0.44	3.54	0.07	0.12	1.11	3.19	4.89	0.30	0.03	0.00	0.00	100.00
GVL-09	256.06	K50	45.45	1.93	1.00	8.17	0.11	41.81	0.17	0.09	0.23	0.05	0.03	0.64	0.31	99.99
GVL-09	262.84	K51	44.77	1.25	1.09	8.89	0.09	42.29	0.15	0.06	0.17	0.03	0.03	0.69	0.48	100.00
GVL-09	287.21	K52	46.56	2.29	1.05	8.52	0.12	37.96	0.82	0.11	0.21	0.07	0.02	1.70	0.57	100.00
GVL-09	326.26	K53	46.51	1.58	0.61	5.01	0.29	44.35	0.21	0.07	0.03	0.06	0.02	1.06	0.21	100.01
GVL-09	343.33	K54	38.20	2.04	1.55	12.57	0.11	39.93	0.04	0.06	0.01	0.06	0.02	4.66	0.74	100.00
GVL-09	352.34	K55	42.52	1.51	0.98	8.24	0.12	45.14	0.02	0.06	0.01	0.03	0.02	1.04	0.29	99.99
GVL-09	380.72	K56	41.48	1.17	1.01	9.57	0.19	44.40	0.47	0.06	0.16	0.04	0.02	1.01	0.44	100.02
GVL-09	398.57	K57	41.48	1.72	1.03	9.26	0.11	43.63	1.16	0.05	0.02	0.05	0.02	1.02	0.44	100.00
GVL-09	414.41	K58	41.19	1.55	1.09	8.82	0.14	45.60	0.03	0.05	0.00	0.05	0.03	1.05	0.40	100.00
GVL-09	439.31	K59	40.65	1.57	1.11	8.93	0.12	44.46	0.01	0.03	0.01	0.05	0.02	2.73	0.32	100.01
GVL-09	471.46	K60	42.25	1.32	1.03	8.35	0.12	44.53	0.44	0.07	0.06	0.03	0.02	1.39	0.40	100.01
GVL-09	506.80	K61	42.19	1.18	1.04	8.91	0.16	44.05	0.77	0.07	0.02	0.05	0.02	1.16	0.42	100.03
GVL-09	516.67	K62	41.93	1.33	1.05	8.52	0.15	44.80	0.66	0.05	0.02	0.04	0.02	1.08	0.36	100.02

Appendix B: Major Element Geochemical Data

Table 3:

BHID	Depth	Sample No.	SiO2	Al_2O_3	Fe_2O_3	FeO	MnO	MgO	CaO	Na_2O	K_2O	TiO_2	P_2O_5	Cr_2O_3	NiO	total
GVL-09	517.47	K63	41.40	1.34	1.06	8.60	0.16	45.11	0.77	0.05	0.02	0.04	0.02	1.06	0.35	100.00
GVL-09	528.31	K64	42.23	0.99	1.12	9.03	0.15	44.51	0.68	0.05	0.01	0.03	0.02	0.73	0.45	100.01
GVL-09	542.58	K65	54.34	2.77	0.86	6.97	0.16	32.26	1.56	0.25	0.10	0.07	0.03	0.53	0.12	100.02
GVL-09	543.77	K66	53.42	1.91	0.89	7.18	0.15	34.28	1.19	0.09	0.06	0.06	0.02	0.58	0.16	99.99
GVL-09	551.31	K67	39.16	1.72	1.24	10.07	0.17	43.25	0.57	0.06	0.01	0.05	0.03	3.12	0.56	100.02
GVL-09	556.16	K68	40.78	0.98	1.14	9.20	0.16	45.12	0.54	0.05	0.01	0.03	0.02	1.68	0.33	100.03
GVL-09	563.19	K69	44.96	1.03	1.08	8.68	0.16	41.81	0.50	0.15	0.06	0.03	0.02	1.26	0.27	100.02
GVL-09	566.03	K70	38.82	1.23	1.11	8.96	0.16	44.34	0.16	0.06	0.01	0.03	0.02	4.64	0.49	100.01
GVL-09	567.30	K71	39.63	1.28	1.13	9.12	0.17	44.28	0.25	0.03	0.07	0.04	0.02	3.52	0.45	100.00
GVL-09	578.07	K72	40.82	1.48	0.96	8.35	0.14	45.13	1.17	0.15	0.03	0.04	0.02	1.29	0.42	100.00
GVL-09	600.74	K73	37.11	1.81	1.28	10.39	0.21	42.86	0.34	0.05	0.11	0.06	0.02	3.62	2.14	100.01
GVL-09	607.48	K74	47.07	1.36	0.93	7.49	0.15	41.48	0.27	0.15	0.07	0.03	0.02	0.58	0.38	99.99
GVL-11	33.39	K75	48.85	29.65	0.18	1.43	0.03	1.17	13.28	2.09	3.13	0.06	0.02	0.00	0.11	100.01
GVL-11	39.54	K76	52.16	10.60	1.17	9.51	0.18	17.92	6.40	1.06	0.11	0.17	0.02	0.23	0.47	100.00
GVL-11	42.05	K77	49.95	29.30	0.20	1.59	0.03	1.72	13.82	2.64	0.60	0.08	0.02	0.02	0.02	100.00
GVL-11	53.74	K78	52.59	14.70	0.89	7.10	0.15	14.86	7.68	1.42	0.16	0.15	0.02	0.20	0.08	100.00
GVL-11	74.52	K79	50.94	21.28	0.58	4.66	0.09	8.95	10.97	1.98	0.27	0.11	0.02	0.11	0.03	100.00
GVL-11	94.66	K80	51.88	18.92	0.73	5.85	0.12	9.81	10.28	1.98	0.18	0.12	0.02	0.09	0.03	100.02
GVL-11	131.62	K81	51.98	17.65	0.79	6.34	0.14	9.63	10.91	1.90	0.25	0.19	0.03	0.17	0.03	100.01
GVL-11	155.23	K82	52.05	19.99	0.65	5.26	0.12	7.78	11.18	2.30	0.35	0.16	0.02	0.11	0.02	100.00
GVL-11	174.40	K83	52.20	19.42	0.69	5.58	0.12	7.76	11.21	2.37	0.37	0.17	0.03	0.09	0.02	100.03
GVL-11	197.23	K84	52.12	19.51	0.74	5.94	0.13	7.62	10.98	2.38	0.24	0.18	0.02	0.13	0.03	100.02
GVL-18	23.67	K85	52.37	22.08	0.53	4.29	0.09	6.36	11.40	2.22	0.31	0.21	0.05	0.08	0.02	100.02
GVL-18	41.73	K86	51.93	22.46	0.51	4.20	0.09	5.72	11.90	2.41	0.48	0.18	0.02	0.07	0.02	100.00
GVL-18	52.95	K87	52.97	15.98	0.83	6.71	0.14	8.67	11.65	2.07	0.46	0.30	0.06	0.14	0.03	100.00
GVL-18	57.45	K88	52.72	17.80	0.84	6.80	0.13	8.81	9.54	2.43	0.48	0.24	0.09	0.08	0.03	100.00
GVL-18	72.41	K89	51.32	23.16	0.51	4.08	0.08	5.51	12.09	2.40	0.60	0.15	0.03	0.06	0.02	100.00
GVL-18	89.80	K90	51.30	20.57	0.71	5.77	0.09	6.80	11.17	2.49	0.67	0.25	0.06	0.10	0.02	100.01
GVL-18	102.02	K91	52.30	21.31	0.60	4.88	0.10	6.26	11.20	2.44	0.56	0.21	0.04	0.07	0.02	100.00
GVL-18	117.93	K92	52.77	25.33	0.34	2.73	0.05	2.61	11.95	2.98	0.92	0.24	0.05	0.03	0.01	100.00

Appendix B: Major Element Geochemical Data

Table 3:

BHID	Depth	Sample No.	SiO2	Al_2O_3	Fe_2O_3	FeO	MnO	MgO	CaO	Na_2O	K_2O	TiO_2	P_2O_5	Cr_2O_3	NiO	total
GVL-18	150.40	K94	53.39	20.11	0.66	5.34	0.11	6.16	10.52	2.57	0.67	0.30	0.06	0.08	0.02	100.00
GVL-05	51.26	K95	43.96	2.83	1.03	8.33	0.14	40.78	1.37	0.08	0.07	0.09	0.03	0.94	0.35	99.99
GVL-05	74.71	K96	41.24	1.65	1.46	11.85	0.15	41.33	0.19	0.03	0.00	0.08	0.02	1.62	0.37	100.00
GVL-05	114.16	K97	40.36	1.95	1.30	10.58	0.09	41.70	0.25	0.05	0.00	0.06	0.02	3.20	0.43	100.00
GVL-05	158.49	K98	53.70	2.26	0.91	7.35	0.17	32.86	1.59	0.15	0.19	0.08	0.02	0.57	0.13	100.00
GVL-05	207.88	K99	42.56	1.21	1.10	8.95	0.18	41.89	2.31	0.09	0.23	0.04	0.03	1.05	0.38	100.00
GVL-05	261.77	K100	43.53	1.65	1.07	8.71	0.11	43.81	0.10	0.05	0.03	0.05	0.03	0.44	0.41	100.00
GVL-05	304.24	K101	45.14	1.28	0.94	7.63	0.14	42.30	0.87	0.07	0.07	0.04	0.02	1.03	0.47	100.00
GVL-05	332.11	K102	41.18	1.01	0.98	8.02	0.13	47.15	0.40	0.07	0.07	0.03	0.02	0.65	0.29	100.01
GVL-05	361.54	K103	43.63	1.27	0.96	7.89	0.13	44.03	0.49	0.06	0.01	0.04	0.02	1.06	0.40	100.00
GVL-05	404.31	K104	42.85	1.15	1.05	8.57	0.14	44.08	0.55	0.08	0.03	0.03	0.02	1.08	0.36	100.00
GVL-05	414.80	K105	15.60	16.05	2.33	18.83	0.46	29.84	0.94	0.18	0.11	0.35	0.11	14.86	0.33	100.00
GVL-05	419.01	K106	40.73	1.51	1.01	8.31	0.11	45.71	0.08	0.08	0.05	0.05	0.02	1.90	0.44	100.01
GVL-05	423.23	K107	45.54	1.31	0.91	7.30	0.17	42.58	0.63	0.06	0.03	0.06	0.02	1.06	0.34	100.00
GVL-05	443.39	K108	43.91	0.99	0.84	6.80	0.09	46.04	0.03	0.08	0.00	0.03	0.02	0.77	0.38	100.01
GVL-05	507.82	K109	52.13	2.46	0.94	7.61	0.16	33.76	1.55	0.20	0.10	0.06	0.03	0.85	0.15	100.00
GVL-05	559.49	K110	41.30	2.12	1.11	9.06	0.16	43.37	1.18	0.10	0.08	0.07	0.04	1.02	0.39	100.00
GVL-05	599.29	K111	55.09	15.93	1.05	8.58	0.15	5.21	8.14	3.73	0.60	1.20	0.29	0.01	0.02	100.00
GVL-03	55.59	K112	53.22	18.65	0.63	5.10	0.12	6.88	11.98	2.29	0.70	0.29	0.06	0.06	0.02	100.00
GVL-03	129.21	K113	52.47	25.80	0.35	2.82	0.05	2.28	12.49	3.01	0.48	0.19	0.04	0.00	0.01	100.01
GVL-03	137.82	K114	51.51	22.82	0.52	4.20	0.09	4.42	12.91	2.74	0.46	0.22	0.05	0.03	0.02	100.00
GVL-03	148.03	K115	50.86	25.55	0.57	4.57	0.06	2.32	12.40	2.54	0.64	0.14	0.03	0.01	0.31	100.00
GVL-03	203.40	K116	48.61	29.76	0.13	1.05	0.03	0.75	15.15	1.85	2.57	0.06	0.02	0.00	0.02	100.00
GVL-03	217.67	K117	54.19	5.30	1.33	10.76	0.25	22.18	4.54	0.64	0.15	0.23	0.02	0.33	0.07	99.99
GVL-03	227.24	K118	51.12	24.90	0.37	2.99	0.07	5.59	11.66	2.45	0.59	0.11	0.03	0.07	0.05	100.00
GVL-03	334.66	K119	51.84	21.22	0.54	4.38	0.11	7.60	10.82	2.58	0.31	0.15	0.02	0.39	0.02	99.99
GVL-03	385.15	K120	51.68	20.04	0.66	5.39	0.12	8.81	10.67	2.07	0.20	0.13	0.02	0.18	0.02	100.01
GVL-03	414.89	K121	51.65	21.97	0.52	4.15	0.09	6.56	11.96	2.48	0.24	0.15	0.02	0.21	0.02	100.02
GVL-03	436.35	K122	49.72	15.58	1.08	8.80	0.14	10.86	11.42	1.77	0.17	0.16	0.02	0.13	0.14	100.00
GVL-03	464.40	K123	44.16	2.75	1.65	13.40	0.15	35.24	0.89	0.06	0.07	0.09	0.03	1.21	0.30	100.00

d

Appendix B: Major Element Geochemical Data

Table 4:

BHID	**Depth**	**Sample No.**	**SiO2**	**Al_2O_3**	**Fe_2O_3**	**FeO**	**MnO**	**MgO**	**CaO**	**Na_2O**	**K_2O**	**TiO_2**	**P_2O_5**	**Cr_2O_3**	**NiO**	**total**
GVL-03	485.56	K125	47.14	16.21	1.90	15.39	0.09	6.77	5.75	4.26	0.64	0.07	0.02	0.06	1.70	100.01
GVL-03	508.67	K126	49.61	5.28	1.18	9.63	0.14	29.13	2.43	0.13	0.12	0.13	0.02	1.97	0.23	99.99
GVL-03	509.98	K127	55.16	4.74	0.92	7.43	0.15	27.08	3.07	0.55	0.14	0.12	0.03	0.51	0.10	100.00
GVL-03	527.57	K128	46.75	4.17	1.17	9.44	0.14	30.55	5.96	0.23	0.02	0.10	0.04	0.89	0.55	100.02
GVL-03	535.46	K129	43.32	4.73	1.03	8.30	0.13	37.67	2.15	0.07	0.10	0.13	0.04	1.73	0.59	99.99
GVL-03	546.93	K130	52.70	15.15	1.28	10.36	0.20	10.43	6.87	2.41	0.22	0.18	0.02	0.11	0.07	100.02
GVL-03	559.69	K131	43.81	3.30	1.06	8.59	0.15	40.23	0.71	0.08	0.12	0.08	0.02	1.37	0.47	100.00
GVL-03	584.19	K132	42.72	3.16	1.03	8.24	0.12	40.76	0.60	0.06	0.02	0.08	0.02	2.83	0.38	100.02
GVL-04	604.58	K133	41.92	3.35	1.06	8.54	0.12	40.96	0.56	0.07	0.01	0.08	0.03	2.92	0.38	100.01

Appendix B: Minor and Trace Element Geochemical Data

Table: 5

			Trace elements (ppm)																	
BHID	**Depth**	**Sample**	**Sc**	**V**	**Cr**	**Co**	**Ni**	**Cu**	**Zn**	**Ga**	**Rb**	**Sr**	**Y**	**Zr**	**Nb**	**Mo**	**Ba**	**Pb**	**Th**	**U**
GVL-04	16.95	K1	20	54.33	707.1	36.73	187.66	19.3	44.71	16.16	14.05	324.1	4.84	13.6	0.05	0.59	138.64	21.6	d.l.	d.l.
GVL-04	30.15	K2	7.19	33.42	433.66	16.51	191.15	35.72	18.08	15.17	25.56	260.25	9.8	80.2	1.94	0.39	220.97	7.98	d.l.	d.l.
GVL-04	76.15	K5	2.14	d.l.	1.83	d.l.	7.36	14.92	7.71	15.81	91.03	49.88	43.9	448	17.2	1.22	1157.5	11.1	16.1	d.l.
GVL-04	83.05	K6	24.8	84.42	787.19	44.01	196.35	33.08	53.72	15.54	12.81	334.62	4.67	16.8	1.66	d.l.	187.32	11	d.l.	d.l.
GVL-04	85.15	K7	91.6	246.59	1071.33	71.93	508.81	307.57	117.26	8.75	16.62	78.06	37.7	53.5	2.77	0.24	144.34	12.2	d.l.	d.l.
GVL-04	104.15	K8	36	1310.6	123177	180.06	1681.6	1902.5	358.49	29.1	15.69	158.18	4.6	13.5	2.86	0.57	263.05	17.1	d.l.	d.l.
GVL-04	105.95	K9	22.1	75.11	1091.31	97.81	1576.6	1881.9	82.2	13.02	30.55	310.07	2.67	8.98	0.47	d.l.	342.21	29.1	d.l.	d.l.
GVL-04	110.15	K10	24.5	83.13	622.4	58.49	454.77	706.98	61.41	14.38	16.46	290.67	4.7	16.5	2.21	d.l.	162.77	25.6	d.l.	d.l.
GVL-04	114.45	K11	30	85.01	689.5	153.55	1669.1	1839.4	75.34	12.67	7.22	210.92	3.85	11.4	3.1	1.81	82.8	23.6	d.l.	d.l.
GVL-04	212.15	K12	20.3	84.84	5157.28	112.7	1773.9	5.41	70.28	4.26	5.67	38.73	4.76	8.59	1.18	0.66	58.75	7.78	0.04	d.l.
GVL-04	227.15	K13	11.5	19.04	1629.81	65.76	1056.3	d.l.	50.06	6.02	29.69	13.48	33.1	214	10.6	0.69	33.08	5.29	7.44	d.l.
GVL-04	254.15	K14	12.5	65.98	7638.21	144.19	2483.1	d.l.	81.28	3.98	7.89	22.29	2.36	3.3	2.15	0.91	26.18	7.74	d.l.	d.l.
GVL-04	264.15	K15	19.5	30.18	2845.62	41.1	1126.3	d.l.	80.74	8.17	85.54	22.76	39.6	294	10.8	0.13	140.59	13.2	8.43	d.l.
GVL-04	272.15	K16	28.9	139.37	3811.08	80.57	632.02	31.98	116.35	5.54	26.35	209.64	7.47	3.19	1.17	1.24	658	4.98	d.l.	d.l.
GVL-04	357.85	K17	27.9	47.75	330.96	14.18	272.63	35.82	31.29	19.48	72.64	1576.4	9.82	5.06	d.l.	0.53	1066.6	12	2	1.9
GVL-04	420.15	K18	4.24	19.21	2379.38	153.48	2767.4	170.02	29.1	0.26	0.7	0.93	1.3	0.73	0.73	d.l.	8.71	8.27	d.l.	d.l.
GVL-04	455.54	K19	7.51	128.25	54501.6	190.54	3609.5	d.l.	255.5	3.23	0.43	0.34	1.32	3.68	1.07	0.91	17.51	11.6	d.l.	d.l.
GVL-04	461.75	K20	14.1	883.67	387822	192.9	2882.6	d.l.	555.29	11.11	1.45	0.73	1.3	2.49	2.84	0.86	37.59	10.9	d.l.	d.l.
GVL-04	467.15	K21	5.28	42.49	11428.2	207.27	3468	363.78	66.89	0.21	d.l.	1.01	0.38	1.24	0.45	0.1	2.19	10.6	d.l.	d.l.
GVL-04	517.95	K22	10	40.83	8376.53	136.84	3854	0.15	100.21	1.95	10.12	12.03	0.73	8.23	0.74	0.11	28.45	7.79	d.l.	d.l.
GVL-04	533.15	K23	21.5	45.52	5166.62	106.4	2115.3	d.l.	83.46	4.02	37.46	38.77	19.7	205	2.76	0.82	159.79	7.25	d.l.	d.l.
GVL-04	538.15	K24	8.13	42.32	7557.87	115.85	1661.7	8.24	116.92	1.86	7	0.92	1.16	2.56	0.28	0.88	7.96	10.7	d.l.	d.l.
GVL-04	542.50	K25	7.19	72.17	19054	172.63	8760.4	d.l.	176.59	3.58	4.14	45.88	0.39	1.23	0.74	0.01	24.97	13.5	d.l.	d.l.
GVL-04	548.15	K26	5.29	44.19	12053.3	143.4	3028.7	d.l.	95.41	1.65	2.11	1.98	1.4	4.83	2.13	1.19	3.73	8.46	0.55	d.l.
GVL-04	566.05	K27	10.2	53.66	5323.53	104.69	2768.1	0.83	87.55	2.58	50.57	14.35	6.5	13.5	3.76	0.61	63	14.3	1.85	d.l.
GVL-04	569.15	K28	6.08	35.88	7248.23	136.48	3052.7	d.l.	109.18	2.35	5.07	0.77	0.01	1.63	1.09	0.02	3.86	12.1	d.l.	d.l.
GVL-02	219.55	K29	30.3	231.52	5451.04	49.77	202.07	81.6	78.42	17.64	26.24	279.16	17.1	84.1	5.66	1.49	347.5	5.45	3.12	d.l.
GVL-02	222.55	K30	38	661.51	33558.9	82.47	461.62	238.28	140	21.02	20.87	269.89	12.1	46.8	5.02	0.98	393.74	10	d.l.	d.l.
GVL-02	231.15	K31	26.1	123.56	1053.3	45.05	158.32	55.58	54.06	15	22.99	276.93	10.5	77.9	4.47	0.03	278.06	10.4	2.38	d.l.

Appendix B: Minor and Trace Element Geochemical Data

Table: 6

			Trace elements (ppm)																	
BHID	**Depth**	**Sample**	**Sc**	**V**	**Cr**	**Co**	**Ni**	**Cu**	**Zn**	**Ga**	**Rb**	**Sr**	**Y**	**Zr**	**Nb**	**Mo**	**Ba**	**Pb**	**Th**	**U**
GVL-02	250.15	K32	28.8	152.71	854.53	46.64	209.17	68.03	66.68	14.3	19.78	284.06	14	58.9	4.55	0.35	267.58	11.1	0.92	d.l.
GVL-02	261.16	K33	20.9	99.11	1346.87	103.07	1412.6	1031.2	67.72	12.9	28.78	260.12	6.03	20.4	1.97	0.11	342.5	10.2	d.l.	d.l.
GVL-02	288.61	K34	39.4	164.43	1499.35	73.67	414.08	4.54	91.41	8.89	22.56	244.55	6.14	28.4	2.26	0.27	268.28	13.2	d.l.	d.l.
GVL-02	294.16	K35	35.7	215.64	362.85	53.71	149.87	112.79	74.72	19	26.48	278.19	18.2	29.6	3.8	0.93	269.22	12	d.l.	d.l.
GVL-04	599.38	K36	16.6	58.85	4984.05	68.05	890.84	11	61.99	3.23	12.1	21.43	5.75	19.9	1.84	0.17	104.55	13.3	d.l.	d.l.
GVL-04	370.87	K37	9.54	28.1	3765.88	52.94	1676.9	45.06	30.16	0.69	0.84	1.29	0.95	3.66	0.7	0	1.39	7.24	1.94	d.l.
GVL-09	16.37	K38	41	610.3	50290.3	127.58	1422.7	849.3	196.7	16.2	2.76	135.88	7.82	9.18	3.67	2.05	66.28	18	d.l.	d.l.
GVL-09	17.88	K39	46.3	172.33	2365.58	228.71	3487.3	1945.6	145.61	6.05	6.49	92.81	18.6	31.2	4.34	0.2	74.7	12	d.l.	d.l.
GVL-09	20.88	K40	17.1	78.21	1345.93	213.47	2179.2	2606.8	70.36	10.9	12.13	300.14	2.83	6.96	2.66	0.35	117.87	26.8	d.l.	d.l.
GVL-09	63.45	K41	24.4	90.03	1306.66	102.94	504.63	440.37	71.02	9.5	68.51	250.4	2.81	5.48	1.36	0.72	260.47	9.92	d.l.	d.l.
GVL-09	74.85	K42	14.6	77.71	4834.02	108.15	1479.2	67	81.36	5.98	10.66	39.22	2.01	9.44	1.66	1.06	42.94	9.01	d.l.	d.l.
GVL-09	78.41	K43	19	83.08	6250.65	528.13	8552	4209.8	182.99	0.3	d.l.	3.34	0.18	2.92	0.63	d.l.	0.49	11.2	d.l.	d.l.
GVL-09	100.50	K44	13.9	55.36	13397.7	120.21	3142.5	87.89	49.61	1.64	4.56	8.32	1.09	14.6	0.22	0.38	22.89	12.2	d.l.	d.l.
GVL-09	129.97	K45	8.99	40.01	4042.56	222	5790.2	1411.6	64.91	0.79	1.44	9.21	1.11	1.69	0.08	0.78	2.19	11.8	d.l.	d.l.
GVL-09	142.71	K46	32.9	156.1	295.35	41.54	150.58	163.72	61.24	17.2	131.59	1182.1	4.77	5.29	0.19	0.24	2168	6.25	2.74	2.1
GVL-09	151.54	K47	28.9	103.82	3812.75	86.96	778.1	17.8	72.44	3.3	17.81	46.45	2.1	5.47	1.21	d.l.	180.04	4.85	d.l.	d.l.
GVL-09	198.62	K48	10.5	50.54	4883.76	119.47	2284.3	8.58	52.98	1.5	5.82	14.36	1.39	2.53	1.11	d.l.	31.94	9.36	d.l.	d.l.
GVL-09	229.02	K49	2.5	d.l.	23.05	0.03	10.28	13.91	72.09	17.2	127.06	87.72	44	460	12.7	1.2	1480.5	23	15.1	1
GVL-09	256.06	K50	5.13	22.05	2616.28	82.59	1982	5.26	69.91	0.88	12.13	12.41	0.52	2.03	1.37	0.51	51.64	9.05	d.l.	d.l.
GVL-09	262.84	K51	8.21	22.26	2850.85	82.06	3171.5	d.l.	58.87	0.59	9.31	8.5	0.5	1.88	0.53	d.l.	19.67	10.3	d.l.	d.l.
GVL-09	287.21	K52	13	42.73	7525.54	143.88	3658.4	143.01	69.1	2.76	12.81	16.09	4.47	39.5	0.51	0.02	52.51	8.5	0.55	d.l.
GVL-09	326.26	K53	11.6	35.4	4261.35	66.59	1288.9	21.49	23.98	1.29	2.39	4.28	0.54	3.4	-1	0.59	9.57	4.02	d.l.	d.l.
GVL-09	343.33	K54	8.71	74.56	22542.4	128.19	4678.8	81.81	167.44	1.96	-0.36	-0.15	-0.3	1.46	-0.9	0.3	4.31	3.2	d.l.	d.l.
GVL-09	352.34	K55	7.77	26.68	3856.3	80.32	1705.7	66.72	36.71	0.2	0.8	0.1	1.37	1.67	0.93	0.25	9.28	3.04	d.l.	d.l.
GVL-09	380.72	K56	5.75	17.63	3691.21	112.85	2989.3	14.8	71.92	1.1	6.75	9.14	0.85	1.1	1.21	0.08	28.76	4.12	d.l.	d.l.
GVL-09	398.57	K57	10.8	22.23	3800.84	77.91	2980.4	12.67	66.8	1.57	0.29	3.9	0.52	3.69	1.69	0.56	0.62	3.29	d.l.	d.l.
GVL-09	414.41	K58	6.99	30.69	4223.65	94.75	2827.6	14.69	48.47	0.68	0.37	0.2	1.25	2.25	1.13	0.32	8.68	2.16	d.l.	d.l.
GVL-09	439.31	K59	6.58	37.08	13276.2	94.03	2278.4	14.53	107	0.76	0.11	0.49	0.03	0.53	1.16	0.38	6.6	4.24	d.l.	d.l.
GVL-09	471.46	K60	8.11	22.88	6123.04	114.91	2887.5	13.84	41.98	0.58	0.35	10.58	0.43	0.97	0.98	0.48	11.78	2.25	d.l.	d.l.

Appendix B: Minor and Trace Element Geochemical Data

Table:7

			Trace elements (ppm)																	
BHID	**Depth**	**Sample**	**Sc**	**V**	**Cr**	**Co**	**Ni**	**Cu**	**Zn**	**Ga**	**Rb**	**Sr**	**Y**	**Zr**	**Nb**	**Mo**	**Ba**	**Pb**	**Th**	**U**
GVL-09	542.58	K65	12.8	50.58	3233.09	79.86	901.5	19.44	60.72	2.13	2.68	33.3	1.42	6.94	0.8	0.48	64.07	7.11	d.l.	d.l.
GVL-09	543.77	K66	13.9	50.85	3590.78	87.78	1212.8	30.36	60.92	1.77	2.11	18.57	0.86	7.37	0.23	0.37	44.69	8.77	d.l.	d.l.
GVL-09	551.31	K67	5.19	68.4	19281.4	154.8	4574	35.49	81.18	1.44	1.81	7.6	0.89	5.18	0.66	0.2	8.24	4.26	d.l.	d.l.
GVL-09	556.16	K68	7.32	35.99	8756.92	167.98	2560.6	15.11	64.46	1.25	1.39	4.06	0.98	2.86	1.05	0.76	17.09	2.44	d.l.	d.l.
GVL-09	563.19	K69	7.38	34.48	6586	101.74	2218.3	4.57	64.72	0.84	1.28	6.95	3.01	5.22	0.5	0.65	19.01	2.94	d.l.	d.l.
GVL-09	566.03	K70	2.64	75.61	23423	156.21	4277.6	21.38	84.56	2.05	1.27	0.05	0.88	2.61	0.39	0.62	8.28	4.19	d.l.	d.l.
GVL-09	567.30	K71	5.03	75.37	25013.3	161.36	3877.1	12.65	91.52	2.2	1.73	2.58	0.4	2.77	1.28	0.54	21.93	4.47	d.l.	d.l.
GVL-09	578.07	K72	6.83	37.04	7028.25	140.63	3333.9	7.35	55.14	1.12	1.21	13.91	0.91	4.85	0.91	0.38	32.09	5.36	d.l.	d.l.
GVL-09	600.74	K73	8.91	112.08	34170.7	219.95	17895	121.61	228.67	2.92	4.23	1.02	0.45	1.78	0.55	0.48	16.89	7.4	d.l.	d.l.
GVL-09	607.48	K74	7.61	17.94	2274.16	87.87	2536.8	10.32	72.03	3.72	3.13	22.09	0.85	0.45	0.35	0.27	28.94	0.14	d.l.	d.l.
GVL-11	33.39	K75	11.4	7.61	55.4	17.93	740.45	78.39	27.06	16.8	148.84	351.24	0.59	4.81	0.68	0.02	580.45	22.7	d.l.	d.l.
GVL-11	39.54	K76	23.1	117	1484.3	128.82	3507.5	2059.1	70.86	8.65	0.34	153.33	4.26	8.54	1	0.45	53.83	8.62	d.l.	0.6
GVL-11	42.05	K77	14.9	22.34	106.04	10.07	109.99	68.69	15.24	19.8	21.43	434.48	1.58	8.39	0.88	0.26	161.63	10.7	d.l.	0.8
GVL-11	53.74	K78	20.7	92.64	1217.26	66.5	604.53	223.26	55.51	11.2	4.66	214.96	2.4	10.8	1.18	0.22	67.71	2.64	d.l.	0.6
GVL-11	74.52	K79	20.9	68.93	685.5	41.68	211.29	30.36	46.66	15	8.47	279.68	1.29	7.43	0.23	0.29	82.35	33.3	d.l.	d.l.
GVL-11	94.66	K80	22.3	82.29	546.09	42.57	212.55	60	48.14	13.4	2.83	283.18	2.12	6.18	1.48	0.8	74.73	1.45	d.l.	d.l.
GVL-11	131.62	K81	27.8	105.39	1028.62	47.45	210.58	52.8	68.33	14.9	3.04	267.04	5.31	12.8	0.52	0.98	120.21	11.2	d.l.	0.7
GVL-11	155.23	K82	25.8	91.44	686.04	37.91	162.94	47.47	45.91	16.5	9.92	313.41	4.13	11.9	0.23	0.03	141.02	4.83	d.l.	0.4
GVL-11	174.40	K83	26.7	102.04	554.13	37.64	155.75	30.96	50.42	16.9	9.7	317.06	5.05	11.5	0.05	0.06	160.35	5.71	d.l.	d.l.
GVL-11	197.23	K84	21.8	110.51	782.93	40.79	164.01	50.32	52.39	17.1	2.32	328.46	5.12	11.4	0.48	0.59	138.54	3.87	d.l.	d.l.
GVL-18	23.67	K85	20.4	67.75	451.74	30.82	140.81	39.35	34.78	16.9	6.24	328.37	5.06	27.4	1.23	0.04	149.22	3.16	d.l.	d.l.
GVL-18	41.73	K86	19.6	73.3	380.7	30.9	119.0	35.4	36.5	16.8	15.2	355.5	5.4	21.9	0.0	d.l.	157.1	3.9	d.l.	d.l.
GVL-18	52.95	K87	37.6	164.3	828.7	44.2	186.7	21.3	142.1	14.7	15.1	231.8	13.8	45.8	0.3	0.1	170.3	14.0	d.l.	d.l.
GVL-18	57.45	K88	24.9	116.6	552.7	46.3	206.9	46.6	66.1	16.7	13.4	260.9	8.9	32.9	0.8	0.0	195.0	8.9	d.l.	d.l.
GVL-18	72.41	K89	20.9	76.8	354.0	28.7	117.5	37.3	41.7	17.4	16.2	346.3	5.4	11.9	0.2	0.5	156.8	4.9	d.l.	0.1
GVL-18	89.80	K90	26.6	95.1	616.4	41.5	172.4	81.2	56.8	15.3	19.5	289.3	8.6	24.7	0.1	d.l.	228.5	22.5	d.l.	d.l.
GVL-18	102.02	K91	21.0	84.2	456.7	28.5	127.4	29.9	43.7	16.1	15.0	323.2	5.4	24.9	d.l.	0.0	204.9	5.1	d.l.	d.l.
GVL-18	117.93	K92	17.1	47.6	170.6	17.7	57.3	25.7	27.4	19.7	29.5	383.7	6.2	36.8	0.4	d.l.	252.0	5.9	d.l.	0.0
GVL-18	126.81	K93	20.8	93.1	477.8	32.5	141.6	47.8	50.0	16.3	15.4	321.9	8.1	39.1	0.2	0.1	236.5	5.0	d.l.	0.1

Appendix B: Minor and Trace Element Geochemical Data

Table: 8

			Trace elements (ppm)																	
BHID	**Depth**	**Sample No.**	**Sc**	**V**	**Cr**	**Co**	**Ni**	**Cu**	**Zn**	**Ga**	**Rb**	**Sr**	**Y**	**Zr**	**Nb**	**Mo**	**Ba**	**Pb**	**Th**	**U**
GVL-05	158.49	K98	17.1	59.9	3303.8	86.0	1042.8	3.2	61.2	2.6	9.3	24.9	3.8	4.7	d.l.	d.l.	30.6	3.4	d.l.	d.l.
GVL-05	207.88	K99	5.6	22.3	3958.8	103.9	2147.1	2.2	53.7	0.1	11.0	110.0	2.7	41.7	d.l.	0.1	64.1	1.2	d.l.	d.l.
GVL-05	261.77	K100	6.2	15.9	1683.2	105.6	2965.7	d.l.	37.7	0.4	0.4	3.3	2.7	1.9	d.l.	d.l.	10.7	3.0	d.l.	d.l.
GVL-05	304.24	K101	13.3	28.4	4204.5	127.8	3067.1	1.1	53.4	1.3	0.9	6.7	1.7	1.3	d.l.	d.l.	5.2	5.2	d.l.	d.l.
GVL-05	332.11	K102	8.5	16.4	2342.8	127.4	2050.0	6.1	50.5	1.0	2.2	6.4	0.4	0.5	d.l.	d.l.	9.3	3.9	d.l.	d.l.
GVL-05	361.54	K103	7.3	24.9	3793.8	115.0	2905.0	d.l.	46.6	1.1	2.3	5.2	2.2	2.4	0.4	d.l.	0.6	7.3	d.l.	d.l.
GVL-05	404.31	K104	7.5	21.9	4381.0	135.5	2647.9	d.l.	55.7	0.2	1.1	6.6	0.9	0.9	0.3	d.l.	9.2	3.1	d.l.	d.l.
GVL-05	414.80	K105	46.6	2009.0	784172.6	230.7	2342.2	d.l.	1111.1	24.8	0.9	8.9	5.4	3.8	1.6	1.5	30.4	7.0	d.l.	d.l.
GVL-05	419.01	K106	7.5	25.4	7336.9	118.4	3118.0	d.l.	55.6	1.4	1.0	0.1	1.7	4.9	d.l.	0.2	15.6	1.9	d.l.	d.l.
GVL-05	423.23	K107	11.6	33.3	4416.6	111.1	2417.5	d.l.	55.3	1.8	1.6	3.8	1.7	1.8	d.l.	0.7	11.8	5.8	d.l.	0.5
GVL-05	443.39	K108	6.1	17.4	2849.8	91.6	2569.3	d.l.	32.9	1.1	1.6	0.4	1.5	1.1	d.l.	d.l.	5.0	4.9	d.l.	d.l.
GVL-05	507.82	K109	15.6	58.1	4480.0	97.0	1055.7	16.0	53.8	0.7	3.0	17.8	1.9	4.3	d.l.	0.4	42.2	4.8	d.l.	d.l.
GVL-05	559.49	K110	10.2	38.1	4384.7	129.6	2819.6	d.l.	50.0	1.3	2.5	16.0	2.5	4.3	d.l.	0.5	52.4	6.1	d.l.	d.l.
GVL-05	599.29	K111	27.6	185.9	65.6	41.4	115.2	39.3	80.0	19.2	20.7	310.2	46.2	206.5	9.9	0.3	438.6	16.6	0.1	2.9
GVL-03	55.59	K112	29.5	133.0	317.1	33.3	154.4	33.5	67.1	16.2	17.2	239.4	8.4	39.2	3.1	1.3	218.0	10.2	2.9	d.l.
GVL-03	129.21	K113	15.6	54.5	49.7	14.2	59.8	37.9	34.9	20.3	10.0	322.7	3.2	26.9	2.2	0.9	150.3	6.8	2.0	d.l.
GVL-03	137.82	K114	21.4	96.9	170.3	26.3	117.8	44.0	43.7	17.7	8.6	283.3	6.7	32.0	2.4	0.0	153.1	3.0	2.1	d.l.
GVL-03	148.03	K115	12.2	43.4	62.9	63.1	2077.6	2743.9	62.8	18.8	17.7	312.0	2.5	26.0	0.8	d.l.	309.1	16.7	d.l.	d.l.
GVL-03	203.40	K116	8.4	14.0	31.9	4.8	155.4	18.4	82.6	21.1	108.6	328.9	0.8	5.7	1.4	0.3	476.4	24.2	2.2	d.l.
GVL-03	217.67	K117	34.3	132.1	2063.6	87.4	566.8	26.7	106.3	6.0	4.6	58.8	6.3	16.5	0.2	d.l.	58.5	13.6	d.l.	d.l.
GVL-03	227.24	K118	11.9	40.6	443.5	28.2	370.2	154.6	27.4	17.1	17.0	379.3	5.0	13.8	0.4	d.l.	208.5	10.4	d.l.	d.l.
GVL-03	334.66	K119	20.1	88.4	1994.9	36.4	195.4	18.5	67.4	17.8	8.2	299.5	8.8	18.1	1.6	d.l.	145.6	4.3	d.l.	d.l.
GVL-03	385.15	K120	25.1	73.0	1052.8	41.3	194.9	30.7	44.7	16.2	2.4	323.0	3.7	7.9	0.6	0.3	100.5	5.5	d.l.	d.l.
GVL-03	414.89	K121	23.3	85.4	1181.0	29.1	135.4	28.6	31.0	18.6	3.7	348.2	4.5	9.6	0.0	d.l.	133.7	2.2	d.l.	d.l.
GVL-03	436.35	K122	34.1	92.9	806.9	106.6	1005.2	1405.0	93.6	13.3	1.8	224.5	7.3	6.7	0.1	d.l.	89.9	226.2	d.l.	d.l.
GVL-03	464.40	K123	11.8	52.5	5052.1	180.8	1755.1	538.6	101.6	1.2	1.9	10.2	3.5	8.7	0.2	d.l.	0.6	11.8	d.l.	d.l.
GVL-03	480.84	K124	38.8	139.0	2440.5	229.1	2307.4	610.6	64.1	9.1	4.6	174.4	9.2	10.7	0.0	d.l.	121.2	10.6	d.l.	d.l.
GVL-03	485.56	K125	19.0	49.9	409.2	436.1	12354.4	1426.6	53.6	16.6	15.6	493.4	3.2	0.7	0.5	1.0	309.9	17.8	d.l.	d.l.
GVL-03	508.67	K126	9.7	88.1	8801.5	107.6	1604.9	11.8	70.7	4.9	5.8	30.4	3.7	10.1	0.7	1.1	51.6	6.7	d.l.	d.l.

Appendix B: Minor and Trace Element Geochemical Data

Table: 9

			Trace elements (ppm)																
BHID	**Depth**	**Sample**	**Sc**	**V**	**Cr**	**Co**	**Ni**	**Cu**	**Zn**	**Ga**	**Rb**	**Sr**	**Y**	**Zr**	**Nb**	**Mo**	**Ba**	**Pb**	**Th**	**U**
GVL-03	509.98	K127	21.30	88.65	3028.57	79.63	764.58	15.19	63.25	3.27	5.08	58.77	3.18	18.20	1.46	0.12	69.37	6.10	0.30	d
GVL-03	527.57	K128	17.05	58.07	4640.30	77.91	3271.07	426.14	68.27	3.89	0.32	10.91	2.30	16.83	0.37	0.05	17.27	7.65	d.l.	d
GVL-03	535.46	K129	10.42	53.51	7870.73	128.83	4083.70	70.27	59.03	2.17	7.99	19.60	2.31	24.89	1.88	0.80	93.57	13.41	0.04	d
GVL-03	546.93	K130	25.06	172.28	707.57	87.16	483.55	######	97.48	16.38	2.82	270.98	1.62	0.96	0.80	0.45	156.18	9.78	1.31	d
GVL-03	559.69	K131	10.50	45.43	5502.87	112.70	2973.06	10.96	45.78	2.09	3.37	5.14	1.04	4.19	1.05	d.l.	14.74	4.80	d.l.	d
GVL-03	584.19	K132	10.14	48.47	11838.95	97.13	2879.46	58.36	45.42	0.88	0.65	2.70	0.09	2.91	0.03	d.l.	1.83	3.81	d.l.	d
GVL-04	604.58	K133	10.99	68.68	12791.52	125.52	2872.60	6.73	50.10	2.36	0.81	4.14	0.20	1.56	0.10	0.04	13.93	3.18	d.l.	d

Appendix C: Assay Data

BHID	From	To	Sample Length	Depth	Pt+Pd
GVL 1	474	474.09	0.09	474.045	0.02
GVL 10	142	143.2	1.2	142.6	0.11
GVL 10	144	144.85	0.85	144.425	1.95
GVL 10	144.9	144.96	0.06	144.93	1.24
GVL 10	145.5	146.55	1.05	146.025	0.75
GVL 10	146.5	148	1.5	147.25	0.88
GVL 10	148	149	1	148.5	0.57
GVL 10	149	150	1	149.5	0.55
GVL 10	150	152	2	151	0.62
GVL 10	152	155	3	153.5	0.8
GVL 10	155	156.72	1.72	155.86	0.14
GVL 10	155.03	156.75	1.72	155.89	0.14
GVL 10	156.75	157.97	1.22	157.36	0.52
GVL 10	157.97	159.23	1.26	158.6	0.6
GVL 10	159.23	160.25	1.02	159.74	0.86
GVL 10	160.25	161.28	1.03	160.765	0.77
GVL 10	161.28	162.3	1.02	161.79	0.73
GVL 10	167	168.8	1.8	167.9	0.27
GVL 10	169	170.95	1.95	169.975	0.34
GVL 10	171	173	2	172	0.41
GVL 10	173	175	2	174	0.4
GVL 10	181	183	2	182	0.23
GVL 10	183	185	2	184	0.15
GVL 10	185	187.4	2.4	186.2	0.07
GVL 10	221	223	2	222	0.2
GVL 10	228.5	230.5	2	229.5	0.39
GVL 10	248.5	250.5	2	249.5	0.32
GVL 10	266.25	268.25	2	267.25	0.47
GVL 10	276	278	2	277	0.69
GVL 10	278	280	2	279	0.39
GVL 10	280	282	2	281	0.37
GVL 10	282	284	2	283	0.48
GVL 10	284	286	2	285	0.28
GVL 10	293.25	295.25	2	294.25	0.34
GVL 10	295	297	2	296	0.2
GVL 10	297.6	298.9	1.3	298.25	0.16
GVL 10	297.3	298.6	1.3	297.95	1.08
GVL 10	300.75	301.75	1	301.25	0.34
GVL 12	26.7	28.68	1.98	27.69	0.05
GVL 12	28.7	29.7	1	29.2	1.565
GVL 12	29.5	30.53	1.03	30.015	1.05
GVL 12	30.5	32.65	2.15	31.575	0.49
GVL 13	125.1	127.02	1.92	126.06	1.27
GVL 14	49	100	51	74.5	1.16
GVL 14	72.75	74.75	2	73.75	1.03
GVL 14	98	100	2	99	0.23
GVL 14	100	101.7	1.7	100.85	0.365
GVL 14	101.65	103.3	1.65	102.48	0.31
GVL 14	103.25	104.9	1.65	104.08	0.17
GVL 14	105.25	107.02	1.77	106.14	0.12
GVL 14	149.7	151	1.3	150.35	1.04
GVL 15	88.5	90	1.5	89.25	1.61
GVL 15	90	92	2	91	0.74
GVL 15	92	94	2	93	1.19
GVL 15	94	95.5	1.5	94.75	0.72
GVL 15	97.5	98.9	1.4	98.2	1.02
GVL 15	99	101	2	100	0.48
GVL 15	101	103	2	102	0.6
GVL 15	103	105	2	104	0.87
GVL 15	105	107	2	106	0.56
GVL 15	138.75	140.4	1.65	139.58	0.47
GVL 15	140.5	140.75	0.25	140.63	1.4
GVL 15	140.75	142.4	1.65	141.58	1
GVL 15	142.25	142.65	0.4	142.45	1.44

Appendix D: Core Logging

BH ID	From	To	Contact	Description	Lithology	Alteration
GVL 01	0	13.85	sharp	m/g to f/g	Quartzite	
GVL 01	13.85	46.53	sharp	dark-grey in colour. Feldspar + pyroxene dominated. F/G Disseminated sulfide specks- possibly Pyrite. Highly Fractured.	Melagabbro	
GVL 01	46.53	48.95	sharp	Crumbly. Extremely fractured core. Quartzite vein?	Quartzite	
GVL 01	48.95	58.36	sharp	dark-grey in colour. Feldspar + pyroxene dominated. F/G Disseminated sulfide specks- possibly Pyrite. Highly Fractured.	Melagabbro	
GVL 01	58.36	71.98	sharp	Pyroxene inclusions-specks. Sharp sub-horizontal contacts	Quartzite	
GVL 01	71.98	74.97	sharp	dark-grey in colour. Feldspar + pyroxene dominated. F/G Disseminated sulfide specks- possibly Pyrite. Highly Fractured.	Melagabbro	
GVL 01	74.97	91.85	sharp	Visable "flows" or flow textured. Shear zone? Melagabbro fragments/blocks within.	Recrystalised Melagabbro	Recrystalised
GVL 01	91.85	109.86	gradational	m/g to f/g. Plag Dominated. Opx + Cpx. Pyrite mineralization along fractures Gabbronorite?	Gabbronorite	
GVL 01	109.86	112.39		Dark green to black with army green patches	Feldspathic pyroxenite	Serpentinised
GVL 01	112.39	127.22	gradational	Massive completely serpentinised	Serpentinite	Serpentinised
GVL 01	127.22	132.3		intercollated with serpentinised Harzburgite	Feldspathic pyroxenite	Serpentinised
GVL 01	132.3	140.56	gradational	intercollated wit pyroxenite. Poikilitic texture. Highly fractured	Poikilitic Serpentinised Harzburgite	Serpentinised
GVL 01	140.56	144.24	gradational	Contains large/coarse Ruby red - copper coloured Mica	Pyroxenite	Altered
GVL 01	144.24	157.07	sharp	Quatrz and feldspar dominated intrusion. Sharp basal contact. Harzburgitic block inclusions	Granofels	
GVL 01	157.07	170.58	sharp	Poikilitic texture. Unmineralised.	Poikilitic Serpentinised Harzburgite	Serpentinised
GVL 01	170.58	173	sharp		Granofels	
GVL 01	173	178.44	gradational	F/G. Opx + Cpx and interstitial feldspar.	Feldspathic pyroxenite	
GVL 01	178.44	180.35	Sharp	Vertical undulatory contact	Pegmatoidal Feldspathic Pyroxenite	
GVL 01	180.35	187.55	sharp	Poikilitic texture, serpentinised. Fractures filled by green-silver Micas	Poikilitic Serpentinised Harzburgite	Serpentinised
GVL 01	187.55	188.35	sharp		Granofels	
GVL 01	188.35	189.24		Harzburgite serpentinised	Serpentinised Harzburgite	Serpentinised
GVL 01	189.24	192.3	sharp	Granofels with brecciated Harzburgite blocks	Granofels	
GVL 01	192.3	193.2	sharp		Serpentinised Harzburgite	
GVL 01	193.2	194.95	sharp	Granofels with brecciated Harzburgite blocks	Granofels	
GVL 01	194.95	198.2		sepentinised harzburgite	Serpentinised Harzburgite	Serpentinised
GVL 01	198.2	199.2	sharp	granofels with intercollated extremely altered Harzburgite	Granofels	
GVL 01	199.2	202.46	sharp	extremely f/g. feldspar + pyroxene dominated. Dyke-Sill? Cut by 20-60cm aplite vein.	Sill	
GVL 01	202.46	208.5			Serpentinised Harzburgite	Serpentinised
GVL 01	208.5	209.56	sharp	intercollated with serpentinised Harzburgite	Granofels	
GVL 01	209.56	287.2	sharp	Poikilitic Harzburgite. Massive	Poikilitic Serpentinised Harzburgite	Serpentinised
GVL 01	287.2	288.2	sharp		Granofels	
GVL 01	288.2	294.68	sharp		Serpentinised Harzburgite	serpentinised
GVL 01	294.68	303.4	sharp	granofels with harzburgite and pyroxenite clasts	Granofels	
GVL 01	303.4	308.02	sharp		Serpentinised Harzburgite	Serpentinised
GVL 01	308.02	311.14	sharp		Granofels	
GVL 01	311.14	311.88	sharp	highly fractured. Sharp contaccts	Serpentinised Harzburgite	Serpentinised
GVL 01	311.88	319.09	sharp		Granofels	
GVL 01	319.09	319.26	sharp	Pyrrhotite + possible chalcopyrite/pentlandite in pyroxenite. 30cm pyroxenite m/g to c/g	Massive Sulphide	
GVL 01	319.26	320.47	gradational		Serpentinised Harzburgite	
GVL 01	320.47	322.34	sharp	brecciated feldspathic pyroxenite. Brecciated by aplite veins.	Granofels	
GVL 01	322.34	338.9		minor Cr. Minor Magnetite. Disseminated sulphide specks	Serpentinised Harzburgite	
GVL 01	338.9	338.98	sharp	3 Chromite stringers bound by pyroxenite	Chromitite	
GVL 01	338.98	348.25	sharp	minor Cr. Minor Magnetite. Disseminated sulphide specks	Serpentinised Harzburgite	Serpentinised
GVL 01	348.25	349.2	sharp	with 30cm granofels inbetween	Granofels	
GVL 01	349.2	353.26	sharp	granopheric texture.	Granofels	
GVL 01	353.26	359.28	sharp		Serpentinised Harzburgite	
GVL 01	359.28	359.76	sharp	Pegmatitic. Granopheric texture. Basal contact 10 inclination.	Granofels	
GVL 01	359.76	373.82	sharp	Poikilitic-mottled	Poikilitic Serpentinised Harzburgite	Serpentinised
GVL 01	373.82	375.42	sharp	Quartz feldspar.	Granofels	
GVL 01	375.42	423.96	sharp	Poikilitic-mottled	Poikilitic Serpentinised Harzburgite	Serpentinised
GVL 01	423.96	426.6	sharp	Quartz feldspar vein. 30 basal contact	Granofels	
GVL 01	426.6	430.68	sharp	Proper poikilitic Harzburgite, more mottles.	Poikilitic Serpentinised Harzburgite	Serpentinised
GVL 01	430.68	432.15	sharp	Mostly greenish. Opx plag + Qtz	Granofels	Chlroritised?
GVL 01	432.15	441.9	sharp	Porphiritic /poikilitic Harzburgite	Poikilitic Serpentinised Harzburgite	Serpentinised
GVL 01	441.9	442.5	sharp	feldspar + opx pegmatoidal vein.	Vein	
GVL 01	442.5	450.7		Poikilitic. Closer opx oikocrysts.	Poikilitic Serpentinised Harzburgite	Serpentinised
GVL 01	450.7	451.74	gradational	M/g sharp basal 30 inclination	Feldspathic pyroxenite	
GVL 01	451.74	454	sharp	Qtz + Feldspar vein. M/G	Granofels	
GVL 01	454	459.9	gradational	M/g to F/g.	Feldspathic pyroxenite	
GVL 01	459.9	462	gradational	M/g	Pyroxenite	

Appendix D: Core Logging

BH ID	From	To	Contact	Description	Lithology	Alteration
GVL 01	462	466.75	sharp	m/g - f/g . Sharp, undulatory basal contact	Feldspathic pyroxenite	
GVL 01	466.75	473.36	sharp	m/g. brecciated pyroxenite blocks within.	Granofels	
GVL 01	473.36	477	sharp	aplite veined. f/g to m/g. disseminated sulphide specks.	Feldspathic pyroxenite	
GVL 01	477	493.9	sharp	cream. Dyke? f/g	Granofels	
GVL 01	493.9	521	sharp	Dyke? Massive. F/g to M/g/ grey. 55 inclination	Diabase	
GVL 01	521	552	sharp	cream. Dyke? f/g. 60 inclination.	Granofels	
GVL 01	552	600.45	Sharp	QUARTZITE, altered, blotchy banded, reddish-grey, finely to medium crystalline, POTASSIC ALTERED PRETORIA GROUP SE	Quartzite	
GVL 02	0.00	22.42	Inferred	highly fragmented core. Plagioclase>Opx. Norite. Brownish colour. Highly weathered	Leuconorite	
GVL 02	22.42	28.51		Dark-green pyroxene. Medium-grained. Highly weathered. Crumbled/rubble.	Leuconorite	
GVL 02	28.51	35.67		highly weathered. Crumbly/rubble. Plagioclase>Opx.	Leuconorite	
GVL 02	35.67	37.85			Leuconorite	
GVL 02	37.85	38.85		Highly weathered zone of homogeneous norite	Norite	
GVL 02	38.85	40.42			Leuconorite	
GVL 02	40.42	43.37		Highly weathered norite. Rubble/crumbly	Norite	
GVL 02	43.37	45.95			Norite	
GVL 02	45.95	61.77		Norite with rusty-red staining (iron staining). Fractured. Cut my multiple Quartzofeldspathic veins.	Norite	
GVL 02	61.77	93		medium to coarse-grained.	Norite	
GVL 02	93.00	101.5		dark-green pyroxene. Greenish-coloured feldspar, altered (chloritisation)	Melanorite	
GVL 02	101.50	101.58		melanorite with rust-red iron staining. Veined and fractured.	Melanorite	
GVL 02	101.58	101.7		fine-grained. Quartzofeldspathic veins. Microfaulted	Granofels	
GVL 02	101.70	102.4		Norite with rusty-red staining (iron staining or K-feldspar staining. Fractured. Cut my multiple subvertical Quartzofeldspa	Norite	
GVL 02	102.40	104		Norite with rusty-red staining (iron staining or K-feldspar staining. Fractured. Cut my multiple subvertical Quartzofeldspa	Norite	
GVL 02	104.00	104.2			Norite	
GVL 02	104.20	104.35		altered. reddish in colour. Quartzofeldspathic veinlets.	Norite	
GVL 02	104.35	104.63			Norite	
GVL 02	104.63	105.8		Altered norite. Reddish colour. Greyish-silver mineral, not magnetic, sulphide? May contribute to the reddish colour	Norite	
GVL 02	105.80	106.02		Quartzofeldspathic veins. 25 degree inclination contact.	Granofels	
GVL 02	106.02	111.3		felsic and reddish coloured veins in norite. Highly veined	Norite	
GVL 02	111.30	124.9		fine to medium-grained. Feldspar>Opx>Cpx. Possibly gabbronorite?	Melanorite	
GVL 02	124.90	126.19		<10 degree inclination.	Granofels	
GVL 02	126.19	127		fine to medium-grained. Feldspar>Opx>Cpx. Possibly gabbronorite?	Melanorite	
GVL 02	127.00	127.74		Reddish altered norite. Pegmatitic feldspathic vein- sub-horizontal	Norite	
GVL 02	127.74	137.9		Interstitially disseminated suphides, lightly disseminated specks.	Melanorite	
GVL 02	137.90	142		Heavily veined.	Leuconorite	
GVL 02	142.00	144.5		Lightly disseminated sulphides. Interstitially disseminated sulphides.	Norite	
GVL 02	144.50	151.1			Leuconorite	
GVL 02	151.10	153.3		Reddish K-spar crystals (15%) Melanorite?	Melanorite	
GVL 02	153.30	160.65		Reddish norite. Altered. Highly weathered. Gradational contacts	Norite	
GVL 02	160.65	168.1		medium-grained. Interstitial scattered sulphide specks. Grades into fine-grained near the base.	Melanorite	
GVL 02	168.10	168.24		Leuconorite or spotted anorthosite? Irregular subhorizontal contacts.	Leuconorite	
GVL 02	168.24	172.53		Fine-grained. Mesonorite	Norite	
GVL 02	172.53	201.78		Coarse-grained norite. Minor phlogophite.	Norite	
GVL 02	201.78	203.52		Coarse-grained norite. Minor phlogophite.	Norite	
GVL 02	203.52	212.7		Opx>Cpx>plagioclase>Phlogophite. Fine-grained. 3 cm magnetite lenses.	Gabbronorite	
GVL 02	212.70	213.8		Opx>Cpx>plagioclase>Phlogophite. Fine-grained. Interstitially disseminated pyrrhotite and pyrite.	Gabbronorite	
GVL 02	213.80	214.02		Quartzofeldspathic intrusion with blocks of Norite/gabbronorite.	Gabbronorite	
GVL 02	214.02	222			Gabbronorite	
GVL 02	222.00	222.9		Chromitiferous rock. Plagioclase and Opx and Cpx. Interstitial disseminated sulphides, pyrrhotite and chalcopyrite. Blebb	Chromitiferous Pyroxenite	
GVL 02	222.90	226.4		Disseminated interstitial suphides, blebby pyrrhotite and chalcopyrite, oxidised to dark yellow. Chromite pods (2 cm) ne	Chromitiferous Pyroxenite	
GVL 02	226.40	232.52		Coarse-grained. Minor phlogophite. Lightly scattered sulphide specks.	Leuconorite	
GVL 02	232.52	259.63		Interstitially disseminated suphides, lightly disseminated specks.	Gabbronorite	
GVL 02	259.63	266.06		pegmatoidal texture. Large interstitial sulphides to blebby (pyrrhotite and chalcopyrite). Intercalated Pegmatoidal and e	Pegmatoidal Feldspathic Pyroxenite	
GVL 02	266.06	268.77		Not mineralised	Leuconorite	
GVL 02	268.77	270.5		highly fractured. Multiple irregular quartzofeldspathic veins.	Melanorite	
GVL 02	270.50	289.2		fine-grained greyish dark-green rock. Cannot identify minerals. (chill zone?)	Unidentifiable	
GVL 02	289.20	298.72		Plagioclase>chromite>Opx (possibly)	Unidentifiable	
GVL 02	298.72	300.1		fine-grained greyish dark-green rock. Cannot identify minerals. (chill zone?)	Unidentifiable	
GVL 02	300.10	301.1		quartz, feldspar and minor Opx. Granofels with assimilated Opx.	Granofels	
GVL 02	301.10	301.52		Plagioclase>chromite>Opx (possibly)	Unidentifiable	
GVL 02	301.52	301.67			Granofels	

Appendix D: Core Logging

BH ID	From	To	Contact	Description	Lithology	Alteration
GVL03	170.15	174.88	Gradational	Medium to coarse-grained. Spotted-Mottled opx 30-40% plagioclase.greenish alteration. Chloritisation?	Leuconorite	
GVL03	174.88	176.49	Sharp	>50% plagioclase.	Mottled Anorthosite	
GVL03	176.49	177.81	Sharp	assimilated mafic material.	Granofels	
GVL03	177.81	178.63	Sharp		Mottled Anorthosite	
GVL03	178.63	178.72	Sharp	Fine-grained. Pinkish-white colour.	Granofels	
GVL03	178.72	179.53	Sharp	Cut by multiple quartzofeldspathic veinlets.	Mottled Anorthosite	
GVL03	179.53	180.26	Sharp		Granofels	
GVL03	180.26	183.86	Gradational	Norite. Medium to coarse-grained. Decreases in plagioclase abundance towards base of unit.	Norite	
GVL03	183.86	189.00	Gradational	Norite increases in plagioclase content towards the base of unit	Spotted Anorthosite	
GVL03	189.00	189.46	Gradational	Medium to coarse-grained.	Mottled Anorthosite	
GVL03	189.46	201.69	Gradational	altered plagioclase with a greenish tinge.	Norite	
GVL03	201.69	203.22	Gradational	Plagioclase, greenish tinge due to alteration -chloritisation. Opx. Minor phlogopite.	Norite	
GVL03	203.22	205.59	Gradational	greenish-white. Altered. Gradational contact.	Anorthosite	
GVL03	205.59	206.00			Mottled Anorthosite	
GVL03	206.00	206.89		Cumulus Opx interstitial plagioclase(<10%). Medium-grained. Brownish-grey. Pods of Quartzofeldspathic material.	Pyroxenite	
GVL03	206.89	208.41		Cumulus Opx, interstitial plagioclase. Minor brown micas (biotite?)	Pyroxenite	
GVL03	208.41	208.59			Granofels	
GVL03	208.59	209.07		Medium-grained.	Pyroxenite	
GVL03	209.07	209.10			Granofels	
GVL03	209.10	210.21			Pyroxenite	
GVL03	210.21	210.24			Granofels	
GVL03	210.24	210.48			Pyroxenite	
GVL03	210.48	210.55			Granofels	
GVL03	210.55	211.02			Pyroxenite	
GVL03	211.02	211.69			Granofels	
GVL03	211.69	221.73			Pyroxenite	
GVL03	221.73	222.28		Quartzofeldspathic materialwith assimilated veilets of Opx-rich material. Fine grained with a few coarse.large quartz cry	Granofels	
GVL03	222.28	222.40		Chloritised plagioclase. Small blebby and interstitiallly disseminated pyrrhotite and chalcopyrote mineralisation.	Pyroxenite	
GVL03	222.40	222.59		Medium-grained. Blebby and interstitially disseminated pyrrhotite rimmed by chalcopyrite.	Pyroxenite	
GVL03	222.59	222.62			Granofels	
GVL03	222.62	225.62		Minor scattered sulphides. Medium-grained	Pyroxenite	
GVL03	225.62	225.86		fine-grained	Granofels	
GVL03	225.86	232.26		20-30% plagioclase. Opx	Norite	
GVL03	232.26	232.56		Minor dark-green veinlets	Anorthosite	
GVL03	232.56	236.24		medium to coarse-grained. 20-30% plagioclase.	Norite	
GVL03	236.24	236.28		irregular pods and veins of noritic material.	Anorthosite	
GVL03	236.28	244.27		Medium to coarse-grained. Multiple veinlets of plagioclase. Minor specks of pyrrhotite and chalcopyrite and possibly pe	Norite	
GVL03	244.27	245.94		>70% feldspar. No mineralisation.	Spotted Anorthosite	
GVL03	245.94	246.74		Gradational contact. 40-50% plagioclase.	Leuconorite	
GVL03	246.74	250.09		20% plagioclase. Multiple hairline veinlets.interstitially disseminated sulphides- pyrrhotite,pentlandite,chalcopyrite (5%	Norite	
GVL03	250.09	250.18			Granofels	
GVL03	250.18	250.16		30% Opx.	Spotted Anorthosite	
GVL03	250.16	255.00		Medium to coarse-grained. interstitially disseminated sulphides- pyrrhotite and chalcopyrite.	Norite	
GVL03	255.00	256.41	Sharp	Medium-grained. No mineralisation	Norite	
GVL03	256.41	256.46	Sharp		Granofels	
GVL03	256.46	266.20	Gradational	Medium-grained. Multiple quartzofeldspathic veinlets.	Leuconorite	
GVL03	266.20	269.36		Medium-grained.	Norite	
GVL03	269.36	269.80		Completely altered. Highly veined.	Norite	
GVL03	269.80	270.60	Gradational	>60 % plagioclase.	Spotted Anorthosite	
GVL03	270.60	273.22		Feldspar altered to a greenish colour. Distinct black to dark brown Opx crystals.	Norite	
GVL03	273.22	279.10		>50% feldspar.	Leuconorite	
GVL03	279.10	283.53		Medium-grained	Norite	
GVL03	283.53	289.23		Medium-grained.	Leuconorite	
GVL03	289.23	301.30		Mottled+spotted texture=Spottled?	Spotted Anorthosite	
GVL03	301.30	309.40		Mottled+spotted texture=Spottled?	Mottled Anorthosite	
GVL03	309.40	317.76		intercalated 10cm leuconorites.	Norite	
GVL03	317.76	319.30			Spotted Anorthosite	
GVL03	319.30	334.00		Opx>Plagioclase>Cpx(10%). Cut by multiple quartzfeldspathic veinlets.	Norite	
GVL03	334.00	415.48		Opx>Plag>Cpx	Feldspathic pyroxenite	
GVL03	415.48	415.60		Shear Zone	Feldspathic pyroxenite	

n

Appendix D: Core Logging

BH ID	From	To	Contact	Description	Lithology	Alteration
GVL03	415.60	417.00			Feldspathic pyroxenite	
GVL03	417.00	417.81		Fine-grained. Dark-green to black veins. Minor interstitial specks of pyrrhotite and chalcopyrite	Pyroxenite	
GVL03	417.81	418.40		Multiple contorted chromite stringers In pyroxenite.	Chromitite	
GVL03	418.40	419.40		Fine-grained. Dark-green to black veins. Minor interstitial specks of pyrrhotite and chalcopyrite	Pyroxenite	
GVL03	419.40	423.00		cut by interconnected multiple quartzofeldspathic veinlets. Interstitially disseminated and blebby Pyrrhotite and chalco	Pyroxenite	
GVL03	423.00	423.80		Interstitially disseminated and blebby Pyrrhotite and chalcopyrite.	Pegmatoidal Feldspathic Pyroxenite	
GVL03	423.80	425.43		Fine-grained. Interstitially disseminated and blebby Pyrrhotite and chalcopyrite.	Pyroxenite	
GVL03	425.43	426.39		Interstitially disseminated and blebby Pyrrhotite and chalcopyrite.	Pegmatoidal Feldspathic Pyroxenite	
GVL03	426.39	428.75		Interstitially disseminated Pyrrhotite	Pyroxenite	
GVL03	428.75	429.94			Feldspathic pyroxenite	
GVL03	429.94	430.04		30 degree inclination angle.	Granofels	
GVL03	430.04	430.59		Medium-grained. Interstitially disseminated pyrrhotite.	Feldspathic pyroxenite	
GVL03	430.59	430.94		No mineralisation.	Pegmatoidal Feldspathic Pyroxenite	
GVL03	430.94	454.06		Fine-grained. Disseminated insterstitial pyrrhotite (6%).	Pyroxenite	
GVL03	454.06	454.39		Highly altered and fractured zone of pyroxenite. Chloritised and or serpentinised.	Pyroxenite	
GVL03	454.39	457.48		Fine-grained. Dark-green to black in colour. Cut by various veinlets, white quartzofeldspathic veins and black mafic veinl	Pyroxenite	
GVL03	457.48	459.92		No mineralisation. Minor Phlogopite.	Feldspathic pyroxenite	
GVL03	459.92	462.30		No mineralisation. Intercalated feldspathic pyroxenite zones	Pegmatoidal Feldspathic Pyroxenite	
GVL03	462.30	463.00		Medium to coarse grained. Highly fractured. Altered black to dark-green.	Pyroxenite	
GVL03	463.00	463.21		Highly bittle pyroxenite zone. Multidisectional S.S . Shear zone?	Pyroxenite	
GVL03	463.21	465.90		Altered black to dark-green. Medium-grained. Interstitially disseminated Pyrrhotite. Netted in places.	Pyroxenite	
GVL03	465.90	469.82		Pyroxenite. Coarse-grained. Dark-green to black in colour. No mineralisation.	Pyroxenite	
GVL03	469.82	472.47	Gradational	Fine-grained. Dark-green to black. Interstitially dissemnated Pyrrhotite.	Pyroxenite	
GVL03	472.47	480.65	Gradational	intercolated Pegmatoidal Zones.	Feldspathic pyroxenite	
GVL03	480.65	489.80	Gradational	Olivine (30%). Opx and Cpx. Interstitially disseminated pyrrhotite (7%)	Olivine bearing Pyroxenite	
GVL03	489.80	491.18	Gradational	medium to coarse-grained/ Minor phlogopite.	Feldspathic pyroxenite	
GVL03	491.18	492.00	Sharp	Fine-grained. Olivine, Opx, Cpx. Interstitially disseminated pyrrhotite	Olivine bearing Pyroxenite	
GVL03	492.00	495.10		Veined anorthosite. Altered.	Pyroxenite	
GVL03	495.10	495.31		Core Broken at contact.	Anorthosite	
GVL03	495.31	497.31		medium to coarse-grained. Serpentinised. Highly fractured.	Pyroxenite	
GVL03	497.31	504.95		Olivine rich serpentinised rock. Too dark/serpentinised to determine other minerals. Disseminated Chromite.	Serpentinised Harzburgite	
GVL03	504.95	507.80		Oikocrysts of Opx. Olivine (60%). Serpentinised. Disseminated chromitite	Poikilitic Serpentinised Harzburgite	
GVL03	507.80	521.00		pyroxenite. Serpentinised. Medium-grained. Pyrrhotite interstitially disseminated.	Pyroxenite	
GVL03	521.00	528.00		Intersitially Disseminated Sulfide.	Serpentinised Harzburgite	
GVL03	528.00	535.26		massive. Completely serpentinised. Lightly mineralised.	Serpentinite	
GVL03	535.26	535.82		almost completely serpentinsed. Harzburgite. Interstitially disseminated pyrrhotite (<5%)	Serpentinite	
GVL03	535.82	539.37		very minor/light pyrrhotite specks. <3%	Serpentinised Harzburgite	
GVL03	539.37	556.29		Fine-grained. Altered. Serpentinised?	Pyroxenite	
GVL03	556.29	568.48		Interstitially disseminated to netted pyrrhotite. <8%.	Serpentinised Harzburgite	
GVL03	568.48	578.53		<2 % interstitially disseminated pyrrhotite and chalcopyrite.	Serpentinised Harzburgite	
GVL03	578.53	578.62		Chloritised plagioclase.	Granofels	
GVL03	578.62	607.57		minor interstitial pyrrhotite specks.	Serpentinised Harzburgite	
GVL 04	0.00	9.98	Gradational	Coarse-grained. Interstitial plagioclase. Cumulus Opx. Minor biotite. Highly weathered, cannot determine exact contactc	leuconorite	
GVL 04	9.98	13.07	Gradational	Plagioclase<Opx . Interstitially lightly dissemintaed Pyrrhotite specks. Highly weathered and fractured.	Melanorite	
GVL 04	13.07	13.08	Sharp	Quartz veinn. 45 degree inclination.	Quartz	
GVL 04	13.08	17.80	Sharp	Plagioclase<Opx. Minor Cpx Cut by multiple steeply dipping quartzofeldspathic veins	leuconorite	
GVL 04	17.80	17.84	Sharp	Quartz + plaioclase . Sharp contacts. Granitic. 55 degree inclination.	Granofels	
GVL 04	17.84	23.41	Sharp	grades into more homogeneous norite. (mesonorite). Equigranular. Cut by multiple quartzofeldspathic veinlets >5mm	Norite	
GVL 04	23.41	27.30	Sharp	Shear zone. 30 degree inclination	Norite	
GVL 04	27.30	27.89	Gradational	homogeneous melanorite with sharp quartzofeldspathic veinlets	Melanorite	
GVL 04	27.89	28.28	Sharp		Anorthosite	
GVL 04	28.28	28.40	Sharp	quartzofeldspathic vein	Granofels	
GVL 04	28.40	28.63	Sharp		Anorthosite	
GVL 04	28.63	28.72	Sharp	quartzofeldspathic vein with anorthosite xenoliths/blocks within it. 45 degree contact.	Granofels	
GVL 04	28.72	28.80	Sharp		Anorthosite	
GVL 04	28.80	29.56	Sharp		Granofels	
GVL 04	29.56	31.60	Gradational		Anorthosite	
GVL 04	31.60	31.92	Sharp	spotted looking texture.	leuconorite	
GVL 04	31.92	32.48	Sharp	Fine-grained quartzofeldspathic vein.	Granofels	
GVL 04	32.48	46.82	Sharp	spotted looking texture. Irregular undulating bottom contact. Multiple quartzofeldspathic veinlets.	leuconorite	

Appendix D: Core Logging

BH ID	From	To	Contact	Description	Lithology	Alteration
GVL 04	46.82	47.20	Sharp	Quartzofeldspathic intrusion. Brecciated norite blocks within intrusive rock. Subhorizontal contacts.	Granofels	
GVL 04	47.20	49.60	Sharp		leuconorite	
GVL 04	49.60	49.74	Sharp	Quartzofeldspathic intrusion in spotted anorthosite.	Granofels	
GVL 04	49.74	51.52	Gradational		leuconorite	
GVL 04	51.52	52.80	Sharp		Anorthosite	
GVL 04	52.80	53.16	Sharp		Granofels	
GVL 04	53.16	53.56	Sharp		Anorthosite	
GVL 04	53.56	54.10	Sharp		Granofels	
GVL 04	54.10	54.18	Gradational		Anorthosite	
GVL 04	54.18	55.44	Gradational		Melanorite	
GVL 04	55.44	56.55	Sharp		leuconorite	
GVL 04	56.55	56.66	Sharp	Sharp undulatory contacts	Granofels	
GVL 04	56.66	57.77	Gradational		Mottled Anorthosite	
GVL 04	57.77	60.34	Gradational	Multiple quartzofeldspathic veinlets and subvertical fractures.	leuconorite	
GVL 04	60.34	60.56	Sharp		Mottled Anorthosite	
GVL 04	60.56	60.68	Sharp	fine-grained dark-green igneous rock. Thin section required. Intrusive contacts. Sill or chill Zone?	Unidentifiable	
GVL 04	60.68	60.88	Sharp		Mottled Anorthosite	
GVL 04	60.88	60.95	Sharp		Granofels	
GVL 04	60.95	61.11	Sharp		Mottled Anorthosite	
GVL 04	61.11	61.14	Sharp		Granofels	
GVL 04	61.14	61.46	Sharp		Mottled Anorthosite	
GVL 04	61.46	61.48	Sharp		Quartz	
GVL 04	61.48	63.00	Sharp		Mottled Anorthosite	
GVL 04	63.00	64.64		Zone of high alteration. Highly fractured. Green unidentified veins and quartzofeldspathic veinlets present too.	Mottled Anorthosite	
GVL 04	64.64	65.05	Sharp		Mottled Anorthosite	
GVL 04	65.05	65.07	Sharp	subhorizontal	Quartz	
GVL 04	65.07	70.74	Sharp		Mottled Anorthosite	
GVL 04	70.74	79.33	Sharp	Quartzofeldspathic vein. 30 degree inclination.	Granofels	
GVL 04	79.33	79.45	Sharp		Melanorite	
GVL 04	79.45	79.68	Sharp	irregular contact.	Granofels	
GVL 04	79.68	81.87	Sharp	subhorizontal contacts.	Granofels	
GVL 04	81.87	84.73			Melanorite	
GVL 04	84.73	86.00	Gradational	Pegmatoidal texture. Interstitially disseminated Pyrrhotite rimmed by chalcopyrite.	Pegmatoidal feldspathic Pyroxenite.	
GVL 04	86.00	86.56		Quartzofeldspathic vein with xenoliths/blocks of Pyoxenite.	Granofels	
GVL 04	86.56	102.08		Quartzofeldspathic vein	Granofels	
GVL 04	102.08	103.08		Quartzofeldspathic vein. Veinlets of assimilated pyroxenitic material	Granofels	
GVL 04	103.08	103.28	Sharp	Pegmatoidal texture. Blebby interstitial Pyrrhotite. Pyrrhotite rimmed by Chalcopyrite. Disseminated chromite.	Chromitiferous Pegmatoidal feldspathic Pyroxenit	
GVL 04	103.28	105.48	Gradational	Pegmatoidal texture. Blebby interstitial Pyrrhotite. Pyrrhotite rimmed by Chalcopyrite. Disseminated chromite.	Pegmatoidal feldspathic Pyroxenite.	
GVL 04	105.48	105.68	Gradational	Pegmatoidal texture. Blebby interstitial Pyrrhotite. Pyrrhotite rimmed by Chalcopyrite. Disseminated chromite.	Chromitiferous Pegmatoidal feldspathic Pyroxenit	
GVL 04	105.68	106.00	Sharp	Blebby interstitial Pyrrhotite. Pyrrhotite rimmed by minor Chalcopyrite.	Feldspathic Pyroxenite	
GVL 04	106.00	106.19	Sharp		Granofels	
GVL 04	106.19	107.52	Sharp	Feldspathic pyroxenite with interstitially disseminated and blebby pyrrhotite and	Feldspathic Pyroxenite	
GVL 04	107.52	107.71	Sharp		Granofels	
GVL 04	107.71	111.64		Interstitially disseminated pyrrhotite and chalcopyrite. Disseminated to blebbly texture of sulphides.	Feldspathic Pyroxenite	
GVL 04	111.64	111.72	Gradational	Blebby interstitial pyrrhotite and chalcopyrite to very fine specks of sulphides.	Pegmatoidal feldspathic Pyroxenite.	
GVL 04	111.72	112.00		medium-grained. Highly mineralised in blebbs of pyrrhotite rimmed by chalcopyrite	Feldspathic Pyroxenite	
GVL 04	112.00	112.15		Large blebby pyrrhotite rimmed by chalcopyrite.	Pegmatoidal feldspathic Pyroxenite.	
GVL 04	112.15	113.30	Gradational	Interstitially disseminated pyrrhotite and chalcopyrite.	Feldspathic Pyroxenite	
GVL 04	113.30	114.25	Gradational	pyroxenite with greater abundance of plagioclase. Cut by quartzofeldspathic veinlets. Large bladed crystals of Cpx? Poss	Feldspathic Pyroxenite	
GVL 04	114.25	119.89	Sharp	Well mineralised. Interstitially disseminated to blebby textured. Cut by quartzofeldspathic veinlets.	Pyroxenite	
GVL 04	119.89	120.59	Sharp	Quartzofeldspathic infrusion with pyroxenitic inclusions.	Granofels	
GVL 04	120.59	121.20		Fine specks of interstitially disseminated sulphides. Too fine to identify.	Pyroxenite	
GVL 04	121.20	121.31		Quartzofeldspathic intrusion with brecciated pyroxenite blocks within it.	Granofels	
GVL 04	121.31	126.20		Highly brecciated by quartzofeldspathic veins. Quartzofeldspathic material with coarse grained plagioclase and quartz. P	Feldspathic Pyroxenite	
GVL 04	126.20	127.00		Grains of (possibly) chromite.	Pyroxenite	
GVL 04	127.00	156.00		feldspathic, brownish-grey, medium crystalline, feldspar veining, veined, scattered sulphides, lightly disseminated sulp	Pyroxenite	
GVL 04	156.00	168.43		feldspathic, brecciated, brownish-grey, medium crystalline, feldspar veining, highly veined, scattered sulphides, lightly	Pyroxenite	
GVL 04	168.43	172.58		broken, greyish-brown, finely crystalline, sheared, fractured, serpentinised, gradational contact, contact angle 30°	Pyroxenite	
GVL 04	172.58	176.61		pyroxenitic, light brownish-grey, medium crystalline, pegmatoidal, veined, scattered sulphides, lightly disseminated sul	Norite	
GVL 04	176.61	176.84		light brown, finely crystalline, veined, gradational contact, contact angle 12°	Hornfels	

Appendix D: Core Logging

BH ID	From	To	Contact	Description	Lithology	Alteration
GVL 04	176.84	181.70		INTERCALATED LEUCONORITE AND MESONORITE, pyroxenitic, light brownish-grey, medium to coarsely crystalline, pegm	Norite	
GVL 04	181.70	193.42		feldspathic, light brownish-grey, medium crystalline, veined, scattered sulphides, lightly disseminated sulphide specks,	Feldspathic Pyroxenite	
GVL 04	193.42	210.13		feldspathic, light brownish-grey, medium crystalline, veined, gradational irregular contact, contact angle 10°	Feldspathic Pyroxenite	
GVL 04	210.13	226.19		Dark-green to blackish-grey with large elipsoidal (long axis horizontal) crystals - possibly Opx. Very fine dispersed inters	Poikilitic Serpentinised Harzburgite	
GVL 04	226.19	232.07		fine-grained, equigranular. Opx>Feldpar>Cpx. Minor reddish-brown mica (biotite?). No visable sulphides	Pyroxenite	
GVL 04	232.07	252.95		Dark-green to blackish-grey with large elipsoidal (long axis horizontal) crystals - possibly Opx. Very fine dispersed inters	Poikilitic Serpentinised Harzburgite	
GVL 04	252.95	263.90		Dark-green to black in colour. Very fine-grained. Very magnetic due to secondary magnetite from serpentinisation. Disse	Serpentinised Harzburgite	
GVL 04	263.90	265.67		Tiger-stripe veined serpentinite. Riddle with man horizontally orientated serpentine veins. Blocks are brecciated in plac	Serpentinised Harzburgite	
GVL 04	265.67	271.74	Sharp	Dark-green to black in colour. Very fine-grained. Very magnetic due to secondary magnetite from serpentinisation. Ddis	Serpentinite	
GVL 04	271.74	272.23	Sharp	sharp contacts. Mint green colour. Xenoliths of unidentified rock.	Unidentifiable	
GVL 04	272.23	286.89	Gradational	Tiger-stripe veined serpentinite. Riddle with man horizontally orientated serpentine veins. Blocks are brecciated in plac	Serpentinised Harzburgite	
GVL 04	286.89	292.58	Sharp	Dark-green to blackish-grey with large elipsoidal (long axis horizontal) crystals - possibly Opx. Very fine dispersed inters	Poikilitic Serpentinised Harzburgite	
GVL 04	292.58	293.82	Sharp		Granofels	
GVL 04	293.82	296.74		Dark-green to blackish-grey with large elipsoidal (long axis horizontal) crystals - possibly Opx. Very fine dispersed inters	Poikilitic Serpentinised Harzburgite	
GVL 04	296.74	297.26		minor reddish grey Mica. Quartzofeldspathic vein	Granofels	
GVL 04	297.26	322.72		Dark-green to black in colour. Very fine-grained. Very magnetic due to secondary magnetite from serpentinisation. Ddis	Serpentinite	
GVL 04	322.72	324.70		Well mineralised interstitially disseminated Pyrrhotite.	Poikilitic Serpentinised Harzburgite	
GVL 04	324.70	344.47		Dark-green to black in colour. Very fine-grained. Very magnetic due to secondary magnetite from serpentinisation. Ddis	Serpentinite	
GVL 04	344.47	349.15		Cannot distinguish between rock types. 55 degree contacts.	Granofels	
GVL 04	349.15	377.61		Dark-green to black in colour. Very fine-grained. Very magnetic due to secondary magnetite from serpentinisation. Ddis	Serpentinite	
GVL 04	377.61	377.86		60 degree contacts, sharp.	Anorthosite	
GVL 04	377.86	397.41	Sharp		Serpentinite	
GVL 04	397.41	397.56	Sharp		Granofels	
GVL 04	397.56	412.95			Serpentinite	
GVL 04	412.95	434.70		Tiger-stripe veined serpentinite. Riddle with man horizontally orientated serpentine veins. Black interstitial magnetite v	Serpentinised Harzburgite	
GVL 04	434.70	455.36		greenishbrown,medium crystalline, sharp contact, contact 50 degree inclination.	Serpentinised Harzburgite	
GVL 04	455.36	455.41		Chromitiferous rock. Thin layer. 45 degree inclination	Chromitite	
GVL 04	455.41	460.74		Chromitiferous Serpentinised Harzburgite. Disseminated interstitial pyrrhotite and chalcopyrite specks.	Serpentinised Harzburgite	
GVL 04	460.74	460.88		thin layer	Chromitite	
GVL 04	460.88	461.26		Chromitiferous Serpentinised Harzburgite. Disseminated interstitial pyrrhotite and chalcopyrite specks.	Serpentinised Harzburgite	
GVL 04	461.26	461.46		thin later	Chromotite	
GVL 04	461.46	462.80		Chromitiferous Serpentinised Harzburgite. Disseminated interstitial pyrrhotite and chalcopyrite specks.	Serpentinised Harzburgite	
GVL 04	462.80	463.40		sharp contacts.	Anorthosite	
GVL 04	463.40	464.64		Chromitite. Friable. Medium to fine-grained. Upper Chromitite Layer	Chromitite	
GVL 04	464.64	469.19		Serpentinised harzburgite? Dark grey to black. Lpoorly mineralised, disseminated sulphides. Disseminated chromite (>3	Harzburgite	
GVL 04	469.19	469.26			Chromitite	
GVL 04	469.26	469.49		Serpentinised harzburgite? Dark grey to black. Lpoorly mineralised, disseminated sulphides. Disseminated chromite (>3	Harzburgite	
GVL 04	469.49	469.68			Chromitite	
GVL 04	469.68	469.81		Serpentinised harzburgite? Dark grey to black. Lpoorly mineralised, disseminated sulphides. Disseminated chromite (>3	Harzburgite	
GVL 04	469.81	469.97			Chromitite	
GVL 04	469.97	471.41		brownish-grey, finely crystalline, gradational contact	Quartzite	
GVL 04	471.41	503.30		brownish-grey, medium crystalline, decomposed, disseminated chromite, gradational contact	Pyroxenite	
GVL 04	503.30	503.83	Undulatory	Black fine-grained rock. Not magnetic. Highly weathered. May be Chromitiferous pyroxenite. Extrely difficult to identify	Pyroxenite	
GVL 04	503.83	504.23	Sharp	Blebbly sulphides (>1 cm). Interstitially disseminated pyrrhotite and chalcopyrite.. Cut by multiple quartzofeldspathic ve	Pegmatoidal feldspathic Pyroxenite.	
GVL 04	504.23	504.59	Sharp	Homogeneous Pyroxenite. Interstitially disseminated sulphides to blebby in places (minor).	Pyroxenite	
GVL 04	504.59	506.26	Sharp	Pegmatoidal Pyroxenite. Interstitially disseminated sulphides to blebby in places (minor). Replacement Pegmatite?	Pegmatoidal feldspathic Pyroxenite.	
GVL 04	506.26	506.80	Sharp	fine to medium-grained. Not mineralised	Pyroxenite	
GVL 04	506.80	506.83	Sharp	feldspathic vein sharp contacts.	Anorthosite	
GVL 04	506.83	510.11	Gradational		Pyroxenite	
GVL 04	510.11	513.07	Sharp	Anorthosite intrusion. Sharp contacts. Weathered.	Anorthosite	
GVL 04	513.07	522.66	Gradational		Pyroxenite	
GVL 04	522.66	524.72	Gradational	intercalated pegmatoidal and homogeneous pyroxenite zones.	Pegmatoidal feldspathic Pyroxenite.	
GVL 04	524.72	526.56	Sharp		Pyroxenite	
GVL 04	526.56	526.66	Sharp	20 degree inclined contacts	Anorthosite	
GVL 04	526.66	532.83	Gradational		Pyroxenite	
GVL 04	532.83	533.06	Gradational	Multiple chromite stringers. Medium to coarse grained.	Dunite	
GVL 04	533.06	533.10		Chromitiferous harzburgite	Serpentinised Harzburgite	
GVL 04	533.10	533.84		Multiple chromite stringers. Medium to coarse grained.	Dunite	
GVL 04	533.84	533.84		Chromite stringer.	Chromitite	
GVL 04	533.84	534.00			Dunite	

q

Appendix D: Core Logging

BH ID	From	To	Contact	Description	Lithology	Alteration
GVL 04	534.00	534.01		Chromite stringer.	Chromitite	
GVL 04	534.01	537.56			Dunite	
GVL 04	537.56	540.88		Pyroxenite with chromite stringers and disseminated chromite amd sulphide specks.	Pyroxenite	
GVL 04	540.88	541.48		Lower Chromitite Layer	Chromite	
GVL 04	541.48	541.63		Multiple chromite stringers within pyroxenite.	Pyroxenite	
GVL 04	541.63	542.18			Pyroxenite	
GVL 04	542.18	542.31	Chromite later		Chromitite	
GVL 04	542.31	542.47		intercalated chromite layers and pyroxenite or harzburgite	Chromitite	
GVL 04	542.47	547.48			Pyroxenite	
GVL 04	547.48	550.00		85% olivine. Disseminated chromite. Multiple intercolated chromitite layers. Finely crystaline. Sugary-textured grains of	Dunite	
GVL 04	550.00	568.60			Pyroxenite	
GVL 04	568.60	570.37	Gradational	Chromite bearing. Fine-grained friable. Gradational contact.	Dunite	
GVL 04	570.37	571.93			Pyroxenite	
GVL 04	571.93	591.00		Interstitial Chromitite.	Harzburgite	
GVL 04	591.00	594.20		little to no Chromite.	Harzburgite	
GVL 04	594.20	600.26		Medium to coarse-grained. Pegmatoidal	Pegmatoidal feldspathic Pyroxenite.	
GVL 04	600.26	601.72		fine to medium-grained. Not mineralised	Feldspathic Pyroxenite	
GVL-05	0	37.3	none	No core recovered	No core recovered	
GVL-05	37.3	38.89	Sharp	Oikocrysts of Opx. Serpentine veins at approximately 30 cm spacing	Poikilitic Serpentinised Harzburgite	
GVL-05	38.89	39.1	Sharp	Granofels vein. Fine-grained.	Granofels	
GVL-05	39.1	43.6		highly fractured.	Serpentinised Harzburgite	
GVL-05	43.6	45.05	Sharp	Crumbly. Comprises feldspar, olivine (unsure)	Unidentifyable	
GVL-05	45.05	56.27		Oikocrysts of Opx. Subvertical veining.	Poikilitic Serpentinised Harzburgite	
GVL-05	56.27	56.75		Highly wathered feldspar and pyroxene bearing rock.	Unidentifyable	
GVL-05	56.75	60.93	Sharp	Opx oikocrysts. Multiple feldspathic veinlets. White and army green pearlecent micas visible within fractures	Poikilitic Serpentinised Harzburgite	
GVL-05	60.93	61.38	Sharp	highly weathered, fine to medium-grained.	Granofels	
GVL-05	61.38	61.8	Sharp		Poikilitic Serpentinised Harzburgite	
GVL-05	61.8	61.93		25 inclination contact.	Granofels	
GVL-05	61.93	97.05		fine to medium-grained. Cut by multiple feldspar rich veins aprroximately 2cm thick.	Serpentinised Harzburgite	
GVL-05	97.05	97.35		Crumbly. Comprises Opx and feldspar.	Unidentifyable	
GVL-05	97.35	98.2			Serpentinised Harzburgite	
GVL-05	98.2	99.77		Crumbly unidentifyable unit comprising feldspar and pyroxene.	Unidentifyable	
GVL-05	99.77	102.55		crumbly/friable.	Serpentinised Harzburgite	
GVL-05	102.55	102.75		Crumbly unidentifyable unit comprising feldspar and pyroxene.	Unidentifyable	
GVL-05	102.75	103.65		highly fractured.	Serpentinised Harzburgite	
GVL-05	103.65	104.25		Crumbly unidentifyable unit comprising feldspar and pyroxene.	Unidentifyable	
GVL-05	104.25	112.8			Serpentinised Harzburgite	
GVL-05	112.8	116		Serpentinised Dunite. Fine to medium-grained. Disseminated chromite.	Dunite	
GVL-05	116	123.57	Sharp	highly fractured.	Poikilitic Serpentinised Harzburgite	
GVL-05	123.57	124.16	Sharp	Greenish colour, fine-grained pyroxenes.irregular vertical fractures.	Granofels	
GVL-05	124.16	155.25		approximately 10 cm Opx oikocrysts.	Poikilitic Serpentinised Harzburgite	
GVL-05	155.25	155.77	Gradational	Medium to coarse grained. Interstitial plagioclase.	Pyroxenite	
GVL-05	155.77	160.67		fine-grained. Cumulus Opx. Interstitial feldspar. Olivine. Disseminated chromite.	Pyroxenite	
GVL-05	160.67	168.15			Poikilitic Serpentinised Harzburgite	
GVL-05	168.15	203.89		intercalated serpentinised Harzburgite and minor dunite. Highly weathered. Dunite is weathered to rubble in places (fri	Serpentinised Harzburgite	
GVL-05	203.89	204.02	Sharp	Fine-grained.	Granofels	
GVL-05	204.02	210.46	Sharp	light-green with dark-green pods. Gritty,friable. Highly weathered.	Dunite	
GVL-05	210.46	210.6	Sharp		Granofels	
GVL-05	210.6	212	Sharp	Crumbly. Weathered.	Dunite	
GVL-05	212	212.14	Sharp		Granofels	
GVL-05	212.14	212.44			Dunite	
GVL-05	212.44	213.88		Opx oikocrysts, Olivine chadocrysts,brecciated look. Closely spaced Oikocrysts of Opx.	Poikilitic Serpentinised Harzburgite	
GVL-05	213.88	218		intercalated serpentinised Harzburgite.	Dunite	
GVL-05	218	218.4			Granofels	
GVL-05	218.4	235.18	Sharp	Intercalated Harzburgite and dunite. Cut by blackish-green-veins. Veins are interconnecting and comprise olivine and op	Serpentinised Harzburgite	
GVL-05	235.18	238.4	Sharp	assimilated Pyroxene and olivine.	Granofels	
GVL-05	238.4	239.15		weathered.	Serpentinised Harzburgite	
GVL-05	239.15	239.4		assimilated Harzburgite.	Granofels	
GVL-05	239.4	260.14		Cut by multiple irregular granite/feldspathic veins ranging in thickness from 10 cm to 0.5 cm. brecciated blocks of harzbu	Poikilitic Serpentinised Harzburgite	
GVL-05	260.14	299.89	Sharp	Chromitiferous. Pyrrhotite bebbs, interstitially disseminated. 8% pyrrhotite.	Serpentinised Harzburgite	

r

Appendix D: Core Logging

BH ID	From	To	Contact	Description	Lithology	Alteration
GVL-05	299.89	297.95	Sharp		Granofels	
GVL-05	297.95	307.47	Gradational	Chromitiferous. Pyrrhotite bebbs, interstitially disseminated. 8% pyrrhotite.	Serpentinised Harzburgite	
GVL-05	307.47	312.42	Sharp	Interstitially disseminated pyrrhotite.	Serpentinised Harzburgite	
GVL-05	312.42	312.72	Sharp		Granofels	
GVL-05	312.72	326.8	Gradational	Interstitially disseminated pyrrhotite. 4%	Serpentinised Harzburgite	
GVL-05	326.8	329.49	Gradational	subvertical granofels veins 2-3 cm thick	Serpentinised Harzburgite	
GVL-05	329.49	346.8	Sharp	fine to medium grained.	Serpentinised Harzburgite	
GVL-05	346.8	350.18	Sharp	highly weathered.friable.	Granofels	
GVL-05	350.18	355.2		F/g	Serpentinised Harzburgite	
GVL-05	355.2	355.27	Sharp contact	Subvertical and sharp contact approximately 30°INCL for both contacts	Quartz Feldspathic Veinlet	
GVL-05	355.27	356.29	Sharp contact	Dominated by olivine with a sugary texture, olivine has been altered to serpentinite (Black). Abundance of small veinlets of serpentine	Serpentinised Dunite	
GVL-05	356.29	356.86	Gradational contacts	Disseminated chrome, veinlets of chrome, dunite dominated by olivine (sugary texture), minor serpentine. 356.55m to 356.63m; Granitic intrusive layer, bottom contact subvertical and sharp with 30°INCL and top contact is sharp and subhorizontal	Chromitifeous serpentinised Dunite	
GVL-05	356.86	356.89	Sharp contact	Subhorizontal contacts	Chrome seam	
GVL-05	356.89	358.05	Sharp contact	Dominated by olivine with a sugary texture.	Serpentinised Dunite	
GVL-05	358.05	358.55	Sharp contact	Sharp and vertical contact/ half core granitic material/ half core serpentinised dunite	Granitic Intrusive Layer	
GVL-05	358.55	375.96	Sharp contact	Dominated by sugary olivine grains, with intervals where the olivine is almost completely altered by serpentinite. Medium to coarse grained	Serpentinised Dunite	
GVL-05	375.96	377.2	Sharp contact	Dominated by opx with minor cpx. Abundance of serpentinised veinlets. Medium to coarse grained. Contacts are both sharp and subhorizontal	Olivine-bearing Pyroxenite	
GVL-05	377.2	384.87	Sharp contact	Dominated by olivine. 383.30m a 2cm thick olivine- pyroxenite unit (sharp suborizontal contact). 383.46m to 383.72m olivine- pyroxenite unit (sharp subhorizontal contact) 383.83m to 383.96m olivine- pyroxenite unit (sharp subhorizontal contact)	Serpentinised Dunite	
GVL-05	384.87	387.52	Sharp contact	Dominated by pyroxene mainly opc and cpx, small/ thin abundance of veinlets of serpentinite, contacts are subhorizontal	Olivine Serpentinised pyroxenite	
GVL-05	387.52	389.39	Gradational contact	Large oikocryst of opx and high amounts of serpentinite	Poikilitic serpentinised Harzburgite	
GVL-05	389.39	389.94	Sharp contact	Has minor olivine, medium to coarse grained, contacts are sharp and subhorizontal	Feldspathic Pyroxenite	
GVL-05	389.94	396.68	Sharp contact	Has large oikocryst of opx, medium to coarse grained	Serpentinised Dunite	
GVL-05	396.68	398.85	Crumbly contact	Medium to coarse grained with thin serpentinisedf veinlets. Bottom contact is sharp and subvertical, 35°INCL and subvertical slickensides	olivine bearing pyroxenite	
GVL-05	398.85	401.8	Sharp contact	Dominated by sugary olivine grains. Abundance of serpentinite small intervals with the unit are completely serpentinised and only relics of olivine remain	Serpentinised Dunite	
GVL-05	401.8	402.32	Sharp contact	Dominated by opx and cpx with thin (less than 1mm thick) serpentinite veinlets medium to coarse grained, subhorizontal contacts	Pyroxenite	
GVL-05	402.32	408.1	Sharp contact	Dominated by sugary olivine grains and minor amounts of serpentinite	Serpentinised Dunite	
GVL-05	408.1	408.89	Sharp contact	Dominated by opx and cpx, with thin seperntinite veinlets. Medium to coarse grained,subhorizontal contacts	Pyroxenite	
GVL-05	408.89	412.1	Sharp contact	Dominated by olivine and minor serpentinite	Serpentinised Dunite	
GVL-05	412.1	412.63	Gradational contact	Large oikocryst of opx and the olivine is mainly altered to serpentinite	Poikilitic serpentinised Harzburgite	
GVL-05	412.63	413.31	Gradational contact	Interval dominated by pyroxenes with minor olivine (15%) mostly altered to serpentinite	olivine bearing pyroxenite	
GVL-05	413.31	414.05	Sharp contact	Dominated by quartz and feldspathic material with minor mafic and amphibole material. Both contacts are sharp and subertical, the bottom contact is 40°INCL and the top contact is 35°ICNL	Granitic Intrusive Layer	
GVL-05	414.05	414.33	Sharp contact	Dominated by olivine with minor serpentinite	Serpentinised Dunite	
GVL-05	414.33	414.92	Sharp contact	Sharp contact both sides, with subhorizontal contacts	Chromitite	

Appendix D: Core Logging

BH ID	From	To	Contact	Description	Lithology	Alteration
GVL-05	414.92	415.66	Sharp contact	Dominated by olivine and minor serpentinisation	Serpentinised Dunite	
GVL-05	415.66	415.79	Sharp contact	Sharp contact with subvertical and 35°INCL	Feldspathic / Mafic Layer (Remobilised norite)	
GVL-05	415.79	420.36	Sharp contact	Dominated by olivine and serpentine. 420.26m two pyroxenite (opx) layers 1cm thick each, both have sharp contacts on both sides and are subhorizontal	Serpentinised Dunite	
GVL-05	420.36	421.52	Sharp contact	Large oikocryst of opx, the olivine grains are altered to serpentinite, although there are relics of olivine	Poikilitic serpentinised Harzburgite	
GVL-05	421.52	421.91	Sharp contact	Dominated by quartz and feldsphatic material with minor mafic and amphimbole material, medium grained with a creamy white colouration. Sharp, subvertical contacts on both side with 35°INCL	Granitic Intrusive Layer	
GVL-05	421.91	425.15	Sharp contact	Large oikocryst of opx, the olivine grains are altered to serpentinite, although there are relics of olivine	Poikilitic serpentinised Harzburgite	
GVL-05	425.15	470.33	Sharp contact	Incalted interval with fresh dunite (fresh 80% small amount of alteration) and serpentinised dunite (olivine grains are mainly altered to serpentine). Medium to coarse grained, olivine grains have a sugary texture, abundance of feldspathic veinlets (1mm thick).	Dunite/ Seperntinised Dunite	
GVL-05	470.33	484	Sharp contact	Interval has a high degree of oxidation (rusty colouration), this unit has a pegmatoidal texture but mainly coarse grained altered serpentinised dunite, dominated by olivine	Serpentinised Dunite	
GVL-05	484	491.37	Gradational Contact	Dominated by olivine, olivine crystals are large (recrystalised). Interval is extremely serpentinised and has high abundance of serpentine veinlets	Pegmatoidal Dunite/Harzburgite	
GVL-05	491.37	491.57	Gradational Contact	Interval with plag (50%), opx (30%), and olivine (20%) medium to coarse grained	Olivine bearing Norite	
GVL-05	491.57	512.13	Gradational contact	Dominated by olivine, medium to coarse grained, serpentinised veinlets are not as abundant in this interval as in the serpentinised dunite. However where the serpentine occurs in this unit are completely serpentinised area (2cm thick) where there are no traces of olivine grains	Altered Dunite	
GVL-05	512.13	515.88	Sharp contact	Medium to coarse grained, the pyroxenes (70%) interval are medium grained, there are extremely altered with high abundances of serpentinite smaller interval with plag/ feldsphathic material highly altered to chlorite	Serpentinised Olivine bearing Pyroxenite	
GVL-05	515.88	517	Sharp contact	Dominated by plag (50%) and opx (50%) medium to coarse grained sharp contact subvertical 30°INCL	Norite	
GVL-05	517	520.26	Sharp contact	Dominated by olivine with serpentinised veinlets	Serpentinised Dunite	
GVL-05	520.26	521.31	Sharp contact	Dominated by plag (50%) and opx (50%) medium to coarse grained sharp contact subvertical 30°INCL. 520.98m a 2cm thick feldspathic/ mafic veinlet (remobilised) material. Sharp contacts brecciated zone below. subvertical 40°INCL on both contacts	Norite	
GVL-05	521.31	531.56	Sharp contact	Dominated by olivine, with abundance of serpentine veinlets	Serpentinised Dunite	
GVL-05	531.56	532.5	Sharp contact	Dominated by quartz and feldspathic material with minor mafic and amphibole material. Both contacts are sharp and subhorizontal	Granofels	
GVL-05	532.5	536.63	Sharp contact	Dominated by olivine with abundance of serpentine veinlets	Serpentinised Dunite	
GVL-05	536.63	538.14	Sharp contact	Dominated by plag (50%) and opx (50%), intervals that are highly serpentinised with relics of olivine crystals. Abundance of veinlets filled with secondary feldspathic material.	Norite	
GVL-05	538.14	539.74	Sharp contact	Dominated by olivine with the abundace of serpentine veinlets. Medium to coarse grained	Serpentinised Dunite	
GVL-05	539.74	540	Sharp contact	Dominated by plag 50% and opx 50%. There are large grains of feldspar with distinct euhedral grains 1-2cm in size.	Norite	
GVL-05	540	541.11	Sharp contact	Dominated by olivine with the abundace of serpentine veinlets. Medium to coarse grained	Serpentinised Dunite	
GVL-05	541.11	541.37	Sharp contact	Dominated by plag 50% and opx 50%. Abundance of veinlets filled with secondary feldspathic material	Norite	
GVL-05	541.37	543.45	Sharp contact	Dominated by olivine with the abundace of serpentine veinlets. Medium to coarse grained. 541.41m to 541.48m - Pegmatoidal unit grains are greater or equal to 2.5cm in size. The unit is afeldspathic pyroxenite dominated by plag and pyroxenes. Contacts with the pegmatoidal unit are sharp and subvertical	Serpentinised Dunite	
GVL-05	543.45	545.21	Sharp contact	Plagioclase 50% and Orthopyroxene 50%, medium to coarse grained. Plag has a geenish tint indicating chloritisation. Minor veinlets within the interval filled with secondary feldspathic material has a pinkish white colouration (2mm thick)	Norite	
GVL-05	545.21	550.25	Sharp contact	Dominated by olivine with the abundance of serpentine veinlets. Abundance of feldspar (15%)? Linked to norite intrusion. Chromite rich.	Serpentinised Dunite	
GVL-05	550.25	550.35	Sharp contact	Veinletsof feldspathic and mafic (pyroxenes) material. Contacts are sharp and subhorizontal	Unidentifyable	

t

Appendix D: Core Logging

BH ID	From	To	Contact	Description	Lithology	Alteration
GVL-05	550.35	552.33	Sharp contact	Dominated by olivine with the abundance of serpentine veinlets. Medium to coarse grained	Serpentinised Dunite	
GVL-05	552.33	552.72	Sharp contact	Thick veinlet, highly fractured filled with secondary feldspathic material with greenish tint	Granofels	
GVL-05	552.72	585.57	Sharp contact	Dominated by sugary textured olivine crystals with abundance of serpentine veinlets. There are small intervals of a pegmatoidal texture less than 2cm thick. The veinlets are rich in quartz/ feldspathic material	Serpentinised Dunite	
GVL-05	585.57	586.09	Sharp contact	Quartz- feldspar rich with minor fractures filled with a secondary (feldspathic/calcite), has a whitish pink colouration	Granofels	
GVL-05	586.09	586.43	Sharp contact	Serpentine veinlets and dominated by olivine	Serpentinised Dunite	
GVL-05	586.43	586.6	Sharp contact	Minor mafic/amphiboles present. Abundance of fractures filled with secondary material (feldspathic/calcite)	Granofels	
GVL-05	586.6	592	Sharp contact	Dominated by olivine with the abundance of serpentine veinlets. Medium to coarse grained	Serpentinised Dunite	
GVL-05	592	592.06	Sharp contact	Noritic material within a veinlet crosscutting the altered Dunite unit, composed of feldspathic material (plag 50%) and mafic (pyroxenes and minor olivine)	Noritic	
GVL-05	592.06	593.43	Sharp contact	Completely serpentinised unit (serpentinite), relics of altered olivine present	Serpentinite	
GVL-05	593.43	594.17	Sharp contact	Dominated by olivine with serpentinised veinlets. Medium to coarse grained	Serpentinised Dunite	
GVL-05	594.17	594.4	Sharp contact	The veinlet has minor mafic material, greenish tint indicating chloritisation	Quartz Feldspathic Veinlet	
GVL-05	594.4	595.92	Sharp contact	Dominated by olivine with the abundance of serpentine veinlets. Medium to coarse grained	Serpentinised Dunite	
GVL-05	595.92	596.48	Sharp contact	Quartz/Mafic/Feldspathic -rich interval. Gradational contact or mixing of the Transvaal Suoergroup (quartzites) and the ultramafic/ mafic rocks of the Bushveld Complex (Dunite)	Unidentifyable	
GVL-05	596.48	599.44	Sharp contact	Dominated by quartz fine to medium grained with a greenish colouration. The quartz crystals are both transparent and milky white	Quartzite (Basement Transvaal Supergroup)	
GVL - 08	0.00	7.74	N/A	weathered reddish, unconsolidated/crummbly	Regolith	
GVL - 08	7.74	16.00	N/A	highly fractured core (extremely). Unable to identify contacts/bounderies or rock type?. Probably serpentinised harzbur	Unidentifiable	
GVL - 08	16.00	37.60		f/g. olive-green to grey. Extremely fractured. Feldspathic veinlets (pervasive)	Pyroxenite	
GVL - 08	37.60	42.00	Gradational	black with feldspar and Opx oikocrysts. Highly fractured core.	Harzburgite	Serpentinise
GVL - 08	42.00	45.22		highly weathered. Disintergrating. m/g to c/g	Pyroxenite	
GVL - 08	45.22	55.18		f/g with opx oikocrysts. Cut (pervasive) by multiple feldspathic veins. Highly fractured.	Harzburgite	Serpentinise
GVL - 08	55.18	60.87		highly altered. Extremely fragile. Disintergrating.	Pyroxenite	
GVL - 08	60.87	70.58		massive. Highly fractured. Feldspar veined	Harzburgite	Serpentinise
GVL - 08	70.58	72.50		highly fractured and weathered.		
GVL - 08	72.50	72.70	sharp	highly veined by cream white feldspar + quartz veins	granofels	
GVL - 08	72.70	84.40	sharp	Poikilitic texture.	Harzburgite	Serpentinise
GVL - 08	84.40	84.60	sharp	granofels vein. Creamy-brown colour.	granofels	
GVL - 08	84.60	97.09	sharp	poikilitic texture. Serpentinised. Secondary Magnetite veinlets.	Harzburgite	
GVL - 08	97.09	97.34	sharp	feldspathic vein (aplite)?	granofels	
GVL - 08	97.34	97.46	sharp	Chromitite block within aplite vein. 30 inclination		
GVL - 08	97.46	104.18	sharp	oikocrysts of opx. Minor disseminated chrome	Harzburgite	Serpentinise
GVL - 08	104.18	105.18	sharp	quartz + feldspar vein	granofels	
GVL - 08	105.18	107.86	sharp		Harzburgite	Serpentinise
GVL - 08	107.86	108.16	sharp		granofels	
GVL - 08	108.16	108.62	sharp	serpentinised poikilitic harzburgite Oikocrysts of opx	Harzburgite	Serpentinise
GVL - 08	108.62	109.38	sharp		granofels	
GVL - 08	109.38	111.10	sharp	serpentinised poikilitic harzburgite Oikocrysts of opx	Harzburgite	Serpentinise
GVL - 08	111.10	111.20	sharp		granofels	
GVL - 08	111.20	114.70	sharp	serpentinised poikilitic harzburgite Oikocrysts of opx	Harzburgite	Serpentinise
GVL - 08	114.70	114.90	sharp		granofels	
GVL - 08	114.90	117.40	sharp	serpentinised poikilitic harzburgite Oikocrysts of opx	Harzburgite	Serpentinise
GVL - 08	117.40	117.80	sharp		granofels	
GVL - 08	117.80	139.20	sharp	serpentinised poikilitic harzburgite Oikocrysts of opx	Harzburgite	Serpentinise
GVL - 08	139.20	139.50	sharp		granofels	
GVL - 08	139.50	147.70	sharp	serpentinised poikilitic harzburgite Oikocrysts of opx	Harzburgite	Serpentinise
GVL - 08	147.70	147.90	sharp		granofels	

Appendix D: Core Logging

BH ID	From	To	Contact	Description	Lithology	Alteration
GVL - 08	147.90	149.10	sharp	serpentinised poikilitic harzburgite Oikocrysts of opx	Harzburgite	Serpentinise
GVL - 08	149.10	154.62	Gradational	Light olive-green to grey. M/g to f/g. highly fractured and weathered.	Pyroxenite	
GVL - 08	154.62	174.17	sharp		Harzburgite	Serpentinise
GVL - 08	174.17	175.10	sharp	feldspathic vein/intrusion. Pyroxenite inclusions/veinlets.	granofels	
GVL - 08	175.10	176.15	sharp	massive.	Harzburgite	Serpentinise
GVL - 08	176.15	177.05	sharp	quartz + feldspar vein. Milky white	granofels	
GVL - 08	177.05	179.32	sharp		Harzburgite	Serpentinise
GVL - 08	179.32	179.72	sharp	quartz + feldspar with pyroxenite blocks included	granofels	
GVL - 08	179.72	186.24			Harzburgite	Serpentinise
GVL - 08	186.24	187.65			granofels	
GVL - 08	187.65	191.45			Harzburgite	Serpentinise
GVL - 08	191.45	192.21			granofels	
GVL - 08	192.21	195.30			Harzburgite	serpentinise
GVL - 08	195.30	195.82			granofels	
GVL - 08	195.82	212.74	Gradational		Harzburgite	serpentinise
GVL - 08	212.74	225.81	Gradational	M/g/ olive-green-grey. Highly fractured. Serpentinised	Pyroxenite	Serpentinise
GVL - 08	225.81	229.20			Harzburgite	Serpentinise
GVL - 08	229.20	229.40	sharp	Pegmatoidal pyroxenite. Caused by intrusion of granofels or cut by granofels.	Pyroxenite	
GVL - 08	229.40	232.70	sharp		granofels	
GVL - 08	232.70	232.90		Pegmatoidal pyroxenite. Caused by intrusion of granofels or cut by granofels.	Pyroxenite	
GVL - 08	232.90	236.10			Harzburgite	
GVL - 08	236.10	237.92		with blocks of harzburgite almost looks intercollated.	granofels	
GVL - 08	237.92	249.50		Khaki-olive green. M/g. possibly serpentinised. Disseminated magnetite.Dunite?	Unidentifiable	
GVL - 08	249.50	261.15	sharp		Harzburgite	
GVL - 08	261.15	261.41	sharp	feldspar + Quartz vein.	granofels	
GVL - 08	261.41	272.76	sharp	m/g to f/g. highly fractured.	Harzburgite	Serpentinise
GVL - 08	272.76	273.12	sharp	feldspar + Quartz vein.	granofels	
GVL09	0	8.85	inferred		Regolith	
GVL09	8.85	15.8	Gradational	Cumulus Opx with plag and minor Cpx. m/g to F/g/ disseminated Chrome	Pyroxenite	
GVL09	15.8	15.81	Sharp	Chromite stringer	Chromitite	
GVL09	15.81	16.5	Sharp	fine-grained. Opx dominated. Chrome Stringers at contacts.	Pyroxenite	
GVL09	16.5	16.51	Sharp	Chromite stringer	Chromite	
GVL09	16.51	19.55	Gradational	coarse-grained. Interstitially disseminated chromite. Interstitially disseminated Pyrrhotite rimmed by chalcopyrite.	Feldspathic Pyroxenite	
GVL09	19.55	23.4	Gradational	Fine-grained. Feldspar rich pyroxenite. Interstitial disseminated sulphides.	Feldspathic Pyroxenite	
GVL09	23.4	27.67	Sharp	Opx>Feldspar>Cpx. Blebby interstitially disseminated pyrrhotite.	Feldspathic Pyroxenite	
GVL09	27.67	30.33	Sharp	Quartz+Feldspar. Pyroxenite assimalated into intrusion.inclusions of pyroxene also present.pegmatoidal texture	Granofels	
GVL09	30.33	35.38	Gradational	Fine to medium-grained. Feldspar 10-15%. Interstitially disseminated pyrrhotite. Blebby in places.	Pyroxenite	
GVL09	35.38	36.89	Sharp	Feldspar rich. 20-30% felspar? Interstitially disseminated pyrrhotite. Quartz+feldspar veined.	Feldspathic Pyroxenite	
GVL09	36.89	37.77	Sharp	milky-white in colour. Quartz + Feldspar. Opx or orthopyroxenitic veinlets.	Granofels	
GVL09	37.77	41.57	Gradational	Fine to medium-grained. Interstitially disseminated Pyrrhotite specks. Multiple granitic veins cutting Pyroxenite.	Pyroxenite	
GVL09	41.57	47.12	Sharp	Opx (Cumulus) and Plagioclase dominated. Blebby Pyrrhotite(6%). Cut by multiple quartzofeldspathic veins.	Pegmatoidal Feldspathic Pyroxenite	
GVL09	47.12	47.78	Sharp	Quartz+ Feldspar vein.	Granofels	
GVL09	47.78	52.41	Sharp	Opx (Cumulus) and Plagioclase dominated. Blebby Pyrrhotite(6%). Cut by multiple quartzofeldspathic veins.	Pegmatoidal Feldspathic Pyroxenite	
GVL09	52.41	53.65	Sharp	Quartz+ Feldspar vein.	Granofels	
GVL09	53.65	55.62	Gradational	interstitially disseminated pyrrhotite specks.	Feldspathic Pyroxenite	
GVL09	55.62	71.6	Sharp	intercalated Feldspathic pyroxenite and minor Pegmatoidal Feldspathic pyroxenite. Pegmatoidal units approx 10 cm. ligh	Feldspathic Pyroxenite	
GVL09	71.6	75.68	Gradational	Cumulus olivine, Opx oikocrysts. Interstitial Pyrrhotite to netted Pyrrhotote and chalcopyrite (3-5%)	Poikilitic Serpentinised Harzburgite	
GVL09	75.68	77.1	Sharp	Medium to coarse-grained. Relict olivine grains. Netted interstitial pyrrhotite (20-30%). Transitions into Poikilitic serpent	Serpentinised Harzburgite	
GVL09	77.1	84.2	Sharp	medium to coarse-grained. Less than 15% plagioclase. Highly fractured. <2% interstitially disseminated Pyrrhotite.	Serpentinised Pyroxenite	
GVL09	84.2	87.96		Interstitially netted pyrrhotite. Oikocrysts if Opx. M/g. riddled with Horizontal-cutting serpentine veins.	Serpentinised Harzburgite	
GVL09	87.96	90.85		Medium-grained. Olivine bearing. Highly cross-cut by horizontal serpentine veins	Serpentinised Pyroxenite	
GVL09	90.85	107.62		intercalated serpentinised Dunite. Disseminated Chromite. Intertitially disseminated pyrrhotite.	Poikilitic Serpentinised Harzburgite	
GVL09	107.62	109.77		recrystalised Opx crystals and interstitial plagioclase. Olivine bearing. Disseminated chromite laths/pods.	Serpentinised Pyroxenite	
GVL09	109.77	125.75		intercalated with serpentinised Dunite. Disseminated chromite. Interstitially disseminated pyrrhotite approx 3%. Serper	Serpentinised Harzburgite	
GVL09	125.75	126.19		Altered to a greenish colour. Recrystalised/remobilised. Hard to identify individual minerals	Serpentinised-Chrloritised feldspathic unit	
GVL09	126.19	138.04	Gradational	intercalated Harzburgite with minor Dunite. Serpentinised. Minor interstitial disseminated pyrrhotite specks <3%.	Serpentinised Harzburgite	
GVL09	138.04	153.1		Fine to medium-grained. Serpentinised with possible chloritisation. Olivine bearing. Cut by multiple quartzofeldspathic	Olivine Bearing Feldspathic Pyroxenite	
GVL09	153.1	220.47	Gradational	m/g intercalated dunitic units. Many serpentine veins. Highly fractured	Poikilitic Serpentinised Harzburgite	
GVL09	220.47	234.63	Gradational	30 % plagioclase. Opx dominated. Fine-grained. Pyrite present within fractures.	Feldspathic Pyroxenite	
GVL09	234.63	239		Highly altered, serpentinised. Highly veined. Interconnected veins of pyroxenite and chlorite.	Feldspathic Pyroxenite	

Appendix D: Core Logging

BH-ID	From	To	Contact	Description	Lithology
GVL09	252.35	255.46		Brecciated blocks of serpentinite.intercalated dunite.	Serpentinite
GVL09	255.46	310.71	Sharp	Extremely to completely serpentinised. Fine to medium-grained.	Serpentinised Harzburgite
GVL09	310.71	312	Sharp	Granofels with sharp 30 inclination contacts.	Granofels
GVL09	312	314.72	Sharp	Fine to Medium-grained. interstitially disseminated Pyrrhotite <2%.	Serpentinised Harzburgite
GVL09	314.72	318.3	Sharp	granofels with sharp contacts. Intrusion has altered Harzburgite at the contacts at about 30 cm aureole.	Granofels
GVL09	318.3	327.36	Sharp	medium-grained. Interstitially disseminated pyrrhotite.	Serpentinised Harzburgite
GVL09	327.36	327.46	Sharp		Granofels
GVL09	327.46	332.47			Serpentinised Harzburgite
GVL09	332.47	332.84			Granofels
GVL09	332.84	369.36		Medium-grained >80% Olivine. Minor interstitial Pyrrhotite. Opx interstitial	Serpentinised Harzburgite
GVL09	369.36	437		mediumgrained. Disseminated chromite. Chromitite lenses 2cm thick Magnetite banding near bottom contact.	Serpentinised Harzburgite
GVL09	437	473		Medium-grained. Olivine dominated. Dissseminated chrome. Riddled with serpentine veinlets. Magnetite bands present. Highly fractured.	Dunite
GVL09	473	478.68		crumbly. Highly weathere/rubble.	Dunite
GVL09	478.68	479.18		Chromitiferous unit. >80% Chromite.	Chromitite
GVL09	479.18	480.15			Dunite
GVL09	480.15	480.48		Chromitiferous unit. >80% Chromite.	Chromitite
GVL09	480.48	486		Disintergrated	Dunite
GVL09	486	486.13		13cm Chromitite stringer	Chromitite
GVL09	486.13	489.25		Disintergrated	Dunite
GVL09	489.25	489.46		chromitite Layer	Chromitite
GVL09	489.46	492.3		Disintergrated	Dunite
GVL09	492.3	492.85		Feldspar and Quartz intrusion or feldspathic Pyroxenite, highly weathered.	Granofels
GVL09	492.85	493.77		Chromitiferous unit >90% Chromite.	Chromitite
GVL09	493.77	498.82			Dunite
GVL09	498.82	499	Sharp		Granofels
GVL09	499	503.82	Sharp		Dunite
GVL09	503.82	504.57	Sharp		Granofels
GVL09	504.57	509.94	Sharp		Dunite
GVL09	509.94	510.14	Sharp		Granofels
GVL09	510.14	539.07	Sharp	Dunite with intercalated darker more serpentinised Dunite	Dunite
GVL09	539.07	544.43	Gradational	medium to course-grained.	Pyroxenite
GVL09	544.43	546.42	Gradational		Poikilitic Serpentinised Harzburgite
GVL09	546.42	555.18		???????	Dunite
GVL09	555.18	555.24		???????	Dunite
GVL09	555.24	559.74		???????	Dunite
GVL09	559.74	562.57		Fresh dunite. Sugary grains with disseminated chromite.	Dunite
GVL09	562.57	564.86	Sharp	serpentinised dunite. Disseminated chromite	Dunite
GVL09	564.86	565.62	Sharp	Chromitite layer. Friable to hard. Fine grained.	Chromitite
GVL09	565.62	585.57	Sharp	Fresh dunite.	Dunite
GVL09	585.57	586.31	Sharp		Granofels
GVL09	586.31	601.04		Fresh dunite	Dunite
GVL09	601.04	601.41	Sharp	Iron-stained dunite	Dunite
GVL09	601.41	601.63			Granofels
GVL09	601.63	602.3		Iron-stained dunite	Dunite
GVL09	602.3	602.8		serpentinised dunite. Cut by interconnecting pyroxenitic veins.	Dunite

Appendix D: Core Logging

BH-ID	From	To	Contact	Description	Lithology
GVL10	75.9	81.7	Gradational	coarse grained. Massive. Interlayered with norite bands. Chloritised veins throughout unit.	Mottled anorthosite
GVL10	81.7	89.43		Medium to coarse grainsed. Massive. Minor felspathic veinlets.	Leuconorite
GVL10	89.43	143.47		Medium to coarse grainsed. Massive.	melanorite
GVL10	143.47	144.2		Medium to coarse grained. Scattered sulphides (pentlandite, pyrrhotite and chalcopyrite) and disseminated chromite.	Feldspathic pyroxenite
GVL10	144.2	145		Massive chromitite. 70 - 80 % chromite.	Chromitite
GVL10	145	145.35		Medium to coarse grained. Scattered sulphides (pentlandite, pyrrhotite and chalcopyrite) and disseminated chromite.	Feldspathic pyroxenite
GVL10	145.35	145.45		Chromitite stringer.	Chromitite
GVL10	145.45	159		Medium to coarse grained. Scattered sulphides (pentlandite, pyrrhotite and chalcopyrite) and disseminated chromite.	Feldspathic pyroxenite
GVL10	159	180		well mineralised. Blebby to disseminated sulphides chalcopyrite and pyrrhotite (3-5%). Plag content increases downwards as mineralisation decreases.	Feldspathic pyroxenite
GVL10	180	193		Medium to coarse grained. Scattered sulphides (pentlandite, pyrrhotite and chalcopyrite) and disseminated chromite. Quartzofeldspathic veins.	Feldspathic pyroxenite
GVL10	193	194.1		heavily aplite veined feldspathic pyroxenite	Feldspathic pyroxenite
GVL10	194.1	205.3	Gradational	Massive. Finely to medium crystaline.	Feldspathic pyroxenite
GVL10	205.3	209.8	Gradational	medium to coarsely crystaline. Massive 60-70% Opx	Norite
GVL10	209.8	218.5		medium to coarse grained. Massive.	Feldspathic pyroxenite
GVL10	218.5	219.1		interstitial pyrrhotite and chalcopyrite. Minor veining throughout.	Feldspathic pyroxenite
GVL10	219.1	234		medium to coarse grained. Massive.	Feldspathic pyroxenite
GVL10	234	237.5	Sharp	fine to coarse grained. Massive, no pyroxenitic texture. Heavily aplite veined. Later quartz veining. Altered.	Granofels
GVL10	237.5	300		sulphide content increses with depth. Scattedred disseminated pyrrhotite and chalcopyrite to blebby at the base.	Feldspathic pyroxenite
GVL10	300	300.5		pyrrhotite and chalcopyrite	Massive sulphide
GVL10	300.5	313.62		sulphide content increses with depth. Scattedred disseminated pyrrhotite and chalcopyrite to blebby at the base.	Feldspathic pyroxenite
GVL11	0.00m	5.00m		Core Missing	
GVL11	5.00m	15.97m		Extrememly weathered, unconsolidated material, large amounts of lost core, the material is mainly pyroxenite with minor amounts of qaurtz-feldspathic material (veinlets). At the top the core there is alluvial reddish sediments associated with the pyroxenite material. the pyroxenites are dominated by opx and cpx with minor amounts of interstitial plagioclase. the pyroxenite material is extremely fractured and crumbly in this interval	
GVL11	15.97m	25.07m	Gradational	Medium to coarse grained, opx and cpx dominate with minor interstitial plagioclase, material is extremely altered and fractured however more consolidated than the material above	Pyroxenite
GVL11	25.07m	27.37m	Gradational	With small intervals where the olivine is extremely altered but dominant mineral. The core is extremely crumbly and fractured, the olivine bearing pyroxenite is meduim to coarse grained. Olivine is extremely altered although still has a surgary texture, minor amounts of plag (interstitial)	Olivine bearing Pyroxenite
GVL11	27.37m	32.00m	Sharp contact	Mainly dominated by creamy white plagioclase with a slightly green tint (chloritisation). Has large oikocryst of opx (1cm)	Mottled Anorthosite
GVL11	32.00m	32.35m	Gradational	Medium to coarse grained. Oikcryst of Opx, has a mottled appearance at the end. At 32 .23m subvertical veinlet, with infill of secondary material	Spotted Anorthosite
GVL11	32.35m	32.46m	Gradational	Greenish tint (chloritisation) minor spotted texture of oikocryst of opx	Anorthosite
GVL11	32.46m	32.70m	Sharp contact	Dominted by Plag	Spotted Norite
GVL11	32.70m	32.71m	Sharp contact	Thin layer of pyroxenite with sulphides (chalcopyrite and pyrrhotite) >3% interstitial.	Pyroxenite
GVL11	32.71m	33.08m	Sharp contact	Dominted by Plag	Leuco spotted Norite
GVL11	33.08m	33.97m	Sharp contact	Greenish tint (chloritisation)	Anorthosite
GVL11	33.97m	34.55m	Sharp contact	Dominated by opx with plag 30-40%	Melo-Norite
GVL11	34.55m	35.42m	Sharp contact	Dominated by plag 55-60%, spotted texture with the oikocryst of opx	Leuco-Norite
GVL11	35.42m	35.46m	Sharp contact	Thin layer of pyroxenite with sulphides (chalcopyrite and pyrrhotite) >7% interstitial. Sulphides are restricted to the pyroxenite layer.	Pyroxenite

Appendix D: Core Logging

BH-ID	From	To	Contact	Description	Lithology
GVL11	35.46m	36.21m	Sharp contact	Has 4 intervals of pure anorthosite (intercalated interval) of norite/ anorthosite. Minor disseminated sulphide (Chalcopyrite and Pyrrhotite) associated with the opx oikcryst. Anorthosite units: 32.52m (2cm); 35.61m (5cm); 35.84m (10cm) 36.04m (2cm)	Spotted Norite
GVL11	36.21m	36.52m	Gradational	Dominated by opx 65%	Melo-Norite
GVL11	36.52m	36.56m	Sharp contact		Spotted Norite
GVL11	36.56m	38.52m	Sharp contact	Dominated by opx, with small intervals of spotted norite, minor disseminated sulphides (chalcopyrite and pyrrhotite) locally, associated generally with the more opx rich intervals.	Melo-Norite
GVL11	38.52m	40.54m	Gradational	Medium to coarse grained, dominated by pyroxenes (opx and cpx) with minor interstitial plag. Disseminated sulphides (chalcopyrite and pyrrhotite) 3% locally	Feldspathic pyroxenite
GVL11	40.54m	41.37m	Sharp contact	Dominated by plag 60%	Spotted Norite
GVL11	41.37m	41.46m	Sharp contact	Thick veinlet filled with remobilised noritic material, filled with both altered and mafic and felsic material	
GVL11	41.46m	41.70m	Sharp contact		Spotted Norite
GVL11	41.70m	42.52m	Sharp contact	Greenish tint due to chloritisation	Mottled Anorthosite
GVL11	42.52m	46.92m	Gradational	Plagioclase up to 60%, minor chlorite veinlet through the interval which are less than 0.5cm thick	Leuco spotted Norite
GVL11	46.92m	47.21m	Gradational	Dominated by opx 60% and more	Melo-Norite
GVL11	47.21m	47.30m	Sharp contact	Minor oickcryst of opx	Anorthosite
GVL11	47.30m	47.63m	Sharp contact		Norite
GVL11	47.63m	47.90m	Gradational	Has greenish tints (chloritisation) minor spotted texture of oikocryst op opx	Anorthosite
GVL11	47.90m	48.76m	Gradational		Melo-Norite
GVL11	48.76m	48.95m	Sharp contact	Minor oickcryst of opx	Spotted Anorthosite
GVL11	48.95m	54.55m	Sharp contact	Dominted by opx	Melo-Norite
GVL11	54.55m	57.37m	Gradational		Spotted Anorthosite
GVL11	57.37m	57.78m	Sharp contact	(Calcite material) minor 1% opx material present	Altered Anorthosite
GVL11	57.78m	94.40m	Sharp contact	Medium to coarse grained dominated by opx and plag (50/50)	Spotted Norite
GVL11	94.40m	95.18m	Gradational	Dominated by opx up to 65%	Melo-Norite
GVL11	95.18m	96.06m	Sharp contact	Dominated by plag up to 60%	Spotted leuco Norite
GVL11	96.06m	99.64m	Gradational		Spotted Anorthosite
GVL11	99.64m	101.00 m	Sharp contact	Dominated by opx and cpx, with 15% cumulus plag	Feldspathic pyroxenite
GVL11	101.00 m	107.60 m	Gradational	Medium to coarse grained dominated by opx and cpx (50%) and plag (50%). Qtz feldspathic veinlet 102.51m to 102.54m	Gabbronorite
GVL11	107.60 m	108.65 m	Sharp contact		Mottled / Spotted Anorthosite
GVL11	108.65 m	111.85 m	Gradational	Othorpyroxene up to 60%	Meso- Norite
GVL11	111.85 m	112.08 m	Gradational	Plagioclase up to 60%, minor chlorite veinlet through the interval which are less than 0.5cm thick	Leuco Norite
GVL11	112.08 m	113.40 m	Gradational	Dominated by opx 60%	Melo-Norite

y

Appendix D: Core Logging

BH-ID	From	To	Contact	Description	Lithology
GVL11	113.40 m	117.36 m	Gradational	Dominated by plag up to 60% and more, where there is an abundance of plag there is a more spotted texture present	Leuco Norite
GVL11	117.36 m	123.41 m	Gradational	Medium to coarse grained with dominant minerals of opx and plag	Norite
GVL11	123.41 m	124.21 m	Gradational	Dominated by palg . The opx forms both a mottled/ spotted texture in small parts of this interval, less than 2cm thick	Leuco spotted Norite
GVL11	124.21 m	150.40 m	Gradational	Meduim to coarse grained	Meso- Norite
GVL11	150.40 m	151.30 m	Gradational	Core is crumbly almost like chip samples	Meso- Norite
GVL11	151.30 m	181.74 m	Gradational		Meso- Norite
GVL11	181.74 m	182.30 m	Sharp contact		Granofic intrusive Material
GVL11	182.30 m	200.55 m	Sharp contact	Medium to coarse grained dominated by opx and plag	Meso- Norite
GVL 12	0	28.6		medium to coarse grained. Massive. Cut by multiple quartzofeldspathic veinlets.	Norite
GVL 12	28.6	25.6		medium to coarse grained. Massive. Cut by multiple quartzofeldspathic veinlets. 90% Opx, 5% Cpx, 5% plag.	Pyroxenite
GVL 12	25.6	29.4		medium to coarse grained. Massive. Cut by multiple quartzofeldspathic veinlets. 90% Opx, 5% Cpx, 5% plag. Disseminate	Pyroxenite
GVL 12	29.4	29.5		Chromitite stringer in pyroxenite.	Chromitite
GVL 12	29.5	29.58		medium to coarse grained. Massive. Cut by multiple quartzofeldspathic veinlets. 90% Opx, 5% Cpx, 5% plag.	Pyroxenite
GVL 12	29.58	29.77		Chromitite stringer in pyroxenite.	Chromitite
GVL 12	29.77	30		medium to coarse grained. Massive. Cut by multiple quartzofeldspathic veinlets. 90% Opx, 5% Cpx, 5% plag.	Pyroxenite
GVL 12	30	30.15		Chromitite stringer in pyroxenite.	Chromitite
GVL 12	30.15	33.16		medium to coarse grained. Massive. Cut by multiple quartzofeldspathic veinlets. 90% Opx, 5% Cpx, 5% plag.	Pyroxenite
GVL 12	33.16	35.73		90% olivine, 10% plagioclase.	Dunite
GVL 12	35.73	39.65		medium to coarse grained. Massive. Minor scattered disseminated sulphides. Poorly mineralised	Feldspathic pyroxenite
GVL 12	39.65	39.75		Chromitite stringer in pyroxenite.	Chromitite
GVL 12	39.75	40.6		medium to coarse grained. Massive. Minor scattered disseminated sulphides. Poorly mineralised	Feldspathic pyroxenite
GVL 12	40.6	40.8		Chromitite stringer in pyroxenite.	Chromitite
GVL 12	40.8	40.85		medium to coarse grained. Massive. Minor scattered disseminated sulphides. Poorly mineralised	Feldspathic pyroxenite
GVL 12	40.85	43.3		fine to medium grained. Friable. Massive.	Dunite
GVL 12	43.3	44.1			Feldspathic pyroxenite
GVL 12	44.1	50		fine to medium grained. Friable. Massive.	Dunite
GVL 12	50	51.5			Feldspathic pyroxenite
GVL 12	51.5	55.6		fine to medium grained. Friable. Massive.	Dunite
GVL 12	55.6	56.2			Feldspathic pyroxenite
GVL 12	56.2	59.3			Dunite
GVL 12	59.3	60			Feldspathic pyroxenite
GVL 12	60	68.9			Dunite
GVL 12	68.9	69.32			Granofels
GVL 12	69.32	74.3			Dunite
GVL 12	74.3	78.1		coarse grained. Massive. 25% plag.	Feldspathic pyroxenite
GVL 12	78.1	83.8		Oikocrysts of Opx (ranging from 1 cm to 5 cm in diameter). Quartzofeldspathic veinlets cutting throughout unit at an obli	Dunite
GVL 12	83.8	84			Granofels
GVL 12	84	93.9		Oikocrysts of Opx (ranging from 1 cm to 5 cm in diameter). Quartzofeldspathic veinlets cutting throughout unit at an obli	Dunite
GVL 12	93.9	94.85		serpentinised. Quartzofeldspathic veinlets cutting unit.	Gabbro
GVL 12	94.85	98.86			Granofels
GVL 12	98.86	103.16		Oikocrysts of Opx (ranging from 1 cm to 5 cm in diameter). Quartzofeldspathic veinlets cutting throughout unit at an obli	Dunite
GVL 12	103.16	103.53			Granofels
GVL 12	103.53	134.1		Oikocrysts of Opx (ranging from 1 cm to 5 cm in diameter). Quartzofeldspathic veinlets cutting throughout unit at an obli	Dunite
GVL 12	134.1	139	sharp	medium to coarse grained massive. Zones of plag and pyroxene enrichment.	Granofels
GVL 12	139	146.09		medium to coarse grained. Massive. Intercalated zones of plag-rich zones. Increased serpentinisation towards the base	Feldspathic pyroxenite
GVL 12	146.09	167.56		Medium to coarse-grained. Massive. Serpentinised. Oikocrysts of Opx of varying size.	Serpentinised Harzburgite
GVL 12	167.56	170.1		Fine to medium grained. Massive.	Pyroxenite
GVL 12	170.1	170.45		Fine to medium grained. Massive. Plagioclase rich zone.	Pyroxenite
GVL 12	170.45	181.8		Fine to medium grained. Massive. Increased serpentinisation.	Pyroxenite
GVL 12	181.8	188		Fine to medium grained. Massive.	Pyroxenite
GVL 12	188	195		medium to coarse grained. Serpentinised. Oikocrysts of Opx varying size (1 cm to 5 cm)	Serpentinised Harzburgite
GVL 12	195	200.45		Extremely weathered and altered zone. Crumbly. medium to coarse grained. Serpentinised. Oikocrysts of Opx varying si	Serpentinised Harzburgite

Appendix D: Core Logging

BH-ID	From	To	Contact	Description	Lithology
GVL 13	0	19	Broken	Medium to coarse grained. Massive. Extensively weathered . Rubble/friable. 60% Plagioclase. 40% Opx.	Norite
GVL 13	19	23.95	Sharp	Greenish tinge. Fine to mediu grained. Massive. Weathered. Rubble/friable. 85% plaioglase. 15 % Opx. Mottles range in s	Mottled Anorthosite
GVL 13	23.95	30.8	Sharp	Medium to coarse grained. Massive. Extensively weathered . Rubble/friable. 60% Plagioclase. 40% Opx.	Norite
GVL 13	30.8	31.8	Sharp		Quartzofeldspathic vein
GVL 13	31.8	32.66	Sharp	Medium to coarse grained. Massive. Extensively weathered . Rubble/friable. 60% Plagioclase. 40% Opx.	Norite
GVL 13	32.66	32.86	Sharp		Quartzofeldspathic vein
GVL 13	32.86	33.47	Sharp	Medium to coarse grained. Massive. Extensively weathered . Rubble/friable. 60% Plagioclase. 40% Opx.	Norite
GVL 13	33.47	33.71	Sharp		Quartzofeldspathic vein
GVL 13	33.71	35.03	Sharp	Medium to coarse grained. Massive. Extensively weathered . Rubble/friable. 60% Plagioclase. 40% Opx.	Norite
GVL 13	35.03	35.18	Sharp		Quartzofeldspathic vein
GVL 13	35.18	40.4	Sharp	Medium to coarse grained. Massive. Extensively weathered . Rubble/friable. 60% Plagioclase. 40% Opx.	Norite
GVL 13	40.4	43.72	Sharp	Massive. Medium grained. 70% Plagioclase. 20% Opx. Cut by multiple quartzofeldspathic veinlets.	Leuconorite
GVL 13	43.72	47	Gradational	Massive. Medium to coarse grained. 60% Plagioclase. 40% Opx.	Norite
GVL 13	47	50.35	Sharp	Massive. Medium to coarse grained. 60% Plagioclase. 40% Opx. Ductile deformation - shearing. Shear zone.	Norite
GVL 13	50.35	52.36	Gradational	Massive. Medium to coarse grained. 70% plagioclase. 30% Opx.	Leuconorite
GVL 13	52.36	52.66	Gradational	Massive. Medium to coarse grained. Increase in pyroxene content.	Norite
GVL 13	52.66	52.76	Gradational	Massive. Medium to coarse grained. Increase in plagioclase content.	Norite
GVL 13	52.76	57	Gradational	Massive. Medium to coarse grained. 70% plagioclase. 30% Opx.	Leuconorite
GVL 13	57	82.12	Gradational	Medium grained. Massive. 70% Plagioclase. 30% Opx.	Mottled Anorthosite
GVL 13	82.12	94.13	Sharp	Medium to coarse grained. Massive. 45% Plagioclase. 55% Opx.	Norite
GVL 13	94.13	95.31	Gradational	Medium to coarse grained. Massive. 60% Plagioclase. 40% Opx.	Mottled Anorthosite
GVL 13	95.31	100.29	Gradational	Medium to coarse grained. Massive. 55% Plagioclase. 45% Opx.	Norite
GVL 13	100.29	102.42	Gradational	Medium to coarse grained. Massive. 50% Plagioclase. 50% Opx.	Norite
GVL 13	102.42	105.13	Gradational	Medium to coarse grained. Massive. 55% Plagioclase. 45% Opx.	Norite
GVL 13	105.13	107.64	Gradational	Medium to coarse grained. Massive. 10% Plagioclase. 60% Opx. 30% Opx.	Pyroxenite
GVL 13	107.64	115.08	Gradational	Medium to coarse grained. Massive. 50% Plagioclase. 50% Opx.	Norite
GVL 13	115.08	125.07	Sharp	Massive. Coarse grained. 70% Plagioclase. 30% Opx.	Mottled Anorthosite
GVL 13	125.07	131.72	Gradational	Massive. Medium to coarse grained. 45% Plagioclase. 55% Opx.	Norite
GVL 13	131.72	143.4		Massive. Medium to coarse grained. 10% Plagioclase. 80% Opx. 10 Cpx.	Pyroxenite
GVL 13	143.4	145.6			Quartzofeldspathic vein
GVL 13	145.6	152.4		Massive. Medium to coarse grained. 10% Plagioclase. 80% Opx. 10 Cpx.	Pyroxenite
GVL 13	152.4	153			Quartzofeldspathic vein
GVL 13	153	158.23		Massive. Medium to coarse grained. 10% Plagioclase. 80% Opx. 10 Cpx.	Pyroxenite
GVL 13	158.23	172.57		Massive. Medium to coarse grained. 40% Plagioclase. 55% Opx. 5 Cpx.	Norite
GVL 13	172.57	176.93		Massive. Medium to coarse grained. 50% Plagioclase. 40% Opx. 10 Cpx.	Norite
GVL 13	176.93	182.86		Massive. Medium to coarse grained. 55% Plagioclase. 55% Opx.	Leuconorite
GVL 13	182.86	183.8			Quartzofeldspathic vein
GVL 13	183.8	185.1		Massive. Medium to coarse grained. 55% Plagioclase. 55% Opx.	Leuconorite
GVL 13	185.1	186.74			Mottled Anorthosite
GVL 13	186.74	200.52		Massive. Medium to coarse grained. 50% Plagioclase. 50% Opx.	Norite
GVL 15	0	14.3	Broken	overburden. Highly weathered. Pyroxenitic material.	Pyroxenite
GVL 15	14.3	14.9	Broken	Quartz and feldspar intrusion. Medium to coarse grained. Massive.	Quartzofeldspathic vein
GVL 15	14.9	15.5	Broken	70% Plag 30% Opx	Mottled anorthosite
GVL 15	15.5	18.4	Sharp	85% Opx 10% Cpx 5 % Plagioclase. Coarse grained. Massive. Magnetite bands throughout (10mm to 30 mm) in thichkness.	Pyroxenite
GVL 15	18.4	19.3	Broken	Very coarse grained. Massive.veins of K-spar throughout. Either K-spar or tinted by magnetite oxidation. Magnetite band	Leuconorite
GVL 15	19.3	20.15	Gradational	medium to coarse grained. Massive. 7% plagioclase. 80% Opx. 13% Cpx. Magnetite band at top contact.	Pyroxenite
GVL 15	20.15	21.3	Sharp	Very coarse grained. Massive. 50% Plagioclase. 40% Opx. 10 % Cpx.	Leuconorite
GVL 15	21.3	22	Gradational	medium to coarse grained. Massive. 7% plagioclase. 80% Opx. 13% Cpx.	Pyroxenite
GVL 15	22	24.77		Coarse grained. Massive. Minor quartzofeldspathic veining. 70 % plagioclase. 20% Opx. 10% Cpx.	Spotted Anorthosite
GVL 15	24.77	36.46		3% plagioclase. 87% Opx. 10% Cpx. Coarse grained. Massive. Plagioclase content increases downwards. Magnetite bande	Pyroxenite
GVL 15	36.46	38		Coarse grained. Massive. Pyroxene content increases downwards. Plagioclase altered (prehnite?). 70 % Plagioclase. 20%	Mottled anorthosite
GVL 15	38	48		Coarse grained. Massive. Pyroxene content increases downwards. Plagioclase altered (prehnite?). 70 % Plagioclase. 20%	Mottled anorthosite
GVL 15	48	55.63		Coarse grained. Massive. Pyroxene content increases downwards. Plagioclase altered (prehnite?). 70 % Plagioclase. 20%	Mottled anorthosite
GVL 15	55.63	57.52	Broken	50 % Plagioclase. 50% Opx. Medium to coarse grained massive. Minor quartzofeldspathic veining.	Norite
GVL 15	57.52	58.12	Gradational	coarse grained. Massive. 70% Plagioclase. 30 % Opx.	Mottled anorthosite
GVL 15	58.12	73.2	Gradational	85% Opx. 10% plagioclase. 5% Cpx. Medium grained. Massive. Plagioclase content increases downwards.	Pyroxenite
GVL 15	73.2	73.7	Sharp	chromitite stringers intercalated with pyroxenite.	Chromitite
GVL 15	73.7	81	Sharp	85% Opx. 10% plagioclase. 5% Cpx. Medium grained. Massive. Plagioclase content increases downwards. Disseminated s	Pyroxenite
GVL 15	81	86.92	Gradational	Medium to coarse grained. Massive. Crumbly. Leucocratic. 55% Plagioclase. 45% Opx.	Norite
GVL 15	86.92	89.42	Gradational	Medium to coarse grained. Massive. 12% Plagioclase. 80% Opx. 12% Cpx.	Pyroxenite

aa

Appendix D: Core Logging

BH-ID	From	To	Contact	Description	Lithology
GVL 15	89.42	95.46	Sharp	Medium to coarse grained. Massive. Minor feldspathic veining. 50% Plagioclase. 50% Opx.	Norite
GVL 15	95.46	97.68	Sharp	Quartz and feldspar intrusion. Fine to medium grained. Massive. Phyllosilicate veinlets with sharp contacts.	Quartzofeldspathic vein
GVL 15	97.68	122.16	Sharp	Medium to coarse grained. Massive. Disseminated sulphide specks . Pyrrhotite and chalcopyrite. Cut by multiple quartzo	Norite
GVL 15	122.16	122.41		Fine grained. Massive.	Quartzofeldspathic vein
GVL 15	122.41	125.43		medium to coarse grained. Massive. 50% plagioclase. 50% Opx.minor quartzofeldspathic veining.	Norite
GVL 15	125.43	126.21		Fine grained. Massive.	Quartzofeldspathic vein
GVL 15	126.21	132.28		medium to coarse grained. Massive. 40% plagioclase. 60 % Opx.	Melanorite
GVL 15	132.28	132.38		Fine grained. Massive.	Quartzofeldspathic vein
GVL 15	132.38	135.48		medium to coarse grained. Massive. 40% plagioclase. 60 % Opx.	Melanorite
GVL 15	135.48	136		Fine grained. Massive.	Quartzofeldspathic vein
GVL 15	136	136.7		medium to coarse grained. Massive. 40% plagioclase. 60 % Opx.	Melanorite
GVL 15	136.7	137			Quartzofeldspathic vein
GVL 15	137	139		medium to coarse grained. Massive. 40% plagioclase. 60 % Opx.	Melanorite
GVL 15	139	140.45		medium to coarse grained. Massive. Plagioclase content increases downwards. 80% Opx. 10% Plagioclase. 10% Cpx.	Pyroxenite
GVL 15	140.45	140.65			Chromitite
GVL 15	140.65	150.5		chromitite stringers intercalated with pyroxenite.	Pyroxenite
GVL 15	150.5	174		medium to coarse grained. Massive. Plagioclase content increases downwards. 80% Opx. 10% Plagioclase. 10% Cpx. Disse	Pyroxenite
GVL 15	174	183		medium to coarse grained. Massive. Plagioclase content increases downwards. 80% Opx. 10% Plagioclase. 10% Cpx. Disse	Pyroxenite
GVL 15	183	195.4		Sheared zone.	Pyroxenite
GVL 15	195.4	201.2		medium to coarse grained. Massive. Plagioclase content increases downwards. 80% Opx. 10% Plagioclase. 10% Cpx. Disse	Feldspathic Pyroxenite
GVL 18	0	10.5	Sharp Contact	Loss of core and unconsolidated seds.	
GVL 18	0.5	29.64	Gradational	Medium to coarse grained. Dominated by plag up to 60%, Greenish tint to plagioclase indication of minor chlorotisation	Leuconorite
GVL 18	29.64	38.34	Sharp Contact	Equal proportions of Opx and Plag	Norite
GVL 18	38.34	38.39	Sharp Contact	Dominate by Opx and Cpx with minor interstitial Plag. Sulphides (Chalcopyrite and Pyrrhotite) associated with the pyroxenite layer, extremely disseminated 2%	Pyroxenite
GVL 18	38.39	51.02	Sharp Contact	Medium to coarse grained, dominant minerals of Opx and Plag, localized with intervals with a mottled/ spotted texture	Norite
GVL 18	51.02	51.26	Sharp Contact	Dominated with Plag up to 90%, Plag has a greenish tint (Chloritisation) within the anorthosite interval there are large oikocryst of Opx (locally)	Anorthosite
GVL 18	51.26	52.15	Gradational	Coarse grained dominated by Opx	Melanorite
GVL 18	52.15	56.3	Gradational	Extremely coarse grained with small intervals within the is unit with a pegmatoidal texture where the grains are larger than 2.5cm in size. These pegmatoidal intervals are recrystallized norite, mainly coposed of Opx and Plag. Small intervals of yroxene-rich layers less than 5cm thick .	Melanorite
GVL 18	56.3	57.35	Sharp Contact	Altered, recrystallized, extremely coarse grained to pegmatoidal with locallised Olivine up to 5%	Melanorite
GVL 18	57.35	57.6	Sharp Contact	medium grained dominated by pyroxenes with minor plag (interstitial)	Pyroxenite
GVL 18	57.6	62	Sharp Contact	Medium grained with qtz and feldspathic material. Interval of mafic material, olivine, opx and plag. Olivine up to 10% small black rounded grains: 58.63m to 58.73m sharp contact. Interval of mafics opx dominate with plagioclase, sharp contact with the granophic material; 60.20m to 60.35m. Interval of Norite (spotted) leuco- plagioclase has greenish tints indicating a high degree of chloritisation: 61.21m - 61.40m. Smaller intervals of veinlets with mafic material probably altered opx.	Granofels
GVL 18	62	64.6	Sharp Contact	Meduim to coarse grained dominated by opx up to 60%.	Norite
GVL 18	64.6	67.7	Sharp Contact	Layer with intercalated mafic layers of noritic texture/ material. Meso- norite interval dominated by opx 65.40m to 64.60m; sharp contacts. Meso-norite interval dominated by opx, plag is extremely chloritised 66.03m to 66.13m, sharp contact. Meso-norite interval dominated by opx, also has a 2cm thick veinlet of remobalised plag 67.17m to 67.57m with sharp contact. Meso-norite interval 67.73m to 67.79m, sharp contact	Granofels
GVL 18	67.7	74.08	Sharp Contact	Plag up 20 %	Leuconorite

Appendix D: Core Logging

BH-ID	From	To	Contact	Discription	Lithology
GVL 18	74.08	85.69	Sharp Contact	An interval of granophic material intruding a noritic package, there is abreccia texture associated with this interval where pieces of noritic material are seen sorrunded by granophic material. The noritic units are medium to coarse grained with opx and plag generally having equal proportions, incase the noritic unit can be more leuco and have a spotted texture. The granitic material is fine to medium grained, however is some veinlets (smaller ones) the granitic material can have a pegmatoidal texture. The granitic matetrial is composed of qtz and K-feldspar (reddish colouration) with minor amphiboles (biotite). The granitic material here has more reddish colour to the granophic material mention above this unit	
GVL 18	85.69	89.73	Sharp Contact	Meduim to coarse grained, equal proportions of plag and opx. Intervals with localised olivine up to 10%	Norite
GVL 18	89.73	90.79	Sharp Contact	Meduim grained composed of qtz and feldspars (reddish colouration)	Granofels
GVL 18	90.79	92.78	Sharp Contact	Meduim to coarse grained in equal proportions of plag and opx with intervals of olivine (locally) up to 10% small subrounded black crystals. 92.00m to 92.10m granitic (pegmatoidal) interval composed of feldspar and qtz.	Norite
GVL 18	92.78	93.37	Sharp Contact	More qtz and plag - rich has a more cream white colouration. Small noritic interval, with sharp contact; 92.97m to 93.02m	Granofels
GVL 18	93.37	96.85	Sharp Contact	Norite (interval with leuco appearance dominated by plag) throughout this interval the plag has a greenish tint indicating choritisation. Granitic intrusive unit 94.90m to 95.10m, medium grained reddish colouration indicating K-feldspar abundance. Granitic intrusive unit 96.03m to 96.15m, medium grained with reddish colouration.	Norite
GVL 18	96.85	97.65	Sharp Contact	Medium to coarse grained in the center of the interval the material is reddish probably because of the K-feldspar and on the side the is a more creamy white colouration due to quartz and plag.	Granofels
GVL 18	97.65	97.95	Sharp Contact	More mafic unit with opx up to 60% and olivine up to 10%	Olivine Norite
GVL 18	97.95	108.05	Gradational	Medium to coarse grained with equal proportions of opx and plag	Norite
GVL 18	108.05	109.24	Sharp Contact	Larger degree of alteration at the top contact, greenish tint- chloritisation and epidotisation	Granofels
GVL 18	109.24	112.65	Sharp Contact	Medium to coarse grained with equal proportions of opx and plag. Granofels 109.60m (2cm thick) reddish colouration (K-feldspar) and qtz. Granofels 110.69m, creamy white at the top and bottom contact and a reddish colouration in the center	Norite
GVL 18	112.65	115.82	Gradational	Opx oikocryst are clustered at the bottom gradational contact.	Mottled Anorthosite
GVL 18	115.82	117.42	Gradational	Equal proportions of Opx and Plag	Norite
GVL 18	117.42	119.08	Sharp Contact	Oikocryst of opx. Plag has a greenish colouration indicating chloritisation	Mottled Anorthosite
GVL 18	119.08	151.14	Sharp Contact	Meduim to coarse grained. Opx and plag are in equal proportions	Norite
GVL 20	2.56	11.35	Broken	Medium to coarse grained. Massive. Greenish grey in colour. Plagioclase degreases downwards. Moderately weathered.	Norite
GVL 20	11.35	12.52	Broken	Medium to coarse grained. Massive. Greenish grey in colour. Plagioclase degreases downwards. Moderately weathered.	Norite
GVL 20	12.52	20.25	Broken	Pinkish grey. Fine grained. Massive. 70% feldspar. 20% Quartz. 10 % amphiboles.	Granophyre
GVL 20	20.25	21.2	Sharp	Pinkish grey. Fine grained. Massive. 70% feldspar. 20% Quartz. 10 % amphiboles. Interfingered with Melanorite.	Granofels
GVL 20	21.2	25.25	Sharp	Medium to coarse grained. Massive. Greenish grey in colour. Plagioclase degreases downwards. Moderately weathered.	Norite
GVL 20	25.25	25.6	Sharp		Quartzofeldspathic vein
GVL 20	25.6	34.2	Sharp	Medium to coarse grained. Massive. Greenish grey in colour. Plagioclase degreases downwards. Moderately weathered.	Norite
GVL 20	34.2	34.6	Sharp		Granofels
GVL 20	34.6	38.12	Sharp	Medium to coarse grained. Massive. Greenish grey in colour. Plagioclase degreases downwards. Moderately weathered.	Norite
GVL 20	38.12	38.32	Sharp	aureole of alteration caused by intrusion.	Granofels
GVL 20	38.32	39.58	Sharp	Dyke. Fine grained. 80% K-Spar. 5 % Plag. 7 % Amphibole. 8% chlorite/epidote.	Granophyre
GVL 20	39.58	39.9	Sharp		Granofels
GVL 20	39.9	40.82	Sharp	Dyke. Fine grained. 80% K-Spar. 5 % Plag. 7 % Amphibole. 8% chlorite/epidote.	Granophyre
GVL 20	40.82	45.12	Sharp	Massive. Medium to coarse grained. 55% Plagioclase. 45% Opx. 5% Cpx.	Norite
GVL 20	45.12	45.17	Sharp		Quartzofeldspathic vein
GVL 20	45.17	46	Gradational	Massive. Medium to coarse grained. 55% Plagioclase. 45% Opx. 5% Cpx.	Norite
GVL 20	46	55.65	Gradational	Massive. Medium to coarse grained. 70% Plagioclase. Quartzofeldspathic veinlets throughout. Intercalated zones of incre	Leuconorite
GVL 20	55.65	63.49	Sharp	Massive. Medium to coarse grained. 60% Plagioclase. 40% Opx. Increase in plagioclase content at the base. Undulatory er	Norite
GVL 20	63.49	65.9	Sharp	Dyke. Fine grained. 80% K-Spar. 5 % Plag. 7 % Amphibole. 8% chlorite/epidote. Chalcopyrite dyke in epidote vein at 64.75	Granophyre
GVL 20	65.9	94	Sharp	Coarse grained. Pyroxene content increases downwards. Cut my multiple quartzofeldspathic veinlets throughout unit.	Norite
GVL 20	94	97.15	Sharp	khaki-red, fine to medium grained. Intrusive contact.	Granophyre
GVL 20	97.15	129		Massive. Medium to coarse grained. 50 % pPlagioclase. 50% Opx.	Norite
GVL 20	129	129.1			Quartzofeldspathic vein

Appendix D: Core Logging

BH-ID	From	To	Contact	Description	Lithology
GVL 20	129.1	129.9		Massive. Medium to coarse grained. 50 % pPlagioclase. 50% Opx.	Norite
GVL 20	129.9	130			Quartzofeldspathic vein
GVL 20	130	139.35		Massive. Medium to coarse grained. 50 % pPlagioclase. 50% Opx.	Norite
GVL 20	139.35	139.45			Quartzofeldspathic vein
GVL 20	139.45	141.2		Massive. Medium to coarse grained. 50 % pPlagioclase. 50% Opx.	Norite
GVL 20	141.2	141.3			Quartzofeldspathic vein
GVL 20	141.3	148.5		Massive. Medium to coarse grained. 50 % pPlagioclase. 50% Opx.	Norite
GVL 20	148.5	148.6			Quartzofeldspathic vein
GVL 20	148.6	149.84		Massive. Medium to coarse grained. 50 % pPlagioclase. 50% Opx.	Norite

dd

Appendix E: Magnetic Susceptibility

BHID	Depth	Reading 1	Reading 2	Reading 3	Average	SI Units	BHID	Depth	Reading 1	Reading 2	Reading 3	Average	SI Units	BHID	Depth	Reading 1	Reading 2	Reading 3	Average	SI Units
GVL3	59.00	0.231	0.210	0.184	0.208	0.000	GVL3	73.70	0.041	0.042	0.033	0.039	0.000	GVL3	88.40	0.048	0.031	0.046	0.042	0.000
GVL3	59.30	0.298	0.304	0.319	0.307	0.000	GVL3	74.00	0.042	0.061	0.060	0.054	0.000	GVL3	88.70	0.014	0.033	0.042	0.030	0.000
GVL3	59.60	0.367	0.341	0.353	0.354	0.000	GVL3	74.30	0.040	0.059	0.032	0.044	0.000	GVL3	89.00	0.033	0.036	0.035	0.035	0.000
GVL3	59.90	0.148	0.136	0.129	0.138	0.000	GVL3	74.60	0.075	0.057	0.046	0.059	0.000	GVL3	89.30	0.055	0.050	0.068	0.058	0.000
GVL3	60.20	0.132	0.184	0.203	0.173	0.000	GVL3	74.90	0.081	0.075	0.071	0.076	0.000	GVL3	89.60	0.069	0.083	0.080	0.077	0.000
GVL3	60.50	0.175	0.159	0.167	0.167	0.000	GVL3	75.20	0.042	0.031	0.036	0.036	0.000	GVL3	89.90	0.095	0.060	0.040	0.065	0.000
GVL3	60.80	0.198	0.182	0.200	0.193	0.000	GVL3	75.50	0.061	0.083	0.055	0.066	0.000	GVL3	90.20	0.050	0.036	0.068	0.051	0.000
GVL3	61.10	0.227	0.223	0.235	0.228	0.000	GVL3	75.80	0.076	0.071	0.052	0.066	0.000	GVL3	90.50	0.069	0.065	0.065	0.066	0.000
GVL3	61.40	0.184	0.176	0.173	0.178	0.000	GVL3	76.10	0.033	0.031	0.074	0.046	0.000	GVL3	90.80	0.035	0.047	0.060	0.047	0.000
GVL3	61.70	0.178	0.157	0.178	0.171	0.000	GVL3	76.40	0.041	0.071	0.072	0.061	0.000	GVL3	91.10	0.046	0.058	0.066	0.057	0.000
GVL3	62.00	0.154	0.140	0.147	0.147	0.000	GVL3	76.70	0.050	0.044	0.036	0.043	0.000	GVL3	91.40	0.037	0.028	0.022	0.029	0.000
GVL3	62.30	0.195	0.195	0.184	0.191	0.000	GVL3	77.00	0.083	0.091	0.082	0.085	0.000	GVL3	91.70	0.011	0.025	0.034	0.023	0.000
GVL3	62.60	0.291	0.281	0.279	0.284	0.000	GVL3	77.30	0.057	0.090	0.063	0.070	0.000	GVL3	92.00	0.023	0.019	0.029	0.024	0.000
GVL3	62.90	0.052	0.051	0.049	0.051	0.000	GVL3	77.60	0.062	0.065	0.072	0.066	0.000	GVL3	92.30	0.015	0.038	0.054	0.036	0.000
GVL3	63.20	0.077	0.061	0.073	0.070	0.000	GVL3	77.90	0.056	0.043	0.087	0.062	0.000	GVL3	92.60	0.058	0.059	0.053	0.057	0.000
GVL3	63.50	0.044	0.059	0.057	0.053	0.000	GVL3	78.20	0.071	0.064	0.060	0.065	0.000	GVL3	92.90	0.049	0.037	0.052	0.046	0.000
GVL3	63.80	0.053	0.056	0.045	0.051	0.000	GVL3	78.50	0.053	0.057	0.062	0.057	0.000	GVL3	93.20	0.029	0.041	0.042	0.037	0.000
GVL3	64.10	0.113	0.104	0.078	0.098	0.000	GVL3	78.80	0.091	0.086	0.070	0.082	0.000	GVL3	93.50	0.021	0.032	0.028	0.027	0.000
GVL3	64.40	0.091	0.064	0.083	0.079	0.000	GVL3	79.10	0.087	0.080	0.080	0.082	0.000	GVL3	93.80	0.089	0.082	0.086	0.086	0.000
GVL3	64.70	0.068	0.084	0.086	0.079	0.000	GVL3	79.40	0.048	0.057	0.061	0.055	0.000	GVL3	94.10	0.068	0.085	0.078	0.077	0.000
GVL3	65.00	0.036	0.042	0.054	0.044	0.000	GVL3	79.70	0.064	0.030	0.067	0.054	0.000	GVL3	94.40	0.088	0.082	0.084	0.085	0.000
GVL3	65.30	0.075	0.069	0.067	0.070	0.000	GVL3	80.00	0.038	0.046	0.034	0.039	0.000	GVL3	94.70	0.073	0.069	0.075	0.072	0.000
GVL3	65.60	0.103	0.086	0.069	0.086	0.000	GVL3	80.30	0.039	0.038	0.570	0.216	0.000	GVL3	95.00	0.091	0.084	0.068	0.081	0.000
GVL3	65.90	0.072	0.063	0.072	0.069	0.000	GVL3	80.60	0.063	0.058	0.055	0.059	0.000	GVL3	95.30	0.069	0.066	0.053	0.063	0.000
GVL3	66.20	0.062	0.073	0.044	0.060	0.000	GVL3	80.90	0.066	0.031	0.059	0.052	0.000	GVL3	95.60	0.087	0.049	0.064	0.067	0.000
GVL3	66.50	0.044	0.075	0.070	0.063	0.000	GVL3	81.20	0.047	0.054	0.064	0.055	0.000	GVL3	95.90	0.055	0.112	0.067	0.078	0.000
GVL3	66.80	0.119	0.097	0.097	0.104	0.000	GVL3	81.50	0.052	0.045	0.053	0.050	0.000	GVL3	96.20	0.014	0.009	0.015	0.013	0.000
GVL3	67.10	0.060	0.053	0.093	0.069	0.000	GVL3	81.80	0.060	0.054	0.056	0.057	0.000	GVL3	96.50	0.005	0.004	0.007	0.005	0.000
GVL3	67.40	0.098	0.070	0.084	0.084	0.000	GVL3	82.10	0.029	0.024	0.024	0.026	0.000	GVL3	96.80	0.056	0.048	0.058	0.054	0.000
GVL3	67.70	0.010	0.080	0.066	0.052	0.000	GVL3	82.40	0.045	0.032	0.025	0.034	0.000	GVL3	97.10	0.022	0.035	0.051	0.036	0.000
GVL3	68.00	0.069	0.064	0.079	0.071	0.000	GVL3	82.70	0.049	0.051	0.058	0.053	0.000	GVL3	97.40	0.042	0.057	0.048	0.049	0.000
GVL3	68.30	0.620	0.061	0.037	0.239	0.000	GVL3	83.00	0.021	0.057	0.040	0.039	0.000	GVL3	97.70	0.053	0.046	0.060	0.053	0.000
GVL3	68.60	0.065	0.053	0.064	0.061	0.000	GVL3	83.30	0.029	0.046	0.039	0.038	0.000	GVL3	98.00	0.046	0.043	0.045	0.045	0.000
GVL3	68.90	0.059	0.082	0.055	0.065	0.000	GVL3	83.60	0.021	0.019	0.018	0.019	0.000	GVL3	98.30	0.073	0.061	0.060	0.065	0.000
GVL3	69.20	0.020	0.046	0.045	0.037	0.000	GVL3	83.90	0.003	0.007	0.010	0.007	0.000	GVL3	98.60	0.021	0.016	0.005	0.014	0.000
GVL3	69.50	0.050	0.020	0.021	0.030	0.000	GVL3	84.20	0.034	0.026	0.025	0.028	0.000	GVL3	98.90	0.067	0.070	0.049	0.062	0.000
GVL3	69.80	0.055	0.046	0.065	0.055	0.000	GVL3	84.50	0.043	0.055	0.029	0.042	0.000	GVL3	99.20	0.070	0.074	0.060	0.068	0.000
GVL3	70.10	0.063	0.056	0.054	0.058	0.000	GVL3	84.80	0.030	0.044	0.024	0.033	0.000	GVL3	99.50	0.000	0.000	0.000	0.000	0.000
GVL3	70.40	0.076	0.075	0.074	0.075	0.000	GVL3	85.10	0.024	0.068	0.053	0.048	0.000	GVL3	99.80	0.020	0.022	0.036	0.026	0.000
GVL3	70.70	0.053	0.053	0.043	0.050	0.000	GVL3	85.40	0.058	0.035	0.044	0.046	0.000	GVL3	100.10	0.058	0.038	0.037	0.044	0.000
GVL3	71.00	0.039	0.059	0.048	0.049	0.000	GVL3	85.70	0.062	0.048	0.051	0.054	0.000	GVL3	100.40	0.064	0.059	0.059	0.061	0.000
GVL3	71.30	0.030	0.042	0.055	0.042	0.000	GVL3	86.00	0.052	0.053	0.064	0.056	0.000	GVL3	100.70	0.036	0.053	0.037	0.042	0.000
GVL3	71.60	0.088	0.048	0.038	0.058	0.000	GVL3	86.30	0.000	0.000	0.000	0.000	0.000	GVL3	101.00	0.007	0.017	0.018	0.014	0.000
GVL3	71.90	0.047	0.039	0.034	0.040	0.000	GVL3	86.60	0.033	0.029	0.059	0.040	0.000	GVL3	101.30	0.064	0.073	0.087	0.075	0.000
GVL3	72.20	0.052	0.044	0.032	0.043	0.000	GVL3	86.90	0.010	0.020	0.019	0.016	0.000	GVL3	101.60	0.030	0.041	0.064	0.045	0.000
GVL3	72.50	0.012	0.007	0.005	0.008	0.000	GVL3	87.20	0.053	0.015	0.024	0.031	0.000	GVL3	101.90	0.067	0.042	0.031	0.047	0.000
GVL3	72.80	0.026	0.025	0.037	0.029	0.000	GVL3	87.50	0.036	0.028	0.030	0.031	0.000	GVL3	102.20	0.082	0.068	0.061	0.070	0.000
GVL3	73.10	0.049	0.059	0.061	0.056	0.000	GVL3	87.80	0.041	0.040	0.003	0.028	0.000	GVL3	102.50	0.063	0.042	0.038	0.048	0.000
GVL3	73.40	0.069	0.092	0.074	0.078	0.000	GVL3	88.10	0.020	0.032	0.450	0.167	0.000	GVL3	102.80	0.025	0.034	0.038	0.032	0.000

ee

Appendix E: Magnetic Susceptibility

BHID	Depth	Reading 1	Reading 2	Reading 3	Average	SI Units	BHID	Depth	Reading 1	Reading 2	Reading 3	Average	SI Units	BHID	Depth	Reading 1	Reading 2	Reading 3	Average	SI Units
GVL3	103.10	0.020	0.033	0.029	0.027	0.000	GVL3	117.80	0.084	0.076	0.080	0.080	0.000	GVL3	132.50	0.077	0.121	0.116	0.105	0.000
GVL3	103.40	0.087	0.060	0.037	0.061	0.000	GVL3	118.10	0.053	0.078	0.088	0.073	0.000	GVL3	132.80	0.073	0.104	0.113	0.097	0.000
GVL3	103.70	0.036	0.034	0.032	0.034	0.000	GVL3	118.40	0.081	0.070	0.070	0.074	0.000	GVL3	133.10	0.089	0.071	0.072	0.077	0.000
GVL3	104.00	0.036	0.027	0.042	0.035	0.000	GVL3	118.70	0.058	0.061	0.055	0.058	0.000	GVL3	133.40	0.083	0.079	0.067	0.076	0.000
GVL3	104.30	0.031	0.030	0.038	0.033	0.000	GVL3	119.00	0.068	0.036	0.049	0.051	0.000	GVL3	133.70	0.046	0.051	0.040	0.046	0.000
GVL3	104.60	0.093	0.063	0.067	0.074	0.000	GVL3	119.30	0.052	0.061	0.063	0.059	0.000	GVL3	134.00	0.081	0.089	0.077	0.082	0.000
GVL3	104.90	0.070	0.045	0.069	0.061	0.000	GVL3	119.60	0.048	0.048	0.071	0.056	0.000	GVL3	134.30	0.094	0.081	0.069	0.081	0.000
GVL3	105.20	0.056	0.033	0.057	0.049	0.000	GVL3	119.90	0.054	0.054	0.051	0.053	0.000	GVL3	134.60	0.138	0.156	0.132	0.142	0.000
GVL3	105.50	0.058	0.040	0.053	0.050	0.000	GVL3	120.20	0.076	0.086	0.069	0.077	0.000	GVL3	134.90	0.096	0.099	0.137	0.111	0.000
GVL3	105.80	0.104	0.090	0.056	0.083	0.000	GVL3	120.50	0.063	0.060	0.058	0.060	0.000	GVL3	135.20	0.070	0.053	0.067	0.063	0.000
GVL3	106.10	0.045	0.056	0.070	0.057	0.000	GVL3	120.80	0.082	0.085	0.075	0.081	0.000	GVL3	135.50	0.247	0.122	0.113	0.161	0.000
GVL3	106.40	0.075	0.066	0.074	0.072	0.000	GVL3	121.10	0.082	0.118	0.077	0.092	0.000	GVL3	135.80	0.245	0.229	0.244	0.239	0.000
GVL3	106.70	0.031	0.030	0.032	0.031	0.000	GVL3	121.40	0.072	0.075	0.101	0.083	0.000	GVL3	136.10	0.193	0.246	0.219	0.219	0.000
GVL3	107.00	0.000	0.000	0.000	0.000	0.000	GVL3	121.70	0.081	0.119	0.109	0.103	0.000	GVL3	136.40	0.087	0.094	0.105	0.095	0.000
GVL3	107.30	0.057	0.060	0.061	0.059	0.000	GVL3	122.00	0.144	0.098	0.098	0.113	0.000	GVL3	136.70	0.175	0.231	0.255	0.220	0.000
GVL3	107.60	0.064	0.062	0.063	0.063	0.000	GVL3	122.30	0.085	0.091	0.098	0.091	0.000	GVL3	137.00	0.426	0.379	0.460	0.422	0.000
GVL3	107.90	0.047	0.060	0.069	0.059	0.000	GVL3	122.60	0.103	0.081	0.093	0.092	0.000	GVL3	137.30	0.268	0.228	0.253	0.250	0.000
GVL3	108.20	0.073	0.055	0.055	0.061	0.000	GVL3	122.90	0.072	0.071	0.099	0.081	0.000	GVL3	137.60	0.120	0.203	0.206	0.176	0.000
GVL3	108.50	0.047	0.069	0.074	0.063	0.000	GVL3	123.20	0.071	0.079	0.079	0.076	0.000	GVL3	137.90	0.141	0.256	0.244	0.214	0.000
GVL3	108.80	0.050	0.074	0.074	0.066	0.000	GVL3	123.50	0.052	0.082	0.057	0.064	0.000	GVL3	138.20	0.130	0.218	0.176	0.175	0.000
GVL3	109.10	0.074	0.069	0.085	0.076	0.000	GVL3	123.80	0.071	0.095	0.082	0.083	0.000	GVL3	138.50	0.189	0.233	0.207	0.210	0.000
GVL3	109.40	0.069	0.053	0.069	0.064	0.000	GVL3	124.10	0.075	0.069	0.078	0.074	0.000	GVL3	138.80	0.153	0.163	0.144	0.153	0.000
GVL3	109.70	0.040	0.057	0.078	0.058	0.000	GVL3	124.40	0.065	0.052	0.066	0.061	0.000	GVL3	139.10	0.187	0.173	0.258	0.206	0.000
GVL3	110.00	0.059	0.086	0.117	0.087	0.000	GVL3	124.70	0.083	0.057	0.068	0.069	0.000	GVL3	139.40	0.159	0.193	0.174	0.175	0.000
GVL3	110.30	0.072	0.079	0.062	0.071	0.000	GVL3	125.00	0.105	0.090	0.071	0.089	0.000	GVL3	139.70	0.173	0.150	0.116	0.146	0.000
GVL3	110.60	0.061	0.044	0.083	0.063	0.000	GVL3	125.30	0.045	0.082	0.088	0.072	0.000	GVL3	140.00	0.145	0.109	0.134	0.129	0.000
GVL3	110.90	0.062	0.078	0.062	0.067	0.000	GVL3	125.60	0.044	0.044	0.063	0.050	0.000	GVL3	140.30	0.081	0.069	0.087	0.079	0.000
GVL3	111.20	0.046	0.048	0.048	0.047	0.000	GVL3	125.90	0.079	0.091	0.077	0.082	0.000	GVL3	140.60	0.000	0.000	0.000	0.000	0.000
GVL3	111.50	0.125	0.157	0.127	0.136	0.000	GVL3	126.20	0.043	0.044	0.049	0.045	0.000	GVL3	140.90	0.062	0.067	0.088	0.072	0.000
GVL3	111.80	0.083	0.087	0.064	0.078	0.000	GVL3	126.50	0.064	0.078	0.064	0.069	0.000	GVL3	141.20	0.067	0.110	0.122	0.100	0.000
GVL3	112.10	0.103	0.132	0.116	0.117	0.000	GVL3	126.80	0.097	0.082	0.069	0.083	0.000	GVL3	141.50	0.174	0.178	0.178	0.177	0.000
GVL3	112.40	0.058	0.080	0.091	0.076	0.000	GVL3	127.10	0.027	0.021	0.021	0.023	0.000	GVL3	141.80	0.147	0.120	0.124	0.130	0.000
GVL3	112.70	0.084	0.094	0.109	0.096	0.000	GVL3	127.40	0.094	0.085	0.101	0.093	0.000	GVL3	142.10	0.267	0.306	0.367	0.313	0.000
GVL3	113.00	0.000	0.000	0.000	0.000	0.000	GVL3	127.70	0.079	0.103	0.108	0.097	0.000	GVL3	142.40	0.184	0.272	0.311	0.256	0.000
GVL3	113.30	0.010	0.010	0.010	0.010	0.000	GVL3	128.00	0.059	0.067	0.108	0.078	0.000	GVL3	142.70	0.322	0.382	0.295	0.333	0.000
GVL3	113.60	0.021	0.020	0.014	0.018	0.000	GVL3	128.30	0.070	0.074	0.061	0.068	0.000	GVL3	143.00	0.134	0.227	0.248	0.203	0.000
GVL3	113.90	0.005	0.002	0.003	0.003	0.000	GVL3	128.60	0.099	0.124	0.168	0.130	0.000	GVL3	143.30	0.110	0.179	0.193	0.161	0.000
GVL3	114.20	0.062	0.059	0.052	0.058	0.000	GVL3	128.90	0.199	0.163	0.195	0.186	0.000	GVL3	143.60	0.191	0.245	0.213	0.216	0.000
GVL3	114.50	0.049	0.036	0.042	0.042	0.000	GVL3	129.20	0.047	0.072	0.120	0.080	0.000	GVL3	143.90	0.272	0.205	0.172	0.216	0.000
GVL3	114.80	0.045	0.041	0.050	0.045	0.000	GVL3	129.50	0.086	0.101	0.080	0.089	0.000	GVL3	144.20	0.048	0.054	0.052	0.051	0.000
GVL3	115.10	0.029	0.050	0.041	0.040	0.000	GVL3	129.80	0.077	0.061	0.063	0.067	0.000	GVL3	144.50	0.079	0.080	0.078	0.079	0.000
GVL3	115.40	0.041	0.055	0.053	0.050	0.000	GVL3	130.10	0.086	0.107	0.070	0.088	0.000	GVL3	144.80	0.088	0.071	0.099	0.086	0.000
GVL3	115.70	0.074	0.068	0.062	0.068	0.000	GVL3	130.40	0.140	0.139	0.072	0.117	0.000	GVL3	145.10	0.150	0.122	0.135	0.136	0.000
GVL3	116.00	0.087	0.047	0.072	0.069	0.000	GVL3	130.70	0.230	0.221	0.221	0.224	0.000	GVL3	145.40	0.098	0.151	0.118	0.122	0.000
GVL3	116.30	0.058	0.081	0.084	0.074	0.000	GVL3	131.00	0.350	0.298	0.294	0.314	0.000	GVL3	145.70	0.164	0.236	0.193	0.198	0.000
GVL3	116.60	0.082	0.061	0.061	0.068	0.000	GVL3	131.30	0.102	0.094	0.086	0.094	0.000	GVL3	146.00	0.005	0.014	0.010	0.010	0.000
GVL3	116.90	0.060	0.080	0.098	0.079	0.000	GVL3	131.60	0.113	0.131	0.139	0.128	0.000	GVL3	146.30	0.168	0.183	0.125	0.159	0.000
GVL3	117.20	0.089	0.102	0.104	0.098	0.000	GVL3	131.90	0.122	0.133	0.134	0.130	0.000	GVL3	146.60	0.177	0.138	0.191	0.169	0.000
GVL3	117.50	0.089	0.072	0.060	0.074	0.000	GVL3	132.20	0.085	0.108	0.134	0.109	0.000	GVL3	146.90	0.111	0.143	0.089	0.114	0.000

ff

Appendix E: Magnetic Susceptibility

BHID	Depth	Reading 1	Reading 2	Reading 3	Average	SI Units	BHID	Depth	Reading 1	Reading 2	Reading 3	Average	SI Units	BHID	Depth	Reading 1	Reading 2	Reading 3	Average	SI Units
GVL3	147.20	0.063	0.067	0.065	0.065	0.000	GVL3	161.90	0.027	0.025	0.018	0.023	0.000	GVL3	176.60	0.000	0.000	0.000	0.000	0.000
GVL3	147.50	0.097	0.099	0.126	0.107	0.000	GVL3	162.20	0.036	0.018	0.033	0.029	0.000	GVL3	176.90	0.017	0.011	0.024	0.017	0.000
GVL3	147.80	0.640	0.435	0.955	0.677	0.001	GVL3	162.50	0.020	0.022	0.018	0.020	0.000	GVL3	177.20	0.000	0.001	0.000	0.000	0.000
GVL3	148.10	0.222	0.436	0.554	0.404	0.000	GVL3	162.80	0.050	0.039	0.250	0.113	0.000	GVL3	177.50	0.074	0.068	0.045	0.062	0.000
GVL3	148.40	0.078	0.112	0.119	0.103	0.000	GVL3	163.10	0.018	0.023	0.044	0.028	0.000	GVL3	177.80	0.035	0.030	0.006	0.024	0.000
GVL3	148.70	0.128	0.120	0.182	0.143	0.000	GVL3	163.40	0.047	0.019	0.026	0.031	0.000	GVL3	178.10	0.052	0.028	0.032	0.037	0.000
GVL3	149.00	0.124	0.089	0.085	0.099	0.000	GVL3	163.70	0.048	0.033	0.041	0.041	0.000	GVL3	178.40	0.024	0.030	0.026	0.027	0.000
GVL3	149.30	0.072	0.101	0.093	0.089	0.000	GVL3	164.00	0.045	0.051	0.040	0.045	0.000	GVL3	178.70	0.059	0.048	0.041	0.049	0.000
GVL3	149.60	0.002	0.004	0.006	0.004	0.000	GVL3	164.30	0.057	0.087	0.060	0.068	0.000	GVL3	179.00	0.015	0.030	0.023	0.023	0.000
GVL3	149.90	0.093	0.086	0.116	0.098	0.000	GVL3	164.60	0.017	0.041	0.032	0.030	0.000	GVL3	179.30	0.016	0.015	0.018	0.016	0.000
GVL3	150.20	0.484	0.545	0.487	0.505	0.001	GVL3	164.90	0.062	0.055	0.430	0.182	0.000	GVL3	179.60	0.000	0.000	0.000	0.000	0.000
GVL3	150.50	0.082	0.081	0.054	0.072	0.000	GVL3	165.20	0.047	0.056	0.063	0.055	0.000	GVL3	179.90	0.000	0.000	0.000	0.000	0.000
GVL3	150.80	0.160	0.185	0.184	0.176	0.000	GVL3	165.50	0.037	0.048	0.045	0.043	0.000	GVL3	180.20	0.022	0.015	0.026	0.021	0.000
GVL3	151.10	0.102	0.135	0.147	0.128	0.000	GVL3	165.80	0.023	0.023	0.027	0.024	0.000	GVL3	180.50	0.021	0.025	0.019	0.022	0.000
GVL3	151.40	0.094	0.085	0.084	0.088	0.000	GVL3	166.10	0.031	0.029	0.038	0.033	0.000	GVL3	180.80	0.020	0.013	0.018	0.017	0.000
GVL3	151.70	0.111	0.079	0.103	0.098	0.000	GVL3	166.40	0.015	0.022	0.026	0.021	0.000	GVL3	181.10	0.025	0.036	0.027	0.029	0.000
GVL3	152.00	0.081	0.037	0.052	0.057	0.000	GVL3	166.70	0.000	0.000	0.000	0.000	0.000	GVL3	181.40	0.038	0.035	0.027	0.033	0.000
GVL3	152.30	0.023	0.040	0.049	0.037	0.000	GVL3	167.00	0.033	0.038	0.037	0.036	0.000	GVL3	181.70	0.023	0.021	0.024	0.023	0.000
GVL3	152.60	0.032	0.040	0.033	0.035	0.000	GVL3	167.30	0.019	0.020	0.014	0.018	0.000	GVL3	182.00	0.027	0.014	0.021	0.021	0.000
GVL3	152.90	0.031	0.034	0.046	0.037	0.000	GVL3	167.60	0.021	0.037	0.050	0.036	0.000	GVL3	182.30	0.000	0.000	0.002	0.001	0.000
GVL3	153.20	0.114	0.096	0.102	0.104	0.000	GVL3	167.90	0.087	0.060	0.055	0.067	0.000	GVL3	182.60	0.032	0.014	0.030	0.025	0.000
GVL3	153.50	0.108	0.189	0.178	0.158	0.000	GVL3	168.20	0.061	0.037	0.045	0.048	0.000	GVL3	182.90	0.030	0.026	0.029	0.028	0.000
GVL3	153.80	0.015	0.022	0.027	0.021	0.000	GVL3	168.50	0.034	0.032	0.044	0.037	0.000	GVL3	183.20	0.032	0.041	0.038	0.037	0.000
GVL3	154.10	0.071	0.042	0.046	0.053	0.000	GVL3	168.80	0.030	0.043	0.039	0.037	0.000	GVL3	183.50	0.057	0.060	0.050	0.056	0.000
GVL3	154.40	0.026	0.035	0.020	0.027	0.000	GVL3	169.10	0.039	0.034	0.028	0.034	0.000	GVL3	183.80	0.024	0.034	0.029	0.029	0.000
GVL3	154.70	0.040	0.051	0.077	0.056	0.000	GVL3	169.40	0.029	0.026	0.017	0.024	0.000	GVL3	184.10	0.032	0.033	0.041	0.035	0.000
GVL3	155.00	0.114	0.088	0.109	0.104	0.000	GVL3	169.70	0.031	0.030	0.025	0.029	0.000	GVL3	184.40	0.023	0.019	0.033	0.025	0.000
GVL3	155.30	0.027	0.011	0.020	0.019	0.000	GVL3	170.00	0.000	0.000	0.000	0.000	0.000	GVL3	184.70	0.114	0.070	0.082	0.089	0.000
GVL3	155.60	0.055	0.022	0.026	0.034	0.000	GVL3	170.30	0.092	0.038	0.045	0.058	0.000	GVL3	185.00	0.025	0.021	0.026	0.024	0.000
GVL3	155.90	0.050	0.051	0.047	0.049	0.000	GVL3	170.60	0.044	0.041	0.050	0.045	0.000	GVL3	185.30	0.030	0.035	0.031	0.032	0.000
GVL3	156.20	0.028	0.009	0.018	0.018	0.000	GVL3	170.90	0.024	0.042	0.029	0.032	0.000	GVL3	185.60	0.008	0.012	0.012	0.011	0.000
GVL3	156.50	0.075	0.104	0.067	0.082	0.000	GVL3	171.20	0.053	0.074	0.053	0.060	0.000	GVL3	185.90	0.004	0.010	0.004	0.006	0.000
GVL3	156.80	0.035	0.035	0.040	0.037	0.000	GVL3	171.50	0.028	0.019	0.037	0.028	0.000	GVL3	186.20	0.030	0.017	0.013	0.020	0.000
GVL3	157.10	0.071	0.079	0.091	0.080	0.000	GVL3	171.80	0.055	0.052	0.071	0.059	0.000	GVL3	186.50	0.022	0.031	0.029	0.027	0.000
GVL3	157.40	0.078	0.069	0.084	0.077	0.000	GVL3	172.10	0.080	0.075	0.053	0.069	0.000	GVL3	186.80	0.037	0.027	0.024	0.029	0.000
GVL3	157.70	0.043	0.058	0.045	0.049	0.000	GVL3	172.40	0.061	0.060	0.047	0.056	0.000	GVL3	187.10	0.159	0.162	0.147	0.156	0.000
GVL3	158.00	0.031	0.026	0.037	0.031	0.000	GVL3	172.70	0.057	0.038	0.054	0.050	0.000	GVL3	187.40	0.077	0.070	0.060	0.069	0.000
GVL3	158.30	0.045	0.073	0.034	0.051	0.000	GVL3	173.00	0.027	0.032	0.027	0.029	0.000	GVL3	187.70	0.085	0.083	0.079	0.082	0.000
GVL3	158.60	0.041	0.021	0.056	0.039	0.000	GVL3	173.30	0.041	0.036	0.040	0.039	0.000	GVL3	188.00	0.093	0.076	0.074	0.081	0.000
GVL3	158.90	0.025	0.032	0.040	0.032	0.000	GVL3	173.60	0.002	0.005	0.004	0.004	0.000	GVL3	188.30	0.038	0.054	0.050	0.047	0.000
GVL3	159.20	0.037	0.062	0.047	0.049	0.000	GVL3	173.90	0.027	0.027	0.033	0.029	0.000	GVL3	188.60	0.064	0.049	0.061	0.058	0.000
GVL3	159.50	0.048	0.051	0.060	0.053	0.000	GVL3	174.20	0.037	0.009	0.046	0.031	0.000	GVL3	188.90	0.063	0.054	0.050	0.056	0.000
GVL3	159.80	0.018	0.026	0.016	0.020	0.000	GVL3	174.50	0.023	0.031	0.052	0.035	0.000	GVL3	189.20	0.068	0.067	0.072	0.069	0.000
GVL3	160.10	0.051	0.025	0.026	0.034	0.000	GVL3	174.80	0.000	0.012	0.000	0.004	0.000	GVL3	189.50	0.073	0.054	0.062	0.063	0.000
GVL3	160.40	0.035	0.030	0.035	0.033	0.000	GVL3	175.10	0.016	0.021	0.007	0.015	0.000	GVL3	189.80	0.088	0.098	0.096	0.094	0.000
GVL3	160.70	0.052	0.045	0.060	0.052	0.000	GVL3	175.40	0.033	0.023	0.036	0.031	0.000	GVL3	190.10	0.115	0.138	0.094	0.116	0.000
GVL3	161.00	0.033	0.038	0.026	0.032	0.000	GVL3	175.70	0.037	0.031	0.035	0.034	0.000	GVL3	190.40	0.070	0.075	0.057	0.067	0.000
GVL3	161.30	0.003	0.005	0.001	0.003	0.000	GVL3	176.00	0.027	0.029	0.035	0.030	0.000	GVL3	190.70	0.030	0.032	0.036	0.033	0.000
GVL3	161.60	0.029	0.039	0.034	0.034	0.000	GVL3	176.30	0.024	0.018	0.035	0.026	0.000	GVL3	191.00	0.067	0.089	0.090	0.082	0.000

gg

Appendix E: Magnetic Susceptibility

BHID	Depth	Reading 1	Reading 2	Reading 3	Average	SI Units	BHID	Depth	Reading 1	Reading 2	Reading 3	Average	SI Units	BHID	Depth	Reading 1	Reading 2	Reading 3	Average	SI Units
GVL3	191.30	0.082	0.055	0.073	0.070	0.000	GVL3	206.00	0.397	0.371	0.349	0.372	0.000	GVL3	220.70	0.074	0.072	0.080	0.075	0.000
GVL3	191.60	0.000	0.000	0.000	0.000	0.000	GVL3	206.30	0.793	0.845	0.795	0.811	0.001	GVL3	221.00	0.089	0.099	0.084	0.091	0.000
GVL3	191.90	0.000	0.000	0.000	0.000	0.000	GVL3	206.60	2.080	2.270	2.400	2.250	0.002	GVL3	221.30	0.132	0.131	0.104	0.122	0.000
GVL3	192.20	0.085	0.070	0.082	0.079	0.000	GVL3	206.90	1.990	2.050	2.010	2.017	0.002	GVL3	221.60	0.014	0.000	0.000	0.005	0.000
GVL3	192.50	0.079	0.066	0.062	0.069	0.000	GVL3	207.20	0.507	0.458	0.396	0.454	0.000	GVL3	221.90	0.000	0.000	0.000	0.000	0.000
GVL3	192.80	0.085	0.070	0.079	0.078	0.000	GVL3	207.50	1.390	1.130	0.906	1.142	0.001	GVL3	222.20	0.008	0.010	0.004	0.007	0.000
GVL3	193.10	0.042	0.059	0.056	0.052	0.000	GVL3	207.80	0.846	0.776	0.883	0.835	0.001	GVL3	222.50	0.676	0.587	0.539	0.601	0.001
GVL3	193.40	0.074	0.080	0.076	0.077	0.000	GVL3	208.10	0.358	0.361	0.338	0.352	0.000	GVL3	222.80	0.086	0.083	0.076	0.082	0.000
GVL3	193.70	0.103	0.115	0.096	0.105	0.000	GVL3	208.40	0.240	0.266	0.254	0.253	0.000	GVL3	223.10	0.139	0.136	0.153	0.143	0.000
GVL3	194.00	0.107	0.180	0.108	0.132	0.000	GVL3	208.70	0.342	0.317	0.309	0.323	0.000	GVL3	223.40	0.072	0.070	0.053	0.065	0.000
GVL3	194.30	0.104	0.166	0.092	0.121	0.000	GVL3	209.00	0.363	0.371	0.333	0.356	0.000	GVL3	223.70	0.073	0.067	0.080	0.073	0.000
GVL3	194.60	0.065	0.056	0.049	0.057	0.000	GVL3	209.30	0.399	0.367	0.375	0.380	0.000	GVL3	224.00	0.089	0.107	0.122	0.106	0.000
GVL3	194.90	0.071	0.086	0.092	0.083	0.000	GVL3	209.60	0.378	0.378	0.413	0.390	0.000	GVL3	224.30	0.055	0.072	0.081	0.069	0.000
GVL3	195.20	0.074	0.072	0.084	0.077	0.000	GVL3	209.90	0.460	0.531	0.506	0.499	0.000	GVL3	224.60	0.055	0.068	0.065	0.063	0.000
GVL3	195.50	0.057	0.073	0.078	0.069	0.000	GVL3	210.20	0.185	0.228	0.151	0.188	0.000	GVL3	224.90	0.068	0.099	0.077	0.081	0.000
GVL3	195.80	0.065	0.071	0.063	0.066	0.000	GVL3	210.50	1.230	1.640	1.730	1.533	0.002	GVL3	225.20	0.052	0.058	0.053	0.054	0.000
GVL3	196.10	0.074	0.093	0.060	0.076	0.000	GVL3	210.80	0.293	0.287	0.285	0.288	0.000	GVL3	225.50	0.017	0.033	0.036	0.029	0.000
GVL3	196.40	0.089	0.094	0.084	0.089	0.000	GVL3	211.10	0.000	0.000	0.000	0.000	0.000	GVL3	225.80	0.000	0.000	0.000	0.000	0.000
GVL3	196.70	0.133	0.139	0.148	0.140	0.000	GVL3	211.40	0.615	0.548	0.584	0.582	0.001	GVL3	226.10	0.000	0.000	0.000	0.010	0.000
GVL3	197.00	0.349	0.323	0.326	0.333	0.000	GVL3	211.70	0.823	0.960	0.900	0.894	0.001	GVL3	226.40	0.000	0.000	0.030	0.010	0.000
GVL3	197.30	0.037	0.041	0.039	0.039	0.000	GVL3	212.00	0.457	0.495	0.461	0.471	0.000	GVL3	226.70	0.000	0.000	0.000	0.000	0.000
GVL3	197.60	0.078	0.055	0.086	0.073	0.000	GVL3	212.30	0.315	0.310	0.282	0.302	0.000	GVL3	227.00	0.026	0.014	0.017	0.019	0.000
GVL3	197.90	0.046	0.057	0.056	0.053	0.000	GVL3	212.60	0.189	0.184	0.156	0.176	0.000	GVL3	227.30	0.009	0.004	0.007	0.007	0.000
GVL3	198.20	0.073	0.059	0.059	0.064	0.000	GVL3	212.90	0.105	0.092	0.115	0.104	0.000	GVL3	227.60	0.016	0.013	0.017	0.015	0.000
GVL3	198.50	0.123	0.129	0.120	0.124	0.000	GVL3	213.20	0.115	0.087	0.099	0.100	0.000	GVL3	227.90	0.000	0.008	0.007	0.005	0.000
GVL3	198.80	0.126	0.119	0.127	0.124	0.000	GVL3	213.50	0.072	0.097	0.071	0.080	0.000	GVL3	228.20	0.000	0.008	0.006	0.005	0.000
GVL3	199.10	0.131	0.123	0.117	0.124	0.000	GVL3	213.80	0.127	0.150	0.144	0.140	0.000	GVL3	228.50	0.010	0.004	0.009	0.008	0.000
GVL3	199.40	0.169	0.162	0.157	0.163	0.000	GVL3	214.10	0.145	0.191	0.134	0.157	0.000	GVL3	228.80	0.024	0.012	0.008	0.015	0.000
GVL3	199.70	0.058	0.057	0.069	0.061	0.000	GVL3	214.40	0.474	0.438	0.438	0.450	0.000	GVL3	229.10	0.012	0.023	0.026	0.020	0.000
GVL3	200.00	0.100	0.106	0.096	0.101	0.000	GVL3	214.70	1.710	1.440	1.330	1.493	0.001	GVL3	229.40	0.028	0.021	0.030	0.026	0.000
GVL3	200.30	0.109	0.101	0.099	0.103	0.000	GVL3	215.00	0.164	0.102	0.110	0.125	0.000	GVL3	229.70	0.025	0.037	0.020	0.027	0.000
GVL3	200.60	0.103	0.114	0.107	0.108	0.000	GVL3	215.30	0.104	0.089	0.078	0.090	0.000	GVL3	230.00	0.020	0.018	0.019	0.019	0.000
GVL3	200.90	0.109	0.099	0.097	0.102	0.000	GVL3	215.60	0.070	0.078	0.077	0.075	0.000	GVL3	230.30	0.007	0.003	0.000	0.003	0.000
GVL3	201.20	0.071	0.072	0.092	0.078	0.000	GVL3	215.90	0.332	0.241	0.243	0.272	0.000	GVL3	230.60	0.025	0.025	0.027	0.026	0.000
GVL3	201.50	0.101	0.109	0.095	0.102	0.000	GVL3	216.20	0.360	0.232	0.276	0.289	0.000	GVL3	230.90	0.025	0.018	0.023	0.022	0.000
GVL3	201.80	0.085	0.110	0.123	0.106	0.000	GVL3	216.50	0.385	0.402	0.398	0.395	0.000	GVL3	231.20	0.040	0.021	0.025	0.029	0.000
GVL3	202.10	0.118	0.115	0.100	0.111	0.000	GVL3	216.80	0.141	0.113	0.101	0.118	0.000	GVL3	231.50	0.026	0.016	0.013	0.018	0.000
GVL3	202.40	0.124	0.112	0.115	0.117	0.000	GVL3	217.10	0.046	0.050	0.041	0.046	0.000	GVL3	231.80	0.000	0.000	0.000	0.000	0.000
GVL3	202.70	0.128	0.138	0.144	0.137	0.000	GVL3	217.40	0.042	0.048	0.048	0.046	0.000	GVL3	232.10	0.087	0.087	0.064	0.079	0.000
GVL3	203.00	0.130	0.134	0.129	0.131	0.000	GVL3	217.70	0.000	0.000	0.000	0.000	0.000	GVL3	232.40	0.010	0.009	0.007	0.009	0.000
GVL3	203.30	0.014	0.000	0.006	0.007	0.000	GVL3	218.00	0.163	0.133	0.136	0.144	0.000	GVL3	232.70	0.011	0.015	0.026	0.017	0.000
GVL3	203.60	0.084	0.080	0.082	0.082	0.000	GVL3	218.30	0.324	0.353	0.394	0.357	0.000	GVL3	233.00	0.005	0.003	0.010	0.006	0.000
GVL3	203.90	0.093	0.089	0.084	0.089	0.000	GVL3	218.60	0.091	0.100	0.101	0.097	0.000	GVL3	233.30	0.028	0.020	0.014	0.021	0.000
GVL3	204.20	0.037	0.025	0.029	0.030	0.000	GVL3	218.90	0.909	1.250	1.150	1.103	0.001	GVL3	233.60	0.015	0.013	0.007	0.012	0.000
GVL3	204.50	0.062	0.061	0.064	0.062	0.000	GVL3	219.20	0.440	0.384	0.381	0.402	0.000	GVL3	233.90	0.032	0.020	0.024	0.025	0.000
GVL3	204.80	0.097	0.100	0.097	0.098	0.000	GVL3	219.50	1.680	1.480	1.800	1.653	0.002	GVL3	234.20	0.012	0.014	0.015	0.014	0.000
GVL3	205.10	0.043	0.073	0.050	0.055	0.000	GVL3	219.80	0.403	0.459	0.377	0.413	0.000	GVL3	234.50	0.032	0.034	0.028	0.031	0.000
GVL3	205.40	0.039	0.049	0.041	0.043	0.000	GVL3	220.10	0.105	0.140	0.096	0.114	0.000	GVL3	234.80	0.026	0.017	0.025	0.023	0.000
GVL3	205.70	0.080	0.085	0.073	0.079	0.000	GVL3	220.40	0.111	0.112	0.116	0.113	0.000	GVL3	235.10	0.028	0.025	0.028	0.027	0.000

hh

Appendix E: Magnetic Susceptibility

BHID	Depth	Reading 1	Reading 2	Reading 3	Average	SI Units	BHID	Depth	Reading 1	Reading 2	Reading 3	Average	SI Units	BHID	Depth	Reading 1	Reading 2	Reading 3	Average	SI Units
GVL3	235.40	0.029	0.028	0.033	0.030	0.000	GVL3	250.10	0.050	0.052	0.044	0.049	0.000	GVL3	264.80	0.016	0.013	0.017	0.015	0.000
GVL3	235.70	0.044	0.016	0.030	0.030	0.000	GVL3	250.40	0.065	0.076	0.069	0.070	0.000	GVL3	265.10	0.037	0.036	0.037	0.037	0.000
GVL3	236.00	0.018	0.019	0.013	0.017	0.000	GVL3	250.70	0.056	0.056	0.068	0.060	0.000	GVL3	265.40	0.022	0.019	0.022	0.021	0.000
GVL3	236.30	0.007	0.004	0.006	0.006	0.000	GVL3	251.00	0.039	0.031	0.046	0.039	0.000	GVL3	265.70	0.027	0.029	0.036	0.031	0.000
GVL3	236.60	0.022	0.017	0.024	0.021	0.000	GVL3	251.30	0.048	0.083	0.073	0.068	0.000	GVL3	266.00	0.028	0.041	0.045	0.038	0.000
GVL3	236.90	0.028	0.017	0.014	0.020	0.000	GVL3	251.60	0.044	0.060	0.050	0.051	0.000	GVL3	266.30	0.082	0.074	0.079	0.078	0.000
GVL3	237.20	0.038	0.032	0.036	0.035	0.000	GVL3	251.90	0.035	0.033	0.049	0.039	0.000	GVL3	266.60	0.081	0.114	0.121	0.105	0.000
GVL3	237.50	0.060	0.056	0.057	0.058	0.000	GVL3	252.20	0.043	0.038	0.048	0.043	0.000	GVL3	266.90	0.091	0.115	0.135	0.114	0.000
GVL3	237.80	0.000	0.008	0.011	0.006	0.000	GVL3	252.50	0.043	0.037	0.044	0.041	0.000	GVL3	267.20	0.081	0.067	0.058	0.069	0.000
GVL3	238.10	0.040	0.027	0.026	0.031	0.000	GVL3	252.80	0.050	0.048	0.033	0.044	0.000	GVL3	267.50	0.074	0.069	0.067	0.070	0.000
GVL3	238.40	0.021	0.009	0.005	0.012	0.000	GVL3	253.10	0.214	0.200	0.226	0.213	0.000	GVL3	267.80	0.096	0.099	0.090	0.095	0.000
GVL3	238.70	0.119	0.129	0.148	0.132	0.000	GVL3	253.40	0.040	0.027	0.042	0.036	0.000	GVL3	268.10	0.061	0.062	0.093	0.072	0.000
GVL3	239.00	0.022	0.021	0.034	0.026	0.000	GVL3	253.70	0.102	0.101	0.100	0.101	0.000	GVL3	268.40	0.075	0.066	0.092	0.078	0.000
GVL3	239.30	0.005	0.000	0.000	0.002	0.000	GVL3	254.00	0.058	0.064	0.088	0.070	0.000	GVL3	268.70	0.006	0.004	0.006	0.005	0.000
GVL3	239.60	0.021	0.021	0.025	0.022	0.000	GVL3	254.30	0.170	0.288	0.236	0.231	0.000	GVL3	269.00	0.021	0.031	0.023	0.025	0.000
GVL3	239.90	0.030	0.013	0.030	0.024	0.000	GVL3	254.60	0.252	0.388	0.411	0.350	0.000	GVL3	269.30	0.000	0.000	0.000	0.000	0.000
GVL3	240.20	0.053	0.060	0.059	0.057	0.000	GVL3	254.90	0.076	0.081	0.086	0.081	0.000	GVL3	269.60	0.000	0.000	0.000	0.000	0.000
GVL3	240.50	0.024	0.024	0.031	0.026	0.000	GVL3	255.20	0.076	0.062	0.096	0.078	0.000	GVL3	269.90	0.000	0.000	0.000	0.000	0.000
GVL3	240.80	0.028	0.041	0.027	0.032	0.000	GVL3	255.50	0.063	0.067	0.043	0.058	0.000	GVL3	270.20	0.000	0.000	0.000	0.000	0.000
GVL3	241.10	0.006	0.012	0.009	0.009	0.000	GVL3	255.80	0.029	0.047	0.025	0.034	0.000	GVL3	270.50	0.002	0.000	0.000	0.001	0.000
GVL3	241.40	0.019	0.026	0.028	0.024	0.000	GVL3	256.10	0.015	0.028	0.011	0.018	0.000	GVL3	270.80	0.017	0.019	0.019	0.018	0.000
GVL3	241.70	0.031	0.015	0.011	0.019	0.000	GVL3	256.40	0.004	0.001	0.013	0.006	0.000	GVL3	271.10	0.024	0.024	0.027	0.025	0.000
GVL3	242.00	0.017	0.018	0.011	0.015	0.000	GVL3	256.70	0.028	0.028	0.028	0.028	0.000	GVL3	271.40	0.003	0.025	0.026	0.018	0.000
GVL3	242.30	0.005	0.007	0.001	0.004	0.000	GVL3	257.00	0.039	0.055	0.063	0.052	0.000	GVL3	271.70	0.034	0.019	0.048	0.034	0.000
GVL3	242.60	0.034	0.014	0.022	0.023	0.000	GVL3	257.30	0.040	0.030	0.041	0.037	0.000	GVL3	272.00	0.005	0.011	0.012	0.009	0.000
GVL3	242.90	0.027	0.043	0.029	0.033	0.000	GVL3	257.60	0.020	0.018	0.028	0.022	0.000	GVL3	272.30	0.010	0.031	0.025	0.022	0.000
GVL3	243.20	0.007	0.010	0.011	0.009	0.000	GVL3	257.90	0.029	0.048	0.044	0.040	0.000	GVL3	272.60	0.019	0.010	0.014	0.014	0.000
GVL3	243.50	0.007	0.008	0.007	0.007	0.000	GVL3	258.20	0.022	0.025	0.041	0.029	0.000	GVL3	272.90	0.027	0.016	0.024	0.022	0.000
GVL3	243.80	0.033	0.019	0.022	0.025	0.000	GVL3	258.50	0.099	0.084	0.101	0.095	0.000	GVL3	273.20	0.017	0.014	0.018	0.016	0.000
GVL3	244.10	0.014	0.017	0.022	0.018	0.000	GVL3	258.80	0.094	0.110	0.130	0.111	0.000	GVL3	273.50	0.022	0.025	0.027	0.025	0.000
GVL3	244.40	0.065	0.056	0.051	0.057	0.000	GVL3	259.10	0.074	0.079	0.103	0.085	0.000	GVL3	273.80	0.023	0.018	0.015	0.019	0.000
GVL3	244.70	0.000	0.000	0.000	0.000	0.000	GVL3	259.40	0.072	0.089	0.102	0.088	0.000	GVL3	274.10	0.010	0.011	0.002	0.008	0.000
GVL3	245.00	0.004	0.007	0.000	0.004	0.000	GVL3	259.70	0.043	0.045	0.045	0.044	0.000	GVL3	274.40	0.018	0.014	0.026	0.019	0.000
GVL3	245.30	0.000	0.003	0.006	0.003	0.000	GVL3	260.00	0.023	0.036	0.019	0.026	0.000	GVL3	274.70	0.016	0.020	0.030	0.022	0.000
GVL3	245.60	0.028	0.028	0.029	0.028	0.000	GVL3	260.30	0.035	0.064	0.066	0.055	0.000	GVL3	275.00	0.021	0.019	0.031	0.024	0.000
GVL3	245.90	0.045	0.034	0.028	0.036	0.000	GVL3	260.60	0.061	0.056	0.092	0.070	0.000	GVL3	275.30	0.009	0.014	0.012	0.012	0.000
GVL3	246.20	0.044	0.041	0.053	0.046	0.000	GVL3	260.90	0.044	0.063	0.080	0.062	0.000	GVL3	275.60	0.000	0.011	0.009	0.007	0.000
GVL3	246.50	0.063	0.066	0.054	0.061	0.000	GVL3	261.20	0.053	0.033	0.050	0.045	0.000	GVL3	275.90	0.017	0.013	0.012	0.014	0.000
GVL3	246.80	0.038	0.059	0.066	0.054	0.000	GVL3	261.50	0.046	0.057	0.054	0.052	0.000	GVL3	276.20	0.011	0.004	0.012	0.009	0.000
GVL3	247.10	0.071	0.063	0.080	0.071	0.000	GVL3	261.80	0.075	0.109	0.131	0.105	0.000	GVL3	276.50	0.000	0.000	0.000	0.000	0.000
GVL3	247.40	0.050	0.075	0.052	0.059	0.000	GVL3	262.10	0.025	0.041	0.049	0.038	0.000	GVL3	276.80	0.009	0.010	0.019	0.013	0.000
GVL3	247.70	0.079	0.084	0.092	0.085	0.000	GVL3	262.40	0.028	0.038	0.034	0.033	0.000	GVL3	277.10	0.039	0.007	0.012	0.019	0.000
GVL3	248.00	0.053	0.056	0.046	0.052	0.000	GVL3	262.70	0.054	0.033	0.023	0.037	0.000	GVL3	277.40	0.005	0.022	0.031	0.019	0.000
GVL3	248.30	0.061	0.058	0.069	0.063	0.000	GVL3	263.00	0.046	0.036	0.038	0.040	0.000	GVL3	277.70	0.030	0.031	0.031	0.031	0.000
GVL3	248.60	0.157	0.142	0.160	0.153	0.000	GVL3	263.30	0.071	0.063	0.074	0.069	0.000	GVL3	278.00	0.029	0.024	0.036	0.030	0.000
GVL3	248.90	0.130	0.122	0.124	0.125	0.000	GVL3	263.60	0.130	0.080	0.113	0.108	0.000	GVL3	278.30	0.016	0.009	0.012	0.012	0.000
GVL3	249.20	0.041	0.019	0.028	0.029	0.000	GVL3	263.90	0.049	0.064	0.077	0.063	0.000	GVL3	278.60	0.040	0.025	0.029	0.031	0.000
GVL3	249.50	0.037	0.031	0.030	0.033	0.000	GVL3	264.20	0.041	0.031	0.031	0.034	0.000	GVL3	278.90	0.029	0.023	0.026	0.026	0.000
GVL3	249.80	0.113	0.116	0.123	0.117	0.000	GVL3	264.50	0.010	0.021	0.022	0.018	0.000	GVL3	279.20	0.020	0.024	0.022	0.022	0.000

Appendix E: Magnetic Susceptibility

BHID	Depth	Reading 1	Reading 2	Reading 3	Average	SI Units	BHID	Depth	Reading 1	Reading 2	Reading 3	Average	SI Units	BHID	Depth	Reading 1	Reading 2	Reading 3	Average	SI Units
GVL3	279.50	0.038	0.037	0.042	0.039	0.000	GVL3	303.00	0.008	0.003	0.002	0.004	0.000	GVL3	327.50	0.320	0.261	0.268	0.283	0.000
GVL3	279.80	0.036	0.042	0.043	0.040	0.000	GVL3	303.50	0.011	0.033	0.011	0.018	0.000	GVL3	328.00	0.313	0.403	0.319	0.345	0.000
GVL3	280.10	0.038	0.025	0.023	0.029	0.000	GVL3	304.00	0.024	0.020	0.038	0.027	0.000	GVL3	328.50	0.322	0.312	0.300	0.311	0.000
GVL3	280.40	0.034	0.024	0.016	0.025	0.000	GVL3	304.50	0.000	0.000	0.000	0.000	0.000	GVL3	329.00	0.429	0.234	0.321	0.328	0.000
GVL3	280.70	0.014	0.020	0.039	0.024	0.000	GVL3	305.00	0.039	0.052	0.028	0.040	0.000	GVL3	329.50	0.373	0.301	0.269	0.314	0.000
GVL3	281.00	0.030	0.038	0.031	0.033	0.000	GVL3	305.50	0.010	0.007	0.014	0.010	0.000	GVL3	330.00	0.155	0.233	0.184	0.191	0.000
GVL3	281.50	0.051	0.044	0.047	0.047	0.000	GVL3	306.00	0.014	0.015	0.020	0.016	0.000	GVL3	330.50	0.225	0.239	0.203	0.222	0.000
GVL3	282.00	0.069	0.063	0.073	0.068	0.000	GVL3	306.50	0.013	0.010	0.000	0.008	0.000	GVL3	331.00	0.328	0.388	0.327	0.348	0.000
GVL3	282.50	0.053	0.042	0.048	0.048	0.000	GVL3	307.00	0.007	0.008	0.004	0.006	0.000	GVL3	331.50	0.225	0.164	0.190	0.193	0.000
GVL3	283.00	0.020	0.037	0.041	0.033	0.000	GVL3	307.50	0.005	0.010	0.016	0.010	0.000	GVL3	332.00	0.282	0.221	0.189	0.231	0.000
GVL3	283.50	0.040	0.045	0.038	0.041	0.000	GVL3	308.00	0.001	0.002	0.000	0.001	0.000	GVL3	332.50	0.201	0.160	0.172	0.178	0.000
GVL3	284.00	0.038	0.037	0.027	0.034	0.000	GVL3	308.50	0.011	0.016	0.014	0.014	0.000	GVL3	333.00	0.231	0.188	0.210	0.210	0.000
GVL3	284.50	0.039	0.049	0.048	0.045	0.000	GVL3	309.00	0.017	0.021	0.022	0.020	0.000	GVL3	333.50	0.291	0.289	0.228	0.269	0.000
GVL3	285.00	0.050	0.069	0.054	0.058	0.000	GVL3	309.50	0.045	0.026	0.060	0.044	0.000	GVL3	334.00	0.415	0.421	0.450	0.429	0.000
GVL3	285.50	0.035	0.035	0.042	0.037	0.000	GVL3	310.00	0.041	0.040	0.048	0.043	0.000	GVL3	334.50	0.373	0.313	0.433	0.373	0.000
GVL3	286.00	0.048	0.034	0.022	0.035	0.000	GVL3	310.50	0.028	0.025	0.018	0.024	0.000	GVL3	335.00	0.214	0.217	0.248	0.226	0.000
GVL3	286.50	0.089	0.079	0.074	0.081	0.000	GVL3	311.00	0.037	0.016	0.013	0.022	0.000	GVL3	335.50	0.432	0.436	0.496	0.455	0.000
GVL3	287.00	0.036	0.031	0.026	0.031	0.000	GVL3	311.50	0.039	0.033	0.029	0.034	0.000	GVL3	336.00	0.642	0.478	0.418	0.513	0.001
GVL3	287.50	0.072	0.056	0.072	0.067	0.000	GVL3	312.00	0.019	0.017	0.014	0.017	0.000	GVL3	336.50	0.329	0.476	0.485	0.430	0.000
GVL3	288.00	0.057	0.058	0.067	0.061	0.000	GVL3	312.50	0.010	0.010	0.031	0.017	0.000	GVL3	337.00	0.348	0.290	0.334	0.324	0.000
GVL3	288.50	0.051	0.045	0.051	0.049	0.000	GVL3	313.00	0.000	0.000	0.000	0.000	0.000	GVL3	337.50	0.284	0.365	0.374	0.341	0.000
GVL3	289.00	0.043	0.051	0.025	0.040	0.000	GVL3	313.50	0.017	0.011	0.012	0.013	0.000	GVL3	338.00	0.306	0.228	0.231	0.255	0.000
GVL3	289.50	0.039	0.030	0.038	0.036	0.000	GVL3	314.00	0.050	0.019	0.030	0.033	0.000	GVL3	338.50	0.356	0.312	0.331	0.333	0.000
GVL3	290.00	0.032	0.021	0.036	0.030	0.000	GVL3	314.50	0.013	0.011	0.020	0.015	0.000	GVL3	339.00	0.317	0.313	0.237	0.289	0.000
GVL3	290.50	0.023	0.027	0.025	0.025	0.000	GVL3	315.00	0.004	0.018	0.014	0.012	0.000	GVL3	339.50	0.267	0.269	0.288	0.275	0.000
GVL3	291.00	0.045	0.032	0.031	0.036	0.000	GVL3	315.50	0.113	0.084	0.072	0.090	0.000	GVL3	340.00	0.368	0.398	0.464	0.410	0.000
GVL3	291.50	0.026	0.031	0.034	0.030	0.000	GVL3	316.00	0.117	0.102	0.131	0.117	0.000	GVL3	340.50	0.564	0.513	0.576	0.551	0.001
GVL3	292.00	0.014	0.011	0.010	0.012	0.000	GVL3	316.50	0.016	0.032	0.029	0.026	0.000	GVL3	341.00	0.551	0.511	0.474	0.512	0.001
GVL3	292.50	0.022	0.007	0.017	0.015	0.000	GVL3	317.00	0.028	0.033	0.033	0.031	0.000	GVL3	341.50	0.210	0.188	0.190	0.196	0.000
GVL3	293.00	0.024	0.023	0.018	0.022	0.000	GVL3	317.50	0.063	0.039	0.053	0.052	0.000	GVL3	342.00	0.428	0.473	0.407	0.436	0.000
GVL3	293.50	0.025	0.038	0.023	0.029	0.000	GVL3	318.00	0.020	0.015	0.020	0.018	0.000	GVL3	342.50	0.334	0.251	0.306	0.297	0.000
GVL3	294.00	0.023	0.016	0.018	0.019	0.000	GVL3	318.50	0.082	0.043	0.042	0.056	0.000	GVL3	343.00	0.343	0.369	0.395	0.369	0.000
GVL3	294.50	0.027	0.028	0.015	0.023	0.000	GVL3	319.00	0.051	0.031	0.057	0.046	0.000	GVL3	343.50	0.196	0.398	0.434	0.343	0.000
GVL3	295.00	0.046	0.021	0.025	0.031	0.000	GVL3	319.50	0.000	0.012	0.007	0.006	0.000	GVL3	344.00	0.157	0.207	0.275	0.213	0.000
GVL3	295.50	0.011	0.009	0.022	0.014	0.000	GVL3	320.00	0.000	0.007	0.002	0.003	0.000	GVL3	344.50	0.262	0.272	0.231	0.255	0.000
GVL3	296.00	0.009	0.016	0.008	0.011	0.000	GVL3	320.50	0.045	0.030	0.034	0.036	0.000	GVL3	345.00	0.276	0.256	0.249	0.260	0.000
GVL3	296.50	0.007	0.008	0.022	0.012	0.000	GVL3	321.00	0.046	0.020	0.023	0.030	0.000	GVL3	345.50	0.260	0.339	0.189	0.263	0.000
GVL3	297.00	0.025	0.010	0.011	0.015	0.000	GVL3	321.50	0.029	0.035	0.045	0.036	0.000	GVL3	346.00	0.181	0.190	0.249	0.207	0.000
GVL3	297.50	0.022	0.033	0.013	0.023	0.000	GVL3	322.00	0.066	0.082	0.059	0.069	0.000	GVL3	346.50	0.269	0.199	0.264	0.244	0.000
GVL3	298.00	0.019	0.012	0.009	0.013	0.000	GVL3	322.50	0.107	0.101	0.142	0.117	0.000	GVL3	347.00	0.530	0.483	0.455	0.489	0.000
GVL3	298.50	0.019	0.002	0.010	0.010	0.000	GVL3	323.00	0.129	0.168	0.118	0.138	0.000	GVL3	347.50	0.279	0.233	0.277	0.263	0.000
GVL3	299.00	0.037	0.016	0.007	0.020	0.000	GVL3	323.50	0.151	0.123	0.145	0.140	0.000	GVL3	348.00	0.336	0.250	0.272	0.286	0.000
GVL3	299.50	0.015	0.022	0.038	0.025	0.000	GVL3	324.00	0.055	0.041	0.031	0.042	0.000	GVL3	348.50	0.309	0.355	0.305	0.323	0.000
GVL3	300.00	0.026	0.024	0.023	0.024	0.000	GVL3	324.50	0.028	0.030	0.038	0.032	0.000	GVL3	349.00	0.352	0.291	0.280	0.308	0.000
GVL3	300.50	0.033	0.017	0.017	0.022	0.000	GVL3	325.00	0.099	0.085	0.117	0.100	0.000	GVL3	349.50	0.327	0.264	0.384	0.325	0.000
GVL3	301.00	0.022	0.024	0.011	0.019	0.000	GVL3	325.50	0.075	0.078	0.072	0.075	0.000	GVL3	350.00	0.423	0.273	0.307	0.334	0.000
GVL3	301.50	0.005	0.006	0.007	0.006	0.000	GVL3	326.00	0.072	0.084	0.071	0.076	0.000	GVL3	350.50	0.424	0.452	0.364	0.413	0.000
GVL3	302.00	0.025	0.034	0.032	0.030	0.000	GVL3	326.50	0.120	0.093	0.107	0.107	0.000	GVL3	351.00	0.439	0.407	0.442	0.429	0.000
GVL3	302.50	0.021	0.040	0.024	0.028	0.000	GVL3	327.00	0.489	0.326	0.273	0.363	0.000	GVL3	351.50	0.317	0.201	0.233	0.250	0.000

jj

Appendix E: Magnetic Susceptibility

BHID	Depth	Reading 1	Reading 2	Reading 3	Average	SI Units	BHID	Depth	Reading 1	Reading 2	Reading 3	Average	SI Units	BHID	Depth	Reading 1	Reading 2	Reading 3	Average	SI Units
GVL3	352.00	0.481	0.429	0.342	0.417	0.000	GVL3	376.50	0.119	0.106	0.108	0.111	0.000	GVL3	401.00	0.679	0.818	0.646	0.714	0.001
GVL3	352.50	0.535	0.434	0.322	0.430	0.000	GVL3	377.00	0.174	0.165	0.198	0.179	0.000	GVL3	401.50	0.851	0.755	0.697	0.768	0.001
GVL3	353.00	0.497	0.433	0.491	0.474	0.000	GVL3	377.50	0.244	0.234	0.216	0.231	0.000	GVL3	402.00	0.662	0.650	0.624	0.645	0.001
GVL3	353.50	0.666	0.723	0.802	0.730	0.001	GVL3	378.00	0.306	0.280	0.212	0.266	0.000	GVL3	402.50	0.757	0.934	0.936	0.876	0.001
GVL3	354.00	0.798	0.804	0.780	0.794	0.001	GVL3	378.50	0.223	0.191	0.189	0.201	0.000	GVL3	403.00	0.297	0.332	0.381	0.337	0.000
GVL3	354.50	0.564	0.463	0.442	0.490	0.000	GVL3	379.00	0.194	0.193	0.187	0.191	0.000	GVL3	403.50	1.030	0.868	1.050	0.983	0.001
GVL3	355.00	0.654	0.460	0.638	0.584	0.001	GVL3	379.50	0.249	0.283	0.339	0.290	0.000	GVL3	404.00	0.741	0.901	1.050	0.897	0.001
GVL3	355.50	0.288	0.309	0.298	0.298	0.000	GVL3	380.00	0.205	0.211	0.192	0.203	0.000	GVL3	404.50	0.532	0.600	0.503	0.545	0.001
GVL3	356.00	0.317	0.311	0.339	0.322	0.000	GVL3	380.50	0.083	0.061	0.065	0.070	0.000	GVL3	405.00	0.637	0.746	0.755	0.713	0.001
GVL3	356.50	0.531	0.559	0.512	0.534	0.001	GVL3	381.00	0.140	0.161	0.153	0.151	0.000	GVL3	405.50	1.030	1.170	0.894	1.031	0.001
GVL3	357.00	0.677	0.562	0.686	0.642	0.001	GVL3	381.50	0.145	0.154	0.173	0.157	0.000	GVL3	406.00	0.844	0.630	1.150	0.875	0.001
GVL3	357.50	0.539	0.482	0.482	0.501	0.001	GVL3	382.00	0.186	0.225	0.235	0.215	0.000	GVL3	406.50	0.859	0.840	1.150	0.950	0.001
GVL3	358.00	0.514	0.354	0.366	0.411	0.000	GVL3	382.50	0.264	0.238	0.302	0.268	0.000	GVL3	407.00	0.684	0.602	0.807	0.698	0.001
GVL3	358.50	0.557	0.367	0.417	0.447	0.000	GVL3	383.00	0.237	0.221	0.229	0.229	0.000	GVL3	407.50	0.426	0.574	0.601	0.534	0.001
GVL3	359.00	0.343	0.346	0.369	0.353	0.000	GVL3	383.50	0.317	0.233	0.414	0.321	0.000	GVL3	408.00	0.737	0.525	0.661	0.641	0.001
GVL3	359.50	0.503	0.507	0.445	0.485	0.000	GVL3	384.00	0.266	0.240	0.240	0.249	0.000	GVL3	408.50	1.060	0.641	0.581	0.761	0.001
GVL3	360.00	0.469	0.433	0.328	0.410	0.000	GVL3	384.50	0.334	0.271	0.305	0.303	0.000	GVL3	409.00	0.398	0.458	0.463	0.440	0.000
GVL3	360.50	0.288	0.289	0.244	0.274	0.000	GVL3	385.00	0.160	0.167	0.158	0.162	0.000	GVL3	409.50	0.689	0.626	0.711	0.675	0.001
GVL3	361.00	0.150	0.143	0.199	0.164	0.000	GVL3	385.50	0.139	0.194	0.122	0.152	0.000	GVL3	410.00	0.546	0.624	0.616	0.595	0.001
GVL3	361.50	0.080	0.084	0.107	0.090	0.000	GVL3	386.00	0.316	0.340	0.335	0.330	0.000	GVL3	410.50	0.326	0.327	0.383	0.345	0.000
GVL3	362.00	0.233	0.300	0.303	0.279	0.000	GVL3	386.50	1.040	0.671	0.961	0.891	0.001	GVL3	411.00	0.512	0.511	0.507	0.510	0.001
GVL3	362.50	0.152	0.242	0.290	0.228	0.000	GVL3	387.00	0.141	0.139	0.199	0.160	0.000	GVL3	411.50	0.621	0.521	0.392	0.511	0.001
GVL3	363.00	0.230	0.220	0.162	0.204	0.000	GVL3	387.50	0.438	0.333	0.407	0.393	0.000	GVL3	412.00	0.181	0.209	0.204	0.198	0.000
GVL3	363.50	0.183	0.177	0.140	0.167	0.000	GVL3	388.00	0.206	0.227	0.274	0.236	0.000	GVL3	412.50	0.477	0.354	0.370	0.400	0.000
GVL3	364.00	0.639	0.450	0.595	0.561	0.001	GVL3	388.50	0.869	0.543	0.605	0.672	0.001	GVL3	413.00	0.398	0.477	0.393	0.423	0.000
GVL3	364.50	0.176	0.152	0.159	0.162	0.000	GVL3	389.00	0.571	0.678	0.639	0.629	0.001	GVL3	413.50	0.341	0.420	0.611	0.457	0.000
GVL3	365.00	0.276	0.248	0.265	0.263	0.000	GVL3	389.50	0.940	0.737	0.629	0.769	0.001	GVL3	414.00	0.460	0.431	0.460	0.450	0.000
GVL3	365.50	0.185	0.198	0.162	0.182	0.000	GVL3	390.00	0.537	0.675	0.439	0.550	0.001	GVL3	414.50	0.380	0.422	0.428	0.410	0.000
GVL3	366.00	0.354	0.355	0.379	0.363	0.000	GVL3	390.50	0.563	0.496	0.504	0.521	0.001	GVL3	415.00	0.380	0.422	0.428	0.410	0.000
GVL3	366.50	0.345	0.318	0.321	0.328	0.000	GVL3	391.00	0.573	0.297	0.431	0.434	0.000	GVL3	415.50	0.133	0.120	0.122	0.125	0.000
GVL3	367.00	0.178	0.168	0.177	0.174	0.000	GVL3	391.50	0.282	0.289	0.356	0.309	0.000	GVL3	416.00	0.257	0.269	0.256	0.261	0.000
GVL3	367.50	0.223	0.266	0.305	0.265	0.000	GVL3	392.00	0.221	0.280	0.196	0.232	0.000	GVL3	416.50	1.090	0.983	1.180	1.084	0.001
GVL3	368.00	0.165	0.121	0.164	0.150	0.000	GVL3	392.50	0.218	0.233	0.263	0.238	0.000	GVL3	417.00	0.713	0.444	0.492	0.550	0.001
GVL3	368.50	0.185	0.211	0.262	0.219	0.000	GVL3	393.00	0.724	0.760	0.651	0.712	0.001	GVL3	417.50	0.364	0.530	0.387	0.427	0.000
GVL3	369.00	0.374	0.283	0.376	0.344	0.000	GVL3	393.50	0.427	0.326	0.381	0.378	0.000	GVL3	418.00	0.223	0.216	0.331	0.257	0.000
GVL3	369.50	0.369	0.273	0.330	0.324	0.000	GVL3	394.00	0.509	0.740	0.613	0.621	0.001	GVL3	418.50	0.142	0.169	0.190	0.167	0.000
GVL3	370.00	0.328	0.311	0.363	0.334	0.000	GVL3	394.50	0.868	0.610	0.831	0.770	0.001	GVL3	419.00	0.233	0.152	0.151	0.179	0.000
GVL3	370.50	0.406	0.393	0.396	0.398	0.000	GVL3	395.00	0.674	0.739	0.857	0.757	0.001	GVL3	419.50	0.339	0.292	0.283	0.305	0.000
GVL3	371.00	0.243	0.304	0.290	0.279	0.000	GVL3	395.50	0.660	0.475	0.609	0.581	0.001	GVL3	420.00	0.179	0.137	0.194	0.170	0.000
GVL3	371.50	0.218	0.222	0.234	0.225	0.000	GVL3	396.00	0.253	0.228	0.313	0.265	0.000	GVL3	420.50	0.197	0.183	0.156	0.179	0.000
GVL3	372.00	0.224	0.219	0.156	0.200	0.000	GVL3	396.50	0.649	0.599	0.543	0.597	0.001	GVL3	421.00	0.199	0.241	0.157	0.199	0.000
GVL3	372.50	0.237	0.279	0.274	0.263	0.000	GVL3	397.00	1.030	1.000	1.220	1.083	0.001	GVL3	421.50	0.076	0.067	0.069	0.071	0.000
GVL3	373.00	0.148	0.175	0.174	0.166	0.000	GVL3	397.50	1.010	1.100	0.863	0.991	0.001	GVL3	422.00	0.051	0.117	0.067	0.078	0.000
GVL3	373.50	0.206	0.210	0.308	0.241	0.000	GVL3	398.00	0.439	0.404	0.527	0.457	0.000	GVL3	422.50	0.063	0.047	0.063	0.058	0.000
GVL3	374.00	0.282	0.230	0.303	0.272	0.000	GVL3	398.50	0.508	0.569	0.441	0.506	0.001	GVL3	423.00	0.110	0.111	0.111	0.111	0.000
GVL3	374.50	0.208	0.203	0.195	0.202	0.000	GVL3	399.00	0.294	0.316	0.405	0.338	0.000	GVL3	423.50	0.091	0.074	0.073	0.079	0.000
GVL3	375.00	0.243	0.225	0.210	0.226	0.000	GVL3	399.50	0.660	0.672	0.571	0.634	0.001	GVL3	424.00	0.080	0.098	0.048	0.075	0.000
GVL3	375.50	0.142	0.198	0.176	0.172	0.000	GVL3	400.00	0.449	0.364	0.445	0.419	0.000	GVL3	424.50	0.087	0.057	0.054	0.066	0.000
GVL3	376.00	0.245	0.227	0.226	0.233	0.000	GVL3	400.50	0.481	0.408	0.539	0.476	0.000	GVL3	425.00	0.057	0.064	0.058	0.060	0.000

kk

Appendix E: Magnetic Susceptibility

BHID	Depth	Reading 1	Reading 2	Reading 3	Average	SI Units	BHID	Depth	Reading 1	Reading 2	Reading 3	Average	SI Units	BHID	Depth	Reading 1	Reading 2	Reading 3	Average	SI Units
GVL3	425.50	0.159	0.152	0.229	0.180	0.000	GVL3	450.00	0.411	0.343	0.392	0.382	0.000	GVL3	474.50	0.035	0.029	0.021	0.028	0.000
GVL3	426.00	0.021	0.024	0.030	0.025	0.000	GVL3	450.50	0.126	0.127	0.161	0.138	0.000	GVL3	475.00	0.016	0.010	0.011	0.012	0.000
GVL3	426.50	0.098	0.070	0.117	0.095	0.000	GVL3	451.00	0.056	0.061	0.055	0.057	0.000	GVL3	475.50	0.042	0.022	0.053	0.039	0.000
GVL3	427.00	0.045	0.081	0.062	0.063	0.000	GVL3	451.50	0.128	0.120	0.130	0.126	0.000	GVL3	476.00	0.244	0.154	0.137	0.178	0.000
GVL3	427.50	0.112	0.149	0.127	0.129	0.000	GVL3	452.00	0.180	0.135	0.192	0.169	0.000	GVL3	476.50	0.111	0.139	0.127	0.126	0.000
GVL3	428.00	0.192	0.257	0.240	0.230	0.000	GVL3	452.50	0.255	0.155	0.176	0.195	0.000	GVL3	477.00	0.824	0.934	0.690	0.816	0.001
GVL3	428.50	0.133	0.154	0.125	0.137	0.000	GVL3	453.00	0.049	0.079	0.079	0.069	0.000	GVL3	477.50	0.533	0.498	0.699	0.577	0.001
GVL3	429.00	0.131	0.107	0.131	0.123	0.000	GVL3	453.50	0.198	0.126	0.174	0.166	0.000	GVL3	478.00	0.807	0.569	0.655	0.677	0.001
GVL3	429.50	0.064	0.067	0.062	0.064	0.000	GVL3	454.00	3.260	1.890	4.520	3.223	0.003	GVL3	478.50	0.687	0.522	0.637	0.615	0.001
GVL3	430.00	0.006	0.007	0.007	0.007	0.000	GVL3	454.50	0.056	0.042	0.063	0.054	0.000	GVL3	479.00	0.416	0.712	0.746	0.625	0.001
GVL3	430.50	0.073	0.081	0.101	0.085	0.000	GVL3	455.00	0.189	0.230	0.103	0.174	0.000	GVL3	479.50	0.326	0.254	0.384	0.321	0.000
GVL3	431.00	0.041	0.046	0.062	0.050	0.000	GVL3	455.50	0.103	0.103	0.105	0.104	0.000	GVL3	480.00	0.020	0.028	0.043	0.030	0.000
GVL3	431.50	0.108	0.087	0.098	0.098	0.000	GVL3	456.00	0.101	0.129	0.112	0.114	0.000	GVL3	480.50	0.037	0.034	0.063	0.045	0.000
GVL3	432.00	0.035	0.049	0.042	0.042	0.000	GVL3	456.50	0.061	0.058	0.075	0.065	0.000	GVL3	481.00	0.136	0.177	0.256	0.190	0.000
GVL3	432.50	0.075	0.088	0.056	0.073	0.000	GVL3	457.00	0.394	0.465	0.348	0.402	0.000	GVL3	481.50	0.361	0.362	0.407	0.377	0.000
GVL3	433.00	0.020	0.023	0.041	0.028	0.000	GVL3	457.50	0.086	0.060	0.059	0.068	0.000	GVL3	482.00	0.053	0.061	0.076	0.063	0.000
GVL3	433.50	0.053	0.045	0.031	0.043	0.000	GVL3	458.00	0.099	0.063	0.057	0.073	0.000	GVL3	482.50	0.062	0.054	0.104	0.073	0.000
GVL3	434.00	0.104	0.081	0.073	0.086	0.000	GVL3	458.50	0.133	0.127	0.159	0.140	0.000	GVL3	483.00	0.073	0.101	0.070	0.081	0.000
GVL3	434.50	0.051	0.031	0.040	0.041	0.000	GVL3	459.00	0.112	0.092	0.112	0.105	0.000	GVL3	483.50	0.075	0.079	0.082	0.079	0.000
GVL3	435.00	0.054	0.089	0.049	0.064	0.000	GVL3	459.50	0.104	0.102	0.062	0.089	0.000	GVL3	484.00	0.037	0.055	0.043	0.045	0.000
GVL3	435.50	0.060	0.051	0.079	0.063	0.000	GVL3	460.00	0.038	0.038	0.030	0.035	0.000	GVL3	484.50	0.030	0.026	0.038	0.031	0.000
GVL3	436.00	0.029	0.017	0.036	0.027	0.000	GVL3	460.50	0.078	0.050	0.058	0.062	0.000	GVL3	485.00	0.047	0.048	0.041	0.045	0.000
GVL3	436.50	0.010	0.015	0.020	0.015	0.000	GVL3	461.00	0.089	0.067	0.049	0.068	0.000	GVL3	485.50	0.092	0.099	0.160	0.117	0.000
GVL3	437.00	0.040	0.029	0.041	0.037	0.000	GVL3	461.50	0.024	0.035	0.046	0.035	0.000	GVL3	486.00	0.213	0.247	0.241	0.234	0.000
GVL3	437.50	0.039	0.039	0.038	0.039	0.000	GVL3	462.00	0.121	0.098	0.085	0.101	0.000	GVL3	486.50	0.170	0.141	0.190	0.167	0.000
GVL3	438.00	0.014	0.018	0.016	0.016	0.000	GVL3	462.50	0.750	0.519	0.512	0.594	0.001	GVL3	487.00	0.171	0.295	0.194	0.220	0.000
GVL3	438.50	0.150	0.008	0.023	0.060	0.000	GVL3	463.00	0.097	0.083	0.091	0.090	0.000	GVL3	487.50	0.353	0.407	0.371	0.377	0.000
GVL3	439.00	0.014	0.026	0.017	0.019	0.000	GVL3	463.50	0.044	0.031	0.057	0.044	0.000	GVL3	488.00	0.276	0.202	0.319	0.266	0.000
GVL3	439.50	0.020	0.031	0.042	0.031	0.000	GVL3	464.00	0.360	0.375	0.298	0.344	0.000	GVL3	488.50	0.180	0.318	0.274	0.257	0.000
GVL3	440.00	0.029	0.015	0.041	0.028	0.000	GVL3	464.50	0.060	0.090	0.060	0.070	0.000	GVL3	489.00	0.267	0.300	0.280	0.282	0.000
GVL3	440.50	0.059	0.050	0.047	0.052	0.000	GVL3	465.00	0.108	0.099	0.099	0.102	0.000	GVL3	489.50	0.237	0.208	0.195	0.213	0.000
GVL3	441.00	0.033	0.036	0.039	0.036	0.000	GVL3	465.50	0.029	0.033	0.056	0.039	0.000	GVL3	490.00	0.675	0.844	0.741	0.753	0.001
GVL3	441.50	0.025	0.026	0.030	0.027	0.000	GVL3	466.00	3.220	2.940	3.140	3.100	0.003	GVL3	490.50	0.424	0.316	0.383	0.374	0.000
GVL3	442.00	0.052	0.059	0.076	0.062	0.000	GVL3	466.50	0.140	0.071	0.089	0.100	0.000	GVL3	491.00	0.184	0.186	0.304	0.225	0.000
GVL3	442.50	0.024	0.024	0.006	0.018	0.000	GVL3	467.00	0.031	0.028	0.019	0.026	0.000	GVL3	491.50	0.055	0.056	0.081	0.064	0.000
GVL3	443.00	0.060	0.059	0.077	0.065	0.000	GVL3	467.50	0.029	0.032	0.032	0.031	0.000	GVL3	492.00	0.037	0.028	0.048	0.038	0.000
GVL3	443.50	0.077	0.098	0.117	0.097	0.000	GVL3	468.00	0.022	0.047	0.048	0.039	0.000	GVL3	492.50	0.081	0.054	0.041	0.059	0.000
GVL3	444.00	0.041	0.055	0.066	0.054	0.000	GVL3	468.50	0.265	0.233	0.288	0.262	0.000	GVL3	493.00	0.040	0.041	0.060	0.047	0.000
GVL3	444.50	0.137	0.102	0.171	0.137	0.000	GVL3	469.00	0.110	0.103	0.090	0.101	0.000	GVL3	493.50	0.021	0.048	0.049	0.039	0.000
GVL3	445.00	0.094	0.095	0.079	0.089	0.000	GVL3	469.50	0.070	0.074	0.084	0.076	0.000	GVL3	494.00	0.125	0.092	0.119	0.112	0.000
GVL3	445.50	0.030	0.026	0.021	0.026	0.000	GVL3	470.00	0.237	0.206	0.237	0.227	0.000	GVL3	494.50	0.036	0.057	0.067	0.053	0.000
GVL3	446.00	0.265	0.193	0.192	0.217	0.000	GVL3	470.50	0.302	0.227	0.275	0.268	0.000	GVL3	495.00	0.000	0.000	0.000	0.000	0.000
GVL3	446.50	0.420	0.315	0.437	0.391	0.000	GVL3	471.00	0.859	0.747	1.120	0.909	0.001	GVL3	495.50	0.033	0.050	0.009	0.031	0.000
GVL3	447.00	0.376	0.279	0.330	0.328	0.000	GVL3	471.50	0.949	1.080	0.790	0.940	0.001	GVL3	496.00	0.030	0.053	0.033	0.039	0.000
GVL3	447.50	0.217	0.282	0.325	0.275	0.000	GVL3	472.00	0.640	0.924	0.570	0.711	0.001	GVL3	496.50	0.109	0.106	0.120	0.112	0.000
GVL3	448.00	0.128	0.096	0.126	0.117	0.000	GVL3	472.50	0.234	0.155	0.142	0.177	0.000	GVL3	497.00	0.065	0.074	0.103	0.081	0.000
GVL3	448.50	0.235	0.216	0.160	0.204	0.000	GVL3	473.00	0.355	0.474	0.637	0.489	0.000	GVL3	497.50	0.022	0.028	0.021	0.024	0.000
GVL3	449.00	0.194	0.198	0.153	0.182	0.000	GVL3	473.50	0.431	0.314	0.284	0.343	0.000	GVL3	498.00	0.017	0.007	0.026	0.017	0.000
GVL3	449.50	0.261	0.198	0.271	0.243	0.000	GVL3	474.00	0.040	0.023	0.016	0.026	0.000	GVL3	498.50	0.026	0.032	0.031	0.030	0.000

Appendix E: Magnetic Susceptibility

BHID	Depth	Reading 1	Reading 2	Reading 3	Average	SI Units	BHID	Depth	Reading 1	Reading 2	Reading 3	Average	SI Units	BHID	Depth	Reading 1	Reading 2	Reading 3	Average	SI Units
GVL3	499.00	0.048	0.520	0.052	0.207	0.000	GVL3	523.50	0.072	0.078	0.058	0.069	0.000	GVL3	548.00	0.043	0.027	0.032	0.034	0.000
GVL3	499.50	0.027	0.023	0.021	0.024	0.000	GVL3	524.00	7.090	7.000	7.240	7.110	0.007	GVL3	548.50	0.085	0.064	0.063	0.071	0.000
GVL3	500.00	0.096	0.115	0.120	0.110	0.000	GVL3	524.50	6.850	5.850	7.460	6.720	0.007	GVL3	549.00	0.081	0.033	0.034	0.049	0.000
GVL3	500.50	0.094	0.233	0.182	0.170	0.000	GVL3	525.00	1.710	1.220	2.240	1.723	0.002	GVL3	549.50	0.092	0.102	0.067	0.080	0.000
GVL3	501.00	0.047	0.074	0.066	0.062	0.000	GVL3	525.50	9.390	10.500	7.240	9.043	0.009	GVL3	550.00	0.005	0.033	0.035	0.024	0.000
GVL3	501.50	0.161	0.084	0.169	0.138	0.000	GVL3	526.00	6.900	8.860	7.960	7.907	0.008	GVL3	550.50	0.033	0.047	0.057	0.046	0.000
GVL3	502.00	0.054	0.066	0.090	0.070	0.000	GVL3	526.50	0.077	0.054	0.073	0.068	0.000	GVL3	551.00	0.042	0.073	0.062	0.059	0.000
GVL3	502.50	0.883	0.644	0.986	0.838	0.001	GVL3	527.00	0.064	0.066	0.040	0.057	0.000	GVL3	551.50	0.039	0.048	0.041	0.043	0.000
GVL3	503.00	0.819	0.653	0.603	0.692	0.001	GVL3	527.50	0.089	0.091	0.091	0.090	0.000	GVL3	552.00	0.065	0.058	0.076	0.066	0.000
GVL3	503.50	0.089	0.086	0.088	0.088	0.000	GVL3	528.00	0.072	0.063	0.061	0.065	0.000	GVL3	552.50	0.078	0.052	0.056	0.062	0.000
GVL3	504.00	0.010	0.094	0.078	0.061	0.000	GVL3	528.50	1.080	1.280	1.030	1.130	0.001	GVL3	553.00	0.041	0.042	0.069	0.051	0.000
GVL3	504.50	0.212	0.341	0.313	0.289	0.000	GVL3	529.00	2.900	2.000	2.650	2.517	0.003	GVL3	553.50	0.047	0.023	0.047	0.039	0.000
GVL3	505.00	0.145	0.080	0.010	0.078	0.000	GVL3	529.50	1.990	1.260	1.570	1.607	0.002	GVL3	554.00	0.016	0.030	0.085	0.044	0.000
GVL3	505.50	7.680	10.300	11.900	9.960	0.010	GVL3	530.00	6.210	5.990	6.360	6.187	0.006	GVL3	554.50	0.008	0.034	0.041	0.028	0.000
GVL3	506.00	5.930	4.030	5.560	5.173	0.005	GVL3	530.50	4.200	6.600	7.920	6.240	0.006	GVL3	555.00	0.010	0.011	0.024	0.015	0.000
GVL3	506.50	5.000	5.230	5.420	5.217	0.005	GVL3	531.00	4.270	4.040	3.180	3.830	0.004	GVL3	555.50	0.047	0.025	0.012	0.028	0.000
GVL3	507.00	0.589	0.041	0.510	0.380	0.000	GVL3	531.50	6.960	7.250	6.760	6.990	0.007	GVL3	556.00	0.063	0.019	0.028	0.037	0.000
GVL3	507.50	3.310	3.660	3.980	3.650	0.004	GVL3	532.00	2.600	2.540	2.550	2.563	0.003	GVL3	556.50	1.530	1.380	1.610	1.507	0.002
GVL3	508.00	0.053	0.054	0.072	0.060	0.000	GVL3	532.50	4.160	2.970	3.410	3.513	0.004	GVL3	557.00	11.800	6.610	9.310	9.240	0.009
GVL3	508.50	0.052	0.055	0.054	0.054	0.000	GVL3	533.00	7.170	6.620	7.330	7.040	0.007	GVL3	557.50	5.050	6.410	8.050	6.503	0.007
GVL3	509.00	0.022	0.021	0.026	0.023	0.000	GVL3	533.50	4.580	5.130	7.020	5.577	0.006	GVL3	558.00	5.670	8.960	9.370	8.000	0.008
GVL3	509.50	0.033	0.054	0.075	0.054	0.000	GVL3	534.00	7.050	8.560	6.460	7.357	0.007	GVL3	558.50	7.700	8.310	9.330	8.447	0.008
GVL3	510.00	0.091	0.057	0.069	0.072	0.000	GVL3	534.50	6.010	6.660	6.530	6.400	0.006	GVL3	559.00	0.090	0.074	0.082	0.082	0.000
GVL3	510.50	0.037	0.037	0.028	0.034	0.000	GVL3	535.00	8.900	8.620	10.200	9.240	0.009	GVL3	559.50	2.800	1.890	2.000	2.230	0.002
GVL3	511.00	0.040	0.034	0.048	0.041	0.000	GVL3	535.50	16.900	19.400	18.800	18.367	0.018	GVL3	560.00	4.830	5.510	5.040	5.127	0.005
GVL3	511.50	0.051	0.054	0.045	0.050	0.000	GVL3	536.00	2.630	3.550	3.780	3.320	0.003	GVL3	560.50	3.550	2.720	3.200	3.157	0.003
GVL3	512.00	0.027	0.045	0.026	0.033	0.000	GVL3	536.50	0.111	0.172	0.140	0.141	0.000	GVL3	561.00	6.360	7.290	5.770	6.473	0.006
GVL3	512.50	0.058	0.051	0.051	0.053	0.000	GVL3	537.00	0.059	0.046	0.057	0.054	0.000	GVL3	561.50	4.830	6.610	6.860	6.100	0.006
GVL3	513.00	0.033	0.049	0.056	0.046	0.000	GVL3	537.50	0.045	0.055	0.060	0.053	0.000	GVL3	562.00	2.450	3.410	2.940	2.933	0.003
GVL3	513.50	0.033	0.049	0.056	0.046	0.000	GVL3	538.00	0.017	0.007	0.009	0.011	0.000	GVL3	562.50	3.450	2.690	2.340	2.827	0.003
GVL3	514.00	0.053	0.044	0.087	0.046	0.000	GVL3	538.50	0.047	0.033	0.031	0.037	0.000	GVL3	563.00	5.590	5.340	3.170	4.700	0.005
GVL3	514.50	0.060	0.064	0.063	0.062	0.000	GVL3	539.00	0.219	0.227	0.242	0.229	0.000	GVL3	563.50	4.880	5.360	5.000	5.080	0.005
GVL3	515.00	0.048	0.051	0.069	0.056	0.000	GVL3	539.50	0.070	0.087	0.067	0.075	0.000	GVL3	564.00	3.250	4.650	4.440	4.113	0.004
GVL3	515.50	0.064	0.072	0.044	0.060	0.000	GVL3	540.00	0.058	0.041	0.045	0.048	0.000	GVL3	564.50	4.720	5.460	4.960	5.047	0.005
GVL3	516.00	0.056	0.072	0.073	0.067	0.000	GVL3	540.50	0.048	0.059	0.045	0.051	0.000	GVL3	565.00	7.360	7.570	8.280	7.737	0.008
GVL3	516.50	0.076	0.065	0.047	0.063	0.000	GVL3	541.00	0.037	0.045	0.040	0.041	0.000	GVL3	565.50	9.040	6.280	6.350	7.223	0.007
GVL3	517.00	0.052	0.088	0.059	0.066	0.000	GVL3	541.50	0.042	0.076	0.070	0.063	0.000	GVL3	566.00	6.910	6.770	6.730	6.803	0.007
GVL3	517.50	0.058	0.069	0.048	0.058	0.000	GVL3	542.00	0.056	0.034	0.022	0.037	0.000	GVL3	566.50	3.970	4.480	5.970	4.807	0.005
GVL3	518.00	0.046	0.102	0.070	0.073	0.000	GVL3	542.50	0.030	0.042	0.028	0.033	0.000	GVL3	567.00	6.260	8.410	6.040	6.903	0.007
GVL3	518.50	0.091	0.132	0.105	0.109	0.000	GVL3	543.00	0.076	0.076	0.095	0.082	0.000	GVL3	567.50	10.600	9.350	8.580	9.510	0.010
GVL3	519.00	0.060	0.053	0.070	0.061	0.000	GVL3	543.50	0.149	0.163	0.177	0.163	0.000	GVL3	568.00	14.000	7.690	10.200	10.630	0.011
GVL3	519.50	0.071	0.105	0.087	0.088	0.000	GVL3	544.00	1.430	0.985	0.634	1.016	0.001	GVL3	568.50	6.020	6.550	7.460	6.677	0.007
GVL3	520.00	0.480	0.486	0.443	0.470	0.000	GVL3	544.50	0.345	0.354	0.438	0.379	0.000	GVL3	569.00	7.070	8.580	7.230	7.627	0.008
GVL3	520.50	0.420	0.365	0.511	0.432	0.000	GVL3	545.00	0.527	0.507	0.384	0.473	0.000	GVL3	569.50	7.290	8.810	14.500	10.200	0.010
GVL3	521.00	0.445	0.345	0.435	0.408	0.000	GVL3	545.50	0.063	0.081	0.076	0.073	0.000	GVL3	570.00	7.960	10.200	12.100	10.087	0.010
GVL3	521.50	0.677	0.577	0.494	0.583	0.001	GVL3	546.00	0.049	0.042	0.081	0.057	0.000	GVL3	570.50	4.150	5.100	7.390	5.547	0.006
GVL3	522.00	0.047	0.049	0.077	0.058	0.000	GVL3	546.50	0.102	0.044	0.055	0.067	0.000	GVL3	571.00	3.270	5.430	5.860	4.853	0.005
GVL3	522.50	0.054	0.076	0.060	0.063	0.000	GVL3	547.00	0.062	0.058	0.063	0.061	0.000	GVL3	571.50	11.100	9.580	11.200	10.627	0.011
GVL3	523.00	0.057	0.067	0.049	0.058	0.000	GVL3	547.50	0.020	0.042	0.024	0.029	0.000	GVL3	572.00	9.350	7.840	12.200	9.797	0.010

Appendix E: Magnetic Susceptibility

BHID	Depth	Reading 1	Reading 2	Reading 3	Average	SI Units	BHID	Depth	Reading 1	Reading 2	Reading 3	Average	SI Units	BHID	Depth	Reading 1	Reading 2	Reading 3	Average	SI Units
GVL3	572.50	12.900	13.100	13.700	13.233	0.013	GVL3	596.50	5.990	6.040	5.440	5.823	0.006	GVL 4	35	0.072	0.061	0.069	0.067333	0.0001
GVL3	573.00	13.400	13.300	14.800	13.833	0.014	GVL3	597.00	8.770	8.400	6.040	7.737	0.008	GVL 4	36	0.083	0.076	0.086	0.081667	0.0001
GVL3	573.50	12.300	11.000	9.180	10.827	0.011	GVL3	597.50	13.100	10.600	12.200	11.967	0.012	GVL 4	37	0.08	0.072	0.074	0.075333	0.0001
GVL3	574.00	9.820	9.620	9.610	9.683	0.010	GVL3	598.00	4.340	5.380	4.400	4.707	0.005	GVL 4	38	0.105	0.096	0.003	0.068	0.0001
GVL3	574.50	10.100	11.700	19.400	13.733	0.014	GVL3	598.50	8.340	5.850	7.590	7.260	0.007	GVL 4	39	0.096	0.093	0.097	0.095333	0.0001
GVL3	575.00	7.720	6.880	6.170	6.923	0.007	GVL3	599.00	3.160	2.970	3.540	3.223	0.003	GVL 4	40	0.118	0.116	0.117	0.117	0.0001
GVL3	575.50	10.000	9.440	8.570	9.337	0.009	GVL3	599.50	9.220	10.500	8.080	9.267	0.009	GVL 4	41	0.107	0.097	0.085	0.096333	0.0001
GVL3	576.00	14.300	13.200	13.200	13.567	0.014	GVL3	600.00	10.900	7.550	10.500	9.650	0.010	GVL 4	42	0.05	0.039	0.058	0.049	0.0000
GVL3	576.50	11.400	7.400	6.770	8.523	0.009	GVL3	600.50	13.900	8.390	10.000	10.763	0.011	GVL 4	43	0.113	0.026	0.028	0.055667	0.0001
GVL3	577.00	8.570	7.450	7.750	7.923	0.008	GVL3	601.00	10.400	9.700	13.200	11.100	0.011	GVL 4	44	0.025	0.231	0.022	0.092667	0.0001
GVL3	577.50	6.220	7.320	8.100	7.213	0.007	GVL3	601.50	12.300	13.000	15.900	13.733	0.014	GVL 4	45	0.126	0.115	0.112	0.117667	0.0001
GVL3	578.00	8.080	8.770	6.820	7.890	0.008	GVL3	602.00	9.000	6.050	5.270	6.773	0.007	GVL 4	46	0	0.091	0.086	0.059	0.0001
GVL3	578.50	0.180	0.190	0.198	0.189	0.000	GVL3	602.50	9.700	6.820	7.950	8.157	0.008	GVL 4	47	0.085	0.092	0.088	0.088333	0.0001
GVL3	579.00	11.300	10.300	10.900	10.833	0.011	GVL3	603.00	18.800	5.530	7.120	10.483	0.010	GVL 4	48	0.1	0.089	0.094	0.094333	0.0001
GVL3	579.50	10.400	9.180	11.400	10.327	0.010	GVL3	603.50	7.090	7.850	10.600	8.513	0.009	GVL 4	49	0.071	0.066	0.067	0.068	0.0001
GVL3	580.00	5.990	6.050	4.030	5.357	0.005	GVL3	604.00	6.710	8.580	7.000	7.430	0.007	GVL 4	50	0.178	0.172	0.174	0.174667	0.0002
GVL3	580.50	12.700	7.850	6.500	9.017	0.009	GVL3	604.50	9.920	9.370	15.000	11.430	0.011	GVL 4	51	0.109	0.125	0.108	0.114	0.0001
GVL3	581.00	7.810	5.240	8.940	7.330	0.007	GVL3	605.00	18.200	15.100	13.500	15.600	0.016	GVL 4	52	0.01	0.01	0.01	0.01	0.0000
GVL3	581.50	14.200	12.900	12.000	13.033	0.013	GVL3	605.50	3.110	3.910	4.830	3.950	0.004	GVL 4	53	0.15	0.009	0.04	0.066333	0.0001
GVL3	582.00	15.400	14.000	13.000	14.133	0.014	GVL3	606.00	14.900	18.100	10.500	14.500	0.015	GVL 4	54	0.065	0.049	0.062	0.058667	0.0001
GVL3	582.50	11.000	11.300	11.400	11.233	0.011	GVL3	606.50	6.660	8.510	7.160	7.443	0.007	GVL 4	55	0.086	0.082	0.082	0.083333	0.0001
GVL3	583.00	17.700	14.800	16.000	16.167	0.016	GVL3	607.00	11.100	11.700	6.820	9.873	0.010	GVL 4	56	0.085	0.079	0.08	0.081333	0.0001
GVL3	583.50	9.080	9.310	9.370	9.253	0.009	GVL3	607.50	12.600	9.060	10.600	10.753	0.011	GVL 4	57	0.085	0.071	0.086	0.080667	0.0001
GVL3	584.00	7.700	6.350	5.670	6.573	0.007	GVL3	608.00	10.900	16.300	10.900	12.700	0.013	GVL 4	58	0.117	0.103	0.102	0.107333	0.0001
GVL3	584.50	7.180	10.000	12.300	9.827	0.010	GVL3	608.50	23.600	20.000	18.000	20.533	0.021	GVL 4	59	0.082	0.066	0.068	0.072	0.0001
GVL3	585.00	11.700	10.200	12.700	11.533	0.012	GVL3	608.82	16.800	12.900	13.700	14.467	0.014	GVL 4	60	0.1	0.089	0.11	0.099667	0.0001
GVL3	585.50	5.100	5.500	6.330	5.643	0.006	**BHID**	**Depth**	**Reading 1**	**Reading 2**	**Reading 3**	**Average**	**SI Units**	GVL 4	61	0.109	0.101	0.112	0.107333	0.0001
GVL3	586.00	11.700	12.300	13.800	12.600	0.013	GVL 4	13	0.085	0.075	0.089	0.083	0.0001	GVL 4	62	0.051	0.055	0.056	0.054	0.0001
GVL3	586.50	9.780	14.500	15.800	13.360	0.013	GVL 4	14	0.164	0.155	0.154	0.157667	0.0002	GVL 4	63	0.095	0.086	0.094	0.091667	0.0001
GVL3	587.00	6.090	7.200	5.680	6.323	0.006	GVL 4	15	0.144	0.137	0.144	0.141667	0.0001	GVL 4	64	0.078	0.072	0.079	0.076333	0.0001
GVL3	587.50	7.590	7.690	7.350	7.543	0.008	GVL 4	16	0.068	0.078	0.092	0.079333	0.0001	GVL 4	65	0.121	0.123	0.172	0.138667	0.0001
GVL3	588.00	9.660	11.300	12.100	11.020	0.011	GVL 4	17	0.125	0.122	0.145	0.130667	0.0001	GVL 4	66	0.109	0.094	0.113	0.105333	0.0001
GVL3	588.50	10.500	10.900	15.500	12.300	0.012	GVL 4	18	0.125	0.122	0.145	0.130667	0.0001	GVL 4	67	0.135	0.127	0.127	0.129667	0.0001
GVL3	589.00	11.300	10.000	10.600	10.633	0.011	GVL 4	19	0.14	0.136	0.123	0.133	0.0001	GVL 4	68	0.105	0.132	0.128	0.121667	0.0001
GVL3	589.50	5.840	3.620	5.100	4.853	0.005	GVL 4	20	0.136	0.136	0.142	0.138	0.0001	GVL 4	69	0.124	0.107	0.115	0.115333	0.0001
GVL3	590.00	7.410	8.110	7.580	7.700	0.008	GVL 4	21	0.056	0.07	0.063	0.063	0.0001	GVL 4	70	0.117	0.126	0.123	0.122	0.0001
GVL3	590.50	4.940	5.260	6.390	5.530	0.006	GVL 4	22	0.101	0.1	0.1	0.100333	0.0001	GVL 4	71	0.013	0.011	0.013	0.012333	0.0000
GVL3	591.00	11.200	9.310	11.100	10.537	0.011	GVL 4	23	0.108	0.112	0.108	0.109333	0.0001	GVL 4	72	0.147	0.151	0.151	0.149667	0.0001
GVL3	591.50	12.900	16.200	13.500	14.200	0.014	GVL 4	24	0.076	0.077	0.078	0.077	0.0001	GVL 4	73	0.248	0.255	0.27	0.257667	0.0003
GVL3	592.00	6.280	9.110	9.860	8.417	0.008	GVL 4	25	0.109	0.105	0.111	0.108333	0.0001	GVL 4	74	0.077	0.001	0.006	0.028	0.0000
GVL3	592.50	12.900	17.500	14.400	14.933	0.015	GVL 4	26	0.127	0.122	0.119	0.122667	0.0001	GVL 4	75	0.012	0.009	0.002	0.007667	0.0000
GVL3	593.00	9.120	13.600	9.350	10.690	0.011	GVL 4	27	0.158	0.157	0.157	0.157333	0.0002	GVL 4	76	0.077	0.001	0.006	0.028	0.0000
GVL3	593.50	3.740	3.620	4.890	4.083	0.004	GVL 4	28	0.033	0.021	0.019	0.024333	0.0000	GVL 4	77	0.012	0.009	0.002	0.007667	0.0000
GVL3	594.00	6.070	6.900	7.120	6.697	0.007	GVL 4	29	0.02	0.016	0.014	0.016667	0.0000	GVL 4	78	0.012	0.009	0.002	0.007667	0.0000
GVL3	594.50	7.350	8.320	14.900	10.190	0.010	GVL 4	30	0.027	0.025	0.025	0.025667	0.0000	GVL 4	79	0.022	0.022	0.022	0.022	0.0000
GVL3	595.00	6.190	4.970	6.400	5.853	0.006	GVL 4	31	0.006	0.008	0.006	0.006667	0.0000	GVL 4	80	0.155	0.135	0.145	0.145	0.0001
GVL3	595.50	9.920	8.750	10.900	9.857	0.010	GVL 4	32	0.006	0.009	0.004	0.006333	0.0000	GVL 4	81	0.155	0.197	0.195	0.182333	0.0002
GVL3	596.00	11.400	8.680	7.720	9.267	0.009	GVL 4	33	0.066	0.053	0.061	0.06	0.0001	GVL 4	82	0.152	0.155	0.153	0.153333	0.0002
							GVL 4	34	0.098	0.085	0.093	0.092	0.0001	GVL 4	83	0.125	0.126	0.128	0.126333	0.0001

nn

Appendix E: Magnetic Susceptibility

BHID	Depth	Reading 1	Reading 2	Reading 3	Average	SI Units	BHID	Depth	Reading 1	Reading 2	Reading 3	Average	SI Units	BHID	Depth	Reading 1	Reading 2	Reading 3	Average	SI Units
GVL 4	84	0.248	0.258	0.253	0.253	0.0003	GVL 4	133	0.339	0.335	0.32	0.331333	0.0003	GVL 4	182	Missing Core				
GVL 4	85	0.95	0.721	0.784	0.818333	0.0008	GVL 4	134	Missing Core					GVL 4	183	Missing Core				
GVL 4	86	0.702	0.698	0.719	0.706333	0.0007	GVL 4	135	Missing Core					GVL 4	184	Missing Core				
GVL 4	87	0	0	0	0	0.0000	GVL 4	136	Missing Core					GVL 4	185	Missing Core				
GVL 4	88	0	0	0	0	0.0000	GVL 4	137	Missing Core					GVL 4	186	Missing Core				
GVL 4	89	0	0	0	0	0.0000	GVL 4	138	Missing Core					GVL 4	187	Missing Core				
GVL 4	90	0	0	0	0	0.0000	GVL 4	139	Missing Core					GVL 4	188	Missing Core				
GVL 4	91	0	0	0	0	0.0000	GVL 4	140	Missing Core					GVL 4	189	Missing Core				
GVL 4	92	0	0	0	0	0.0000	GVL 4	141	Missing Core					GVL 4	190	Missing Core				
GVL 4	93	0	0	0	0	0.0000	GVL 4	142	Missing Core					GVL 4	191	Missing Core				
GVL 4	94	0	0	0	0	0.0000	GVL 4	143	Missing Core					GVL 4	192	Missing Core				
GVL 4	95	0	0	0	0	0.0000	GVL 4	144	Missing Core					GVL 4	193	Missing Core				
GVL 4	96	0	0	0	0	0.0000	GVL 4	145	Missing Core					GVL 4	194	Missing Core				
GVL 4	97	0	0	0	0	0.0000	GVL 4	146	Missing Core					GVL 4	195	Missing Core				
GVL 4	98	0	0	0	0	0.0000	GVL 4	147	Missing Core					GVL 4	196	Missing Core				
GVL 4	99	0	0	0	0	0.0000	GVL 4	148	Missing Core					GVL 4	197	Missing Core				
GVL 4	100	0	0	0	0	0.0000	GVL 4	149	Missing Core					GVL 4	198	Missing Core				
GVL 4	101	0	0	0	0	0.0000	GVL 4	150	Missing Core					GVL 4	199	Missing Core				
GVL 4	102	0	0	0	0	0.0000	GVL 4	151	Missing Core					GVL 4	200	Missing Core				
GVL 4	103	0	0	0	0	0.0000	GVL 4	152	Missing Core					GVL 4	201	Missing Core				
GVL 4	104	0.25	0.249	0.233	0.244	0.0002	GVL 4	153	Missing Core					GVL 4	202	Missing Core				
GVL 4	105	0.416	0.429	0.414	0.419667	0.0004	GVL 4	154	Missing Core					GVL 4	203	Missing Core				
GVL 4	106	0.281	0.282	0.282	0.281667	0.0003	GVL 4	155	Missing Core					GVL 4	204	Missing Core				
GVL 4	107	0.142	0.15	0.159	0.150333	0.0002	GVL 4	156	Missing Core					GVL 4	205	Missing Core				
GVL 4	108	0.152	0.156	0.154	0.154	0.0002	GVL 4	157	Missing Core					GVL 4	206	Missing Core				
GVL 4	109	0.157	0.157	0.178	0.164	0.0002	GVL 4	158	Missing Core					GVL 4	207	Missing Core				
GVL 4	110	0.091	0.094	0.095	0.093333	0.0001	GVL 4	159	Missing Core					GVL 4	208	Missing Core				
GVL 4	111	0.214	0.211	0.211	0.212	0.0002	GVL 4	160	Missing Core					GVL 4	209	Missing Core				
GVL 4	112	0.238	0.238	0.234	0.236667	0.0002	GVL 4	161	Missing Core					GVL 4	210	1.58	1.6	1.62	1.6	0.0016
GVL 4	113	0.396	0.386	0.406	0.396	0.0004	GVL 4	162	Missing Core					GVL 4	211	7.18	8.66	9.04	8.293333	0.0083
GVL 4	114	0.313	0.304	0.305	0.307333	0.0003	GVL 4	163	Missing Core					GVL 4	212	8.71	4.05	3.67	5.476667	0.0055
GVL 4	115	0.23	0.203	0.23	0.221	0.0002	GVL 4	164	Missing Core					GVL 4	213	19.7	19.7	20	19.8	0.0198
GVL 4	116	0.234	0.217	0.217	0.222667	0.0002	GVL 4	165	Missing Core					GVL 4	214	11.9	11.7	11.4	11.66667	0.0117
GVL 4	117	0.216	0.23	0.235	0.227	0.0002	GVL 4	166	Missing Core					GVL 4	215	0.421	0.398	0.387	0.402	0.0004
GVL 4	118	0.305	0.311	0.321	0.312333	0.0003	GVL 4	167	Missing Core					GVL 4	216	9.2	8.71	8.75	8.886667	0.0089
GVL 4	119	0.275	0.278	0.27	0.274333	0.0003	GVL 4	168	Missing Core					GVL 4	217	0.172	0.163	0.164	0.166333	0.0002
GVL 4	120	0.3	0.299	0.291	0.296667	0.0003	GVL 4	169	Missing Core					GVL 4	218	1.39	1.37	1.48	1.413333	0.0014
GVL 4	121	0.206	0.213	0.211	0.21	0.0002	GVL 4	170	Missing Core					GVL 4	219	18.9	19.2	19.5	19.2	0.0192
GVL 4	122	0.207	0.207	0.205	0.206333	0.0002	GVL 4	171	Missing Core					GVL 4	220	0.544	0.551	0.529	0.541333	0.0005
GVL 4	123	0.287	0.307	0.203	0.265667	0.0003	GVL 4	172	Missing Core					GVL 4	221	0.18	0.178	0.186	0.181333	0.0002
GVL 4	124	0.301	0.298	0.298	0.299	0.0003	GVL 4	173	Missing Core					GVL 4	222	28.3	28.2	28.2	28.23333	0.0282
GVL 4	125	0.341	0.33	0.32	0.330333	0.0003	GVL 4	174	Missing Core					GVL 4	223	13.1	12	11.9	12.33333	0.0123
GVL 4	126	0.293	0.281	0.286	0.286667	0.0003	GVL 4	175	Missing Core					GVL 4	224	0.477	0.527	0.531	0.511667	0.0005
GVL 4	127	0.241	0.249	0.236	0.242	0.0002	GVL 4	176	Missing Core					GVL 4	225	30.6	30.6	29.9	30.36667	0.0304
GVL 4	128	0.323	0.344	0.341	0.336	0.0003	GVL 4	177	Missing Core					GVL 4	226	31.6	33.2	32.9	32.56667	0.0326
GVL 4	129	0.543	0.549	0.559	0.550333	0.0006	GVL 4	178	Missing Core					GVL 4	227	0.187	0.197	0.189	0.191	0.0002
GVL 4	130	0.283	0.293	0.354	0.31	0.0003	GVL 4	179	Missing Core					GVL 4	228	0.545	0.758	0.775	0.692667	0.0007
GVL 4	131	0.68	0.696	0.74	0.705333	0.0007	GVL 4	180	Missing Core					GVL 4	229	0.254	0.267	0.275	0.265333	0.0003
GVL 4	132	0.339	0.354	0.357	0.35	0.0004	GVL 4	181	Missing Core					GVL 4	230	0.284	0.299	0.289	0.290667	0.0003

Appendix E: Magnetic Susceptibility

BHID	Depth	Reading 1	Reading 2	Reading 3	Average	SI Units	BHID	Depth	Reading 1	Reading 2	Reading 3	Average	SI Units	BHID	Depth	Reading 1	Reading 2	Reading 3	Average	SI Units
GVL 4	231	0.224	0.226	0.221	0.223667	0.0002	GVL 4	280	0.91	0.202	0.185	0.432333	0.0004	GVL 4	329	25	24.2	23.9	24.36667	0.0244
GVL 4	232	0.166	0.162	0.164	0.164	0.0002	GVL 4	281	0.211	0.212	0.209	0.210667	0.0002	GVL 4	330	68.3	65.9	66.5	66.9	0.0669
GVL 4	233	0.221	0.23	0.222	0.224333	0.0002	GVL 4	282	0.191	0.195	0.196	0.194	0.0002	GVL 4	331	0.396	0.309	0.32	0.341667	0.0003
GVL 4	234	0.497	0.485	0.479	0.487	0.0005	GVL 4	283	0.256	0.258	0.262	0.258667	0.0003	GVL 4	332	0.125	0.134	0.134	0.131	0.0001
GVL 4	235	12.7	13.1	12.1	12.63333	0.0126	GVL 4	284	0.25	0.23	0.235	0.238333	0.0002	GVL 4	333	0.063	0.061	0.06	0.061333	0.0001
GVL 4	236	13.4	13.3	13.2	13.3	0.0133	GVL 4	285	34.3	34.2	35.9	34.8	0.0348	GVL 4	334	0.229	0.229	0.229	0.229	0.0002
GVL 4	237	18.1	18.1	18.4	18.2	0.0182	GVL 4	286	0.195	0.193	0.197	0.195	0.0002	GVL 4	335	0.267	0.296	0.293	0.285333	0.0003
GVL 4	238	20.4	22.1	22	21.5	0.0215	GVL 4	287	0.683	0.694	0.852	0.743	0.0007	GVL 4	336	0.226	0.225	0.24	0.230333	0.0002
GVL 4	239	19.5	19.7	19.6	19.6	0.0196	GVL 4	288	0.197	0.189	0.189	0.191667	0.0002	GVL 4	337	0.927	0.867	0.55	0.781333	0.0008
GVL 4	240	20.6	20.4	20.3	20.43333	0.0204	GVL 4	289	26.9	26.5	26.3	26.56667	0.0266	GVL 4	338	0.38	0.403	0.397	0.393333	0.0004
GVL 4	241	23.4	23.8	23.6	23.6	0.0236	GVL 4	290	0.125	0.167	0.128	0.14	0.0001	GVL 4	339	0.225	0.231	0.218	0.224667	0.0002
GVL 4	242	42.2	42.8	43.1	42.7	0.0427	GVL 4	291	0.145	0.143	0.149	0.145667	0.0001	GVL 4	340	31.6	28.2	29	29.6	0.0296
GVL 4	243	27.5	27.6	27.6	27.56667	0.0276	GVL 4	292	0.149	0.149	0.131	0.143	0.0001	GVL 4	341	0.238	0.231	0.229	0.232667	0.0002
GVL 4	244	23.1	24.5	24.6	24.06667	0.0241	GVL 4	293	0.128	0.125	0.127	0.126667	0.0001	GVL 4	342	66.7	64	39.5	56.73333	0.0567
GVL 4	245	3.37	3.39	3.4	3.386667	0.0034	GVL 4	294	0.174	0.168	0.166	0.169333	0.0002	GVL 4	343	55.1	46.5	50.9	50.83333	0.0508
GVL 4	246	28.2	28.1	27.9	28.06667	0.0281	GVL 4	295	0.71	0.691	0.675	0.692	0.0007	GVL 4	344	0.3	0.297	0.3	0.299	0.0003
GVL 4	247	37.7	32.7	35.5	35.3	0.0353	GVL 4	296	0.221	0.227	0.227	0.225	0.0002	GVL 4	345	0.212	0.2	0.215	0.209	0.0002
GVL 4	248	23.4	25	26.2	24.86667	0.0249	GVL 4	297	0.116	0.129	0.13	0.125	0.0001	GVL 4	346	0.212	0.2	0.215	0.209	0.0002
GVL 4	249	30.3	29.3	29.5	29.7	0.0297	GVL 4	298	0.234	0.246	0.253	0.244333	0.0002	GVL 4	347	0.075	0.073	0.084	0.077333	0.0001
GVL 4	250	3.82	4.23	0.444	2.831333	0.0028	GVL 4	299	0.193	0.19	0.188	0.190333	0.0002	GVL 4	348	0.296	0.296	0.301	0.297667	0.0003
GVL 4	251	0.389	0.391	0.392	0.390667	0.0004	GVL 4	300	0.203	0.214	0.211	0.209333	0.0002	GVL 4	349	0.178	0.174	0.179	0.177	0.0002
GVL 4	252	0.399	0.403	0.409	0.403667	0.0004	GVL 4	301	0.27	0.286	0.269	0.275	0.0003	GVL 4	350	16.1	13.1	12.9	14.03333	0.0140
GVL 4	253	0.3	0.283	0.305	0.296	0.0003	GVL 4	302	27	25	31.1	27.7	0.0277	GVL 4	351	22.1	19.5	22.8	21.46667	0.0215
GVL 4	254	30.5	31.2	35.9	32.53333	0.0325	GVL 4	303	44.8	53.2	58.7	52.23333	0.0522	GVL 4	352	81.2	85.5	87.7	84.8	0.0848
GVL 4	255	0.355	0.357	0.359	0.357	0.0004	GVL 4	304	0.257	0.285	0.27	0.270667	0.0003	GVL 4	353	27.4	32.7	20.1	26.73333	0.0267
GVL 4	256	32.1	33	31.9	32.33333	0.0323	GVL 4	305	0.777	0.748	0.899	0.808	0.0008	GVL 4	354	30.1	28.4	30.9	29.8	0.0298
GVL 4	257	41	42.9	39.8	41.23333	0.0412	GVL 4	306	0.247	0.228	0.232	0.235667	0.0002	GVL 4	355	128	128	129	128.3333	0.1283
GVL 4	258	62.7	63.8	64.4	63.63333	0.0636	GVL 4	307	0.13	0.144	0.155	0.143	0.0001	GVL 4	356	31	30.9	36.2	32.7	0.0327
GVL 4	259	53.1	42.9	40.4	45.46667	0.0455	GVL 4	308	9.19	10.6	9.96	9.916667	0.0099	GVL 4	357	87.1	86.4	89.7	87.73333	0.0877
GVL 4	260	52.3	51.3	50.8	51.46667	0.0515	GVL 4	309	0.195	0.292	0.402	0.296333	0.0003	GVL 4	358	15.7	14.6	16.8	15.7	0.0157
GVL 4	261	0.203	0.211	0.224	0.212667	0.0002	GVL 4	310	0.216	0.205	0.207	0.209333	0.0002	GVL 4	359	47	48.7	50.1	48.6	0.0486
GVL 4	262	36.4	32	22	30.13333	0.0301	GVL 4	311	0.139	0.152	0.188	0.159667	0.0002	GVL 4	360	59.1	50.6	59.5	56.4	0.0564
GVL 4	263	20.7	13.8	19.9	18.13333	0.0181	GVL 4	312	0.265	0.269	0.262	0.265333	0.0003	GVL 4	361	24.8	27.7	27.7	26.73333	0.0267
GVL 4	264	0.194	0.192	0.191	0.192333	0.0002	GVL 4	313	0.196	0.207	0.244	0.215667	0.0002	GVL 4	362	40.7	37.8	40.6	39.7	0.0397
GVL 4	265	0.192	0.2	0.195	0.195667	0.0002	GVL 4	314	0.224	0.227	0.229	0.226667	0.0002	GVL 4	363	55.3	56.6	55.6	55.83333	0.0558
GVL 4	266	32.4	32.5	32.7	32.53333	0.0325	GVL 4	315	0.172	0.169	0.17	0.170333	0.0002	GVL 4	364	75.2	67.2	65.3	69.23333	0.0692
GVL 4	267	25	25.5	24.7	25.06667	0.0251	GVL 4	316	0.178	0.173	0.18	0.177	0.0002	GVL 4	365	56.1	56.7	55.4	56.06667	0.0561
GVL 4	268	20.2	16.6	16.8	17.86667	0.0179	GVL 4	317	0.117	0.115	0.114	0.115333	0.0001	GVL 4	366	58.6	59.8	63.9	60.76667	0.0608
GVL 4	269	53.6	54.5	56.6	54.9	0.0549	GVL 4	318	0.161	0.162	0.162	0.161667	0.0002	GVL 4	367	1.73	2.42	2.39	2.18	0.0022
GVL 4	270	48.4	43.8	42.2	44.8	0.0448	GVL 4	319	0.128	0.127	0.126	0.127	0.0001	GVL 4	368	46.6	47.2	47.9	47.23333	0.0472
GVL 4	271	3.85	3.79	3.79	3.81	0.0038	GVL 4	320	0.248	0.249	0.249	0.248667	0.0002	GVL 4	369	41.8	40	48.1	43.3	0.0433
GVL 4	272	0.087	0.095	0.093	0.091667	0.0001	GVL 4	321	28.3	21.7	19.4	23.13333	0.0231	GVL 4	370	44.4	55.9	56.9	52.4	0.0524
GVL 4	273	42.3	44.8	45.6	44.23333	0.0442	GVL 4	322	116	115	112	114.3333	0.1143	GVL 4	371	41.3	49.1	49.5	46.63333	0.0466
GVL 4	274	32.6	34.8	34.7	34.03333	0.0340	GVL 4	323	0.617	0.193	0.682	0.497333	0.0005	GVL 4	372	41.9	45.8	34.1	40.6	0.0406
GVL 4	275	24.9	21.3	25.5	23.9	0.0239	GVL 4	324	50.4	52.9	55.9	53.06667	0.0531	GVL 4	373	20.1	20.2	22	20.76667	0.0208
GVL 4	276	8.54	9.81	11.3	9.883333	0.0099	GVL 4	325	0.264	0.269	0.269	0.267333	0.0003	GVL 4	374	85.8	90.3	91.4	89.16667	0.0892
GVL 4	277	0.421	0.441	0.426	0.429333	0.0004	GVL 4	326	47.6	65.8	65.3	59.56667	0.0596	GVL 4	375	71.7	66.5	61.2	66.46667	0.0665
GVL 4	278	0.896	0.875	0.848	0.873	0.0009	GVL 4	327	0.264	0.264	0.266	0.264667	0.0003	GVL 4	376	45.3	43.9	44.3	44.5	0.0445
GVL 4	279	0.395	0.397	0.393	0.395	0.0004	GVL 4	328	0.12	0.116	0.118	0.118	0.0001	GVL 4	377	45.3	43.9	44.3	44.5	0.0445

Appendix E: Magnetic Susceptibility

BHID	Depth	Reading 1	Reading 2	Reading 3	Average	SI Units	BHID	Depth	Reading 1	Reading 2	Reading 3	Average	SI Units	BHID	Depth	Reading 1	Reading 2	Reading 3	Average	SI Units
GVL 4	378	112	116	114	114	0.1140	GVL 4	427	60.4	59.9	60.4	60.23333	0.0602	GVL 4	476	CC	CC	CC		
GVL 4	379	36.5	36.5	37	36.66667	0.0367	GVL 4	428	56.5	54.8	56.1	55.8	0.0558	GVL 4	477	CC	CC	CC		
GVL 4	380	56.8	56.7	58.6	57.36667	0.0574	GVL 4	429	62.2	63.3	63.3	62.93333	0.0629	GVL 4	478	CC	CC	CC		
GVL 4	381	50.8	50.8	51.5	51.03333	0.0510	GVL 4	430	94.1	98.5	99.2	97.26667	0.0973	GVL 4	479	CC	CC	CC		
GVL 4	382	54.8	56.8	58.2	56.6	0.0566	GVL 4	431	73.2	73.1	76.4	74.23333	0.0742	GVL 4	480	CC	CC	CC		
GVL 4	383	43.2	43	43	43.06667	0.0431	GVL 4	432	32.8	38.1	37.4	36.1	0.0361	GVL 4	481	CC	CC	CC		
GVL 4	384	72.2	71.9	71.3	71.8	0.0718	GVL 4	433	85	88.4	89.3	87.56667	0.0876	GVL 4	482	CC	CC	CC		
GVL 4	385	53.5	52	53.3	52.93333	0.0529	GVL 4	434	44.1	42.1	40.4	42.2	0.0422	GVL 4	483	CC	CC	CC		
GVL 4	386	35	35.2	35	35.06667	0.0351	GVL 4	435	43	45.2	46.7	44.96667	0.0450	GVL 4	484	CC	CC	CC		
GVL 4	387	37.9	38	38	37.96667	0.0380	GVL 4	436	40.3	40	38.3	39.53333	0.0395	GVL 4	485	CC	CC	CC		
GVL 4	388	3.24	3	3.23	3.156667	0.0032	GVL 4	437	30.5	39.5	32	34	0.0340	GVL 4	486	CC	CC	CC		
GVL 4	389	0.193	0.186	0.189	0.189333	0.0002	GVL 4	438	35.6	33.6	38.5	35.9	0.0359	GVL 4	487	CC	CC	CC		
GVL 4	390	0.686	0.72	0.629	0.678333	0.0007	GVL 4	439	10.5	9.42	9.62	9.846667	0.0098	GVL 4	488	CC	CC	CC		
GVL 4	391	0.263	0.261	0.258	0.260667	0.0003	GVL 4	440	95	89.9	103	95.96667	0.0960	GVL 4	489	CC	CC	CC		
GVL 4	392	0.223	0.235	0.235	0.231	0.0002	GVL 4	441	46.6	50.5	51.3	49.46667	0.0495	GVL 4	490	CC	CC	CC		
GVL 4	393	0.38	0.351	0.42	0.383667	0.0004	GVL 4	442	43	43	42.1	42.7	0.0427	GVL 4	491	CC	CC	CC		
GVL 4	394	22.6	22.5	23.7	22.93333	0.0229	GVL 4	443	78	71	77.3	75.43333	0.0754	GVL 4	492	CC	CC	CC		
GVL 4	395	0.172	0.174	0.184	0.176667	0.0002	GVL 4	444	59.5	57.1	53.1	56.56667	0.0566	GVL 4	493	CC	CC	CC		
GVL 4	396	0.359	0.407	0.388	0.384667	0.0004	GVL 4	445	50.8	50.8	51.2	50.93333	0.0509	GVL 4	494	CC	CC	CC		
GVL 4	397	0.183	0.189	0.19	0.187333	0.0002	GVL 4	446	1.8	1.59	1.27	1.553333	0.0016	GVL 4	495	CC	CC	CC		
GVL 4	398	73.6	84.1	82.4	80.03333	0.0800	GVL 4	447	71.8	62.3	74.1	69.4	0.0694	GVL 4	496	CC	CC	CC		
GVL 4	399	46.3	46.5	45.1	45.96667	0.0460	GVL 4	448	75.2	74.7	74.2	74.7	0.0747	GVL 4	497	CC	CC	CC		
GVL 4	400	47.5	85.1	84.9	72.5	0.0725	GVL 4	449	74.4	75.3	74.6	74.76667	0.0748	GVL 4	498	CC	CC	CC		
GVL 4	401	25.4	21.3	19.6	22.1	0.0221	GVL 4	450	60.6	59.1	60.6	60.1	0.0601	GVL 4	499	CC	CC	CC		
GVL 4	402	67.7	70.2	70	69.3	0.0693	GVL 4	451	155	89.5	95.6	113.3667	0.1134	GVL 4	500	CC	CC	CC		
GVL 4	403	48.1	48.1	46.3	47.5	0.0475	GVL 4	452	51.8	50.5	46.2	49.5	0.0495	GVL 4	501	CC	CC	CC		
GVL 4	404	82.1	80.7	80.8	81.2	0.0812	GVL 4	453	50.1	48.1	47	48.4	0.0484	GVL 4	502	CC	CC	CC		
GVL 4	405	72.5	76.7	77.8	75.66667	0.0757	GVL 4	454	32.4	31.3	30.7	31.46667	0.0315	GVL 4	503	0.57	0.57	0.564	0.568	0.0006
GVL 4	406	53	53.9	53.7	53.53333	0.0535	GVL 4	455	17	17.1	16	16.7	0.0167	GVL 4	504	CC	CC	CC		
GVL 4	407	51.9	59.7	62.8	58.13333	0.0581	GVL 4	456	46.7	49.7	50.9	49.1	0.0491	GVL 4	505	CC	CC	CC		
GVL 4	408	63.5	64.7	62.6	63.6	0.0636	GVL 4	457	50.3	57.1	56.4	54.6	0.0546	GVL 4	506	1.89	1.9	1.87	1.886667	0.0019
GVL 4	409	59.2	59.9	60.1	59.73333	0.0597	GVL 4	458	27.3	27.4	29.1	27.93333	0.0279	GVL 4	507	1.74	1.83	1.83	1.8	0.0018
GVL 4	410	74.7	72.1	68.7	71.83333	0.0718	GVL 4	459	99.9	101	102	100.9667	0.1010	GVL 4	508	0.624	0.611	0.584	0.606333	0.0006
GVL 4	411	71.8	72.9	74.4	73.03333	0.0730	GVL 4	460	130	129	130	129.6667	0.1297	GVL 4	509	0.533	0.551	0.679	0.587667	0.0006
GVL 4	412	50.2	53.9	53.7	52.6	0.0526	GVL 4	461	58.5	59	55.8	57.76667	0.0578	GVL 4	510	0.6	0.589	0.602	0.597	0.0006
GVL 4	413	63.2	63.6	63.3	63.36667	0.0634	GVL 4	462	CC	CC	CC			GVL 4	511	0.11	0.11	0.113	0.111	0.0001
GVL 4	414	70.2	76.8	71.6	72.86667	0.0729	GVL 4	463	12.3	12	10.9	11.73333	0.0117	GVL 4	512	1.32	1.82	1.3	1.48	0.0015
GVL 4	415	43.7	44	44.3	44	0.0440	GVL 4	464	43.8	36.2	47.4	42.46667	0.0425	GVL 4	513	14.1	13.6	13	13.56667	0.0136
GVL 4	416	58.9	60.8	60.3	60	0.0600	GVL 4	465	27.6	28.8	26.6	27.66667	0.0277	GVL 4	514	0.129	0.13	0.155	0.138	0.0001
GVL 4	417	54.8	57.4	55.8	56	0.0560	GVL 4	466	22.2	19.3	15.6	19.03333	0.0190	GVL 4	515	0.2	0.203	0.209	0.204	0.0002
GVL 4	418	68.1	69.8	68.8	68.9	0.0689	GVL 4	467	22	21.7	21.3	21.66667	0.0217	GVL 4	516	0.309	0.31	0.309	0.309333	0.0003
GVL 4	419	60.5	56.3	59.1	58.63333	0.0586	GVL 4	468	38.8	37.2	38.8	38.26667	0.0383	GVL 4	517	0.428	0.426	0.439	0.431	0.0004
GVL 4	420	32	32.7	31.9	32.2	0.0322	GVL 4	469	40.2	40.6	39.9	40.23333	0.0402	GVL 4	518	0.49	0.492	0.483	0.488333	0.0005
GVL 4	421	53.3	53.6	51.1	52.66667	0.0527	GVL 4	470	41.6	39.9	37.4	39.63333	0.0396	GVL 4	519	0.573	0.642	0.657	0.624	0.0006
GVL 4	422	72.7	61.5	66.5	66.9	0.0669	GVL 4	471	CC	CC	CC			GVL 4	520	0.618	0.657	0.589	0.621333	0.0006
GVL 4	423	68.9	72	69.3	70.06667	0.0701	GVL 4	472	CC	CC	CC			GVL 4	521	0.639	0.638	0.597	0.624667	0.0006
GVL 4	424	68	73.9	73.7	71.86667	0.0719	GVL 4	473	CC	CC	CC			GVL 4	522	0.176	0.174	0.173	0.174333	0.0002
GVL 4	425	71.8	71.4	71.7	71.63333	0.0716	GVL 4	474	CC	CC	CC			GVL 4	523	0.067	0.061	0.062	0.063333	0.0001
GVL 4	426	58.1	55.3	57.6	57	0.0570	GVL 4	475	CC	CC	CC			GVL 4	524	0.409	0.412	0.414	0.411667	0.0004

qq

Appendix E: Magnetic Susceptibility

BHID	Depth	Reading 1	Reading 2	Reading 3	Average	SI Units	BHID	Depth	Reading 1	Reading 2	Reading 3	Average	SI Units	BHID	Depth	Reading 1	Reading 2	Reading 3	Average	SI Units
GVL 4	525	0.687	0.688	0.675	0.683333	0.0007	GVL 4	574	0.513	0.483	0.502	0.499333	0.0005	GVL2	56	0.193	0.281	0.243	0.239	0.000
GVL 4	526	0.67	0.672	0.663	0.668333	0.0007	GVL 4	575	1.3	1.43	1.43	1.386667	0.0014	GVL2	57	0.479	0.501	0.536	0.505	0.001
GVL 4	527	0.424	0.43	0.446	0.433333	0.0004	GVL 4	576	0.518	0.516	0.5	0.511333	0.0005	GVL2	58	0.619	0.561	0.725	0.635	0.001
GVL 4	528	0.359	0.348	0.354	0.353667	0.0004	GVL 4	577	0.681	0.599	0.607	0.629	0.0006	GVL2	59	0.335	0.494	0.456	0.428	0.000
GVL 4	529	0.363	0.348	0.347	0.352667	0.0004	GVL 4	578	0.953	1.02	1.03	1.001	0.0010	GVL2	60	0.192	0.242	0.26	0.231	0.000
GVL 4	530	0.362	0.381	0.39	0.377667	0.0004	GVL 4	579	0.462	0.538	0.513	0.504333	0.0005	GVL2	61	0.333	0.427	0.46	0.407	0.000
GVL 4	531	0.557	0.503	0.57	0.543333	0.0005	GVL 4	580	1.05	0.964	0.765	0.926333	0.0009	GVL2	62	0.575	0.681	0.87	0.709	0.001
GVL 4	532	0.319	0.33	0.3	0.316333	0.0003	GVL 4	581	0.425	0.426	0.412	0.421	0.0004	GVL2	63	0.771	0.706	0.565	0.681	0.001
GVL 4	533	0.989	0.999	0.997	0.995	0.0010	GVL 4	582	0.525	0.534	0.513	0.524	0.0005	GVL2	64	0.557	0.612	0.593	0.587	0.001
GVL 4	534	0.557	0.54	0.531	0.542667	0.0005	GVL 4	583	0.781	0.765	0.785	0.777	0.0008	GVL2	65	0.719	0.783	0.676	0.726	0.001
GVL 4	535	0.664	0.682	0.67	0.672	0.0007	GVL 4	584	0.538	0.539	0.566	0.547667	0.0005	GVL2	66	0.703	0.469	0.694	0.622	0.001
GVL 4	536	0.618	0.588	0.626	0.610667	0.0006	GVL 4	585	0.43	0.433	0.449	0.437333	0.0004	GVL2	67	0.478	0.497	0.438	0.471	0.000
GVL 4	537	1.18	1.14	1.18	1.166667	0.0012	GVL 4	586	0.381	0.398	0.425	0.401333	0.0004	GVL2	68	0.966	1.31	1.15	1.142	0.001
GVL 4	538	0.383	0.37	0.357	0.37	0.0004	GVL 4	587	0.739	0.424	0.426	0.529667	0.0005	GVL2	69	0.513	0.911	0.988	0.804	0.001
GVL 4	539	0.359	0.36	0.36	0.359667	0.0004	GVL 4	588	0.426	0.59	0.591	0.535667	0.0005	GVL2	70	0.721	0.654	0.822	0.732	0.001
GVL 4	540	0.622	0.591	0.572	0.595	0.0006	GVL 4	589	1.2	1.17	1.12	1.163333	0.0012	GVL2	71	0.997	1.15	1.45	1.199	0.001
GVL 4	541	0.63	0.57	0.541	0.580333	0.0006	GVL 4	590	3.21	2.69	2.7	2.866667	0.0029	GVL2	72	0.978	1.3	0.953	1.077	0.001
GVL 4	542	0.88	0.898	0.88	0.886	0.0009	GVL 4	591	1.46	1.46	1.61	1.51	0.0015	GVL2	73	1.02	0.978	0.995	0.998	0.001
GVL 4	543	0.495	0.481	0.46	0.478667	0.0005	GVL 4	592	0.811	0.805	0.726	0.780667	0.0008	GVL2	74	0.996	0.902	0.912	0.937	0.001
GVL 4	544	0.406	0.404	0.402	0.404	0.0004	GVL 4	593	0.277	0.342	0.331	0.316667	0.0003	GVL2	75	1.01	0.845	0.746	0.867	0.001
GVL 4	545	0.123	0.131	0.133	0.129	0.0001	GVL 4	594	0.17	0.169	0.167	0.168667	0.0002	GVL2	76	1.04	0.887	0.815	0.914	0.001
GVL 4	546	0.565	0.553	0.55	0.556	0.0006	GVL 4	595	0.18	0.18	0.185	0.181667	0.0002	GVL2	77	0.7	0.843	0.932	0.825	0.001
GVL 4	547	0.448	0.379	0.388	0.405	0.0004	GVL 4	596	0.161	0.151	0.152	0.154667	0.0002	GVL2	78	0.858	0.972	0.916	0.915	0.001
GVL 4	548	1.57	1.15	1.5	1.406667	0.0014	GVL 4	597	1.3	1.31	1.3	1.303333	0.0013	GVL2	79	0.835	0.891	0.872	0.866	0.001
GVL 4	549	0.415	0.41	0.423	0.416	0.0004	GVL 4	598	5.2	5.49	5.31	5.333333	0.0053	GVL2	80	0.265	0.271	0.313	0.283	0.000
GVL 4	550	0.437	0.428	0.439	0.434667	0.0004	GVL 4	599	0.342	0.353	0.343	0.346	0.0003	GVL2	81	1.3	0.886	0.885	1.024	0.001
GVL 4	551	0.462	0.464	0.465	0.463667	0.0005	GVL 4	600	0.37	0.343	0.326	0.346333	0.0003	GVL2	82	0.738	1.05	1.16	0.983	0.001
GVL 4	552	0.652	0.664	0.617	0.644333	0.0006	GVL 4	601	1.02	0.99	1.01	1.006667	0.0010	GVL2	83	1.06	0.825	1.02	0.968	0.001
GVL 4	553	0.474	0.487	0.474	0.478333	0.0005	**BHID**	**Depth**	**Reading 1**	**Reading 2**	**Reading 3**	**Average**	**SI Units**	GVL2	84	1.39	1.37	1.46	1.407	0.001
GVL 4	554	0.277	0.289	0.29	0.285333	0.0003	GVL2	36	0.441	0.441	0.387	0.423	0.000	GVL2	85	0.824	1.05	0.961	0.945	0.001
GVL 4	555	0.316	0.334	0.341	0.330333	0.0003	GVL2	37	0.445	0.482	0.634	0.520	0.001	GVL2	86	0.934	0.878	1.1	0.971	0.001
GVL 4	556	0.102	0.102	0.104	0.102667	0.0001	GVL2	38					0.000	GVL2	87	1.15	1	0.886	1.012	0.001
GVL 4	557	0.547	0.517	0.514	0.526	0.0005	GVL2	39	0.32	0.388	0.506	0.405	0.000	GVL2	88	1.1	1.11	1.18	1.130	0.001
GVL 4	558	5.98	5.54	5.5	5.673333	0.0057	GVL2	40	0.434	0.352	0.41	0.399	0.000	GVL2	89	1.34	1.14	1.25	1.243	0.001
GVL 4	559	0.257	0.26	0.263	0.26	0.0003	GVL2	41					0.000	GVL2	90	1.33	1.17	1.15	1.217	0.001
GVL 4	560	0.533	0.576	0.561	0.556667	0.0006	GVL2	42	0.347	0.217	0.258	0.274	0.000	GVL2	91	0.874	1.06	1.14	1.025	0.001
GVL 4	561	0.341	0.364	0.358	0.354333	0.0004	GVL2	43	0.407	0.313	0.291	0.337	0.000	GVL2	92	1.34	1.56	1.52	1.473	0.001
GVL 4	562	0.617	0.618	0.61	0.615	0.0006	GVL2	44	0.347	0.262	0.344	0.318	0.000	GVL2	93	1.75	1.69	1.87	1.770	0.002
GVL 4	563	1.17	1.17	1.05	1.13	0.0011	GVL2	45	0.359	0.22	0.231	0.270	0.000	GVL2	94	2.7	2.06	2.08	2.280	0.002
GVL 4	564	0.184	0.182	0.187	0.184333	0.0002	GVL2	46	0.18	0.141	0.202	0.174	0.000	GVL2	95	2.21	1.91	2.15	2.090	0.002
GVL 4	565	0.586	0.568	0.586	0.58	0.0006	GVL2	47					0.000	GVL2	96	2.04	1.9	1.88	1.940	0.002
GVL 4	566	0.266	0.232	0.23	0.242667	0.0002	GVL2	48	0.196	0.217	0.263	0.225	0.000	GVL2	97	1.3	1.55	1.73	1.527	0.002
GVL 4	567	0.849	0.862	0.808	0.839667	0.0008	GVL2	49	0.693	0.576	0.824	0.698	0.001	GVL2	98	2.04	2.1	1.95	2.030	0.002
GVL 4	568	0.575	0.592	0.59	0.585667	0.0006	GVL2	50	0.162	0.162	0.187	0.170	0.000	GVL2	99	2.29	2.28	2.25	2.273	0.002
GVL 4	569	73.4	73.8	75.1	74.1	0.0741	GVL2	51	0.413	0.208	0.249	0.290	0.000	GVL2	100	1.67	2.14	1.91	1.907	0.002
GVL 4	570	0.562	0.46	0.584	0.535333	0.0005	GVL2	52	0.099	0.111	0.103	0.104	0.000	GVL2	101	1.82	1.82	1.95	1.863	0.002
GVL 4	571	0.654	0.569	0.541	0.588	0.0006	GVL2	53	0.212	0.213	0.208	0.211	0.000	GVL2	102	1.15	1.18	1.15	1.160	0.001
GVL 4	572	0.7	0.764	0.78	0.748	0.0007	GVL2	54	0.189	0.233	0.185	0.202	0.000	GVL2	103	1.01	1.06	1.05	1.040	0.001
GVL 4	573	0.483	0.524	0.582	0.529667	0.0005	GVL2	55	0.23	0.188	0.214	0.211	0.000	GVL2	104	1.77	1.73	1.73	1.743	0.002

rr

Appendix E: Magnetic Susceptibility

BHID	Depth	Reading 1	Reading 2	Reading 3	Average	SI Units	BHID	Depth	Reading 1	Reading 2	Reading 3	Average	SI Units	BHID	Depth	Reading 1	Reading 2	Reading 3	Average	SI Units
GVL2	105	0.689	0.701	0.699	0.696	0.001	GVL2	154	0.366	0.328	0.37	0.355	0.000	GVL2	203	0.656	0.603	0.771	0.677	0.001
GVL2	106	0.679	0.678	0.667	0.675	0.001	GVL2	155	0.231	0.265	0.282	0.259	0.000	GVL2	204	0.17	0.147	0.172	0.163	0.000
GVL2	107	1.46	1.53	1.54	1.510	0.002	GVL2	156	0.37	0.362	0.381	0.371	0.000	GVL2	205	9.1	9.1	9.52	9.240	0.009
GVL2	108	1.12	1.18	1.16	1.153	0.001	GVL2	157					0.000	GVL2	206	3.16	3.32	3.17	3.217	0.003
GVL2	109	1.08	1.07	1.07	1.073	0.001	GVL2	158					0.000	GVL2	207	0.725	0.801	0.906	0.811	0.001
GVL2	110	0.754	0.79	0.853	0.799	0.001	GVL2	159	0.326	0.325	0.325	0.325	0.000	GVL2	208	2.75	2.98	2.79	2.840	0.003
GVL2	111	0.87	0.905	0.883	0.886	0.001	GVL2	160	1.05	1.11	1.08	1.080	0.001	GVL2	209	2.96	2.91	2.99	2.953	0.003
GVL2	112	2.06	1.94	1.95	1.983	0.002	GVL2	161	2.76	2.86	2.88	2.833	0.003	GVL2	210	8.74	8.66	8.7	8.700	0.009
GVL2	113	0.936	1.05	1.02	1.002	0.001	GVL2	162	1.46	1.44	1.45	1.450	0.001	GVL2	211	6.62	6.39	6.2	6.403	0.006
GVL2	114	1.85	2.09	2.22	2.053	0.002	GVL2	163	2.28	2.34	2.31	2.310	0.002	GVL2	212	9.27	7.77	9.04	8.693	0.009
GVL2	115	1.74	1.95	1.97	1.887	0.002	GVL2	164	2.58	2.45	2.62	2.550	0.003	GVL2	213	9.98	9.3	10	9.760	0.010
GVL2	116	1.77	1.79	1.78	1.780	0.002	GVL2	165	2.32	2.26	2.34	2.307	0.002	GVL2	214	4.47	4.87	4.57	4.637	0.005
GVL2	117	1.92	2.07	2.12	2.037	0.002	GVL2	166	2.3	2.26	2.29	2.283	0.002	GVL2	215	6.23	6.03	5.82	6.027	0.006
GVL2	118	1.54	1.52	1.52	1.527	0.002	GVL2	167	2.31	2.08	2.39	2.260	0.002	GVL2	216	7.61	8.27	8.6	8.160	0.008
GVL2	119	1.53	1.39	1.47	1.463	0.001	GVL2	168	1.61	1.64	1.63	1.627	0.002	GVL2	217	10.3	9.87	10	10.057	0.010
GVL2	120	1.4	1.43	1.49	1.440	0.001	GVL2	169	1.17	1.15	1.14	1.153	0.001	GVL2	218	11.1	10.8	10.9	10.933	0.011
GVL2	121	2.08	2.14	2.13	2.117	0.002	GVL2	170	1.59	1.64	1.6	1.610	0.002	GVL2	219	12.7	11.6	12.1	12.133	0.012
GVL2	122	1.83	1.73	1.8	1.787	0.002	GVL2	171	1.22	1.25	1.2	1.223	0.001	GVL2	220	14	13.6	13.9	13.833	0.014
GVL2	123	1.34	1.3	1.29	1.310	0.001	GVL2	172	1.91	2	2.04	1.983	0.002	GVL2	221	10.7	10.7	10.8	10.733	0.011
GVL2	124	0.898	1.03	1.07	0.999	0.001	GVL2	173	1.91	1.89	1.97	1.923	0.002	GVL2	222	31.7	30.9	28.5	30.367	0.030
GVL2	125	1.12	1.19	1.23	1.180	0.001	GVL2	174	1.46	1.6	1.56	1.540	0.002	GVL2	223	19.1	18.9	15.6	17.867	0.018
GVL2	126	1.26	1.26	1.27	1.263	0.001	GVL2	175	1.98	2	2.04	2.007	0.002	GVL2	224	7.79	8.66	9.17	8.540	0.009
GVL2	127	0.764	0.768	0.775	0.769	0.001	GVL2	176	1.94	2.01	2.02	1.990	0.002	GVL2	225	1	0.984	0.973	0.986	0.001
GVL2	128	1.1	1.25	1.22	1.190	0.001	GVL2	177	1.01	1.01	1.03	1.017	0.001	GVL2	226	19.5	19.4	19.5	19.467	0.019
GVL2	129	1.25	1.18	1.15	1.193	0.001	GVL2	178	2.16	2.2	2.25	2.203	0.002	GVL2	227	0.825	0.829	0.826	0.827	0.001
GVL2	130	1.9	1.14	1.741	1.594	0.002	GVL2	179	0.72	0.707	0.699	0.709	0.001	GVL2	228	4.99	4.64	4.31	4.647	0.005
GVL2	131	1.98	2.01	1.96	1.983	0.002	GVL2	180	4.6	4.93	4.63	4.720	0.005	GVL2	229	10.1	9.63	10.3	10.010	0.010
GVL2	132	2.13	2.06	2.08	2.090	0.002	GVL2	181	3.01	2.89	2.82	2.907	0.003	GVL2	230	0.989	1.04	1.05	1.026	0.001
GVL2	133	1.77	1.95	1.89	1.870	0.002	GVL2	182	5.46	5.32	5.47	5.417	0.005	GVL2	231	0.702	0.774	0.721	0.732	0.001
GVL2	134	1.56	1.26	1.52	1.447	0.001	GVL2	183	7.55	7.66	7.97	7.727	0.008	GVL2	232	0.752	0.708	0.682	0.714	0.001
GVL2	135	2.21	2.27	2.25	2.243	0.002	GVL2	184	2.78	2.88	2.84	2.833	0.003	GVL2	233	0.497	0.546	0.502	0.515	0.001
GVL2	136	2.49	2.54	2.48	2.503	0.003	GVL2	185	4.79	4.68	4.95	4.807	0.005	GVL2	234	1.31	1.35	1.36	1.340	0.001
GVL2	137	1.71	1.65	1.66	1.673	0.002	GVL2	186	2.51	2.53	2.52	2.520	0.003	GVL2	235	2.57	2.43	2.61	2.537	0.003
GVL2	138	1.52	1.44	1.52	1.493	0.001	GVL2	187	5.31	5.42	5.36	5.363	0.005	GVL2	236	2.07	2.24	2.2	2.170	0.002
GVL2	139	1.73	1.76	1.75	1.747	0.002	GVL2	188	3.55	3.6	3.6	3.583	0.004	GVL2	237	2.62	2.44	2.4	2.487	0.002
GVL2	140	1.72	1.93	1.88	1.843	0.002	GVL2	189	4.74	4.68	4.7	4.707	0.005	GVL2	238	2.5	2.55	2.56	2.537	0.003
GVL2	141	1.18	1.25	1.28	1.237	0.001	GVL2	190	2.59	2.63	2.66	2.627	0.003	GVL2	239	2.44	2.44	2.5	2.460	0.002
GVL2	142	2.55	2.54	2.41	2.500	0.003	GVL2	191	3.06	3.27	3.08	3.137	0.003	GVL2	240	2.6	2.66	2.66	2.640	0.003
GVL2	143	2.27	2.25	1.66	2.060	0.002	GVL2	192	4.67	4.85	5.07	4.863	0.005	GVL2	241	2.27	2.24	2.25	2.253	0.002
GVL2	144	3.41	3.4	3.37	3.393	0.003	GVL2	193	5.52	5.54	5.08	5.380	0.005	GVL2	242	5.19	5.11	5.1	5.133	0.005
GVL2	145	3.32	3.34	3.33	3.330	0.003	GVL2	194	2.03	1.89	2.19	2.037	0.002	GVL2	243	3.5	3.55	3.6	3.550	0.004
GVL2	146	2.96	3.09	3.06	3.037	0.003	GVL2	195	2.93	3	3.18	3.037	0.003	GVL2	244	4.7	4.7	4.69	4.697	0.005
GVL2	147	2.95	2.99	2.98	2.973	0.003	GVL2	196	3.19	3.55	3.83	3.523	0.004	GVL2	245	4.97	4.74	4.83	4.847	0.005
GVL2	148	3.13	3.21	3.14	3.160	0.003	GVL2	197	4.54	4.83	4.98	4.783	0.005	GVL2	246	5.64	5.76	5.74	5.713	0.006
GVL2	149	2.19	2.19	2.22	2.200	0.002	GVL2	198	3.57	3.51	3.67	3.583	0.004	GVL2	247	1.76	1.92	2.04	1.907	0.002
GVL2	150	4.17	4.26	4.3	4.243	0.004	GVL2	199	4.02	4.31	4.3	4.210	0.004	GVL2	248	1.34	1.38	1.45	1.390	0.001
GVL2	151	1.01	0.856	0.959	0.942	0.001	GVL2	200	2.77	2.8	2.86	2.810	0.003	GVL2	249	0.886	0.881	0.885	0.884	0.001
GVL2	152	3.23	3.23	3.19	3.217	0.003	GVL2	201	2.33	2.51	2.62	2.487	0.002	GVL2	250	1.02	1	0.98	1.000	0.001
GVL2	153	3.06	3.01	3.02	3.030	0.003	GVL2	202	13.9	13.5	13.9	13.767	0.014	GVL2	251	1.28	1.31	1.32	1.303	0.001

SS

Appendix E: Magnetic Susceptibility

BHID	Depth	Reading 1	Reading 2	Reading 3	Average	SI Units	BHID	Depth	Reading 1	Reading 2	Reading 3	Average	SI Units	BHID	Depth	Reading 1	Reading 2	Reading 3	Average	SI Units
GVL2	252	1.24	1.24	1.18	1.220	0.001	GVL2	301	0.078	0.076	0.076	0.077	0.000	GVL6	42.00	0.066	0.059	0.056	0.060	0.000
GVL2	253	1.14	1.12	1.08	1.113	0.001	GVL2	302	0.085	0.088	0.083	0.085	0.000	GVL6	43.00	0.075	0.079	0.063	0.072	0.000
GVL2	254	2.7	2.91	3.24	2.950	0.003	GVL2	303	0.014	0.022	0.023	0.020	0.000	GVL6	44.00	0.081	0.062	0.065	0.069	0.000
GVL2	255	1.47	1.42	1.44	1.443	0.001	GVL2	304	0.27	0.232	0.227	0.243	0.000	GVL6	45.00	0.029	0.031	0.034	0.031	0.000
GVL2	256	1.53	1.86	2.02	1.803	0.002	GVL2	305	0.009	0.016	0.016	0.014	0.000	GVL6	46.00	23.200	16.300	15.900	18.467	0.018
GVL2	257	0.482	0.503	0.545	0.510	0.001	GVL2	306	0.018	0.015	0.017	0.017	0.000	GVL6	47.00	0.073	0.077	0.079	0.076	0.000
GVL2	258	0.282	0.292	0.287	0.287	0.000	GVL2	307	0.016	0.012	0.012	0.013	0.000	GVL6	48.00	C.C				0.000
GVL2	259	1.17	1.11	1.33	1.203	0.001	GVL2	308	0.013	0.016	0.013	0.014	0.000	GVL6	49.00	C.C				0.000
GVL2	260	2.6	3.37	3.81	3.260	0.003	GVL2	309	0.03	0.029	0.026	0.028	0.000	GVL6	50.00	C.C				0.000
GVL2	261	0.149	0.146	1.47	0.588	0.001	GVL2	310	0.016	0.013	0.015	0.015	0.000	GVL6	51.00	C.C				0.000
GVL2	262	0.309	0.262	0.271	0.281	0.000	GVL2	311	0.043	0.045	0.046	0.045	0.000	GVL6	52.00	C.C				0.000
GVL2	263	1.35	1.54	1.61	1.500	0.002	**BHID**	**Depth**	**Reading 1**	**Reading 2**	**Reading 3**	**Average**	**SI Units**	GVL6	53.00	C.C				0.000
GVL2	264	0.228	0.304	0.25	0.261	0.000	GVL6	5.50	0.116	0.248	0.289	0.218	0.000	GVL6	54.00	C.C				0.000
GVL2	265	0.735	0.777	0.738	0.750	0.001	GVL6	6.00	0.138	0.206	0.204	0.183	0.000	GVL6	55.00	C.C				0.000
GVL2	266	2.56	2.75	2.74	2.683	0.003	GVL6	7.00	0.134	0.195	0.132	0.154	0.000	GVL6	56.00	C.C				0.000
GVL2	267	0.289	0.293	0.288	0.290	0.000	GVL6	8.00	0.307	0.293	0.362	0.321	0.000	GVL6	57.00	C.C				0.000
GVL2	268	1.36	1.4	1.4	1.387	0.001	GVL6	9.00	0.252	0.216	0.256	0.241	0.000	GVL6	58.00	C.C				0.000
GVL2	269	3.01	3.16	3.19	3.120	0.003	GVL6	10.00	0.059	0.082	0.073	0.071	0.000	GVL6	59.00	C.C				0.000
GVL2	270	1.32	1.37	1.39	1.360	0.001	GVL6	11.00	0.076	0.074	0.074	0.075	0.000	GVL6	60.00	C.C				0.000
GVL2	271	3.28	3.43	3.28	3.330	0.003	GVL6	12.00	0.122	0.151	0.127	0.133	0.000	GVL6	61.00	C.C				0.000
GVL2	272	1.95	1.91	1.9	1.920	0.002	GVL6	13.00	0.080	0.074	0.074	0.076	0.000	GVL6	62.00	C.C				0.000
GVL2	273	0.687	0.683	0.71	0.693	0.001	GVL6	14.00	0.114	0.105	0.097	0.105	0.000	GVL6	63.00	C.C				0.000
GVL2	274	0.346	0.347	0.349	0.347	0.000	GVL6	15.00	0.016	0.042	0.033	0.030	0.000	GVL6	64.00	C.C				0.000
GVL2	275	1.65	1.75	1.81	1.737	0.002	GVL6	16.00	0.059	0.085	0.079	0.074	0.000	GVL6	65.00	C.C				0.000
GVL2	276	7.66	7.58	7.55	7.597	0.008	GVL6	17.00	0.094	0.062	0.070	0.075	0.000	GVL6	66.00	C.C				0.000
GVL2	277	2.23	2.28	2.28	2.263	0.002	GVL6	18.00	0.071	0.067	0.035	0.058	0.000	GVL6	67.00	C.C				0.000
GVL2	278	0.011	0.006	0.012	0.010	0.000	GVL6	19.00	0.093	0.067	0.103	0.088	0.000	GVL6	68.00	C.C				0.000
GVL2	279	0.88	0.995	0.979	0.951	0.001	GVL6	20.00	0.011	0.014	0.015	0.013	0.000	GVL6	69.00	C.C				0.000
GVL2	280	1.34	1.26	1.47	1.357	0.001	GVL6	21.00	0.022	0.022	0.016	0.020	0.000	GVL6	70.00	C.C				0.000
GVL2	281	0.24	0.24	0.24	0.240	0.000	GVL6	22.00	0.047	0.058	0.050	0.052	0.000	GVL6	71.00	C.C				0.000
GVL2	282	0.249	0.235	0.213	0.232	0.000	GVL6	23.00	0.084	0.065	0.090	0.080	0.000	GVL6	72.00	C.C				0.000
GVL2	283	0.88	0.87	0.9	0.883	0.001	GVL6	24.00	0.168	0.121	0.187	0.159	0.000	GVL6	73.00	C.C				0.000
GVL2	284	0.032	0.032	0.035	0.033	0.000	GVL6	25.00	0.104	0.099	0.127	0.110	0.000	GVL6	74.00	C.C				0.000
GVL2	285	0.039	0.038	0.037	0.038	0.000	GVL6	26.00	0.121	0.105	0.121	0.116	0.000	GVL6	75.00	C.C				0.000
GVL2	286	0.112	0.111	0.112	0.112	0.000	GVL6	27.00	0.107	0.063	0.090	0.087	0.000	GVL6	76.00	C.C				0.000
GVL2	287	0.072	0.076	0.077	0.075	0.000	GVL6	28.00	0.331	0.299	0.235	0.288	0.000	GVL6	77.00	C.C				0.000
GVL2	288	28.8	28.9	29	28.900	0.029	GVL6	29.00	0.089	0.075	0.094	0.086	0.000	GVL6	78.00	C.C				0.000
GVL2	289	12.2	12.1	12.2	12.167	0.012	GVL6	30.00	0.084	0.058	0.050	0.064	0.000	GVL6	79.00	C.C				0.000
GVL2	290	10.6	11.3	10.7	10.867	0.011	GVL6	31.00	0.081	0.083	0.103	0.089	0.000	GVL6	80.00	C.C				0.000
GVL2	291	19.7	21	23.8	21.500	0.022	GVL6	32.00	0.102	0.065	0.061	0.076	0.000	GVL6	81.00	C.C				0.000
GVL2	292	25.2	25.9	26	25.700	0.026	GVL6	33.00	0.089	0.074	0.094	0.086	0.000	GVL6	82.00	C.C				0.000
GVL2	293	26.7	27	26.4	26.700	0.027	GVL6	34.00	0.044	0.050	0.057	0.050	0.000	GVL6	83.00	C.C				0.000
GVL2	294	16.7	17.3	17.5	17.167	0.017	GVL6	35.00	0.058	0.072	0.080	0.070	0.000	GVL6	84.00	0.109	0.093	0.100	0.101	0.000
GVL2	295	33.2	33.3	33.2	33.233	0.033	GVL6	36.00	0.093	0.081	0.066	0.080	0.000	GVL6	84.80	174.000	139.000	577.000	296.667	0.297
GVL2	296	40.1	42	42.5	41.533	0.042	GVL6	37.00	0.050	0.063	0.062	0.058	0.000	GVL6	85.00	1.200	1.180	1.120	1.167	0.001
GVL2	297	40.2	40.1	40.3	40.200	0.040	GVL6	38.00	0.061	0.062	0.064	0.062	0.000	GVL6	86.00	0.267	0.239	0.192	0.233	0.000
GVL2	298	36	36.3	36.1	36.133	0.036	GVL6	39.00	0.094	0.082	0.108	0.095	0.000	GVL6	87.00	0.179	0.211	0.211	0.200	0.000
GVL2	299	35.8	35.3	35.8	35.633	0.036	GVL6	40.00	0.079	0.058	0.064	0.067	0.000	GVL6	88.00	0.175	0.165	0.147	0.162	0.000
GVL2	300	11.4	11.4	9.67	10.823	0.011	GVL6	41.00	0.118	0.121	0.134	0.124	0.000	GVL6	89.00	0.497	0.347	0.369	0.404	0.000

tt

Appendix E: Magnetic Susceptibility

BHID	Depth	Reading 1	Reading 2	Reading 3	Average	SI Units	BHID	Depth	Reading 1	Reading 2	Reading 3	Average	SI Units	BHID	Depth	Reading 1	Reading 2	Reading 3	Average	SI Units
GVL6	90.00	0.158	0.176	0.166	0.167	0.000	GVL6	138.00	0.048	0.041	0.032	0.040	0.000	GVL6	187.00	0.127	0.096	0.067	0.097	0.000
GVL6	91.00	0.181	0.141	0.156	0.159	0.000	GVL6	139.00	0.094	0.085	0.095	0.091	0.000	GVL6	188.00	0.085	0.122	0.094	0.100	0.000
GVL6	92.00	0.127	0.138	0.137	0.134	0.000	GVL6	140.00	0.074	0.071	0.051	0.065	0.000	GVL6	189.00	0.218	0.240	0.245	0.234	0.000
GVL6	92.70	214.000	125.000	174.000	171.000	0.171	GVL6	141.00	0.030	0.029	0.019	0.026	0.000	GVL6	190.00	0.124	0.075	0.079	0.093	0.000
GVL6	93.00	0.504	0.441	0.357	0.434	0.000	GVL6	142.00	0.037	0.045	0.043	0.042	0.000	GVL6	191.00	0.089	0.076	0.090	0.085	0.000
GVL6	94.00	0.111	0.130	0.121	0.121	0.000	GVL6	143.00	0.074	0.068	0.056	0.066	0.000	GVL6	192.00	0.093	0.081	0.059	0.078	0.000
GVL6	95.00	0.095	0.091	0.106	0.097	0.000	GVL6	144.00	0.057	0.062	0.059	0.059	0.000	GVL6	193.00	0.073	0.042	0.080	0.065	0.000
GVL6	96.00	0.212	0.126	0.104	0.147	0.000	GVL6	145.00	0.033	0.031	0.030	0.031	0.000	GVL6	194.00	0.051	0.068	0.050	0.056	0.000
GVL6	97.00	0.140	0.154	0.168	0.154	0.000	GVL6	146.00	0.090	0.101	0.115	0.102	0.000	GVL6	195.00	0.390	0.354	0.290	0.345	0.000
GVL6	98.00	0.211	0.203	0.183	0.199	0.000	GVL6	147.00	0.088	0.101	0.102	0.097	0.000	GVL6	196.00	0.141	0.155	0.100	0.132	0.000
GVL6	99.00	0.357	0.354	0.351	0.354	0.000	GVL6	148.00	0.131	0.117	0.115	0.121	0.000	GVL6	197.00	0.027	0.060	0.086	0.058	0.000
GVL6	100.00	0.170	0.145	0.148	0.154	0.000	GVL6	149.00	0.067	0.074	0.091	0.077	0.000	GVL6	198.00	0.076	0.086	0.081	0.081	0.000
GVL6	101.00	0.132	0.086	0.121	0.113	0.000	GVL6	150.00	0.102	0.120	0.116	0.113	0.000	GVL6	199.00	0.039	0.030	0.023	0.031	0.000
GVL6	102.00	0.410	0.411	0.412	0.411	0.000	GVL6	151.00	0.102	0.108	0.113	0.108	0.000	GVL6	200.00	0.061	0.102	0.148	0.104	0.000
GVL6	103.00	0.208	0.250	0.276	0.245	0.000	GVL6	152.00	0.072	0.077	0.084	0.078	0.000	GVL6	201.00	0.099	0.106	0.118	0.108	0.000
GVL6	104.00	0.109	0.116	0.127	0.117	0.000	GVL6	153.00	0.157	0.164	0.186	0.169	0.000	GVL6	202.00	0.052	0.063	0.085	0.067	0.000
GVL6	105.00	0.298	0.331	0.292	0.307	0.000	GVL6	154.00	0.163	0.181	0.180	0.175	0.000	GVL6	203.00	0.063	0.088	0.163	0.105	0.000
GVL6	106.00	0.672	0.340	0.294	0.435	0.000	GVL6	155.00	0.087	0.094	0.078	0.086	0.000	GVL6	204.00	0.173	0.234	0.142	0.183	0.000
GVL6	107.00	0.652	0.707	0.694	0.684	0.001	GVL6	156.00	0.115	0.112	0.128	0.118	0.000	GVL6	205.00	1.880	0.352	0.215	0.816	0.001
GVL6	108.00	0.074	0.068	0.066	0.069	0.000	GVL6	157.00	0.082	0.045	0.082	0.070	0.000	GVL6	206.00	0.271	0.547	0.697	0.505	0.001
GVL6	109.00	0.027	0.030	0.030	0.029	0.000	GVL6	158.00	0.060	0.079	0.084	0.074	0.000	GVL6	207.00	0.542	0.473	0.503	0.506	0.001
GVL6	110.00	0.032	0.040	0.038	0.037	0.000	GVL6	159.00	0.088	0.097	0.064	0.083	0.000	GVL6	208.00	0.235	0.194	0.250	0.226	0.000
GVL6	111.00	0.088	0.084	0.068	0.080	0.000	GVL6	160.00	0.021	0.034	0.032	0.029	0.000	GVL6	209.00	0.652	0.589	0.532	0.591	0.001
GVL6	112.00	0.052	0.077	0.062	0.064	0.000	GVL6	161.00	0.066	0.074	0.068	0.069	0.000	GVL6	210.00	1.120	0.947	1.150	1.072	0.001
GVL6	113.00	0.072	0.069	0.064	0.068	0.000	GVL6	162.00	0.094	0.076	0.074	0.081	0.000	GVL6	211.00	1.760	1.110	1.030	1.300	0.001
GVL6	114.00	0.041	0.039	0.043	0.041	0.000	GVL6	163.00	0.054	0.087	0.081	0.074	0.000	GVL6	212.00	0.000	0.000	0.000	0.000	0.000
GVL6	115.00	0.032	0.025	0.026	0.028	0.000	GVL6	164.00	0.098	0.105	0.095	0.099	0.000	GVL6	213.00	0.391	0.432	0.379	0.401	0.000
GVL6	116.00	0.023	0.028	0.029	0.027	0.000	GVL6	165.00	0.278	0.322	0.350	0.317	0.000	GVL6	214.00	0.070	0.102	0.065	0.079	0.000
GVL6	117.00	0.050	0.047	0.039	0.045	0.000	GVL6	166.00	14.900	12.200	12.200	13.100	0.013	GVL6	215.00	0.165	0.203	0.191	0.186	0.000
GVL6	118.00	0.078	0.052	0.039	0.056	0.000	GVL6	167.00	0.073	0.108	0.076	0.086	0.000	GVL6	216.00	0.159	0.188	0.128	0.158	0.000
GVL6	119.00	0.054	0.061	0.060	0.058	0.000	GVL6	168.00	0.070	0.069	0.055	0.065	0.000	GVL6	217.00	0.748	0.732	1.070	0.850	0.001
GVL6	120.00	0.041	0.036	0.059	0.045	0.000	GVL6	169.00	0.112	0.125	0.163	0.133	0.000	GVL6	218.00	0.170	0.180	0.218	0.189	0.000
GVL6	121.00	0.068	0.048	0.064	0.060	0.000	GVL6	170.00	0.062	0.081	0.111	0.085	0.000	GVL6	219.00	0.248	0.296	0.204	0.249	0.000
GVL6	122.00	0.035	0.030	0.026	0.030	0.000	GVL6	171.00	0.129	0.131	0.154	0.138	0.000	GVL6	220.00	0.692	0.666	0.813	0.724	0.001
GVL6	123.00	0.013	0.020	0.011	0.015	0.000	GVL6	172.00	0.188	0.185	0.165	0.179	0.000	GVL6	221.00	0.573	0.552	0.531	0.552	0.001
GVL6	124.00	0.032	0.034	0.041	0.036	0.000	GVL6	173.00	0.087	0.082	0.090	0.086	0.000	GVL6	222.00	0.287	0.207	0.365	0.286	0.000
GVL6	125.00	0.042	0.055	0.044	0.047	0.000	GVL6	174.00	0.235	0.281	0.268	0.261	0.000	GVL6	223.00	1.270	1.440	1.430	1.380	0.001
GVL6	126.00	0.034	0.051	0.052	0.046	0.000	GVL6	175.00	0.304	0.242	0.214	0.253	0.000	GVL6	224.00	0.182	0.247	0.333	0.254	0.000
GVL6	127.00					0.000	GVL6	176.00	0.197	0.251	0.235	0.228	0.000	GVL6	225.00	0.360	0.282	0.240	0.294	0.000
GVL6	128.00					0.000	GVL6	177.00	0.106	0.125	0.136	0.122	0.000	GVL6	226.00	0.990	1.230	1.200	1.140	0.001
GVL6	129.00					0.000	GVL6	178.00	0.015	0.015	0.021	0.017	0.000	GVL6	227.00	0.109	0.076	0.087	0.091	0.000
GVL6	130.00					0.000	GVL6	179.00	0.118	0.114	0.121	0.118	0.000	GVL6	228.00	0.221	0.255	0.209	0.228	0.000
GVL6	131.00	0.028	0.036	0.032	0.032	0.000	GVL6	180.00	0.264	0.548	0.288	0.367	0.000	GVL6	229.00	0.028	0.005	0.011	0.015	0.000
GVL6	132.00	0.032	0.031	0.040	0.034	0.000	GVL6	181.00	0.583	0.541	0.587	0.570	0.001	GVL6	230.00	0.029	0.019	0.055	0.034	0.000
GVL6	133.00	0.040	0.027	0.040	0.036	0.000	GVL6	182.00	0.003	0.004	0.002	0.003	0.000	GVL6	231.00	0.006	0.013	0.010	0.010	0.000
GVL6	134.00	0.039	0.033	0.032	0.035	0.000	GVL6	183.00	0.150	0.199	0.201	0.183	0.000	GVL6	232.00	0.000	0.009	0.015	0.008	0.000
GVL6	135.00	0.036	0.033	0.042	0.037	0.000	GVL6	184.00	0.163	0.154	0.177	0.165	0.000	GVL6	233.00	1.000	0.800	0.939	0.913	0.001
GVL6	136.00	0.049	0.030	0.030	0.036	0.000	GVL6	185.00	0.217	0.245	0.190	0.217	0.000	GVL6	234.00	0.024	0.021	0.036	0.027	0.000
GVL6	137.00	0.025	0.028	0.023	0.025	0.000	GVL6	186.00	0.228	0.225	0.218	0.224	0.000	GVL6	235.00	4.910	4.580	6.330	5.273	0.005

uu

Appendix E: Magnetic Susceptibility

BHID	Depth	Reading 1	Reading 2	Reading 3	Average	SI Units	BHID	Depth	Reading 1	Reading 2	Reading 3	Average	SI Units	BHID	Depth	Reading 1	Reading 2	Reading 3	Average	SI Units
GVL6	236.00	0.224	0.246	0.251	0.240	0.000	GVL6	285.00	missing core				0.000	GVL6	334.00	missing core				0.000
GVL6	237.00	0.043	0.101	0.103	0.082	0.000	GVL6	286.00	missing core				0.000	GVL6	335.00	missing core				0.000
GVL6	238.00	0.192	0.520	0.091	0.268	0.000	GVL6	287.00	missing core				0.000	GVL6	336.00	missing core				0.000
GVL6	239.00	0.038	0.023	0.060	0.040	0.000	GVL6	288.00	missing core				0.000	GVL6	337.00	missing core				0.000
GVL6	240.00	0.019	0.011	0.056	0.029	0.000	GVL6	289.00	missing core				0.000	GVL6	338.00	missing core				0.000
GVL6	241.00	0.023	0.015	0.056	0.031	0.000	GVL6	290.00	missing core				0.000	GVL6	339.00	missing core				0.000
GVL6	242.00	0.015	0.000	0.010	0.008	0.000	GVL6	291.00	missing core				0.000	GVL6	340.00	missing core				0.000
GVL6	243.00	0.030	0.043	0.049	0.041	0.000	GVL6	292.00	missing core				0.000	GVL6	341.00	missing core				0.000
GVL6	244.00	0.165	0.127	0.094	0.129	0.000	GVL6	293.00	missing core				0.000	GVL6	342.00	missing core				0.000
GVL6	245.00	0.038	0.030	0.032	0.033	0.000	GVL6	294.00	missing core				0.000	GVL6	343.00	missing core				0.000
GVL6	246.00	0.920	0.514	0.429	0.621	0.001	GVL6	295.00	missing core				0.000	GVL6	344.00	missing core				0.000
GVL6	247.00	0.140	0.152	0.143	0.145	0.000	GVL6	296.00	missing core				0.000	GVL6	345.00	missing core				0.000
GVL6	248.00	0.087	0.129	0.194	0.137	0.000	GVL6	297.00	missing core				0.000	GVL6	346.00	missing core				0.000
GVL6	249.00	0.351	0.404	0.379	0.378	0.000	GVL6	298.00	missing core				0.000	GVL6	347.00	missing core				0.000
GVL6	250.00	0.723	0.659	0.703	0.695	0.001	GVL6	299.00	missing core				0.000	GVL6	348.00	missing core				0.000
GVL6	251.00	0.422	0.517	0.414	0.451	0.000	GVL6	300.00	missing core				0.000	GVL6	349.00	missing core				0.000
GVL6	252.00	0.332	0.321	0.366	0.340	0.000	GVL6	301.00	missing core				0.000	GVL6	350.00	missing core				0.000
GVL6	253.00	1.260	0.778	1.040	1.026	0.001	GVL6	302.00	missing core				0.000	GVL6	351.00	missing core				0.000
GVL6	254.00	0.771	0.975	0.657	0.801	0.001	GVL6	303.00	missing core				0.000	GVL6	352.00	missing core				0.000
GVL6	255.00	0.540	0.555	0.439	0.511	0.001	GVL6	304.00	missing core				0.000	GVL6	353.00	missing core				0.000
GVL6	256.00	0.772	0.687	0.724	0.728	0.001	GVL6	305.00	missing core				0.000	GVL6	354.00	missing core				0.000
GVL6	257.00	0.244	0.130	0.229	0.201	0.000	GVL6	306.00	missing core				0.000	GVL6	355.00	missing core				0.000
GVL6	258.00	missing core				0.000	GVL6	307.00	missing core				0.000	GVL6	356.00	missing core				0.000
GVL6	259.00	missing core				0.000	GVL6	308.00	missing core				0.000	GVL6	357.00	missing core				0.000
GVL6	260.00	missing core				0.000	GVL6	309.00	missing core				0.000	GVL6	358.00	missing core				0.000
GVL6	261.00	missing core				0.000	GVL6	310.00	missing core				0.000	GVL6	359.00	missing core				0.000
GVL6	262.00	missing core				0.000	GVL6	311.00	missing core				0.000	GVL6	360.00	missing core				0.000
GVL6	263.00	missing core				0.000	GVL6	312.00	missing core				0.000	GVL6	361.00	missing core				0.000
GVL6	264.00	missing core				0.000	GVL6	313.00	missing core				0.000	GVL6	362.00	missing core				0.000
GVL6	265.00	missing core				0.000	GVL6	314.00	missing core				0.000	GVL6	363.00	missing core				0.000
GVL6	266.00	missing core				0.000	GVL6	315.00	missing core				0.000	GVL6	364.00	missing core				0.000
GVL6	267.00	missing core				0.000	GVL6	316.00	missing core				0.000	GVL6	365.00	missing core				0.000
GVL6	268.00	missing core				0.000	GVL6	317.00	missing core				0.000	GVL6	366.00	missing core				0.000
GVL6	269.00	missing core				0.000	GVL6	318.00	missing core				0.000	GVL6	367.00	missing core				0.000
GVL6	270.00	missing core				0.000	GVL6	319.00	missing core				0.000	GVL6	368.00	missing core				0.000
GVL6	271.00	missing core				0.000	GVL6	320.00	missing core				0.000	GVL6	369.00	missing core				0.000
GVL6	272.00	missing core				0.000	GVL6	321.00	missing core				0.000	GVL6	370.00	missing core				0.000
GVL6	273.00	missing core				0.000	GVL6	322.00	missing core				0.000	GVL6	371.00	missing core				0.000
GVL6	274.00	missing core				0.000	GVL6	323.00	missing core				0.000	GVL6	372.00	missing core				0.000
GVL6	275.00	missing core				0.000	GVL6	324.00	missing core				0.000	GVL6	373.00	missing core				0.000
GVL6	276.00	missing core				0.000	GVL6	325.00	missing core				0.000	GVL6	374.00	missing core				0.000
GVL6	277.00	missing core				0.000	GVL6	326.00	missing core				0.000	GVL6	375.00	missing core				0.000
GVL6	278.00	missing core				0.000	GVL6	327.00	missing core				0.000	GVL6	376.00	missing core				0.000
GVL6	279.00	missing core				0.000	GVL6	328.00	missing core				0.000	GVL6	377.00	missing core				0.000
GVL6	280.00	missing core				0.000	GVL6	329.00	missing core				0.000	GVL6	378.00	missing core				0.000
GVL6	281.00	missing core				0.000	GVL6	330.00	missing core				0.000	GVL6	379.00	missing core				0.000
GVL6	282.00	missing core				0.000	GVL6	331.00	missing core				0.000	GVL6	380.00	missing core				0.000
GVL6	283.00	missing core				0.000	GVL6	332.00	missing core				0.000	GVL6	381.00	missing core				0.000
GVL6	284.00	missing core				0.000	GVL6	333.00	missing core				0.000	GVL6	382.00	missing core				0.000

Appendix E: Magnetic Susceptibility

BHID	Depth	Reading 1	Reading 2	Reading 3	Average	SI Units	BHID	Depth	Reading 1	Reading 2	Reading 3	Average	SI Units	BHID	Depth	Reading 1	Reading 2	Reading 3	Average	SI Units
GVL6	383.00	missing core				0.000	GVL6	432.00	missing core				0.000	GVL6	481.00	missing core				0.000
GVL6	384.00	missing core				0.000	GVL6	433.00	missing core				0.000	GVL6	482.00	missing core				0.000
GVL6	385.00	missing core				0.000	GVL6	434.00	missing core				0.000	GVL6	483.00	missing core				0.000
GVL6	386.00	missing core				0.000	GVL6	435.00	missing core				0.000	GVL6	484.00	missing core				0.000
GVL6	387.00	missing core				0.000	GVL6	436.00	missing core				0.000	GVL6	485.00	missing core				0.000
GVL6	388.00	missing core				0.000	GVL6	437.00	missing core				0.000	GVL6	486.00	missing core				0.000
GVL6	389.00	missing core				0.000	GVL6	438.00	missing core				0.000	GVL6	487.00	missing core				0.000
GVL6	390.00	missing core				0.000	GVL6	439.00	missing core				0.000	GVL6	488.00	missing core				0.000
GVL6	391.00	missing core				0.000	GVL6	440.00	missing core				0.000	GVL6	489.00	missing core				0.000
GVL6	392.00	missing core				0.000	GVL6	441.00	missing core				0.000	GVL6	490.00	missing core				0.000
GVL6	393.00	missing core				0.000	GVL6	442.00	missing core				0.000	GVL6	491.00	missing core				0.000
GVL6	394.00	missing core				0.000	GVL6	443.00	missing core				0.000	GVL6	492.00	missing core				0.000
GVL6	395.00	missing core				0.000	GVL6	444.00	missing core				0.000	GVL6	493.00	missing core				0.000
GVL6	396.00	missing core				0.000	GVL6	445.00	missing core				0.000	GVL6	494.00	missing core				0.000
GVL6	397.00	missing core				0.000	GVL6	446.00	missing core				0.000	GVL6	495.00	missing core				0.000
GVL6	398.00	missing core				0.000	GVL6	447.00	missing core				0.000	GVL6	496.00	missing core				0.000
GVL6	399.00	missing core				0.000	GVL6	448.00	missing core				0.000	GVL6	497.00	missing core				0.000
GVL6	400.00	missing core				0.000	GVL6	449.00	missing core				0.000	GVL6	498.00	missing core				0.000
GVL6	401.00	missing core				0.000	GVL6	450.00	missing core				0.000	GVL6	499.00	missing core				0.000
GVL6	402.00	missing core				0.000	GVL6	451.00	missing core				0.000	GVL6	500.00	missing core				0.000
GVL6	403.00	missing core				0.000	GVL6	452.00	missing core				0.000	GVL6	501.00	missing core				0.000
GVL6	404.00	missing core				0.000	GVL6	453.00	missing core				0.000	GVL6	502.00	missing core				0.000
GVL6	405.00	missing core				0.000	GVL6	454.00	missing core				0.000	GVL6	503.00	missing core				0.000
GVL6	406.00	missing core				0.000	GVL6	455.00	missing core				0.000	GVL6	504.00	missing core				0.000
GVL6	407.00	missing core				0.000	GVL6	456.00	missing core				0.000	GVL6	505.00	missing core				0.000
GVL6	408.00	missing core				0.000	GVL6	457.00	missing core				0.000	GVL6	506.00	missing core				0.000
GVL6	409.00	missing core				0.000	GVL6	458.00	missing core				0.000	GVL6	507.00	missing core				0.000
GVL6	410.00	missing core				0.000	GVL6	459.00	missing core				0.000	GVL6	508.00	missing core				0.000
GVL6	411.00	missing core				0.000	GVL6	460.00	missing core				0.000	GVL6	509.00	missing core				0.000
GVL6	412.00	missing core				0.000	GVL6	461.00	missing core				0.000	GVL6	510.00	missing core				0.000
GVL6	413.00	missing core				0.000	GVL6	462.00	missing core				0.000	GVL6	511.00	missing core				0.000
GVL6	414.00	missing core				0.000	GVL6	463.00	missing core				0.000	GVL6	512.00	missing core				0.000
GVL6	415.00	missing core				0.000	GVL6	464.00	missing core				0.000	GVL6	513.00	missing core				0.000
GVL6	416.00	missing core				0.000	GVL6	465.00	missing core				0.000	GVL6	514.00	missing core				0.000
GVL6	417.00	missing core				0.000	GVL6	466.00	missing core				0.000	GVL6	515.00	missing core				0.000
GVL6	418.00	missing core				0.000	GVL6	467.00	missing core				0.000	GVL6	516.00	missing core				0.000
GVL6	419.00	missing core				0.000	GVL6	468.00	missing core				0.000	GVL6	517.00	missing core				0.000
GVL6	420.00	missing core				0.000	GVL6	469.00	missing core				0.000	GVL6	518.00	missing core				0.000
GVL6	421.00	missing core				0.000	GVL6	470.00	missing core				0.000	GVL6	519.00	missing core				0.000
GVL6	422.00	missing core				0.000	GVL6	471.00	missing core				0.000	GVL6	520.00	missing core				0.000
GVL6	423.00	missing core				0.000	GVL6	472.00	missing core				0.000	GVL6	521.00	missing core				0.000
GVL6	424.00	missing core				0.000	GVL6	473.00	missing core				0.000	GVL6	522.00	9.550	9.540	11.500	10.197	0.010
GVL6	425.00	missing core				0.000	GVL6	474.00	missing core				0.000	GVL6	523.00	14.100	10.400	11.200	11.900	0.012
GVL6	426.00	missing core				0.000	GVL6	475.00	missing core				0.000	GVL6	524.00	17.800	17.600	18.800	18.067	0.018
GVL6	427.00	missing core				0.000	GVL6	476.00	missing core				0.000	GVL6	525.00	7.260	7.110	9.730	8.033	0.008
GVL6	428.00	missing core				0.000	GVL6	477.00	missing core				0.000	GVL6	526.00	16.100	11.400	9.150	12.217	0.012
GVL6	429.00	missing core				0.000	GVL6	478.00	missing core				0.000	GVL6	527.00	15.300	15.500	17.500	16.100	0.016
GVL6	430.00	missing core				0.000	GVL6	479.00	missing core				0.000	GVL6	528.00	8.820	6.340	7.760	7.640	0.008
GVL6	431.00	missing core				0.000	GVL6	480.00	missing core				0.000	GVL6	529.00	16.600	20.100	21.500	19.400	0.019

Appendix E: Magnetic Susceptibility

BHID	Depth	Reading 1	Reading 2	Reading 3	Average	SI Units	BHID	Depth	Reading 1	Reading 2	Reading 3	Average	SI Units	BHID	Depth	Reading 1	Reading 2	Reading 3	Average	SI Units
GVL6	530.00	31.400	31.200	31.000	31.200	0.031	GVL6	579.00	0.566	0.401	0.384	0.450	0.000	GVL 09	33	0.367	0.368	0.363	0.366	0.000366
GVL6	531.00	4.810	6.350	5.050	5.403	0.005	GVL6	580.00	0.348	0.185	0.554	0.362	0.000	GVL 09	34	0.59	0.607	0.629	0.608667	0.000609
GVL6	532.00	21.700	17.500	32.100	23.767	0.024	GVL6	581.00	2.260	2.530	1.770	2.187	0.002	GVL 09	35	0.377	0.402	0.419	0.399333	0.000399
GVL6	533.00	1.050	0.799	0.544	0.798	0.001	GVL6	582.00	1.330	1.220	1.080	1.210	0.001	GVL 09	36	0.594	0.586	0.618	0.599333	0.000599
GVL6	534.00	1.000	0.547	0.670	0.739	0.001	GVL6	583.00	0.060	0.064	0.060	0.061	0.000	GVL 09	37	0.032	0.031	0.03	0.031	0.000031
GVL6	535.00	9.490	9.040	8.890	9.140	0.009	GVL6	584.00	0.468	0.526	0.481	0.492	0.000	GVL 09	38	0.578	0.588	0.585	0.583667	0.000584
GVL6	536.00	8.280	6.500	8.520	7.767	0.008	GVL6	585.00	0.619	0.562	0.586	0.589	0.001	GVL 09	39	2.26	2.53	2.3	2.363333	0.002363
GVL6	537.00	21.200	15.100	17.300	17.867	0.018	GVL6	586.00	0.757	1.120	0.793	0.890	0.001	GVL 09	40	1.23	1.37	1.37	1.323333	0.001323
GVL6	538.00	19.200	14.700	22.700	18.867	0.019	GVL6	587.00	0.779	0.844	0.780	0.801	0.001	GVL 09	41	1.67	1.7	1.69	1.686667	0.001687
GVL6	539.00	14.400	11.700	12.700	12.933	0.013	GVL6	588.00	0.571	0.637	0.741	0.650	0.001	GVL 09	42	4.74	4.77	4.7	4.736667	0.004737
GVL6	540.00	15.900	18.300	13.100	15.767	0.016	GVL6	589.00	0.703	0.579	0.490	0.591	0.001	GVL 09	43	0.548	0.565	0.558	0.557	0.000557
GVL6	541.00	18.300	14.000	12.200	14.833	0.015	GVL6	590.00	1.790	2.000	1.950	1.913	0.002	GVL 09	44	0.589	0.695	0.708	0.664	0.000664
GVL6	542.00	44.200	30.400	39.600	38.067	0.038	GVL6	591.00	1.750	1.110	1.250	1.370	0.001	GVL 09	45	0.344	0.35	0.304	0.332667	0.000333
GVL6	543.00	7.930	5.680	4.650	6.087	0.006	GVL6	592.00	1.570	1.730	1.780	1.693	0.002	GVL 09	46	0.3	0.315	0.323	0.312667	0.000313
GVL6	544.00	9.710	11.900	12.900	11.503	0.012	GVL6	593.00	1.560	1.930	2.450	1.980	0.002	GVL 09	47	0.197	0.195	0.196	0.196	0.000196
GVL6	545.00	19.500	21.800	14.900	18.733	0.019	GVL6	594.00	0.519	0.566	0.603	0.563	0.001	GVL 09	48	0.384	0.386	0.391	0.387	0.000387
GVL6	546.00	1.910	1.870	1.410	1.730	0.002	GVL6	595.00	0.366	0.401	0.420	0.396	0.000	GVL 09	49	0.186	0.183	0.18	0.183	0.000183
GVL6	547.00	20.600	20.600	27.200	22.800	0.023	GVL6	596.00	0.940	1.100	1.160	1.067	0.001	GVL 09	50	0.253	0.244	0.234	0.243667	0.000244
GVL6	548.00	16.900	13.600	16.500	15.667	0.016	GVL6	597.00	0.305	0.338	0.452	0.365	0.000	GVL 09	51	0.3	0.312	0.325	0.312333	0.000312
GVL6	549.00	6.910	9.390	9.900	8.733	0.009	GVL6	598.00	0.722	0.557	0.457	0.579	0.001	GVL 09	52	0.265	0.276	0.285	0.275333	0.000275
GVL6	550.00	10.100	9.650	9.770	9.840	0.010	GVL6	599.00	0.266	0.272	0.275	0.271	0.000	GVL 09	53	0.062	0.059	0.056	0.059	0.000059
GVL6	551.00	18.500	16.800	15.400	16.900	0.017	GVL6	600.00	0.127	0.122	0.117	0.122	0.000	GVL 09	54	0.216	0.226	0.23	0.224	0.000224
GVL6	552.00	6.870	7.630	5.840	6.780	0.007	GVL6	601.00	0.216	0.163	0.186	0.188	0.000	GVL 09	55	0.231	0.236	0.23	0.232333	0.000232
GVL6	553.00	27.400	36.000	32.900	32.100	0.032	GVL6	602.00	0.198	0.249	0.343	0.263	0.000	GVL 09	56	0.813	0.782	0.79	0.795	0.000795
GVL6	554.00	11.300	8.380	7.150	8.943	0.009	BHID	Depth	Reading 1	Reading 2	Reading 3	Average	SI Units	GVL 09	57	0.635	0.658	0.649	0.647333	0.000647
GVL6	555.00	5.680	6.460	5.460	5.867	0.006	GVL 09	9	0.926	0.746	0.886	0.852667	0.000853	GVL 09	58	4.4	4.42	4.42	4.413333	0.004413
GVL6	556.00	13.700	10.100	6.980	10.260	0.010	GVL 09	10	0.366	0.365	0.363	0.364667	0.000365	GVL 09	59	3.09	3.23	3.27	3.196667	0.003197
GVL6	557.00	8.130	8.340	8.080	8.183	0.008	GVL 09	11	0.306	0.327	0.323	0.318667	0.000319	GVL 09	60	2.21	2.23	2.17	2.203333	0.002203
GVL6	558.00	4.090	3.080	2.680	3.283	0.003	GVL 09	12	0.274	0.271	0.268	0.271	0.000271	GVL 09	61	1.54	1.42	1.5	1.486667	0.001487
GVL6	559.00	2.250	3.370	4.860	3.493	0.003	GVL 09	13	0.372	0.362	0.376	0.37	0.00037	GVL 09	62	0.368	0.365	0.378	0.370333	0.00037
GVL6	560.00	7.700	5.520	5.560	6.260	0.006	GVL 09	14	0.332	0.302	0.323	0.319	0.000319	GVL 09	63	0.082	0.077	0.091	0.083333	8.33E-05
GVL6	561.00	6.190	12.000	11.200	9.797	0.010	GVL 09	15	0.584	0.575	0.522	0.560333	0.00056	GVL 09	64	0.87	0.877	0.875	0.874	0.000874
GVL6	562.00	7.570	6.240	6.830	6.880	0.007	GVL 09	16	0.35	0.399	0.376	0.375	0.000375	GVL 09	65	0.329	0.324	0.319	0.324	0.000324
GVL6	563.00	0.973	0.726	1.040	0.913	0.001	GVL 09	17	0.496	0.489	0.506	0.497	0.000497	GVL 09	66	1.84	1.66	1.64	1.713333	0.001713
GVL6	564.00	1.910	2.420	2.170	2.167	0.002	GVL 09	18	2.44	2.48	2.48	2.466667	0.002467	GVL 09	67	0.536	0.502	0.528	0.522	0.000522
GVL6	565.00	3.060	2.370	2.190	2.540	0.003	GVL 09	19	0.991	0.973	0.99	0.984667	0.000985	GVL 09	68	0.355	0.369	0.351	0.358333	0.000358
GVL6	566.00	2.270	1.910	1.960	2.047	0.002	GVL 09	20	0.26	0.261	0.27	0.263667	0.000264	GVL 09	69	0.43	0.455	0.514	0.466333	0.000466
GVL6	567.00	2.330	2.050	3.260	2.547	0.003	GVL 09	21	0.12	0.119	0.119	0.119333	0.000119	GVL 09	70	0.843	0.869	8.884	3.532	0.003532
GVL6	568.00	2.090	1.680	1.550	1.773	0.002	GVL 09	22	0.212	0.198	0.202	0.204	0.000204	GVL 09	71	0.359	0.386	0.464	0.403	0.000403
GVL6	569.00	2.380	2.230	2.730	2.447	0.002	GVL 09	23	0.336	0.369	0.341	0.348667	0.000349	GVL 09	72	0.699	0.858	0.855	0.804	0.000804
GVL6	570.00	3.380	3.130	3.400	3.303	0.003	GVL 09	24	0.113	0.145	0.204	0.154	0.000154	GVL 09	73	0.365	0.372	0.36	0.365667	0.000366
GVL6	571.00	4.850	3.890	3.300	4.013	0.004	GVL 09	25	0.245	0.18	0.272	0.232333	0.000232	GVL 09	74	0.412	0.467	0.46	0.446333	0.000446
GVL6	572.00	1.130	1.670	1.340	1.380	0.001	GVL 09	26	0.238	0.283	0.276	0.265667	0.000266	GVL 09	75	12.6	12.8	13.1	12.83333	0.012833
GVL6	573.00	0.635	0.649	1.010	0.765	0.001	GVL 09	27	0.139	0.234	0.248	0.207	0.000207	GVL 09	76	39.4	62.6	67.1	56.36667	0.056367
GVL6	574.00	1.310	0.326	0.422	0.686	0.001	GVL 09	28	0.23	0.225	0.237	0.230667	0.000231	GVL 09	77	22.3	23.2	23.1	22.86667	0.022867
GVL6	575.00	3.080	4.240	2.730	3.350	0.003	GVL 09	29	0.075	0.081	0.079	0.078333	7.83E-05	GVL 09	78	95.6	95.7	92.3	94.53333	0.094533
GVL6	576.00	2.630	2.290	1.960	2.293	0.002	GVL 09	30	0.09	0.082	0.081	0.084333	8.43E-05	GVL 09	79	0.401	0.406	0.398	0.401667	0.000402
GVL6	577.00	1.600	0.986	1.000	1.195	0.001	GVL 09	31	0.187	0.185	0.197	0.189667	0.00019	GVL 09	80	0.839	0.878	0.874	0.863667	0.000864
GVL6	578.00	1.650	1.000	1.270	1.307	0.001	GVL 09	32	0.537	0.545	0.549	0.543667	0.000544	GVL 09	81	0.278	0.286	0.287	0.283667	0.000284

Appendix E: Magnetic Susceptibility

BHID	Depth	Reading 1	Reading 2	Reading 3	Average	SI Units	BHID	Depth	Reading 1	Reading 2	Reading 3	Average	SI Units	BHID	Depth	Reading 1	Reading 2	Reading 3	Average	SI Units
GVL 09	82	0.423	0.37	0.385	0.392667	0.000393	GVL 09	131	23.5	24	23.8	23.76667	0.023767	GVL 09	180	2.1	2.14	2.06	2.1	0.0021
GVL 09	83	0.398	0.414	0.436	0.416	0.000416	GVL 09	132	15.3	15.9	15.6	15.6	0.0156	GVL 09	181	1.38	1.34	1.32	1.346667	0.001347
GVL 09	84	2.78	2.76	2.68	2.74	0.00274	GVL 09	133	23.2	23.8	22.4	23.13333	0.023133	GVL 09	182	9.57	9.61	9.82	9.666667	0.009667
GVL 09	85	1.13	1.15	1.11	1.13	0.00113	GVL 09	134	19.6	17	17	17.86667	0.017867	GVL 09	183	58.7	57.3	58.7	58.23333	0.058233
GVL 09	86	0.463	0.625	0.616	0.568	0.000568	GVL 09	135				#DIV/0!	#DIV/0!	GVL 09	184	31.1	30.1	28.2	29.8	0.0298
GVL 09	87	0.463	0.508	0.447	0.472667	0.000473	GVL 09	136	0.15	0.153	0.152	0.151667	0.000152	GVL 09	185	46.6	41.7	45	44.43333	0.044433
GVL 09	88	0.163	0.153	0.168	0.161333	0.000161	GVL 09	137	0.226	0.222	0.223	0.223667	0.000224	GVL 09	186	1	0.985	1.1	1.028333	0.001028
GVL 09	89	0.367	0.363	0.356	0.362	0.000362	GVL 09	138	0.219	0.25	0.241	0.236667	0.000237	GVL 09	187	39.9	41.3	38.7	39.96667	0.039967
GVL 09	90	0.438	0.459	0.467	0.454667	0.000455	GVL 09	139	0.28	0.245	0.253	0.259333	0.000259	GVL 09	188	17.9	16.1	17.4	17.13333	0.017133
GVL 09	91	0.234	0.246	0.247	0.242333	0.000242	GVL 09	140	0.276	0.274	0.269	0.273	0.000273	GVL 09	189	22.9	25.2	23.9	24	0.024
GVL 09	92	0.437	0.436	0.415	0.429333	0.000429	GVL 09	141	0.258	0.263	0.259	0.26	0.00026	GVL 09	190	5.64	5.23	5.12	5.33	0.00533
GVL 09	93	0.449	0.523	0.629	0.533667	0.000534	GVL 09	142	0.213	0.215	0.214	0.214	0.000214	GVL 09	191	5.64	5.3	5.09	5.343333	0.005343
GVL 09	94	0.366	0.362	0.369	0.365667	0.000366	GVL 09	143	0.201	0.199	0.191	0.197	0.000197	GVL 09	192	35.6	36.2	35.9	35.9	0.0359
GVL 09	95	0.48	0.544	0.911	0.645	0.000645	GVL 09	144	0.158	0.16	0.164	0.160667	0.000161	GVL 09	193	0.587	0.605	0.487	0.559667	0.00056
GVL 09	96	9.6	9.8	9.8	9.733333	0.009733	GVL 09	145	0.192	0.184	0.199	0.191667	0.000192	GVL 09	194	24.6	25	23.8	24.46667	0.024467
GVL 09	97	0.177	0.154	0.172	0.167667	0.000168	GVL 09	146	0.184	0.183	0.184	0.183667	0.000184	GVL 09	195	57.7	55.2	51.2	54.7	0.0547
GVL 09	98	33	32.8	32.6	32.8	0.0328	GVL 09	147	0.512	0.48	0.513	0.501667	0.000502	GVL 09	196	17.2	18	18.4	17.86667	0.017867
GVL 09	99	18.4	20.1	19.4	19.3	0.0193	GVL 09	148	0.169	0.65	0.647	0.488667	0.000489	GVL 09	197	28.2	28.2	28.8	28.4	0.0284
GVL 09	100	22.4	23.1	23	22.83333	0.022833	GVL 09	149	0.235	0.253	0.259	0.249	0.000249	GVL 09	198	32.5	33.4	34.7	33.53333	0.033533
GVL 09	101	14.3	14.3	14.6	14.4	0.0144	GVL 09	150	16.8	17.2	17.2	17.06667	0.017067	GVL 09	199	16.8	21.5	20.3	19.53333	0.019533
GVL 09	102	19.9	19.1	19.1	19.36667	0.019367	GVL 09	151	0.173	0.178	0.174	0.175	0.000175	GVL 09	200	0.305	0.31	0.296	0.303667	0.000304
GVL 09	103	11.1	11	10.8	10.96667	0.010967	GVL 09	152	0.332	0.303	0.311	0.315333	0.000315	GVL 09	201	0.209	0.194	0.204	0.202333	0.000202
GVL 09	104	14.1	14.6	14	14.23333	0.014233	GVL 09	153	0.179	0.182	0.172	0.177667	0.000178	GVL 09	202	0.203	0.205	0.193	0.200333	0.0002
GVL 09	105	17.1	16.9	16.9	16.96667	0.016967	GVL 09	154	0.066	0.067	0.064	0.065667	6.57E-05	GVL 09	203	0.216	0.246	0.25	0.237333	0.000237
GVL 09	106	16	15.1	14.2	15.1	0.0151	GVL 09	155	0.636	0.639	0.642	0.639	0.000639	GVL 09	204	0.851	0.848	0.911	0.87	0.00087
GVL 09	107	40.9	41.7	41.6	41.4	0.0414	GVL 09	156	0.233	0.222	0.219	0.224667	0.000225	GVL 09	205	0.2	0.196	0.197	0.197667	0.000198
GVL 09	108	0.198	0.2	0.2	0.199333	0.000199	GVL 09	157	0.321	0.315	0.303	0.313	0.000313	GVL 09	206	26.7	26.4	26.9	26.66667	0.026667
GVL 09	109	0.818	0.839	0.791	0.816	0.000816	GVL 09	158	0.057	0.055	0.054	0.055333	5.53E-05	GVL 09	207	0.308	0.306	0.3	0.304667	0.000305
GVL 09	110	2.73	2.19	2.25	2.39	0.00239	GVL 09	159	0.283	0.279	0.274	0.278667	0.000279	GVL 09	208	0.134	0.113	0.125	0.124	0.000124
GVL 09	111	15.7	13.5	14.3	14.5	0.0145	GVL 09	160	0.412	0.422	0.4	0.411333	0.000411	GVL 09	209	0.227	0.274	0.297	0.266	0.000266
GVL 09	112	2.86	2.76	2.78	2.8	0.0028	GVL 09	161	0.436	0.444	0.436	0.438667	0.000439	GVL 09	210	42.4	43.2	45.2	43.6	0.0436
GVL 09	113	0.215	0.215	0.218	0.216	0.000216	GVL 09	162	0.209	0.219	0.219	0.215667	0.000216	GVL 09	211	0.179	0.181	0.193	0.184333	0.000184
GVL 09	114	0.223	0.232	0.226	0.227	0.000227	GVL 09	163	0.234	0.24	0.041	0.171667	0.000172	GVL 09	212	20.6	19.9	18.5	19.66667	0.019667
GVL 09	115	0.183	0.183	0.186	0.184	0.000184	GVL 09	164	0.239	0.246	0.251	0.245333	0.000245	GVL 09	213	48.1	49.7	47.1	48.3	0.0483
GVL 09	116	0.195	0.188	0.185	0.189333	0.000189	GVL 09	165	30	32.2	34.5	32.23333	0.032233	GVL 09	214	28.7	28.7	25.8	27.73333	0.027733
GVL 09	117	0.503	0.461	0.498	0.487333	0.000487	GVL 09	166	0.304	0.303	0.306	0.304333	0.000304	GVL 09	215	2	2.49	2.57	2.353333	0.002353
GVL 09	118	1.43	1.51	1.55	1.496667	0.001497	GVL 09	167	0.24	0.239	0.235	0.238	0.000238	GVL 09	216	0.171	0.178	0.181	0.176667	0.000177
GVL 09	119	5.35	5.21	5.29	5.283333	0.005283	GVL 09	168	0.196	0.202	0.198	0.198667	0.000199	GVL 09	217	0.215	0.209	0.193	0.205667	0.000206
GVL 09	120	0.44	0.448	0.446	0.444667	0.000445	GVL 09	169	0.258	0.258	0.267	0.261	0.000261	GVL 09	218	0.145	0.154	0.142	0.147	0.000147
GVL 09	121	0.65	0.647	0.646	0.647667	0.000648	GVL 09	170	0.331	0.338	0.372	0.347	0.000347	GVL 09	219	0.202	0.217	0.214	0.211	0.000211
GVL 09	122	1.01	1.01	1.05	1.023333	0.001023	GVL 09	171	0.312	286	0.325	95.54567	0.095546	GVL 09	220	0.194	0.191	0.191	0.192	0.000192
GVL 09	123	0.665	0.615	0.606	0.628667	0.000629	GVL 09	172	0.121	0.114	0.114	0.116333	0.000116	GVL 09	221	0.136	0.128	0.122	0.128667	0.000129
GVL 09	124	0.639	0.704	0.734	0.692333	0.000692	GVL 09	173	0.223	0.235	0.263	0.240333	0.00024	GVL 09	222	0.097	0.096	0.101	0.098	0.000098
GVL 09	125	0.193	0.207	0.186	0.195333	0.000195	GVL 09	174	36.2	36.4	36.6	36.4	0.0364	GVL 09	223	0.089	0.093	0.093	0.091667	9.17E-05
GVL 09	126	0.104	0.108	0.114	0.108667	0.000109	GVL 09	175	0.312	0.319	0.316	0.315667	0.000316	GVL 09	224	0.08	0.08	0.081	0.080333	8.03E-05
GVL 09	127	0.155	0.162	0.168	0.161667	0.000162	GVL 09	176	0.322	0.327	0.348	0.332333	0.000332	GVL 09	225	0.123	0.122	0.126	0.123667	0.000124
GVL 09	128	1.26	1.27	1.24	1.256667	0.001257	GVL 09	177	0.846	0.836	0.818	0.833333	0.000833	GVL 09	226	0.07	0.07	0.073	0.071	0.000071
GVL 09	129	24.3	23.6	22.5	23.46667	0.023467	GVL 09	178	0.287	0.273	0.294	0.284667	0.000285	GVL 09	227	1.74	0.155	1.47	1.121667	0.001122
GVL 09	130	11.2	12.1	11.7	11.66667	0.011667	GVL 09	179	0.82	0.822	0.894	0.845333	0.000845	GVL 09	228	0.104	0.102	0.101	0.102333	0.000102

yy

Appendix E: Magnetic Susceptibility

BHID	Depth	Reading 1	Reading 2	Reading 3	Average	SI Units	BHID	Depth	Reading 1	Reading 2	Reading 3	Average	SI Units	BHID	Depth	Reading 1	Reading 2	Reading 3	Average	SI Units
GVL 09	229	2.32	2.56	2.54	2.473333	0.002473	GVL 09	278	0.345	0.408	0.359	0.370667	0.000371	GVL 09	327	24	28.1	26.3	26.13333	0.026133
GVL 09	230	0.118	0.119	0.123	0.12	0.00012	GVL 09	279	0.11	0.112	0.106	0.109333	0.000109	GVL 09	328	35.4	33.9	34.1	34.46667	0.034467
GVL 09	231	0.1	0.1	0.102	0.100667	0.000101	GVL 09	280	0.202	0.2	0.201	0.201	0.000201	GVL 09	329	22.7	22.4	21.4	22.16667	0.022167
GVL 09	232	0.208	0.213	0.212	0.211	0.000211	GVL 09	281	0.45	0.415	0.439	0.434667	0.000435	GVL 09	330	38.6	37.8	36.1	37.5	0.0375
GVL 09	233	0.1	0.103	0.099	0.100667	0.000101	GVL 09	282	0.187	0.183	0.183	0.184333	0.000184	GVL 09	331	41.3	39.3	42.9	41.16667	0.041167
GVL 09	234	CC			#DIV/0!	#DIV/0!	GVL 09	283	0.182	0.186	0.18	0.182667	0.000183	GVL 09	332	31.4	31.1	30.2	30.9	0.0309
GVL 09	235	0.178	0.183	0.181	0.180667	0.000181	GVL 09	284	0.12	0.124	0.119	0.121	0.000121	GVL 09	333	20.7	21.5	20.5	20.9	0.0209
GVL 09	236	0.749	0.743	0.654	0.715333	0.000715	GVL 09	285	0.232	0.246	0.246	0.241333	0.000241	GVL 09	334	9.83	10.1	11	10.31	0.01031
GVL 09	237	0.955	0.854	0.914	0.907667	0.000908	GVL 09	286	0.233	0.234	0.296	0.254333	0.000254	GVL 09	335	81.1	81.3	81	81.13333	0.081133
GVL 09	238	0.175	0.176	0.144	0.165	0.000165	GVL 09	287	8.86	8.88	9.28	9.006667	0.009007	GVL 09	336	83	79	83.7	81.9	0.0819
GVL 09	239	0.623	0.601	0.537	0.587	0.000587	GVL 09	288	12.8	12.9	13.4	13.03333	0.013033	GVL 09	337	48.3	49.5	51.1	49.63333	0.049633
GVL 09	240	0.189	0.19	0.197	0.192	0.000192	GVL 09	289	22.1	20.6	21.3	21.33333	0.021333	GVL 09	338	108	109	109	108.6667	0.108667
GVL 09	241	0.211	0.207	0.206	0.208	0.000208	GVL 09	290	36.1	34.8	36.4	35.76667	0.035767	GVL 09	339	41.4	41.7	39.1	40.73333	0.040733
GVL 09	242	0.215	0.21	0.199	0.208	0.000208	GVL 09	291	8.07	8.01	7.74	7.94	0.00794	GVL 09	340	68.8	79.8	89.9	79.5	0.0795
GVL 09	243	0.229	0.213	0.2	0.214	0.000214	GVL 09	292	0.231	0.202	0.204	0.212333	0.000212	GVL 09	341	15.5	15.2	15.4	15.36667	0.015367
GVL 09	244	0.164	0.171	0.173	0.169333	0.000169	GVL 09	293	0.237	0.239	0.227	0.234333	0.000234	GVL 09	342	61.7	79.3	64.8	68.6	0.0686
GVL 09	245	cc					GVL 09	294	0.154	0.155	0.152	0.153667	0.000154	GVL 09	343	58.5	57.1	59.1	58.23333	0.058233
GVL 09	246	cc					GVL 09	295	0.229	0.196	0.23	0.218333	0.000218	GVL 09	344	15.7	14.7	12.5	14.3	0.0143
GVL 09	247	cc					GVL 09	296	0.134	0.132	0.135	0.133667	0.000134	GVL 09	345	44.1	42.8	43	43.3	0.0433
GVL 09	248	cc					GVL 09	297	0.163	0.157	0.162	0.160667	0.000161	GVL 09	346	39.1	38.7	39.1	38.96667	0.038967
GVL 09	249	cc					GVL 09	298	1.32	1.33	1.34	1.33	0.00133	GVL 09	347	61.9	63.2	62.4	62.5	0.0625
GVL 09	250	cc					GVL 09	299	2.48	2.77	2.85	2.7	0.0027	GVL 09	348	35.5	36.6	36.9	36.33333	0.036333
GVL 09	251						GVL 09	300	23.1	23.3	23.6	23.33333	0.023333	GVL 09	349	66.3	61.2	62.2	63.23333	0.063233
GVL 09	252	0.185	0.167	0.156	0.169333	0.000169	GVL 09	301	7.61	7.77	7.96	7.78	0.00778	GVL 09	350	28.7	30.4	20.2	26.43333	0.026433
GVL 09	253	0.242	0.217	0.23	0.229667	0.00023	GVL 09	302	4.54	4.2	4.25	4.33	0.00433	GVL 09	351	43	40	47.9	43.63333	0.043633
GVL 09	254	0.313	0.313	0.324	0.316667	0.000317	GVL 09	303	34.3	34	33.9	34.06667	0.034067	GVL 09	352	51.2	42.6	41.9	45.23333	0.045233
GVL 09	255	0.971	0.92	1	0.963667	0.000964	GVL 09	304	25.8	26.1	26.4	26.1	0.0261	GVL 09	353	51.1	49.2	38.8	46.36667	0.046367
GVL 09	256	0.16	0.157	0.16	0.159	0.000159	GVL 09	305	10.3	9.33	9.55	9.726667	0.009727	GVL 09	354	68	71.6	71	70.2	0.0702
GVL 09	257	0.179	0.172	0.188	0.179667	0.00018	GVL 09	306	46.6	46.8	46.6	46.66667	0.046667	GVL 09	355	35	32.5	34.3	33.93333	0.033933
GVL 09	258	0.253	0.249	0.243	0.248333	0.000248	GVL 09	307	34.1	34.6	34.8	34.5	0.0345	GVL 09	356	57.5	59.7	58.3	58.5	0.0585
GVL 09	259	0.754	1.13	1.16	1.014667	0.001015	GVL 09	308	25.4	20.4	21.9	22.56667	0.022567	GVL 09	357	32.6	31.7	31.7	32	0.032
GVL 09	260	0.16	0.159	0.156	0.158333	0.000158	GVL 09	309	15.5	17.7	17.5	16.9	0.0169	GVL 09	358	71	75.4	75	73.8	0.0738
GVL 09	261	18.8	18.7	18.7	18.73333	0.018733	GVL 09	310	0.928	0.896	0.981	0.935	0.000935	GVL 09	359	40.5	42.8	39.8	41.03333	0.041033
GVL 09	262	36.8	37.6	37.2	37.2	0.0372	GVL 09	311	0.09	0.092	0.1	0.094	0.000094	GVL 09	360	46.9	49.9	48.4	48.4	0.0484
GVL 09	263	37.6	43.4	46.7	42.56667	0.042567	GVL 09	312	83.6	77.4	81.8	80.93333	0.080933	GVL 09	361	66.8	66.6	65.4	66.26667	0.066267
GVL 09	264	4.56	4.53	4.66	4.583333	0.004583	GVL 09	313	49.2	47.5	48.1	48.26667	0.048267	GVL 09	362	26.4	26.5	25.7	26.2	0.0262
GVL 09	265	24.2	23.9	24.4	24.16667	0.024167	GVL 09	314	55.5	56	54.8	55.43333	0.055433	GVL 09	363	23.4	23.3	23.4	23.36667	0.023367
GVL 09	266	8.97	8.91	8.54	8.806667	0.008807	GVL 09	315	1.13	1.07	1.18	1.126667	0.001127	GVL 09	364	32.9	31.7	30.6	31.73333	0.031733
GVL 09	267	0.365	0.363	0.359	0.362333	0.000362	GVL 09	316	0.008	0.008	0.009	0.008333	8.33E-06	GVL 09	365	74.2	69.7	69.6	71.16667	0.071167
GVL 09	268	0.212	0.207	0.182	0.200333	0.0002	GVL 09	317	0.153	0.156	0.137	0.148667	0.000149	GVL 09	366	56.7	56.2	57.2	56.7	0.0567
GVL 09	269	0.237	0.22	0.227	0.228	0.000228	GVL 09	318	0.369	0.402	0.444	0.405	0.000405	GVL 09	367	61.3	60.6	62.7	61.53333	0.061533
GVL 09	270	0.793	0.717	0.691	0.733667	0.000734	GVL 09	319	15.8	15.6	15.8	15.73333	0.015733	GVL 09	368	0.185	0.215	0.19	0.196667	0.000197
GVL 09	271	21.8	19.6	22.1	21.16667	0.021167	GVL 09	320	51.3	59.6	52.4	54.43333	0.054433	GVL 09	369	18.7	19	17.6	18.43333	0.018433
GVL 09	272	0.18	0.178	0.193	0.183667	0.000184	GVL 09	321	10.9	11	10.8	10.9	0.0109	GVL 09	370	45.7	47.7	46.7	46.7	0.0467
GVL 09	273	0.211	0.214	0.196	0.207	0.000207	GVL 09	322	66.9	67	66.3	66.73333	0.066733	GVL 09	371	71.6	71.4	70.7	71.23333	0.071233
GVL 09	274	0.219	0.229	0.223	0.223667	0.000224	GVL 09	323	84.5	76.1	76.3	78.96667	0.078967	GVL 09	372	60.9	63.7	65.8	63.46667	0.063467
GVL 09	275	0.106	0.081	0.057	0.081333	8.13E-05	GVL 09	324	108	111	111	110	0.11	GVL 09	373	51.3	49.8	50	50.36667	0.050367
GVL 09	276	0.106	0.081	0.057	0.081333	8.13E-05	GVL 09	325	12.4	12.6	12.6	12.53333	0.012533	GVL 09	374	43.5	46.8	46.2	45.5	0.0455
GVL 09	277	0.202	0.201	0.203	0.202	0.000202	GVL 09	326	60.5	61.7	61	61.06667	0.061067	GVL 09	375	44	41.6	46.8	44.13333	0.044133

zz

Appendix E: Magnetic Susceptibility

BHID	Depth	Reading 1	Reading 2	Reading 3	Average	SI Units	BHID	Depth	Reading 1	Reading 2	Reading 3	Average	SI Units	BHID	Depth	Reading 1	Reading 2	Reading 3	Average	SI Units
GVL 09	376	8.57	7.64	8.31	8.173333	0.008173	GVL 09	425	87.7	84.2	83.1	85	0.085	GVL 09	474	c.c				
GVL 09	377	39.3	43.8	43.8	42.3	0.0423	GVL 09	426	77.7	63.3	74.2	71.73333	0.071733	GVL 09	475	c.c				
GVL 09	378	44.9	45.5	45.7	45.36667	0.045367	GVL 09	427	79.5	80.1	79.9	79.83333	0.079833	GVL 09	476	c.c				
GVL 09	379	42.6	41.5	42.5	42.2	0.0422	GVL 09	428	95.1	101	103	99.7	0.0997	GVL 09	477	c.c				
GVL 09	380	46.8	36.1	40.8	41.23333	0.041233	GVL 09	429	96.6	96.2	97.5	96.76667	0.096767	GVL 09	478	c.c				
GVL 09	381	23	22.6	21.4	22.33333	0.022333	GVL 09	430	98.5	102	102	100.8333	0.100833	GVL 09	479	c.c				
GVL 09	382	0.187	0.203	0.199	0.196333	0.000196	GVL 09	431	103	105	107	105	0.105	GVL 09	480	c.c				
GVL 09	383	45.2	50.1	52	49.1	0.0491	GVL 09	432	71.2	73.5	72.6	72.43333	0.072433	GVL 09	481	c.c				
GVL 09	384	0.225	0.223	0.24	0.229333	0.000229	GVL 09	433	80.5	84.8	85.9	83.73333	0.083733	GVL 09	482	c.c				
GVL 09	385	45.4	49	49.6	48	0.048	GVL 09	434	47.2	47.1	41.7	45.33333	0.045333	GVL 09	483	c.c				
GVL 09	386	48.6	49	48.2	48.6	0.0486	GVL 09	435	78.3	77.5	70.1	75.3	0.0753	GVL 09	484	c.c				
GVL 09	387	45.2	46	46.7	45.96667	0.045967	GVL 09	436	101	103	104	102.6667	0.102667	GVL 09	485	c.c				
GVL 09	388	37.5	46.7	47.1	43.76667	0.043767	GVL 09	437	70	71.8	72	71.26667	0.071267	GVL 09	486	3.31	3.21	3.3	3.273333	0.003273
GVL 09	389	33.9	34.3	34.2	34.13333	0.034133	GVL 09	438	98.3	97.5	90.7	95.5	0.0955	GVL 09	487	c.c				
GVL 09	390	34.4	36.8	36.2	35.8	0.0358	GVL 09	439	71.7	78.2	74.9	74.93333	0.074933	GVL 09	488	c.c				
GVL 09	391	50.5	50.3	51.8	50.86667	0.050867	GVL 09	440	52	58.3	61	57.1	0.0571	GVL 09	489	c.c			#DIV/0!	#DIV/0!
GVL 09	392	37	40.5	40.7	39.4	0.0394	GVL 09	441	61.7	55.4	50.7	55.93333	0.055933	GVL 09	490	16.2	16.3	15.9	16.13333	0.016133
GVL 09	393	27.7	26.7	26.5	26.96667	0.026967	GVL 09	442	56.5	81.5	90.4	76.13333	0.076133	GVL 09	491	c.c				
GVL 09	394	36.7	36	37	36.56667	0.036567	GVL 09	443	40.1	32.2	37.6	36.63333	0.036633	GVL 09	492	c.c				
GVL 09	395	51.6	49.3	46	48.96667	0.048967	GVL 09	444	57.3	49.3	49.4	52	0.052	GVL 09	493	c.c				
GVL 09	396	44	46.6	45.6	45.4	0.0454	GVL 09	445	98.9	104	103	101.9667	0.101967	GVL 09	494	c.c				
GVL 09	397	62.5	67.5	67.9	65.96667	0.065967	GVL 09	446	110	118	121	116.3333	0.116333	GVL 09	495	c.c				
GVL 09	398	51.2	49	47.1	49.1	0.0491	GVL 09	447	110	109	98.7	105.9	0.1059	GVL 09	496	8.47	8.08	8.65	8.4	0.0084
GVL 09	399	75.2	75.3	74	74.83333	0.074833	GVL 09	448	91.3	101	95.9	96.06667	0.096067	GVL 09	497	c.c				
GVL 09	400	43	44	54.4	47.13333	0.047133	GVL 09	449	92.3	93.2	95.9	93.8	0.0938	GVL 09	498	2.72	2.32	2.36	2.466667	0.002467
GVL 09	401	74.8	75.1	75.5	75.13333	0.075133	GVL 09	450	83.6	85.2	87.3	85.36667	0.085367	GVL 09	499	0.001	0	0	0.000333	3.33E-07
GVL 09	402	43.3	46.4	46.3	45.33333	0.045333	GVL 09	451	84.1	88.2	86	86.1	0.0861	GVL 09	500	4.43	4.96	5	4.796667	0.004797
GVL 09	403	51.8	51.9	50.2	51.3	0.0513	GVL 09	452	84.4	86	87.1	85.83333	0.085833	GVL 09	501	2.23	2.4	2.4	2.343333	0.002343
GVL 09	404	38.3	46	41.2	41.83333	0.041833	GVL 09	453	59.6	67.4	62.6	63.2	0.0632	GVL 09	502	5.19	5.23	5.11	5.176667	0.005177
GVL 09	405	57.1	57.8	57	57.3	0.0573	GVL 09	454	74.1	71.7	73.3	73.03333	0.073033	GVL 09	503	3.17	3.5	3.63	3.433333	0.003433
GVL 09	406	63.5	62.8	62.5	62.93333	0.062933	GVL 09	455	83.8	83.2	85.4	84.13333	0.084133	GVL 09	504	0.009	0.001	0.008	0.006	0.000006
GVL 09	407	57.6	57.2	57.6	57.46667	0.057467	GVL 09	456	84	83	81.3	82.76667	0.082767	GVL 09	505	4.45	4.46	4.54	4.483333	0.004483
GVL 09	408	37.6	35.2	35.1	35.96667	0.035967	GVL 09	457	18.5	18	17.7	18.06667	0.018067	GVL 09	506	2.29	2.05	2.09	2.143333	0.002143
GVL 09	409	44.6	44.9	44.9	44.8	0.0448	GVL 09	458	63.4	66.2	67.5	65.7	0.0657	GVL 09	507	1.27	1.27	1.26	1.266667	0.001267
GVL 09	410	22.1	22.4	22.6	22.36667	0.022367	GVL 09	459	124	112	100	112	0.112	GVL 09	508	2.07	2.13	2.15	2.116667	0.002117
GVL 09	411	96.7	95.2	96.7	96.2	0.0962	GVL 09	460	61.1	57.9	58.4	59.13333	0.059133	GVL 09	509	2.69	2.75	2.46	2.633333	0.002633
GVL 09	412	52.9	44.1	52.8	49.93333	0.049933	GVL 09	461	258	214	219	230.3333	0.230333	GVL 09	510	0.083	0.085	0.083	0.083667	8.37E-05
GVL 09	413	47.4	49.2	52.3	49.63333	0.049633	GVL 09	462	65.1	62.2	60.4	62.56667	0.062567	GVL 09	511	1.86	1.78	1.8	1.813333	0.001813
GVL 09	414	57.8	40.2	59.9	52.63333	0.052633	GVL 09	463	70.1	67.4	71.8	69.76667	0.069767	GVL 09	512	2.32	3.3	3.71	3.11	0.00311
GVL 09	415	79.4	77.4	78.4	78.4	0.0784	GVL 09	464	95.2	89.9	91.2	92.1	0.0921	GVL 09	513	2.69	2.53	2.6	2.606667	0.002607
GVL 09	416	77.8	77.9	76	77.23333	0.077233	GVL 09	465	45.7	46.2	44.7	45.53333	0.045533	GVL 09	514	2.61	2.65	2.81	2.69	0.00269
GVL 09	417	38.8	41.1	39.8	39.9	0.0399	GVL 09	466	3.7	3.61	3.53	3.613333	0.003613	GVL 09	515	1.82	2	1.84	1.886667	0.001887
GVL 09	418	72.6	73.9	73.9	73.46667	0.073467	GVL 09	467	14.4	14.7	13.2	14.1	0.0141	GVL 09	516	2.39	2.07	2.3	2.253333	0.002253
GVL 09	419	35.8	36.4	37.2	36.46667	0.036467	GVL 09	468	32.2	32.3	32.9	32.46667	0.032467	GVL 09	517	2.3	2.28	2.37	2.316667	0.002317
GVL 09	420	70.2	69.1	72	70.43333	0.070433	GVL 09	469	36.1	36.5	31.9	34.83333	0.034833	GVL 09	518	2.09	2.39	2.84	2.44	0.00244
GVL 09	421	100	98.4	95.7	98.03333	0.098033	GVL 09	470	21.3	19.1	21	20.46667	0.020467	GVL 09	519	5.72	5.05	5.2	5.323333	0.005323
GVL 09	422	45.6	47.4	46.3	46.43333	0.046433	GVL 09	471	27.4	26.1	26.3	26.6	0.0266	GVL 09	520	1.15	0.94	1.19	1.093333	0.001093
GVL 09	423	40.5	42.1	38.8	40.46667	0.040467	GVL 09	472	26.6	26.5	26	26.36667	0.026367	GVL 09	521	1.88	1.95	1.92	1.916667	0.001917
GVL 09	424	49	49.7	49.2	49.3	0.0493	GVL 09	473	25.5	35.4	34.6	31.83333	0.031833	GVL 09	522	2.65	2.79	3.06	2.833333	0.002833

aaa

Appendix E: Magnetic Susceptibility

BHID	Depth	Reading 1	Reading 2	Reading 3	Average	SI Units	BHID	Depth	Reading 1	Reading 2	Reading 3	Average	SI Units	BHID	Depth	Reading 1	Reading 2	Reading 3	Average	SI Units
GVL 09	523	cc					GVL 09	572	0.599	0.615	0.613	0.609	0.000609	GVL 11	40.5	0.121	0.095	0.099	0.105	0.000
GVL 09	524	cc					GVL 09	573	0.373	0.328	0.335	0.345333	0.000345	GVL 11	41	0.053	0.071	0.06	0.061	0.000
GVL 09	525	cc					GVL 09	574	0.482	0.522	0.634	0.546	0.000546	GVL 11	41.5	0.047	0.039	0.043	0.043	0.000
GVL 09	526	cc					GVL 09	575	0.387	0.39	0.416	0.397667	0.000398	GVL 11	42	0.013	0.014	0.016	0.014	0.000
GVL 09	527	cc					GVL 09	576	1.28	1.17	1.15	1.2	0.0012	GVL 11	42.5	0.059	0.05	0.043	0.051	0.000
GVL 09	528	0.785	0.961	0.714	0.82	0.00082	GVL 09	577	0.363	0.319	0.318	0.333333	0.000333	GVL 11	43	0.095	0.099	0.103	0.099	0.000
GVL 09	529	0.754	0.662	0.639	0.685	0.000685	GVL 09	578	0.329	0.338	0.345	0.337333	0.000337	GVL 11	43.5	0.071	0.065	0.077	0.071	0.000
GVL 09	530	2.37	1.46	2.88	2.236667	0.002237	GVL 09	579	0.326	0.291	0.304	0.307	0.000307	GVL 11	44	0.066	0.068	0.074	0.069	0.000
GVL 09	531	4.49	4.64	4.56	4.563333	0.004563	GVL 09	580	0.617	0.657	0.704	0.659333	0.000659	GVL 11	44.5	0.093	0.083	0.108	0.095	0.000
GVL 09	532	1.07	0.964	1.07	1.034667	0.001035	GVL 09	581	0.489	0.527	0.465	0.493667	0.000494	GVL 11	45	0.086	0.084	0.097	0.089	0.000
GVL 09	533	2.03	1.81	1.78	1.873333	0.001873	GVL 09	582	0	0.205	0.241	0.148667	0.000149	GVL 11	45.5	0.039	0.041	0.057	0.046	0.000
GVL 09	534	1.83	2.62	2.21	2.22	0.00222	GVL 09	583	1.25	1.12	1.43	1.266667	0.001267	GVL 11	46	0.074	0.087	0.07	0.077	0.000
GVL 09	535	2.09	2.17	2.21	2.156667	0.002157	GVL 09	584	0.933	0.822	0.935	0.896667	0.000897	GVL 11	46.5	0.112	0.093	0.112	0.106	0.000
GVL 09	536	2.65	2.73	2.66	2.68	0.00268	GVL 09	585	0.779	0.854	0.851	0.828	0.000828	GVL 11	47	0.099	0.099	0.099	0.099	0.000
GVL 09	537	1.7	1.64	1.68	1.673333	0.001673	GVL 09	586	0.38	0.366	0.389	0.378333	0.000378	GVL 11	47.5	0.118	0.124	0.119	0.120	0.000
GVL 09	538	1.89	1.63	1.61	1.71	0.00171	GVL 09	587	0.646	0.59	0.626	0.620667	0.000621	GVL 11	48	0.096	0.097	0.084	0.092	0.000
GVL 09	539	0	0.131	0.137	0.089333	8.93E-05	GVL 09	588	0.697	0.693	0.679	0.689667	0.00069	GVL 11	48.5	0.135	0.146	0.123	0.135	0.000
GVL 09	540	0.17	0.94	0.157	0.422333	0.000422	GVL 09	589	0.566	0.559	0.548	0.557667	0.000558	GVL 11	49	0.054	0.061	0.08	0.065	0.000
GVL 09	541	0.293	0.313	0.258	0.288	0.000288	GVL 09	590	0.568	0.691	0.682	0.647	0.000647	GVL 11	49.5	0.158	0.149	0.152	0.153	0.000
GVL 09	542	0.288	0.281	0.25	0.273	0.000273	GVL 09	591	0.479	0.497	0.405	0.460333	0.00046	GVL 11	50	0.117	0.115	0.158	0.130	0.000
GVL 09	543	0.339	0.343	0.264	0.315333	0.000315	GVL 09	592	0.458	0.449	0.472	0.459667	0.00046	GVL 11	50.5	0.146	0.132	0.165	0.148	0.000
GVL 09	544	0.363	0.335	0.346	0.348	0.000348	GVL 09	593	0.389	0.386	0.3387	0.371233	0.000371	GVL 11	51	0.113	0.141	0.164	0.139	0.000
GVL 09	545	2.12	2.33	2.86	2.436667	0.002437	GVL 09	594	0.132	0.107	0.119	0.119333	0.000119	GVL 11	51.5	0.095	0.129	0.124	0.116	0.000
GVL 09	546	1.85	1.71	1.99	1.85	0.00185	GVL 09	595	0.136	0.608	0.782	0.508667	0.000509	GVL 11	52	0.095	0.14	0.135	0.123	0.000
GVL 09	547	2.67	2.76	2.79	2.74	0.00274	GVL 09	596	0.463	0.464	0.454	0.460333	0.00046	GVL 11	52.5	0.13	0.127	0.109	0.122	0.000
GVL 09	548	2.49	2.37	2.53	2.463333	0.002463	GVL 09	597	0.378	0.466	0.464	0.436	0.000436	GVL 11	53	0.148	0.14	0.111	0.133	0.000
GVL 09	549	1.69	1.72	2.08	1.83	0.00183	GVL 09	598	0.698	0.61	0.62	0.642667	0.000643	GVL 11	53.5	0.076	0.078	0.114	0.089	0.000
GVL 09	550	1.01	1.05	1.01	1.023333	0.001023	GVL 09	599	0.392	0.346	0.373	0.370333	0.00037	GVL 11	54	0.113	0.11	0.123	0.115	0.000
GVL 09	551	0.676	0.63	0.753	0.686333	0.000686	GVL 09	600	0.307	0.476	0.474	0.419	0.000419	GVL 11	55	0.04	0.042	0.049	0.044	0.000
GVL 09	552	1.18	1.1	1.07	1.116667	0.001117	GVL 09	601	0.77	0.655	0.571	0.665333	0.000665	GVL 11	56					0.000
GVL 09	553	0.808	0.867	0.839	0.838	0.000838	GVL 09	602	0.6	0.582	0.627	0.603	0.000603	GVL 11	57	0.039	0.042	0.052	0.044	0.000
GVL 09	554	1.96	1.86	1.93	1.916667	0.001917	**BHID**	**Depth**	**Reading 1**	**Reading 2**	**Reading 3**	**Average**	**SI Units**	GVL 11	58	0.032	0.038	0.042	0.037	0.000
GVL 09	555	0.291	0.289	0.3	0.293333	0.000293	GVL 11	32	0.223	0.187	0.166	0.192	0.000	GVL 11	59	0.027	0.025	0.024	0.025	0.000
GVL 09	556	1.2	1.22	1.14	1.186667	0.001187	GVL 11	32.5	0.058	0.081	0.078	0.072	0.000	GVL 11	60	0.052	0.056	0.048	0.052	0.000
GVL 09	557	1.5	1.51	0.188	1.066	0.001066	GVL 11	33	0.043	0.04	0.066	0.050	0.000	GVL 11	61	0.02	0.056	0.059	0.045	0.000
GVL 09	558	0.277	0.275	0.313	0.288333	0.000288	GVL 11	33.5	0.017	0.025	0.03	0.024	0.000	GVL 11	62	0.039	0.035	0.037	0.037	0.000
GVL 09	559	0.285	0.347	0.355	0.329	0.000329	GVL 11	34	0.112	0.138	0.215	0.155	0.000	GVL 11	63	0.057	0.07	0.08	0.069	0.000
GVL 09	560	0.565	0.589	0.572	0.575333	0.000575	GVL 11	34.5	0.287	0.356	0.351	0.331	0.000	GVL 11	64	0.053	0.056	0.062	0.057	0.000
GVL 09	561	0	1.14	0.798	0.646	0.000646	GVL 11	35	0.09	0.149	0.155	0.131	0.000	GVL 11	65	0.044	0.05	0.042	0.045	0.000
GVL 09	562	cc					GVL 11	35.5	0.141	0.222	0.38	0.248	0.000	GVL 11	66	0.095	0.083	0.084	0.087	0.000
GVL 09	563	0.735	0.668	0.617	0.673333	0.000673	GVL 11	36	0.076	0.091	0.095	0.087	0.000	GVL 11	67	0.031	0.04	0.04	0.037	0.000
GVL 09	564	0.407	0.415	0.382	0.401333	0.000401	GVL 11	36.5	0.055	0.058	0.063	0.059	0.000	GVL 11	68	0.05	0.048	0.056	0.051	0.000
GVL 09	565	0.6	0.617	0.465	0.560667	0.000561	GVL 11	37	0.192	0.2	0.216	0.203	0.000	GVL 11	69	0.035	0.031	0.029	0.032	0.000
GVL 09	566	0.876	0.93	0.882	0.896	0.000896	GVL 11	37.5	0.167	0.184	0.184	0.178	0.000	GVL 11	70	0.039	0.042	0.056	0.046	0.000
GVL 09	567	0.89	0.844	0.856	0.863333	0.000863	GVL 11	38	0.154	0.156	0.187	0.166	0.000	GVL 11	71	0.071	0.051	0.068	0.063	0.000
GVL 09	568	1.34	1.65	1.53	1.506667	0.001507	GVL 11	38.5	0.278	0.273	0.221	0.257	0.000	GVL 11	72	0.085	0.092	0.09	0.089	0.000
GVL 09	569	1.21	1.16	1.3	1.223333	0.001223	GVL 11	39	0.188	0.19	0.195	0.191	0.000	GVL 11	73	0.052	0.062	0.053	0.056	0.000
GVL 09	570	1.52	1.52	1.31	1.45	0.00145	GVL 11	39.5	0.117	0.131	0.162	0.137	0.000	GVL 11	74	0.017	0.034	0.033	0.028	0.000
GVL 09	571	0.727	0.823	0.926	0.825333	0.000825	GVL 11	40	0.197	0.165	0.201	0.188	0.000	GVL 11	75	0.032	0.04	0.046	0.039	0.000

bbb

Appendix E: Magnetic Susceptibility

BHID	Depth	Reading 1	Reading 2	Reading 3	Average	SI Units	BHID	Depth	Reading 1	Reading 2	Reading 3	Average	SI Units	BHID	Depth	Reading 1	Reading 2	Reading 3	Average	SI Units
GVL 11	76	0.083	0.077	0.077	0.079	0.000	GVL 11	125	0.259	0.299	0.298	0.285	0.000	GVL 11	174	0.12	0.148	0.147	0.138	0.000
GVL 11	77	0.001	0.002	0.001	0.001	0.000	GVL 11	126	0.313	0.213	0.259	0.262	0.000	GVL 11	175	0.269	0.272	0.227	0.256	0.000
GVL 11	78	0.094	0.07	0.087	0.084	0.000	GVL 11	127	0.189	0.217	0.206	0.204	0.000	GVL 11	176	0.336	0.477	0.471	0.428	0.000
GVL 11	79	0.138	0.065	0.144	0.116	0.000	GVL 11	128	0.176	0.247	0.239	0.221	0.000	GVL 11	177	0.123	0.142	0.164	0.143	0.000
GVL 11	80	0.112	0.105	0.066	0.094	0.000	GVL 11	129	0.2	0.192	0.164	0.185	0.000	GVL 11	178	0.159	0.119	0.141	0.140	0.000
GVL 11	81	0.181	0.161	0.184	0.175	0.000	GVL 11	130	0.099	0.144	0.124	0.122	0.000	GVL 11	179	0.129	0.15	0.116	0.132	0.000
GVL 11	82	0.113	0.134	0.131	0.126	0.000	GVL 11	131	0.187	0.237	0.2	0.208	0.000	GVL 11	180	0.289	0.264	0.279	0.277	0.000
GVL 11	83	0.103	0.073	0.11	0.095	0.000	GVL 11	132	0.254	0.268	0.249	0.257	0.000	GVL 11	181	0.28	0.361	0.393	0.345	0.000
GVL 11	84	0.092	0.103	0.089	0.095	0.000	GVL 11	133	0.193	0.164	0.18	0.179	0.000	GVL 11	182	0.002	0.003	0.001	0.002	0.000
GVL 11	85	0.04	0.062	0.064	0.055	0.000	GVL 11	134	0.288	0.361	0.337	0.329	0.000	GVL 11	183	0.318	0.246	0.204	0.256	0.000
GVL 11	86	0.041	0.05	0.04	0.044	0.000	GVL 11	135	0.223	0.205	0.158	0.195	0.000	GVL 11	184	0.14	0.22	0.188	0.183	0.000
GVL 11	87	0.102	0.08	0.091	0.091	0.000	GVL 11	136	0.131	0.203	0.199	0.178	0.000	GVL 11	185	0.232	0.22	0.212	0.221	0.000
GVL 11	88	0.081	0.087	0.09	0.086	0.000	GVL 11	137	0.684	0.423	0.494	0.534	0.001	GVL 11	186	0.383	0.369	0.43	0.394	0.000
GVL 11	89	0.107	0.126	0.089	0.107	0.000	GVL 11	138	0.381	0.291	0.387	0.353	0.000	GVL 11	187	0.416	0.412	0.481	0.436	0.000
GVL 11	90	0.064	0.057	0.055	0.059	0.000	GVL 11	139	0.205	0.235	0.212	0.217	0.000	GVL 11	188	0.446	0.559	0.502	0.502	0.001
GVL 11	91	0.116	0.107	0.136	0.120	0.000	GVL 11	140	0.212	0.239	0.224	0.225	0.000	GVL 11	189	0.334	0.362	0.37	0.355	0.000
GVL 11	92	0.064	0.061	0.071	0.065	0.000	GVL 11	141	0.251	0.264	0.252	0.256	0.000	GVL 11	190	0.493	0.685	0.711	0.630	0.001
GVL 11	93	0.068	0.056	0.068	0.064	0.000	GVL 11	142	0.26	0.198	0.272	0.243	0.000	GVL 11	191	0.382	0.426	0.452	0.420	0.000
GVL 11	94	0.096	0.091	0.097	0.095	0.000	GVL 11	143	0.19	0.289	0.259	0.246	0.000	GVL 11	192	0.496	0.516	0.447	0.486	0.000
GVL 11	95	0.139	0.133	0.157	0.143	0.000	GVL 11	144	0.011	0.011	0.01	0.011	0.000	GVL 11	193	0.335	0.329	0.39	0.351	0.000
GVL 11	96	0.049	0.045	0.05	0.048	0.000	GVL 11	145	0.262	0.226	0.226	0.238	0.000	GVL 11	194	0.52	0.402	0.369	0.430	0.000
GVL 11	97	0.048	0.059	0.046	0.051	0.000	GVL 11	146	0.151	0.16	0.17	0.160	0.000	GVL 11	195	0.381	0.376	0.382	0.380	0.000
GVL 11	98	0.081	0.083	0.095	0.086	0.000	GVL 11	147	0.212	0.221	0.235	0.223	0.000	GVL 11	196	0.462	0.507	0.41	0.460	0.000
GVL 11	99	0.067	0.065	0.062	0.065	0.000	GVL 11	148	0.194	0.145	0.167	0.169	0.000	GVL 11	197	0.383	0.314	0.463	0.387	0.000
GVL 11	100	0.23	0.234	0.262	0.242	0.000	GVL 11	149	0.121	0.188	0.123	0.144	0.000	GVL 11	198	0.567	0.547	0.644	0.586	0.001
GVL 11	101	0.132	0.133	0.176	0.147	0.000	GVL 11	150	0.113	0.147	0.156	0.139	0.000	GVL 11	199	0.409	0.508	0.532	0.483	0.000
GVL 11	102	0.235	0.24	0.252	0.242	0.000	GVL 11	151					0.000	GVL 11	200	0.286	0.256	0.342	0.295	0.000
GVL 11	103	0.127	0.232	0.229	0.196	0.000	GVL 11	152	0.146	0.136	0.146	0.143	0.000	GVL 11	201	0.218	0.228	0.269	0.238	0.000
GVL 11	104	0.156	0.171	0.204	0.177	0.000	GVL 11	153	0.121	0.11	0.094	0.108	0.000							
GVL 11	105	0.128	0.118	0.127	0.124	0.000	GVL 11	154	0.193	0.076	0.122	0.130	0.000							
GVL 11	106	0.192	0.192	0.262	0.215	0.000	GVL 11	155	0.125	0.127	0.139	0.130	0.000							
GVL 11	107	0.184	0.182	0.156	0.174	0.000	GVL 11	156	0.131	0.151	0.162	0.148	0.000							
GVL 11	108					0.000	GVL 11	157	0.204	0.169	0.243	0.205	0.000							
GVL 11	109	0.156	0.116	0.15	0.141	0.000	GVL 11	158	0.162	0.184	0.231	0.192	0.000							
GVL 11	110	0.233	0.205	0.2	0.213	0.000	GVL 11	159	0.128	0.147	0.126	0.134	0.000							
GVL 11	111	0.312	0.284	0.299	0.298	0.000	GVL 11	160	0.178	0.148	0.17	0.165	0.000							
GVL 11	112	0.222	0.221	0.19	0.211	0.000	GVL 11	161	0.103	0.086	0.113	0.101	0.000							
GVL 11	113	0.265	0.236	0.278	0.260	0.000	GVL 11	162	0.173	0.244	0.17	0.196	0.000							
GVL 11	114	0.595	0.489	0.528	0.537	0.001	GVL 11	163	0.122	0.078	0.133	0.111	0.000							
GVL 11	115	0.116	0.133	0.128	0.126	0.000	GVL 11	164	0.258	0.219	0.253	0.243	0.000							
GVL 11	116	0.189	0.142	0.203	0.178	0.000	GVL 11	165	0.238	0.214	0.27	0.241	0.000							
GVL 11	117	0.1	0.141	0.156	0.132	0.000	GVL 11	166	0.254	0.175	0.197	0.209	0.000							
GVL 11	118	0.123	0.141	0.121	0.128	0.000	GVL 11	167	0.205	0.179	0.133	0.172	0.000							
GVL 11	119	0.145	0.108	0.12	0.124	0.000	GVL 11	168	0.292	0.202	0.156	0.217	0.000							
GVL 11	120	0.125	0.098	0.213	0.145	0.000	GVL 11	169	0.103	0.073	0.088	0.088	0.000							
GVL 11	121	0.143	0.139	0.142	0.141	0.000	GVL 11	170	0.148	0.115	0.17	0.144	0.000							
GVL 11	122	0.15	0.156	0.16	0.155	0.000	GVL 11	171	0.267	0.253	0.217	0.246	0.000							
GVL 11	123	0.169	0.152	0.142	0.154	0.000	GVL 11	172	0.125	0.12	0.129	0.125	0.000							
GVL 11	124	0.1	0.097	0.105	0.101	0.000	GVL 11	173	0.156	0.197	0.159	0.171	0.000							

ccc

Appendix F: Pt/Pd ratios across the Bushveld Complex

Limb	Location	Reef	Pt	Pd	Au	Pt/Pd	Limb	Location	Reef	Pt	Pd	Au	Pt/Pd
Western	Amandabult	Merensky	56	30	4	1.9	Eastern	Booysendal	Merensky	58.4	30.9	8.2	1.9
Western	Amandabult	UG2	55	19	2	2.9	Eastern	Booysendal	UG2	55.3	35.1	1.2	1.6
Western	Rustenburg Area	Merensky	58	24	5	2.4	Eastern	Der Brochen	Merensky	58.2	31	8	1.9
Western	Rustenburg Area	UG2	54	20	2	2.7	Eastern	Der Brochen	UG2	53	37.4	1.2	1.4
Western	Rustenburg Area	UG2	62	27	1	2.3	Eastern	Spitzkop	Merensky	57	32	7	1.8
Western	Pandora	UG2	56.9	31.6	1.4	1.8	Eastern	Spitzkop	UG2	54	35	1	1.5
Western	Marikana	UG2	58.4	29.4	1	2.0	Eastern	Kennedy's Vale	Merensky	57	33	6	1.7
Western	Marikana Lonmin	Merensky	63.8	27.7	5.1	2.3	Eastern	Kennedy's Vale	UG2	53	35	1	1.5
Western	Marikana Lonmin	UG2	60.6	28.1	0.7	2.2	Eastern	Tubase	Merensky	45	43	2	1.0
Western	Marikana Lonmin	UG2	47.5	23	0.5	2.1	Eastern	Tubase	UG2	60	26	9	2.3
Western	RPM Rustenburg	Merensky	67.3	24.4	3.9	2.8	Eastern	Garatau	Merensky	44	45	2	1.0
Western	RPM Rustenburg	UG2	54.9	34.4	0.7	1.6	Eastern	Garatau	UG2	59	28	8	2.1
Western	Impala	Merensky	56.9	24.9	25.8	2.3	Eastern	Modikwa	Merensky	59.2	30.9	5.7	1.9
Western	Impala	UG2	47.6	25.8	0.7	1.8	Eastern	Modikwa	UG2	43.8	46	1.4	1.0
Western	BRPM	Merensky	64.3	26.9	4.9	2.4	Eastern	Smokey Hills	UG2	45	45	1	1.0
Western	BRPM	UG2	58.5	30.3	0.7	1.9	Eastern	Marula	Merensky	53.4	31	6.8	1.7
Western	Styldrift	Merensky	63.8	27.3	4.8	2.3	Eastern	Marula	UG2	37.1	38	1	1.0
Western	Styldrift	UG2	59.2	30.1	0.6	2.0	Eastern	Twickenham	Merensky	60	30	6.3	2.0
Western	WBJV Project 3	Merensky	64	27	5	2.4	Eastern	Twickenham	UG2	43.1	47.2	1.5	0.9
Western	WBJV Project 3	UG2	62	28	1	2.2	Eastern	Ga-Pasha	Merensky	61	29.3	6.2	2.1
Western	Wesizwe Core	UG2	61.8	28	0.46	2.2	Eastern	Ga-Pasha	UG2	42.1	47.9	1.8	0.9
Western	WBJV Project 1	Merensky	64	27	5	2.4	Eastern	Lebowa	Merensky	62.9	27.4	5.9	2.3
Western	WBJV Project 1	UG2	63	26	1	2.4	Eastern	Lebowa	UG2	41.1	48.8	1.9	0.8
Western	Rooderand	Merensky	60.7	27.5	0.6	2.2	Eastern	Phosiri		56.9	32.9	7	1.7
Western	Rooderand	UG2	61.7	29	2	2.1	Eastern	Phosiri		48.3	42.1	2	1.1
Western	RPM Union	Merensky	62.2	28.5	3.7	2.2	Eastern	Mphalele		51.5	37.5	4	1.4
Western	RPM Union	UG2	59.2	28.4	0.5	2.1	Eastern	Mphalele		51.5	37.5	4	1.4
Western	RPM Amandebult	Merensky	62	28.9	3.6	2.1	Eastern	Limpopo		56.7	31.9	4.2	1.8
Western	RPM Amandebult	UG2	60.4	27.1	0.7	2.2	Eastern	Limpopo		47.1	42.8	2.2	1.1
Western	Northam	Merensky	63	29.2	2.6	2.2	Eastern	Maandagshoek	Merensky	60	21	5	2.9
Western	Northam	UG2	57.8	30.9	1	1.9	Eastern	Maandagshoek	UG2	40	35	1	1.1
Eastern	Sheba's Ridge	UG2	23.83	69.46	5.45	0.3	Northern	Warsprings	B Reef	34	58	8	0.6
Eastern	Blue Ridge	UG2	50.3	23.5	1	2.1	Northern	Warsprings	B Reef	34	58	8	0.6
Eastern	Kliprivier	UG2	53	37	1.1	1.4	Northern	Akanani	Platreef	42.6	48.1	5.7	0.9
Eastern	Everest	UG2	59	29.5	1	2.0	Northern	Mogalakwena	Platreef	42.65	47.57	6.8	0.9
Eastern	Mareesburg	UG2	55.1	34.8	1.1	1.6	Northern	Boikgansho	Platreef	42.25	51.2	7.01	0.8
Eastern	Mototolo	UG2	55.1	34.8	1.1	1.6	Northern	Grasvalley		42.3	48.8	2.4	0.9
Eastern	Two Rivers	Merensky	56.6	27.4	6.4	2.1	Northern	Platreef Area	Merensky-li	42	40	7	1.1
Eastern	Two Rivers	UG2	46	27.8	0.8	1.7							

Appendix G: Map of Grasvally area with available structural data adapted from Hulbert (1983)

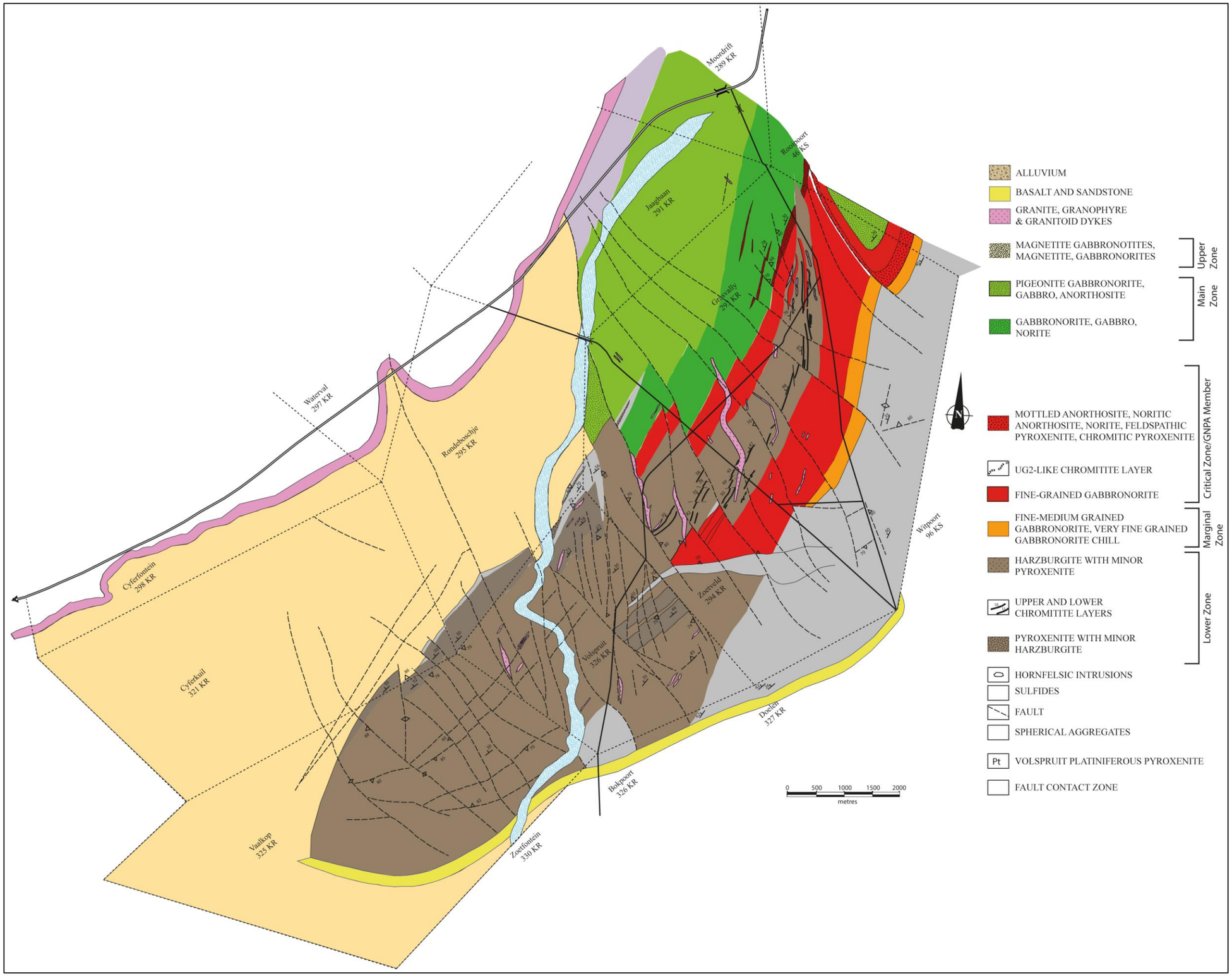

a